15–20 September
1975
Budapest, Hungary

Edited by
E. Wolfram

Volume 1
PREPRINTS OF
CONTRIBUTED
PAPERS

Akadémiai Kiadó
Budapest

PROCEEDINGS
of the
INTERNATIONAL CONFERENCE ON COLLOID AND SURFACE SCIENCE

Proceedings of the
INTERNATIONAL CONFERENCE
ON COLLOID AND SURFACE SCIENCE

Edited by
E. WOLFRAM

Volume 1
Preprints of Contributed Papers

This volume contains papers presented at the International Conference on Colloid and Surface Science held in September, 1975 in Budapest, Hungary. The purpose of this IUPAC-sponsored meeting was to cover as many subjects as possible of this broad field of science. Thus, the reader is provided with a survey of the present status of research work carried out in a great number of laboratories in twenty countries on seemingly different topics having one essential feature in common: they are concerned with materials possessing large surface area and/or supermolecular structure elements.

The following areas have been dealt with: surface structure and surface chemistry of solids; adsorption at solid/gas and solid/liquid interfaces; wetting; thin liquid films; adsorption of polymers; adsorption of surfactants; formation of disperse systems; stability and structure of disperse systems; electrical phenomena; rheology; gels; micellization and related phenomena; monolayers and foams; molecular interactions; applications; methods.

The second volume containing the discussions of the Conference will follow at a later date.

AKADÉMIAI KIADÓ
Publishing House of the Hungarian Academy of Sciences
Budapest

PROCEEDINGS

OF THE

INTERNATIONAL CONFERENCE ON COLLOID AND SURFACE SCIENCE

sponsored by the

INTERNATIONAL UNION OF PURE AND APPLIED CHEMISTRY

15–20 September, 1975
Budapest, Hungary

COLLOIDS
BUDAPEST
1975

PROCEEDINGS OF THE

INTERNATIONAL CONFERENCE ON COLLOID AND SURFACE SCIENCE

SPONSORED BY THE

INTERNATIONAL UNION
OF PURE AND APPLIED CHEMISTRY

15–20 September, 1975
Budapest, Hungary

Edited by
E. WOLFRAM

VOLUME 1
Preprints of contributed papers



AKADÉMIAI KIADÓ, BUDAPEST 1975
PUBLISHING HOUSE OF THE HUNGARIAN ACADEMY OF SCIENCES

CONFERENCE ORGANIZED BY

HUNGARIAN CHEMICAL SOCIETY
AND
COMMISSION ON COLLOID AND SURFACE SCIENCE,
HUNGARIAN ACADEMY OF SCIENCES

HONORARY PRESIDENT

PROFESSOR T. ERDEY-GRÚZ
PRESIDENT OF THE HUNGARIAN ACADEMY OF SCIENCES

CHAIRMAN

PROFESSOR G. SCHAY
MEMBER OF THE HUNGARIAN ACADEMY OF SCIENCES
HONORARY PRESIDENT OF THE HUNGARIAN CHEMICAL SOCIETY
PRESIDENT OF THE HUNGARIAN NATIONAL ADHERING COMMITTEE, IUPAC
TITULAR MEMBER OF THE COMMISSION ON COLLOID AND SURFACE CHEMISTRY, IUPAC

SCIENTIFIC COMMITTEE

PROFESSOR G. SCHAY, CHAIRMAN, PROFESSOR E. WOLFRAM, SECRETARY,
PROFESSOR L. G. NAGY, DR. F. SZÁNTÓ, DR. T. SZEKRÉNYESY,
DR. G. SZÉKELY, DR. J. TÓTH, PROFESSOR F. TÜDŐS

ORGANIZING COMMITTEE

PROFESSOR E. WOLFRAM, CHAIRMAN, DR. T. SZEKRÉNYESY, SECRETARY,
DR. G. FÓTI, DR. G. GÁTI, DR. A. LŐRINC, DR. M. NAGY,
DR. L. OPOCZKY, MRS. É. SZEPESVÁRY

© Akadémiai Kiadó, Budapest 1975

Joint edition published by
Akadémiai Kiadó, The Publishing House of the Hungarian Academy of Sciences,
Budapest, Hungary and
Elsevier Scientific Publishing Company, Amsterdam,
The Netherlands
Printed in Hungary

Series: ISBN 963 05 0877 X
Volume: ISBN 963 05 0845 1

PREFACE

The science of colloid and surface chemistry belongs to those areas that are predominantly interdisciplinary, moreover, multidisciplinary in character. This is due to the fact that it is most difficult to find any material systems in Nature or among artifasts having structures which might be described on a purely molecular level without taking into account supermolecular textural elements, such as dispersed particles of any kind, more or less coherent networks with mostly individual (or, at least, specific) physical properties, and/or interfacial boundary layers between macroscopic phases or submicroscopic particles.

Even in the earliest stages this inherent multidisciplinarity resulted in a higher degree of specialization than did other branches of chemistry thereby giving rise to the quick and relatively separate development of a number of further disciplines: initially surface science, which was followed by structural rheology, and in recent decades aerosol science, emulsion science, powder science or, as a synthesis of knowledge on disperse structures, solid state physics and rheology namely: materials science in general. Added proof of this specialization is shown by the great number of meetings being held on topics devoted to selected fields that are connected, to varying extents, with problems involving supermolecular structures and interfacial layers.

On the other hand, there is no doubt that the more progressed the splitting into highly specialized fields, the more pronounced and urgent the need for integration which is the means of allowing the recognition of a comparatively small number of basic principles that govern an astonishingly broad spectrum of phenomena intimately related to colloidal structures and interfaces.

The tendency to sum up and the need for integrating the various disciplines have been the leading principles governing the organization of the present conference so, instead of limiting the subjects of papers to a few selected topics we have endeavored to accept contributions from an as broad horizon as possible not excluding those of technological character. In referring to a broad horizon the term should be understood not only in the professional sense but also geographycally – as shown by the fact that the 130 papers or so originated from 22 countries, including 6 from overseas.

This book – which is volume one of the Proceedings of the Budapest conference – contains all contributed papers presented at the meeting except for those

the manuscripts of which arrived after June 15, 1975. Texts were photoprinted in the form submitted. The views expressed in the papers are, therefore, those of the contributors, and errors resulting from language difficulties, typing or drawing have not been corrected. For the same reason, it was beyond the possibilities of the editor to ensure even a formal homogeneity in nomenclature and symbols used. Nevertheless, it should be noted that the apparent thematical heterogeneity of this collection has been the natural result of the intention to cover colloid and surface science as a whole as outlined above.

In order to make the survey easier for the reader the papers have been classified into four sections, comprising sixteen narrower groups. Needless to say that this classification serves but a rough orientation in that overlapping between the subjects dealt with has been inevitable.

Volume two of the Proceedings of this conference, containing the discussions that are expected to take place during the sessions, is due to appear early in 1976. The whole printed material of the Budapest conference will be completed by the plenary, main and invited lectures to be published partly as a separate issue of Pure and Applied Chemistry, and partly in the Progress of Colloid and Polymer Science.

The organizers of this conference are indebted to the International Union of Pure and Applied Chemistry. This body has honoured the conference by granting its sponsorship for a meeting held in a country where colloid science has a long tradition.

The editor wishes to express sincere thanks to Dr. M. Nagy for his valuable help in the editorial work. He is also indebted to Akadémiai Kiadó, Publishing House of the Hungarian Academy of Sciences for the rapidity and care with which this book was prepared and printed.

Finally, sincere thanks are due to all contributors whose assistance enabled this book to appear by the beginning of the conference.

June 30, 1975 E. WOLFRAM

CONTENTS

I. SURFACE CHEMISTRY

I/1 SURFACE STRUCTURE AND SURFACE CHEMISTRY OF SOLIDS 1

M. L. HUGGINS
Some challenges to surface chemists 3

D. YATES and T. W. HEALY
Surface charge and tritium exchange studies of the iron oxide (Goethite) – solution interface 7

H. LEIDHEISER, JR. and M. W. KENDIG
Electrical model for interfacial failure of polybutadiene-coated steel 15

H. G. VASILJEV and F. D. OVCHARENKO
The study of the surface chemistry of natural alumosilicates 19

YU. I. TARASEVICH
The investigation of coordination compounds on the surface of layer silicates 27

L. G. NAGY, G. TÖRÖK and G. FÓTI
Investigations on the structure and sorption properties of hydrated antimony pentoxide used for the selective removal of radiosodium 33

J. TÓTH
The specific surface area and the energy distribution of heterogeneous solid surfaces 41

J. BODNÁR, J. GAJÁRI and L. G. NAGY
Study of carbon type sorbents by structural chemical analysis and immersional calorimetry 49

Z. JUHÁSZ and L. OPOCZKY
Surface and mechanochemical activation of silicates 57

I/2 ADSORPTION AT SOLID/GAS AND SOLID/LIQUID INTERFACES 65

A. ENAULT and Y. LARHER
Triple point of the first monomolecular layer of nitric oxide adsorbed on the cleavage face of lamellar halides 67

J. VANDERDEELEN and L. BAERT
Adsorption of phosphate ions onto an amorphous ferric hydroxide 75

W. RUDZINSKI, B. W. WOJCIECHOWSKI and A. DABROWSKI
Adsorption from dense fluids and their mixtures 83

R. S. ROY and A. PANDA
Adsorption of organic molecules on activated charcoal 91

F. SZÁNTÓ, I. DÉKÁNY and L. G. NAGY
Adsorption from solution and sediment volumes of organophilic montmorillonites . . 99

L. G. NAGY, G. FÓTI, H. KUTY and G. SCHAY
Equilibrium and kinetic studies of liquid adsorption on porous activated carbon . . 107
I. PÁSZLI
Formation and structure of solid/vapour boundary layers 115

I/3 WETTING 123

A. I. RUSANOV
The contact angle theory for elastic solids 125
M. UENO, K. TSUBAKI and K. MEGURO
Wettability studies of methyl group rich surface and benzene ring rich surface by the aqueous solutions of nonionic surfactants with homogeneous ethylene oxide chain length 133
J. VAN BRAKEL and P. M. HEERTJES
Capillary rise and the contact angle glass-hexane 141
O. N. GRIGOROV and E. V. GRIBANOVA
The influence of concentration and composition changes in ascending meniscus region on the capillary rise of solution in porous systems 149
CH. FIEBER and H. SONNTAG
Some problems in determination of interfacial tension by measuring the forces exerted on solid bodies 157
E. WOLFRAM and É. BOROSS-VARGH
Effect of preadsorbed surfactant on the wettability of polymers 163
A. LŐRINC and K. STERYOPOULOS
The modification of copper-phtalocyanine pigment surfaces by surfactant adsorption 169

I/4 THIN LIQUID FILMS 177

H. J. SCHULZE
Stability of thin liquid films on hydrophobic quartz surfaces 179
G. PESCHEL and P. BELOUSCHEK
Disjoining forces in thin layers of aqueous electrolyte solutions 187

I/5 ADSORPTION OF POLYMERS 195

T. VAN VLIET and J. LYKLEMA
Conformational transitions in free and adsorbed polymethacrylates 197
W. NORDE and J. LYKLEMA
Adsorption of human plasma albumin and bovine ribonuclease at charged polystyrene-water interfaces 205
YU. A. ELTEKOV
Structure of polymer adsorption layers 213
K. FURUSAWA, H. NAKANISHI and A. KOTERA
Polymer adsorption onto the porous glass from theta solvent 221

I/6 ADSORPTION OF SURFACTANTS 229

G. KRETZSCHMAR
Studies on different models of adsorption kinetics of surface active substances 231

J. KLOUBEK
Kinetics of the surfactant adsorption on the solution surface 239
M. J. SCHWUGER and H. G. SMOLKA
Mixed adsorption of ionic and nonionic surfactants on active carbon 247

II. DISPERSE SYSTEMS

II/1 FORMATION OF DISPERSE SYSTEMS 255

B. SUBOTIC
The influence of constitutive and nonconstitutive components on colloids "in statu nascendi" 257
R. DESPOTOVIC, N. FILIPOVIC-VINCEKOVIC, D. MAYER, S. POPOVIC and M. SZVOBODA
The influence of surfactants on the formation and properties of some inorganic colloids 265
B. PURGARIC and H. FÜREDI-MILHOFER
The kinetics of precipitation of dicalcium phosphate dihydrate 273

II/2 STABILITY AND STRUCTURE OF DISPERSE SYSTEMS 281

A. A. BARAN, O. D. KURILENKO, I. M. SOLOMENTSEVA and I. I. KOCHERGA
Stabilization of hydrophobic sols by water-soluble polymers 283
O. D. KURILENKO, A. A. BARAN and YA. YA. VASKO
An investigation of gold and silver iodide hydrosols flocculation by polyethylenoxide additions by flow ultramicroscopy method 291
S. ROHRSETZER, M. KABAI-FAIX, F. CSEMPESZ
Surface properties of sol particles 299
P. RICHMOND and R. P. KEAVEY
Radial distribution functions for concentrated colloidal dispersions 307
I. MÁDI
Study of the heteroadagulation of lyophobic sols by a radioactive tracer method . . 315
R. J. CAIRNS and E. L. NEUSTADTER
Mechanism by which dispersant additives stabilise carbon dispersions in non-polar media 323
E. L. NEUSTADTER, K. P. WHITTINGHAM and D. M. GRIST
The role of demulsifiers in water/crude oil emulsions 331
L. MUKHIN, S. SHALYT, L. OGNYEVA, E. FEDOROVA and I. KAZAKOVA
The role of structural-mechanical barrier in water-in-oil emulsions stability 339

II/3 ELECTRICAL PHENOMENA 347

S. S. DUKHIN, V. N. SHILOV and YU. YA. YEREMOVA
Induced dipole moments of colloid particles 349
M. P. SIDOROVA, M. FAZYLOVA and D. A. FRIDRIKHSBERG
Electrokinetic studies of some model systems: quartz-electrolyte solutions 357
B. V. EREMENKO and B. E. PLATONOV
Electrokinetic potential of colloid precipitations in aqueous (poly)ethylen oxide . . . 363

K. P. TIKHOMOLOVA
Investigation of liquid movement in electric fields through multilayer diaphragms 371

S. P. STOYLOV
Electrooptic study of the colloid stability of anisodiametric particles 379

S. SOKEROV and T. VOROBEVA
Electrooptical investigations of the interaction among spherical particles 387

II/4 RHEOLOGY 395

K. STRENGE and H. SONNTAG
The modification of the elastic behaviour and the interpretation of the interparticulate interaction of structured suspensions 397

A. A. TRAPEZNIKOV and V. G. TARANENKO
Deformation strengthening of colloid and polymer solutions filled with aerosil 405

M. GILDE, F. SZÁNTÓ and B. VÁRKONYI
Sedimentation and rheological properties of flocculated kaolinite suspensions 413

U. F. DEINEGA and N. YA. KOVGANICH
Strong electric field influence on rheological properties of disperse systems 421

Z. DÁRDAI and A. MAGYARITS
Electro-rheological investigation of suspensions 429

II/5 GELS 437

D. BARGEMAN, E. J. VAN EMMERIK and C. A. SMOLDERS
The gelation of iron-oxide sols 439

M. NAGY, E. WOLFRAM, T. VÁRADI
Formation of disperse structures in polymer gels 447

I. TAR and E. WOLFRAM
The effect of co-solved substances on the gel-sol transition in gelatin 455

III. SURFACTANTS, MONOLAYERS AND FOAMS

III/1 MICELLIZATION AND RELATED PHENOMENA 463

Z. N. MARKINA, O. P. BOVKUN, N. N. TSIKURINA and A. V. SINEVA
Micelle formation in aqueous solutions of surface-active substances 465

K. S. BIRDI
A study of mixed micelles of cationic and nonionic surfactants by membrane osmometry 473

H. CHRISTEN, H. F. EICKE and J. REHAK
Equilibrium considerations on micelle formation in apolar media in the presence of solubilized water 481

H. F. EICKE, H. CHRISTEN and R. HOPMANN
Stability considerations with respect to conformational transformations during micelle formation in apolar media 489

A. S. KERTES, O. LEVY and G. Y. MARKOVITS
Aggregation of alkylammonium bisulfate in benzene 497

W. U. MALIK, A. K. JAIN and M. J. SIDDIQUI
Solutions of cobalt hexammine soaps in organic solvents 501

J. B. BROWN, I. LAPCZYNSKA and S. FRIBERG
Microemulsions from nonionic emulsifiers 507

ZS. BEDŐ, E. BERECZ and M. SZAKSZON
Investigation of micellar solutions (microemulsions) 517

III/2 MONOLAYERS AND FOAMS 525

M. LANDUYT-CAUFRIEZ, J. CASPERS, J. M. RUYSSCHAERT and J. JAFFÉ
Interaction lipid-gramicidin s at the air-water interface 527

W. RETTING, H.-D. DÖRFLER and H. SACKMANN
The penetration of homologous sodium alkyl sulfates into lipid monolayers 535

A. POSS, C. BERLINER, J. M. RUYSSCHAERT and J. JAFFÉ
Properties of antamanide at the air-water interface 543

H.-D. DÖRFLER and E. MÜLLER
On the electrosorption behaviour of phospholipids: measurements of differential capacity and inhibition 551

M. TOMOAIA, A. IOANETTE and E. CHIFU
Behaviour of β-apo-8′-carotenal at the oil/water and air/water interfaces 559

D. VOLLHARDT and L. ZASTROW
Some new results on the surface diffusion in spread monolayers at the gas/liquid interface using the radiotracer technique 567

D. EXEROVA, I. PENEV and CHR. CHRISTOV
Investigation of black films by alpha-particles 575

I. B. IVANOV, B. P. RADOEV, T. TR. TRAYKOV, D. ST. DIMITROV, E. D. MANER and CHR. ST. VASSILIEFF
Hydrodynamics of foam and emulsion films 583

D. PLATIKANOV and N. RANGELOVA
Investigation of black foam films of different structures by electric impulses 591

III/3 MOLECULAR INTERACTIONS 599

K. MEGURO, S. MUTO, K. DEGUCHI and M. UENO
The mechanism of charge transfer solubilization of 7,7,8,8-tetracyanoquinodimethane in surfactant solution 601

S. HAYANO and M. FUJIHARA
Distribution of dye in surfactant micelle systems 609

V. N. IZMAILOVA, G. P. YAMPOL'SKAYA and V. K. MAZO
Interaction of surface-active macromolecules with non-polar substances in aqueous solutions 617

H. GUSTAVSSON and B. LINDMAN
Alkali and halide ion nuclear magnetic relaxation and shielding in surfactant systems 625

T. GILÁNYI and E. WOLFRAM
Interaction of polymers with surfactants in aqueous solution 633

C. HOLT
The stability of bovine casein micelles 641

GY. INZELT and P. GRÓF
Studies on molecular process in poly vinyl-alcohol/water systems 645

IV. APPLICATIONS AND METHODS

IV/1 APPLICATIONS 653

Z. R. ULBERG and U. F. DEINEGA
Simultaneous electrodeposition of polymer dispersions and metals 655

J. SNUPÁREK, JR.
Some aspects of semicontinuous emulsion polymerization-particle size and water absorption of latex films 663

G. KARAGOUNIS, I. PANDI-AGATHOKLI and E. KONTARAKI
The synthesis of polymeric catena compounds by interfacial reactions 671

E. VÁMOS
Tribology as a branch of surface chemistry 679

H. MÁTTYUS, I. RUSZNÁK, L. GY. NAGY, P. LENGYEL and J. GAJÁRI
Effect of beating on the sorption capacity of bleached sulfate pulp 687

V. FRAKNÓY-KŐRÖS and K. LUTTER
The role of adherence in the preparation of phosphor coating of fluorescent lamps . 695

M. RÉDLY
Ion-exchange studies in soil columns 703

J. BOZZAY, Z. CSŰRÖS, D. ÁGOSTON and R. SOÓS
Study of the dissolution rate of pharmaceutical agents suspended in lipoids in varying composition 711

IV/2 METHODS 719

W. BAUMEISTER and M. HAHN
High resolution electron microscopy and the molecular structure of monolayers . . . 721

H. J. PURZ
Electron microscopic investigations of colloid and polymer systems 729

YU. M. CHERNOBEREZHSKII, K. I. OMAROVA and M. SH. SHUKROEV
Development of new methods in electroanalytical and surface chemistry on the basis of the suspension effect 737

A. VÉRTES, E. KUZMANN, S. NAGY, F. NAGY, L. DOMOKOS and Z. HEGEDÜS
Mössbauer study of the corrosion products of iron and iron alloys 745

S. LEVINE and G. R. FÉAT
The double layer interaction of two charged colloidal spheres of a concentrated dispersion in a hydrocarbon medium (Received 14. August, 1975) 753

S. LEVINE and G. NEALE
Theoretical aspects of the rate of wetting of a porous medium (Received 14. August, 1975). . 761

Author index 769

Subject index 773

I. SURFACE CHEMISTRY

Group I/1
Surface structure and surface chemistry of solids

SOME CHALLENGES TO SURFACE CHEMISTS

Maurice L. Huggins

Arcadia Institute for Scientific Research, 135 Northridge Lane, Woodside, California 94062, U.S.A.

Here are some problems that to me seem interesting and capable of being solved by intelligent application of known principles and procedures. Moreover, I think that their solution would lead to important results.

How can you prepare two-dimensional (sheet) polymers on a liquid or solid surface? Inorganic sheet polymers have been known, in crystals, at least since 1922. [1] How can you make single sheet polymer molecules, organic or inorganic? Some attempts to do this, using reactions in the liquid state, have led to 3-dimensional network polymers [2,3], but, performing the reactions at appropriate interfaces with the proper reagents and conditions, it should be possible to synthesize polymeric sheet molecules. Some will have structures with holes of uniform size, as in chicken wire. What would you do with them?

Considering, for example, that many aromatic compounds of the type RAB can be condensed to stable trimers

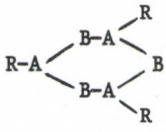

it seems likely that similar procedures, using disubstituted para derivatives of benzene or 4,4' derivatives of biphenyl, can yield 2- and 3-dimensional polymers -- the former if made at a suitable interface.

I have discussed procedures for making certain types of coordination polymers of the sheet and network classes elsewhere. [2,3]

In the crystalline state many compounds form rings or chains or networks of hydrogen bonds [4,5], in which these hydrogen bonds are coupled together [5-7], either directly through the bridgehead atoms or through resonating, conjugated systems between the bridgehead atoms. It should not be difficult to make similarly coupled hydrogen bond sheet polymers at suitable interfaces. Of course these polymers would not remain stable at high temperatures, but they might be useful nevertheless. What would you do with them?

How would you prepare hydrogen bond sheet polymers in which the hydrogen bonds are symmetrical (with only a single minimum in the potential energy curve) or nearly so? Most hydrogen bonds are quite unsymmetrical, the hydrogen being held much more tightly by one bridgehead atom than by the other. Some, however, are symmetrical, with the hydrogen held equally by the two bridgehead atoms. (If the two bridgehead atoms are different, it is better to differentiate between hydrogen bonds with two potential energy minima and those with only one.) Other hydrogen bonds are only slightly unsymmetrical, with the hydrogen in either of two locations (at potential energy minima) but capable of shifting readily to the other, because the potential energy barrier between them is very low. If the potential energy curve for the hydrogen is very flat in this region and if the coupling between hydrogen bonds is sufficiently good, all the hydrogen bonds in a chain would tend to be polarized alike and to shift together (or sequentially) when forced to shift by an external field. Such coupled hydrogen bond systems are very highly polarizable. Ferroelectrics such as KH_2PO_4 are of this sort. The degree of symmetry and the polarizability of hydrogen bonds can be altered in predictable ways [8,9] by changing the groups attached to the bridgehead atoms. Either reasoning from theoretical considerations or by studying known structures, it should be possible to predict and to make two-dimensional polymeric systems of coupled, very polarizable hydrogen bonds. What would you do with them?

How could you make a catalyst system on a crystal surface that would function like a nucleic acid in the synthesis of polypeptides? Important biological syntheses, such as the formation of polypeptide chains, are catalyzed by appropriately spaced and oriented chemical units (of the right kinds) on a rigid substrate (e.g., in a nucleic acid molecule). It should be possible, by the choice of suitable crystal surfaces or by chemical modification of ordinary crystal surfaces, to produce substrates that will catalyze reactions in much the same way. Perhaps Ziegler-Natta catalysis of the synthesis of stereoregular polymers on chemically modified titanium halide crystal surfaces is a simple example of this. I think that the time is right for scientists to start research in this potentially important field. How would you start?

How can you change clouds to rain? It seems likely that the water droplets in a cloud do not coalesce to form rain drops because their surfaces are charged (all with the same sign). The removal of a proton from a surface oxygen (either by itself or by interaction with a water molecule from the surroundings) might well result in a decrease of the (Gibbs) free energy, even for a droplet containing nothing but water. The proton removal might be still easier if CO_2 had been adsorbed. Simplifying the situation somewhat, one might say that the proton is removed from an H_2CO_3 molecule, leaving behind the negative HCO_3^- ion. Of course, that ion must be incorporated into the hydrogen-bonded network extending throughout the droplet.

Following Langmuir's brilliant researches in this field, silver iodide particles have been shown to be effective in producing coalescence (with growth of ice crystals) under certain very special conditions. It seems to me, however, that there must be some more generally applicable means for neutralizing the droplet charges and so inducing coalescence to liquid drops. Perhaps research along these lines has been done, but I have not heard of it. Substances dissociating into strongly adsorbing positive ions and weakly adsorbing (or nonadsorbing) negative ions should be investigated. Research on this problem by intelligent knowledgeable surface scientists might be very fruitful, with beneficial results for mankind. Have you thought seriously about it?

REFERENCES

[1] M. L. Huggins, J. Amer. Chem. Soc. 44, 1841 (1922).

[2] M. L. Huggins, Pure Appl. Chem. 12, 427 (1966).

[3] M. L. Huggins, in "Kinetics and Mechanism of Polyreactions", F. Tüdős, Ed., Akadémiai Kiadó, Budapest, 1971.

[4] M. L. Huggins, Thesis in Advanced Inorganic Chemistry course, University of California, 1919.

[5] M. L. Huggins, Angew. Chem. 83, 163 (1971); Intern. Ed. 10, 147 (1971).

[6] M. L. Huggins, Nature 139, 550 (1937).

[7] M. L. Huggins, Amer. Scientist 31, 338 (1943).

[8] M. L. Huggins, J. Phys. Chem. 40, 723 (1936).

[9] M. L. Huggins, Acta Cryst. B26, 219 (1970).

SURFACE CHARGE AND TRITIUM EXCHANGE STUDIES OF THE IRON OXIDE (GOETHITE) - SOLUTION INTERFACE

D.E. Yates and T.W. Healy

Department of Physical Chemistry, University of Melbourne, Parkville 3052, Australia.

Introduction. The hydrous metal oxides, typified by TiO_2, Al_2O_3, Fe_2O_3, FeOOH, etc., exhibit markedly larger surface charge densities than observed for mercury or the classical hydrophobic colloid silver iodide[1]. As argued in detail elsewhere[2], the behaviour of SiO_2 is unique in that it has a lower charge than AgI near the point of zero charge (p.z.c.), but a high oxide-like charge, far from the p.z.c.; the relationship of SiO_2 to the other oxides can be accounted for in detail[2,3]. The electrical double layer properties of the iron oxides and in particular goethite (α-FeOOH) have been studied by several groups of workers and it is still uncertain as to whether or not α-FeOOH has a planar impenetrable interface or one with a penetrable gel layer. We can, with reasonable certainty rule out the possibility of "physical porosity" since goethite exhibits no significant porosity to N_2, Ar and Kr[4,5].

The present study is aimed at obtaining experimental information on the α-FeOOH-water interface by complimentary titration, tritium exchange and dissolution rate studies.

Goethite is a good model oxide. The crystal structure is well known[6] and for acicular goethite crystals, the crystal faces present at the surface and their proportions, have been determined[7,8]. Hence the theoretical surface density of exchangeable protons, N_H, can be calculated. Using the method developed by Hockey and co-workers[9,10] the theoretical value of 16.8 exchangeable protons per nm^2 is obtained[11]. This value is higher than the N_H value for most oxides because bulk lattice OH groups are exposed and make a contribution to N_H which does not occur for the simple oxides.

Experimental. The α-FeOOH samples, all identified as such by X-ray

diffraction and electron microscopy, were prepared by the method of Atkinson, Posner and Quirk[7,12]. B.E.T. nitrogen (16.2 $\AA^2$) surface areas were determined after outgassing overnight at 75-120°C; the mean of duplicate determinations gave areas as follows - Sample A 48±2 m^2g^{-1}, Sample B 54±2m^2g^{-1} and Sample C 39±2 m^2g^{-1}. Geometric surface areas, estimated from electron micrographs were in reasonable agreement with these values. The samples were freeze dried and stored in a dessicator.

Triply distilled water was used; after outgassing with purified nitrogen it gave a pH of 7.0±0.5 at 20°C. All reagents were analytical grade and the KNO_3 was recrystallized and baked overnight at 300°C prior to use.

The surface charge pH isotherms were determined by potentiometric titration of goethite suspensions with HNO_3 and KOH in the presence of KNO_3. The technique has been described elsewhere[11]. The isotherms determined on a series of goethite suspensions were reproducible to better than ±0.5 $\mu C.cm^{-2}$ over the pH range 4-10.

The tritium exchange method developed by Bérubé, Onoda and de Bruyn[13] was used to determine the number of available protons per unit area of interface. The physically adsorbed water was removed by outgassing at room temperature for 4 days. Other experimental details are described elsewhere[11,14]

To examine quantitatively the amount of rapidly dissolving non-crystalline material present on the surface of the goethite samples, the ammonium oxalate extraction method[15] was used. This method has been shown to extract the non-crystalline iron oxide material[16]. The concentration of dissolved Fe(III) was measured by Atomic Absorption Spectroscopy. The dissolution was followed as a function of time and the fraction of rapidly dissolved material determined by extrapolation of the straight line obtained to zero time.

Results and Discussion. The σ_o-pH isotherms for two of the three goethite are shown in Figure 1. These results are from rapid titrations and the intersection at zero surface charge, independent of KNO_3 concentration yields a point of zero charge (p.z.c.) of 7.5±0.1. Both the values of the p.z.c. and the magnitude of the surface charges are in reasonable agreement with published data of other workers[12] and with the results for other goethite samples studied in this laboratory[11]. The rapid rate at which dry goethite attains its surface charge after wetting is shown in Figure 2 from sample B.

The tritium exchange-time curve for FeOOH shown in Figure 3 for sample B indicates that exchange occurs in two steps: the first rapid exchange is practically instantaneous and is completed within the 5 minute shaking before the sample was centrifuged. The second slower step continues for several days. The extrapolation of the less than 30 min. rapid steps yields a value of N_H, the surface density of rapidly-exchangeable protons of 16.4 nm^{-2} in good agreement with the value calculated from the crystal structure[11]. But as shown in Figure 3 extrapolation of the curve for greater than 30 mins. yields a slightly higher value. Such an extrapolation is probably more realistic when the time to wet the titrated FeOOH and centrifuge the samples for counting is considered.

The results of tritium exchange studies of this kind on three samples of FeOOH are given in Table 1.

TABLE 1. Surface density of rapidly exchangeable protons (N_H) on three samples of α-FeOOH.

Sample	BET Area $m^2 g^{-1}$	Experimental N_H/nm^{-2}		Theoretical N_H/nm^{-2}
		$t < 30^{\neq}$	$t > 30^{\neq}$	
A	48	-	20.1±0.7	
B	54	16.4±0.7	18.0±0.7*	16.8
C	39	-	18.8±0.5	

≠ $t < 30$, $t > 30$ refers to extrapolation to zero time of data for exchange times of less than and greater than 30 mins respectively.

* Includes experiments done at different labelling times, pH values and ionic strengths.

The labelling and extracting conditions for α-FeOOH sample B were varied by changing the labelling time and by adding HNO_3, KOH and KNO_3 to the solutions. Within experimental error the only difference observed was that longer labelling times gave an increased amount of the slow tritium exchange. This is because the slow exchange is due to bulk exchange[17] and long labelling times are necessary to tritiate the internal OH groups of α-FeOOH.

In the dissolution experiments which reveal the presence or otherwise of amorphous material all samples of α-FeOOH showed an initial rapid dissolution followed by the much slower dissolution of crystalline material. The details of the dissolution experiments are summarized in Table 2 below. Each value given is the mean of at least two determinations. The sample listed as B(titrated) was taken, without drying, from a suspension of goethite B which had previously been titrated to obtain the charge data of Figure 1.

TABLE 2. Dissolution studies of α-FeOOH samples in pH 3.0 ammonium oxalate.

Sample	Rapidly dissolved Fe ($/10^{-6}$ mol m^{-2})	Crystalline (Slow) Dissolution Rate ($/10^{-7}$ mol m^{-2} hr^{-1})
A	1.21±0.10	2.2±0.1
B	3.8 ±0.1	10.0±1.0
B(titrated)	3.0 ±0.2	6.4±0.6
C	1.18±0.08	2.0±0.3

The dissolution rates are similar to those reported by Quirk et al[8,18] who used 0.5 M HCl as reagent; their dissolution rates and rapidly dissolved fractions were slightly lower than observed in the present study.

The data for sample B is quite different from the other samples. The higher amount of rapidly dissolved iron was confirmed by electron microscopy wherein some amorphous material was observed precipitated along with the crystalline α-FeOOH particles.

It must be stressed that the amount of rapidly dissolving Fe is small in each case. The data of Table 2 can be recalculated to give rapidly dissolvable fractions corresponding to 0.7, 2.3 and 1.0 iron atoms per square manometer for samples A, B and C respectively. These values are less than 20% of a monolayer if we assume the rapidly dissolved iron is evenly spread on the surface. This is clearly not the case for sample B where amorphous material was observed in electron micrographs as clumps of precipitate rather than as a surface layer. The higher surface area of sample B may also reflect the presence of discrete amorphous material.

The surface charge (σ_o), tritium exchange (N_H) and dissolution studies on the three α-FeOOH samples exhibit a consistent pattern viz. that the interface is closely approximated by a plane rather than a gel and that the typical high surface charge is a characteristic of this plane. It is worth noting that there is no correlation between the σ_o-pH behaviour and the small amounts of rapidly dissolving amorphous material; sample B with three times as much amorphous material as sample A gives approximately the same high charge and the same number of rapidly exchanging protons. This also confirms that the rapidly dissolving fraction is a small fraction of the total titratable and/or exchangeable surface.

Summary and Conclusions. The surface charge-pH behaviour of three α-FeOOH samples yields characteristic high oxide like charges. That this charge arises from crystal planes rather than a gel layer was confirmed by

tritium exchange studies which established close correlation between the experimental and theoretical numbers of exchangeable protons. Dissolution rate experiments showed that small amounts of rapidly dissolving amorphous material was present in each sample and that this small amount did not contribute to either the tritium exchange or surface charge.

Acknowledgements. This work was supported by the Australian Research Grants Commission. A Commonwealth Post-Graduate Award to D.E.Y. is gratefully acknowledged.

References

1. G.R. Wiese, R.O. James, D.E. Yates and T.W. Healy, MTP Int.Rev.Sci., Vol.6 (in press).
2. S. Levine and A.L. Smith, Disc.Faraday Soc., 52, 290 (1971).
3. D.E. Yates, S. Levine and T.W. Healy, J.Chem.Soc. Faraday I. 70, 1807 (1974).
4. G.C. Bye and C.R. Howard, J.Appl.Chem.Biotechnol., 21, 324 (1971).
5. L.A.G. Aylmore, Clays and Clay Minerals, 22, 175 (1974).
6. L. Bragg and G.F. Claringbull, "The Crystal Structures of Minerals", Bell, London, 1965.
7. R.J. Atkinson, A.M. Posner and J.P. Quirk, J.Inorg.Nuclear Chem., 30, 2371 (1968).
8. R.M. Cornell, A.M. Posner and J.P. Quirk, J.Inorg.Nuclear Chem., 36, 1937 (1974).
9. P. Jones and J.A. Hockey, Trans.Faraday Soc., 67 2679 (1971).
10. K. Atherton, G. Newbold and J.A. Hockey, Disc.Faraday Soc. 52, 33 (1971)
11. D.E. Yates, Ph.D. Thesis, University of Melbourne, 1975.
12. R.J. Atkinson, A.M. Posner and J.P. Quirk, J.Phys.Chem., 71, 555 (1967).
13. Y.G. Bérubé, G.Y. Onoda, Jr. and P.L. de Bruyn, Surface Sci., 8, 448 (1967).
14. D.E. Yates and T.W. Healy, J.Colloid Interface Sci., in press.
15. U. Schwertmann, Z.Pflang.Bodenk., 105, 194 (1964).
16. E.R. Landa and R.G. Gast, Clays and Clay Minerals, 21, 121 (1973).
17. K.J. Gallagher and D .N. Phillips, Trans.Faraday Soc., 64, 785 (1968).
18. R.M. Cornell, A.M. Posner and J.P. Quirk, Soil Sci.Soc.Amer.Proc., 38 377 (1974).

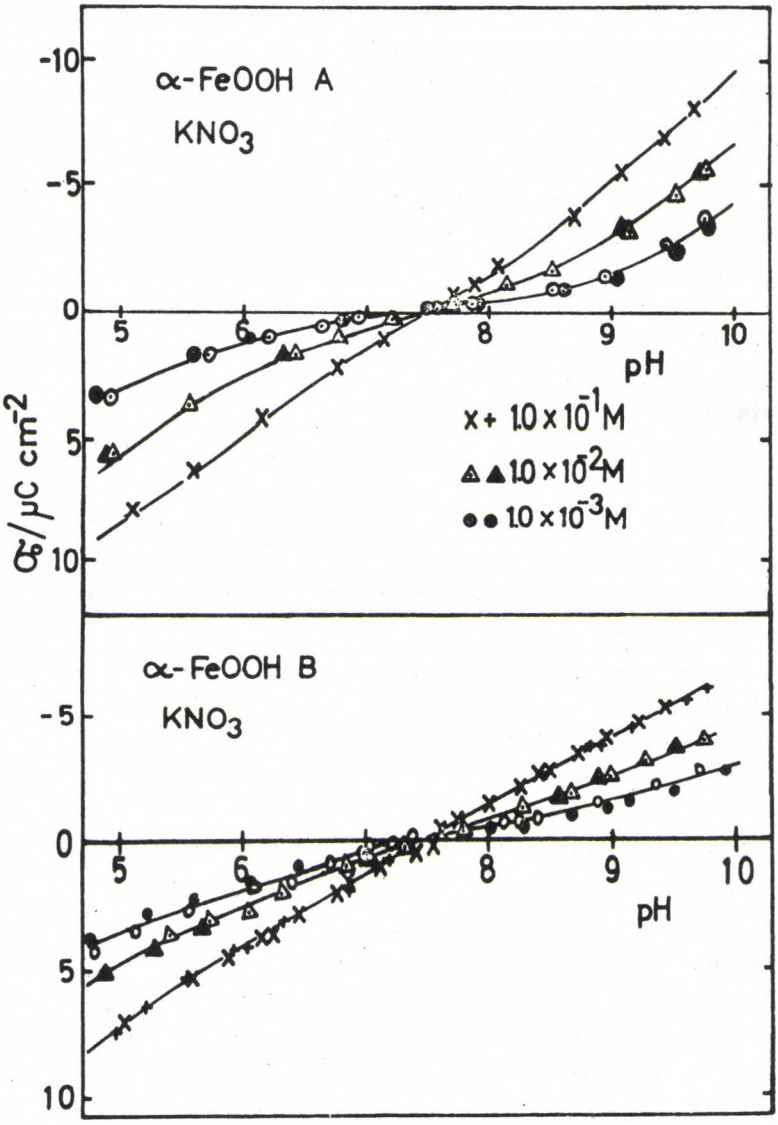

Figure 1. The surface charge density, σ_o, of goethite samples A and B as a function of pH in aqueous solutions of KNO_3.

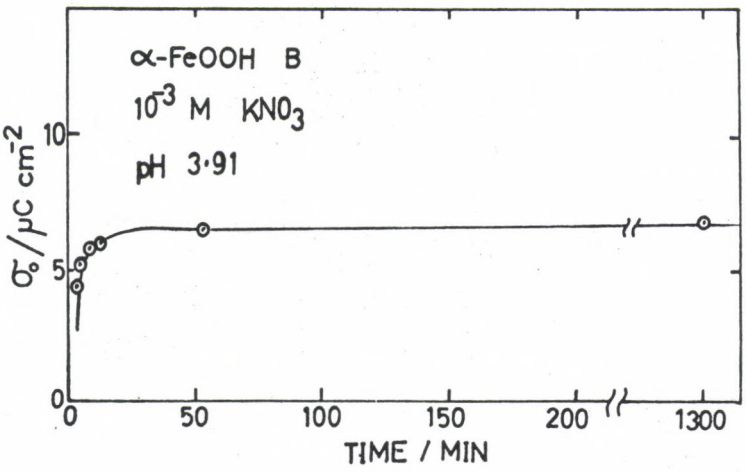

Figure 2. The surface charge, σ_o, of goethite B as a function of time after adding the oxide to 10^{-3} M KNO_3 solution. The pH was maintained at 3.91 by titrating with 0.10 M HNO_3.

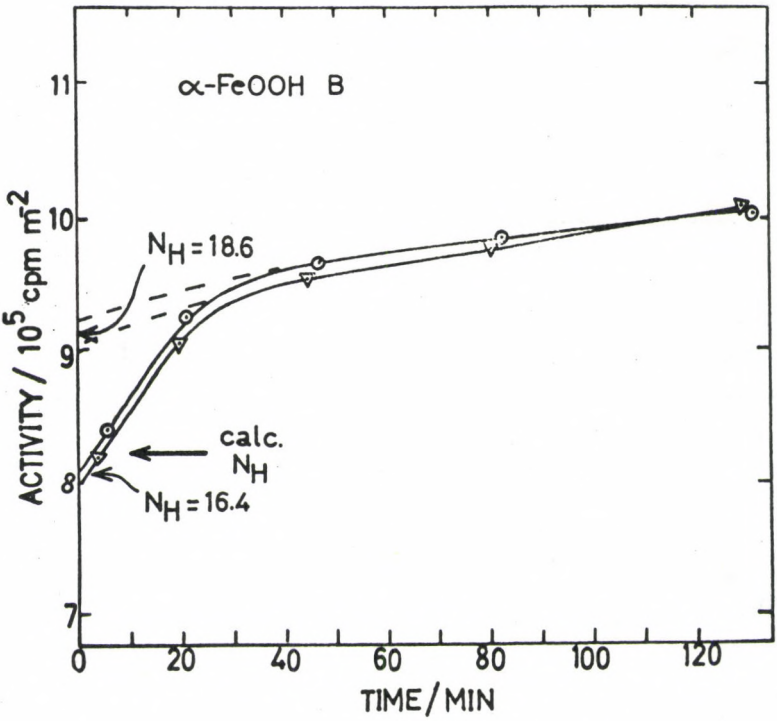

Figure 3. Solution radioactivity as a function of extraction time for goethite B, short extraction times. Activity of labelling solution, 3.27×10^9 cpm cm^{-3}; labelling time, 4 days. The calculated N_H value of 16.8 nm^{-2} is included for comparison.

ELECTRICAL MODEL FOR INTERFACIAL FAILURE OF POLYBUTADIENE-COATED STEEL

Henry Leidheiser, Jr., and Martin W. Kendig

Center for Surface and Coatings Research, Lehigh University, Bethlehem, Pennsylvania, U. S. A.

Previous work has shown that the electrical properties of protective polymer coatings provides useful information about the corrosion properties of the system (1, 2). A mechanism has been proposed previously for the corrosion of polybutadiene-coated steel (3). This paper proposes a model that qualitatively describes the electrical behavior as a function of the frequency at which the measurements are made. The model applies particularly to the practical case where base metal is exposed at the base of pores in the coating.

The electrical impedance across polymer-coated steel may be described in terms of the effective permittivity of the polymer coating. This effective permittivity is a function of the frequency of the applied field and the time of exposure of the coated substrate to a model corrosion medium, 0. 5M NaCl (4).

The conductivity of polymer coatings is proposed to be determined by the conductivity of electrolyte in pores. The impedance, Z, across an electrolyte-impregnated polymer on a steel substrate thus becomes:

$$Z = Z_{pore} + Z_{interface}$$

The pores contribute a component, ϵ_{pore}, to the effective permittivity of the polymer coating:

$$\epsilon_{pore} = L/A \, \epsilon_{\circ} \, \omega \, Z$$

where L = coating thickness

A = cross sectional area of pore

ϵ_o = permittivity of free space

ω = angular frequency of applied field

Under conditions where the pores in the coating are the dominating influence ϵ_{pore} is inversely proportional to the angular frequency:

$$\epsilon_{pore} \quad \alpha \quad \frac{\sigma}{\epsilon_o \omega}$$

where σ = the conductivity of the penetrating electrolyte.

Under conditions where the electrical properties of the interface dominate, the contribution by pores to the permittivity can be utilized to obtain information about the permittivity of the interface:

$$\epsilon_{pore} = r_1 r_2 (\epsilon''_{interface} + j\epsilon'_{interface})$$

where r_1 = ratio of interface thickness to the polymer coating thickness

r_2 = ratio of the exposed interfacial area to the cross sectional area of the pore

$\epsilon''_{interface}, \epsilon'_{interface}$ = complex permittivity of the interface

Figures 1 and 2 show schematically the qualitative behavior of the logarithm of the electrical permittivity vs. the logarithm of the frequency of the applied field for two special situations which are often seen in practical steel-coating systems exposed to corrosive electrolytes.

Examples will be shown of the electrical response as a function of frequency for various polymer thicknesses, various polymer systems, and various degrees of coating delamination.

References

1. H. Leidheiser, Jr., and R. Touhsaent, Corrosion 28, 435 (1972).
2. H. Leidheiser, Jr., and D. Wallace, J. Electrochem. Soc. 120 (8), 230c (1973).
3. H. Leidheiser, Jr., and M. W. Kendig, Meeting, Natl. Assocn. Corrosion Engrs., Toronto, Canada, April 15, 1975; to be published.
4. M. W. Kendig and H. Leidheiser, Jr., J. Electrochem. Soc. 121 (8), 275c (1974).

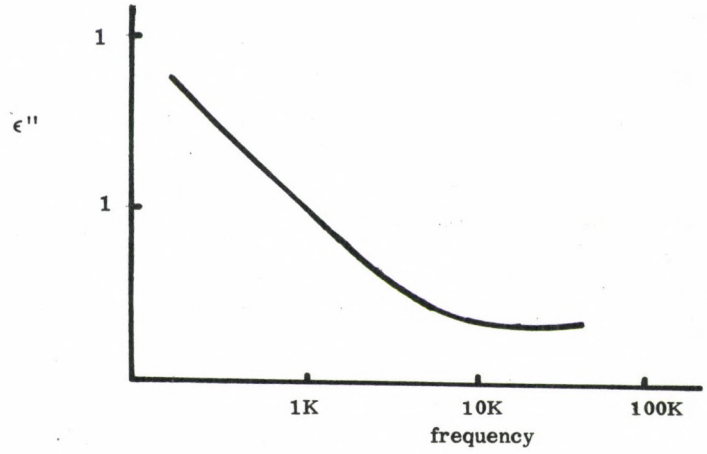

Figure 1. Schematic representation of log ϵ'' vs. log frequency in the case of a polymer coating containing a pore continuous to a low-impedance interface at the metal surface. Slope is -1 at low frequencies.

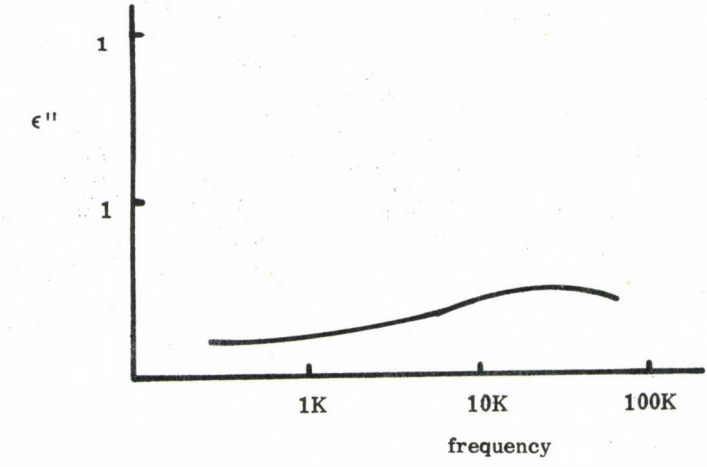

Figure 2. Schematic representation of log ϵ'' vs. log frequency in the case of a polymer coating containing a pore continuous to a high-impedance interface at the metal surface.

THE STUDY OF THE SURFACE CHEMISTRY OF NATURAL ALUMOSILICATES

H.G.Vasiljev, F.D.Ovcharenko

Institute of Colloid Chemistry and Water Pollution Control, Academy of Sciences of the Ukrainian SSR,
252142, Kiev - 142, Vernadsky Street, 42, USSR

According to the modern considerations on the structure of natural layer silicates their surface has a number of active centres/1-4/. The most important of them for the investigation of surface reactivity with organic and inorganic substances are exchange cations, surface OH-groups and coordination-unsaturated ions of metals located on the edges of crystals(fig.1). In addition, it should be noted that in contradistinction to other silicates the kaolinite structure has the stable radical which can affect surface properties/5/.

In the neutral medium the exchange capacity of natural alumosilicates is caused by two reasons: non-stoichiometric isomorphous substitutions in octahedral and tetrahedral networks and by oxygen excess negative charge on the edges of particles (broken bonds)/4/. In the first case the bond of exchange cation with surface depends on both the nature of ion and the arragement of isomorphous substitutions in structure. Under the equal conditions the bond is the strongest if non-stoichiometric substitutions occur in the tetrahedral lattice/6/. In the swelling minerals the large singly-charged cations belong only to one of two adjacent layers in interlayer space. They distribute in the hexagonal holes formed by oxygen atoms. Doubly-charged ions seem to occupy the positions near the plane of symmetry which is between the adjacent layers/7/.

It was shown in paper/8/ that during the hydration process of Na-form of montmorillonite and the formation of just a single layer of water molecules on surface Na^+-ions remain in holes

coordinating with H_2O molecules from the direction of interlayer space only.By the NMR technique we have investigated the state of this ion (as well as Al^{3+}-ion) with further hydration of samples.Figures 2,b and c show the NMR spectra of Na- and Al-forms of Pyzhevsk montmorillonite saturated by water within a maximum.As it should be expected,the intensity of the line of Na^+- is approximately by 3 times greater than that of the line of Al^{3+}.Since the latter is weak we failed to trace the variations of its form and width.

The NMR line of Na^+-ions becomes distinct just at 20% moisture of the sample when the width is 3.5±0.1 G.With the increasing of moisture it vanishes monotonously and at 30% moisture it is 1.0±0.1 G,i.e. practically equal to the linewidth for aqueous solutions of sodium salts(fig.2,a).Further increasing of moisture does not lead to a sufficient decreasing of its width.The data obtained may be explained in the following way. In dehydrated mineral Na^+-ions distributing in the hexagonal holes of oxygen atoms are in the electric field of low symmetry.Owing to the great contribution of quadrupole interactions to the linewidth the NMR spectrum of Na^+-ions is difficult to observe.The symmetry is low up to 20% moisture,it corresponds to the singly-layer adsorption of water molecules/8/.The formation of the second layer leads to the displacement of Na^+--ions towards the plane of symmetry of interlayer space,they attain the environment of the electric field of the higher symmetry.At the moisture of 30% Na^+-ions are hydrated completely and distribute in the centre of octahedron of H_2O molecules.In this case the electric field symmetry is of the kind that the contribution of quadrupole interactions to the NMR linewidth is minimum.

Therefore,with moisture increase, Na^+-ions leave hexagonal holes.In this case the energy of bond between them and H_2O molecules must be greater than the bond with oxygen atoms of silicate layer.To estimate the latter quantitatively the calculation of this energy has been made by us by means of extended Hükkel method/9/.The values of effective nuclear charges of sodium and oxygen atoms were determined according to Slater rules.The orbital potentials of ionization of these atoms

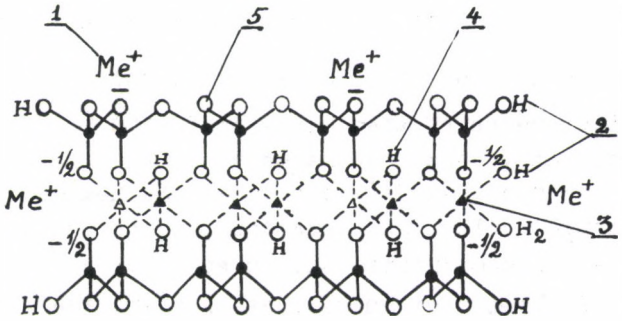

Fig.1.Active centres of layer silicates: 1 - exchange cations; 2 - surface hydroxylic groups; 3 - coordination-unsaturated Al^{3+}-,Fe^{3+}-and Mg^{2+}-ions; 4 - structural hydroxylic groups of octahedrons; 5 - oxygen of tetrahedral network.

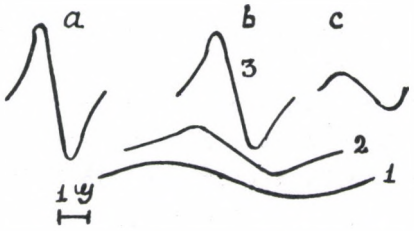

Fig.2.The NMR spectra of Na^{+}- and Al^{3+}-ions. a - aqueous solution of NaCl; b - Na-montmorillonite at moisture of 20% (1),25 (2),40% (3); c - - Al-montmorillonite saturated by H_2O.

were taken from paper/10/ and their coordinates - from paper /11/.Nondiagonal elements of effective Hamiltonian matrix were calculated according to the formula:

$$H_{pq} = \frac{K}{2}(I_p + I_q)S_{pq} ,$$

where K=1.75 /12/, I_p-are ionization potentials of states, S_{pq}-overlapping integrals.

The calculations showed that the energy of bond of Na^+-ion located in a hexagonal hole is 74.2 kcal/mol.Because the complete hydration value of these ions is 85-102 kcal/mol /13,14/ the comparison of the calculated value and the given one allows to conclude that Na^+-ions leave the hexagonal holes of the structure during the hydration process (with increasing of a number of coordinated molecules of H_2O).From the data obtained it follows that on silicate surface the exchange Na^+-ions preserve the properties which they possess in aqueous solutions.It,probably,relates to other exchange cations.Along with it,the effect of non-stoichiometric isomorphous substitutions in layer silicates structure on thermal stability of their cation-substituted forms (table 1) has been investigated. The table shows that if such substitutions occur in the octahedral network of dioctahedral structures the cations H^+ and Li^+,small in size,migrate into octahedral holes and interstices/15/ at 200-300°C.

As the result of it the mineral loses the abiluty for ion-exchange.In addition it is of interest to note that H^+-ions absorbed by the lattice at certain electric donor centres are not localized but diffuse through the crystal structure of silicate.It is evident from the data given in fig.3.The figure shows that in contradistinction to Al-forms (fig.3,1a) in the NMR spectrum of H-mineral heated during an hour at 200°C against the background of OH-group a narrow line with $\Delta H \simeq 0.5$ E (fig. 3,1b) which we attribute to exchange H^+-ions/16/ becomes distinct.This line is being observed even at 500°C.It diminishes above this temperature when the loss of structural hydroxylic groups just occurs (fig.3,2).

In this case if non-stoichiometric substitutions occur in the tetrahedral network cation-exchange forms of such minerals are stable to high temperature (table1).Here it should be underlined that it is impossible to make H-form for such minerals.As the exchange cations are substituted by H^+-ions the latter destroy the defective tetrahedrons in which silica is substituted isomorphously by aluminium or Fe^{3+} .In consequence,on the surface of silicates the exchange Al^{3+} and Fe^{3+}-ions/17/ are

always present.

Table 1

The effect of heating temperature of cation-substituted forms of layer silicates on their exchange capacity; τ = 1 hour, $d < 40\mu$.

Salt form	100	200	300	400	500
	C, μequiv/g				
1	2	3	4	5	6
	Pyzhevsk montmorillonite /O/				
H	760	480	40	0	0
Li	1050	40	34	10	0
Na	1060	1060	1060	1050	980
Mg	1100	1100	1100	990	370
Ba	1150	1150	1150	1140	990
Al	1130	1130	1120	1100	750
	Kovdorsky vermiculite /T/				
Li	1280	1280	1280	1280	1270
Na	1280	1280	1230	1280	1280
Mg	1400	1400	1400	1400	1400
Ba	1420	1420	1420	1420	1420
Al	1390	1390	1390	1390	1380
	Glukhovsky kaolinite /O/				
H	90	60	10	0	0
Li	242	34	34	46	48
Na	240	240	240	230	90
Mg	245	245	245	220	100
Ba	250	250	250	240	110
Al	240	240	240	230	90
	Cherkasky palygorskite /O,T/				
H	62	36	10	0	0
Li	150	120	80	208	210
Na	151	151	151	280	283
Mg	150	150	150	280	270
Ba	155	155	155	275	285
Al	145	145	145	280	280

Note: /O/ is isomorphism in octahedrons, /T/ - in tetrahed-

rons; for H-form C is given without Al^{3+}-,Fe^{3+}-,Mg^{2+}-ions.

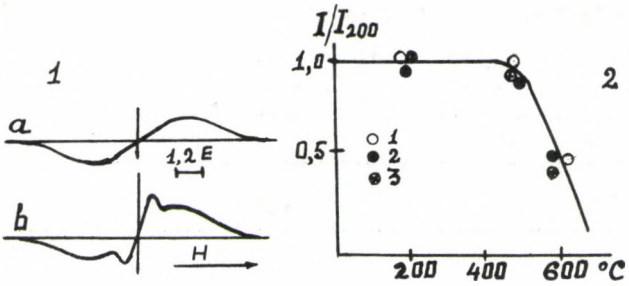

Fig.3. (1) The NMR spectra of protons of the samples of Al- (a) and H-form (b) of montmorillonite dehydrated at 200°C; (2) The variation of integral intensities of the NMR spectra of protons of hydroxylic groups and H^+-ions in acid forms of montmorillonite depending on temperature: 1 - OH-group of H-form;2 - OH-group of H-form;3 - H^+-ions; heating temperature - 1 hour.

In order to determine surface OH-groups quantitatively we have made use of the method of methoxylation of the surface of CH_2N_2 as well as the method of inverse conductometric titration of aqueous suspensions of K-forms of silicates by acid and alkali solutions/3/.In both cases the samples were purified thoroughly from additions of organic substances,oxides and carbonates.The data obtained are listed in table 2.

The table indicates that the chemical data provided show the content of the surface OH- groups to be too high.By using the method of inverse conductometric titration of suspensions an additional information both on the nature and the quantity of the surface OH-groups of layer silicates may be obtained.From the data obtained (table 2) it follows that in alkali medium the surface ≡SiOH groups provide the minerals with additional CEC, and the hydroxylic groups of the base character cause their anion-exchange.

Coordination-unsaturated ions of metals located at the edges of the octahedral network (fig.1) can affect sufficiently the properties of the surface of natural alumosilicates.As water molecules and hydroxylic groups are being removed aluminium (Fe,Mg) transfers from six into four coordinated ones and beco-

mes a strong Lewis centre.Along with the protons of the silanol group these centres bring about adsorbed and catalytic properties of the edges of minerals.The quantity of them on surface seems to correspond to the value of OH-group of the base character (table 2).

Table 2

The content of hydroxylic groups (μmol/g) on surface of layer silicates

Mineral	methoxylation of CH_2N_2	Conductometric method		
		≡SiOH	=Al-OH =FeOH	$=Al(OH)^{-1/2}$ $=Fe(OH)^{-1/2}$ $-Mg(OH)^{-1/2}$
Kaolinite	106	60	50	22
Montmorillonite	310	245	130	-
Nontronite	330	250	120	50
Palygorskite	390	340	200	130

As it has already been mentioned,a small part of exchange cations is located on the edges of minerals (fig.1).The behavior of some ions on this surface deserves special attention.In order to obtain the salt form of alumosilicate usually the suspension of mineral is repeatedly treated by the concentrated solution of the metal chloride/18/.Under such conditions the anion-exchange process occurs parallel to the cation-exchange one:

$$=Al - OH + MeCl \rightarrow =AlCl + MeOH \qquad (2)$$

During the process of washing of the sample and after the removal of electrolytes the cations weakly-bonded with surface, =AlCl-groups,too,are exposed to hydrolysis:

$$/mineral/^{-}Na^{+} + H_2O \rightarrow /mineral/^{-}H^{+} + NaOH; =Al - Cl + H_2O \rightarrow$$
$$\rightarrow =AlOH + HCl \qquad (3)$$

As a result of the reaction of neutralization in the intermicellar liquid the neutral salt is observed.In case of acid excess its H^+-ions can substitute the exchange cations from the surface with further formation of the same salt.The processes mentioned readily occur when the exchange complex has well-hydrated cations,such as Li^+,$Na^+$and Ca^{2+}.

Because H^+-ions (3) destroy the mineral according to the well-

-known mechanism/4/ the exchange Al^{3+}-,Fe^{3+}- or Mg^{2+}-ions are always observed on its surface or their compounds with silica acid.Therefore,it is difficult to obtain the homoionic form of silicate by the method described.

R e f e r e n c e s

1.Rentgenovsky metody izucheniya i structura glinistykh minera-lov,pod red.G.Browna,"Mir",M.,1965.

2.Yu.I.Tarasevich,F.D.Ovcharenko,Adsorbtsiya na glinistykh mi-neralakh,"Naukova dumka",Kiev,1975.

3.N.G.Vasiljev,F.D.Ovcharenko,L.V.Golovko,DAN SSSR,217,830(1974).

4.N.G.Vasiljev,M.A.Buntova,F.D.Ovcharenko,Colloid.Zh.,37,16(1975)

5.V.V.Mank,F.D.Ovcharenko,A.Ya.Karushkina,N.G.Vasiljev,DAN SSSR,218,921 (1974).

6.V.E.Polyakov,Ionny obmen,gidrofilnost i electrokinetichesky svojstva glinistykh mineralov,Avtoref.cand.dissert.,Kiev,1972.

7.I.V.Matyash,A.S.Litovchenko,N.G.Vasiljev,Colloid.Zh.,36,576 (1974).

8.J.Mamy,Recherches sur l'hydration de la montmorillonite. Thesses Gr.doct.es-scien.Phys.,Inst.SNRA,Paris,1968.

9.Yu.A.Kruglyak,G.G.Dyadyusha,V.A.Kuprievich,L.M.Podolskaya, G.I.Kagan,Metody rascheta electronnoj structury i spectrov molecul,"Naukova dumka",Kiev,1969.

10.O.P.Charkin,G.V.Bobykina,M.E.Dyatkina,sb.Stroeniye molecul i kvantovaya khimiya,"Naukova dumka",Kiev,1970.

11.Von R.Rothbouer,News Jahrbuch fur Mineralogie,N°4,143(1971).

12.R.Hoffman,J.Chem.Phys.,39,1397 (1963).

13.K.P.Mischenko,G.P.Poltoratsky,Voprosy thermodynamiki i stro-eniya vodnykh i nevodnykh rastvorov electrolitov,"Khimiya", M.,1968.

14.I.V.Matyash,Voda v condensirovannykh sredakh,"Naukova dum-ka",Kiev,1972,

15.N.G.Vasiljev,F.D.Ovcharenko,M.A.Buntova,DAN SSSR,213,1113 (1973).

16.N.G.Vasiljev,F.D.Ovcharenko,V.V.Mank,N.A.Ovramenko,Kinetika i kataliz.,15,773 (1974).

17.N.G.Vasiljev,F.D.Ovcharenko,M.A.Buntova,DAN SSSR,216,1048(1974)

18.V.E.Polyakov,Yu.I.Tarasevich,O.L.Alekseev,Ukr.khim.zh.,34, 526 (1968).

THE INVESTIGATION OF COORDINATION COMPOUNDS ON THE SURFACE OF LAYER SILICATES

Yu.I.Tarasevich

Institute of Colloid Chemistry and Water Pollution Control,
Academy of Science of the Ukrainian SSR
252142, Kiev-142, Vernadsky Street, 42, USSR

It is known /1-3/ that exchange cations of layer silicates with extending structural cell (montmorillonite and vermiculite) influence greatly on adsorption of polar molecules of water, alcohols and other substances by these minerals. To elucidate the mechanism of interaction of water with montmorillonite and vermiculite the IR-spectra of different cation-substituted forms of these minerals with adsorbed ordinary and heavy water have been studied.

The analysis of results obtained (table 1) and their comparison with infrared spectra of liquid water, aqueous electrolyte solutions and crystallohydrates /4/ permits to confirm that a considerable part of molecules of water adsorbed by montmorillonite and vermiculite participate in specific interaction with exchange cations and form simultaneously hydrogen bonds with surface oxygen atoms and water molecules from the second coordination sphere of cations.

The molecules of such substances as acetonitrile and pyridine being sensitive spectral probes on electron accepting centres are not capable at the same time to specific interaction with each other and with surface oxygen atoms of adsorbents. Consequently, the investigation of adsorption of these substances by means of IR-spectroscopy permits to prove unambiguously the formation of coordination compounds of polar molecules with exchange cations on surface of montmorillonite and vermiculite.

Table 2 shows frequences of valent CN-vibrations of acetoni-

trile molecules coordinated by cations of different metals in solution /5/ and on montmorillonite surface. The table indicates a good quantitative agreement between frequences ν(CN)-vibrations of complex cations $[Me(CH_3CN)n]^{m+}$ in two states.

Table I

The effect of exchange cations on frequency (ν , cm^{-1}) of central maximum in the region of valent OH(OD)-vibrations of ordinary and heavy water adsorbed by montmorillonite and vermiculite at P/Ps $\approx$ 1,0

Exchange Cations	Montmorillonite		Vermiculite	
	ν(OH)	ν(OD)	ν(OH)	ν(OD)
Na^+	3440	2560	3400	2530
Li^+	3425	2540	3380	2510
Ca^{2+}	3410	2525	3390	2515
Mg^{2+}	3390	2500	3355	2490
Ca^{2+}	3385	2500	-	-
Cu^{2+}	3375	2505	3370	2495

Table 2

Frequences of valent CN-vibrations (cm^{-1}) of acetonitrile molecules bound coordinately with cations of metals.

Liquid CH_3CN	Cations					
	Na^+	Li^+	Ca^{2+}	Mg^{2+}	Co^{2+}	Cu^{2+}
	Solution					
2253	2265	2278	-	2290	2315	2325
	Montmorillonite					
	2264	2280	2274	-	2313	2330

In order to determine composition and structure of coordination compounds on surface of montmorillonite and vermiculite

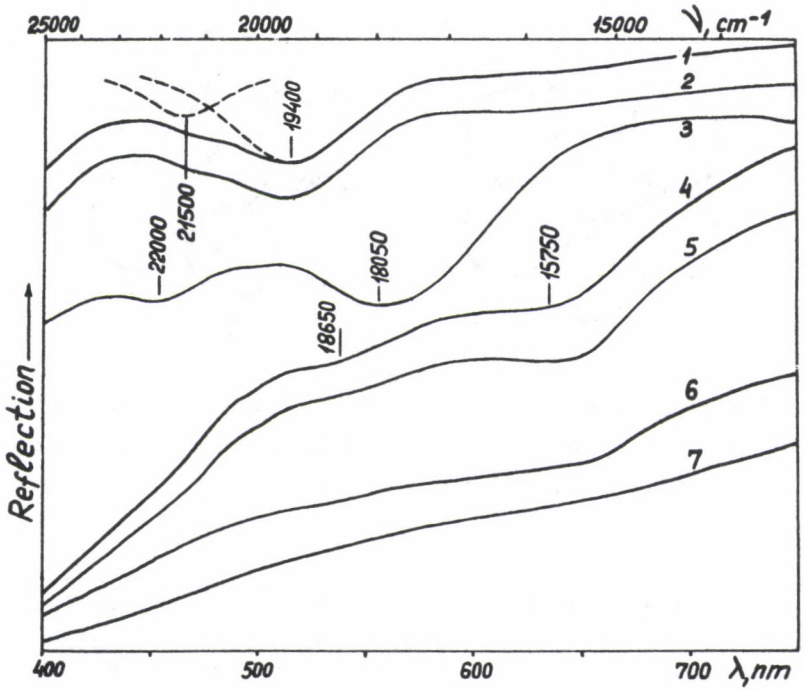

Fig. 1. Reflection spectra in visible region of Co-montmorillonite : 1 - saturated by water vapour, 2 - air-dry, 3-7 - dehydrated at 70, 150, 200, 250 and 300°C

along with X-ray analysis and electronic paramagnetic resonance technique (the results of these investigations have been published in paper /6, 7/) we have used electronic spectroscopy in ultraviolet, visible and near IR-regions of spectrum..As an example, fig. 1 shows reflection spectra in visible region of Co-montmorillonite with different amounts of adsorbed water. The analysis of spectra of both samples saturated with water vapours and air-dry shows that in hydrated montmorillonite exchange cations Co^{2+} are surrounded by octahedron of water molecules. Analogous environment is also ty-

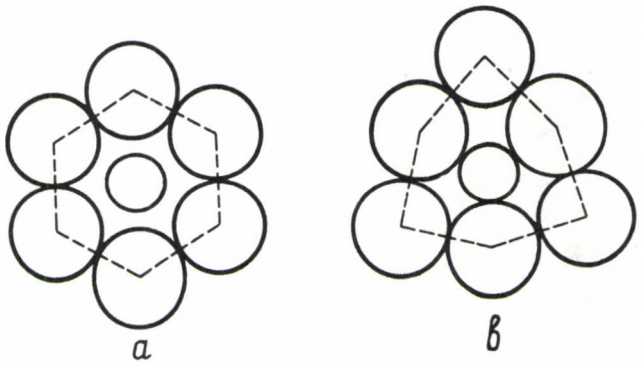

Fig. 2. Diagrams of exchange cations Co^{2+} and Ni^{2+} arrangement in hexagonal (a) and ditrigonal (b) holes of layer silicates structure

Table 3

Value of splitting by crystal field 10Dq, Raha's parameter B and nedheloauxetic parameter β for octahedral and tetrahedral aquacations Co^{2+} and Ni^{2+} adsorbed by montmorillonite.

Cation	Environment	Chemical Bond Parameters		
		10Dq, cm^{-1}	B, cm^{-1}	β
Co^{2+}	Octahedron	9420	785	0,81
	Tetrahedron	4210	765	0,79
Ni^{2+}	Octahedron	8650	885	0,86
	Tetrahedron	3900	655	0,64

pical for exchange cations of Ni^{2+} in hydrated montmorillonite. Calculated according to method /8/ the parameters of chemical bond for adsorbed cations $\left[Co(H_2O)_6\right]^{2+}$ and $\left[Ni(H_2O)_6\right]^{2+}$ (table 3) are near to parameters typical for hexaaquacations Co^{2+} and Ni^{2+} in aqueous solution /9/.

With heating of Co and Ni-montmorillonite up to 150-200°C octahedral environment of Co^{2+} and Ni^{2+} ions changes into tet-

rahedral one. In case of Co-sample it testifies to the appearance of distinct 15750 cm^{-1} band typical for transition from ground state $^4A_2$ into $^4T_1(P)$ state in visible region of spectrum and triplet of 8000-7250-6320 cm^{-1} bound with transition of $^4A_2 \longrightarrow 4T_1(F)$ in near IR-region. These results may be interpreted easily keeping in mind that with dehydration exchange cations submerge into ditrigonal holes of mineral structure.

Thus, in samples of Co- and Ni-montmorillonite partially dehydrated by heating at 150-200°C exchange cations Co^{2+} and Ni^{2+} are in environment of three neigbouring oxygen atoms of ditrigonal holes (fig. 2). The fourth coordination position in tetrahedron is occupied by a molecule of bound water.

In conclusion we shall note that the amount of data obtained permits to develop an approach to hydration (solvation) of layer silicates of montmorillonite and vermiculite as to formation of surface coordination compounds.

Literature.

1. Yu.I.Tarasevich, V.M.Valitskaya, F.D.Ovcharenko, Colloid J., 30, 889 (1968).
2. Yu.I.Tarasevich, V.M.Rudenko, E.V.Sharkina, F.D.Ovcharenko Colloid J., 32, 266 (1970).
3. Yu.I.Tarasevich, V.P.Telichkun, F.D. Ovcharenko, Colloid J., 34, 412 (1972).
4. G.Zundel, Hydration and Intermolecular Interaction, Academic Press, N.Y.-London, 1969.
5. Z.Keçki, J.Woitczak, Roczn.Chem., 44, 847 (1970).
6. Yu.I.Tarasevich, F.D.Ovcharenko, Proceed. 1972 Internat. Clay Conference, Madrid, 1973, p.627.
7. E.V.Sharkina, Yu.I.Tarasevich, Ukr.Chem. J., 39, 163, 309 (1973).
8. A.B.P.Lever, Inorganic Electronic Spectroscopy Elsevior Publishing Company, Amsterdam-London-N.Y., 1968.
9. F.A.Cotton, G.Wilkinson, Advanced Inorganic Chemistry, Interscience Publishers, N.Y.-London-Sydney, 1966.

INVESTIGATIONS ON THE STRUCTURE AND SORPTION PROPERTIES OF HYDRATED ANTIMONY PENTOXIDE USED FOR THE SELECTIVE REMOVAL OF RADIOSODIUM

L.G. Nagy, G. Török and G. Fóti

Department of Physical Chemistry, Technical University of Budapest, 1521. Budapest, Hungary

Introduction

The presence of ^{24}Na often causes serious difficulties in the radiochemistry especially in the neutron activation analysis.

Because of the well-known difficulties of the analytical separation processes of the alkali metal ions, the only useful method /first proposed by GIRARDI[1] and his coworkers/ is based on the selective or semiselective sorption of the sodium ions on hydrated antimony pentoxide /HAP/. According to their results nearly absolute selectivity can be achieved if the solution is made to 9-12 M for hydrochloric acid.

Some negative aspects, such as inhomogeneities of the commercial preparations, and thus some inconsistency in the results, further the empirical character of the procedure and the unknown mechanism of the sorption directed our attention to the preparation and qualification of the sorption material, and to the investigation of the mechanism of the sorption process.

Preparation and qualification of the sorption material

Based on some initial data given by Girardi a method was elaborated to prepare the HAP preparations and an elution chromatographic method was selected to determine the

sorption properties of the products, or with other words to qualify our preparations. The details of the preparation and qualification procedure are given elsewere /2,3/.

Based on the investigations on the sodium sorption the following conclusions could be made

- In highly acidic solutions - first of all in hydrochloric acid solutions - selective or semiselective sorption is observed. Under these circumstances ion-exchange can be excluded as sorption-mechanism, because of the high proton or better to say hydronium concentration.
- In these solutions specific, practically irreversible sorption is obtained at column loadings less then 5-10 mg ion/g HAP, whereas at column loadings above 10 mg ion/g HAP the observed changes on the sorption isotherms are indicating the presence of other mechanism.
- This change of the mechanism is supported by other conclusions made on the basis of the sorption isotherms. The linear semilogarithmic plot of the F_t values are to be interpreted with energetical inhomogeneities, that is the most active groups or places - which are reacting with the first amount of ions- are forming much more irreversible bonds as the groups or places which will react later. This means, that the bond strength shows large inhomogeneities. Based on the sorption isothermthe bond strength decreases monotonously from an initial value - down to zero.
- Furthermore it is well known, that in solutions of moderate acidity or in neutral solutions HAP may be treated as an inorganic ion exchanger, in which case the sorption process should be a reversible ion exchange process.

It could be further that the kinetics of the sorption process is a so-called diffusion controlled kinetics.Furthermore the upper limit of the rate of sorption may be set at 1 min. as the average contact time did not exceed this value.

Thus the general conclusion may be drawn, that HAP is a polyfunctional sorption material, and depending on the experimental parameters general ion exchange or selective and irreversible sorption process occurs.

Let us define the term: irreversible for our case. Irreversible means, that the ion in question - in our case sodium - can not be eluted with eluting agent volumes several ten to hundred times higher than the column-volume. Furthermore according to our investigations the sodium ions - bound to the HAP - can not be eluted with solutions of other ions, using frontal chromatographic technics. Investigations were made with K^+, Li, Cs^+, and Ca^{2+} ions. The first three are alkali metal ions, their chemical properties are rather similar to the sodium. The Ca^{2+} ions have an ionic radius, which is nearly the same as that of the sodium. This means, that the geometrical parameters are nearly the same.

Sodium bound to HAP is however easily exchangeable with sodium, at least in strongly acidic media. The sodium ions in the solution thus have a free access to the bound sodium ions, and the activation energy is rather small. It can be concluded, that the sorption is a surface process.

Investigations on the structure and sorption properties of the preparations.

Investigations on the structure of HAP preparations were already made by BEATSLE et al. /4/ and MITSUO ABE et al /5,6,7/, but other preparation techniques were used, and preparations for ion-exchange applications were made.

Because of these reasons some investigations were made to determine the structure - and in first of all the surface structure - of the preparations.

Thermoanalysis

The thermoanalytical results can be demonstrated on Fig. 1.

Three rather indistinct steps can be observed; the first one is between 20-100°C the second one is between 250-450°C and third one is about 550-600°C.

The first step is possibly due to the loss of the physically bound water, the second, or better to say the height of the second one may be correlated to the sorption

properties of the preparations, whereas the third one is a rather small weight loss.

Some important conclusions may be drawn, if we consider, that the preparations were already preheated at 270°C for several hours during the preparation process. As more than 5% absolute /about 40% relative/ weight loss occurs under this temperature it can be assumed that some mobile and volatile groups are existing in the preparations. As the HAP consists of the following elements: antimony, oxygen, hydrogen, the weight loss is most probably due to the loss of water. This means that the water content of the preparation is partly mobile water.

Moessbauer spectroscopy

However the thermoanalytical investigations did not give on answer on the question, whether the weight loss is due only to the loss of water or the loss of oxygen should be considered too. Because of these reason the Moessbauer spectra were taken of the standard preparations and of preparations made with less oxydizing agent /HNO_3/. According to the results more than 97 % of the antimony is in the +5 oxidation state, and the preparations show a pure antimony oxide structure. Thus the conclusion may be drawn, that at least in the first and second step the weight loss is due to the water loss of the preparation.

Crystal structure

X-ray diffraction methods were used to determine the crystal structure of the preparations /Fig. 2 /. Both the "good" and "poor" preparations possessed a pyrochlor structure with a cell-constant of 10,3 Å. However the results indicate, that crystalline structure is an essential factor for the sodium-sorption, with other words sodium sorption occurs only in the presence of pyrochlor structure. This observations and earlier conclusions on the surface reactions lead us to the conclusion, that the surface structure of the pyrochlor cells should be investigated in details.

Furthermore the well known fact was to be considered, that the pyrochlor structure is a typical zeolitic structure with ion-deficiency. In the case of the HAP crystal positions may be partly or full vacant, thus allowing the uptake of various ions with appropriate geometric properties. The ion--sorption in general may be explained in this way, but neither the selectivity nor other details can be solely attributed to this zeolitic character.

IR-spectroscopy

IR-spectra were made in order to determine the characteristic bonds in the preparations. On the basis of the IR-spectra shown on Fig. 3. the following conclusions may be drawn:

- Beside the Sb-O band at 770 cm^{-1} and the broad absorption maximum 2500-3700 cm^{-1} only some small peaks can be observed.
- Because of some missing peaks, the low intensity of the Sb-OH vibration at 1250 cm^{-1}, and because of the rather large band width at 2500-3700 cm^{-1} at may be assumed, that only negligible amounts of Sb-OH groups are present, that is the preparation consists of SbO bonds, and hetero-energetically bounded water. These water molecules are occupying some of the lattice points, between which a rather free exchange may occur. This assumption was supported by numerous IR spectra of HAP preparations where in various stages of the preparation process deuterium compounds /D_2O and DCl/ were used. The standard shift of about 600 cm^{-1} was not observable, that means D_2O was exchanged during processing.

IR spectra of untreated, with water and hydrochloric acid treated and finally with sodium loaded HAP were also determined /Fig. 4./. The first three spectra are practically the same, but after the sorption of sodium the broad absorption band between 2500 and 3600 cm^{-1} shows a well defined absorption maximum. This observation may be caused by a partial inmobilization of the lattice water. This observation was interpreted as the solvation of the sodium ions, which

was assumed as the basic chemical process of the sorption of the sodium ions.

The specific surface area determined via gas adsorption technique was between 20-30 m²/g, the "good" preparations showed a somehow smaller specific surface area than the preparations with "poor" sorption properties. The preparations did not show a porous structure.

The heat of solvation was determined by microcalorimetry. An equilibrium could be reached within 2 minutes with the good preparations, whereas with the other ones the curves showed a monotonous ascending character even after 10 minutes /Fig. 5./. The specific heat of solvation - calculated on unit mass - was about 50% higher for the "poor" preparations, than for the good ones. However if the differences in the specific surface area taken into consideration, too, nearly the same value: 0,5 cal/m² is obtained. This value compared to 0,025 cal/m² the heat of solvation on activated carbon determined under similar conditions indicates, that the solvation is not a pure physical sorption, since at least on the good preparations the rate of the process excludes the possibility of transport processes in the solid phase.

The large specific surface area of the "poor" preparations and the slow but constant uptake of water may be explained by an "non ideal" surface; i.e. the crystal structure on the surface lattices is to a greater extent demolished during the preparation process, than on the "good" preparations.

As the reaction-heat of the sorption process at least for aqueous solutions of NaCl is within the deviation of some ten percent equal with the heat of solvation with H_2O the conclusion may be drawn, that similar processes are occuring in both case.

The final conclusion and hypothesis is thus EQUIVALENT SORPTION. The sodium ions may be bound to the vacant surface positions, via solvation i.e. by hydrogen bonds. The counter ion is bound to the sodium via electrostatic forces.

1., Girardi F., Sabbioni E.J., Journal of Radioanal. Chem. 1, 169-178 /1968/
2., Török G., Diehl J.F.: Radiochim Acta 15 96-100 /1971/
3., Török G., Schelenz R., Fischer E.: BFL-Bericht 2/1973 165 pp.
4., Baetsle L.H., Huys D.: J. inorg. Nucl. Chem. 30 639-649 /1968/.
5., Mitsuo Abe, Takuji Ito: Bull. Chem. Soc. Jap. 41 333-342 /1968/
6., " " ibid 41 2366-2371 /1968/
7., Mitsuo Abe: Bull. Chem. Soc. Japan 42 2683-2685 /1969/

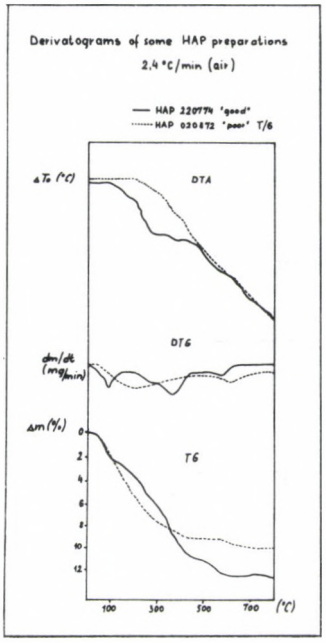

Fig. 1.

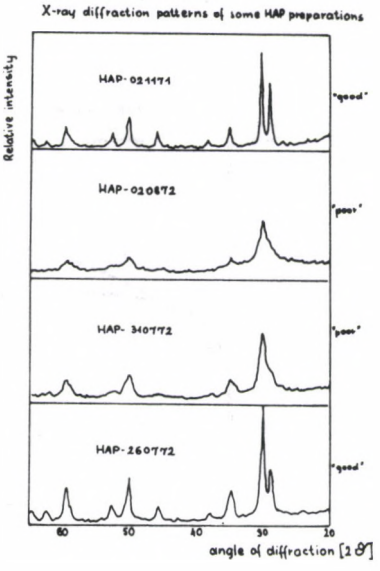

Fig. 2.

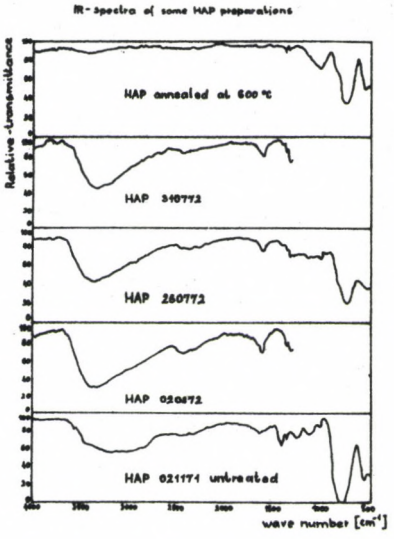

Fig. 3.

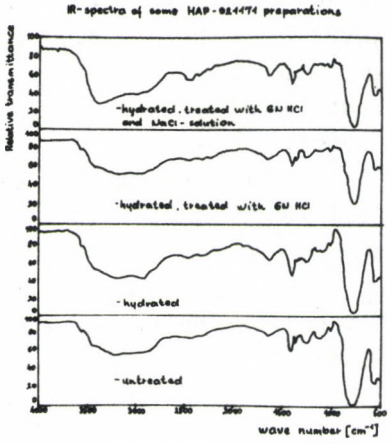

Fig. 4.

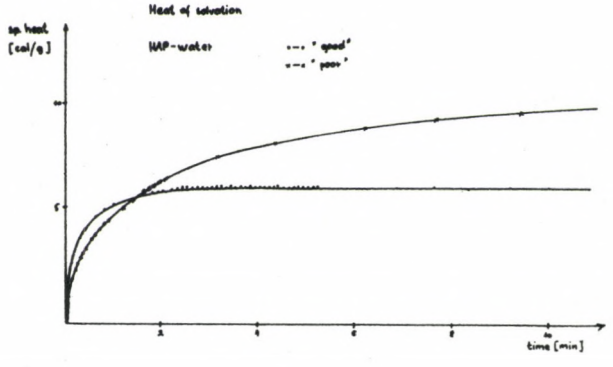

Fig. 5.

THE SPECIFIC SURFACE AREA AND THE ENERGY DISTRIBUTION OF THE HETEROGENEOUS SOLID SURFACES

J. Tóth

Petroleum Engineering Research Laboratory
of the Hungarian Academy of Sciences,
3515 Miskolc, P.O.B. 2. Hungary

Stepwise model of adsorption on heterogeneous surfaces.

In principle, an energetically heterogeneous surface can be divided into an infinitely great number or a given number /z/ of homogeneous patches of size a_i and energy ε_i. Let us suppose that on a heterogeneous surface the monolayer adsorption of gases /vapours/ takes place stepwise, i.e., if

$$\varepsilon_1 > \varepsilon_2 > \ldots\ldots \varepsilon_i > \ldots\ldots \varepsilon_z$$

then the patches are saturated in the sequence of their increasing energy with increasing equilibrum pressure /p/. The energy ε_i is related to a given pair of adsorbent-adsorptive, thus it also implies the interaction energies. Let the quantity adsorbed up to the energy-level ε_i be n_i^s, and the equilibrum pressure p_i. On the basis of the stepwise model, the energy ε_i corresponding to the patch a_i can be regarded as identical with the energy of a homogeneous surface on which a similar quantity of n_i^s is adsorbed at equilibrum pressure p_i. The Langmuir' equation corresponding to the above mentioned homogeneous adsorption fits to the point /n_i^s, p_i/ of the heterogeneous isotherm according to Fig. 1. At the fitting point, it is also valid

$$n_i^s = \frac{n_{u,i}^s \, p_i}{b_i + p_i} \qquad /1/$$

where the extent of the homogeneous surface can be calculated from $n_{u,i}^s$. Write Eq. /1/ in the form of a differential

equation, i.e.:

$$\Psi_i - 1 = \frac{1}{b_i} p_i \qquad /2/$$

where

$$\Psi_i = \frac{n_i^s}{p_i} \frac{dp_i}{dn_i^s} . \qquad /3/$$

Since

$$b_i = k \exp / - \frac{\varepsilon_i}{RT} / \qquad /4/$$

therefore, taking into account Eq. /2/, the energy of the patch a_i is:

$$\varepsilon_i = RT \ln \left[k \frac{/\Psi_i - 1/}{p_i} \right] \qquad /5/$$

On the basis of the theoretical considerations of DeBoer /1/ and Hobson /2/, the value of $\underline{k}$ in Eq. /5/ may be written to a good approximation in the form of

$$k = 1{,}76 \, /MT/^{1/2} . \, 10^4 \qquad /6/$$

if p is expressed in torrs. /M is the molecular weight of the adsorptiv./

Since the Langmuir' equation may be fitted to any point $/n^s$, p/ of the heterogeneous isotherm, we generally get

$$\varepsilon = RT \ln \left[k \frac{/\Psi - 1/}{p} \right] \qquad /7/$$

If the temperature of the heterogeneous isotherm is under the critical temperature of the adsorptive then it is valid for the vapour pressure $/p_o/$ that

$$p_o = k_1 \exp /- \frac{\lambda}{RT} / \qquad /8/$$

On the basis of Eqs /7-8/ with the condition of $k \approx k_1$ the net adsorption energy /difference between the energy ε and the heat of condensation / can be simply calculated:

$$\varepsilon - \lambda = \Delta\lambda = RT \ln \left[p_o \frac{/\Psi - 1/}{p} \right] \qquad /9/$$

Specific surface area $/a^s/$ of heterogeneous adsorbents.

The $\Psi - 1$ vs. p functions of the heterogeneous isotherms usually change stepwise, according to Fig. 2. The surface is practically homogeneous in the proportional sections of these functions, according to Fig. 2 /see dashed straight lines/. The energies ε belonging to the homogeneous patches decrease with increasing coverage /with increasing p/. The

determination of the specific surface area is given possible by the fact that on the function $\Psi - 1$ vs. p can be marked off accurately the last proportional section, namely the interval of the final homogenisation of the surface beyond which - as a result of multilayer adsorption - the $\Psi - 1$ function decreases. The total monolayer capacity $/n_u^s/$ of the heterogeneous surface can be determined from the Langmuir' isotherm belonging to the last proportional section and fitting to it /see Fig. 2/. Despite the conventionally used neglections /spherical molecules, closest fitting/, an identical and real specific surface area can be calculated to a fairly good approximation /within a maximum error of 10 %/ from the isotherms of various adsorptives measured at various temperatures. Our statement is backed up by the data in Table I, where the specific surface areas calculated from the isotherms of Szepesy and Illés /3-4/, measured on a Nuxit-AL microporous activated carbon are presented.

T a b l e I

①	C_2H_6	CO_2	C_3H_8				C_3H_6		
②	20	20	20	40	60	90	20	40	90
③	28,7	21,5	30,2	31,6	33,4	35,9	28,7	30,1	34,8
④	130,3	170,6	111,4	106,1	101,1	95,3	121,8	110,8	102,9
⑤	999	987	905	902	907	919	938	906	963

① Adsorptive,
② Temperature of isotherm $/^oC/$
③ The space required for a molecule $/Å^2/$,
④ Monolayer adsorption capacity $/n.cm^3\ g^{-1}/$,
⑤ Specific surface area $/m^2\ g^{-1}/$

The isotherm equation of monolayer adsorption on a heterogeneous surface.

If the "stepwise" $\psi - 1$ vs. p function presented in Fig. 2 is approximated by the power function

$$\psi - 1 = \frac{1}{b'} p^m \qquad /10/$$

than by solving the differential equation /10/ we get following isotherm equation:

$$n^s = \frac{n^s_\infty p}{/b' + p^m/^{1/m}} \qquad /11/$$

where b', n^s_∞ and m are constants, and for m always holds that

$$0 < m < 1$$

In connection with Eq. /11/ we have thus far pointed out the following:

1./ By using the linear form of the equation, i.e. the relationship

$$\left(\frac{p}{n^s}\right)^m = \frac{1}{/n^s_\infty/^m} p^m + \frac{b'}{/n^s_\infty/^m} \qquad /12/$$

the isotherms of the type I. measured on a heterogeneous surface can be described in an exceedingly wide pressure range /from 1-2 torr to several at./, more accurately then it is possible by using the Dubinin-Raduskevich equation /5-6/.

2./ The value of m depends - within the mentioned accuracy of Eq. /12/ - on the quality of the adsorbent only. Thus the value of m should be considered as a number suitable for characterizing the energetical heterogeneity of the adsorbent. /m = 1 is a homogeneous surface, $m \to o$ is an "infinite" heterogeneous one /5/.

3./ The constant b' figuring in Eqs /11-12/ can be interpreted by the relationship

$$b' = p_o p^{m-1} \exp / - \frac{\Delta\lambda}{RT} /$$

while the relation

$$n^s \approx n_u^s$$

applies to the condition $b' \ll p_o^m$.

4./ On the basis of Eq. /11/ and the Gibbs' relationship, the state equation of the monolayer may be calculated. This equation can be given in dimensionless form, and the explicite form of which depending only on the adsorbent's quality /i.e. on $\underline{m}$ /5//.

Characteristics functions of heterogeneous surfaces.

Allowing for Eq. /7/ and Eq. /10/, we have the relation

$$\mathcal{E} = RT \ln\left[\frac{k}{b'} p^{m-1}\right] \quad p \neq o \qquad /13/$$

By introducing the symbols

$$\alpha = \frac{n_u^s}{n_\infty^s} \text{ and } \Theta = \frac{n^s}{n_u^s}$$

we get, from Eq. /11/, that

$$p = \left[\frac{\Theta^m b'}{\alpha^m - \Theta^m}\right]^{\frac{1}{m}} \qquad /14/$$

After inserting Eq. /14/ into Eq. /13/ and subsequently solving for Θ, the following relationship results

$$\Theta = \frac{\alpha}{\left[1+k_1 \exp\left(\frac{\mathcal{E}}{n\,RT}\right)\right]^{1/m}} \qquad /15/$$

where $n = \frac{1-m}{m}$ and $k_1 = b'^{\,1/1-m}\; k^{-1/n}$

Similar considerations and the use of Eq. /9/ and /10/ lead to

$$\Theta = \frac{\alpha}{\left[1+k_2 \exp\left(\frac{\Delta\lambda}{n\,RT}\right)\right]^{1/m}} \qquad /16/$$

where

$$k_2 = \left[b'/p_o^m\right]^{1/1-m}$$

In Eqs /15/ and /16/, definite energy values /$\mathcal{E}$ or $\Delta\lambda$/ are assigned to a given degree of coverage, thus if the stepwise model of the adsorption and Eqs /1/ through /9/

related to the model are approximately correct, the relationship Θ vs. ε or Θ vs. $\Delta\lambda$ relating to each adsorptive must be a temperature-independent characteristic function. This fact is supported by the upper part of Fig. 3 where the ε-characteristics of carbon dioxide, ethane, ethylene, propane, propylene, buthane calculated by means of Eqs /15-16/ and of the isotherms measured on Nuxit-AL charcoal at different temperatures are presented.

For the ε-characteristics, it is typical that

a./ a value of ε greater than 0 and increasing with the molecular weight of the adsorptive is involved with the value $\Theta = 1$ /total coverage/. This energies which may be denoted by ε_h are characteristic for the totally homogenized surface.

b./ If greater the value of ε_h, than greater and wider is the energy interval covered by the ε-characteristics, too.

Energy distribution of heterogeneous surfaces.

Based on the stepwise model of the adsorption, we are able to calculate approximately the differential distribution of the energy of adsorption, that is

$$-\frac{d\theta}{d\varepsilon} = \chi/\varepsilon/ \qquad /17/$$

The explicite form of Eq. /17/ can be derived by differentiating from Eq. /15/:

$$\chi/\varepsilon/ = \frac{1}{/1-m/\alpha^m\ RT}\theta/\varepsilon/\left[\alpha^m - \theta^m/\varepsilon/\right] \qquad /18/$$

The functions of /18/ are shown in the lower part of Fig. 3. The specific feature of the distribution functions follows from the properties of the ε-characteristics:

The $\chi/\varepsilon/$ values pertaining to $\Theta > 1$ have no physical meaning whereas for $\Theta = 1$, $\chi/\varepsilon/ > 0$. For that reason, the Gaussian distribution functions - on the basis of the stepwise model of the monolayer adsorption - "break off" at ε_h. Thus, the $\chi/\varepsilon/$ functions belong definite lowe energy limits /ε_h/. The calculation on the function $\chi/\varepsilon/$ as defined by Eq. /18/ is much simpler than the solution of the physically more exact and, consequently, often used equation

$$\Theta(p,T) = \int_{\Omega} \Theta_L(\varepsilon,p,T)\, \chi(\varepsilon)\, d\varepsilon \qquad /19/$$

where Θ_L is the local adsorption isotherm /valid for a single patch/ Ω is the range of possible variation of ε. The $\chi(\varepsilon)$ pertaining to isotherms /11/ has also been calculated by using Eq. /19/ [6], but in our opinion, the energy distribution - for microporous adsorbents - according to /18/ is more representative, due to the fictive lower limit $\varepsilon = 0$ indispensable for the solution of Eq. /19/.

References

[1] J.H. DeBoer, The Dynamical Character of Adsorption. Chapt. IV. Clarendon Press, Oxford 1953

[2] J.P. Hobson, Canad. J. Phys. 43, 1934 /1965/

[3] L. Szepesy, V. Illés, Acta Chim. Hung. 35, 37 /1963/

[4] L. Szepesy, V. Illés, Acta Chim. Hung. 35, 53 /1963/

[5] J. Tóth, Acta Chim. Hung. 69, 311 /1971/

[6] J. Tóth, W.Rudzinski, A.Waksmundzki, M.Jaroniec, S. Sokolowski, Acta Chim. Hung. 82, 11 /1974/

Figures

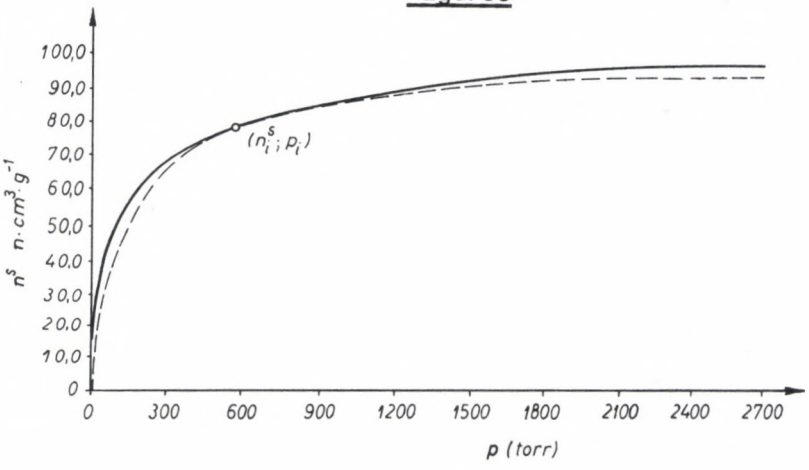

Fig.1 Propane 40 °C isotherm on Nuxit-AL charcoal /solid line/ and the Langmuir' equation fitting to point $/n_i^s, p/$ of the isotherm /dashed line/.

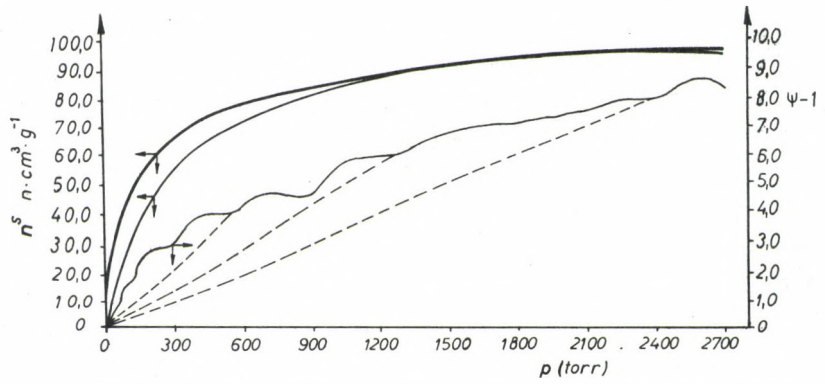

Fig.2 Determination of the specific surface area of the Nuxit-AL charcoal on the basis of the propane 40 °C isotherm

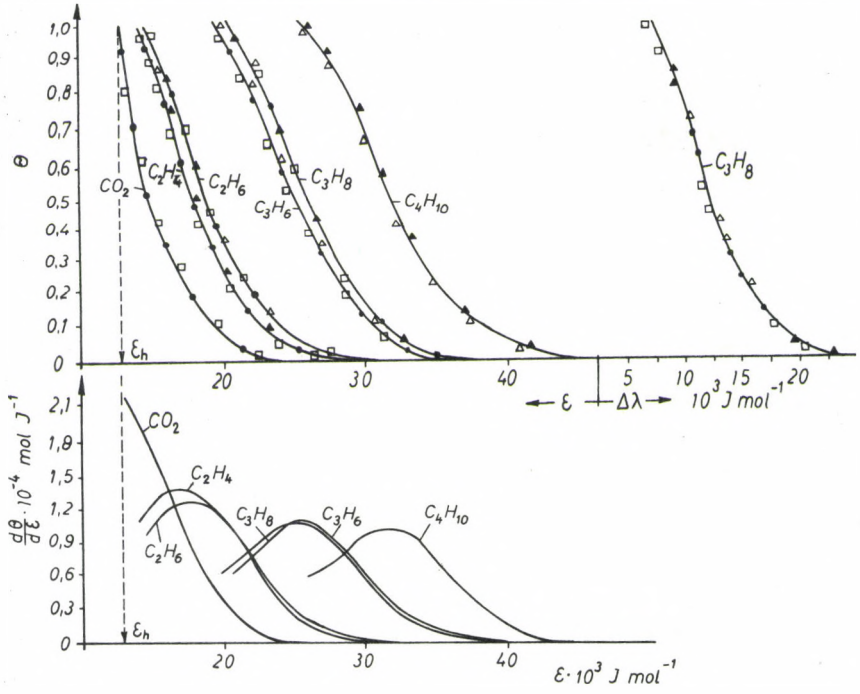

Fig.3 Characteristics-functions /upper part/ and energy distributions /lower part/ for the Nuxit-Al charcoal. Data as calculated from isotherms at temperatures:
• 20 °C ▫ 40 °C ▲ 60 °C ▵ 90 °C

STUDY OF CARBON TYPE SORBENTS BY STRUCTURAL CHEMICAL ANALYSIS AND IMMERSIONAL CALORIMETRY

J. Bodnár, J. Gajári[*] and L.G. Nagy

Department of Physical Chemistry, [*]Institute of Agriculture Chemical Technology, Technical University of Budapest, 1521. Budapest, Hungary.

We have studied the decisive surface properties of systems having practical importance.

The relative values of apparent adsorption capacity calculated from the adsorption isotherms of phenol-water/activated carbon systems /Fig.1./ don't agree in every case with those of specific surface area determined by the BET method.

The great differences in the adsorption of phenol from dilute aqueous solutions on carbons having approximately the same high B.E.T. surface area /about 1000 m^2/g/ and activated by steam or chemically, respectively, show the importance of surface oxides /1/.

Data given by the thermoanalytical method were used for the study of the oxidation degree. Comparing the derivatograms /measured in the atmosphere of argon and air/ of chemically and steam activated carbons it can be established, that the chemically activated carbon, having a lower oxidation degree reacts to the oxygen of the air at 250-300°C in an exotherm process. /Fig. 2./. According to the thermogravimetrical curve the oxidation proceeding at low temperature is not followed by weight decrease causing irreversible changes in the other surface properties of the adsorbent and the recrystallization of the carbon structure is also hindered at this relatively low temperature. The considerable

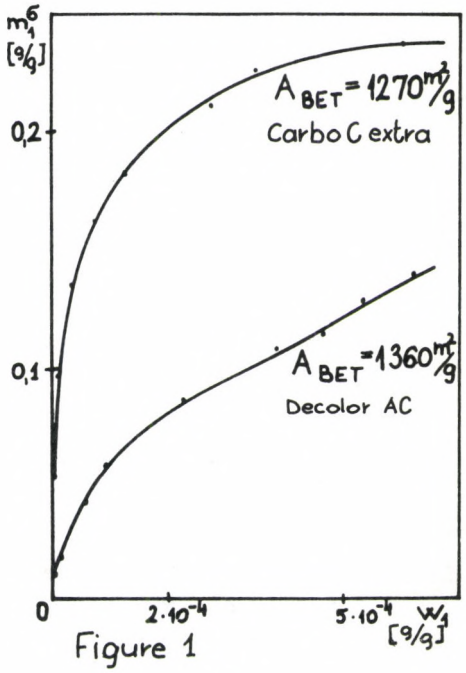

Figure 1

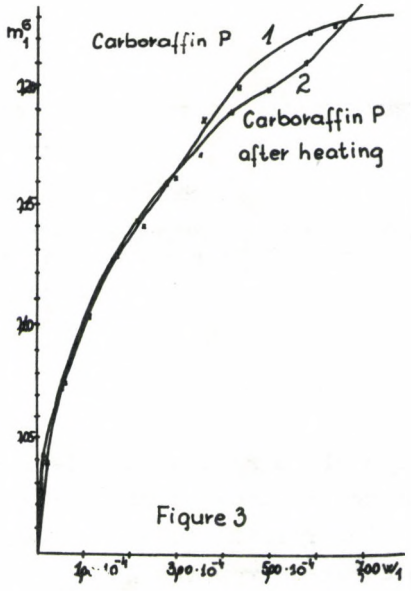

Figure 3

Carboraffin P

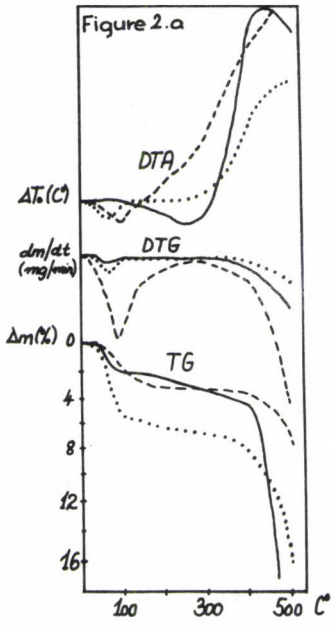

Carbo C Extra

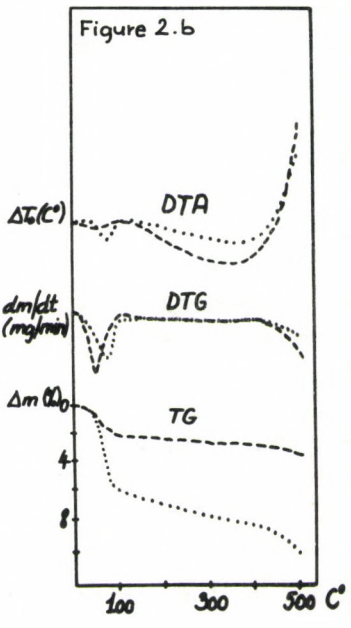

Derivatograms in air /broken/, in argon /dotted/ and in air after heating /continuous/

similarity in the derivatograms of the chemically and steam activated carbon samples /the former after having been heated to 300°C and recooling/ refers to the fact, that the oxide structure of surface, formed as a result of the exotherm process is approximately the same as the original structure of the steam activated carbons. At the same time the adsorption of phenol is not affected considerably by the change of the oxidation degree, as it can be seen in Fig. 3., therefore the rule of surface oxides in the preferential adsorption of the studied systems is negligible.

With regard to the possibility, that chemisorption can proceed at the faults of the carbon structure, we studied the framed structure of carbon black, steam and chemically actived carbons. The diffractograms in Fig. 4. point uniformly to amorphous structure, though a small quantity of graphite is determinable in the steam activated sample. The small difference among the samples can be explained by the different quality of the raw material of carbons, and by the possible order in structure.

Comparing the pore distribution data determined by gas adsorption /2/ with the saturation values given by the adsorption isotherms of dilute solutions /Fig. 5./, it can be established, that the preferential adsorption of the studied systems can be attributed to the effect of the processes taking place in the pores having a smaller diameter than 10 Å. Adsorbing gases at a low pressure, Dubinin observed a similar phenomena /3/.

Clearing up the determinative role of the ultramicropores the problem arose, that the inorganic impurities of the industrial active carbons have practically no effect on the preferential sorption from dilute solutions of partially mixable liquids. The hydrophility of surface, which depend on the quantity of function groups, can't be neglected and

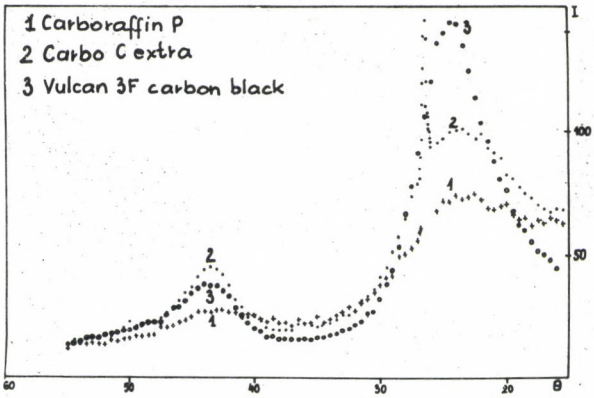

Figure 4

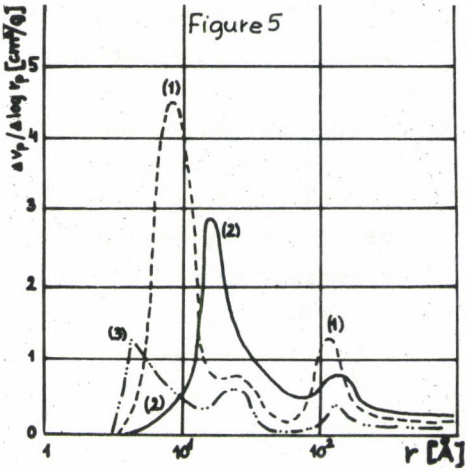

Pore distributions of H_3PO_4-activated /1/, $ZnCl_2$-activated /2/, and steam activated /3/ carbons.

Figure 6

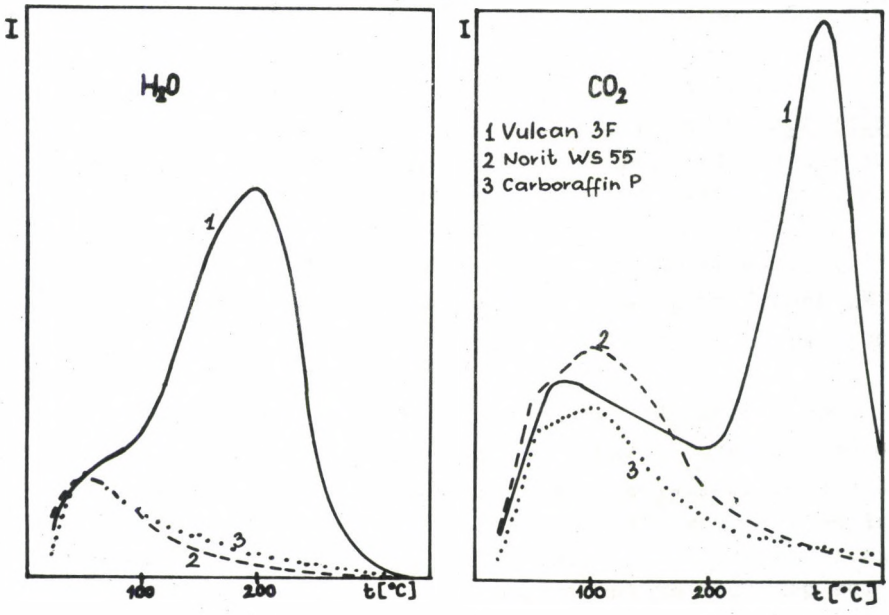

in the other hand these groups have a cation- or/and an anion exchange capacity being measurable as usual in the case of ion exchange resins. Though the data in the 1st table show the low number of these groups, the addition of the chemical bonding to the ion exchange groups and the wall action observed in ultramicropores is expectable at a uniform arrangement of the function groups. At the same time there is not any connection among the sorption data of oxalic acid and the value of ion exchange capacity.

Table 1.

Adsorbent	A_{BET} /m²/g/	Ion exchange capacity cation /mequiv/g/	anion	Oxalic acid adsorbed /g/g carbon/
Norit WS 55	910	0,15	0,45	0,098
Norit Carbo C extra	1270	0,35	0,35	0,108
Decolor AC	1360	0,40	0,35	0,028
Carboraffin P	2400	0,55	0,40	0,054
Sugar charcoal	150	0,60	0,00	-

Since the addition of the effects mentioned above is expectable, we tried to get informations about the arrangement of the function groups

At different temperatures we measured the quantity of water and carbon dioxide resulting from the decomposition of the function groups /containing oxygen/ of carbon black and steam and chemically activated carbons by mass spectrometry. As it can be seen in Fig. 6. the decomposition process yielding water and carbon dioxide is separable in time, on the other hand the decomposition of the surface oxides of carbon reaches its maximum until 100°C. In case of carbon black having a probably considerable oxide structure inside of the grains in consequence of its way

of preparing, the decomposition curve reaches its maximum value only at 300°C. From results the conclusion can be drawn, that the majority of the function groups of active carbons is on the surface. Carbon monoxide didn't form under the experimental circumstances.

Further informations on the function groups of surface can be obtained by infrared spectroscopy /4/. Though a monomolecular layer is sorbed on the surface of each activated carbon from cyclohexane according to the data of adsorption from binary mixtures, the spectrophotometrical measurements indicate bimolecular adsorption of acetic acid on a double /steam and chemically/ activated carbon /Fig.7./. The possible explanation is the measurability of only those processes, which proceed on the external surface. Considering the facts, that the dimer sorption is not observable by spectrophotometry in the H or OH form of carbons and there is a small amount of ion exchange groups, we can establish a much greater probability of the function groups on the external surface, than in the pores.

Since the anion exchange capacity of sugar charcoal is equal to zero, its value measured on industrial activated carbons is attributable to the effect of inorganic contaminations . The chemisorption among the residue of $ZnCl_2$ used as an activating agent and the π -sextett of benzene as well as among the basic metal oxides and the nitro group of nitro-benzene is also shown by the specific immersional heats measured in a Pászli-Wolfram type microcalorimeter. /Table 2./

Comparing the time dependence of the immersional heat with that of the heat evolving in a prompt reaction we can establish, that the cause of lasting is the hindered wetting of surface beside the inertia of equipment /Fig. 8./. Representing lg w against lg Q /Q=heat of immersion; $w = \frac{dQ}{dt}$; t = time/ the curve obtained is divisable into for sections of different and practically constant slope /Fig. 9./.

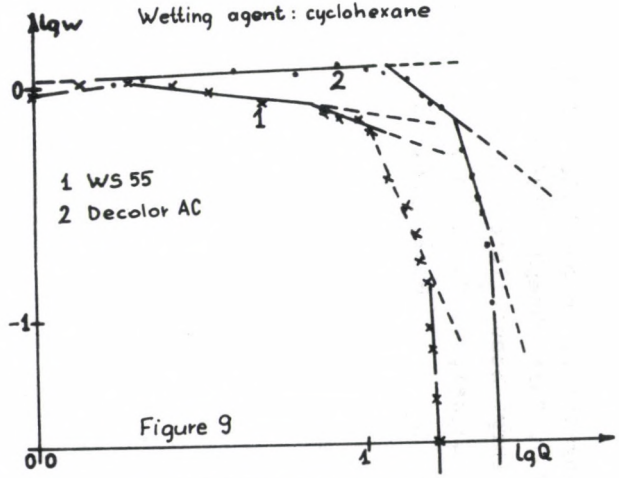

Figure 9

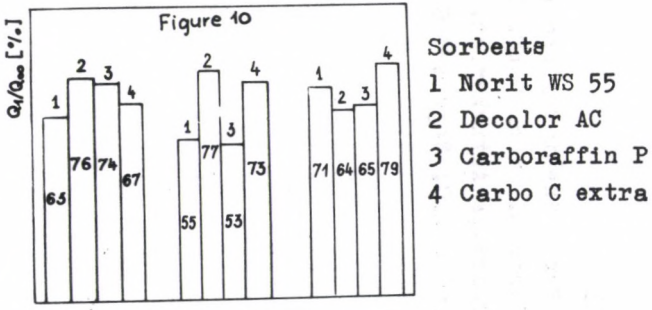

Figure 10

Sorbents
1 Norit WS 55
2 Decolor AC
3 Carboraffin P
4 Carbo C extra

cyclohexane benzene nitrobenzene
Wetting agent

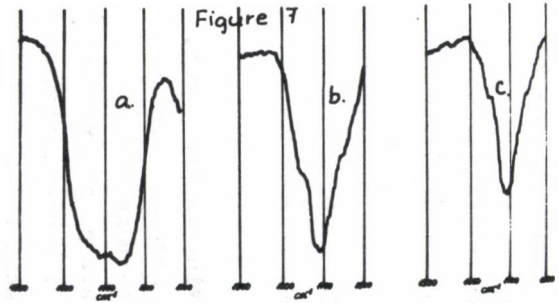

Figure 7

Infrared spectra of acetic acid adsorbed on Carbo C extra /a/, after basic /b/ and after acidic treatment of sorbent.

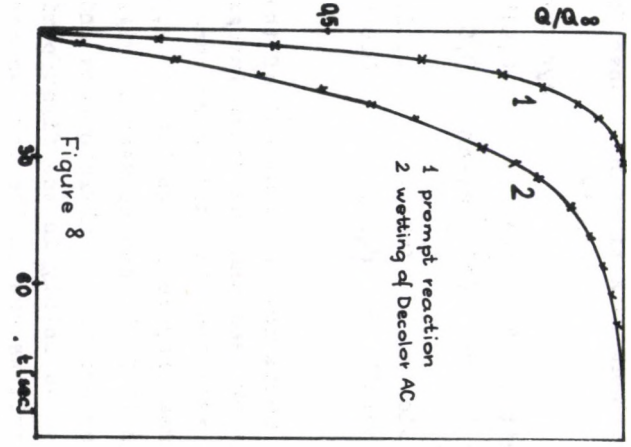

Figure 8

Table 2.

Adsorbent	Activating agents	Specific heats of immersion /cal/m²/ Wetting agents		
		cyclohexane	benzene	nitrobenzene
Norit WS 55	steam	0,019	0,018	0,035
Norit Carbo C extra	$ZnCl_2$+steam	0,023	0,024	0,034
Decolor AC	$ZnCl_2$	0,021	0,023	0,027
Carboraffin P	H_3PO_4	0,020	0,018	0,025

Comparing the quotient of the heat evolving in the first, fast process and the total integral heat of immersion in cyclohexane the obtained values are lower for carbons having ultramicropores, than for those, which contain pores greater than 15 Å. It can be seen in Fig. 10., that the chemisorption among benzene or nitrobenzene and the inorganic impurities proceeds mainly in the first period. Consequently these impurities are on the more accessible parts of surface as it follows from the results of spectrophotometry, too.

References

1. B. R. Puri, Chemistry and Physics of Carbon Vol.6 /1970/
2. M.M. Dubinin, Proc. Conf. Ind. Carb. Graph. /1958/
3. Pulverförmige Aktivkohlen. Lurgi Schnellinformation
4. J. Bodnár, L.G. Nagy and G. Lugosi, J. Coll. Int. Sci. 49 No.2. 326. /1974/

SURFACE AND MECHANOCHEMICAL ACTIVATION OF SILICATES

Z. Juhász[x] and L. Opoczky[xx]

[x]Technical University, Budapest, IX. Kinizsi u.1.

[xx]Central Research and Design Institute for the Silicate Industry, Budapest, III. Bécsi u.126-128

Introduction

Rather than the dispersity degree of the system alone, during the dry grinding of solids, the surface quality and inner crystalline structure of the particles, hence the free energy of the system is altered. Accordingly, the grinding operation is considered as a mechanical activation.

Upon activation, the solid reacts on mechanical, thermal and chemical influences else than in the original condition. Such processes are encountered in silicates and actually they are of industrial importance.

In the following, some model substances will be quoted to illustrate main characteristics of mechanical activation.

Test materials and methods

Test materials included:

- washed silica sand /98,1% of SiO_2/;
- -dicalcium silicate /termed C_2S/ burnt at 1450°C and stabilized by quenching; /34,68% of SiO_2, 65,11% of CaO/.

Test materials were activated by dry grinding for various times in laboratory vibrating and ball mills.

Dispersity degrees of grindings have been described partly by the specific surfaces determined by permeability measurement / ω cm^2/g/ and partly, by the "total" specific surface calculated from water vapour and nitrogen absorption iso-products by means of the BET balance /Ω_v and Ω_N, sq.m/g, resp./.

Variations of the crystalline structure of the grinding have been tested by X-ray diffractometry /RTG/ and by thermoanalytic methods /derivatography, DTG, TG, DTA/. For quarz, also the NaOH-soluble SiO_2 content /l_{Si}/ has been determined. The surface hydration degree of quarz / α / has been calculated from the thermal weight loss curves /TG/.

Technological characteristics have been described by the relative compressive strength / σ_r/ of specimens made of lime hydrate and ordinary silica sand in case of silica grindings, and for C_2S, by the heat of hydration Q^H_{28} and the compressive strength of standard specimens / σ_{28}/, besides, also the chemically bound water quantity W_{28} has been determined.

Test results

Test curves of silica sand have been plotted in Fig. 1. Dispersity degree of the grindings varied vs. time according to a maximum curve, hence after a prolonged grinding, the system coarsened. Also the surface hydration degree varied similarly. Increase of the hydration degree is due to the amorphous layer on the particle surface thickening with time, and of a high OH content. The hydration decrease after prolonged grinding is due to the interaction between silanol /Si-OH/ groups present on adjacent particle surfaces upon chemical reaction by condensation, concomitant to the formation of siloxane /Si-O-Si/ groups /agglomeration/. Appearance of the amorphous material, or decomposition of the crystalline structure of quarz can be followed by taking

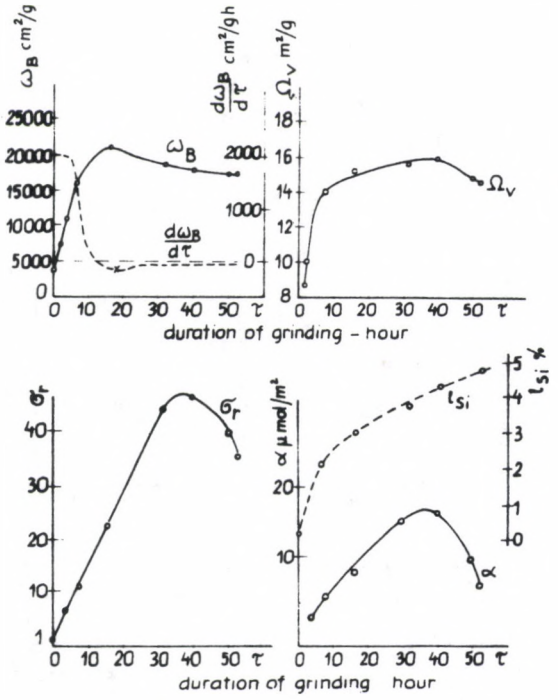
ω_B cm²/g
$\frac{d\omega_B}{d\tau}$ cm²/gh
Ω_V m²/g
ω_B
$\frac{d\omega_B}{d\tau}$
Ω_V
duration of grinding - hour
σ_r
σ_r
l_{Si}
l_{Si} %
α
duration of grinding hour

Fig.1.

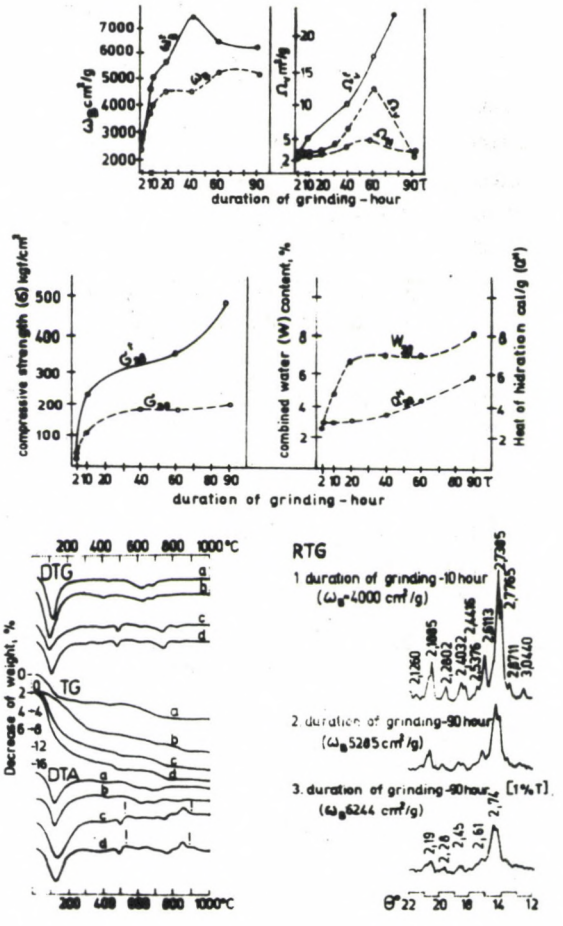
duration of grinding - hour
compressive strength (G) kgf/cm²
combined water (W) content, %
Heat of hidration cal/g (Q')
duration of grinding - hour
DTG
TG
DTA
Decrease of weight, %
RTG
1. duration of grinding -10 hour
(ω_s-4000 cm²/g)
2. duration of grinding-90 hour
(ω_s 5285 cm²/g)
3. duration of grinding-90 hour
(ω_s 6244 cm²/g)
[1%T]

Fig.2.

X-ray diffractogram /RTG/ of C_2S much changed after prolonged grinding. The decrease of the line intensity, disappearance of some peaks, and thicknening of some lines in case of grinding in the presence of a tenside /1% of triethanolamine / is still more conspicuous.

Alongside with the variation of the crystalline structure, - in spite of the important agglomeration - also the hydraulicity of grindings grew /Q_{28}^{H}, W_{28}^{H}/. Mechanochemical activation contributed to the formation of calcium hydrosilicates, at the same time accelerated the C_2S hydration known to be slow /see in the derivatogram: a = 1 h, b = 1o h, c = 4o h, d = 9o h of grinding and hydration/.

Discussion

Test results presented as an example show three, essentially different, often overlapping processes in course of the mechanical activation of silicates:

- mechanical dispersion concomitant to the particle size refinement;
- surface activation concomitant to the free surface energy increase;
- mechanochemical activation concomitant to the inner desorganization, amorphization within the inner atomic structure of solids.

Surface activation coarsens the system, while mechanochemical activation is often observed to entrain chemical reactions inside or interfacially of the particles.

Two kinds of coarsening processes are typical for the mechanical activation of silicates:

X-radiograms, while the quoted chemical reaction between particle surfaces can be concluded on from the TG and dissolution curves, by calculation. Upon feeding humid air into the mill chamber during grinding the adsorbed water acted as a surface active grinding aid, and contributed to the increase of dispersity degree. At the same time, growth of the surface hydration, then of the described reaction by condensation, and simultaneously, of the agglomeration could be observed.

After mechanical activation, an important increase of the hidden hydraulicity of grindings could be observed. The decrease of surface hydration was, however, accompanied by strength loss of the specimens.

Test curves of C_2S are seen in Fig. 2. External and "total" specific surfaces are quite different, the latter are lower by orders of magnitude as a rule.

The flattening of the C_2S dispersity curve after 10 hours of grinding is concomitant to the increasing aggregation of the particles. At last, aggregates got a structure too solid to be penetrated by either nitrogen or water molecules. These particles of solid structure are termed agglomerates. The different accessibility of the inner agglomerate surface to the two adsorbents, and the variable ratio of surfaces determined by both leads to the conclusion that in different grinding stages particles of different compactnesses develop.

Agglomeration, reducible to the chemical interaction between surfaces also for C_2S, was responsible for the reduction of the "active" hence "water-bound" specific surfaces and for the strength loss of grinding specimens.

Admixture of a surfactant reduced the agglomeration as shown by the increase of the "active" surface $/\Omega_T^{\downarrow}/$ and the strength $/\sigma_{28}^{T}/$.

- "aggregation" appearing after relative short grinding periods, hence clinging of particles upon adhesive forces, counteracting the subsequent mechanical dispersion /loss of validity for the Rittinger formula/;
- "agglomeration" for prolonged grinding, i.e. very solid adherence, recrystallization, welding of particles upon chemical forces. Agglomerates are formed in the mill between adjacent grinding bodies owing to high compressions at the contact spots.

In general, crystalline structure amorphization is facilitated by reducing the agglomeration /e.g. by surfactants/.

References

Juhász,Z.: Aufbereitungs-Technik 1o. 558-562. /1974/
Rehbinder,P.A.-G.S. Chodakow: Silikattechnik 13 29o /1962/
Schrader,R.-R.Wissing, H. Kubsch: Z.anorg.all.Chem.365.171. /1969/
Beke,B.-Opocky L.: Dechama Monographien Bd 57. Verlag Chemie 495-5o8.
Opoczky,L.-Z.Juhász: VI. Int. Congress on the Chem. of Cement. Moscow, 1974.

Group I/2

Adsorption at solid/gas and solid/liquid interfaces

TRIPLE POINT OF THE FIRST MONOMOLECULAR LAYER OF NITRIC OXIDE ADSORBED ON THE CLEAVAGE FACE OF LAMELLAR HALIDES.

A. ENAULT and Y. LARHER

DRA/SRIRMa, CEN.SACLAY, B.P. N° 2, 91190 GIF SUR YVETTE, France.

INTRODUCTION

We present and discuss sets of adsorption isotherms of nitric oxide on the cleavage face of lamellar halides. Because of the propensity of this gas to dimerise the results appear more complex than those observed for the adsorption of simple gases(Ar, Kr, Xe and CH_4) on the same substrate (1-4).

I. EXPERIMENTAL DETAILS

The experimental techniques has been described in detail elsewhere (1). The adsorption isotherms are measured volumetrically using a modified McLeod gauge. The temperature of the sample is kept constant to better than $\pm$ 0.02 K by evaporating oxygen or nitrogen under constant pressure. The pressure of nitric oxide is corrected for thermal effusion using the empirical formula of TAKAISHI and SENSUI (5) and for mercury drag effect, which we estimated with a capacitance manometer.

The adsorbents were prepared by sublimation in a rapid current of dry nitrogen (1). Frèquent purifications of nitric oxide were made : the gas was frozen at 77 K, repeatedly degassed at 77 K and distilled off at 90 K.

II - EXPERIMENTAL RESULTS. DISCUSSION

II - 1 General aspect of the sets of adsorption isotherms : 2D triple points.

We have measured sets of adsorption isotherms of NO on the cleavage face of 14 lamellar halides : $NiCl_2$, $CoCl_2$, $FeCl_2$, $NiBr_2$, $CoBr_2$, $FeBr_2$, $MgBr_2$, $CdCl_2$, CoI_2, $CdBr_2$, MnI_2, CdI_2, CaI_2, and PbI_2. A typical set, for NO on $FeCl_2$, is shown in figure 1. Below a temperature which we call T_t a single phase transition is observed from a dilute 2D phase g to a dense 2D phase β. Above T_t there are two phase-transitions : firstly from g to a dense 2D phase α, then from α to β . Clearly T_t

is the temperature of a 2D triple point where the three 2D phases g, α and β coexist.

From sets of adsorption isotherms we are able to determine the equations of the log p versus 1/T curves for the three observed transitions and therefrom the triple point temperatures, as well as energy and entropy data concerning the adsorbed phases. For NO on $MgBr_2$, $CdCl_2$, $CdBr_2$ and CdI_2, we observe only the g → β transition , the triple point staying above 94 K the upper temperature accessible to our cryostat. However for NO on the cadmium halides independant measurements of the triple points have been made by MATECKI, THOMY and DUVAL (6). We shall include these results in our discussion.

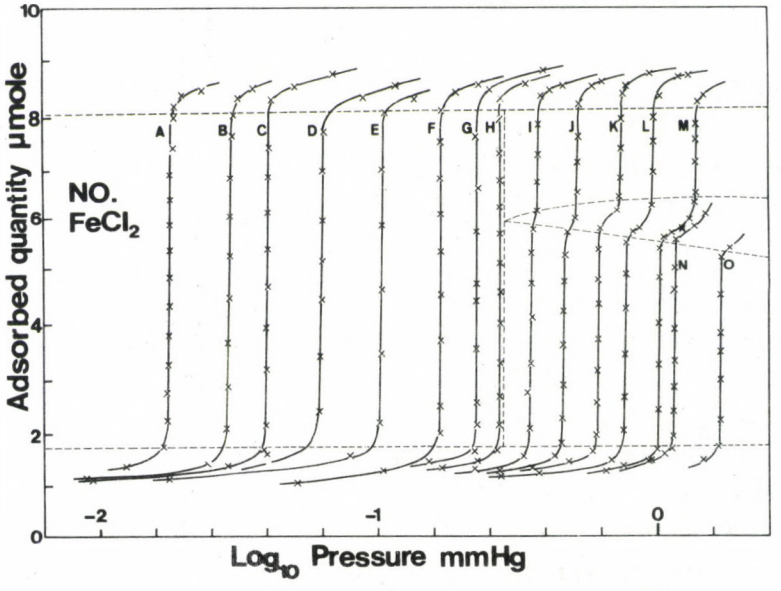

Figure 1 : Adsorption isotherms of nitric oxide on the cleavage face of ferrous chloride.

A, 75.74 K ; B, 77.27 K ; C, 78.16 K ; D, 79.54 K ; E, 81.29 K; F, 82.48 K ; G, 85.42 K ; H, 84.08 K ; I, 85.05 K ; J, 86.10 K; K, 87.20 K ; L, 88.11 K ; M, 89.28 K ; N, 89.82 K ; O, 91.53 K.

II-2 Densities of the α and β phases

Among the parameters which we shall discuss to try to infer the structure of the α and β 2D phases, their densities are the simplest and the most directly available. Clearly a prerequisite for handling such data is that the adsorbents have uniform surfaces. At least for one half of them, v.z. $NiCl_2$, $FeCl_2$, $NiBr_2$, $FeBr_2$, $CdCl_2$, $CdBr_2$, MnI_2, PbI_2, the adsorption isotherms show very little convexity towards the positive ordinates and one may reasonably suppose that the cleavage face represents at least 90 % of the total surface. In all these cases, we have determined one xenon isotherm. Supposing that a xenon atom has in a monolayer the same packing as in its bulk crystalline phase, i.e. $\sigma = 16.8$ Å^2, we find that $\sigma^\beta = 12.7 \pm 0.7$ Å^2 and $\sigma^\alpha = 18.7 \pm 0.5$ Å^2 per molecule of $(NO)_2$. We intentionally express the values for the nitric oxide dimer, which is its normal form in its bulk dense phases. A sketch of this planar dimer, as it exists in the bulk crystal is given in figure 2 (7). In its densest crystallographic plane, the (001), $(NO)_2$ occupies an area of 13.23 Å^2 the N-N bond being almost perpendicular to it. The nearness of σ^β to this value strongly suggests that the adsorbed β phase is

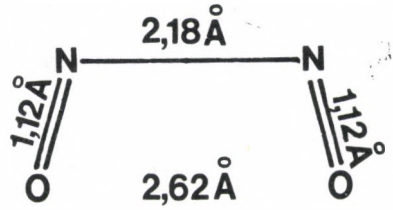

Figure 2 : Structure of the dimer in the bulk solid phase.

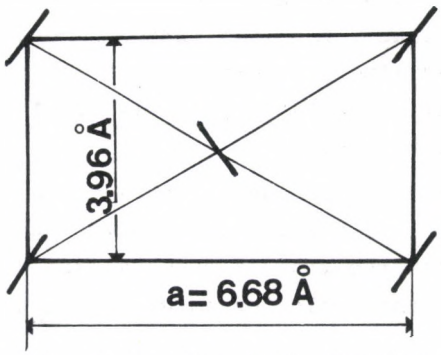

Figure 3 : The $(NO)_2$ lattice in the (001) crystallographic plane. For a compact arrangement one would have $\frac{a}{b} = 1.732$ instead of 1.687.

a crystalline monolayer with a structure close to that of the (001) plane of crystalline $(NO)_2$, i.e. the quasi-parallelipiped dimers standing on their smaller side almost perpendicular to the surface of the substrate. It is of interest to note here that in the (001) plane the dimers are in a quasi compact arrangment as shown by figure 3.

Given this structure for the β phase, many possibilities remain for the α phase. The most common type of triple points for one component 3D systems concerns the gas-liquid-solid equilibrium. For 2D equilibrium such points have been obtained only for xenon (8) and krypton (9) on graphite. Comparison of adsorption data for simple gases on graphite and lamellar halides suggests that, due to surface structure, the 2D liquid is an exceptional type of 2D phase, observable only on very smooth surfaces like the cleavage face of graphite. This makes it very improbable that the α phase is a liquid. In any case, were the β → α transition a melting transition, it would be necessary to imagine for it a structural change quite different from that of the 3D melting which involves a density change of only 12 % (10), definitely lower than the 45 % observed for the β → α transition. We may think of an α layer where the dimers are lying flat on the surface. Given the structure of the dimer, the transition of a 2D phase where the molecules lie flat to a phase where they are almost perpendicular to the surface, involves indeed a density variation of the order of magnitude of that effectively observed. In the following we will show that the analysis of other data supports this interpretation.

II-3 Adsorption energies and entropies

For a 2D condensation in an nth layer it may be shown that the transition pressure $p^{(n)}$ is related to the temperature by the following equations (1,2,9) :

$$R \frac{d \log p^{(n)}}{d\, 1/T} = - (h^{(g)} - u^{(n)})$$

$$R \log p^{(n)} = - \frac{h^{(g)} - u^{(n)}}{T} + s_o^{(g)} - s^{(n)}$$

where R is the gas constant, $h^{(g)}$ and $s_o^{(g)}$ are the molar enthalpy and entropy of the gaseous adsorbate at unit pressure. $u^{(n)}$ and $s^{(n)}$ can be considered as yielding approximate values of the molar energy and entropy of the dense layer (n) formed during the transition. Using these relations we have estimated $u^{(\alpha)}$, $u^{(\beta)}$, $s^{(\alpha)}$ and $s^{(\beta)}$.

For the systems studied we find $6.1 \leq s^{\beta} \leq 8.9$ cal.mol.$^{-1}$ K^{-1}, and $10.3 \leq s^{(\alpha)} \leq 13.5$ cal.mol.$^{-1}K^{-1}$, to be compared to the entropy of the bulk adsorbate $s^{(\infty)} \simeq 7.5$ cal.mol.$^{-1}K^{-1}$. Previous studies of the adsorption of rare gases on the same substrates led us to think that values of $s^{(n)}$ close to $s^{(\infty)}$ indicated a structure of the adlayer close to that of the densest plane of the bulk adsorbate. Consequently the values of $s^{(\beta)}$ observed here, support our previous conjecture that the β phase has a structure close to that of the (001) plane of crystalline $(NO)_2$, which is its densest plane. It is also satisfying that comparatively high values of $s^{(\alpha)}$ are found for the relatively low density α layer.

On the other hand $u^{(\beta)}$ and $u^{(\alpha)}$ are rather close to each other. We find $3972 \leq h^{g)} - u^{(\beta)} \leq 4242$ cal.mol^{-1} (of NO) $3539 \leq h^{(g)} - u^{(\alpha)} \leq 3903$ cal.mol^{-1}, $u^{(\alpha)} - u^{(\beta)}$ being lower than 300 cal.mol^{-1}. Since the energy of the bulk adsorbate $h^{(g)} - u^{(\infty)} = 4000$ cal.mol^{-1}, the attraction of the β layer by the substrate is hardly higher than the attraction of the (001) plane of $(NO)_2$ by bulk nitric oxide. Of course in the α phase, the $(NO)_2$ molecules lying flat on the surface should be more attracted by it than in the β phase, but it is not at all surprising that the loss in lateral attraction should be the prevailing factor, making thus $|u^{\alpha}|$ somewhat lower than $|u^{\beta}|$.

A possibility which could be considered for the $\alpha \rightarrow \beta$ transition, is that of a transition from a monomeric to a dimeric layer. However it can be discarded on the basis of the energy difference $|u^{(\beta)} - u^{(\alpha)}|$ which appears to be much lower than the absolute value of the estimated dimerisation enthalpy of NO in its liquid phase, v.z. 1800 cal.mol^{-1} (of NO).

II - 4 Adsorption energy

In figure 4 we have plotted the free energy difference $f^{(\infty)} - f^{(\beta)} = RT \log(P^{(\infty)}/p^{(\beta)})$, as a function of the parameter a, the distance between two halide ions on the cleavage face of the adsorbent. Since $s^{(\infty)} - s^{(\beta)}$ is close to zero, this quantity depends very little on the temperature. Two points are suggested by this figure. Firstly, there seems to be a maximum in $f^{(\infty)} - f^{(\beta)}$ at $a = 3.9$ Å a value close to 3.96 Å and 3.885 Å, the distances of closest approach of two $(NO)_2$ molecules in the (001) plane of bulk nitric oxide (see fig. 3). We interpret this maximum as corresponding to an optimum of the lateral interaction of the $(NO)_2$ molecules in the β phase. Secondly, it appears that at comparable values of the compatibility, the attraction of $(NO)_2$ by the halides is the more important, the higher the atomic number of the anion. We note that for simple gases both these points have been more firmly established (1-4). Clearly we have ignored $MgBr_2$ in our reasoning. This can be justified, since rare gas adsorption studies have shown that, due to their higher ionic character, $MgBr_2$ and CaI_2 attract the molecules less than the other lamellar halides (4,11).

II - 5 Triple point temperature

They are plotted in figure 5, again as a function of the parameter a of the adsorbent. There is a certain similarity between figures 4 and 5. We interpreted the maximum in figure 5 as corresponding to an optimum lateral interaction in the β phase. That this manifests itself in a higher value of the triple point temperature, i.e. a larger domain of existence of the β phase, seems quite plausible. Of course lateral interactions are expected to have less importance for the α phase than for the β phase.

On the other hand the situation should be reversed for the interaction with the substrate. Consequently, the differences between the attraction energies of $(NO)_2$ by the various classes of halides, that we have shown for the β phase, should be more important for the α phase. Thus the higher the attraction by the substrate, the higher the stability of the

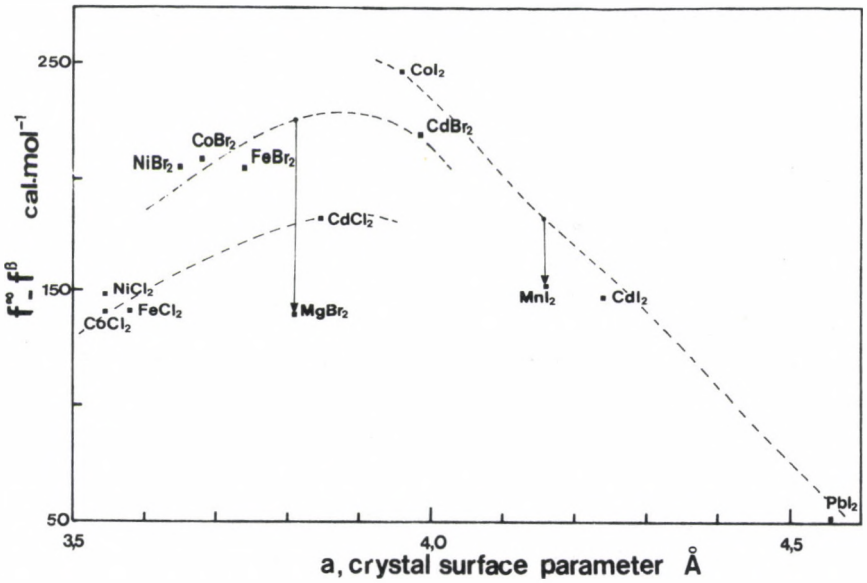

Figure 4 : Variation of the free energy of the β phase with the surface parameter a.

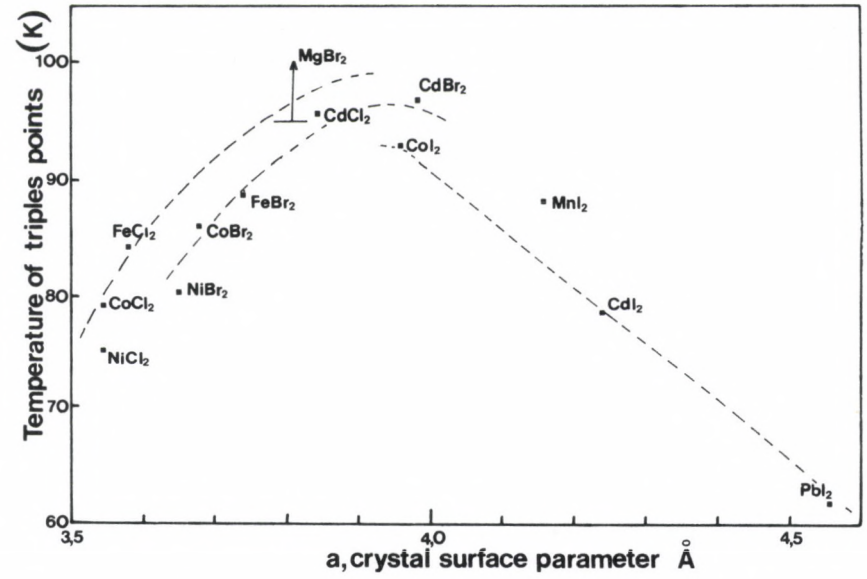

Figure 5 : Variation of the triple point temperature with the surface parameter a.

α phase and the lower the triple point temperature, as indeed seems to be the case. The exceptional case, $MgBr_2$, supports this point.

REFERENCES

1. Y. LARHER, Thesis, Orsay 1970 ; CEA report 4089, 1970
2. Y. LARHER, J. Coll. Interface Sci. (1971), 37, 836
3. Y. NARDON, Thesis, Nancy 1972 ; CEA note 1574, 1973
4. F. MILLOT, unpublished data
5. T. TAKAISHI and Y. SENSUI, Trans. Faraday Soc. (1963), 59 2503
6. M. MATECKI, A. THOMY and X. DUVAL, J. Chim. Phys. (1974), 71, 1484
7. W.N. LIPSCOMB, F.E. WANG, W.R. MAY and E.L. LIPPERT, Acta. Cryst. (1961), 14, 1100
8. A. THOMY and X. DUVAL, J. Chim. Phys. (1970), 67, 1101
9. Y. LARHER, J. Chem. Soc. Faraday Trans. I (1974), 70, 320
10. E.C. KERR, University microfilms, Ann Arbor, Michigan, Publi. n° 21480
11. Y. LARHER and Y. NARDON, Le Vide, (1973), 167, 209

ADSORPTION OF PHOSPHATE IONS ONTO AN AMORPHOUS FERRIC HYDROXIDE

J.Vanderdeelen and L.Baert

Radiobiological and Physical Chemistry, State University of Ghent, Coupure 533 , Ghent, Belgium

1.INTRODUCTION

Some hypotheses and theories which represent a diagnostic picture of the reaction between sesquioxides or soils and phosphate ions are deduced from the analysis and interpretation of classical or complex adsorption isotherms(1-11).Besides the indirect character of such methodology it has been shown that this procedure may lead to some uncertainties due to the fact that theoretical basis for the application of these laws is not fully developed(12).

Our approach to the problem has been different : together with the analytical side of the phosphate adsorption onto an amorphous ferric hydroxide, the heat evolved during this reaction has been measured calorimetrically.

2.EXPERIMENTAL

The preparation of the sample, the description of both cell and calorimeter, and the course of the experimental run are described elsewhere (13,14)

3.RESULTS AND DISCUSSION

The measured heats versus the amounts of phosphorus fixed, defined as μmole P per 200 mg of the sample,are represented in figure 1.

To evaluate these results the pH shift of the suspensions after equilibrium as compared to the added phosphate solutions must be taken into account (columns 3 and 4 of table 1).

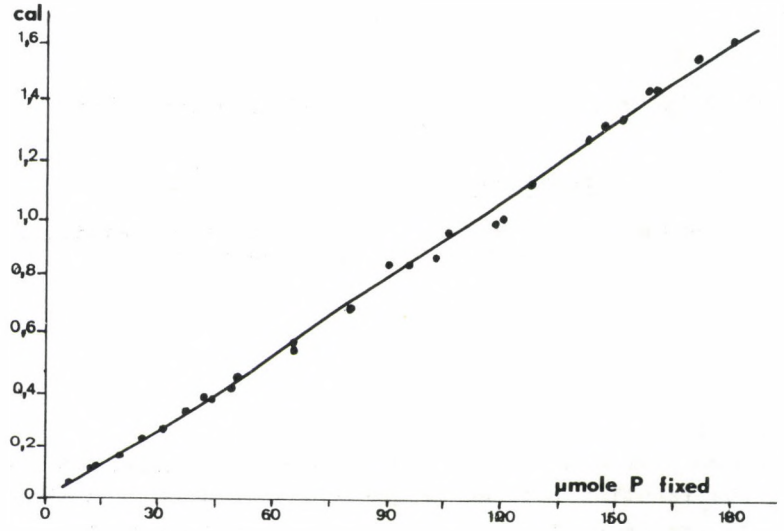

Fig.1. Measured heats (cal) as function of the amounts of P fixed (µmole P per 200 mg)

As the pH of the suspension without any P treatment is about 5 , it may be stated qualitatively that the phosphate adsorption onto this product involves a substitution of surface hydroxylgroups. The ions thus released are consumed according to the following reactions : -neutralisation of $H_2PO_4^-$ to HPO_4^{--}, because KH_2PO_4 was added;
-neutralisation of hydroxylgroups onto the surface of the solid.

Of course if these reactions proceed with an heat exchange, this will be included in the measured heat, as indicated in figure 1.

3.1. Heat evaluation of site reactions

3.1.1. Neutralisation of $H_2PO_4^-$

Starting with an arbitrary chosen value of ionic strength, I, the activity coefficient,f, of each phosphate species with charge Z, is given by the Robinson equation :

$$\log f = -Z^2\left(\frac{0.5115\sqrt{I}}{1+1.5\sqrt{I}} - 0.2\ I\right) \qquad (1)$$

Using the thermodynamic protolytic constants of H_3PO_4 at 38.7°C, being respectively $K_1=10^{-2.20}$, $K_2=10^{-7.19}$ and $K_3=10^{-12.18}$, the "mixed acidity constant", $K_i(15)$ is calculated using the following equation, wherein HB and B represent the conjugate acid and base :

$$K_i' = K_i \frac{f_{HB}}{f_B} \qquad (2)$$

Because the pH and the concentration a, of both the added phosphate solution and the suspension after equilibrium are experimentally fixed, the distribution of the species is obtained by :

$$\frac{[H_3PO_4]}{a} = \frac{(H^+)^3}{N} \qquad (3)$$

$$\frac{[H_2PO_4^-]}{a} = \frac{(H^+)^2 K_1'}{N} \qquad (4)$$

$$\frac{[HPO_4^{--}]}{a} = \frac{(H^+) K_1' K_2'}{N} \qquad (5)$$

$$\frac{[PO_4^{---}]}{a} = \frac{K_1' K_2' K_3'}{N} \qquad (6)$$

wherein $N=(H^+)^3 + (H^+)^2 K_1' + (H^+) K_1' K_2' + K_1' K_2' K_3'$ (7)

Using the concentrations a new value of ionic strenght is then computed and this iterative method is processed till the concentration of the species does not change anymore. The concentration of neutralised HPO_4^{--} is then obtained bij difference as compared to the added solution. Finally the heat of neutralisation due to this site reaction is evaluated as the product of the above-calculated concentration and the heat of neutralisation of an acid and a base(14), taking into account the

heat of ionisation of $H_2PO_4^-$ (16).

3.1.2. Neutralisation of surface hydroxylgroups

The pH response of the suspension after adding known amounts of OH^- under experimental conditions comparable with those in the calorimetric run, is recorded.The heat evolved during this reaction is measured calorimetrically.

3.2.Corrected results

Columns 1 and 2 of table 1 show the phosphate concentrations (µmole P/200 mg) which are added and fixed by the solid during the calorimetric run. The pH values of stock solutions and suspensions are given in columns 3 and 4. The concentrations of neutralised HPO_4^{--}, as calculated according to 3.1.1. are listed in column 5. Finally taking into account the two corrections, the net heats of adsorption, in calories per mole are tabulated in the last column. An examination of this spectrum of energy indicates that it holds no certainty to trace a diagnostic picture concerning the mechanism of interaction. From the course of the values of the heats of adsorption at low phosphate densities(<50µmole) it seems indeed premature to conclude for a surface heterogeneity. Because of the important pH jump in that region, the correction for neutralisation of surface hydroxylgroups becomes appreciable. Moreover taking into account the implications for this correction as well as a reproductibility, of about 5 to 10% (14) of the calorimetric results, some skepticism arises. For larger occupancies (50 to 80µmole) a manifest discontinuity appears : an adsorption region of phosphate without any heat exchange should occur. This looks doubtful, knowing a priori the high specificity of phosphate for this kind of adsorbent. For the largest phosphate concentrations (>140 µmole), an obvious stabilisation has arisen. It has to be noted that this occurs in the region where the pH jump is gradually depressed, due to the large excess of $H_2PO_4^-$, so that only the neutralisation of these ions must be taken into account. The considerations derived from these results have intended us to elaborate an appropriate method, providing more reliable results with regard to the thermochemical side of this heterogeneous reaction.

Table 1. Results of the phosphate adsorption onto an amorphous iron hydroxide.

P added (μmole)	P fixed (μmole)	pH stock	pH equil.	HPO_4^{--} neutr. (μmole)	cal/mole
16.1	13.1	5.09	7.22	1.5	7035
24.2	19.3	4.97	7.83	3.8	4295
32.3	25.0	4.93	8.22	5.3	4152
48.4	37.0	4.84	7.72	8.9	4344
80.6	43.0	4.74	7.29	23.2	1597
112.9	52.0	4.70	7.19	35.0	-
161.3	66.0	4.67	6.95	42.8	353
258.0	82.0	4.62	6.65	53.6	392
322.0	96.0	4.58	6.48	56.5	1258
483.0	102.0	4.55	6.22	57.1	1575
806.0	120.0	4.50	5.97	65.3	2327
1451.0	146.0	4.45	5.66	66.2	3431
1935.0	157.0	4.42	5.55	71.0	3584
2419.0	170.0	4.40	5.48	76.3	3552
3000.0	173.0	4.38	5.40	78.1	3582

Concerning the mode of interaction between phosphate and the solid, the analytical results provide useful data. Out of the pH shifts (table 1) it follows that phosphate adsorption is related to a substitution, wherein, as function of the pH of the medium, surfacegroups of type $-OH_2^+$ or -OH are involved. The relation of the concentration of fixed P versus that of released OH^- is represented in figure 2. The concentration of OH^- is defined as the sum of the increase in concentration of HPO_4^{--} as compared to the stock solution, and the concentration of OH^-, added to the suspension to bring it up to the considered pH level. It seems logical that, when approaching the isoelectric point of the substrate (pH=7.9), the ratio will reach about 1. At decreasing pH values the ratio $\frac{P}{OH}$ increases (fig.2).This may be explained by the fact that in this pH region surfacegroups of type $-OH_2^+$ and -OH exist. These considerations lead us to propose the following reactions, as suggested by Breeuwsma (17) in case of hematite and being valid here too :

$$-OH_2^+ + H_2PO_4^- \rightleftharpoons -H_2PO_4 + H_2O$$

$$-OH + H_2PO_4^- \rightleftharpoons -H_2PO_4 + OH^-$$

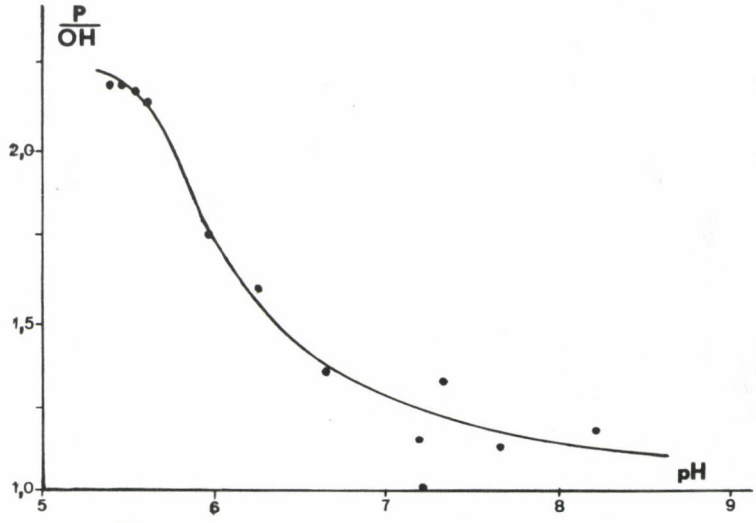

Fig.2. Ratio $\frac{P}{OH}$ as function of the pH

4.ADAPTED METHOD

Regarding to the above-mentioned objections, the solid has been treated prior to the calorimetric run.Therefore,samples of the same batch are eluted with KNO_3 solutions; the concentrations and pH values are identical to those of the phosphate solutions which will be used in the calorimetric run. Once the pH of the eluate equals that of the eluens, the suspension is filtered off and the humid paste is used as such. It has been tried to weigh for each experiment 250 mg into the cup ; further the same procedure of calorimetric run as for the untreated material is used (13,14)

4.1. Results and discussion

The results are given in table 2. If the pH values of the suspensions after equilibrium(table 2) are compared with the untreated suspensions (table 1) it has to be noted that in this case the pH jump is considerably reduced.

Nevertheless the pH shift is such that the neutralisation of the excess of $H_2PO_4^-$ must be taken into account. Because this calculated correction amounted to at most 20% of the experimentally observed value, one can state that reliability on the results is enhanced.

Table 2. Results of phosphate with the treated amorphous iron hydroxide.

P added (μmole)	P fixed (μmole)	pH stock	pH equil.	$\frac{cal}{mole}$
100	57	4.75	6.42	5266(376)
200	74	4.62	6.06	4747(180)
500	111	4.59	5.57	5136(347)
1000	137	4.54	5.09	4969(493)
2000	182	4.42	5.03	5757(233)

Referred to the same amount of substrate, it has to be stated that for the same added dose, the fixed quantities of P are always higher for the treated than for the untreated product. The reason therefore lies probably into the fact that the pH values of the suspensions are always lower in this case as compared to the untreated product. It has already been shown that as the pH drops, the adsorption of P is increased (9).

The molar heats of adsorption being the mean of 6 repetitions figure in the last column of table 2. The standard deviations are given within brackets ; some of them represent a valuable estimation of the fluctuations which may be attended with this apparatus and the used methodology (13). If we exclude the value of 5757 calories per mole, it has to be noted that within a concentration range from 57 till 137μmoles P a constant heat of adsorption is observed. This would imply that based on these heat exchanges the reaction occurs homogeneously in the controlled range. This hypothesis seems to be consistent with the one already formulated : a monotone substitution of surfacegroups by phosphate ions.

Finally, it might be mentioned that these results are consistent with the valuable and experimentally controlled theory of the Australian reseachers (18,19), that has been deduced on a non-energetic basis.

REFERENCES

1.OLSEN S.R.,WATANABE F.S. Soil Sci.Soc.Am.Proc.21,144,1957.
2.HSU P.H., RENNIE D.A. Can.J.Soil Sci. 42, 197, 1962.
3.DE HAAN F.A.H. Ph.D.Thesis, Wageningen, 1965.
4.MULJADI D.,POSNER A.M., QUIRK J.P. J.Soil Sci.17, 212,1966.
5.GUNARY D. J. Soil Sci. 21, 72,1970.
6.HINGSTON F.J., POSNER A.M. QUIRK J.P. Disc.Farad.Soc.52, 334, 1971.
7.LOPEZ-HERNANDEZ I.D., BURNHAM C.P. J.Soil Sci.25,207,1972.
8.UDO E.J., UZU F.O. Soil Sci.Soc.Am.Proc. 36, 879, 1972.
9.VANDERDEELEN J.,BAERT L. Meded. Fak. Landbouw 37,53,1972.
10.HOLFORD C.R.,WEDDERBURN R.W.M.,MATTINGLY G.E.G. J.Soil Sci. 25,242,1974.
11.KUO S., LOTSE E.G. Soil Sci., 116, 400, 1974.
12.KILIMANN F., ECKART R. Proc. Symp.Guilford, 1969.
13. VANDERDEELEN J., ROUQUEROL J., BAERT L. Coll.C.N.R.S. 201 Marseille, 465, 1970.
14.VANDERDEELEN J., BAERT L. Meded. Fak. Landbouw, to be published
15.STUMM W., MORGAN J.J. Aquatic chemistry, John Wiley & Sons, Inc,N.Y. 1970.
16.PITZER K.S. J. Am. Chem. Soc. 59, 2365, 1937.
17.BREEUWSMA A. Ph.D. Thesis, Wageningen, 1973.
18.HINGSTON F. J. and Coll. Nature 215, 1459, 1967.
19.HINGSTON F. J., POSNER A.M., QUIRK J.P. J. Soil Sci. 23,177, 1972.

ADSORPTION FROM DENSE FLUIDS AND THEIR MIXTURES

W.Rudzinski, B.W.Wojciechowski and A.Dabrowski*

Department of Chemical Engineering
Queen's University at Kingston
Ontario , Canada

The three-dimensional treatment of mobile, high-density adsorbed phases is still one of the great unresolved problems of adsorption.This problem becomes especially difficult in the case of mixed adsorbed phases, which are also considered in this paper.

We begin by considering the adsorption of a single component on a flat surface. This surface provides an external force field acting on the semi-infinite adsorbed phase above it. We are accepting here Brunet's approach[1] which states that the functional properties such as $\mu(\rho(\underline{r}),\underline{r})$ remain unaffected by the density gradient due to the external force field $\mathcal{E}$,

$$\mu(\rho(\underline{r}),\underline{r}) = \mu(\rho(\underline{r})) \qquad (1)$$

For the system defined above we may write,

$$\mu - \mu_o + \mathcal{E}(\underline{r}) = 0 \qquad (2)$$

where the subscript "o" denotes the bulk phase, i.e., adsorbed phase at infinite distance from surface.(We shall assume further that $\mathcal{E}(\underline{r})$ is only function of the distance from the surface z).

---

* Department of Physical Chemistry, MCS University at Lublin ul.Nowotki 12, 20-031 Poland

According to the standart notations, μ, ρ and f mean here the chemical potential, density and fugacity, respectively. With the above assumptions the theoretical description of mobile adsorption reduces to the following two problems:

a.) Evaluation of the relations between the density and fugacity of ordinary bulk phases,

b.) evaluation of the adsorption potential function $\mathcal{E}(z)$.

The second problem has been studied extensively and several methods have been proposed[2].Thus, we shall concentrate our discussion on the relations between density, fugacity and pressure of ordinary bulk phases.

In his illustrative numerical calculations Brunet[1] used the Tonk's theory of dense fluids in its form modified by Hill[3].The modified Tonk's equation of state generates correct expressions for the second and third, virial coefficients in the hard-sphere approximation.This equation provides a comparatively good agreement with experimental data at very high densities, but a poor agreement in the first-order phase transition region.The latter is very important because, due to the variation of adsorption potential, the local state in the adsorbed phase may well correspond to the phase transition region. This is especially true at lower coverages of surface where the adsorbed phase remembers a thin film rather than a three-dimensional bulk liquid.In our oppinion, this is the main reason for which Brunet's theory fails at lower coverages of surface.

An another reason is the assumption expressed by eq.(1) which states that the molecular enviriment in the adsorbed phase is a same as in the bulk phase having the same density. This is probably true at very high coverages of surface. At low and mediate coverages the molecular enviroment is rather like that when admolecules are arranged two-dimensionally. (At the distance of the minimum of adsorption potential).

We shall avoid the above discussed disadvantages by applying the recent results of Rudzinski[4] for the summation of the virial expansion for the equation of state.

On the basis of Holleran's Unit Compressibility Law[5], Rudzinski[4] has summed up to infinity the virial expansion for the equation of state. This procedure led him to a simple and good working equation of the form,

$$\frac{pV}{NkT} = 1 + \frac{\varrho}{2}\int_0^{\infty}\left\{\exp\left(\frac{-u(r)}{kT_B(\Delta + \Theta)}\right) - 1\right\} 4\pi r^2 dr \qquad (4)$$

where $\Delta = N/Vd_o$ is a reduced density, d_o being the Holleran's density characteristic constant[5]. Further, $\Theta = T/T_B$, where T_B is the Boyle temperature. In eq.(4) u(r) is the pair intermolecular potential which, for the purpose of the present paper, is assumed to be unperturbed by the presence of the solid surface.

Rudzinski's equation of state (4) generates the fully correct, most general form of the second virial coefficient. The illustrative calculations performed by Rudzinski showed the first-order phase transition region, and a good agreement with experiment in predicting critical densities of simple gases.

The eq.(4) is valid for all substances obeying the Holleran's Unit Compressibility Law, but the recent results reported by Holleran[6] suggest that this is the case of all substances interacting via simple intermolecular potentials. With the assumption of pair-additivity of intermolecular interactions, which underlines the eq.(4), we arrive at the following form of the radial distribution function[7],

$$g(r) = \frac{3kT}{r}\left[u'(r)\right]^{-1}\left\{\exp\left(\frac{-u(r)}{kT_B(\Delta + \Theta)}\right) - 1\right\} \qquad (5)$$

This function must yet properly be normalized by the condition;

$$\lim_{r \to +\infty} g(r) = 1 \qquad (6)$$

It is easy to check that both for Lennard-Jones (12-6), and the Sutherland potential of the form

$$u(r) = \begin{cases} +\infty, & r \leqslant \sigma \\ -cr^{-6}, & r > \sigma \end{cases} \qquad (7)$$

the normalization constant is equal to $2(\Delta + \Theta)/\Theta$.

The activity and fugacity can be easily expressed in terms of the coupled radial distribution function $g(r,\xi)$ [7]

$$\ln \frac{f}{kT} = \ln\varrho + \frac{\varrho}{kT}\int_0^1 d\xi \int_0^\infty dr\, u(r)\cdot g(r,\xi)\cdot 4\pi r^2 \qquad (8)$$

We arrive at the function $g(r,\xi)$, associated with the function $g(r)$, by replacing $u(r)$ by $\xi\cdot u(r)$ in eq.(5).This is, however, true only for $r > \sigma$ .The contribution to the thermodynamic properties of the system from the attractive part of the Sutherland potential does not depend upon the coupling parameter ξ Therefore, when accepting the potential (7), the integration with respect to ξ is running only in the region $r > \sigma$.

The purpose of introducing the Sutherland potential (7) ,is, that the integration in eq.(8) can be performed analytically.This is very important, since it makes numerical calculations hundreds times shorter.Some difficulty appears when evaluating the term $u(r)/u'(r)$ for the Sutherland potential in the region of repulsive intermolecular forces. We shall omit this difficulty by assuming at this moment that $u(r)$ is given by the repulsive part of the Lennard-Jones potential. With this meanwhile assumption the value of the term $u(r)/u'(r)$ is constant and equal to $(-1/12)$. After integration in eq.(8) we have,

$$\ln \frac{f}{kT} = \ln \; + \frac{2\pi\sigma^3}{3}\varrho\left[\frac{1}{2} - \sum_{j=1}^{\infty} \frac{1}{j!\,j(2j+1)}\left(\frac{c}{\sigma\, k\, T_B(\Delta+\Theta)}\right)^j\right] \qquad (9)$$

The above equation ,combined with equation (3) yields the density profile from which the adsorption isotherm $N_A(\varrho_0)$ can be evaluated according to the equation,

$$N_A(\varrho_0) = \int_V \left[\varrho(z) - \varrho(z=\infty)\right] d\underline{r} \qquad (10)$$

Following the Brunet's approach, from this density profile we can evaluate the pressure profile using eq.(4). Next, the pressure profile enables us to calculate the spreading pressure φ according the following equation:

$$\varphi = \int_0^{\infty} \left[p(z) - p(z = \infty) \right] dz \qquad (11)$$

We have arrived now at the moment when we can extend our treatment for the mixed condensed phases. To this purpose we shall apply some theoretical results reported recently by Sircar and Myers[8].

In the case of mixed adsorbed phases the surface excess is the thermodynamic quantity, used to describe the adsorption effect. Assuming that the mixed adsorbed phase behaves as an ideal solution, Sircar and Myers have developed the following three equations giving the surface excess n_1^e as a function of the molar concetration x_1 :

$$n_1^e = \frac{x_1 \cdot x_2 (1 - K)}{\frac{x_1}{m_1} + K \frac{x_2}{m_2}} \qquad (12)$$

where

$$K = \frac{\gamma_2}{\gamma_1} \exp\left[\frac{\varphi_m - \varphi_2}{m_2 k T} - \frac{\varphi_m - \varphi_1}{m_1 k T} \right] \qquad (13)$$

and

$$\gamma_1 x_1 \exp \frac{\varphi_m - \varphi_1}{m_1 k T} - \gamma_2 x_2 \exp \frac{\varphi_m - \varphi_2}{m_2 k T} = 0 \qquad (14)$$

Above, γ_i's are the activity coefficients in the bulk phase and φ_m is the parameter which is eliminated by solving the equations (12) - (14). Its physical meaning is described in the original paper by Sircar and Myers[8]. Further, m_i's are the surface capacities of the components of the mixture. According to the Brunet's approach, these surface capacities are given by the equation

$$m = \frac{\sigma^2}{s\sqrt{2}} \qquad (15)$$

in which s is the adsorbent area per one adsorbed molecule. The activity coefficients can be evaluated unequivocally, and the values φ_i's are given by eq.(11). Thus, we can see that both ordinary and excess isotherms may be evaluated fully theoretically from molecule-molecule and surface-molecule potentials.

We shall be interested further in the region of low and mediate coverages of surface where Brunet's theory fails.

As we have said above the adsorbed phase is then like a thin film rather than a three-dimensional bulk phase. We shall express this fact by replacing the three-dimensional Boyle temperature by its corresponding two-dimensional value, when evaluating the fugacity-density interrelation in eq.(9). Of course, such a procedure seems to be justified only for distances around the density peak maximum, but this region contributes predominantingly to the overall adsorption effect.

The two-dimensional Boyle temperature is called sometimes as the "second characteristic gas-solid temperature".For the admolecules interacting via LJ(12-6) potential, Sams, Constabaris and Halsey[9] have found the following relation,

$$T_B' = 1.6 \frac{u_o}{k} \qquad (16)$$

where T_B' is the two-dimensional Boyle temperature, and u_o is the attraction parameter in LJ(12-6) potential.

We shall further accept the relation (16) in our illustrative calculations for argon adsorbed on graphite at 77.5°K, for which temperature experimental data exist for this kind of adsorption system.We shall also accept the gas-surface interraction parameters reported by Sams, Constabaris and Halsey[9]. The gas-gas interaction parameters for both the Suthrland and LJ(12-6) potential have been reported elsewhere[10].

Two density profiles have been evaluated; one, corresponding to the bulk density Δ_o equal to $0.5 \cdot 10^{-6}$, in the units of the reduced density Δ ,and the other one for $\Delta_o = 0.1 \cdot 10^{-5}$. They are shown in Fig.1 as the dashed ,and the solid line, respectively.

Their form seems to be an impressive check of the correctness of our approach. The evaluated density profiles do not exceede the value $\Delta = 2.0$; this value is only by about 5% different from the hexagonal close packing density of argon, when evaluated by using the Sutherland hard-core parameter.[10].

Our approach is being investigated; more detailed discussion and the agreement with experimental data will be presented in our future publication.

References

1.J.Brunet, Chem.Engng.Sci.,27,685,(1972)

2.T.L.Hill,J.Phys.Chem.,63,456,(1959)

3.T.L.Hill,J.Chem.Phys.,20,141,(1952)

4.W.Rudzinski,J.Phys. A: Gen.Phys.,5,1642,(1972)

5.E.M.Holleran,J.Chem.Phys.,47,5318,(1967)

6.E.M.Holleran,ibid.,49,39,(1968)

7.T.L.Hill,"Statistical Mechanics",p.190,(McGraw-Hill,N.Y.,1956)

8.S.Sircar and A.L.Myers,AIChE J.,19,159,(1973)

9.J.R.Sams,G.Constabaris and G.D.Halsey,J.Chem.Phys.,36,1334, (1962)

10.T.M.Reed and K.E.Gubbins, "Applied Statistical Mechanics", pp.117-118,(McGraw-Hill,N.Y.,1973)

Acknowledgement

The authors would like to express their thanks to Professor C.C.Hsu from Queen's University for reading the manuscript and helpfull comments.

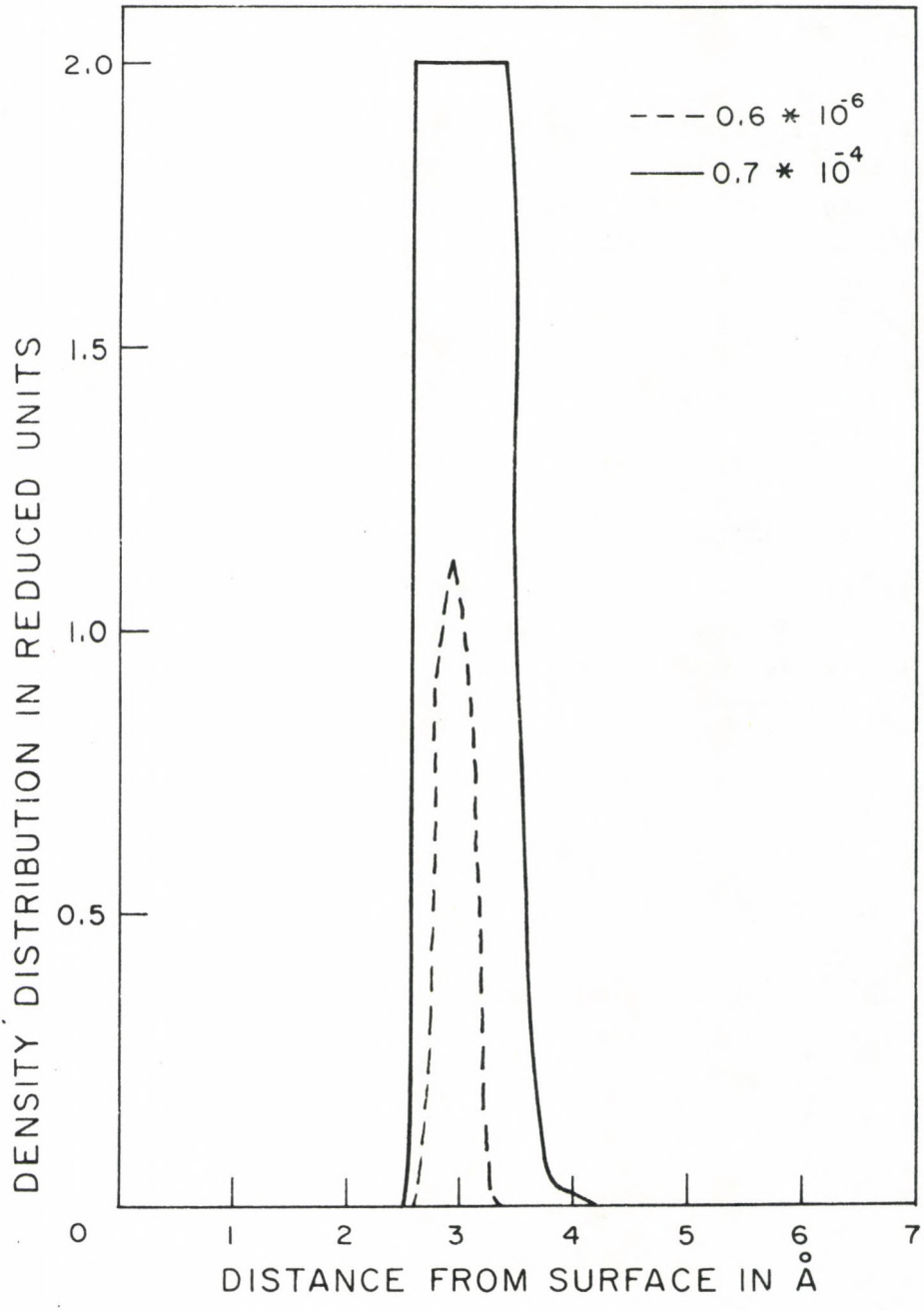
2.0
1.5
1.0
0.5
0
1
2
3
4
5
6
7
DENSITY DISTRIBUTION IN REDUCED UNITS
DISTANCE FROM SURFACE IN Å
--- 0.6 * 10^-6
—— 0.7 * 10^-4

Fig. 1

ADSORPTION OF ORGANIC MOLECULES ON ACTIVATED CHARCOAL

R.S.Roy and A.Panda

Postgraduate Chemistry Department, Sambalpur University, Burla, Orissa, India

Adsorption of organic compounds from solution phase by carbon is influenced by a number of factors, most important being the nature of (1) the compound (2) the substituent active group and its position in the molecule (3) the solvent and (4) the adsorbent surface.

In the purification on substances containing impurities of organic molecules activated charcoal is generally used as the purifier, the amount and nature of the organic impurities adsorbed on adsorbent carbon particle surface being the significant factors in controlling the purification. A knowledge of the adsorption properties of organic molecules containing common functional groups individual and combined may therefore be useful in controlling the purification.

Adsorption of a molecule with a functional group on activated charcoal has been observed to be reduced in the presence of a molecule with another functional group. The latter molecule is said to 'poison' the charcoal surface. This reduction in adsorption may be due to the competition between the two groups of molecules for the charcoal surface in the surface condensation. This view suggests that the adsorption of a molecule with a functional group can be controlled by the amount of another molecule with a different functional group on the adsorbent.

Theory:

Consider the equilibrium

Adsorbate 1 + Adsorbate 2 + Free surface $\rightleftharpoons$ Adsorbed adsorbate

If C_1 and C_2 are the concentrations of 1 and 2 in the solution in contact with the adsorbent, a_1 and a_2 the fractions of 1 and 2 that actually come in contact with the adsorbent per unit time, θ_1 and θ_2 the positions covered by 1 and 2 respectively, then it follows that the rate of adsorption

$$r_1 = \left[1 - (\theta_1 + \theta_2)\right] a_1 C_1 a_2 C_2 \qquad (1)$$

where a_1 and a_2 are constants $k' = a_1 a_2$, and from kinetic theory of gases for the gas phase adsorption

$$a = \sigma (2 \pi m k T)^{-\frac{1}{2}} \exp\left(- E_{ad} / R T\right) \qquad (2)$$

where σ is sticking coefficient, m mass of adsorbed molecules, and E_{ad} activation energy of adsorption.
The rate of escaptin out from the adsorbent

$$r_2 = (v_1 + v_2)(\theta_1 + \theta_2) \qquad (3)$$

where v the rate constant from the gas theory

$$v = A \exp\left(- E_{des} / R T\right) \qquad (4)$$

where A is specific rate constant for desorption and E_{des} energy of desorption.
For similar molecules A remaining almost constant with the assumption that the energy of desorption remains constant equation (3) assumes the form

$$r_2 = v (\theta_1 + \theta_2) \qquad (5)$$

where $v = (v_1 + v_2) / 2 = k''$
At equilibrium

$$r_1 = r_2 \qquad (6)$$

Hence, from equations (1) and (5)

$$\left[1 - (\theta_1 + \theta_2)\right] a_1 C_1 a_2 C_2 = v (\theta_1 + \theta_2) \qquad (7)$$

or $$C_1 C_2 = (v / a_1 a_2) \left[1 / 1 - (\theta_1 + \theta_2)\right](\theta_1 + \theta_2) \qquad (8)$$

If x_1 and x_2 are the amounts of 1 and 2, respectively, that actually get adsorbed on m, the amount of adsorbent, then for separate specific adsorption sites for adsorbates 1 and 2

$$\theta_1 = k_1 (x_1 / m) \qquad (9a)$$

$$\theta_2 = k_2 \left(x_2 / m \right) \qquad (9b)$$

Substituting equations (9_a) and (9_b) in (9), and on rearrangement

$$1 / C_1 C_2 = \left(a_1 a_2 / v \right) \; m / \left(k_1 x_1 + k_2 x_2 - 1 \right) \qquad (10)$$

If equation (10) is valid, plot of $1 / C_1 C_2$ vs $m / (k_1 x_1 + k_2 x_2)$, values of k_1, k_2, x_1, x_2, m being determined experimentally, should give a straight line with a slope and a negative intercept, each of $a_1 a_2 / v$. Values of x_1 and x_2 can be obtained analytically while that of a_1, a_2, k_1, k_2 can be determined using equation (11) from experiments containing each of the adsorbates.

$$1 / C_{1(2)} = a_{1(2)} / v_{1(2)} \; m / k_{1(2)} x_{1(2)} - 1 \qquad (11)$$

Experimental:

The activated charcoal used in this work was supplied by German Merck. Acetone, acetic acid, oxalic acid, iodine and sodium hydroxide used was of B.D.H. Analar grade. Acetone was distilled twice before use.

Adsorption isotherms of acetic acid and oxalic acid were determined at the room temperature by the method described by Kipling and Wright[1]. The solutions were shaken for one and a half hours by means of an electric shaker (Ganson's horizontal model sh. 2) and analyzed for acetic and oxalic acids by alkalimetry and for acetone by iodometry.

Adsorption isotherms for the mixed systems acetic acid - acetone and oxalic acid - acetone, were determined using different concentrations of the adsorbates on 0.5 gm of activated charcoal by the usual procedure. Concentration of the acid in the mixture was determined taking into account the acid concentration of the phenol due to its acidity.

Results:

The concentrations of acetic acid and acetone in the individual

and mixed systems are presented in Tables I, II, III and IV, which also contain the amounts adsorbed in each case. Figure 1 shows the adsorption isotherm for acetic acid, and Figure 2 presents that for acetone. The plots of values of $1 / C$ vs. m / x listed in Tables I and II are linear yielding k values of 4 and 1 for the acetic acid and acetone adsorption, respectively. Figure 3 gives the composite isotherm for the mixed acetic acid - acetone system described in Table III, values of $1 / C_1 C_2$ varying linearly with those of $m / (k_1 x_1 + k_1 x_2)$ as expected of equation (10).

Adsorption of both adsorbated in the mixed system with varying concentrations, decreases with increasing concentration of the added adsorbates, but that due to acetic acid is more. The ratio between acid to acetone is maintained at 6 to 1. In Figure 4 are shown the isotherms due to acetic acid and acetone adsorption from the mixture summarized in Table IV. Acetic acid adsorption follows the usual L - shaped curve, while that of acetone changes to the S - shape.

Table I : Adsorption of acetic acid on charcoal at 24 $\pm$ 2°C

C' (N)	C_1 (N)	x_1 (gm)	m (gm)	m / x_1
0.20	0.1560	0.1320	0.500	3.797
0.10	0.0734	0.0798	0.500	6.334
0.05	0.0275	0.0675	0.500	7.409
0.02	0.0092	0.0324	0.500	15.430

C' = Total concentration, C_1 = Equilibrium concentration, x_1 = amount adsorbed, m = Amount of adsorbent.

Table II ; Adsorption of acetone on charcoal at 24 $\pm$ 2°C

C' (N)	C_2 (N)	x_2 (gm)	m (gm)	m / x_2
1.20	0.7391	0.002230	0.504	2.270

0.60	0.3540	0.1190	0.500	4.202
0.30	0.1664	0.0644	0.500	7.731
0.12	0.0621	0.280	0.500	17.860

C' = Total concentration, C_2 = Equilibrium concentration, x_2 = = amount adsorbed, m = amount of adsorbent.

Table III : Adsorption of acetic acid - acetone on charcoal at 29 ± 2°C

C' (N)	C_1(N)	C_1(N)	C_2(N)	m(gm)	$m/ k_1x_1 + k_2x_2$
0.4	1.2	0.3688	0.7413	0.500	0.8388
0.3	1.2	0.2738	0.7413	0.500	0.9328
0.2	1.2	0.1689	0.7413	0.502	0.8403
0.1	1.2	0.0785	0.7413	0.500	1.0430

C' = Total concentration of acetic acid, C = Total concentration of acetone, C_1 = Equlibrium concentration of acetic acid, C_2 = Equlibrium concentration of acetone, m = Amount of the adsorbent.

Table IV : Adsorption of acetic acid - acetone on charcoal at 24 ± 2°C

C'(N)	C(N)	C_1(N)	C_2(N)	m(gm)	x_1/m	x_2/m
0.20	1.20	0.1689	0.7413	0.502	0.1866	0.4434
0.10	0.60	0.0752	0.4492	0.503	0.1488	0.1508
0.05	0.30	0.0294	0.1943	0.500	0.1276	0.1054
0.02	0.12	0.0057	0.0421	0.502	0.0900	0.0778

Discussion:

The adsorption of individual and mixed adsorbates of acetic acid, acetone, acetic acid - acetone and oxalic acid - acetone on charcoal is of Langmuir type. The composite isotherm, equation (10) has been applied to (1) acetic acid - acetone and (2) oxalic acid - acetone mixed systems on activated charcoal. The assumptions which are implicit in the derivation are that (I) the adsorption occurs at specific localized sites, (II) each site can adsorb only one adsorbed species, and (III) the energy of the adsorbed species remains the same throughout the surface independent of other adsorbed species at sites without involving any lateral interaction between the adsorbing species. Experiments in general, obey the isotherm, plots of $1 / C_1C_2$ vs $m / (k_1x_1 + k_2x_2)$ giving straight lines with negative intercepts.

It is to be expected from the isotherm that the intercept should be equal to the slope, but experimental results being not in conformity with this, a correction factor F called the "adsorption coefficient" is introduced to account for the discrepancy, and the modified isotherm then becomes

$$1 / C_1 C_2 = (F a_1 a_2 / v)[m / (k_1x_1 + k_2x_2)] - a_1 a_2 / v \quad (12)$$

The significance of K may qualitatively be put proportional to the difference in adsorption of the adsorbates. F value comes out to be 1.28 and 1.32 for the acetic acid - acetone and oxalic acid - acetone systems, respectively, while the K value is 0.25.

Carboxylic acid and acetone contain the - C O O H and O H functional groups, respectively. For the acetic acid - acetone mixture in the ratio of 6 to 1 N, with a total concentration of 1.4 N, the fractions adsorbed are 15 to 45%, while for the mixture ten times less concentrated i.e., 0.14 N the fractions adsorbed are in 74 to 65 %. This observation clearly indicates that the preferential adsorption of acetic acid is more in dilute solutions, but decreases with increasing concentration and eventually becomes less, as shown in Figure 4.

Constant k, for the oxalic acid - acetone system is deter-

mined to be 3.9. Under comparable conditions the amount of acetic acid adsorbed from the acid - acetone system is about 1.4 times more than oxalic acid.

Adsorption of molecules of acidic and basic nature depends on the surface chemistry of oxides, as has been shown[2] by the adsorption of acidic and basic substances on hydroxylated metal oxide surfaces. Constant k, is the inverse value for the maximum coverage in a monolayer of the specific adsorption sites for adsorbate and can be determined by the molecular area of the adsorbed molecule

$$k = \left(x / m\right)^{-1}_{max}$$

From the Langmuir plots the saturation values $\left(x / m\right)_{max}$ for the adsorption of acetic acid, oxalic acid and acetone are found to be 4.2, 3.0 and 17.3 m mol / gm, respectively. These values correspond well to the content of basic surfaces oxides on activated charcoal, showing thereby that the main mechanism probably is the ion exchange adsorption on basic sites, and is equimolar and not an equivalent reaction, expressed as

$$C - O\,H^{-} + C\,H_3C\,O\,O\,H \rightleftharpoons C - C\,H_3C\,O\,O^{-} + H_2O$$

Pauling's rule of electrostatic valency can also explain[3] the phenamenon pointing to the importance of sites of basicity.

References:

1. J.J.Kipling and E.H.M.Wright, J.Chem. Soc., 3382 1963 , 3535 1964 , 4340 1965 .
2. H.P.Boehm, Kolloid Z., 227, 171 1968 . H.P.Boehm and M. Hermann Z. anarg. Chem., 352, 156 1967 , M.Hermann and H.P.Boehm, Z. anorg. Chem., 368, 173 1969 .
3. A.Weiss, Z. anorg. Chem., 299, 92 1959.

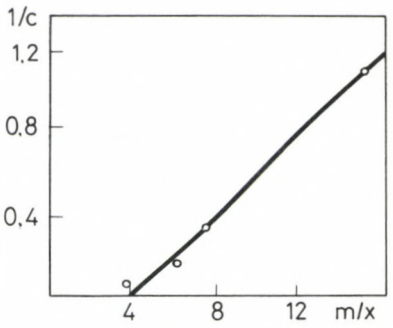

Fig. 1: 1/c vs. m/x, Acetic Acid

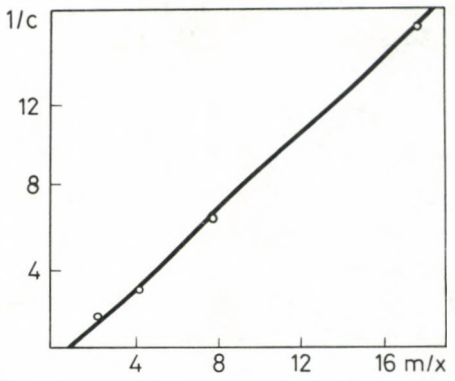

Fig. 2: 1/c vs. m/x, Acetone

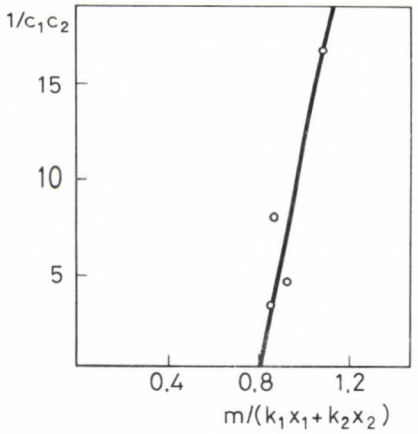

Fig. 3: $1/c_1c_2$ vs. $m/(k_1x_1+k_2x_2)$

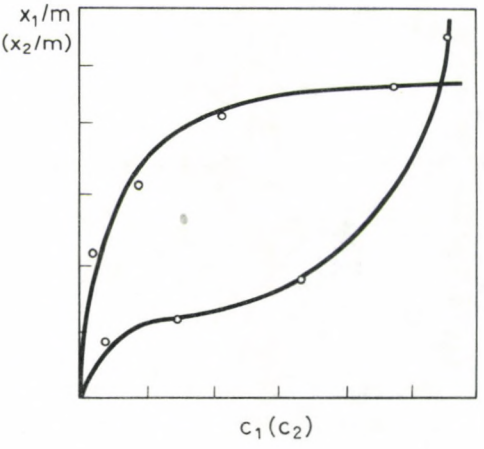

Fig. 4: c vs. x/m

ADSORPTION FROM SOLUTION AND SEDIMENT VOLUMES OF ORGANOPHILIC MONTMORILLONITES

F. Szántó[x], I. Dékány[x] and L. G. Nagy[xx]

[x] Department of Colloid Chemistry, József Attila University, 6720 Szeged, Hungary
[xx] Department of Physical Chemistry, Technical University, 1521 Budapest, Hungary

As a continuation of our earlier investigations /2,10/ with original and industrial organophilic bentonites, liquid adsorption and sedimentation studies have been carried out with "organophilic" /in part lipophilic/ montmorillonites, the surfaces of which were covered to systematically increasing extents with an organic cation-active compound, hexadecylpyridinium chloride /HPCl/. Such investigations may provide theoretical support for the results of practically-important sedimentation and rheological experiments, and in addition may result in the extension of the liquid adsorption theory on non-swelling solid surface to swelling adsorbents. In this lecture we summarize the liquid adsorption results, and then turn briefly to the parallel obtained by sediment-volume measurement and to the probability of theoretical interpretation of this.

Experimental

The experimental material was a colloid fraction obtained by a several-step peptization and sedimentation procedure from Mád bentonite; X-ray diffraction examinations showed it to be pure montmorillonite. The organophilic products were precipitated from a dilute montmorillonite sol with the cation-active substance, washed by repeated decantation, dried at 80° C in a vacuum-oven, ground, extracted for 50 hours in a Soxhlet apparatus with a 1:1 isopropanol-water mixture, redried as before, and ground. Data relating to the starting substance

and the organophilic stages are shown in Table I.
The X-ray diffraction examinations were carried out by the Department of Mineralogy, Petrography and Geochemistry of the József Attila University.
Analytically-pure methanol and benzene were used in the liquid adsorption measurements. After estabilishment of the adsorption equilibrium at $t=25\pm0,5^{o}$ C, for which 48 hours was sufficient in practice, the adsorbent was removed from the liquid mixture by centrifugation. The concentration change resulting from the adsorption was determined with a Zeiss liquid-interferometer. The sediment volumes were measured as previously /10/ in 20 ml calibrated test-tubes.

Results and Discussion

The specific adsorption excess was calculated via the definition $n_1^{\sigma} = n_o/x_{1,o}-x_1$ /4,6/.
Adsorption excess isotherms for methanol/1/-benzene/2/ mixtures on the adsorbents in question are shown in Fig. 1.

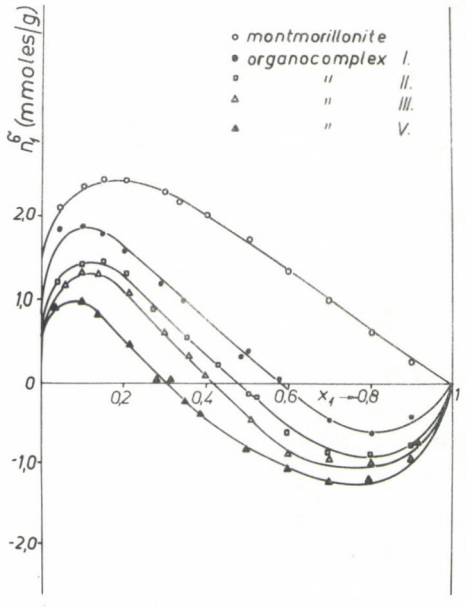

Fig. 1.
Adsorption excess isotherms for methanol/1/-benzene/2/ mixtures

Similar ones can be found in the literature for industrial organophilic bentonites too /5,10/. From the n_1^{σ} vs. x_1 excess isotherms the adsorption capacities were determined by the Schay-Nagy extrapolation method /7/. The material content of the interfacial layer was calculated referred to the individual pure components /$n^s_{1,o}$/. In the knowledge of the molar volumes of the components, the adsorption capacities were also given in terms of the specific volume /v^s/ of the interfacial layer. From the adsorption capacities and the cross-sectional areas of the components, the equivalent specific surface area was calculated /a^s_{equiv}/ /10/. From the determination of the adsorption excess isotherm /i.e. from the fact that the system is examined from the liquid-phase side/, it follows that information is obtained only on the overall adsorption capacities, but not on the structure of the phase-transition in the event of a complex phase-transition.Because of the nature of the organocomplex, it is assumed that the solid/liquid phase-transition is of a complex character. In the knowledge of this, we use the term interfacial phase. The excess isotherm determined on montmorillonite belongs to type II in the Schay-Nagy isotherm classification /4/. The methanol is thus preferentially adsorbed on the silicate surface. The equivalent specific surface area obtained for the montmorillonite is 323 m^2/g, and the BET surface area was 51 m^2/g. This means that the methanol penetrates to some extent into the interlamellar space and is also adsorbed on the internal surfaces, but it does not exploit the entire internal surface.

The excess isotherms determined on the organocomplexes belong to isotherm type IV. The results show that with the increase of the organophilic character of the adsorbent the positive adsorption of the methanol decreases, while at the same time the benzene is adsorbed to an ever larger extent. The equilibrium diagrams /x^s_1 vs. x_1/ in Fig. 2. clearly illustrate how the amount of methanol in the adsorption layer decreases with the increase of the organophilic character in the range where the average composition of the interfacial phase /x^s_1/

is constant. It can be seen from the equilibrium diagrams and from the excess isotherms determined on the organocomplexes that with the increase of the organophilic character the azeotropic composition is shifted towards smaller methanol mole fractions. In the knowledge of the azeotropic composition therefore, we can characterize the extent of the surface modification /organophilization/ too /Table I./.

The adsorption capacities calculated from the excess isotherms /$n^s_{1,o}$ and v^s/ increase practically linearly up to about 85 % saturation /compared with grade V/ with the extent of the organophilic character. This means that in methanol-benzene mixtures the internal surfaces of the organocomplex become increasingly accessible, the higher the organophilic charac - ter of the complex. If it is assumed that the adsorption layer is monomolecular, then the specific surface area of samples with higher organophilic character /III-V/ is 733-778 m^2/g. This value agrees well with that calculated from the crystallographic data /3/ for the specific surface area of montmorillonite: 752 m^2/g, and that given on the basis of electronmicroscope measurements: 842 m^2/g /3,9/ /Fig. 3./.

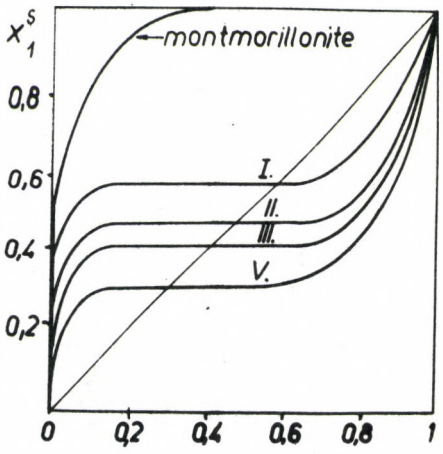

Fig. 2.
See in the text

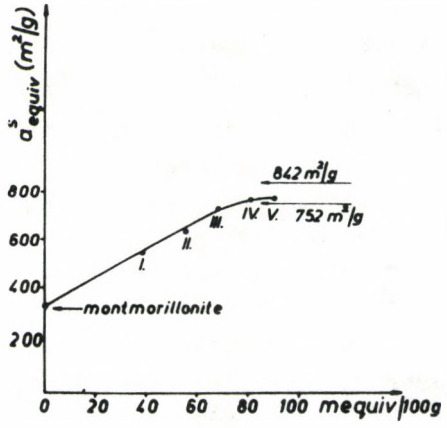

Fig. 3.
Variation of the equivalent specific surface area as a function of the organophilic character

Table I.

adsorbents	montm.	organophilic montmorillonites				
		I.	II.	III.	IV.	V.
HP-ion /mequiv/100g/	0,00	39,7	55,50	68,30	81,20	90,10
d_{ool} /Å/	12,36	14,36	15,16	17,31	18,60	18,80
$n^s_{1,o}$ /mmole/g/	3,40	5,69	6,69	7,72	8,04	8,19
v^s /cm^3/g/	0,139	0,253	0,302	0,350	0,367	0,376
a^s_{equiv} /m^2/g/	323	541	636	733	764	778
x^a_1	-	0,58	0,47	0,41	0,37	0,30

In the study of the sediment volumes, characteristic maximum curves were obtained as a function of the composition of the mixture /Fig. 4./. Such an effect of alcohols in the case of organophilic bentonites has been known since the publications of Jordan et al. /1/. Here we see the phenomenon in the case of hexadecylpyridinium montmorillonites with various organophilic characters in methanol-benzene mixtures. The position of the maxima is practically at an equilibrium mole fraction of x_1 = 0.1, which agrees well with the composition starting from which the composition of the interfacial layer is constant in a wide interval /Figs. 1-2./, and thus the interfacial layer is saturated with alcohol. The height of the maxima increases characteristically with the increase of the extent of organophilic character. There is a good linear relation between the maximum sediment volume and the adsorption capacity up to about 85 % saturation /Fig. 5./. Up to this point there is also a linear relation between the degree of organophilic character and the specific surface area calculated from the adsorption capacity /Fig. 3./.

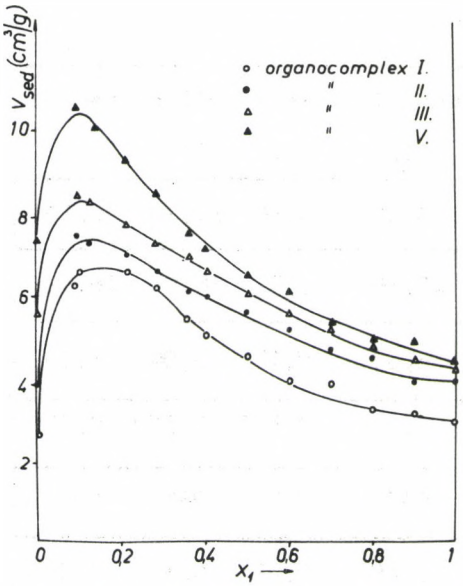

Fig. 4.

Sediment volumes as a function of the equilibrium mole fraction

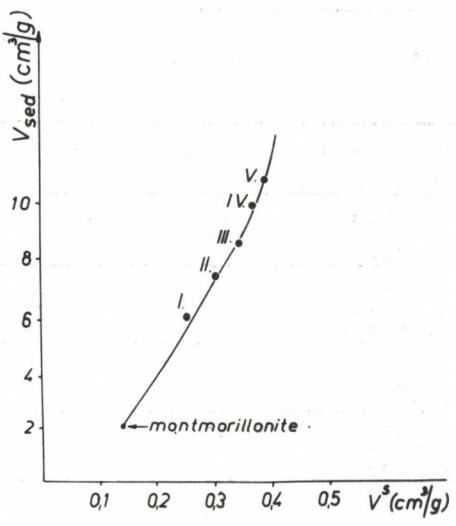

Fig. 5.

Maximum sediment volumes as a function of the adsorption capacity

The phenomenon can be explained as follows : the maximum disaggregation /dispersion/ relating to the given organophilic character is attained by the establish ment of the composi - tion of the interfacial layer said to be optimum, i. e. an appropriate proportion of the whole surface is exploited /this is shown by the results of the adsorption measurements/, and the "packs of cards" are disoriented to a certain extent. The sediment volume and the specific surface area proceed in parallel with this process, and are correlated linearly. If, as the basis of a very simplified card-house structure is taken the "T model", i. e. two lamellae or two packs of lamellae in edge-to-face contact then /as demonstrated by our calculations/ the specific sediment volume is given by the following relation:

$$V_{sed}\ /cm^3/g/ = \frac{1}{2}\ /\frac{h}{d}+1+\frac{d_a}{d}/\frac{1}{\varrho}$$

where h is the greater dimension of the lamellae, d is the thickness of the lamella or "pack of cards", d_a is the thickness of the adsorption layer, and ϱ is the density of the solid material. The quotient h/d, which can be regarded as an disaggregation /dispersion/ factor too, is the predominant factor determining the sediment volume. If h/d = 2-3 / in strongly aggregated systems /, then the quotient d_a/d /the extent of "swelling"/ may be the governing factor, but in any event the specific sediment volume is low /1-2 cm^3/g/. However, if the organocomplex is in a completely disaggregated state, then the known crystallographic and electronmicroscope data indicate a value of 35-40 for this factor; it is then practically this which determines the sediment volume, the specific value of which lies around 10 cm^3/g. This in fact corresponds to the maximum measured values.

All this refers to the extracted HP-montmorillonites, within the limits mentioned. It can be seen from Fig. 5. that, beginning from a saturation of about 85 %, the sediment volume function inclines upwards from linear. It may be presumed that with a high degree of organophilic character it is not a simple card-house structure which develops; instead, it is necessary to reckon with cellular-foamy structures, the existence of which was assumed by van Olphen /3/, and was demonstrated on the stereo-electronmicroscope pictures of freezedried thixotropic bentonite gels /8/.

The outlined results and considerations may sooner or later provide systematic and factual support for our practical knowledge relating to clay-mineral suspensions.

Acknowledgements

The authors wish to express their thanks to Prof. Dr.A.Weiss for his kind interest and valuable discussions in connection with this work.

References

1. J. W. Jordan, B. J. Hook and C. M. Finlayson, J. Phys. Chem. 54, S 1196 /1950/
2. F. Szántó and S. Veres, Acta Phys. Chem. Szeged, 9, S 157 /1963/
3. H. van Olphen, "An Introduction to Clay Colloid Chemistry", Interscience Publ. J. Wiley, New York, /1963/
4. J. J. Kipling, "Adsorption from Solutions of Non-Electrolytes", Academic Press, London, /1965/
5. W. H. Slabaugh and D. B. Hanson, J. Colloid Interface Sci. 29, S 460 /1969/
6. D. H. Everett, "IUPAC Manual Appendix II," S 592 Butterworths, London, /1972/
7. G. Schay and L. G. Nagy, J. Colloid Interface Sci. 38, S 302 /1972/
8. J. Blaha,/Zentrum für Elektronenmikroskopie, Graz/ private communication, /1973/
9. H. Stange, Inaugural-Dissertation, München, /1973/
10. I. Dékány, F. Szántó, L. G. Nagy and G. Fóti, J.Colloid Interface Sci. 50, S 265 /1975/

EQUILIBRIUM AND KINETIC STUDIES OF LIQUID ADSORPTION ON POROUS ACTIVATED CARBON

L.G. Nagy, G. Fóti, H. Kuty* and G. Schay**

Department of Physical Chemistry, Technical University of Budapest, 1521. Budapest, Hungary
* Chinoin Pharmaceutical Works, 1325. Budapest P.O.B.110. Hungary
** Central Res. Inst. for Chemistry, Hungarian Academy of Sciences, 1525. Budapest, P.O.B.17, Hungary

Conventional characterization of the sorption properties of activated carbons is based mainly on their behaviour in solid/gas interfacial phenomena. The generally accepted standard method for the estimation of specific surface areas of solid adsorbents is computation by the well-known BET equation, and the determination of the pore volume distribution of an adsorbent is also based on calculations from gas adsorption isotherms. The aim of our work is to show that the solid/liquid interfacial phenomena studied more and more intensively also offer possibilities for investigating the above-mentioned surface properties of porous adsorbents, and there are liquid adsorption methods having more or less equivalent applicability comparing with the conventional gas adsorption ones. Since the estimation method of the surface area of adsorbents using adsorption measurements from liquid phase is well-known in the literature, this equilibrium adsorption technique will not be described in detail, in contrary to the so-called isotope molecular exchange method elaborated for the study of the kinetic behaviour of solid/liquid interfacial phases, which is effected mostly by the pore structure of the solid adsorbent.

Equilibrium method

Three types of chemically and/or steam activated carbons have been tested to compare the gas adsorption and liquid

adsorption techniques, namely NUXIT BD, NUXIT AL III, NUXIT LBS. The binary liquid mixtures used in the equilibrium adsorption measurements were methanol-benzene, ethanol--benzene, acetic acid - benzene, acetic acid - water. The specific surface area values determined from the reduced surface excess isotherms using Schay and Nagy's "graphical" method /1/ were found to be in good agreement with each other and with the BET values /see Table I/. Molar areas used in the calculations were 180 m^2/mmole for benzene, 94 m^2/mmole for methanol, 120 m^2/mmole for ethanol, 120 m^2/mmole for acetic acid, 60 m^2/mmole for water /2/.

Table I

Comparison of the results of the BET and the "graphical" method

Specific surface area values in m^2/g

adsorbent / method	NUXIT BD	NUXIT AL III	NUXIT LBS
BET	1080	860	510
methanol-benzene	1040	870	540
ethanol-benzene	1110	890	490
acetic acid-benzene	1120	810	510
acetic acid-water	1020	830	530

Comparison of the BET and "graphical" method leads to excellent agreement even in case of porous activated carbons having extremely large /1000-2000 m^2/g/ specific surface area values, thus the equilibrium measurement of adsorption from liquids can be applied in a wide range for surface area estimation.

Kinetic method

The isotope molecular exchange is a useful technique for the kinetic study of the S/L adsorption equilibrium on porous adsorbents. Using this method quantitative data can be obtained on the exchange rate of molecules of various species between the bulk liquid phase and the adsorbate.

The experimental technique consists of three consecutive steps: 1/ equilibration of the solid/liquid adsorption system, 2/ change of the bulk liquid phase to another one of the same chemical composition but of a different isotope ratio, 3/ observation of time dependence of the isotope ratio in the liquid phase. In case of a one-component liquid phase the first two steps are very simple, but using liquid mixtures some sources of error should be taken into consideration. After separation of the phases weighed amount of the liquid with a different isotope concentration is added to the wet adsorbent and this time is the start point of the exchange process. A simple way to determine the time dependence of the isotope ratio in the liquid phase is the application of the radioisotope tracer technique, when specific intensity of the liquid phase should be measured either using fractional sampling technique or in a fluid flow system having the liquid circulated through a column packed with the adsorbent as well as in front of a detector.

Data evaluation

Plotting the data of the isotope molecular exchange measurements in $\lg/1-\frac{i}{i_\infty}/$-t form /where i and i_∞ are specific intensity values of the liquid phase at time t and in equilibrium of the exchange process, respectively/ two types of exchange curves can be obtained according to our experiences /see Fig. 1./. Linear exchange curves of type I have been obtained for example for both components from benzene-n--heptane mixtures on silica gels having macropore structure

and a relatively small /~100 m²/g/ specific surface area. From the slope of the exchange curves of type I half-time of the exchange process and - knowing the amounts of the phases - the exchange rate can be calculated /3/.

Our measurements on porous activated carbons have resulted in exchange curves of type II only. In this case the total exchange process can be described as superimposition fof parallel processes of different rate. The decomposition of the total exchange curve can be made assuming that rates of the part-processes differ in an order of magnitude. Our experimental exchange curve obtained on porous activated carbons could be described as superimposition of two processes having finite rate. Evaluation of the exchange curve of type II allows the determination of the half-times of the part--processes as well as the concerning exchange volumes, which can be considered as a so-called kinetic pore volume distribution. Parameters of the exchange curve /slopes and sections of the linear components representing the separate part-processes/ as well as material- and radiointensity--balances should be known to carry out the calculation.

Possible sources of error

- Sampling error due to inhomogeneity of the sorbent
- Incomplete equilibration
- Errors at changing the liquid phase

In our experiments only one-component liquid phases have been studied, so the above listed sources of error could be negligible. Further sources of error in measurement of the specific intensity at the fractional sampling technique used by us are:

- Error of the time measurement depending on the rate of the exchange process
- Error of weighing, mainly in the case of volatile liquids
- Error because of the decrease in amount of the liquid phase, when the exchange rate depends remarkably on the amount of the liquid phase

- Error of the radiointensity measurement. Reproducibility of the exchange curve describing the isotope molecular exchange is determined mainly by the reliability of the radiointensity measurements. If every radiointensity measurement lasts one unit of time and standard deviation of the mass measurement is negligible compared with that of the intensity measurement, standard deviation of the specific intensity $(sd)_i = \pm\sqrt{\frac{i}{m}}$, where m is the mass of the liquid sample. Based on this value and according to the propagation of errors

$$(sd)_{lg(1-i/i_\infty)} = \pm \frac{1}{2,3} \frac{\sqrt{i/i_\infty\,(1+i/i_\infty)}}{1-i/i_\infty} \cdot \frac{(sd)_{i_\infty}}{i_\infty}$$

During the exchange process, i.e. with increasing value of the i/i_∞ ratio, the percentage value of this standard deviation varies according to a minimum curve /see Table II/.

Table II

Standard deviation of $lg(1-i/i_\infty)$ as a function of the exchange ratio at $(sd)_{i_\infty} = 1\%$

i/i_∞	$(sd)_{lg(1-i/i_\infty)}$ %	i/i_∞	$(sd)_{lg(1-i/i_\infty)}$ %
0,1	1,51	0,7	1,32
0,2	1,19	0,8	1,59
0,3	1,08	0,9	2,80
0,4	1,06	0,95	3,97
0,5	1,08	0,99	13,2
0,6	1,15		

Results and discussion

Our isotope molecular exchange experiments have been carried out on the same three NUXIT type porous active carbon adsorbents, which had been used in the equilibrium adsorption measurements. Carbon-14-labelled ethanol was used for

equilibration as liquid phase and inactive ethanol for changing the liquid phase. Beta radiation of the C-14 in the fractional samples was detected by liquid scintillation technique.

Specific intensity of the liquid phase as a function of time can be seen in Fig. 2. All of the exchange curves obtained are of type II /see for example Fig. 3./. Having decomposed the total exchange curves the half-times of the part-processes and the concerning exchange volumes have been resulted.

All of the total exchange curves have axial sections at finite values of exchange ratio, i.e. a part of the liquid wetting the adsorbent can be exchanged in a prompt process. Thus three sorts of exchange volumes exist, one of them corresponds to a prompt process, the second to the fast, and the third to the slow one. It seems to be probable, that the prompt exchange process is caused not only by the incomplete separation of the phases at the phase change, but this volume - at least partly - is a part of the adsorbate volume because it is in good correlation with the pore volume distribution determined using gas adsorption technique, and its reliability is not worse than that of the part-processes of finite rate. The average half-time and exchange volume values have been summarized in Table III. On basis of the measured exchange volumes and the pore volume distributions of the activated carbon samples correlations can be found between the pore size intervals and the rates of the corresponding part-processes /see Fig.4./. It can be seen that the exchange volume corresponding to the slow part-process has generally a small value, not more than 10-20% of the total exchange volume. So the first step of the data evaluation, i.e. calculation of parameters of the slow process has appreciable uncertainty, because in this range - close to the equilibrium - the reliability of the data is relatively poor. This poor reliability of the slow process causes, of course, an increasing uncertainty in parameters of the faster

ones, because their calculation is based on parameters of the slowest process.

Table III

Half-times of the separate processes and the corresponding exchange volumes

$t_{1/2}$ /min/	process	NUXIT BD		NUXIT AL III		NUXIT LBS	
	fast	6,5+0,5		9,0+0,5		10,5+0,5	
	slow	200±10		190±10		160±10	
exhange volume/100 g of adsorbent		v/cm³/	v_{rel}	v/cm³/	v_{rel}	v/cm³/	v_{rel}
	prompt	101	56%	85	55%	55	50%
	fast	63	35%	47	30%	33	30%
	slow	16	9%	23	15%	22	20%
	total	180 ±20		155 ±17		110 ±13	
pore volume /cm³/100g/		115±10		90±10		80±10	

To sum upt it can be stated that the isotope molecular exchange method is able to give useful informations about kinetics of sorption processes. The total exchange process can be decomposed to its parts and thus a model can be constructed on the time dependence of accessibility of the porous solid surface. On porous adsorbents the exchange rate of the isotope molecules is determined by adsorption - mainly chemisorption - interactions and by the diffusion in the pores. Differences observed among systems containing the same liquid and adsorbents of the same chemical nature can be explained by different pore diffusion processes determined by different pore structure.

1. G.Schay, L.G.Nagy.: J. Coll. Interface Sci. 36 /3/ 302 /1972/
2. A.Blackburn, J.J.Kipling, D.A.Tester.: J. Chem. Soc. 2373 /1957/
3. L.G.Nagy: Progress Report 1971, CSCR Lehingh Univ. Pa, USA

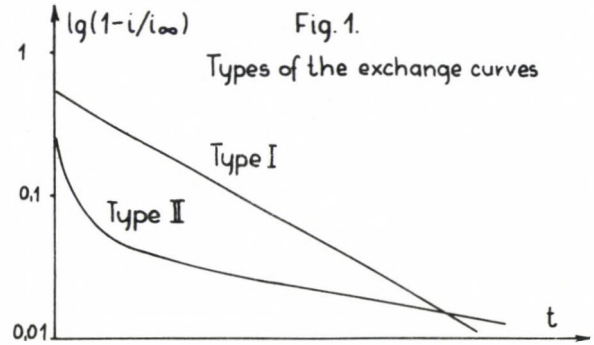

Fig. 1.
Types of the exchange curves

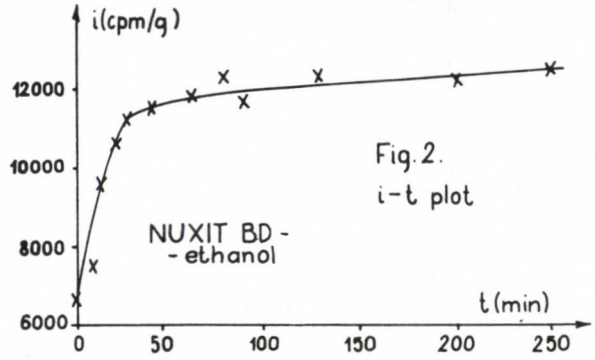

Fig. 2.
i-t plot

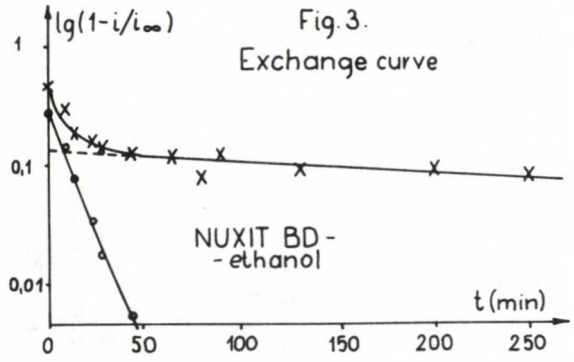

Fig. 3.
Exchange curve

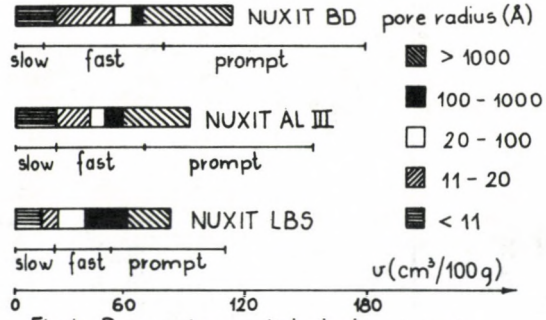

Fig. 4. Pore volume distributions and the exchange volumes

FORMATION AND STRUCTURE OF SOLID/VAPOUR BOUNDARY LAYERS

I.Pászli

Department of Colloid Science, L. Eötvös University, Budapest, Hungary

Introduction

The calorimetric study of the adsorption of pure vapours provides the same type of information about the van der Waals forces determining the structure of solid/vapour and solid/liquid interfacial layers as do other techniques permitting the direct measurement of these forces.

Studies performed at relative vapour pressures /p_r/ less than unity are of special interest since for $p_r = 1$, both experimental and theoretical evidence is available to prove that the solid/vapour interfacial layer has a duplex structure in the sense given by Harkins[1]. The existence of a duplex film has been recognized earlier by Everett[2], although on a heuristic basis.

The aim of this paper is to show under what conditions the van der Waals forces acting in the solid/vapour interfacial layer may be determined using solid/liquid heat of immersion /q_w/, and solid/vapour adsorption data.

State of adsorbed molecules in the S/V and S/L surface layers

In a thermodynamic system at equilibrium, the intensity parameters of the system as a whole /e.g. temperature $\mathcal{T}$, mechanical strain $-\mathcal{P}$, the chemical potentials of the components μ_i, etc./ can be given as quantities independent of the position coordinates. These will be referred to as global intensities. It is also possible to define so-called local intensities

for given points of the system. The former can be expressed for any point of the system through the position-dependent local intensive quantities /Y_k/. By definition, the global intensity, $\mathcal{Y}_k$, of an arbitrary type of interaction can be expressed in the form

$$\mathcal{Y}_k = Y_k(\xi, \eta, \zeta) + \psi_k(\xi, \eta, \zeta) \qquad /1/$$

where ψ_k is the intensity of the external potential field, which is a function of position coordinates ξ, η and ζ. The above equation correlates the global data characteristic of the system as a whole with the local data actually characterizing an arbitrary point. /The potential fields ψ_k are usually known from other branches of physics./ It is evident from eq. /1/ that in the vicinity of the phase boundary surface the local pressure $P(\xi, \eta, \zeta)$ will vary as a result of the position-dependent van der Waals forces $\psi(\xi, \eta, \zeta)$ operative in these same regions, even at constant $-\mathcal{P}$, i.e. in mechanical equilibrium. Previously, a formula has been given[3] to describe the density distribution of a continuous medium placed in an anisotropic field:

$$\varrho = \varrho_0 \frac{1}{1 - A} \; ; \qquad A = \frac{\chi_0 \iint_{(0)}^{(\Delta P)} \chi \, d(\Delta P) \, d(\Delta P)}{1 + \varrho_0 \Delta P} \qquad /2/$$

Here ϱ_0 is the density in an arbitrary reference state, χ_0 is the compressibility factor and ΔP is the difference in local pressure between the given point and the reference state, i.e. the difference between the corresponding van der Waals forces. The position-dependence of the latter implies that the density obtained from eq. /2/ is also a function of the position coordinates. Thus, if the average densities referring to a given adsorption volume are determined, eq. /2/ permits calculation of the van der Waals forces. It should be noted that if ϱ is the average density of the layer, then ΔP is the <u>average</u> van der Waals force assigned to the layer.

The interfacial layer has different average densities at

different relative equilibrium pressures. The reason of this is that the form of the interaction field at the surface changes with the amount adsorbed /i.e. with p_r/ and, according to the equipartition theorem, the same is true for the kinetics energy of the adsorptive molecules. It is these two effects that determine the distance from the surface within which vapour molecules are "captured" by the solid surface. Obviously, this distance is nothing else but the thickness of the sorption layer at its vapour side. It should be noted that the "thickness" at the solid-phase side is also subject to changes.

The average density of the S/V layer can be written as

$$\varrho = \left(n^{S/V} / V^{S/V} \right) M \qquad /3a/$$

where $n^{S/V}$ is the amount of material adsorbed in volume $V^{S/V}$ and M is the molecular weight. In principle, the molecules in this layer cannot be expected to assume a close-packed arrangement. Certainly, the density of this layer should be lower than the average density of the duplex film formed at $p_r = 1$ /this is always true for adsorbents with narrow pores/, but it should exceed the density of the equilibrium vapour phase at the given relative pressure. This, of course defines a rather wide interval for the value of volume $V^{S/V}$:

$$\varrho_{duplex} > \varrho \geq \varrho^{v}(p_r) \qquad /4/$$

The lower limit, $\varrho^{v}(p_r)$, corresponds to unrealistically large thickness; over such distances, the van der Waals forces no doubt decay insignificant levels. Thus, the calculation of the average density ϱ, by all means requires determination of the relationship between the layer volume $V^{S/V}$ and the relative pressure.

Volume $V^{S/V}$ can be calculated from the following considerations. Assume an isolated thermodynamic system that contains an adsorbent of unit mass and, separated from it, a liquid and a vapour phase in equilibrium with one another at pressure p^o. Let part of the vapour be adsorbed on the solid phase so that the adsorption equilibrium should be achieved at relative pressure p_r presorption .

Now let immerse the solid covered by presorbed vapour into the bulk liquid phase being in equilibrium with the vapour at $p_r=1$. The amount of heat that will be free then is in a good approximation equal to the residual heat of immersion, q_r^w, which may be expressed as

$$q_r^w = p^o\left(V^{S/L} - p_r V^{S/V}\right) + n^{S/V} .RT \ln p_r + u^{s(S/V)} - u^{s(S/L)} \qquad /5/$$

Here the term

$$u^{s(S/V)} - u^{s(S/L)} = Q_{def}^s$$

is the energy change of the solid due to the transition from the presorption to the wetted state. The value of Q_{def}^s is connected with the deformation of the solid; at $p_r=1$, $Q_{def}^s = 0$. $V^{S/L}$ is the volume of the solid/liquid boundary layer at equilibrium. The value for $V^{S/V}$ may be expressed as

$$V^{S/V} = \frac{1}{p_r}\left[\frac{n^{S/V} .RT \ln p_r + \left(Q_{def}^s - q_r^w\right)}{p^o} + V^{S/L}\right]. \qquad /6/$$

For at $p_r=1$, Q_{def}^s being equal to zero, owing to the duplex structure

$$V^{S/V} = V^{S/L} + V^{L/V},$$

so that

$$V^{L/V} = -\frac{q_r^w}{p^o}$$

Taking into account that the absolute value of the heat of immersion at $p_r=1$ is exactly equal to the surface energy of the wetting liquid (which is the principle of the Harkins-Jura method), the following is true for $V^{L/V}$

$$V^{L/V} = -\frac{A_s^{L/V} \cdot u^{L/V}}{p^o},$$

where $A_s^{L/V}$ is the external surface area of the adsorbent and $u^{L/V}$ the specific surface energy of liquid. From this expression the thickness $/\tau/$ of the free liquid surface layer can

be obtained

$$\tau = - \frac{u^{L/V}}{p^o} ,$$

if $A_s^{L/V}$ is known.

Numerous systems are known for which it is fairly reasonable to assume that the S/L layer has a compact monomolecular structure. In this case, term $V^{S/L}$ in eq. /6/ immediately becomes definite; using the values of Q^s_{def} (these can be calculated), the actual layer volume $V^{S/V}$ can thus be calculated at least in a certain interval of relative pressures.
Thus

$$\varrho = n^{S/V} \frac{M}{\frac{1}{p_r}\left[\frac{n^{S/V} RT \ln p_r - \left(q_r^w - Q^s_{def}\right)}{p^o} + \frac{a^s M}{a_m \varrho_L}\right]} \qquad /7/$$

where a^s is the specific surface area of the adsorbent, a_m is the space requirement of the adsorbate and ϱ_L is the density of the liquid. The layer densities calculated from eq. /7/ are either much smaller than, or nearly equal to, the density of the adsorbate in the liquid state. Consequently, the adsorbate can be regarded as being in the vapour or liquid state.

If the adsorbate is regarded as a vapour, the compressibility can be calculated from the state equation for ideal gases. In this case, the van der Waals forces are given by the formula

$$\left(1 - \frac{\varrho_v}{\varrho}\right) + \left(1 - \frac{\varrho_v}{\varrho}\right) \frac{(\Delta p)}{(p^o)} + \frac{p_r}{2} \frac{(\Delta p)^2}{(p^o)^2} - \frac{p_r}{3} \frac{(\Delta p)^3}{(p^o)^3} + \frac{p_r}{4} \frac{(\Delta p)^4}{(p^o)^4} - \ldots = 0$$

If the adsorbate is regarded as a liquid, the isothermal compressibility can be expressed by Tait's formula[4]

$$\chi = \frac{C_1}{C_2 + \Delta p} = \frac{C_1}{C_2} \frac{1}{1 + \frac{\Delta p}{C_2}}$$

where C_1 and C_2 are constants.

For most liquids $C_1 \sim 10^{-1}$ and $C_2 \sim 10^3$ atm approximately /e.g. C_2 for acetone is 826, for benzene 970 and for carbon tetrachloride 867 atm, at 25°C/, thus, up to a pressure of $\Delta P \approx 800$ atm, the above fraction can be expanded into a binomial series, i.e.

$$\chi = \frac{C_1}{C_2}\left(1 - \frac{\Delta P}{C_2} + \frac{(\Delta P)^2}{C_2^2} - \frac{(\Delta P)^3}{C_2^3} + \ldots\ldots\right)$$

Hence the value of the double integral is

$$C_1\left(\frac{1}{2C_2}(\Delta P)^2 - \frac{1}{6C_2^2}(\Delta P)^3 + \frac{1}{12C_2^3}(\Delta P)^4 - \ldots\right)$$

Finally, by expressing from eq. /2/ the power series determining ΔP, one obtains

$$\left(1 - \frac{\varrho_L}{\varrho}\right)C_2 + \left(1 - \frac{\varrho_L}{\varrho}\right)(1 + C_1)(\Delta P) - \tfrac{1}{2} C_1 (\Delta P)^2 -$$
$$- \tfrac{1}{2} C_1\left(\frac{1}{C_2} - \frac{1}{3C_2}\right)(\Delta P)^3 - \tfrac{1}{2}C_1\left(\frac{1}{6C_2^2} - \frac{1}{3C_2^2}\right)(\Delta P)^4 - \ldots = 0$$

In a given range of ΔP, the higher-order terms in the above equation can be neglected and thus ΔP can be calculated from the average layer density obtained from thermodynamic data, using tabulated values of C_1 and C_2.

It is apparent from the latter equation that the van der Waals forces actually depend on the layer density. Taking into account that the actual van der Waals force operative in the layer at equilibrium is the superposition of the forces acting between pairs of the individual lattice elements and adsorbed molecules, the variation of the average value with the presorbed amount can only be interpreted if the thickness of the solid part of the layer also varies during sorption. The actual density distribution at a given p_r is shown in the Figure. With increasing p_r, the density distribution curves at the

vapour $\left(\varrho_V^{S/V}\right)$ and the solid $\left(\varrho_s^{S/V}\right)$ side are shifted upwards and downwards, respectively, accompanied by the simultaneous increase of layer thicknesses $\tau_S(p_r)$ and $\tau_v(p_r)$. The $\varrho_V^{S/V}$ curve at one point surpasses the value corresponding to the density of the liquid ϱ_L. The layer between the point of intersection shown in the Figure and the geometrical surface of the solid layer, including the inhomogeneous space from the solid phase, is the so-called archetype of the solid/liquid interfacial layer, as this is the preformed variant of the regular S/L layer to be found in the duplex film.

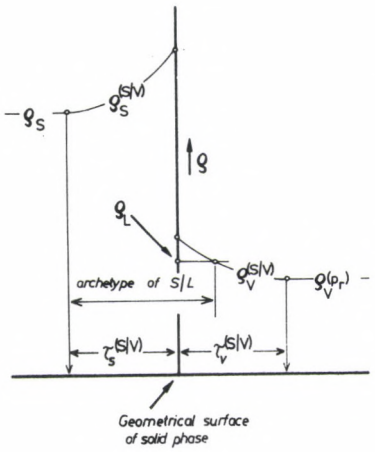

References

1. Pászli, I.: Mitteilungsblatt, Chem. Ges. der DDR, 20, 187 /1973/
2. Everett, D.H.: Trans. Faraday Soc. 60 1803 /1964/
3. Pászli, I.: Distributions of component-densities in anisotropic, equilibrium systems, Lecture helt at the meeting of the comission on Colloid and Surface Science, Hung. Acad. Sci., May, 1974.
4. Moelwyn-Hughes, E.A.: Physikalische Chemie, G.Thieme Verlag, Stuttgart, 1970, p. 385.

Group I/3
Wetting

THE CONTACT ANGLE THEORY FOR ELASTIC SOLIDS

A.I.Rusanov

Department of Chemistry, Leningrad State University,
Leningrad, USSR

The existing theories of wetting refer mainly to non-deformable solids. Though some questions of wetting of deformable solids were broached in the works [1-5], there is no thermodynamic theory of incomplete wetting of elastic deformable solids so far. The formulation of such a theory and the derivation of relationships for the contact angle were the task of this investigation.

We consider a liquid drop on the surface of an elastic solid occupying the low half-space $z > 0$. We adopt the usual notations S, L, V for the bulk phases and the double symbols SL, SV, LV, for the interfaces. As usual, the relationships for the equilibrium contact angle may be derived from the condition of the minimum of free energy. This leads to the equation

$$\sigma_{LV} dA_{LV} + \sigma_{SL} dA_{SL} + \sigma_{SV} dA_{SV} + dW + d\mathcal{U} = 0 \quad (V_L = const) \qquad (1)$$

where σ is surface tension, A is surface area, W is the work of deformation of a solid, $\mathcal{U}$ is the energy of a system in gravitational field, V_L is the volume of a liquid drop.

The work of deformation was calculated by the formula

$$W = \pi \int (\vec{P}\vec{u})\, r\, dr \qquad (2)$$

where $\vec{P}$ is the vector of stresses applied to the surface of the solid, $\vec{u}$ is the displacement vector for the solid surface points, r is the distance from the center of the region of wetting. For the initial state of a not

deformed solid with the radius of the wetting perimeter and the contact angle θ, the vector $\vec{P}$ is given by the conditions

$$P_z = P \equiv (P_L - P_V)_{z=0}\,, \quad P_r = 0$$

$$P_z = -\sigma_{LV}\sin\theta/t\,, \quad P_r = -\sigma_{LV}\cos\theta/t \quad (a \le r \le a+t) \qquad (3)$$

$$\vec{P} = 0 \quad (r \ge a+t)$$

where P_z and P_r are the normal and radial components of $\vec{P}$, z is counted from the not deformed surface of the solid.

It is assumed here that the surface tension force of the liquid, applied to the solid surface, is uniformly distributed along the circular stripe of width t. This means that the real profile of tangential pressure in the surface layer LV is approximated by a step profile with the respective choice of an effective thickness, τ (evidently, $t = \tau / \sin\theta$). An analogous model was used by Lester [1], but he considered the normal forces only (in reality, this corresponds to the value $\theta = 90^\circ$). In the general case, the normal and tangential components of the surface tension of a liquid are equal to $\sigma_{LV}\sin\theta$ and $\sigma_{LV}\cos\theta$. The tangential component is partly compensated by the surface tensions σ_{SL} and σ_{SV}, so that the resulting force, causing the tangential deformation, equals

$$\sigma_{LV}\cos\theta + \sigma_{SL} - \sigma_{SV} \equiv \sigma_{LV}\left(\cos\theta - \frac{\sigma_{SV} - \sigma_{SL}}{\sigma_{LV}}\right) \equiv \sigma_{LV}\,\Delta\cos\theta \qquad (4)$$

where $\Delta\cos\theta$ is the deviation of $\cos\theta$ from the value corresponding to the Young equation.

With a given vector of stresses $\vec{P}$, a displacement vector $\vec{u}$ for various points of the surface may be found by the methods of the theory of elasticity. The problem has been solved in this work, and the following solutions have

been obtained for the case of small deformation:

$$u_z(r) = \frac{4(1-\nu^2)}{\pi E}\left\{ P a E\left(\frac{r}{a}\right) + \frac{\sigma \sin\theta}{t}\left[a E\left(\frac{r}{a}\right) - \right.\right.$$

$$\left.\left. - (a+t) E\left(\frac{r}{a+t}\right)\right] + \frac{\pi(1-2\nu)}{4(1-\nu)} \sigma \Delta \cos\theta \right\} \quad (r \le a) \tag{5}$$

$$u_z(r) = \frac{4(1-\nu^2)}{\pi E}\left\{ P r G\left(\frac{a}{r}\right) + \frac{\sigma \sin\theta}{t}\left[r G\left(\frac{a}{r}\right) - \right.\right.$$

$$\left.\left. - (a+t) E\left(\frac{r}{a+t}\right)\right] + \frac{\pi(1-2\nu)}{4(1-\nu)} \cdot \frac{\sigma \Delta \cos\theta}{t}(a+t-r) \right\} \tag{6}$$

$$(a \le r \le a+t)$$

$$u_z(r) = \frac{4(1-\nu^2) r}{\pi E}\left\{ P G\left(\frac{a}{r}\right) + \frac{\sigma \sin\theta}{t}\left[G\left(\frac{a}{r}\right) - G\left(\frac{a+t}{r}\right)\right]\right\}$$

$$(r \ge a+t) \tag{7}$$

$$u_r(r) = -\frac{4(1-\nu^2) r}{\pi E}\left\{ \frac{r \sigma \Delta \cos\theta}{3at}\left[\frac{a+t}{r} H\left(\frac{r}{a+t}\right) - \right.\right.$$

$$\left.\left. - \frac{a}{r} H\left(\frac{r}{a}\right)\right] + \frac{\pi(1-2\nu)}{8(1-\nu)} P \right\} \quad (r \le a) \tag{8}$$

$$u_r(r) = -\frac{4(1-\nu^2) r}{\pi E}\left\{ \frac{r \sigma \Delta \cos\theta}{3at}\left[\frac{a+t}{r} H\left(\frac{r}{a+t}\right) - 2G\left(\frac{a}{r}\right) + \right.\right.$$

$$\left.\left. + \frac{a^2}{r^2} F\left(\frac{a}{r}\right)\right] + \frac{\pi(1-2\nu)}{8(1-\nu)}\left[P \frac{a^2}{r^2} - \frac{\sigma \sin\theta}{t}\left(1 - \frac{a^2}{r^2}\right)\right]\right\}, \tag{9}$$

$$(a \le r \le a+t)$$

$$u_r(r) = -\frac{4(1-\nu^2)r}{\pi E}\left\{\frac{r\sigma\Delta\cos\theta}{3at}\left[2G\left(\frac{a+t}{r}\right) - \frac{(a+t)^2}{r^2}F\left(\frac{a+t}{r}\right) - \right.\right.$$

$$\left.\left. - 2G\left(\frac{a}{r}\right) + \frac{a^2}{r^2}F\left(\frac{a}{r}\right)\right] + \frac{\pi(1-2\nu)}{8(1-\nu)}\left[P\frac{a^2}{r^2} - \sigma\sin\theta\frac{2a+t}{r^2}\right]\right\} \quad (10)$$

$$(r \geq a+t)$$

where E is the Young modulus for a solid, ν is the Poisson coefficient, $G(k) \equiv E(k) - (1 - k^2)K(k)$, $H(k) \equiv (2 - 1/k^2)E(k) - (1 - 1/k^2)K(k)$, $K(k)$ and $E(k)$ are the elliptic integrals of the first and second kind respectively.

Eqs.(5)-(10) characterize completely the shape of the deformed surface of a solid. They predict the sag of the surface in the central region and the ridge formation along the three-phase contact line. Eqs.(5)-(10) are considerably simplified if the condition $t \ll a$ is used which is practically true for all observable contact angles in the case of a macroscopic drop.

Inserting (3),(5)-(10) into (2) and taking into account the smallness of t/a, it follows the expression for the deformation work

$$W = \frac{2(1-\nu^2)a}{E}\left[\frac{4}{3}P^2a^2 - 4Pa\sigma_{LV}\sin\theta + \sigma_{LV}^2\sin^2\theta\left(\frac{3}{2} + \right.\right. \quad (11)$$

$$\left.\left. + 3\ln 2 - \ln\frac{t}{a}\right) + \sigma_{LV}^2(\Delta\cos\theta)^2\left(3\ln 2 - \frac{1}{2} - \ln\frac{t}{a}\right)\right] \cdot$$

$$\cdot\left[1 + O\left(\frac{t}{a}\right)\right]$$

where O(t/a) denotes a negligible quantity of the order of magnitude of t/a.

Eqs.(5)-(10) allow also to calculate all the geometrical characteristics of the system under consideration, in particular, the quantities A_{LV}, A_{SL}, A_{SV} and V_L in (1). This make possible to solve two tasks: 1) to find a connection between the contact angles θ and θ' for the not deformed and deformed surface from the condition V_L=const.; 2) to determine the equilibrium values of this angles from condition (1). Both the tasks have been solved separately for the cases of absence and presence of the gravitational field.

The solution of the first task in absence of external field (when $Pa = 2\sigma_{LV}\sin\theta$) is

$$\cos\theta' \simeq \cos\theta - \frac{3\sigma_{LV}(1+\cos\theta)^2}{2\pi E a}\left[\frac{\Delta\cos\theta(1-\cos\theta)(2+\cos\theta)}{1+\cos\theta} \times \right. \qquad (12)$$

$$\left. \times\left(4\ln 2 - 1 + \ln\frac{a\sin\theta}{\alpha}\right) - \sin^2\theta\left(4\ln 2 - \frac{5}{3} + \ln\frac{a\sin\theta}{\alpha}\right)\right]$$

The angles θ and θ' are strictly defined as limiting slope angles of Gibbs' surface of tension for the boundary LV on the line where this surface intersects the surface of a solid, the angles being taken with respect to the not deformed (plane) surface of a solid. It means that the angle θ' is a directly observable angle, but not a true contact angle. The latter cannot be determined from an experiment and is an impractical parameter for the case of deformable solids.

We point out three consequences following from Eq.(12): 1) $\theta' \to \theta$ if $\sigma_{LV}/E \to 0$; 2) at given σ_{LV} and E $\theta' \to \theta$ if $a \to \infty$; 3) $\theta' < \theta$ if $\Delta\cos\theta \le 0$. The first consequence is trivial, it shows the transition to the case when deformation is absent. The second one means that an observable contact angle practically coincides with an initial contact angle for a drop of sufficiently large size.

Eq.(12) demonstrates the change in the slope of a liquid surface in the place of three-phase contact during the deformation of a solid. Eq.(12) is true for any values of

θ • In order to find the equilibrium value of θ' and the corresponding value of θ , Eq.(1) is to be used. The application of (5)-(10) allows to solve this task completely, but the result is too cumbrous. Therefore, we confine ourselves here by a graphic example.

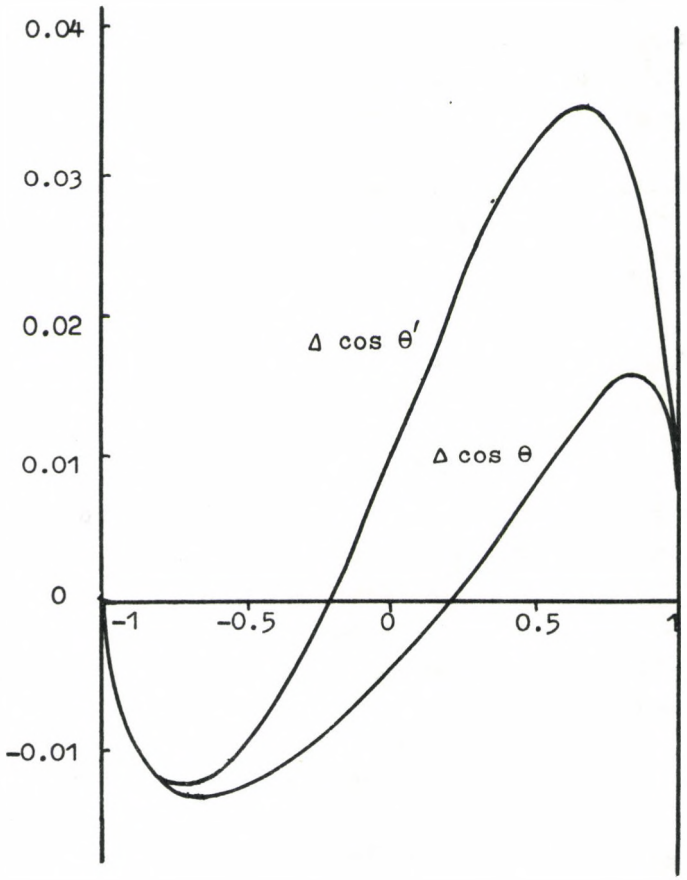

Fig. 1

On Fig. 1 the dependence has been given of the equilibrium quantities $\Delta\cos\theta = \cos\theta - \cos\theta_0$ and $\Delta\cos\theta' = \cos\theta' - \cos\theta_0$ on $\cos\theta_0 = (\sigma_{SV} - \sigma_{SL}) / \sigma_{LV}$ for $a/\mathcal{R} = 10^6$, $3\sigma_{LV}/2\pi E\mathcal{R} = 10^3$, $\sigma_{SV}/\sigma_{SL} = 2$ in absence of external field. It is seen that inside the interval $0 < \theta_0 < \pi$ there is a value of $\cos\theta$ and $\cos\theta'$ (in the case under consideration $\cos\theta_1 = 0.25$ and $\cos\theta_1' = -0.21$) coinciding with the value $\cos\theta_0$ predicted by the Young equation. The angles θ and θ' for the equilibrium state depend not only on the combination $(\sigma_{SV} - \sigma_{SL}) / \sigma_{LV}$ as in the Young equation, but also on each of these quantities separately. Besides, the angles θ and θ' depend on the size of a drop.

In real conditions for a large drop, the gravitational effect becomes very important. In the case when the drop size is much more than the capillary constant, Eqs. (1), (5)-(11) allow to obtain very simple formulas. In presence of the gravitational field

$$P = (\rho_L - \rho_V) g h \qquad (13)$$

where ρ is density, g is the acceleration due to gravity, h is the height of a drop before the deformation of a solid. Some results for this case are given below.

The connection between the angles θ' and θ for small deformations is

$$\cos\theta' = \cos\theta + \frac{2a(\rho_L - \rho_V) g}{\pi E}(1 - \cos\theta) \qquad (14)$$

The equilibrium value of θ' and the corresponding value of θ for small deformations are determined from the equations

$$\cos\theta' - \frac{3a(\rho_L - \rho_V) g}{\pi E}(1 - \cos\theta') \approx \frac{\sigma_{SV} - \sigma_{SL}}{\sigma_{LV}} \qquad (15)$$

$$\cos\theta - \frac{a(\rho_L - \rho_V) g}{\pi E}(1 - \cos\theta) \approx \frac{\sigma_{SV} - \sigma_{SL}}{\sigma_{LV}} \qquad (16)$$

It is seen from (15) and (16) that both θ' and θ prove to be less than the equilibrium contact angle for non-deformable solids.

The theory presented here has been formulated in terms of an observable contact angle and this is very important for practice. But a true contact angle is also of interest in the theory, especially for the verification of the Young equation. It may be shown that an observable and a true contact angles coincide at a limit of $a \to \infty$ and both the angles satisfy the Young equation at this limit. According to (6), the deformation in the three-phase contact region increases infinitely at $a \to \infty$. If the Young equation remains true for this case, it may be supposed to be true for any other deformation state. As for force interpretation of the three-phase contact equilibrium, it is evident that the utilization of the theory of elasticity in our calculations implies the share of the volume stresses of a solid (together with surface tensions) in the total balance of forces in the region of the three-phase contact.

References

1. G.R.Lester, J. Colloid Sci. 16, 315, 1961.
2. G.R.Lester, Nature 209 (5028), 1126, 1966.
3. G.R.Lester, in "Wetting", S.C.I. Monograph No.25, London, 1967, p.57.
4. E.E.Braudo, E.N.Michailow, W.B.Tolstogusow, Z.phys. Chem., Leipzig, 253 , 369, 1973.
5. A.I.Rusanov, in "Structure and Properties of Surface Layers of Polymers" (in Russ.), Publ. "Naukova Dumka" Kiev, 1972, p.3.

WETTABILITY STUDIES OF METHYL GROUP RICH SURFACE AND BENZENE RING RICH SURFACE BY THE AQUEOUS SOLUTIONS OF NONIONIC SURFACTANTS WITH HOMOGENEOUS ETHYLENE OXIDE CHAIN LENGTH

M. Ueno, K. Tsubaki and K. Meguro

Department of Chemistry, Science University of Tokyo, Kagurazaka, Shinjuku-ku, Tokyo, Japan.

Wettabilities of hard solids and polymers with low-energy surfaces by organic liquids and aqueous solutions of surfactants have been extensively studied by many workers.[1~18]

Bernett and Zisman[1,2] have reported the wetting of polyethylene and Teflon by aqueous solutions of nonylphenoxypolyoxyethylene -ethanol mixture and other various surfactants on the same basis as wetting by pure organic liquids. They have established that the critical surface tension values are in reasonable agreement with those found with pure organic liquids, but a narrow spread at $\cos\theta = 1$ exists for the various solutions on each of these surfaces. This narrow spread may be caused by the heterogeneity of polyoxyethylene chain length for nonionic surfactants. Therefore, the study of wetting phenomena by the aqueous solutions of nonionic surfactants with homogeneous polyoxyethylene chain length can be expected.

In this paper, the wettabilities of the close-packed methyl surface of 39 layers of barium stearate multilayer by the aqueous solutions of a series of polyethyleneglycol n-dodecylethers with homogeneous polyoxyethylene chain length are discussed on the basis of the results of contact angle measurements, and the value of the critical surface tension is also compared to that of the surface obtained with n-alkanes. Furthermore, the critical surface tensions of two polyvinylbenzal multilayers built up by the Langmuir-Blodgett method[19~22] on the barium stearate multilayers are estimated by this method using the nonionic surfactants as wetting agent.

EXPERIMENTAL

Materials

Polyethyleneglycol n-dodecylethers, $C_{12}H_{25}O(CH_2CH_2O)_nH$, (for convenience, abbreviated hereafter as $C_{12}E_5$, $C_{12}E_6$, $C_{12}E_7$, $C_{12}E_8$ and $C_{12}E_{10}$ for n = 5, 6, 7, 8, and 10, respectively), were obtained from Nikko Chemical Co., Ltd.

The samples except $C_{12}E_{10}$ containing 20% $C_{12}E_8$ were confirmed to have homogeneous polyoxyethylene chain length by the results of thin-layer chromatography and gas-liquid chromatography ,respectively.

Stearic acid, required to build up 39 layers of barium stearate on a chrome-finished metal plate, was purified by repeated crystallization from ethanol to give a purity above 99.8%. The water substrate was prepared by distilled, ion-exchanged water.

The piston oils required for building up the stearic acid and two polyvinylbenzals on the metal plate were oleic acid (29.5 dyne/cm) and ethyl myristate (20.7 dyne/cm).

Mirror-clean chrome-finished stainless steel metal plates required for bearing a multilayer of barium stearate were degreased by extracting contaminants with hot toluene for about 4 hr in a Soxhlet extractor and washed thoroughly with distilled water. In this way, hydrophilic plates were obtained.

Poly(vinylalcohol)(PVA) required for synthesis of poly(vinyl benzal) was supplied by Nihon Gosei Kagaku Co., Ltd. The product was purified by repeated precipitation from aqueous solution with addition of a large excess of methanol, then by extraction of traces of poly(vinyl acetate) with metanol in a Soxhlet extractor, and finally by drying under vacuum. The purity of the PVA, as checked by infrared spectroscopy and elemental analysis, was found to be above 99.8% . The viscosity-average molecular weight was 7.96×10^4.

Two poly(vinyl benzals), (PVBen-A) and (PVBen-B) with different mole% of benzal group were prepared by acetalization of the PVA in HCl solution with benzaldehyde, respectively.
These polymers thus obtained were washed thoroughly with dilute ammonia to remove traces of acid, then with water. PVBen-A and B were precipitated from dimethylsulfoxide solution with addition of hot water and were finally dried under vacuum. The con-

tents of benzal groups in these polymers were 52.0 and 67.0 mole-%, respectively.

Barium Stearate and Polymer Multilayers.

The polymer monolayers were found to be easily deposited on the hydrophobic close-packed methyl surface of 39 layers of barium stearate ; a 2.0×10^{-2}M benzene solution of stearic acid was used as the spreading solution. The aqueous substrate was 1.0×10^{-3}m $BaCl_2$ solution. The pH of the substrate was adjusted at about 9.2 by addition of a small amount of aqueous ammonia.

At this pH, 90% of the stearic acid in monolayers spread on $BaCl_2$ solution is known to be converted to barium stearate.[23,24]

A freshly prepared metal plate was immersed in the aqueous substrate; the monolayer was spread and immediately pressed with the appropriate piston oil and hereafter was aged for 5 -10 min to permit evaporation of the solvent, and then successive barium stearate layers, up to 39 layers, were deposited on the plate by repeated dipping and withdrawal processes using a synchronous motor. The rate of dipping and withdrawal was usually 1.2 cm/min. In all of cases, Y-type films were produced,that is, films composed of alternating monolayers.

On this plate bearing 39 layers of barium stearate, two layers of each polymer were built up. Deposition resulted in the multilayer structure where adhesion between adjacent monolayers is brought about by alternating benzal-benzal and hydroxyl-hyroxyl contact for polymers. The deposition ratio showed a value of 1.0 corresponding to complete transfer of the monolayer from trough to the plate during both dipping and withdrawal.

Surface Pressure Measurements

Surface pressure-area measurements were carried out by using a Wilhelmy-type surface balance at 20° ± 0.5°C. The stainless steel trough were lightly waxed, and paraffin wax-molded barriers were used to confine and compress the polymer monolayers.

The surface balance was completely enclosed in a protective box. The sensitivity of the apparatus was 0.1 dyne/cm, and surface areas were estimated within an accuracy of 0.1%.

The spreading solutions of polymers were prepared at 90 mg/100 ml for PVBen-A and -B from a mixed solvent consisting of

benzene and dimethyl sulfoxide (60/40 v/v). The spreading solutions were delivered precisely to 0.0002 ml from an Agla microsyringe. Usually pressure-area curve measurements were begun 30 min after adding the spreading solution. This allowed elimination of the solvent and complete spreading. To ensure that equilibrium was attained, surface pressure measurements were made 7 min after each compression and the rate of compression was 1.0 cm/min. Under these conditions, the reproducibility was satisfactory.

Contact Angle Measurements

Contact angles were measured by the drop-on-plate method by use of a goniometer (Erma Kogaku Co, Ltd. M-2010) which was enclosed in a protective box fixed to a universal table mount. Here the sensitive control of the drop volume is accomplished by using an Agla microsyringe. To form the equilibrium advancing contact angle, the fine needle point was lowered to within 1 mm of the multilayer surface and liquid was slowly pushed out by the pressure of its piston until the drop approached 2mm in diameter, at which point the needle was slowly raised at such a rate that the drop continued to advance after removal of the needle. The drop was observed through a horizontal microscope with a goniometer eyepiece. Contact angles, θ, were slightly dependent on time. Where time dependence was more pronounced, θ values were taken at a fixed interval after placement of the drop. The temperature in the chamber was maintained at $20^{\circ} \pm 0.1^{\circ}C$. Values of θ could generally be measured to a small fraction of a degree with an average deviation for six drops of $\pm 1^{\circ}$.

Surface Tension Measurements

Surface tensions, γ_L, of the wetting liquids and the aqueous solutions of the surfactants were measured at $20^{\circ} \pm 0.1^{\circ}C$ by using a Wilhelmy-type surface tensiometer (SIMAZU ST-1). Where observed surface tensions deviated by more than about 0.5 dyne/cm from the published values, the liquids were further purified by distillation to bring them into coincidence with reported values. Otherwise, the liquids were used as received.

A list of those liquids employed together with measured surface tension values are given in Table I.

TABLE I

Measured Surface Tensions of Liquids Used for Contact Angle Measurements.

Liquids	γ_L (dyne/cm)
n-Alkanes	
n-Nonane	23.0
n-Decane	24.0
n-Dodecane	25.5
n-Tetradecane	26.5
n-Hexadecane	27.7

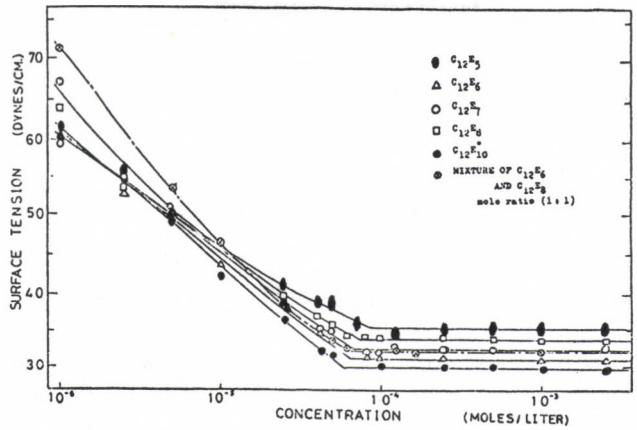

Fig. 1. The surface tension versus concentration curves of aqueous solutions of a series of polyethylenegycol n-dodecylethers.

On the other hand, the surface tension versus concentration curves for aqueous solutions of these nonionic surfactants are shown in Fig. 1.

RESULTS AND DISCUSSION

The contact angle data with n-alkanes and the aqueous solutions measured for barium stearate multilayers are shown separately in Figs. 2 (a) and (b), which show upper and lower parts in the curves, respectively. As shown in Fig.2(a), at COS θ = 1, the values of critical surface tensions, γ_c, for these n-alkanes observed according to Zisman's relation were found to be in the range from 21.0 to 22.0 dyne/cm. This is very close to the value

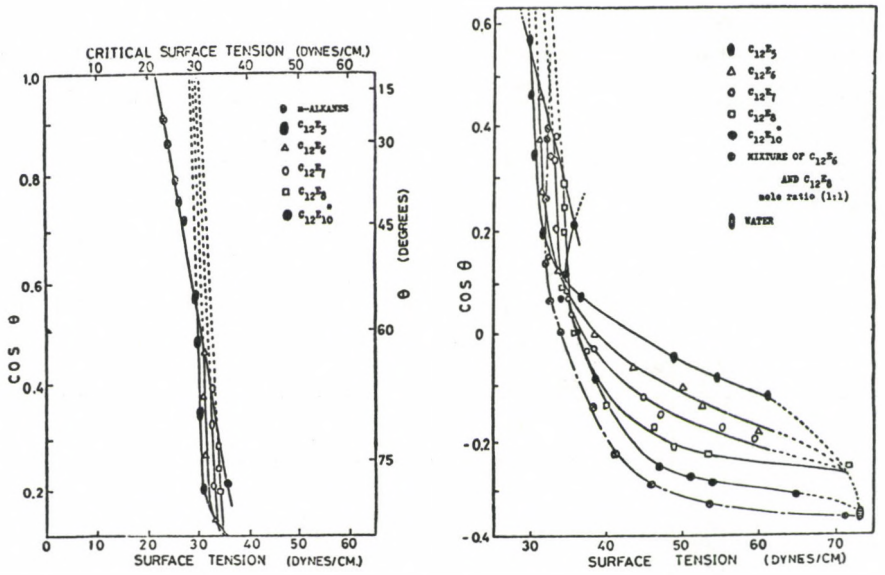

Figs. 2 (a) and (b). Surface tension versus COS θ curves obtained with n-alkanes and aqueous solutions of polyethyleneglycol n-dodecylethers. (a) : upper part in the curves, (b) : lower part in the curves.

for γ_c of close-packed methyl groups (22 dyne/cm), which is the minimum value found for crystalline hydrocarbon[3]. Therefore, this suggests that the multilayer surface consists of homogeneous close-packed methyl groups. However, at COS θ = 1, the values of the intercepts obtained by dotted lines of each curves do not coincide with that (21-22 dyne/cm) obtained with n-alkanes as shown in Figs. 2(a) and (b), and show narrow spread for the intercepts in the range from 28 to 30 dyne/cm. This means that a γ_c value can not be obtained by the same method as previously reported by Bernett[1,2] Fig.3 show a plot of COS θ against various concentrations of the nonionic surfactants. As with Figs.2(a) and (b), the values for COS θ gradually increase with increase of the concentration, i.e., with depression of surface tension, up to cmc, and subsequently approach the constant values characteristic of each of the surfactants in all ranges of the concentrations above cmc, as shown in Fig. 3. When these constant values for COS θ were plotted against their corresponding

surface tensions according to Zisman's relation[3], a linear relation could be obtained as shown in Figs.2(a) and 4, and then the γ_c value obtained with the surfactant solutions was found to agree very closely with that obtained by extrapolating the curve with n-alkanes to COS θ = 1. Such a fact has not been so far reported.

Furthermore, these aqueous solutions of the nonionic surfactants above cmc were applied to estimate the γ_c values for PVBen-A and -B.

Contact angle data with the surfactants for multilayers of PVBen-A and -B are shown in Fig. 4 together with those for barium stearate multilayers. These observed γ_c values for two multilayers are 33.0 and 32.0, respectively.

It can be seen that all results for γ_c values of the PVBens are very close to those of benzene ring-rich surfaces[11,12] (33-35 dyne/cm) and almost coincide with the γ_c value (33 dyne/cm) for amorphous polystyrene, where the edge contribution of the benzene ring must be important for steric reasons[1,2].

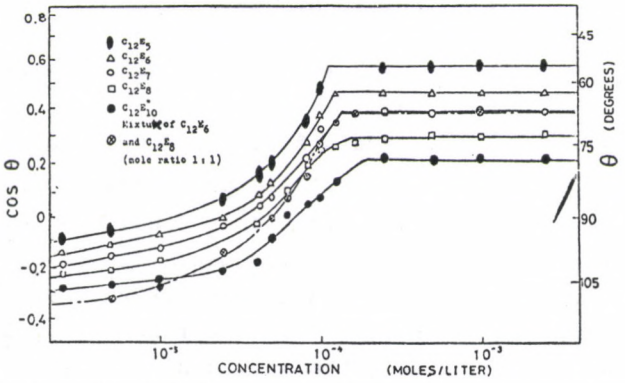

Fig. 3. COS θ versus concentration curves obtained with the nonionic surfactant solutions.

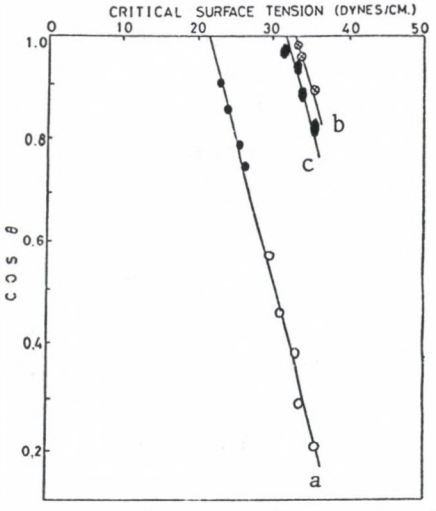

Fig. 4. Surface tension versus COS θ curves for barium stearate(a), PVBen-A(b) and PVBen(c) multilayers obtained with n-alkanes and nonionic surfactants.

Thus, PVBen multilayers might produces the close-packed benzene ring-rich surface due to strong intermolecular cohesion between benzene rings.

REFERENCES

1). M.K. Bernett and W.A.Zisman, J.Phys. Chem.,63,1241(1959).
2). M.K. Bernett and W.A.Zisman, J.Phys. Chem.,63,1911(1959).
3). W.A. Zisman , Contact Angle, Wettability and Adhesion (Advan. Chem. Ser. 43),American Chemical Society,Washington, D.C.,1964.
4). H.W. Fox and W.A.Zisman,J.Colloid Sci.,5,514(L950).
5). H.W.Fox and W.A.Zisman,J.Colloid Sci.,7,109(1952).
6). H.W.Fox and W.A.Zisman,J.Colloid Sci.,7,428(1952).
7). E.F.Hare and W.A.Zisman,J.Phys.Chem.,59,335(1955).
8). H.W.Fox and W.A.Zisman,J.Phys.Chem.,59,1097(1955).
9). S.Newman,J.Colloid Interface Sci.,25,341(1967).
10). F.M.Forkes,Chemistry and Physics of Interfaces,American Chemical Society.Washington,D.C.,1965.
11). H.W.Fox,E.F.Hare and W.A.Zisman,J.Colloid Sci.,8,194(1953)
12). A.E.Ellison and W.A.Zisman,J.Phys.Chem.,58,503(1954).
13). D.K.Owens,J.Appl.Polymer Sci.,13,1741(1969).
14). J.R.Dann,J.Colloid Interface Sci.,32,302(1970).
15). S.Wu,J.Polymer Sci.,part C,34,19(1971).
16). W.R.Good,J.Colloid Interface Sci.,44,63(1972).
17). J.Panzer,J.Colloid Interface Sci.,44,142(1973).
18). A.El-Shimi and E.D. Goddard,J.Colloid Interface Sci.,48, 242(1974).
19). I.Langmuir,Trans.Faraday Soc.,15,68(1920).
20). K.B.Blodgett,J.Amer.Chem.Soc.,56,495(1934).
21). K.B.Blodgett,J.Amer.Chem.Soc.,57,1007(1934).
22). K.B.Blodgett and I.Langmuir,Phys.Rev.,51,964(1937).
23). J.A.Spink and J.V.Sanders,Trans.Faraday Soc.,51,1154(1955)
24). J.W.Ellis and J.L.Paully,J.Colloid Sci.,19,755(1964).

CAPILLARY RISE AND THE CONTACT ANGLE GLASS - HEXANE

J. van Brakel and P.M. Heertjes

Delft University of Technology, Laboratorium voor Chemische Technologie, Julianalaan 136, Delft (The Netherlands)

Capillary rise of a liquid in a homogeneous packing of spherical or rotund particles cannot be described in a simple way |1|. The phenomena observed fall under four classes, to be described below. The same solid-liquid combination can come under more than one class. This depends on the value of the contact angle, θ, and on the fact whether the latter changes during capillary rise.

It appears that for glass-hexane θ may take various values. Most of the available knowledge |2,3| suggests that the contact angle glass-hexane should be equal to zero. Possible secondary phenomena that might explain apparent finite contact angles will be discussed as well as the possibility of true finite contact angles for glass-hexane.

Experimental methods

Capillary rise experiments are performed by submerging a packing of 300-400 μm glass beads 2 mm below a *n*-hexane surface, which is kept at a constant level. The packing is contained by a glass tube of 23 mm diameter and supported by a glass filter, or it is slightly sintered, in which case no support is needed. The packing is prepared using a controlled deposition and vibration technique. The homogeneity is checked by means of x-ray absorption. The capillary rise is observed visually or by x-rays. When there is a sharp liquid front both methods give the same result. The packing, x-ray absorption, and sintering techniques have been described in detail elsewhere |4|.

Results

Two criteria are used in classifying the observed phenomena. The first is whether a saturation gradient is observed in the equilibrium situation after capillary rise. That is to say, whether, at equilibrium, there is a sharp front or a gradual change between the completely saturated and the dry part of the porous medium.(Hence, an equivalent radius model predicts no saturation gradient and a "pore size distribution" model predicts a saturation

gradient.)

The second criterion is whether the movement of the sharp liquid front can be described by the Kozeny equation |1|,

$$\frac{dh}{dt} = \frac{k}{h} (h_c - h) \qquad (1)$$

with h the height of capillary rise at time t, and k and h_c constants for a certain solid-liquid combination, k representing the resistance to viscous flow and h_c the capillary force. (This equation can be compared with the Poiseuille or Darcy equation.) For packings of rotund particles eq.(1) can be chequed on two points : (i) the relation between dh/dt and $1/h$ should be linear, (ii) the value of k should be approximately correct.

The characteristics of the four classes are as follows :

Class Ia. At first there is a rapid capillary rise of a sharp liquid front, for which eq. (1) is valid (see Fig. 1). After a few minutes a

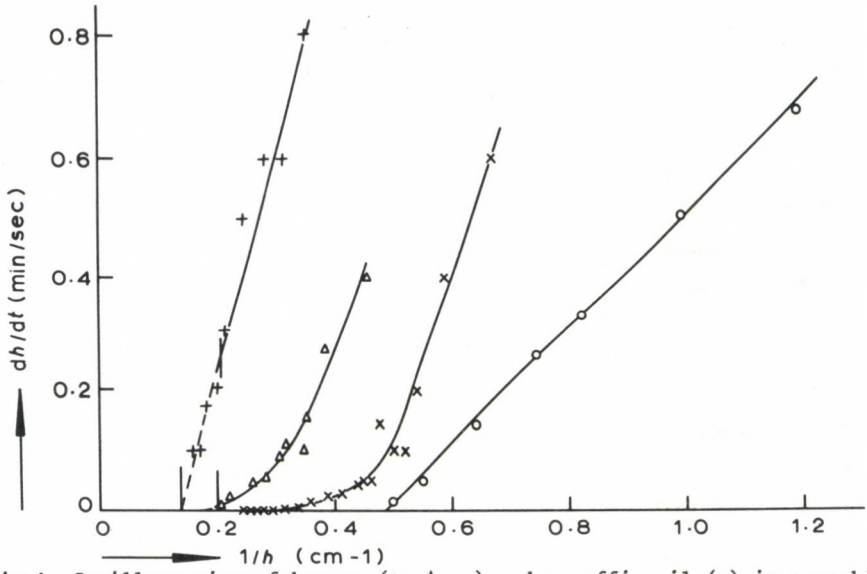

Fig.1. Capillary rise of hexane (+, Δ, x) and paraffin oil (o) in a packing of 300-400 μm glass beads.

+, class Ia, between vertical strokes development of a saturation gradient (see Fig. 2).

Δ, class Ib, after vertical stroke development of a saturation gradient

o, class IIa, coordinates on vertical scale have to be multiplied by 100.

x, class IIb, cf Fig. 2.

saturation gradient starts to develop (see Fig. 2).

Class Ib. At first there is a more slow capillary rise of a sharp liquid front, for which eq (1) does not hold (see Fig. 1). After a number of hours a saturation gradient starts to develop.

Class IIa. Rapid capillary rise of a sharp liquid front is observed, for which eq. (1) is valid. At equilibrium there is no saturation gradient. This behaviour has not been observed for glass-hexane. In Fig. 1 the results are given for glass beads - paraffin oil, which system displays IIa behaviour.

Class IIb. Eq. (1) does not hold (see Fig. 1). At equilibrium no saturation gradient is observed (see Fig 2). The maximum capillary rise for IIa and IIb systems is always lower than that for the corresponding Ia or Ib system.

In the sequel Ia, etc will be used as adjectives, referring to the characteristics as described above.

The capillary rise for many other solid-liquid combinations has been

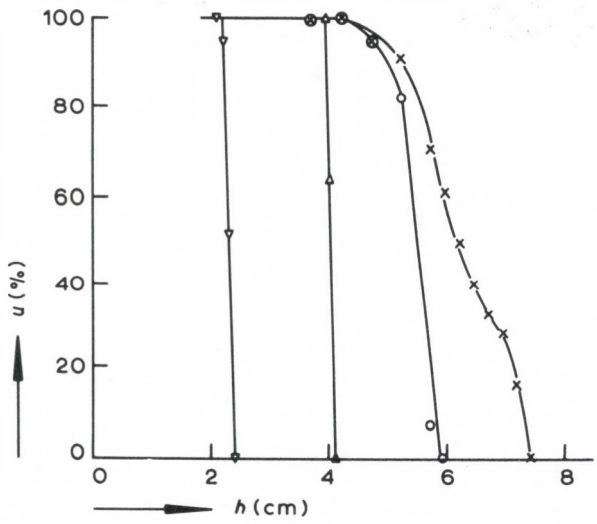

Fig. 2. Capillary rise of hexane in a packing of 300-400 μm glass beads.
u is the %vol of porespace saturated with liquid.
Experiment from class IIb : ∇, 30 min; Δ, 50 h (equilibrium)
Experiment from class Ia : Δ, 1 min; o, 3 min; x,30 min (equilibrium). No saturation gradient means, operationally, a saturation gradient not wider than 1 mm.

studied. It appears that IIa behaviour is extremely rare. This is of interest because various experimental techniques, e g the Bartell and Washburn methods to determine the contact angle, presuppose IIa behaviour.

Capillary rise and the contact angle

Given the occurrence of four kinds of capillary rise a large number of ad hoc hypotheses can be invoked, concerning matters such as : consolidation of the packing, various aspects of non-homogeneity, evaporation, capillary condensation, presence of phase to be displaced |5|. These subjects cannot be discussed here, but it should be noted that the *same* packing with the same rising liquid can come under different classes.

The results are interpreted as follows. A wide saturation gradient (class Ia and Ib) will be observed when $\theta = 0$. No saturation gradient (class IIa and IIb) will be observed when θ is above some critical value |6|. When eq. (1) does not hold, as for class Ib and IIb, this can be ascribed to a contact angle which decreases during capillary rise |5|.

The consequence of this interpretation is that, apparently, glass-hexane, which shows Ia, Ib, and IIb behaviour, does not necessarily have $\theta = 0$. Possible explanations for this fact are discussed in the next section. The further question as to which mechanisms may cause the contact angle to decrease with time will not be discussed in the present paper.

Contact angle glass - hexane

If hexane sometimes yields $\theta = 0$ (class Ia), while in other cases $\theta >> 0$ (class IIb), or a contact angle decreasing during capillary rise from some finite value to approximately zero (class Ib), this may be due to the presence of other components or to the fact that the glass surfaces are not identical. For an evaluation of these points the following experimental data are relevant.

As yet it is not possible to induce a certain class behaviour for a given batch of glass beads. Experiments have been performed with various kinds of soda glass, various kinds of lead glass, a borosilicate glass, and an alumina silicate glass. Without surface treatment most glass beads display Ib behaviour. Numerous cleaning procedures have been applied. In general these tend to increase the contact angle.

Ia behaviour, hence $\theta = 0$, has been observed for soda glass treated with hydrogen fluoric acid and for lead glass that had been subjected to a heat treatment. But Ia behaviour cannot be thus obtained for all soda and lead

glasses. Hence the unknown part of the history of the glass is more important than the surface treatment.

Subsequent experiments performed upon the same packing give reproducible results. That is to say that, in a Ib or IIb experiment, the surface does not undergo irreversible changes.

Ia glass beads lose their Ia behaviour when cleaning procedures involving sulfo-chromic acid are applied. They also lose their Ia behaviour after being exposed to the atmosphere for two years. Sand, which always yields a Ia behaviour with hexane, does not lose its Ia behaviour when subjected to the same treatments.

Hexane of different sources has been used, distilled and dried under various conditions. This does not influence the results for a given batch of glass beads. Similar results as for hexane are found for heptane and toluene. Glass beads yielding a IIb behaviour give the same maximum capillary rise for hexane and toluene (after correction for the density and the surface tension).

On the basis of these results it is concluded that no unknown components interfere at the interface glass-water-hexane. The contact angle is a function of the nature of the water layer on the glass surface. This result does not seem to be in concordance with existing knowledge on contact angles. The approaches of Zisman and Fowkes will be mentioned briefly.

Critical surface tensions of glass are reported to be in the range 19-44 dynes/cm |7|. Therefore hexane, with a surface tension of 18 should yield $\theta = 0$, not being an autophobic liquid. Small concentrations of contaminants may lower the critical surface tension, γ_c, of a solid. However, from the extensive studies of Zisman et al it follows that all organic molecules, except fluorinated compounds, yield $\gamma_c > 22$ |2| and give $\theta = 0$ for alkanes below nonane |8|.

Fowkes approach |3|, assuming a negligible film pressure, predicts $\theta > 0$ when $\gamma_S^d < 18$, γ_S^d being the contribution of the dispersion forces to the solid surface tension, in this case equal to the γ_L^d of water, which has been reported as 21.8 |3|. Although the latter value may be disputed |9|, it would seem that also on this account $\theta = 0$ for glass-hexane.

There is some controversy in the literature as to whether the value of the film pressure is significant for systems that display $\theta > 0$. The present results suggest that the value of the film pressure can be significant for oxide surfaces under normal conditions (i e with a hydratation layer) and that lower alkanes may form non-duplex films on these surfaces.

This implies that alkanes can form structured polymolecular adsorption layers on hydrated glass. Other experimental data and theoretical considerations supporting this have been reported [9,10].

Conclusions

From capillary rise experiments it appears that hexane in contact with hydrated glass may display a finite contact angle. During capillary rise the contact angle may decrease.

It is improbable that this finite contact angle is due to unknown contaminants.

The lower alkanes may yield significant film pressures and non-duplex films on hydrated surfaces.

Acknowledgements

The experimental work was carried out by Monsieur D.R.Y. Karboviac and Mr. A.H.A.P. Veer.

References

1. J. van Brakel, Powder Technol. 11 (1975) 205.
2. W.A. Zisman, Adv.Chem.Series 43 (1964) 1.
3. F.M. Fowkes, Adv.Chem.Series 43 (1964) 99.
   F.M. Fowkes, Wetting, S.C.I. Monograph (25)(1967) 3, 42.
4. J. van Brakel and P.M. Heertjes, Powder Technol. 9 (1974) 263.
5. to be published.
6. J. van Brakel and P.M. Heertjes, Nature 254 (1975) 585.
7. D.H. Kaelble, Physical Chemistry of Adhesion, Wiley-Interscience, New York (1971) 180.
   K. Tesařík and M. Nečasová, J.Chrom. 65 (1972) 39.
   A. Liberti, in : Gas Chromatography (A.B. Littlewood, Ed.), Elsevier, Amsterdam (1966) 95.
   F. Farré-Rius, J. Henniker, and G. Guiochon, Nature 196 (1962) 63.
8. F. Schulman and W.A. Zisman, J.Colloid Sci. 7 (1952) 465.
   E.G. Shafrin and W.A. Zisman, J.Colloid Sci. 7 (1952) 166.
9. J.N. Israelschvili, J.Chem.Soc., Far.Trans. II 69 (1973) 1729.
10. D.H. Bangham and Z. Saweris, Trans.Far.Soc. 34 (1938) 554.
    D.H. Bangham and R.I. Razouk, Trans.Far.Soc. 33 (1937) 1459.
    K.W. Bewig and W.A. Zisman, J.Phys.Chem. 68 (1964) 1804.
    A.W. Adamson, J.Colloid Interf.Sci. 27 (1968) 180.
    M. Blank and R.H. Ottewil, J.Phys.Chem. 68 (1964) 2206.
    G. Curthoys, V. Ya. Davydov, A.V. Kiselev, S.A. Kiselev, and B.V. Kuznetsov, J.Colloid Interf.Sci. 48 (1974) 58.
    T.D. Blake and W.H. Wade, J.Phys.Chem. 76 (1972) 675.
    T.D. Blake, J.L. Cayias, W.H. Wade, and J.Z. Zerdecki, J.Colloid Interf. Sci. 37 (1971) 678.
    I.E. Dzyaloshinskii, E.M. Lifshitz, and L.P. Pitaevskii, Adv.Physics 10 (1961) 165.
    A.D. Read and J.A. Kitchener, Wetting, S.C.I. Monograph (25) (1967) 300.

THE INFLUENCE OF CONCENTRATION AND COMPOSITION CHANGES IN ASCENDING MENISCUS REGION ON THE CAPILLARY RISE OF SOLUTION IN POROUS SYSTEMS

O.N.Grigorov and E.V.Gribanova

Leningrad State University, Chemical Faculty, Leningrad, 199004, Sredny pr. 41/43, USSR

As has been shown /1/ concentration of interaction products of the capillary ascending solution with the solid surface was observed even in such a weak interacting system as quartz - 10^{-3}N KCl solution /2/. This necessitates taking osmotic and electrokinetic phenomena into account in estimating the whole process of capillary rise.

The study of the KCl solution rising in quartz powder diaphragms /2/ shows that there is a total increase of electrolyte concentration due to Cl^- negative adsorption and also a change in cationic composition (a decrease of K^+ concentration and increase of H^+ concentration) owing to the ionic exchange between the quartz surface and KCl solution. The interaction product concentration in a relatively small volume of solution adjoining the meniscus leads to a marked influence of the capillary osmosis (owing to the concentration gradient) and electroosmosis (due to liquid junction potential) on the capillary rise process /1,2/.

The theory of the capillary (anomalous) osmosis was developed by Deryaguin and others /3/. According to this theory, the velocity of osmotic sliding in porous systems is composed of capillary osmosis velocity v_c and electroosmotic velocity v_e(when electrolytes are present):

$$v = v_c + v_e$$

In a general case, the solution sliding velocity along the solid wall due to the tangential concentration gradient is equal to:

$$v_c = -\frac{c_o \operatorname{grad} \mu}{\eta}\xi = \frac{RT}{\eta}\frac{\Delta c}{\Delta l}\xi \,, \qquad (1)$$

where η-the viscosity of the liquid; c_o-the bulk concentration of dissolved molecules; μ-the chemical potential; $\frac{\Delta c}{\Delta l}$-the concentration gradient; $\xi = \int_o^\infty (c - c_o)h\, dh/c_o$: here c - the concentration of dissolved molecules at the distance h from the plane of sliding, ξ-the value characterizing the thickness of the double layer.

In the case of dilute electrolyte solutions, ξ can be expressed according to Bolzmann's distribution through ζ-potential:

$$\xi^+ = \frac{\varepsilon\zeta}{4\pi F c z^+ z^-} \,; \qquad \zeta^- \ll |\xi^+| \quad (-\zeta \gg 25\text{mV}) \qquad (2)$$

where ε-the dielectric constant; F -Faraday number; z^+, z^--ion valences.

If there is a liquid junction potential in the system ($\Delta\varphi$) the electroosmosis velocity is equal to :

$$v_e = \frac{\varepsilon\zeta}{4\pi\eta l}\Delta\varphi \qquad (3)$$

Taking the meniscus region concentration changes into account, the capillary rise equation may be written as follows:

$$\frac{W(h\eta + h_a\eta_a)}{D_h}\frac{dh}{dt} + hg\gamma_l - P'_{cap}\cos\theta - P_{eo} - P_{co} = 0 \qquad (4)$$

where h and h_a - are the heights of the wetted and dry parts of the diaphragm; η_a- the air viscosity; W - porosity; D_h-permeability; γ_l- liquid density; g - the gravity acceleration; P'_{cap}- the equilibrium capillary pressure in the diaphragm; θ- the contact angle; P_{eo} and P_{co}- the electroosmotic and capillaryosmotic pressures, respectively.

The present work was carried out to investigate the kinetics of the capillary rise in quartz powder diaphragms in the presence or absence of concentration changes in the meniscus region. To estimate the capillaryosmotic and electroosmotic components of the process we have studied the influence of identical concentration gradients of electrolyte (HCl) and nonelectrolyte (saccharose).

Experimental

Experiments were carried out with quartz powder diaphragms

(fraction 20-50μ). To purify the quartz surface, the powder was preliminary treated with HNO_3 solution (1:3), then washed out with a large excess of distilled water to a constant pH-value, and dried at 105°C.

To create the concentration gradient in the zone of ascending liquid, one part of the quartz powder was treated with 5.10^{-3}N HCl solution and another with the solution of saccharose (5.10^{-3}M). The treated powders were sucked off on the Buchner funnel and then dried at 105°C.

The experiments on capillary rise were carried out according to Jamin's counterpressure method, described in /1/. The equation of the capillary rise process for Jamin's method may be written as follows:

$$\frac{W(h\rho + h_a \rho_a)}{D_h} \frac{dh}{dt} + hg\gamma_1 + P_{cp} - P'_{cap}\cos\theta - P_{eo} - P_{co} = 0 \quad (5)$$

where P_{cp} is the value of counterpressure at the time t.

During the experiments dependences P_{cp} - t and h - t were measured. The values of D_h and ζ-potential were measured in separate experiments by standard methods /4/. Also, analytical determination of K^+, Cl^-, pH, dissolved silica and saccharose was carried out according to /2/.

The study of kinetics of capillary rise of water and 10^{-3}N KCl solution was made in diaphragms of the pure quartz, of the quartz treated with HCl and the quartz treated with saccharose. The measurement results show that the curves of capillary rise in quartz treated with saccharose in all cases lie considerably higher than those of the rise in pure quartz and quartz treated with HCl. The curves of the capillary rise in the quartz treated with HCl at the beginning of the experiment lie lower, than the curves for pure quartz during the capillary rise both for water and KCl solution.

These experiments allow to estimate the total value of the active pressure at different velocities of the capillary rise by the equation (5):

$$P = P'_{cap}\cos\theta + P_{eo} + P_{co} = \frac{W(h\rho + h_a \rho_a)}{D_h} \frac{dh}{dt} + hg\gamma_1 + P_{cp} \quad (6)$$

The results of the calculation in the form of dependences ΣP on $\lg\frac{dh}{dt}$ are given in Fig.1(a and b). In Fig.1 one sees a

marked scattering of the points obtained in parallel experiments, but the character of the dependences for each separate treatment is preserved. Similar dispersion was observed earlier as well /5/, and it may be connected with the different packing of particles in the diaphragms and also with changes in the air moisture, which is known to influence strongly /6/ the contact angle.

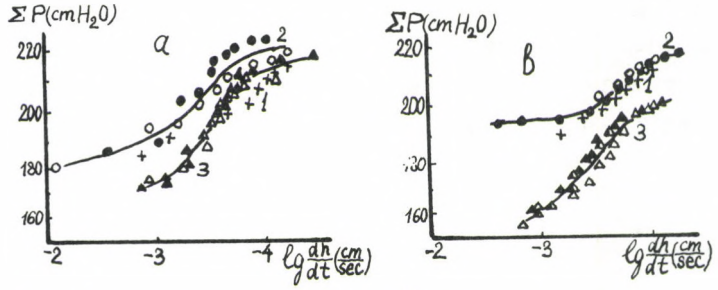

Fig.1. Dependence $\Sigma P - \lg\frac{dh}{dt}$ in capillary rise of water (a) and KCl solution (b): 1 - pure quartz (+); 2 - quartz treated with saccharose (o,●); 3 - quartz treated with HCl (△,▲,▲).

In /1/ it is shown, that the $\cos\theta$ values calculated by eq. (5) from the experiments on capillary rise of water in the diaphragms of pure quartz (fractions 20-50 and 50-100μ) for different rise velocities correspond to the values of $\cos\theta$, which were measured in the quartz slit with the same meniscus velocities. Thus, the capillary rise of water in pure quartz sand, measured by Jamin's method is to be considered as being free from the influence of concentration changes. Dependences $\Sigma P - \lg\frac{dh}{dt}$ for capillary rise in pure quartz are linear in all cases (Fig.1). Fig.1 also shows that treating with saccharose increases considerably the process of capillary rise, especially at small heights (at great velocities), but treating with acid decreases it.

Fig.2(a,b,c) shows the influence of electrolyte on capillary rise process with different preliminary treatments of the quartz. It is seen quite clearly the influence of electrolyte on rising in the quartz treated with acid and saccharose. The curve characters for KCl solution is like that for water, but they are situated lower, especially for acid treated quartz

(Fig.2b). In pure quartz the presence of electrolyte does not practically influence the capillary rise (Fig.2a).

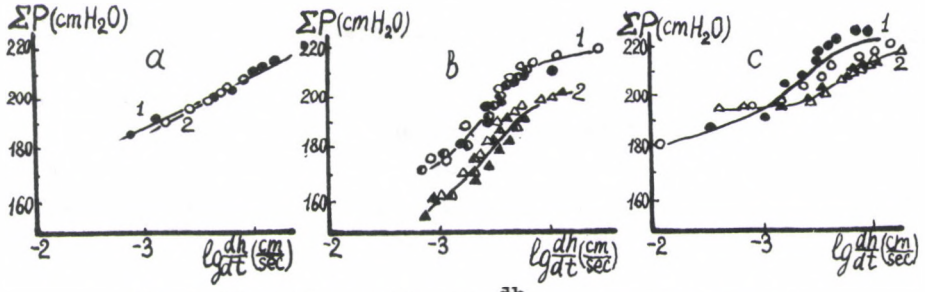

Fig.2. Dependence $\Sigma P - \lg\frac{dh}{dt}$ in capillary rise in diaphragms of pure quartz (a), quartz treated with HCl (b) and quartz treated with saccharose (c): 1 - water; 2 - KCl solution.

Analytical determination of the component content in a rising solution gives the results, that are in agreement with our previous data /2/. The greatest concentration of acid and saccharose are observed in the first portion of the solution, i.e. in the zone 3-5cm below the meniscus and reaches the values of 25-30mg.eq/L.

The results obtained show, that in the upper part of capillary ascending liquid the considerable concentration gradients of dissolved substances arise. Unfortunately the methods of analytical determination of solute composition don't allow to obtain a sufficiently small portion of the solution to receive more exact the concentration distribution in a thin layer of solution near meniscus.

However, determinations of potentials appearing in the process of capillary rise /2/ permit to conclude that in meniscus region we can observe considerably greater concentration gradients than the results of analytical determination show. Thus, the calculation of concentration gradients from the measured values of liquid junction potentials at capillary rise of 10^{-3}N HCl solution in pure quartz (fraction 50-100μ) gives the value of 0,012gr.eq/Lcm, whilst the analytical determination of Cl^- in the first portion corresponding to 5cm of the height of diaphragm gives the value of 0,0011gr.eq/L only. It

is natural to suppose that in the quartz preliminary treated with 5.10^{-3}N HCl solution or saccharose the concentration gradients arising in the ascending meniscus region should be considerably greater, than in pure quartz,and can reach the values of 0,1 - 1gr.eq/L.cm in order.

The Table1 gives the calculated results of capillaryosmotic flow velocities for different gradients of concentration by eqs.(1) and (2). In a separate column of the Table the values of capillaryosmotic pressure estimated by the following formula are given:

$$P_{co} = \frac{W\rho l}{D_h} v_c \qquad (7)$$

Table 1. Results of calculation of capillaryosmotic velocity and pressure.

grad c(gr.eq/L.cm)	$v_c.10^4$(cm/sec)	P_{co}(cm H_2O)
0.01	2.02	2.28
0.02	4.03	4.58
0.04	8.07	9.17
0.08	16.10	18.34

The Table 1 shows that the appearance of the concentration gradients observed experimentally in the meniscus region can stimulate sufficiently great velocities of the capillaryosmotic flow therefore invoke a considerable change in kinetics of capillary rise. The deviation of dependence $\Sigma P - \lg\frac{dh}{dt}$ for quartz pretreated with saccharose from that for pure quartz (Fig.1,2) is 5-20cm H_2O and is in accordance with the values of P_{co} given in Table 1.

The character of the dependence $\Sigma P - \lg\frac{dh}{dt}$ (Fig.1,2) for the quartz treated with acid can seem unexpected. In fact, with the same concentration gradients of HCl and saccharose in the meniscus region the capillary rise in quartz treated with HCl should be even greater than that for the quartz which was pretreated with saccharose, HCl being electrolyte. But the values of total pressure developing in the process in this case were much smaller, than even for the pure quartz. Such behaviour of the system is probably to be explained by assuming that the

surface of quartz in this process receives an effective positive charge owing to slowing down of the process of HCl desorption from the quartz surface. In fact, as was shown in /7/, during the capillary rise of 10^{-3}N KCl solution in the quartz preliminary treated with HCl the positive values of streaming potential were measured, in spite of the fact that the pH-value of the solution displaced from the diaphragm exceeded the isoelectric point. In the case of positive surface charge the electroosmotic flow, caused by liquid junction potential, is directed downward and thus slowed the process of capillary rise that we have observed experimentally.

Much greater negative effect in the case of capillary rise of KCl solution in quartz treated with HCl (Fig.2b) perhaps may be connected with the slowing down of desorption of HCl molecules from the quartz surface in KCl solution, as compared with desorption in water, which increased the effective positive charge of the surface.

Fig.1,2 also show that the efficiency of surface treatment is connected not so much with the height of capillary rise, as it may be expected (with the increase of height the total value of dissolved substances also grows) but with the velocity of solution boundary. This may probably be explained by greater velocities of rising in the narrow part of meniscus region which lead to greater gradients of concentration, the process of diffusion being less active here. This gives a greater effect of capillaryosmotic flow on the capillary rise at the beginning of the process when comparatively greater velocities take place.

The experiments carried out allow to conclude that the interaction of a solid body with a liquid influences considerably the kinetics of capillary rise, the nature of the interacting substances determining the type of the influence.

References

/1/. E.V.Gribanova, O.N.Grigorov, "Pore structure and properties of materials", Proceedings of the International Symposium, Prague, 1973, Part 2, C-341.

/2/.E.V.Gribanova, L.V.Grabek, O.N.Grigorov,"Electro poverkhnostnye yavleniya v dispersnykh sistemakh", collection, Moskva, Nauka, 1972, S.103.

/3/ B.V.Deryaguin, S.S.Dukhin, M.M.Koptelova, Kolloidn.Zh. 31, 3, 1969, 359-369.

/4/ Electrokinetitscheskiye svoystva capillarnykh sistem (Electrokinetic properties of capillary systems), collection, Moskva-Leningrad, Izd. AN SSSR, 1956.

/5/ O.N.Grigorov, E.V.Gribanova, L.M.Kalyuzhnaya, Zh.Prikl. Khim., 41, 3, 1968, 557-562.

/6/ S.A.Vladychenskii, Pochvoved., 10, 1962, 62.

/7/ E.V.Gribanova, Candidate's dissertation, Leningrad, 1970.

SOME PROBLEMS IN DETERMINATION OF INTERFACIAL TENSION BY MEASURING THE FORCES EXERTED ON SOLID BODIES

Ch. Fieber, H. Sonntag

Zentralinstitut für physikalische Chemie der
Akademie der Wissenschaften der DDR,
1199 Berlin, Rudower Chaussee 5,
German Democratic Republic

Among the various methods to determine interfacial tension, those based on force measurement with bodies immersed into the phase boundary are most suitable in respect to expense in experimental performance and evaluation. A deciding disadvantage, however, arises from the uncertainity of contact angle, and, in some cases, from lack in theorie. To overcome these difficulties solid spheres are used recently as immersing bodies. By measuring the maximum force exerted on a small glass sphere, combined with an optical angle measurement, Sheludko /1/ obtained very accurate values of surface tension using the tables of Chun and Scriven /2/ for computation.

The following theoretical analysis of forces acting on a sphere /3/ offers the possibility of a simultaneous estimation of interfacial tension and contact angle. Starting point for this elaboration was the reflection, that the direction of the force vector of interfacial tension may be altered at choice by varying the depth of immersion.

The figure shows the geometrical relations necessary to understand the following statement. A sphere of radius R is situated in the phase boundary between two fluid phases. The origin of coordinates is fixed to the centre of the sphere. Because of rotational symmetry only the vertical components of forces are to be considered. Provided that the sphere has been tared in phase 1, the net force in the phase boundary is

$$P = P_\sigma + P_A + P_H \qquad (1)$$

The interfacial tension σ acts on the three-phase contact line $2\pi r_0$ under the contact angle ϑ and causes a force $P_{0,\sigma}$. Its vertical component is

$$P = 2\pi r_0 \sigma \cos(\alpha + \vartheta) \qquad (2)$$

or, together with

$$r_0 = R \cos\alpha \qquad (3)$$

$$P = 2\pi R \sigma \cos\alpha \cos(\alpha + \vartheta) \qquad (4)$$

Using the relation

$$s + h = R \sin\alpha \qquad (5)$$

the buoyancy P_A may be expressed in terms of α

$$-P_A = \frac{\pi}{3} R^3 \Delta\varrho\, g\, (2 + 3\sin\alpha - \sin^3\alpha) \qquad (6)$$

where $\Delta\varrho$ is the difference in density between the two phases and g is the acceleration due to gravity.

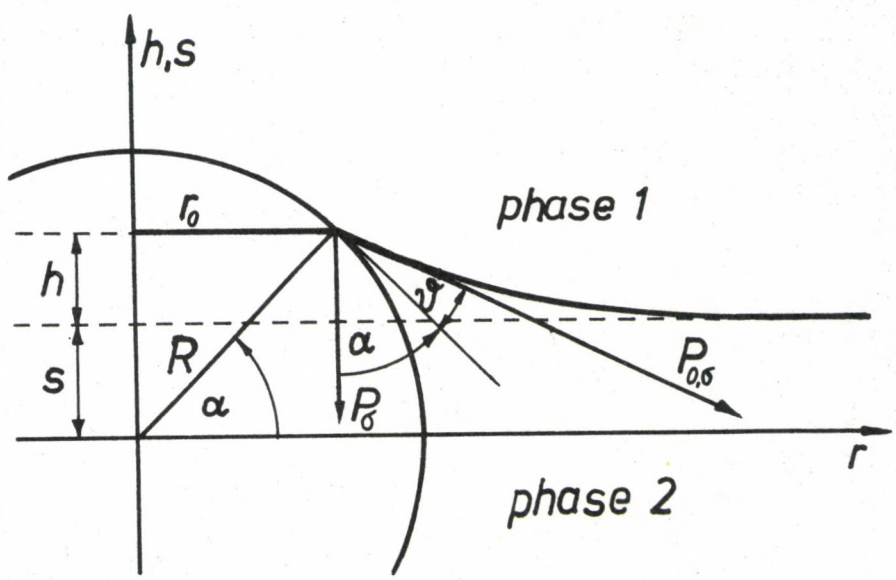

The last term of equation (1) is the hydrostatic pressure originating from the difference in level between the three-phase contact line and the fluid interface. This pressure acts on an effective area $\pi r_0^2 = \pi R^2 \cos^2$.

Hence

$$P_H = \pi R^2 \Delta\varrho \; g \; h \cos^2 \tag{7}$$

Substituting for h leads to

$$P_H = \pi R^3 \Delta\varrho \; g \cos^2\alpha \; (\sin\alpha - z) \tag{8}$$

whre $z = s/R$.

Now equ. (1) can be written in detailed form

$$P = 2\pi R\sigma \cos\alpha \cos(\alpha+\vartheta) - \frac{\pi}{3} R^3 \Delta\varrho \; g \; (2 + 3\sin\alpha - \sin^3\alpha)$$

$$+ \pi R^3 \Delta\varrho \; g \cos^2\alpha \; (\sin\alpha - z) \tag{9}$$

If P is measured as a function of z equ. (9) contains the unknown quantities α, ϑ and σ. The contact angle ϑ, however, can be estimated from the measured function $P = f(z)$ by an operation initiated by Yarnold /4/.

There is a special position of the sphere in which the height h is equal to zero, i.e. the menisque shows no curvature. Then

$$\alpha + \vartheta = \frac{\pi}{2} \tag{10}$$

$$\sin\alpha = z \tag{11}$$

and the forces P and P_H vanish.

The remaining buoyancy becomes

$$- P_{A(h=0)} = \frac{\pi}{3} \Delta\varrho \; g \; R^3 \; (2 + 3z - z^3) \tag{12}$$

The point of intersection of the calculable function (12) with the measured function $P = f(z)$ gives the value of z at $h = 0$.

Hence follows from equations (10) and (11)

$$\cos \vartheta = z_{(h=0)} \tag{13}$$

Actually, α is related to z by Laplace's equation

$$\frac{\cos (\alpha + \vartheta)}{r} + \frac{d \sin (\alpha + \vartheta)}{d h} - \frac{\Delta \varrho g h}{\sigma} = 0 \tag{14}$$

but it is not possible to eliminate α in equ. (9) because there is no analytical solution of equation (14). In recent times advances have been made in integrating Laplace's equation numerically /2/, /5/. Chun and Scriven have presented tables containing pairs of values x,y for different values of ϕ . (These quantities are related to our system by $x^2 = r^2 \Delta \varrho \, g/\sigma$, $y^2 = h^2 \Delta \varrho \, g/\sigma$, $\phi = \frac{\pi}{2} - (\alpha + \vartheta)$). The use of these tables allows, on principle, the determination of σ from equ. (9), starting with an initial approximation of σ and reaching its final value iteratively. However, a complete table work including the whole scale of values is not at disposal yet.

Therefore we will take a new line in calculation to dispense the aid of tables. We make use of the possibility to measure not only P = f (z) but dP/dz = f (z), too.

The differentiation of equation (9) yields

$$- dP/d\alpha = 2\pi R \sigma \sin (2\alpha + \vartheta)$$

$$+ \pi R^3 \Delta \varrho \, g \left[\sin 2\alpha \, (\sin\alpha - z) + \cos^2\alpha \, dz/d\alpha \right] \tag{15}$$

and, after multiplication by $d\alpha /dz$

$$- dP/dz = \pi R^3 \Delta \varrho g \cos^2\alpha$$

$$+ \left\{ 2\pi R \sigma \sin (2\alpha + \vartheta) + \pi R^3 \Delta \varrho \, g \left[\sin 2\alpha \, (\sin\alpha - z) \right] \right\} d\alpha /dz \tag{16}$$

Solving Laplace's equation (14) for $dh/d\alpha$ leads to

$$\frac{dh}{d\alpha} = \frac{r \cos (\alpha + \vartheta)}{\frac{\Delta \varrho g h r}{\sigma} - \cos (\alpha + \vartheta)} \tag{17}$$

In case of $r = r_o$, the relations (3) and (5) can be applied to equation (17)

$$\left(\frac{dh}{d\alpha}\right)_{(r=r_o)} = \frac{R\, d\,(\sin\alpha - z)}{d\alpha}$$

$$= \frac{R \cos\alpha \cos(\alpha+\vartheta)}{\frac{\Delta\varrho\, g}{\sigma} R^2 \cos\alpha\,(\sin\alpha - z) - \cos(\alpha+\vartheta)} \qquad (18)$$

and, finally, we obtain

$$\frac{dz}{d\alpha} = \cos\alpha\left[1 - \frac{1}{\frac{\Delta\varrho\, g}{\sigma} R^2 \frac{\cos\alpha\,(\sin\alpha - z)}{\cos(\alpha+\vartheta)}}\right] \qquad (19)$$

Substituting for $d\alpha/dz$ in equ. (16) at last leads to a second equation containing just the same unknown quantities α and σ as equation (9) does,

$$-dP/dz = \pi R^3 \Delta\varrho\, g \cos^2\alpha$$

$$+ \frac{2\pi R\sigma \sin(2\alpha+\vartheta) + \pi R^3 \Delta\varrho\, g \sin 2\alpha\,(\sin\alpha - z)}{\cos\alpha\left[1 - \frac{1}{\frac{\Delta\varrho\, g}{\sigma} R^2 \frac{\cos\alpha\,(\sin\alpha - z)}{\cos(\alpha+\vartheta)} - 1}\right]} \qquad (20)$$

Form the pair of equations (9) and (20) both unknown quantities α and σ can readily be calculated.

A set of values R, g, $\Delta\varrho$, ϑ, P, dP/dz, z, is given to a computer to find out

Thus, the above analysis shows that the measurable function $P = f(z)$ includes all informations to determine σ exactly without any knowledge of numerical solutions of Laplace's equation. The equations /6/ used for calculation do not include any limiting conditions except the contact angle to be constant during the time of measurement.

For the sake of lucidity the equations may be finally written in a suitable, dimensionless form

$$\frac{P}{\pi R^3 \Delta\varrho g} =$$

$$2\,B\cos\alpha\cos(\alpha+\vartheta) - \tfrac{1}{3}(2 + 3\sin\alpha - \sin^3\alpha)$$

$$+ \cos^2\alpha\,(\sin\alpha - z) \qquad (21)$$

$$-\frac{dP}{\pi R^3 \Delta\varrho g\, dz} = \cos^2\alpha + \frac{2B\sin(2\alpha+\vartheta) + \sin 2\alpha\,(\sin\alpha - z)}{\cos\alpha\left[1 - \dfrac{1}{\dfrac{\cos\alpha\,(\sin\alpha - z)}{B\cos(\alpha+\vartheta)} - 1}\right]} \qquad (22)$$

where $B = \dfrac{\sigma}{\Delta\varrho g R^2}$

Experimental results will be presented in brief, when this paper is read.

/1/ A. Sheludko, Colloid and Polymer Sci. (to be published)

/2/ H. Chun and L. E. Scriven, J. Colloid Interface Sci. 30 (1969)

/3/ H. M. Princen, in Surface and Colloid Science vol. II Wiley-Interscience (New York) 1969

/4/ G. D. Yarnold, Proc. Phys. Soc. 58 (1946)

/5/ J. F. Padday, Phil. Trans. A 269 (1971)

/6/ Ch. Fieber and H. Sonntag, Colloid and Polymer Sci. (in press)

EFFECT OF PREADSORBED SURFACTANT ON THE WETTABILITY OF POLYMERS

E.Wolfram and É.Boross-Vargha

Department of Colloid Science, L. Eötvös University, Budapest, Hungary

Introduction

The wettability of low-energy surfaces is usually interpreted in terms of either the critical surface tension, γ_c, or the polar and non-polar components of the surface free energy of the solid (1 - 9). Even in case of pure liquids, some uncertainty arises from the fact that the amount adsorbed from the vapour phase on the solid is mostly unknown although there is some evidence that the film pressure at the solid/vapour phase is likely to be small enough to be neglected for truly hydrophobic surfaces, like Teflon.

The situation is evidently more complicated when the wetting liquid is a surfactant solution, and it was very early shown that in this case the adsorption of the solute on each of the three interfaces involved, including the solid/vapour interface, is to be taken into account.

As a continuation of earlier studies in this Laboratory (10,11) in a recent work of one of us (12) the wettability of polytetrafluoroethylene (PTFE) and polyethylene terephthalate (PET) surfaces by aqueous solutions of ionic surfactants has been found to depend significantly on both the ionic character of the surfactant and the apparent polarity as characterized by the γ_c of the polymer. The advancing contact angle *vs.* surfactant concentration curves have been similar in type insofar that the contact angle decreases with increasing concentration up to the c_M then reaching a more or less constant value,

The surprising feature of these curves is that the said constant value does depend on the chain length for anionics on both surfaces as well as for cationics on PET but it does not for cationics on the non-polar Teflon.

There is no doubt that this finding is intimately related to the adsorbability of the surfactant at the solution/polymer interface. Unfortunately, a direct measurement of surfactant adsorption on the corresponding particulate polymers having a sufficiently large surface area for getting detectable amounts adsorbed from solution seems to be impracticable as there is no experimental procedure to prepare small polymer particles with the same surface properties as macroscopic sheets used for contact angle measurements do have.

The basic idea of the present work has been to check how a pretreatment of the polymer surface with the surfactants used earlier does effect the wettability of them by pure liquids. For characterizing the change in surface polarity due to modification by preliminary surfactant adsorption, the calculation procedures of Good, Fowkes and Wu have been used.

Experimental

PTFE (Teflon®, Du Pont) and PET (Hostaphan, Hoechst) sheets were used after washing them free from impurities. The removing of contaminations was controlled by measuring water contact angles. The alkyl sulfates from C_{12} to C_{18} (Marchon, Ltd., Whitehaven) were repeatedly recrystallized from a mixture (1 : 1) of ethyl alcohol and benzene, filtered and washed with acetone. The alkyl trimethyl ammonium bromides from C_{12} to C_{18} (Schuchardt) were recrystallized from a mixture of acetone and diethyl ether. The pure liquids (glycerol, formamide and methylene iodide) used in the experiments were "Anal. reagent" grade (E. Merck).

Surface tension γ_{LV} was determined by a du Noüy tensiometer (A. Krüss, Hamburg, accuracy $\pm$o,1 dynes.cm^{-1}). The advancing contact angle was measured using the projection goniometer described previously (10). The reproducibility of the contact angle measured on drops of o,o2 ml was $\pm$ 1°. The experiments were carried out at 25 $\pm$o,5°C.

The pretreatment of the surfaces has been performed as follows:
The PTFE and PET sheets were kept for 48 hours in the aqueous surfactant solutions the concentrations of which were equal to the c_M of each surfactant. After this treatment the sheets had been carefully dried in vacuo then the contact angle measurements were repeated with the four pure liquids and with solutions corresponding to the c_M of each of the detergents.

Results

From the data summarized in Table 1 it can be seen that the contact angles of the test liquids do not change systematically on the PTFE surface treated with either anionic or cationic solutions. For $\theta(c_M)$, i.e. the contact angle of the surfactant solution with $c = c_M$ almost the same values were obtained both on treated and untreated Teflon surface.

On treated PET surfaces the contact angle of the pure liquids decreases nearly to the same angle ($\theta \simeq 44^\circ$) independently of the liquid and the character of the surfactant. The drops of solutions with a concentration equal to, or larger than, the c_M, however, spread on the surface so that no contact angle could be observed. C_{18} homologs behaved exceptionally, here a very small contact angle (about 8-10 degrees) could be measured. The data given in Table 1 are the mean values of 10-20 measurements with a standard deviation from 1 to 9 per cent. It should be mentioned that the values of the cationics show a larger variance.

Discussion

Using the data of Table 1 and those for γ_{LV} calculations were made on the basis of the Good-Girifalco-Fowkes-Young (GGFY) and the Wu equations to estimate the non-polar (γ_s^d) and the polar (γ_s^p) component of the solid surface free energy, the total surface free energy of the solid ($\gamma_s = \gamma_s^d + \gamma_s^p$) and the apparent polarity ($P = \gamma_s^p / \gamma_s$). The results of the calculations are summarized in Table 2.

From these calculations it can be established that there is

Table 1

Contact angle of pure liquids on polymer surfaces at 25°C

a untreated

b treated with solutions of anionics, $c=c_M$

c treated with solutions of cationics, $c=c_M$

Liquid	Contact angle (degrees)					
	Teflon			PET		
	a	b	c	a	b	c
Water	116±1,5	118±1,3	107±4,4	77±0,6	47±3,0	37±6,7
Glycerol	103±0,6	110±3,7	103±8,6	60±1,4	48±3,0	44±1,2
Formamide	94±0,6	99±1,0	96±4,2	53±0,8	45±2,9	37±3,2
Methylene iodide	78±1,0	92±7,0	78±4,8	30±0,8	46±1,9	45±2,6

Table 2

Calculated surface energy components of polymers

solid		Teflon				PET			
		γ_s^d	γ_s^p	γ_s	p	γ_s^d	γ_s^p	γ_s	p
clean	a)	15,12	0,38	15,50	0,025	38,60	4,08	42,68	0,096
	b)	18,75	0,32	19,07	0,017	38,34	7,18	45,52	0,158
	c)	14,58	1,02	15,60	0,065	36,59	2,88	39,47	0,073
treated	a)	15,76	1,01	16,77	0,060	26,14	22,34	48,48	0,461

a) calculated from GGFY equation

b) calculated from the Wu equation

c) from reference (3)

no change in the calculated values of the surface energy components for the clean and treated PTFE surfaces. This indicates that no adsorption of the surfactants occurs on Teflon surfaces. For PET, however, the calculated values of γ_s^p and P increase after treating with surfactant solutions. The increase of P is more than fourfold. This phenomenon is attributed to the preferential adsorption of the surfactant molecules from the solution on the polar PET. The polar groups of the molecules at the S/L interface are oriented towards the aqueous solution and this gives rise to a surface with a higher value of the polar component of the solid surface energy than that of the original clean solid surface.

References

1. Contact Angle, Wettability and Adhesion, Advan. Chem.Ser. 43, (1964)
2. Wetting, S.C.I. Monograph No. 25, London (1967)
3. D.H. Kaelble, "Physical Chem. of Adhesion" Wiley, New York (1971)
4. L.A. Girifalco, R.J. Good, J. Phys. Chem. 61, 904 (1957)
5. F.M. Fowkes, Ind. Eng. Chem. 56, 40 (1964)
6. S. Wu, J. Polymer Sci. Part C. 34, 19 (1971)
7. J.R. Dann, J. Colloid Interface Sci. 32, 302 1970 ; ibid. 32, 321 (1970)
8. D.K. Owens, R.C. Wendt, J. Appl. Polymer Sci. 13, 1741 (1969)
9. Y. Tamai, H.J. Kobayashi, J. Colloid Interface Sci. 32, 369 (1970)
10. E. Wolfram, Kolloid-Z. Z. Polymere 182, 75 (1962)
11. E. Wolfram, É. Boross-Vargha, Annales Univ.Sci.Budapestin. Sect. Chim. 10, 43 1968 ; ibid. 11, 37 (1969) ; Fortschr. Kolloide u. Polymere 55, 143 (1971)
12. E. Wolfram, Croatica Chim. Acta 45, 137 (1973)

THE MODIFICATION OF COPPER-PHTHALOCYANINE PIGMENT SURFACES BY SURFACTANT ADSORPTION

A.Lőrinc and K. Steryopoulos
Research Laboratory for Applied Chemistry
and Colouristics, Budapest

The aim of our investigations was to increase the wettability by water of copper-phthalocyanine pigments by surfactant adsorption. By this modification of the surface it is possible to exert an advantageous influence on the colloid-chemical and applied-technological characteristics of the aqueous dispersions of the pigments.

We determined the adsorption of sodium dodecylsulphate and dodecyltrimethylammonium bromide on characteristical copper-phthalocyanine pigments and their chlorinated derivates.

We characterised the modification of the surface by the Harkins spreading coefficient as a function of the surfactant amount adsorbed on the basis of contact wetting measurements with liquids of different polarities and with the surface polarity calculated from the Young and the Fowkes equation; the latter was adapted to solid/liquid interface.

The contact-configurational state of equilibrium ensuing on the interaction between non-deformed solids and liquids, can be described by the Young equation:

$$\gamma_{LV} \cdot \cos\Theta = \gamma_{SV} - \gamma_{SL} - \gamma_{SO} - \pi_{SV} - \gamma_{SL} \qquad (1)$$

where γ = interfacial tension corresponding to the indices; S = solid phase; L = liquid phase; V = vapour phase; O = vacuum; Θ = contact angle; π_{SV} = surface pressure of the vapour layer adsorbed / experimentally it can be determined by vapour adsorption measurements/.

The degree of the spreading of the liquid can be given by Harkins' coefficient of spreading /S_{LSV}/ /1/:

$$S_{LSV} = \gamma_{SV} - \gamma_{SL} - \gamma_{LV} = \gamma_{SO} - \pi_{SV} - (\gamma_{SL} + \gamma_{LV}) = \gamma_{LV}(\cos\Theta - 1) + \pi_{SV} \quad (2)$$

For the characterisation of low-energy solid substrates the critical surface tension / γ_c/ suggested by Zisman /2/ could only be considered as an informative approximation. By combining Young's equation and Fowkes' one - the latter applied to the solid/liquid interface - the following correlation is obtained /3/:

$$\cos\Theta + 1 = 2\sqrt{\gamma_S^d}\,\frac{\sqrt{\gamma_L^d}}{\gamma_{LV}} + 2\sqrt{\gamma_S^p}\,\frac{\sqrt{\gamma_L^p}}{\gamma_{LV}} - \frac{\pi_{SV}}{\gamma_{LV}} \quad (3)$$

From this correlation - by using readily measurable values / $\gamma_{LV} = \gamma_L^d + \gamma_L^p$/ /5/, Θ, π_{SV}/ - the specific free energy of the solid surface / $\gamma_S = \gamma_S^d + \gamma_S^p$/ can be calculated.

The surface pressure / π_{SV}/ of the adsorbed vapour layer of the measuring liquids, under close scrutiny, in contrast with general assumptions, does not equal zero. If it is negligible or not, can only be decided if its actual value is known /4/.

Experimental

The adsorbed amount of surfactant was determined over a wide range of concentrations. Based on preliminary experiments it was found that the adsorption equilibrium was attained in about 15 hrs. The concentrations of the NaDS-solutions were determined by "Two-phase" titration, with hexadecyl-trimethylammonium bromide standard solution in the presence of Bromophenol Blue indicator. The concentrations of the DTAB-solutions were calculated by the back titration of the NaDS-solution of given volume and concentration, which had been added in excess /5/. The accuracy of the concentration determination was $\pm$ 1%.

The adsorbents used were C.I. Pigment Blue 15 /Heliogen Blau 7181-D; BASF/ and C.I.Pigment Green 7 /Monastral Green GN;ICI/. The latter was also applied after heat treatment at 240 °C for 5 hours in oxygen atmosphere. The specific surfaces of the pigment adsorbents were determined from the nitrogen isotherms by the BET-method.

The NaDS and DTAB were purified by recrystallization from organic solvent mixtures /6/. Their critical micelle concentration /c_M/ determined at 25,0 °C by surface tension and electric conductivity measurements, is as follows:

Surfactant	Measurement by	
	surface tension	electric conductivity
	c_M mmoles/l	
NaDS	8,1	8,2
DTAB	15,2	15,3

Determination of the contact angle

In order to carry out the contact wetting measurements, the pigment samples with modified surface had to prepared in "dry" state. The pigments were separated by centrifuging and the supernatant was removed by suction. The surfactant-modified pigment sediment as well as the non-modified pigments were dried at 80 °C in vacuum until constant weight was obtained.

The surface of the pigment samples prepared in this manner contained slightly more surfactant than the quantity adsorbed at equilibrium. This condition was disregarded. In oder to determine the contact angle in a precise and reliable way, pellets having smooth, coherent surfaces were prepared from the pigment powders and the contact angles were measured goniometrically. The surface of the pellets obtained by pressing is equivalent to a "real" coherent surface, from the measuring-technical point of view.

In order to scan the apolar and polar sites of the surface, distilled water and methylene iodide were used as measuring liquids. On each pellet the contact angles of 2-3 drops of both measuring liquids were determined. The mean value was calculated from the data determined on several pellets.

Results

Figures 1 and 2 show the adsorption isotherms of NaDS and DTAB.

Fig. 1

Adsorption of Sodium Dodecylsulfate on Copper Phthalocyanines Pigments

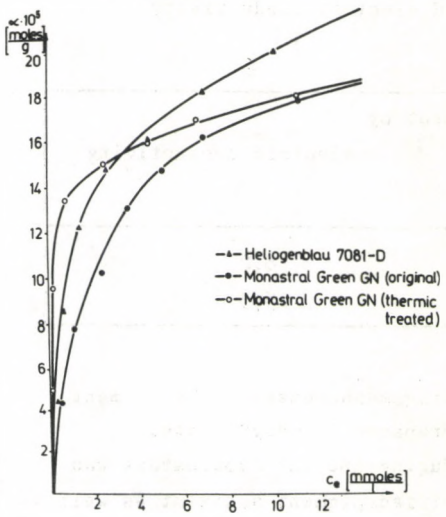

Fig. 2

Adsorption of Dodecyltrimethylammonium Bromide on Copper Phthalocyanine Pigments

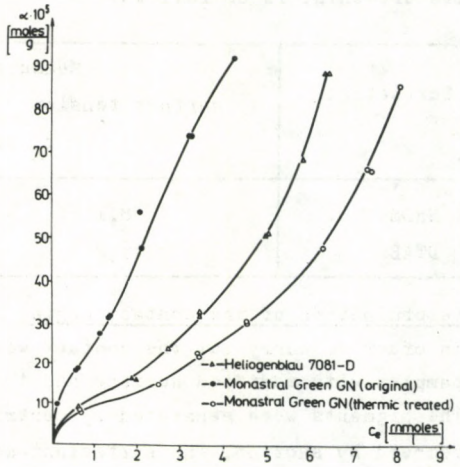

In some cases, at surfactant concentrations exceeding the critical micelle concentration, a small part of the pigment may become so highly dispersed that it can not be separated even by centrifuging for 3-4 hrs at 4500-5000 rpm. When determining the concentration of the supernatant, the small amount of surfactant desorbed from these particles may cause error, but this is negligible. Though such particles would be removable by ultra-filtration this technique was not applied because of the expected adsorption of the surfactant on the membrane. To calculate the spreading coefficient and the "surface polarity", the most obvious contact angle value $\bar{\Theta} = f(\alpha)$ was used. This was read from the curves pertaining to identical adsorbed surfactant quantities / $\bar{\Theta}$ = mean value of contact angle; α = adsorbed quantity of surfactant/.

The π_{SV} value related to methylene iodide vapour could not be determined on account of technical reasons. Therefore the π_{SV} values of both the methylene iodide and water vapours were taken to be zero, although the π_{SV} of water vapour measured on the pigments was found higher than nil.

a/ Wetting with water

Upon the increase of the quantity of surfactant adsorbed, S_{LVS} will increase /Fig.3 and 4/.

Fig. 3

The Change of the Spreading Coefficient of Water as a Function of the Sodium Dodecylsulfate Adsorption on Copper Phthalocyanine Pigments

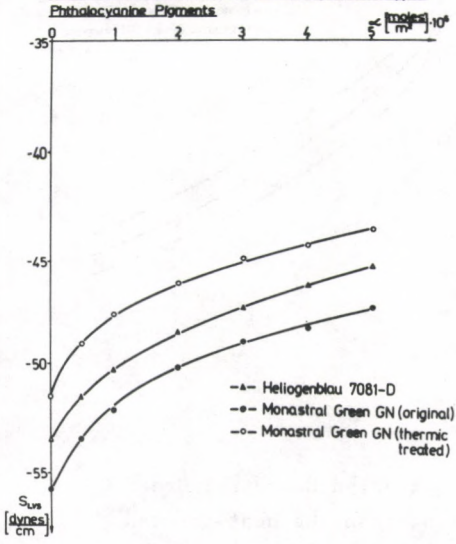

Fig. 4

The Change of the Spreading Coefficient of Water as a Function of the Dodecyltrimethylammonium Bromide Adsorption on Copper Phthalocyanine Pigments

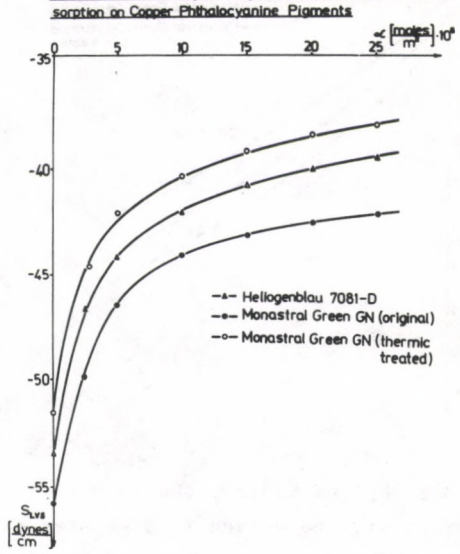

Uncovered pigments are wetted the least, whereas those covered by the largest amount of surfactant will be wetted most.

In the interaction between water and pigment the major part is played by dispersion forces. The heat treated Monastral Green GN pigment - at identical surfactant adsorption - will be wetted better than the thermally untreated sample. This is probably due to changes in crystal modification taking place during thermal treatment.

b/ Wetting with methylene iodide

With the increase of the quantity of surfactant adsorbed, the spreading coefficient /S_{LVS}/ is decreased /Fig. 5 and 6/. Best wetting is obtained on the uncovered pigments, whereas those covered with the highest amounts of adsorbed NaDS or DTAB will be wetted the least. In the interaction between the pigment and methylene iodide - similarly to water - the dispersion forces are of greatest importance.

Fig. 5

The Change of the Spreading Coefficient of Methylene Iodide as a Function of the Sodium Dodecylsulfate Adsorption on Copper Phthalocyanine Pigments

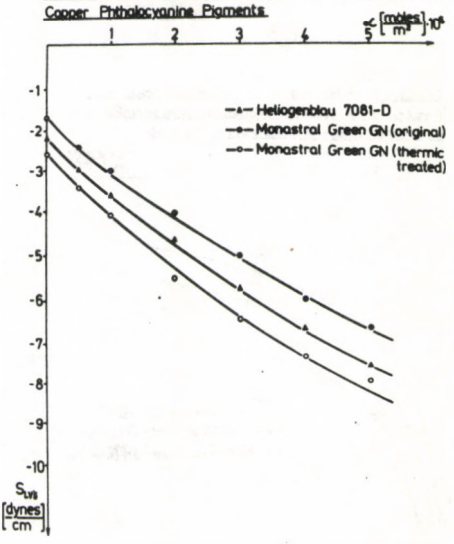

Fig. 6

The Change of the Spreading Coefficient of Methylene Iodide as a Function of the Dodecyltrimethylammonium Bromide Adsorption on Copper Phthalocyanine Pigments

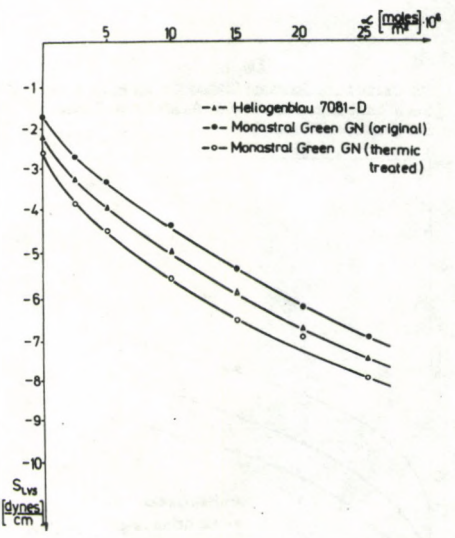

With methylene iodide, the thermally non-treated Monastral Green GN pigment will be wetted to a greater extent than the heat-treated sample. The "surface polarity" of pigments increases with the increase of surfactant adsorption /highest polarity is observed for the heat-treated Monastral Green GN, and the lowest for the thermally non-treated pigment; Heliogen Blau 7081-D is between the two/.

The value $\gamma_S = \gamma_S^d + \gamma_S^p$, within the experimental limits of error was found independent of the quantity of surfactant adsorbed.

Discussion

Role of surfactant adsorption

On the copper-phthalocyanine-blue pigments having different crystal modifications, used in former measurements /7/ and, on copper-phthalocyanine- and chlorinated copper-phthalocyanine pigments studied in the present work, both anionic and cationic surfactants are adsorbed oriented, by physisorption, the polar group being oriented towards the solution. The wettability of the pigments with surfactant-covered surfaces changes unambiguously with the structure of the adsorption layer. The vertical orientation of the surfactant molecules increases with the increase of the surfactant adsorption. On the increase of

the vertical ion orientation and the degree of coverage, the surface polarity of the pigment will become higher. The spreading coefficient of water, as well as its adhesion energy, increases upon increasing the adsorbed quantity of the surfactant, whereas that of methylene iodide is deminished. In addition to the nature of the pigment /chemical structure, crystal modification/, the wettability of copper-phthalocyanines is mainly determined by the structure of the adsorption layer. As a result of oriented surfactant adsorption, their wettability by water is increased. The stability of their suspensions increases up to the equilibrium concentration corresponding to c_M.
At equilibrium concentrations higher than c_M the particle aggregates will disintegrate.

As a result of thermal treatment the specific surface of copper-phthalocyanine pigments - as a function of the temperature and the time of treatment - will be considerably reduced. Their crystal structure is partly or totally altered and is some cases chemical changes also occur.

References

1./ D.H. Kaelble, Physical Chemistry of Adhesion. New York, 1971.
E. Wolfram, Kontaktnedvesedés. Budapest, 1971.

2./ W.S. Zisman, Advan. Chem. Ser. 43, 1 /1964/

3./ F.M. Fowkes, Soc. Chem. Ind. Monograph: 25, 3 /1967/
F.M. Fowkes, Advan Chem. Ser. 43, 99 /1964/
D.K. Owens, J. Appl. Polymer Sci. 13, 1741 /1969/
Y.Tamay,K.Makuuchi,M.Suziki,J.Phys.Chem: 71, 4176 /1967/
Y.Tamay,H.Kobayashi,J.Colloid Interface Sci: 32, 369 /1970/

4./ D.H. Bangham., R.I. Razouk, Trans. Faraday Soc.: 33, 1453 /1937/
B. Vincent, Proceedings of the VI th International Congress on Surface Active Substances. Zürich, 1972. II/2.p.581

5./ S. Wu., K.J. Brzozowski, Colloid Interface Sci.: 37, 686 /1971/

6./ K. Szterjopulosz., E. Wolfram, Annales Univ.Scien.Budapestinensis Sect.Chim. 11, 9 /1969/

7./ A. Lőrinc, K.Szterjopulosz, E.Wolfram, Kémiai Közlemények 42, 224 /1974/
A. Lőrinc, K.Szterjopulosz, Kol.Ért. 16, 338 /1974/

Group I/4
Thin liquid films

STABILITY OF THIN LIQUID FILMS ON HYDROPHOBIC QUARTZ SURFACES

H.J.Schulze

Research Institute of Mineral Dressing of the Academy of Sciences of the GDR, 92 Freiberg, GDR

The stability of thin liquid films on solid surfaces has a great practical importance for dispersion properties and wettability. The system investigated by us represents a model for the flotation of oxidic solids, for the wetting behaviour of optic glasses, and for the problem of silicosis.

The measurements were carried out with single crystals of quartz and quartz glass in aqueous solutions of dodecylamine hydrochloride (DCA). The thickness of the thin liquid film being formed by pressing an air bubble against a plane solid surface (capillary pressure in the bubble during the measurement of far-reaching electrostatic forces of interaction 400-700 dyne/cm^2, during the measurement of critical thickness depending on concentration about 2000 dyne/cm^2) was interferometrically recorded. In each case a surface section of about 10-20 μm^2 of the border of the thin film (5-15 μm broad) was photometrically measured. Film radius was about 100 μm. In this narrow border single holes are forming which lead to the rupture of the film. Equilibrium films, on the other hand, after efflux of dimple are completely homogeneous.

At polar, e.g. oxide surfaces there are aqueous equilibrium films with a thickness of between 100 and 1000 Å. They are stabilized by electrostatic forces of repulsion of the ion-double layers /1/. At quartz surfaces and

even at thicknesses below 100 Å stable films occur by structuring of the bordering water phase by the quartz crystal lattice. DERJAGUIN characterized the latter as αfilms /2/.

Other authors, too, e.g. PESCHEL /3/, underlined the existence of a structurally limited component of the disjoining pressure of liquid films at quartz surfaces.

If the quartz surface is reversely charged or surfactants are adsorbed at it, then unstable liquid films occur which spontaneously rupture at a certain critical thickness, h_{crit}. This process is the precondition for the development of coagulation structures in dispersions, for the attachment of mineral particles to air bubbles during flotation, and for the water-repellant effect of solid surfaces.

The reverse charging and thus labilization of film, as we could show it /4/, may be accomplished already by multivalent cations, e.g. Al^{3+}. The critical thickness of rupture is e.g. 350–450 Å in 10^{-4} M $AlCl_3$ solutions. But the adsorption of cation-active surfactants, too, leads only by a reverse charging of the liquid-gas interface to the development of electrostatic forces of attraction between the interface and the negatively charged oxide surfaces. The range of action of these forces is very wide at low ionic strengths ($< 10^{-3}$ mole/l) so that aqueous DCA-solution films already rupture at thicknesses above 1000 Å (Fig. 1, upper curves). The differential change of the electrostatic forces of interaction per unit area according to the thickness h_{crit}, $\partial \Pi_{el} / \partial h_{crit}$ is about $0.6 \cdot 10^8$ up to $24 \cdot 10^8 \cdot \frac{dyne}{cm^2} \cdot \frac{1}{cm}$. If we increase the ionic strength either by decreasing or increasing pH in solution or by adding an indifferent electrolyte, e.g. 10^{-2}...10^{-1} m/l KCl, the range of action of the electrostatic forces mentioned above is very strongly suppressed. Now they are no longer responsible for film instability and the critical thickness, therefore, drops below 450 Å (Fig. 1, lower curve). Our measurements show that in this case h_{crit} is above all dependent on pH

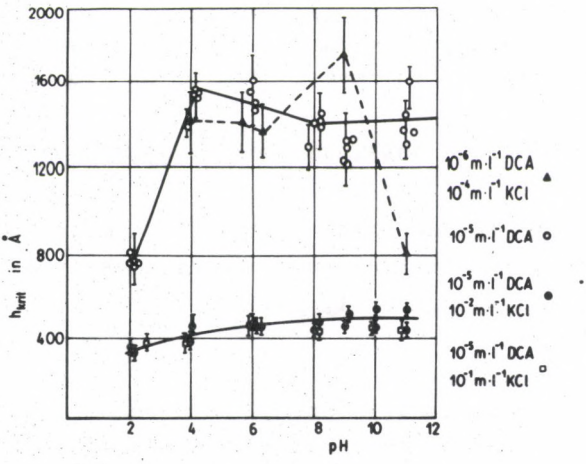

Fig. 1
Critical thickness in the system:
quartz/H_2O/air bubble

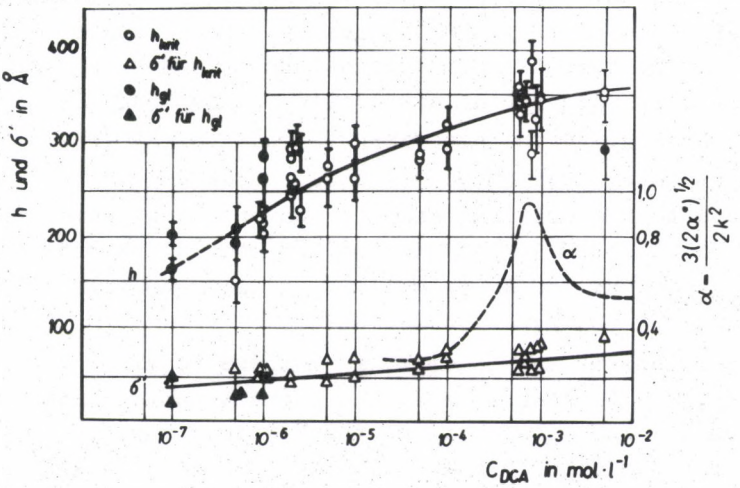

Fig. 2
Film thickness h, standard deviation δ', and damping coefficient

value in solution (Fig. 1) and on amine concentration (Fig. 2). With increasing pH value /5/ and increasing amine concentration critical thickness rises from 150 up to 450 Å.

Up to this point we obtained the following four remarkable <u>results</u>:

1) There is a continuous transfer of equilibrium films to unstable films in the range of thicknesses between 150 and 200 Å with extremely low DCA concentrations of about $5 \cdot 10^{-7}$ m/l.
2) In the present system we did not observe an influence of the damping coefficient of surface waves of amine solutions. We can see from Fig. 2 that h_{crit} as well as the standard deviation of the normally distributed critical thicknesses within the limits of error do not show any special deviations in the near of the maximum damping coefficient of DCA /7/.
   At free foam films, on the other hand, the influence of h_{crit} by the damping coefficient could clearly be proved. That is obviously, because first of all surface fluctuations lead to the rupture of film. With maximum damping coefficient a very low critical thickness and a very narrow distribution of critical thickness are developed.
3) Surfactant adsorption at the SiO_2 phase boundary leads, in contrast to the experimental results, at free foam films to an increase of critical thickness.
4) Close to the critical micelle concentration (cmc) (in 10^{-2} KCl at pH 3 about $5\text{–}8 \cdot 10^{-3}$ mole/l) unstable films (h_{crit} about 350 Å) as well as equilibrium films (h_{equ} about 250–300 Å) are co-existing.

What conclusions may be drawn from these results?
Firstly, the existence of a continuous transfer from equilibrium thickness to critical thickness of rupture shows that previously too a high value for the wave length of film surface deflection was assumed:
SCHELUDKO as well as VRIJ /8/ previously stated about 20 µm.

After SCHELUDKO critical thickness is proportional to the Hamaker constant $A^{1/4}$ and to the wave length $\lambda^{1/2}$ and inversely proportional to the surface tension of liquid $\sigma^{1/4}$ /6/:

$$h_{crit} = \left(\frac{A\lambda^2}{128\pi\sigma}\right)^{1/4}$$

Assuming the Hamaker constant of pure water ($A_{H_2O} \approx 7.5 \cdot 10^{-13}$ erg) being valid in the range of transfer from h_{equ} to h_{crit} in the first approximation you may calculate a mean deflection wave length $\lambda^* \approx 3.7...7.5$ /um. A similar value for free films from the extrapolation of their critical thickness as a function of the film radius R = 0 was recently given by MANEV /6/.

(We should mention in this connection that the diameter of our photometrically measured film area is nearly the same as the above mentioned deflection wave length λ^*).

Secondly, interpretation of the concentration and pH dependence on h_{crit} at this point of investigation is still difficult. The obtained results above all seem to contradict our opinions concerning the interaction of dispersions in heterogenous systems, according to which an adsorbed layer in general must lead to a decrease of the Hamaker constant. If you consider e.g. only the interaction of dispersions with a completely homogenous and dense adsorbed layer and you assume this to be equal in the first approximation to the interaction between water and hydrocarbon, a Hamaker constant $A_{H_2O/hydrocarbon} \approx 3...5 \cdot 10^{-14}$ erg could be obtained after the calculations made by NINHAM and PARSEGIAN /9/.

In reference /5/ we tried to give an explanation based on the change of the forces of dispersion in presence of an adsorbed layer of certain thickness. The uncertain data concerning the required Hamaker constants and the doubts in respect to the validity of the geometric mean unfortunately do not allow a clear conclusion.

However in these cases we do not know what effect the damping of the micro-waves of dispersion forces /10/ by the very high ionic strength in the present system has. For the interpretation of results, therefore, it is necessary, in my opinion, to consider the peculiarities of the formation of water structure at silicate surfaces and their modification by adsorbed layers. In this connection not only the far-reaching structure-forming effects of the pure SiO_2-lattice matrix have to be considered, but also the increase of the order of water molecules in the neighbourhood of aliphatic molecules leading to the so-called hydrophobic interaction after NEMETHY and SCHERAGA /11/. Here some reflections may be of interest, which already a few years ago were made by WEISS /12/: The problem of the formation of hydrophobic silicates with layer lattice does not consist in the prevention of single water molecules from contacting the interface, but it consists in the prevention of a stable water structure from being formed at this interface. The pure quartz surface is hydrophilic, when a special water structure can be formed. WEISS assumes that at silicates with layer lattice very close to the phase boundary water clusters with an area of 40 - 60 $Å^2$ and at a distance of more than 6 Å clusters of 95 - 120 $Å^2$ must be present. Small alkyl groups of adsorbed molecules, doubtlessly, may be integrated in this structure, but greater unpolar chains destroy them and the surface becomes hydrophobic. In this case the positive component of disjoining pressure could be rapidly reduced.
NEMETHY and SCHERAGA postulate that the assumption firstly proposed by FRANK and EVANS is valid, which states that the structural order of water in the neighbourhood of unpolar parts of solution increases because the number of hydrogen bondings per mole of water increases too. If, on the contrary, water is desplaced from the neighbourhood of such aliphatic groups, so the order of the system is decreasing, which leads to better proportions of entropy and

thus to a negative free energy of formation.
In the interpretation of the stability of thin films therefore both effects have to be considered: The pure quartz surface causes a molecular wide-range order in water. Therefore stable films are occurring. Lowest surfactant concentrations (at present we do not yet know the required degree of coverage and the necessary chain length) destroy these orders, the positive, structure-depending component of disjoining pressure disappears, and a labilization of the film leads to its rupture already at very low surfactant concentrations, but at low critical thicknesses. With increasing adsorption density of surfactant at the SiO_2 surface film stability is further increased, because entropy of water decreases caused by the present unpolar groups. If a dense adsorbed layer is built up it seems to occur an upper limiting value of critical thickness. The pH dependence, furthermore, does not show an influence of the composition of the amine adsorbed layer, because it is known that the proportion between undissociated and dissociated amines is changing as pH value changes.
Based on the adsorption of micelles, finally, a partial stabilization of the film in the near of cmc is caused by electrostatic forces of interaction. They are formed between the polar groups of micelles entering the liquid and the polar groups of surfactant adsorbed at the liquid-gas interface. Therefore we could observe at these concentrations unstable as well as stable films.
The results presented here can give only a small contribution to the interpretation of stability of thin liquid films. I was supposed to show that in comparison to free films a number of other variables has to be considered, which can be of remarkable practical importance, but must still be subjected to a detailed investigation.

References

/1/ Schulze, H.J., Cichos, Chr.
Z. phys. Chem., Leipzig, 251 (1972) p. 252-268

/2/ Derjag in, B.V., Curaev, N.V.
J. Coll. Interf. Sci., 49 (1974) p. 249-255

/3/ Peschel, G., Adlfinger, K.H.
Z. phys. Chem. NF 59 (1968) p. 27,
Special Disc. Farad. Soc. 1 (1970) p. 89-97

/4/ Schulze, H.J., Cichos, Chr.
Z. phys. Chem., Leipzig 252 (1972) p. 145-151

/5/ Schulze, H.J.
Coll. and Polymer Sci, Darmstadt, (1975) in press

/6/ Manev, E.; Scheludko, A.; Exerowa, D.
Coll. and Polymer Sci., Darmstadt 252 (1974) p.586
-593

/7/ Lucassen, J.; Hansen, R.S.
J. Coll. Interf. Sci. 22 (1966) p. 32-44

/8/ Vrij, A.
Disc. of Farad. Soc. No 42 (1966) p. 23-33

/9/ Ninham, B.W.; Parsegian, V.A.
J. chem. Phys. 52 (1970) p. 4578-4587

/10/ Smith, E.R.; Mitchell, D.J.; Ninham, B.V.
J. Coll. Interf. Sci. 45 (1973) p. 55-68

/11/ Memethy, G.; Scheraga, A.A.
J. Chem. Phys. 36 (1962) p. 3382-3417

/12/ Weiss, A.
CJD-Congress, Brüssel (1964), Band III./7 (preprint)

DISJOINING FORCES IN THIN LAYERS OF AQUEOUS ELECTROLYTE SOLUTIONS

G.Peschel and P. Belouschek

Institute of Physical Chemistry, University Würzburg, 87 Würzburg, Federal Republic Germany

Introduction

The subject of the electrical double layer at the solution/solid interface has been studied by a number of authors carrying out experimental and theoretical investigations. If a solid is immersed in an aqueous electrolyte solution its surface will become charged and exert an attraction force on the ions of opposite charge in the vicinal solution. The mutual approach of charge bearing solid surfaces in electrolyte solution will involve the overlapping of the diffuse ion layers of both surfaces at sufficiently close distances and give rise to repulsion forces which become larger with decreasing distance. This effect,which, e.g., determines the stability of disperse systems, is assumed to follow the electrostatic theory of DERYAGIN and LANDAU [1] and VERWEY and OVERBEEK [2] (DLVO-theory).

To be exact, the electrostatic repulsion effect is superimposed by a long-range attraction due to dispersion forces [2].

Since the problem of particle interaction is very important in the field of colloid science,the direct measurement of the repulsive forces in thin aqueous electrolyte layers between two solid surfaces appears to be desirable as a rigorous test of the DLVO-theory. Though this task turned out to be very difficult some authors succeeded in obtaining reliable results.

ROBERTS[3] pressed an optically smooth rubber surface

on to a flat glass surface being immersed in an aqueous NaCl solution. Interference fringes served as a means for measuring the plate distances. Unlike the predictions of the DLVO-theory according to which a monotonous fall of the film thickness with concentration had to be anticipated the equilibrium film thickness exhibited a maximum value in the concentration range of 10^{-2} - 10^{-1} m.

Precise measurements of the disjoining pressure between sodium montmorillonite plates at surface separations down to 20 Å with a low concentrated 1:1 electrolyte are due to BARCLAY et al. [4]. The disjoining pressure turned out to be higher than predicted by theory and the authors believe that the additional repulsive forces arise from the interaction of extended hydrate layers at both interfaces.

Some more effects are known from literature which likewise support the idea of the existence of a hydration component of the disjoining pressure. The present work aims at presenting a new test for the validity of the DLVO-theory and substantiating the real existence of hydration layers at solid surfaces.

The Interaction between Flat Surfaces

Let us assume two flat solid plates immersed in an electrolyte solution, being parallel to each other and separated by a distance h. At small distances, say $h < 10^{-5}$ cm, the electrolyte double layers will interact with each other and generate a positive disjoining pressure given by the well-known expression

$$\Pi_{el} = 2nKT\,(\cosh u - 1) \qquad (1)$$

with $u = ev\psi_m/KT$. ψ_m is the potential mid-way between the plates, v is the ion valency and k the BOLTZMANN constant. The equation is based on the presumption that the surface potential ψ_0 remains constant during the approach of the plates.

In practice, however, specific adsorption of ions at the plate surfaces will take place and lead to the formation of STERN-layers which display the potential ψ_δ at the very small distance δ from the plate surface.

The dispersion interaction between the solid plates of unit area, the thickness of which is by far greater than the gap width, follows the relation [2]

$$\Pi_D = - \frac{A}{6 \pi h^3} \qquad (2)$$

if retardation effects are disregarded.

The net HAMAKER constant A is given by

$$A = (\sqrt{A_{11}} - \sqrt{A_{22}})^2 \qquad (3)$$

A_{11} is the HAMAKER constant of the fused silica material, which was used in the present work, A_{22} is that of the aqueous layer. Putting $A_{11} = 2 \ 10^{-12}$ erg [5] and $A_{22} = 5.6 \times 10^{-13}$ erg (the value for water [6]), one yields $A = 4.4 \times 10^{-13}$ erg. Taking $h = 10^{-6}$ cm Π_D according to Eq.(2) amounts to $- 2.3 \ 10^4$ dyne/cm^2. Subtracting this value from the net disjoining pressures experimentally found one would obtain the sum of the electrostatic and hydration components of the disjoining pressure, when a gap width of 100 Å is taken as a basis.

The Experimental Method

The disjoining pressure measurements were carried out with a spherical/planar fused silica plate system. This was chosen to avoid the serious problem of plane-parallelity of the plates during measurement. The essential part of the experimental device is shown in Fig.1.

The planar fused silica plate A_2 is placed on the bottom of a container C which can be filled with the solution to be investigated over a membrane filter MF. The spherically formed plate A_1 is attached to the one end of a balance system BS which can be operated via a magnetic coil and

thus allow to adjust the contact forces in the plate system. The gap width can be recorded by a displacement transducer DT which is connected to a strain gauge measuring bridge. The apparatus is placed in a large vacuum chamber which guarantees an overall and uniform thermostating.

It proved to be useful to introduce the distance dependence of the disjoining pressure obtained by experiment to be

$$\Pi = C \cdot e^{-nh} \qquad (4)$$

with C and n being parameters which can be calculated by a special theory [7,8] on the basis of experimental data.

Results and Discussion

Aqueous solutions of LiCl,NaCl,and KCl were investigated in a concentration range of 10^{-4} - 1 m. In Fig.2 the disjoining pressure Π found in experiment is plotted against the logarithm of the electrolyte concentration for a plate distance of 100 Å. The broken line indicates the disjoining pressure calculated by the simple Eq.(1) and assuming the (rather high) surface potential ψ_o = 250 mv.

Even in the low concentration range the agreement between experimental and theoretical data is very poor, though the experimental curves follow roughly the trend marked by the theoretical one. Particularly the maxima at about 10^{-2}m and 0.5 - 0.8 m are left unexplained by the DLVO-theory.

A contribution relevant to our findings stems from DERYAGIN and RABINOVICH [9]. They measured the force barriers in aqueous solutions of LiCl,NaCl,and KCl when bringing into contact two crossed platinum and gold filaments, respectively. Maximum force barriers were found in the concentration range 0.5 - 1 m.

In this connection it is interesting to note that alkali halides in aqueous solution exhibit a break in their partial

molar volumes at about 0.8 m,as was found by VASLOW [10]. The author supposed that this is a critical concentration where all water molecules in the solution participate more or less in extended hydration clusters (FRANK-WEN clusters) surrounding the ions. By increasing the electrolyte concentration the clusters will suffer a cooperative break down or at least a structural transition.

Evidence given by the present author [11,12] shows that a number of pure liquids (e.g., halogenobenzenes,nitrobenzene, acetonitrile) display a disjoining pressure maximum in thin layers within a close temperature range where a structural transition is established by other methods to occur. The enhanced disorder in the molecular arrangements within this range seems to favor an epitaxial influence of the solid surface on the neighbouring solvent molecules which are subjected to a long-range ordering deep into the bulk phase. The disjoining pressure maximum at about 0.5 - 0.8 m as found in the present work might be attributed to a similar effect.

Simple calculations show that this critical concentration may be achieved for the cations near the negatively charged fused silica surface in the outer HELMHOLTZ plane when the electrolyte concentration far distant from the wall is still about 10^{-2} m. Under these conditions the water neighbouring this layer might be particularly immobilized and act as a matrix for a cooperatively extending immobilization of more distant water molecules leading to the very disjoining pressure maxima at about 10^{-2} m.

VASLOW's interpretation suggests the occurrence of rather large hydration numbers for the ions. That these can be obtained by sufficiently precise methods was reviewed by DROST-HANSEN [13].

These results,on the other hand, support the hydration model proposed by HORNE and BIRKETT [14] according to

which the first hydration layer surrounding the ion is not followed directly by a disordered zone as postulated by the FRANK-WEN model but by extended clusters of water molecules.

The solid surface via adsorption phenomena is known to act as a momentum sink by damping thermal fluctuations. Hence the hydration clusters proposed by HORNE and BIRKETT which in the case of simple alkali halide ions are surely highly unstable in bulk solution might get stabilized near the solid surface as was emphasized by DROST-HANSEN [15].

All these facts may serve to strengthen our view about the generation of the unexpected disjoining pressure maxima which is outlined in the foregoing.

It must be emphasized that the relatively large structural effects found by our method might be due to the overlap of two structurally changed aqueous zones each bounded by a solid surface, which is apt to induce strong molecular orientations in vicinal liquid layers.

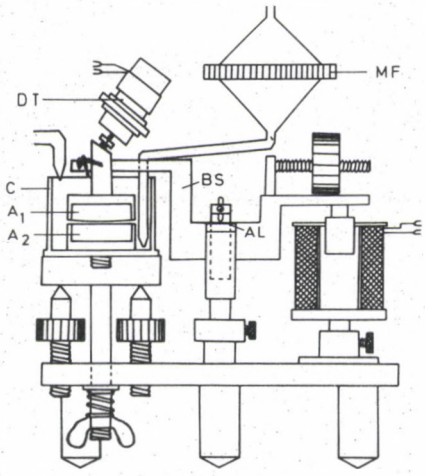

Fig.1. Experimental apparatus for the determination of the disjoining pressure in thin layers.

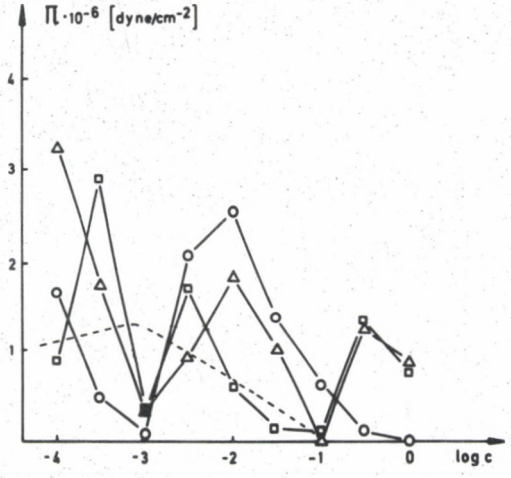

Fig.2. Disjoining pressure vs. electrolyte concentration for LiCl (○), NaCl (△), and KCl (□). Plate distance h = 100 Å; t = 20 °C ; --- theoretical curve.

References

[1] DERYAGIN,B.V., LANDAU,L.D.,Acta physicochim. URSS 14, 633 (1941).

[2] VERWEY,E.J., OVERBEEK,J.Th.G.,"Theory of the Stability of Lyophobic Colloids", Elsevier Publ. Comp., Amsterdam 1948.

[3] ROBERTS,A.D. J.Colloid Interf.Sci.,41, 23 (1972).

[4] BARCLAY,L.,HARRINGTON,A.,OTTEWILL,R.H., Kolloid Z. Z. Polymere 250, 655 (1972).

[5] BLACK,W., de JONGH,J.G.V.,OVERBEEK,J.Th.G.,SPARNAAY, M.G., Trans.Faraday Soc. 56, 1597 (1960).

[6] KRUYT,H.R.,"Colloid Science ", Elsevier,Amsterdam Vol. 1, 1952.

[7] ADLFINGER,K.H.,SCHNORRER,R.,PESCHEL,G., Z. angew. Physik 29, 136 (1970).

[8] ADLFINGER,K.H.,PESCHEL,G., Z. physik.Chem.(N.F.) 70, 151 (1970).

[9] DERYAGIN,B.V.,RABINOVICH,Ya.I., Kolloidn.Zh. 31, 37 (1969).

[10] VASLOW,F., J.Phys.Chem. 70, 2286 (1966).

[11] ADLFINGER,K.H.,PESCHEL,G., Spec. Discuss. Faraday Soc. 1, 89 (1970).

[12] PESCHEL,G.,SCHNORRER,R.,Z.physik.Chem. (N.F.) 75, 97 (1971).

[13] DROST-HANSEN,W.,Advances in Chemistry Series,No.67, 70 - 120 (1967).

[14] HORNE,R.A.,BIRKETT,J.D., A.D. Little,Inc.,Tech.Rept. 18 ONR Contract No. Nonr-4424(00).

[15] DROST-HANSEN,W., in "Chemistry of the Cell Interface", Part B,pp. 1 - 184, ed. H.D. BROWN,Academic Press , N.Y.,1971.

Group I/5
Adsorption of polymers

CONFORMATIONAL TRANSITIONS IN FREE AND ADSORBED POLYMETHACRYLATES

T. van Vliet and J. Lyklema

Laboratory for Physical and Colloid Chemistry of the
Agricultural University, De Dreijen 6, Wageningen, Netherlands

Polyelectrolytes of the polymethacrylate (PMA) type have the interesting property that they occur in two different conformations. At low pH, they occur in a compact form, the hyper-coiled or a-conformation. Above pH $\sim$ 5.5 (the precise value depending on the nature and concentration of the low-MW electrolyte) the molecule expands rapidly towards the more extended b-conformation. Several authors, employing various experimental techniques have found this transition[1-8]. It is the occurrence of the a-conformation that distinguishes polymethacrylates from most other polyelectrolytes, including polyacrylates. Van der Waals attraction[5] and hydrophobic[9,10] bonding have been forwarded as explanations, but hitherto no consensus of opinion has been reached.

In this article, we want to show that, under suitable conditions, the conformational transition is also observed if the polymethacrylate is in the adsorbed state. Indications of this are found in work by Böhm and Lyklema[11-13]. As will be shown, the occurrence of the transition in PMA layers, adsorbed on paraffin drops emulsified in aqueous solution can be monitored rheologically, a feature that in turn can be advantageously exploited to obtain useful additional information on the nature of the underlying interaction forces.

EXPERIMENTAL

Our polyelectrolyte was a copolymer of methacrylic acid and its methyl ester in the molar ratio 2:1, further abbreviated as PMA-pe. It has been described before[11,12]. Paraffin oil and water were of the same quality as those described by Lankveld and Lyklema[14]. The aqueous solutions contained 0.05 M NaCl except where otherwise stated. Experiments in solutions of $CaCl_2$ have also been performed but they will be reported elsewhere[15].

The emulsification process of paraffin in aqueous solutions of PMA-pe was essentially identical to that described in ref[12,16].
Potentiometric titrations have been carried out under nitrogen at 22°C. Three types of rheological measurements have been done. Emulsion viscosities have been obtained at 20.0 ± 0.2 °C using a Haake Rotovisko at a shear rate D = 7.05 s^{-1} and a shearing time (t ∿ 10-40 min) taken so long that the observed viscosity did not change any more. PMA-pe solution viscosities at various temperatures were obtained using a Ubbelohde-type viscometer. The extrapolation of η_{sp}/c to c=0, in order to obtain the intrinsic viscosity $[\eta]$, was done isoionically in 0.05 M Na^+. Dynamic moduli of emulsions have been measured in a rheometer, developed and described by Duiser[17] and den Otter[18]. Essentially it consists of two coaxial cylinders between which the sample is contained. The inner one is brought in a harmonic oscillation and from an observed phase shift and amplitude difference between inner cylinder and driving system, the loss and storage moduli, G" and G' respectively, can be calculated. The amplitudes were sufficiently low to ensure linear vicoelasticity. The temperature was 20.0 ± 0.2 °C except in experiments where T was variable.

RESULTS

Titration of free and adsorbed PMA-pe If titration data of dissolved polyelectrolytes are plotted as pH - log $(1-\alpha)/\alpha$ graphs (so-called Henderson-Hasselbalch (HH)-plots) usually a straight line or continuous curve is obtained. However, in the case of PMA-pe the HH-plots consist of *two* lines, separated by a transition region. The two lines reflect the two conformations occurring with this polyelectrolyte. The data can be replotted[4] to give the fraction f_b of PMA-pe in the b-conformation as a function of α. See fig. 1, curve 1.

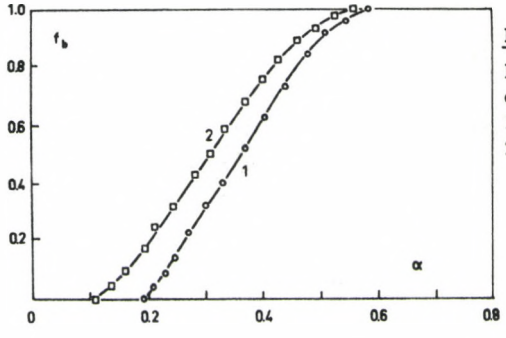

Fig. 1

Fraction of PMA-pe in the expanded or b-conformation
1) free PMA-pe
2) PMA-pe, adsorbed at the paraffin oil-aqueous solution interface.

Obtaining the corresponding graphs for adsorbed PMA-pe is more difficult. PMA-pe covered emulsions contain also some dissolved PMA-pe. This was discarded by twice centrifuging the emulsion and redispersion in 0.05 M NaCl. The thus obtained emulsion was then titrated with HCl to $\alpha \sim 0$ and backwards to $\alpha = 1.0$ with NaOH. The exact value of α at the lower end of the titration could not be established but it was found that, by allowing this value of α to vary within narrow limits, only with one particular value the characteristic HH-plots were obtained[15]. We used this feature as an additional means of positioning the curves. The result is shown in fig. 1, curve 2. The difference between duplo's is less than 0.03 in f_b.
From fig. 1 it is concluded that the conformational transition occurs also in adsorbed PMA-pe. The transition range is somewhat broadened and moved to lower α. It follows from a balance count of the total number of titrable groups that down to $\alpha = 0.05$ a small part of the adsorbed PMA-pe is not yet titrated. This "lost" amount roughly corresponds to the amount that can be accomodated in a monolayer, suggesting that only loops and tails partake in the interaction, leading to the a-conformation. In view of the largely irreversible binding of the train segments this is not surprising. In connection with our finding we note that Caspers et al.[19] observed a conformational transition as a function of pH in polypeptides, spread at the air-water interface.

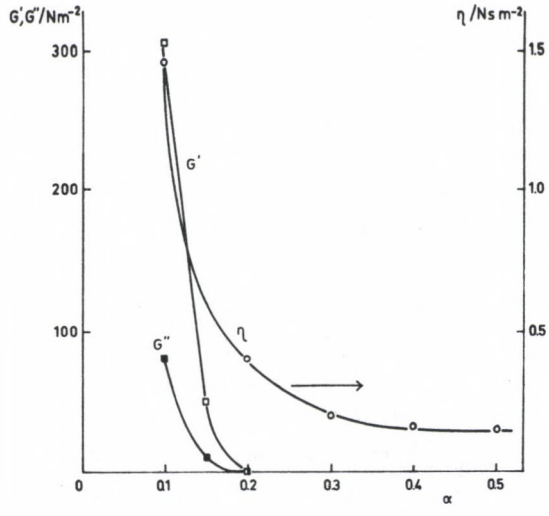

Fig. 2. Dynamic moduli and viscosity of paraffin oil in water emulsions, stabilized by PMA-pe.
Electrolyte 0.05 M NaCl.
Volume fraction of oil 0.5.
Polymer adsorption 2.2 mg/m^2.

Rheology. The interaction between polyelectrolyte-covered paraffin droplets is reflected in the rheological properties of the emulsions (12, 20, 21). It can be concluded from fig. 2, both from the G' and the η-curve, that such interaction occurs only at low α, that is if a substantial part of the adsorbed PMA-pe is in the a-conformation. At high α the emulsions are very fluid with little or no indication for attraction between adsorbed polyelectrolyte sheets.

The titration data (fig. 1) and the rheological results (fig. 2) complement each other. Fig. 1 reflects attraction at low α between loops and/or tails adsorbed on *one* emulsion droplet. On the other hand, the high values of G' and η at low α are due to attraction between extending loops and/or trains, anchored onto *different* droplets. The two types of interaction seem to be very similar.

In this connection it is interesting to note that the interaction between adsorbed PMA-pe layers makes itself also felt in the drainage behaviour of free liquid films, stabilized by this polyelectrolyte. At $\alpha \sim 0.1$ the films are rigid, draining towards equilibrium over days whereas at $\alpha \geq 0.3$ the films are mobile and drain rapidly.

Having concluded that rheological measurements constitute a rewarding approach to the establishment of the occurrence of the a-conformation, we performed two sets of experiments, in order to get some insight in the nature of the interaction force. In one set we investigated the effect of methanol (MeOH) in another set we varied the temperature. The results are collected in figs 3 and 4.

It depends very strongly on α how the viscosity of an emulsion is affected by the addition of MeOH. If α is low and a sufficient fraction occurs in the a-conformation (that is in the region of enhanced viscosity (fig. 2)), η passes through a maximum at $x_{MeOH} \sim 0.13$-0.17 (fig. 3). However, if the greater part of the adsorbed layer is in the b-conformation η is low and MeOH has virtually no effect. In our picture, this is thus interpreted that small amounts of MeOH increase the attraction that gives rise to the a-conformation whereas larger supplies of MeOH disrupt any bonds.

Our finding can be compared with intrinsic viscosity [η] measurements of polymethacrylic acid in 2×10^{-3} N HCl by Priel and Silberberg[22]. These authors found that as a function of x_{MeOH} [η] first decreased, then passed through a minimum at $x_{MeOH} \sim 0.1$, followed by an increase till a maximum at $x_{MeOH} \sim 0.4$. We recall that the interaction force, which in our case is measured between different adsorbed layers, leads to an *enhanced* emulsion *viscosity*, whereas in bulk the same force acts only inside one molecule

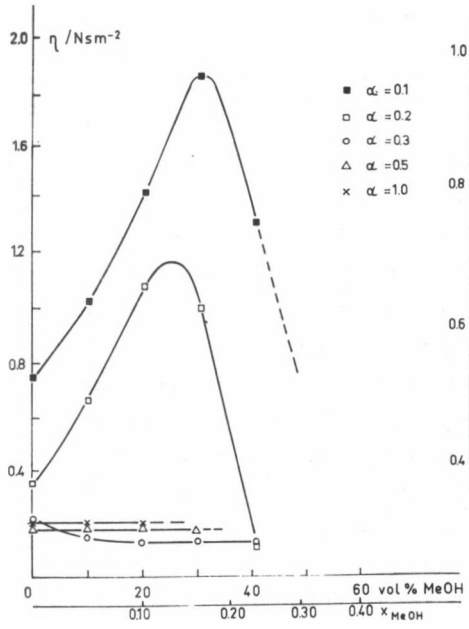

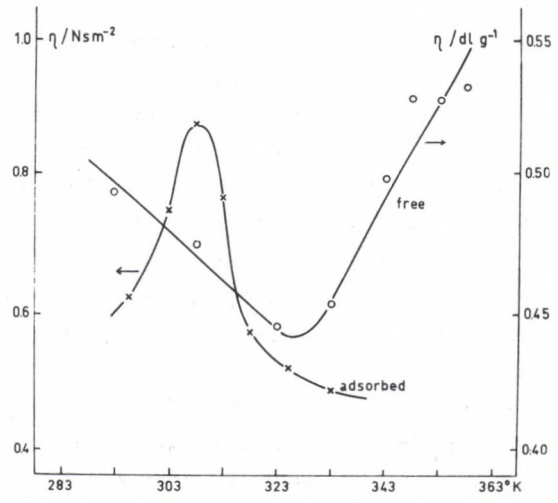

Fig. 3 (left). Viscosities of paraffin oil emulsions in water-methanol mixtures. Stabilizer: Na-PMA-pe. Emulsification time 1 min, polyelectrolyte supply 2 mg per cm^3 of paraffin oil. Electrolyte 0.05 M NaCl. The degree of neutralization is given. T = 20°C.

Fig. 4 (right). Influence of temperature on the intrinsic viscosity of dissolved PMA-pe and on the viscosity of the polyelectrolyte stabilized emulsions of fig. 3 at α = 0.1. No methanol added.

(provided the solution is dilute) and hence leads to compaction and subsequent *reduction of* [η]. Thus, our maximum is in perfect qualitative agreement with the minimum observed in [22]. Perhaps it is even allowed to invoke the fact that the bulk minimum and the emulsion maximum are not too far apart as an indication of much similarity between the nature of the interaction in free and adsorbed polyelectrolytes, a conclusion which we have also drawn from fig. 1. After all, complete agreement may not be expected since the polyelectrolytes used are not identical.

The disrupture of bonds by MeOH has been used as an argument that these bonds were due to hydrophobic interaction[5,23,28]. This may perhaps apply to large volume fractions and hence e.g. explain the reduction of η beyond the maximum (fig. 3) or the increase of [η] of bulk PMA beyond the minimum

(ref[22]). However, small amounts of MeOH behave apparently in a different way. Also for ethanol it has been established that small volume fractions can behave differently from larger contents [24,25]. Our insight in the structural details of the interaction with alcohol molecules is not yet far enough developed to arrive at incontestible conclusions. At any rate it appears that our results are not incompatible with the idea that hydrophobic bonding plays an important role in the occurrence of the a-conformation. The temperature-dependence measurements tell the same story. Fig. 4 shows that, as a function of T, the emulsion viscosity passes through a maximum at $\sim 308^{\circ}K$. This maximum is also obtained with the dynamic moduli (not shown). On the other hand, the intrinsic viscosity of the free polyelectrolyte has a minimum at $T \sim 325^{\circ}K$. Silberberg et al.[26] observed a similar minimum with free PMA. Both extrema are interaction *maxima* and again in agreement with hydrophobic bonding. Némethy and Scheraga[27] theoretically predicted interaction maxima at $331^{\circ}K$ for aliphatic groups and at $315^{\circ}K$ for aromatic ones. Again, quantitative agreement, neither with the theory nor between the two sets of experiments may be anticipated, but the semi-quantitative analogy is convincing enough to point to hydrophobic interaction as a main factor in the establishment of the a-conformation.

CONCLUSION

Our main conclusion is that rheological measurements with PMA-pe stabilized emulsions are a powerful means of obtaining information on interaction between adsorbed polyelectrolyte layers. It was shown that the thus measured interaction is very similar to the interaction occurring inside free dissolved polyelectrolyte. The conformational transition, occurring in polymethacrylates at low α is probably to a large extent due to hydrophobic bonding.

ACKNOWLEDGEMENTS

This work was financially supported by the Unilever Research Laboratory, Vlaardingen, Netherlands. The technical assistance of Mr. T. van Hooydonk and Mr. R.G. van Driel is gratefully acknowledged.

REFERENCES

1. R. Arnold, and J.Th.G. Overbeek, Recl. Trav. Chim. 69, 192 (1950).
2. A. Katchalsky, J. Polym. Sci. 7, 393 (1951).
3. H.P. Gregor, and M. Frederick, J. Polym. Sci. 23, 451 (1957).
4. J.C. Leyte, and M. Mandel, J. Polym. Sci. A, 2, 1879 (1964).
5. M. Mandel, J.C. Leyte, and M.G. Stadhouder, J. Phys. Chem. 71, 603 (1967).
6. A. Silberberg, and P.F. Mijnlieff, J. Polym. Sci. A-2, 8, 1089 (1970).
7. V. Crescenzi, F. Quadrifoglio, and F. Delben, J. Polym. Sci. A-2, 10, 357 (1972).
8. W.H.J. Stork, J.A.M. van Boxsel, A.F.P.M. de Goeij, P.L. de Haseth, and M. Mandel, Biophys. Chem. 2, 127 (1974).
9. J. Eliassaf, J. Polymer Sci. B, 3, 767 (1965).
10. F. Delben, V. Crescenzi, and F. Quadrifoglio, Eur. Polym. J. 8, 933 (1972).
11. J.T.C. Böhm, Meded. Landbouwhogeschool Wageningen 74, 5 (1974).
12. J.T.C. Böhm, and J. Lyklema, in "Theory and Practice of Emulsion Technology" (A.L. Smith, Ed.). Academic Press, London/New York (1975).
13. J.T.C. Böhm, and J. Lyklema, 5th Int. Congress Surface Active Substances, Zürich, Proc. Carl Hansen Verlag, München II, 2, 459 (1972) (in German) and J.T.C. Böhm, and J. Lyklema, J. Colloid Interface Sci. 50, 559 (1975).
14. J.M.G. Lankveld, and J. Lyklema, J. Colloid Interface Sci. 41, 454 (1972).
15. T. van Vliet, and J. Lyklema, to be published.
16. J.M.G. Lankveld, and J. Lyklema, J. Colloid Interface Sci. 41, 475 (1972).
17. J.A. Duiser, Thesis, Leiden, Netherlands (1965).
18. J.L. den Otter, Thesis, Leiden, Netherlands (1967).
19. J. Caspers, C. Berliner, J.M. Ruysschaert, and J. Jaffe, J. Colloid Interface Sci. 49, 433 (1974).
20. M. van den Tempel in "Rheology of Emulsions" (P. Sherman Ed.) Pergamon Press, London, Ch 1 (1963).
21. J.M.P. Papenhuizen, Rheol. Acta. 11, 73 (1972).
22. Z. Priel, and A. Silberberg, J. Polymer Sci. A-2, 8, 705 (1970).
23. W. Kauzmann, Advan. Protein Chem. 14, 1 (1959).

24. M. Yaacobi, and A. Ben-Naim, J. Solution Chem. 2, 425 (1973).
25. D.G. Oakenfull, and D.E. Fenwick, J. Phys. Chem. 78, 1759 (1974).
26. A. Silberberg, J. Eliassaf, and A. Katchalsky, J. Polymer Sci. 23, 259 (1957).
27. G. Némethy, and H.A. Scheraga, J. Phys. Chem. 66, 1773 (1962).
28. E.V. Anufrieva, T.M. Birshtein, T.N. Nekrasova, O.B. Ptitsyn and T.V. Sheveleva, J. Polymer Sci. C, 16, 3519 (1968).

ADSORPTION OF HUMAN PLASMA ALBUMIN AND BOVINE RIBONUCLEASE AT CHARGED POLYSTYRENE-WATER INTERFACES

W. Norde and J. Lyklema

Laboratory for Physical and Colloid Chemistry of the Agricultural University, De Dreijen 6, Wageningen, Netherlands

The adsorption of biopolymers is a matter of considerable theoretical interest and it has widespread applications in biochemistry, bioengineering, immunochemistry, medicine and other fields. One of the main problems is always what the conformation of the adsorbed biopolymer is and how it depends on relevant variables such as the nature of the sorbent, pH, ionic strength and nature of any buffer that may have been added.

Usually, less emphasis is laid on kinetic factors. However, it should be realized that polymer adsorption is more often than not irreversible. The consequence of this is that the final state of an adsorbed macromolecule may be influenced by the way along which the adsorption process has proceeded.

For biopolymers, the extent to which the molecules can unfold themselves is an important factor. The more they unfold, the lower the adsorbed amount Γ_p. For a given biopolymer, the extent of unfolding may depend on the available adsorbing area and hence diminish with increasing degree of occupancy of the sorbent by polymer. It can also depend on the nature of the sorbent. All of this renders biopolymer adsorption an extremely complex problem that is far from solved.

In a previous publication[1)] on the adsorption of human plasma albumin (HPA) on polystyrene (PS) latices it was concluded that the platform value of the isotherm is related to the ability of the dissolved HPA molecule to unfold. In other words, the platform adsorption is related to the internal coherence of the biopolymer.

As a sequel to this finding we describe below a comparative study of the adsorption on PS latices of HPA and ribonuclease (RNase). The reason for the

choice of these two proteins is that the RNase molecule has substantial internal coherence with respect to variations of pH[2] whereas the HPA molecule relatively easily adapts itself to variations in acidity[3,4]. As will be shown, this difference of reconformational ability reflects itself in the adsorption behaviour.

EXPERIMENTAL

The albumin and the latices have been described before[1]. We recall that the latices have been prepared without using surfactants[5]. Their surface charge is entirely due to $-OSO_3^-$ groups and ranges between -2.3 and -15.5 $\mu C/cm^2$. Crystalline RNase from bovine pancreas (5 x crystallized, protease-free, salt-free and roughly chromatographed to increase the 'A' fraction[6]) and electrophoretically pure HPA were obtained from Sigma Chemical Company. Aqueous solutions of the proteins were prepared and dialyzed against water for some days. Just before use, the RNase solutions were adjusted to pH 6.5 and heated for 10 minutes at 62°C to disrupt possible aggregates[6].

Adsorption measurements have been described elsewhere[7]. It be recalled that, prior to adding them together, the protein solution and the latex were brought to the same pH and KNO_3 concentration without using buffers.

RESULTS AND DISCUSSION

Upon adsorption on PS latex, both HPA and RNase produce adsorption isotherms with well-developed platforms at sufficiently high bulk concentration c_p. However, the way in which these platform-values Γ_{pm} depend on pH and the latex surface charge σ_o differs significantly between the two. Figure 1 illustrates this. These results are typical.

The first point to recall is that the isoelectric point (i.e.p.) of HPA in 0.05 M KNO_3 is ca. 4.7[3,8], that of RNase ca. 9.3[9]. To the left of the i.e.p. the surface and biopolymer have an opposite charge whereas to the right of it they repel each other electrostatically. However, the trends of the Γ_{pm} (pH) curves do not reflect this overall-electrostatic interaction between sorbent and protein. In stead of that, for HPA the curves are more or less symmetrical with respect to the i.e.p., with a pronounced maximum around the i.e.p., whereas with RNase Γ_{pm} is very little dependent on pH. It must be concluded that, at least for HPA, the platform adsorption is predominantly determined by the net charge of the molecule in solution.

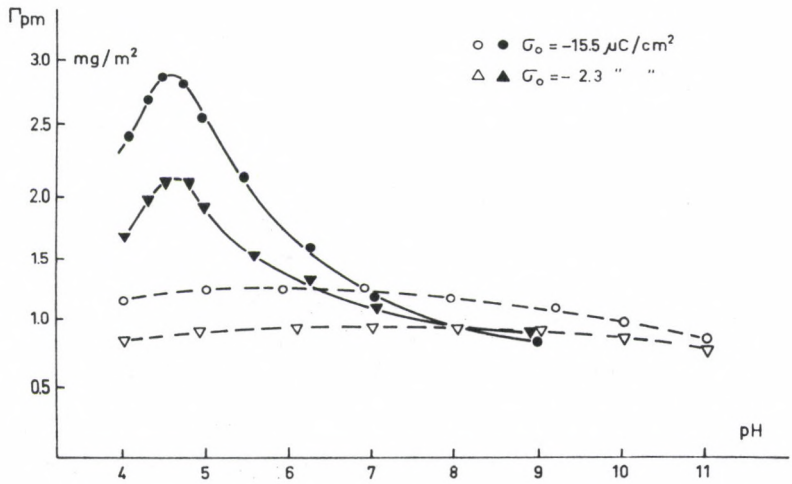

Figure 1. Platform adsorption of HPA (——) and RNase (– – –) on polystyrene latices with different surface charges.
Electrolyte: 0.05 M KNO_3; T = 22°C.

We tend to interpret the observed curves in terms of the internal coherence or, for that matter, flexibility of the molecule, rather than in terms of the formation of an incomplete monolayer[1]. For HPA molecules, the conformational stability is maximal around the i.e.p.[4], where the total negative charge just compensates the total positive charge. However, the more the pH differs from the i.e.p., either to the acid or to the alkaline side, the higher the net charge on the molecule and the likelier it is to unfold. In this picture, HPA adsorbs in the isoelectric region in a thicker layer than outside it and in a conformation that more resembles the conformation in solution. However, as compared to HPA, the dissolved RNase molecule has a more rigid structure, its conformation is less sensitive to pH changes and so is Γ_{pm}. Consequently it is expected that, accepting completion of the monolayer, over a wide pH-region the conformation of the RNase molecules is not drastically changed upon adsorption. Hence, the thickness of the RNase film is little dependent on the pH of adsorption.

The obvious next step is to compare Γ_{pm} with the amounts of protein that can be accomodated in a complete monolayer of molecules of unperturbed dimensions.

The hydrodynamic shape of the dissolved HPA molecule is often referred to as an ellipsoid of rotation having axes of 14 nm, 4 nm and 4 nm[10]. Based on these values and on a molecular weight of 69,000 values of 2.1 mg/m^2 and 7.2 mg/m^2 are calculated for close-packed monolayers in which the molecules are oriented side-on and end-on, respectively.

The RNase molecule is also considered to be an ellipsoid. It has hydrodynamic dimensions of 2.5 x 4.5 x 4.5 nm. Its molecular weight is 13,680[9]. Thus, a close-packed layer of side-on adsorbed RNase molecules would correspond to 1.1 mg/m^2 whereas the end-on orientation would result in 2.0 mg/m^2. Mainly because of the uncertainties in the molecular dimensions, the uncertainty in these calculations are of the order of 25%.

If in the isoelectric region the adsorbed HPA molecules have more or less retained their native conformation, the values found for Γ_{pm} suggest a side-on rather than an end-on orientation. Except at high pH-values (i.c. pH ca. 11), the maximum amount of RNase adsorbed can also be accounted for by assuming a close-packed monolayer of side-on native molecules. However, the finding that Γ_{pm} for the isoelectric HPA and for RNase depends on σ_o, indicates that either those proteins do not adsorb in exactly their native conformation or are tilted to a different degree.

Deželić and Deželić[11] observed that HPA is still immunochemically active when adsorbed on PS latices from a solution of pH 8. In spite of this, in agreement with the ideas presented here, the same authers[12] concluded that at pH 8 the adsorbed HPA molecules are partially unfolded. Apparently, either the conformation of the HPA molecule is not very crucial with respect to its immunochemical activity or the active site is not impaired appreciably.

In the present study it has been observed that upon adsorption at polystyrene surfaces the enzymatic activity of RNase is reduced to virtually zero. Besides to conformational changes this may be due to the inaccessibility of the active site for the large substrate molecule in the adsorbed state.

It is noteworthy that both with HPA and RNase the adsorbed amounts are larger at the more negatively charged PS surface, even at pH > i.e.p. where the net charges of both the protein and the latex are negative. To explain this, we envisage two possibilities which are not mutually exclusive. First, an interpretation can be sought in terms of the relative hydrophobicity of the PS surface and the protein.

Since the $-OSO_3^-$ groups at the PS-surface are monovalent and relatively large, they are expected to break the structure of the vicinal water, i.e. increase its entropy. The number of K^+-ions bound per unit area of PS surface increases with σ_o [13]. Also K^+-ions are assumed to be structure-breakers [14]. In this sense, the hydrophobicity of the PS surface decreases with increasing σ_o.

When an adsorbing protein molecule unfolds at a hydrophobic surface the loss of internal hydrophobic interaction, contributing to the conformational stability of the protein in solution, is more or less compensated for by the gain in hydrophobic interaction between protein and surface. Therefore, it is expected that, under otherwise identical conditions, the tendency to unfold is greater the more hydrophobic the nature of the surface is.

The second possibility for the interpretation of the higher adsorbed amounts at the more negatively charged interface is based on the distribution of the charge in the protein molecule. The likeliness of the charge in the HPA molecule being unevenly distributed and some of the consequences with respect to the adsorption mechanism have been indicated in a previous paper [1]. It is imaginable that local excesses of charge in the protein molecules lead to a more end-on orientation towards the PS surface the more negative σ_o is.

Some representative adsorption isotherms are depicted in figures 2 (HPA series) and 3 (RNase series).

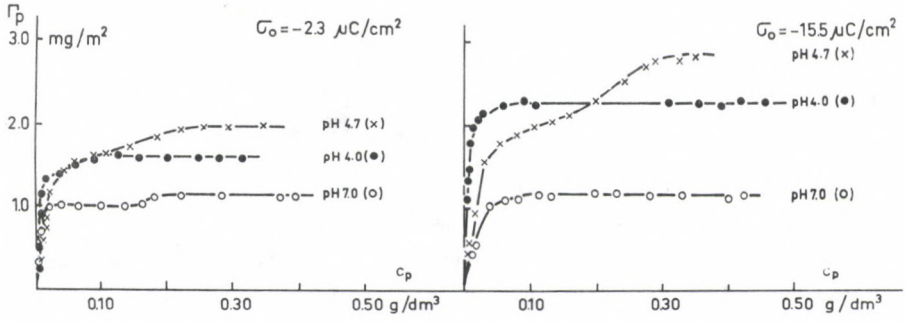

Figure 2. Examples of adsorption isotherms of HPA on polystyrene latices of different surface charge. Electrolyte: 0.05 M KNO_3; T = 22°C.

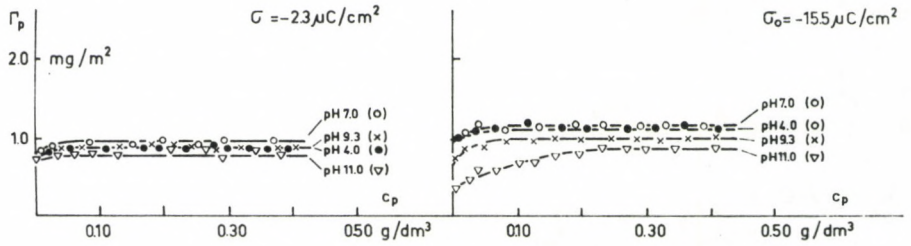

Figure 3. Examples of adsorption isotherms of RNase on polystyrene latices of different surface charge. Electrolyte: 0.05 M KNO_3; T = 22°C.

For both proteins, the adsorption is highly irreversible towards dilution.

Unlike the situation with RNase, the shapes of the isotherms for HPA are very sensitive to the pH (i.e. to the charge of the protein) and to σ_o. This sensitivity for HPA has already been discussed in detail elsewhere[1,7].

Another interesting point of difference between the adsorption behaviour of the two proteins is that the isotherms for HPA sometimes show a step or an inflection point. The occurrence of such transitions suggests different adsorption mechanisms at low and high degree of occupancy. In view of what has been said above concerning the effect of the surface occupancy on the extent of unfolding, the occurrence of transition regions in the isotherms for HPA is not surprising. However, the transitions are most clearly observed for HPA adsorbed from its isoelectric solution where the extent of unfolding upon adsorption is relatively small, a feature for which we have no satisfactory interpretation.

The main point we want to make is that, with due allowance for the complexity of the biopolymer adsorption process, some trends emerge relating adsorption behaviour to the coherence of the dissolved molecules.

This conclusion is important enough to warrant a more detailed study and to that order we have, in addition to the work described above, used ellipsometry, micro-calorimetry and titration as additional techniques. It is our intention to publish this in some detail elsewhere but for the moment it suffices to note that the results of these additional measurements are in general support of the picture developed.

ACKNOWLEDGEMENT. The authors thank Mrs. E. Eikelboom for technical assistance with the RNase adsorption measurements.

REFERENCES

1. J. Lyklema and W. Norde, Croat. Chem. Acta 45, 67 (1973).
2. J.G. Buzzell and C. Tanford, J. Phys. Chem. 60, 1204 (1956).
3. J.F. Foster, 'Plasma Albumin' in The Plasma Proteins, Vol. I, F.W. Putnam, Ed., Academic Press, New York (1960).
4. W.G.M. Braam, Thesis, University of Nijmegen (1972).
5. K. Furusawa, W. Norde and J. Lyklema, Kolloid-Z.u.Z. Polym. 250, 908 (1972).
6. R.G. Fruchter and A.M. Crestfield, J. Biol. Chem. 240, 3875 (1965).
7. W. Norde, K. Furusawa and J. Lyklema, Proc. 6th Int. Congress Surface Active Substances, Zürich, 1972, Carl Hanser Verlag, München (1973).
8. J. Steinhardt, J. Krijn and J.G. Leidy, Biochemistry 10, 4005 (1971).
9. F.M. Richards and H.W. Wyckoff, 'Bovine Pancreas Ribonuclease' in The Enzymes, Vol. IV, P. Boyer, Ed., Academic Press, New York (1971).
10. P.G. Squire, P. Moser and C.T. O'Konski, Biochem. J. 7, 4261 (1968).
11. N. Dežélić and G. Dežélić, Croat. Chem. Acta 42, 457 (1970).
12. G. Dežélić, N. Dežélić and Z. Telišman, Eur. J. Biochem. 23, 575 (1971).
13. W. Norde, Mededelingen Landbouwhogeschool, in preparation.
14. J.L. Kavanau, 'Water and Solute-Water Interactions', Holden-Day Inc., San Francisco, 1964.

STRUCTURE OF POLYMER ADSORPTION LAYERS

Yu.A.Eltekov

Institute of Physical Chemistry U.S.S.R. Academy of Sciences, Leninsky Prospect, 31, Moscow, USSR

The structure of adsorption layers of linear macromolecules on the surface of non-porous bodies were studied by adsorption, chromatographic and spectral methods. It has been shown that for preferential adsorption of macromolecules from diluted solutions in solvents, the molecules of which weakly interact with the adsorbent surface, the thickness of the adsorption layers does not, as a rule, exceed 2 nm. During adsorption of this type, coils of macromolecules strongly deformate and the macromolecule tends to arrange all its segments on the surface. On the basis of the monolayer model of polymer adsorption, the constants of adsorption equilibrium were estimated for certain systems.

The contempary molecular-statistical theory of polymer adsorption uses the lattice model of solution structure. One of the problems of the adsorption theory is calculation of the constants of adsorption equilibrium and determination of the adsorption layer structure. From structual data of adsorp tion layers the molecular parameters of adsorption particles can be estimated. According to the statistical theory of polymer adsorption developed by Simha, Eirich and Frisch (1-3), only certain segments of the macromolecular chain attach to the adsorbent surface and, consequently, the thickness of the polymer adsorption layer can be considerable. According to recent statistical theories of polymer adsorption (4-7) the amount of adsorbed segments of the chain depends on the interaction energy of the segments ε , and at values $\varepsilon > \frac{1}{4}kT$

practically all the segments of the macromolecule are attachned to the adsorbent surface. In this case the thickness of the layer corresponds to the thickness of the monolayer of macromolecules stretched out along the surface. Experimental studies of polymer adsorption on various solid bodies give different values of thickness of polymer adsorption layers. In the present work adsorption of linear macromolecules on non-porous adsorbents was studied to determine the structure of the adsorption layers of these polymers.

EXPERIMENTAL

Pigment-grade rutile (s = 4 m^2/g), aerosil (s = 170 m^2/g) and carbon black of the graphon type (s = 85 m^2/g) were used as the non-porous adsorbents. The specific surface (s) was determined by the BET method from data of low-temperature nitrogen adsorption. The adsorbents were vacuum treated for 8 hr at 180°C prior to the tests.

The following oligomers and polymers were studied: polyoxyethylene (POE) with molecular weight (MW) 300, 3,000, 15,000; polystyrenes (PS) with MW 40,000 and 300,000; polyvinylacetate (PVA) with MW 180,000; polydimethylsiloxane (PDMS) with MW 350,000; polyacrylamide (PAA) with MW 30,000; polymethylmethacrylate (PMMA) with MW 300,000 and 330,000.

The solvents used were double-distilled water, methylethylketone, chloroform, carbon tetrachloride and n-hexane. The organic solvents were distilled and kept over granulated NaA zeolite without binder. Adsorption tests were carried out in adsorption ampoules using diluted polymers (8). The solutions were mixed with the adsorbents for 7-10 days. Values of Gibbs' (excessive) adsorption were determined from expression

$$\Gamma = \frac{(C_o - C) \cdot m}{m_a s} \qquad (1)$$

where C_o and C are polymer concentrations before and after adsorption, m is the amount of polymer solution and m_a and

s are the amount and the specific surface of the adsorbent. Variation of polymer concentration in the solution caused by adsorption was determined on an interferometer and in certain cases on an IR-spectrometer.

Spectral (9) and gas-chromatographic (10) methods were also used to determine the structure of the polymer adsorption layer. Maximum adsorption values (Γ_m) of the polymers studied from diluted solutions are presented in Table 1.

Table 1

Maximum values of polymer adsorption

Polymer	MW	Solvent	Adsorbent	Γ_m mg/m^2
POE	30,000	H_2O	carbon black, 3000°	0.6
-"-	15,000	-"-	-"- -"-	0.7
PAA	30,000	-"-	-"- -"-	0.3
PS	40,000	CCl_4	-"- -"-	0.7
-"-	300,000	-"-	-"- -"-	0.8
-"-	-"-	-"-	Rutile	0.7
-"-	-"-	-"-	Aerosil	0.9
PVA	180,000	-"-	-"-	0.8
PDMS	350,000	n-hexane	-"-	0.7
PMMA	300,000	$CHCl_3$	-"-	0.4
-"-	330,000	$CH_3COC_2H_5$	carbon black, 3000°	0.6

Similar values of corresponding parameters of adsorption of linear polymers are reported by other researchers (Table 2).

In Tables 1 and 2 the values of Gibbs' adsorption are presented as the excess of polymer in the adsorption phase as compared with its content in solution bulk. At low concentrations of polymer in solution bulk these values are close to the total content of polymer on the adsorbent surface. To estimate τ - the thickness of the adsorption layer,

$$\tau = \frac{\Gamma_m}{\rho_a} \qquad (2)$$

Table 2.

Maximum values of polymer adsorption. (Publisched data).

Polymer	MW	Solvent	Adsorbent	Γ_m, mg/m^2	Ref.
POE	5,000	H_2O	carbon black, 3000°	0.6	11
-"-	18,000	-"-	-"- -"-	0.8	11
-"-	-"-	C_6H_6	aerosil	0.9	11
-"-	5,000	-"-	-"- -"-	0.8	11
PMMA	33,000	-"-	-"- -"-	0.9	12
-"-	290,000	-"-	-"- -"-	0.9	12
-"-	822,000	-"-	-"- -"-	0.9	13
PS	105,000	-"-	-"- -"-	0.6	13
-"-	32,000	-"-	-"- -"-	0.5	14
-"-	135,000	-"-	-"- -"-	0.6	14
PVA	465,000	-"-	-"- -"-	0.9	15

the density of the adsorbed polymer is assumed equal to the density of the polymer in block. The model is also based on the assumption that at $\Gamma = \Gamma_m$, molecules of the solvent are practically entirely forced out of the adsorption layer by the macromolecules of the polymer. This assumption is apparently correct, since further increase of polymer concentration in solution does not result in increase of adsorption.

It is of interest to analyse the dependence of Γ_m on M - the molecular weight of polymerhomologues. For adsorption of non-deformated macromolecular coils

$$\Gamma_m = AM^{1/3} \qquad (3)$$

And for vertical arrangement of the adsorbed macromolecules

$$\Gamma_m = AM \qquad (4)$$

In the case of adsorption of macromolecules stretched out along the surface the exponent n at M is close to 0. A slight increase of Γ_m with M is due to densening of the

adsorption layer as a result of substitution of van der Waals (molecular) radii for interatomic distances.

Values of n for adsorption of linear polymers are presented in Table 3.

Table 3

Values of n in $\Gamma_m = AM^n$

Polymer	Range of M	Adsorbent	n	Reference
POE	300-15,000	carbon black,3000°	0.15	10,11
POE	600-15,000	aerosil	0.07	11
PS	40,000-300,000	-"- -"-	0.06	8
PVA	140,000-900,000	tin powder	0.09	16
PMMA	230,000-2560,000	aerosil	0.01	17
-"-	33,000-290,000	-"-	0.00	2

It follows from data of Table 3 that values $n < 0.2$ are typical for linear polymers. This indicates considerable deformation of macromolecular coils in the field of adsorption forces and prevailing parallel arrangement of macromolecules in the adsorption layer. The value of p for excited carbonyl groups in the chains of PVA and PMMA macromolecules adsorbed on the surface of aerosil was estimated by the IR--spectroscopic method (9). Values of p for PVA, PMMA and polylaurylmethacrylate (PLMA) are given in Table 4. Thus, more than one-third of the carbonyl groups of PVA, PMMA and PLMA macromolecules directly interact with hydroxyl groups of the aerosil surface. These data indicate that the macromolecular coils are strongly deformated and stretch out along the surface.

Gas-chromatographic data of molecules on adsorbents with various polymers pre-adsorbed on their surface indicate that with increase of the content of adsorbed polymer the value of V_e (retention volume) at first sharply decreases, then at a certain value of polymer adsorption it becomes independent of the amount of polymer adsorbed (Fig.1).

Table 4

Values of p for adsorption on aerosil.

Polymer	MW	Solvent	p	Reference
PVA	180,000	$CHCl_3$	0.4	9
PMMA	300,000	$CHCl_3$	0.3	9
-"-	320,000	C_2HCl_3	0.35	13
PLMA	330,000	$C_{12}H_{26}$	0.36	18
-"-	1190,000	$C_{12}H_{26}$	0.36	18

The amount of adsorbed polymer at which V_e does not further depend on Γ corresponds to formation of a dense monolayer of the adsorbed polymer. However, data obtained by other methods give higher values of the thickness of adsorption layers of linear polymers . The thickness of polymer layers on glass surface were estimated by measurement of polymer viscosity in narrow capillaries (Table 5).

Table 5.

Thickness of polymer layer on glass according to viscosimetric data.

Polymer	MW	Solvent	concentration, mg/g	τ, A	Ref.
PS	110,000	cyclohexane	1.0	200	19
-"-	950,000	-"-	1.0	550	19
-"-	-"-	benzene	1.0	250	19
-"-	110,000	-"-	1.0	600	19
-"-	400,000	toluene	0.5	750	20
-"-	800,000	-"-	0.5	1500	21
PVA	880,000	-"-	0.1	4700	22
-"-	-"-	-"-	0.1	1200	21
PMMA	230,000	benzene	0.1	140	19
-"-	1430,000	-"-	0.1	740	19

The values of τ calculated from polymer viscosity are high and apparently, are due not to adsorption but to other factors.

The rheological method of estimating the thickness of polymer adsorption layers developed in (23) is valid for non-interacting spherical practicles, uniformally covered by the polymer layer. It is hard to expect that these conditions are fulfilled and therefore the values of τ determined by this method are considerably overstated.

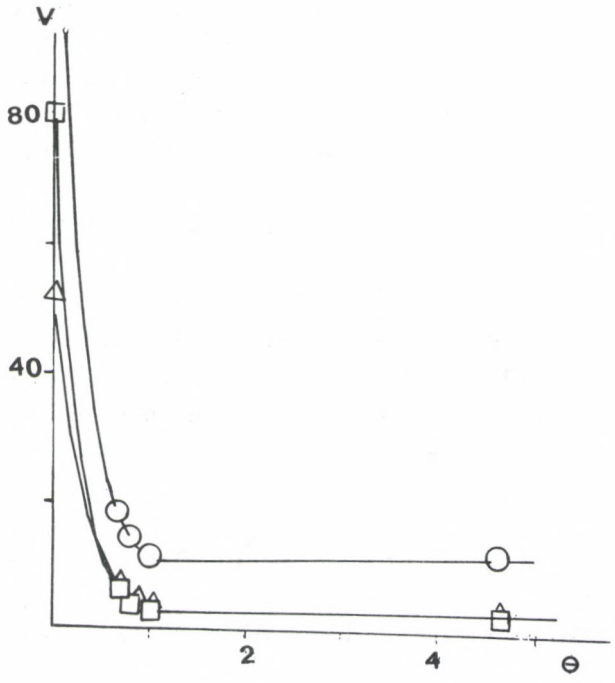

Fig.1.

Dependence of V_e - retention volume of benzene (circle), n-pentane (square) and ether (triangle) on the value of polymer adsorption.

REFERENCES

1. H.L.Frisch, R.Simha, F.R.Eirich, J.Chem.Phys. 21, 365(1953)
2. R.Simha, H.L.Frisch, F.R.Eirich, J.Phys.Chem.57, 584(1953)
3. H.L.Frisch, R.Simha, J.Chem.Phys. 27, 702 (1957).
4. W.G.Huguchi, J.Phys.Chem. 65, 487 (1962).
5. A.Silberberg, J.Phys.Chem. 66, 1873, 1884 (1962).
6. A.Silberberg, J.Phys.Chem. 46, 1105 (1967).
7. K.Motomura, R.Mutuura, J.Chem.Phys. 50, 1281 (1969).
8. A.V.Kiselev, V.N.Novikova, Yu.A.Eltekov, Dokl. AN SSSR 149, 131 (1963).
9. A.V.Kiselev, V.I.Lygin, I.N.Solomonova, D.O.Usmanova, Yu. A.Eltekov, Kolloidn.Zh. 30, 386 (1968).
10. Yu.A.Eltekov, V.V.Khopina, A.V.Kiselev, N.V.Kovaleva, J.Colloidn.Interface Sci. 47, 795 (1974).
11. G.L.Howard, P.Mc Counell, J.Phys.Chem. 71, 2974, 2981 (1967).
12. J.M.Herd, A.J.Hopkins, G.L.Howard, J.Polym.Sci. C-34, 211 (1971).
13. C.Thies, J.Phys.Chem. 70, 3783 (1966).
14. G.L.Howard, S.J.Wood, J.Polym.Sci. A-2, 10, 1023 (1973).
15. G.Thies, J.Colloid.Interface Sci. 27, 734 (1968).
16. J.Koral, R.Ullman, F.R.Eirich, J.Phys.Chem. 62, 541(196)
17. C.Thies, P.Peysen, R.Ullman, Proc. 4th, Intern.Congress Surface
18. B.J.Fontana, J.R.Thomas, J.Phys.Chem. 65, 480 (1961).
19. F.W.Rowland, R.Bules, E.Rothstein, F.R.Eirich, Ind. Eng. Chem. 57, 46 (1965).
20. H.G.Fendler, H.Rohlender, H.A.Stuart, Macromol.Chemie 18, 383 (1955).
21. O.E.Ohren, J.Polymer Sci. 19, 199 (1951).
22. C.A.F.Tuijnman, J.J.Hermans, J.Polymer Sci. 25, 385(1957).
23. A.Doroszkwski, R.Lambourne, J.Colloid. Interface Sci. 26, 210 (1968).

POLYMER ADSORPTION ONTO POROUS GLASS FROM THETA SOLVENT

K. Furusawa, H. Nakanishi, and A. Kotera

Department of Chemistry, Tokyo Kyoiku University,
Otsuka, Bunkyo, Tokyo, Japan

Introduction

The adsorption phenomenon of polymer from dilute solution on the solid surface has not been sufficiently understood in spite of numerous experimental and theoretical studies[1]. Progress in this field has been slowed by a lack of experimental data on the adsorption from theta solvents using well defined polymers and adsorbents. The present study reports the adsorption of narrow distributed polystyrens from cyclohexane solution at 35 °C onto porous glass which has been characterized by using mercury porosimeter and nitrogen adsorption.

Experimental

Materials) Narrow distribution polystyrene samples used in this study were anionically polymerized and commercially distributed by Pressure Chemicals(U.S.A.) as standard samples of gel permeation chromatography(GPC). The ratios of weight and number average molecular weight M_w/M_n were found to be approximately less than 1.1 by light scattering and osmotic pressure measurements. The molecular weight data for these samples are listed in Table 1. Cyclohexane, employed as the theta solvent, was purified by the usual procedures and were freshly distilled prior to use. Physical constants of the solvent were as follows;

$$n_{25°C}^{D} = 1.4233, \quad d_{35°C} = 0.7642, \quad d_{40°C} = 0.7689$$

The theta temperature in polystyrene-cyclohexane system was

Table 1, Molecular weight data for the polystyrene standards used in this study.

Polymer designation	$M_w \times 10^{-4}$	$M_n \times 10^{-4}$	M_w/M_n
PS-0.4	-	0.37 ±0.04	<1.10
PS-1	1.00 ±0.10	1.09 ±0.05	<1.06
PS-5	5.01 ±0.25	5.05 ±0.20	<1.06
PS-11	11.3 ±0.50	11.2 ±0.40	<1.06
PS-20	20.0 ±1.0	19.3 ±0.8	<1.06
PS-50	50.7 ±2.0	49.4 ±0.20	<1.20
PS-67	67.0 ±3.2	64.0 ±3.2	<1.10

determined as 35 °C by light scattering measurements. This value is in good agreement with the reported one, for example, 34.8°C by Orofino et.al.[2].

The adsorbent used in this study was commercial porous glass beads with a particle size of 200 ∿ 400 mesh which were supplied by Bio Rad Laboratory(Richmond, California, U.S.A.) as GPC column packing material and was designated as Bio-Glass-500. The pore size and the surface area of the glass beads were determined by the mercury porosimeter and BET methods, respectively, and it was shown that the average pore size is 175 ±17A in radius and the surface area per one gram of glass beads 95.43 m^2/gr. They were washed for 24 hrs., using the refluxing method with cyclohexane, dried in a vaccum oven at 130 °C for 48 hrs., and stored in a dry atomosphere.

Viscosity measurement) Viscosities were measured with an Ubbelohde viscometer in the temperature range of 31.0 ∿ 40.0°C. Intrinsic viscosity ,$[\eta]$, was obtained by Huggins equation. $[\eta]_\theta$ at the theta temperature was determined by way of interpolation to 35 °C.

Adsorption measurement) Adsorption measurements were conducted as follow; a given quantity of a polymer solution containing known concentration of the polymer was introduced into an adsorption tube which contained a weighed quantity of the porous glass. After the tube was stoppered and sealed,

they were mounted in a shaker and agitated slowly for a desired period of time in a thermostat controlled at 35 ±0.05 °C. After completion of the adsorption period, the adsorbents were separated from the solution and the remaining concentrations were determined by a Narumi differential refractometer using the calibration curve. From these measurements, the amounts of polymer present in the solution before and after being in contact with the adsorbent were determined and the amount of adsorption , A_S, in milligrams of adsorped polymer per square meter of adsorbent, was calculated.

Results and Discussion

Rate of adsorption) To estimate the rate of adsorption, the quantity of adsorbed polymer was determined, after agitating the tubes at various time intervals from 0.1 to 24 hrs., at an initial polymer concentration of 4 mg/ml. As shown in Fig.1, the time required to reach the equilibrium adsorption

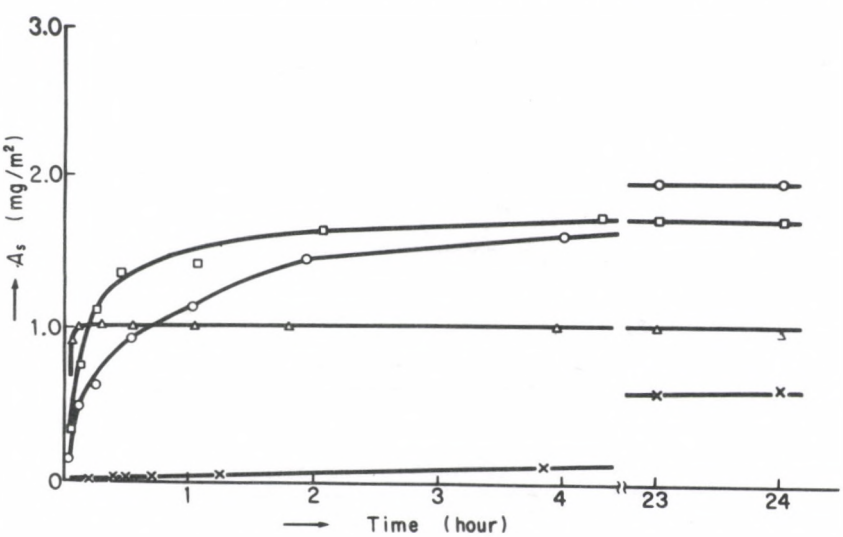

Fig.1, Rate of adsorption of polystyrene on porous glass from cyclohexane solution at 35 °C.

(X); PS-50, M_W = 507,000 (o); PS-20, M_W = 200,000
(□); PS-11, M_W = 113,000 (△); PS-1, M_W = 10,000

greatly depended upon the molecular weight of the polymer. This tendency presumably represents in the reduced diffusion rate into the narrow pores of the surface and effective surface area of the adsorbent due to the increase in the molecular weight of polymer. Particularly, the highest molecular weight sample(PS-5, M_W = 507000) required a longer time to reach the equilibrium and an apparent equilibrium was established scarcely after 24 hrs, but a subsequent slight increase in adsorption, barely detectable within the experimental error, appears to continue for several days. In the present work, however, 24 hrs. was employed as a standard adsorption time, since no difference in the amount of adsorption between the contact time 23 and 24 hrs. was found in all samples except for the highest molecular weight sample.

Adsorption isotherm) Fig.2 shows adsorption isotherms for the series of polymers of different molecular weight. It is evident that the amount of adsorption at the plateau region

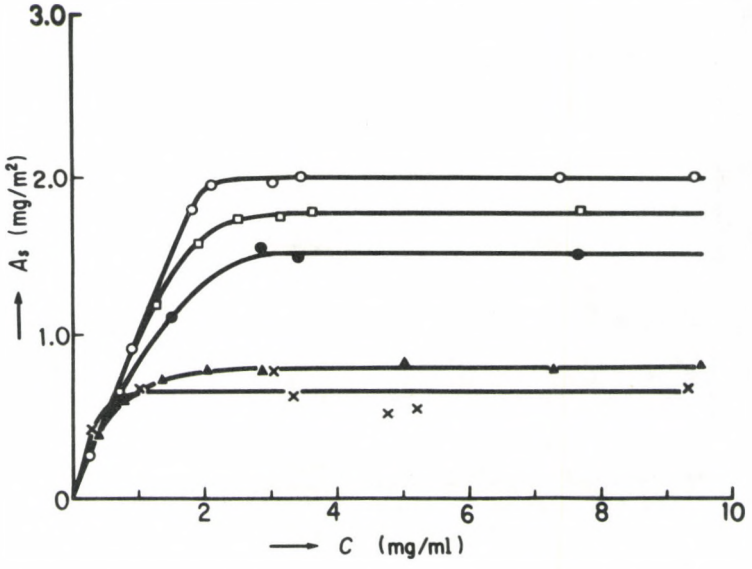

Fig.2, Adsorption isotherms of polystyrene on porous glass from cyclohexane solution at 35 °C.

(x); PS-50, M_W = 507,000 (o); PS-20, M_W = 200,000
(□); PS-11, M_W = 110,000 (◉); PS-5, M_W = 50,100
(▲); PS-1, M_W = 10,000

depends significantly upon molecular weight and increases with increasing molecular weight except that of the highest molecular weight sample. Discluding the highest molecular weight sample, this behavior is a manner expected theoretically in polymer adsorption on solid surfaces[3]. The initial slope of the isotherm reflects more clearly the interactions between the adsorbate and the adsorbed polymer, as the lateral order interaction among the adsorbed molecules in this region can be disregarded. In the present work, the initial slope does not generally show a very high affinity character, as is often observed for a synthetic polar polymer[4], though an obvious molecular weight dependency is observed, i.e., the initial slope of isotherm increases with increasing the molecular weight of polymer. The quantities of adsorbed polymer measured at the plateau region for each polymer were very close to the recent measurements of G.H.Howard et.al.[5] for the adsorption of polystyrene on Areosil silica from theta solvents.

Molecular weight dependence) Generally, in polymer adsorption onto nonporous and homogeneous solid surface, the relation between maximum adsorption ,A_S, and molecular weight of adsorbed polymer ,M, is written over a wide range of molecular weight as follows;

$$A_S = KM^{\alpha} \qquad (1)$$

Where K and α are constants. According to R.Ullman[6], the conformation of adsorbed polymer chain at the solution-solid interface can be determined from the application of Ullman's three models corresponding to the α-value obtained experimentally. These models of polymer chain adsorbed were

(1) $\alpha = 0$, Maximum adsorption is independent of molecular weight. In this case, the polymer molecule is tightly adsorbed onto solid surface with all segments.

(2) $\alpha = 1$, Maximum adsorption is directly proportional to molecular weight. Here, the polymer chain is adsorbed with a few segments at interface and other segments extended into solution.

(3) $0 < \alpha < 1$. Maximum adsorption increases exponentially

with the increase of molecular weight. Adsorbed polymer chain consists of sequences and loops, which is designated as the loop adsorption.

Molecular weight dependence of A_S obtained in the present work is shown in Fig.3 by log A_S - log M plot. The sharp fall in A_S for the high molecular weight samples may be attributed to the porous nature of the adsorbate, i.e., the relation between the radius of gyration of polymer chain in solution and the radius of pore of the adsorbate effects on the effective adsorption area at solid surface for adsorption. Discluding A_S of the high molecular weight samples, $\alpha = 0.26$ was determined from the gradient of straight line. This value suggests that the adsorption in the present system will be a loop adsorption in the Ullman's models.

The mean radius of gyration of an isolated polymer chain in thata state, $\langle s_0^2 \rangle^{1/2}$, can be estimated from the intrinsic

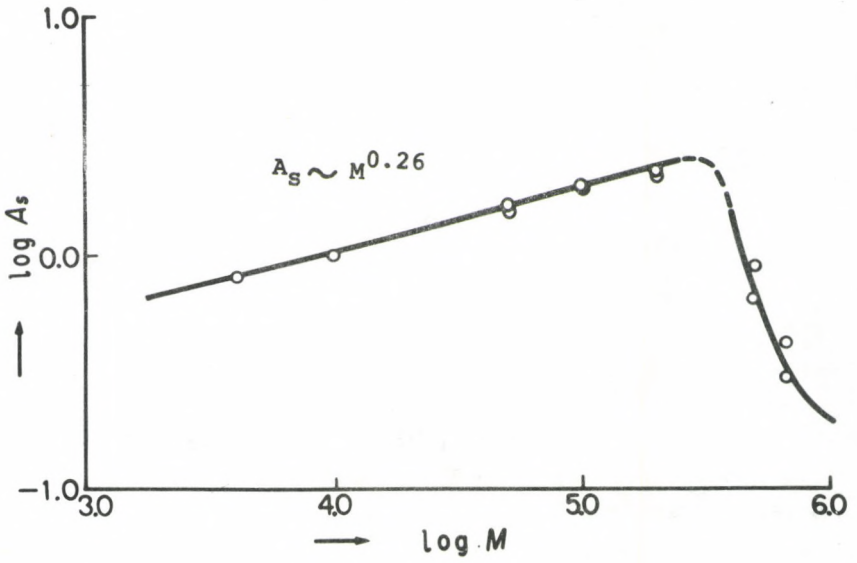

Fig.3, Molecular weight dependence of maximum adsorption of polystyrene on porous glass from cyclohexane solution at 35 °C.

viscosity ,[η], using Flory-Fox[7] equation. The intrinsic viscosity in theta state, $[\eta]_\theta$, may be related to the molecular weight as follows;

$$[\eta]_\theta = K_\theta M^{1/2} \qquad (2)$$

and

$$K_\theta = \Phi \left(\frac{6 \langle s_0^2 \rangle}{M}\right)^{3/2} \qquad (3)$$

Where Φ is the universal Flory constant and assumed to have its usual value of 2.87×10^{21}. On the other hand, K_θ in above equations may be determined experimentally from the viscosity measurements in theta state using narrow-distribution polystyrene samples and the following viscosity equation was obtained;

$$[\eta]_\theta = 7.69 \times 10^{-4} M^{1/2} \qquad (4)$$

The numerical result in equation (4) is close to the previously found value[8], $K_\theta = 7.6 \times 10^{-4}$. The root mean square radius of gyration of polystyrene in theta state can be expressed explicitly as follows;

$$\langle s_0^2 \rangle^{1/2} = 0.263 \times 10^{-8} M^{1/2} \qquad (5)$$

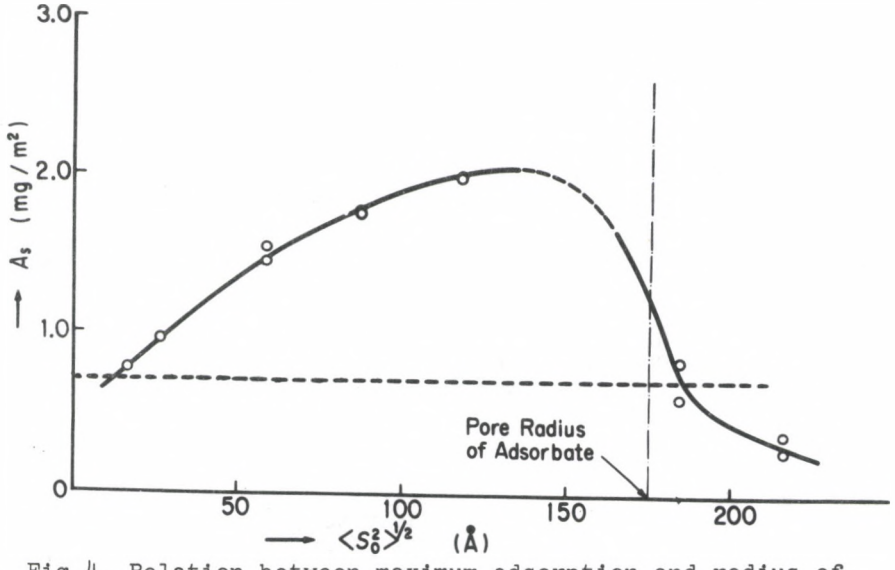

Fig.4, Relation between maximum adsorption and radius of gyration of polystyrene in solution.

From equation (5), we can find a relation between $\langle s_\theta^2 \rangle^{1/2}$ and A_s and plotted the results in Fig.4 by a solid line. While, assuming that a monolayer consisting of randamly coiled polymer chain in solution was formed at adsorption saturation, then the relation between $\langle s_\theta^2 \rangle^{1/2}$ and A_s is given in a horizontal dotted line showing in Fig.4. Comparison of these two lines in the figure reveals that the dotted line is always much smaller than the solid one, especially in high molecular weight region the difference is remarkable. This suggests that there was considerable compression of the polymer chain upon adsorption and the tendency is seen markedly in high molecular weight sample. This results are in accordance with the deduction obtained from the initial slope of adsorption isotherm, i.e., the affinity of polymer molecule for adsorbent increased with increasing molecular weight.

References

1) e.g., A.Silberberg, J.Phys.Chem.,66,1884(1962); F.Patat, E.Killmann and C.Schliebener,Fortschr.Hochpolym. Forsch.3,332(1964)

2) T.A.Orofino and J.W.Mickey, J. Chem. Phys.,38,2512 (1963)

3) R.Simha, H.L.Frisch and F.R.Eirich, J. Phys. Chem., 57, 584(1953)

4) E.Hamori, W.C.Forsman and R.E.Hughes, Macromolecules, 4, 193(1971)

5) G.J.Howard and S.J.Woods, J. Polym. Sci., Part A-2, 10, 1023(1972)

6) R.Ullman, in Encyclopedia of Polymer Science and Technology, Vol.1, H.F.Mark, N.G.Gaylord and N.Bikales, Eds., Interscience, New York, 1964, pp 551

7) T.G.Fox and P.J.Flory, J. Amer. Chem. Soc., 73, 1909 (1951)

8) H.Utiyama, Dissertation Kyoto Univ., Kyoto, Japan (1962)

Group I/6
Adsorption of surfactants

Studies on different models of adsorption kinetics of surface active substances

G.Kretzschmar

Central Institute of Organic Chemistry, Academy of Sciences of the German Democratic Republic, 1199 Berlin-Adlershof

The rate of adsorption of surface active substances at a liquid-air interface is usually measured by the vibrating jet method in the range at low times, while in the case at long times the adsorption is determined by a direct investigation of surface tension.

The analysis of experimental results leads to different interpretations. Addison [1], Rideal and Sutherland [2] , Posner and Alexander [3] ,proposed a barrier-limited adsorption mechanism to explain their results with some surface active substances.

On the other hand Defay and Hommelen [4] , found a diffusion-limited process by investigations of the adsorption of short chain alcohols. Similar calculations were made by Netzel and Hoch [5] on the adsorption of polyglycol ether. Lange [6,7] studied the long time adsorption of dodecyl heptaglycol ether and explained his results in terms of a diffusion-limited process with a remarkable dependence of the coefficient of diffusion by the concentration. His treatment on the inequivalence of spread and adsorbed films is a basic fact. Already Fordham [8] , has explained[a] theory on the influence of concentration gradients at surface tension. Essential for this problem is the work of Hansen [9] . He analysed his own work with Wallace [10] and the results in the paper of Defay and Hommelen [4] and concluded, that the influence of the concentration gradient may be respected in the following way:

$$\pi_{dyn} = \pi_{stat.} + RT\int_0^\infty (c_{x,t} - c_0)\,dx = \overline{\pi}_{st.} - \Gamma RT \quad (1)$$

The interpretation of our own results Kretzschmar and Vollhardt [11] , Kretzschmar [12] is based on the theory of Fordham and Hansen.
In this report we shall explain a treatment for an equation of state of Langmuir-type, which encloses the concentration gradient. This equation is practicable for dynamic adsorption systems.

Experiments

The rate of adsorption was measured by registration the change of the dynamic electric potential, which depends on time. The apparate for this purpose we have described at another place [13] .
α-dodecyl-ω-hydroxy-hexa(oxyethylene) is suitable for this experiments, because its surface potential is already big in the range of a small film pressure. This is shown by the two curves in fig.1. In fig. 2 is plotted the dynamic surface potential of the same substance against the time of adsorption.
By comparing fig.1 and fig.2 we can see, that the maximum values of dynamic potentials are in same order with the static ones.
In the present instance we assume, that a fixed surface potential taking place, corresponds to the same surface state. From this conclusion it is possible, to calculate the density of adsorption Γ by using the laws of diffusion, for instance the equation of Ward and Tordai [14] , or in the simplest case

$$\Gamma_t = 2C_0\sqrt{\frac{Dt}{\pi}} \qquad (2)$$

Without going through all the details of the arguments, we suppose the equilibrium between the interface a and the sublayer l , in terms of diffusion the coordinate x=0, and write $\mu_a = \mu_l$ (μ=chemical potential)
A useful equation of state in surface chemistry is given by a van der Waals analogous form:

$$\left(\pi + \frac{a}{A^2}\right)(A - A_0) = RT \qquad (3)$$

π =film pressure, a=coefficient of interaction, A=area of adsorbed film, $A_0 = \frac{1}{\Gamma_\infty}$

Hückel [15] and Cassel [16] combined equ.(3) with the equation of Gibbs $\Gamma = -\frac{a}{RT}\frac{d\sigma}{d\ln a}$ and got the isotherm

$$c = K' \frac{\theta}{1-\theta} \exp \theta/1-\theta \exp -2a\Gamma/RT \qquad (4)$$

We can write

$$\ln\left[\left(\frac{1-\theta}{\theta}\right)\frac{c}{K'}\right] = \left[\frac{\theta}{1-\theta}\right] - \frac{2a\Gamma}{RT} \qquad (5)$$

Without energy-barrier we calculate the mass transfer at interface by using equ.(2), q by the critical values of equ. (3) and $c=c_{x=0}$ with the aide of fig.1.

According to this, we can construct the curves in fig.3. From the theoretical point of view we expect straight lines in the case of a normal diffusion limited adsorption.

An analysis of possible reasons of this deviation leads to remarkable results. If the time of adsorption becomes smaller, the deviation from a straight line is increasing. Take we into account an energy barrier, we have a discrepance by comparing our results with Hansen's criterion. Starting from the work of Sutherland [17] , Hansen notes, that diffusion-limited mechanism have at low time a dependence of $\Gamma = f(t^{1/2})$, whereas the function of a barrier-limited adsorption is $\Gamma = f(t)$.

We shall begin in an elementary way by finding a new correlation between the $c_{x=0}$-values in the equation of state for static and dynamic systems. The derivation is based on the same simplification of statistical thermodynamics, which leads to the Langmuir-equation.

The chemical potential of a particle in solution is by van Laar:

$$\mu_i = \mu_i^\circ + kT \ln\left(\frac{N_1}{N_1+N_2}\right) + \left(\frac{N_2}{N_1+N_2}\right)\Delta u^\circ \qquad (6)$$

μ° =chemical standard potential

N_1, N_2 =number of species 1 or 2

u° =potential energy between two particles

with $\mu_l^o = kT \ln f_1 + u_o^1 + pv_1$ (1= partition function).
In the adsorbed state:

$$\mu_a = kT \ln f_a + kT \ln \left(\frac{\theta}{1-\theta}\right) \mu_a \qquad (7)$$

In the state of equilibrium between interface and sublayer it results:

$$\theta = \frac{1}{1 + \frac{N_1+N_2}{N_1} \cdot \frac{f_2}{f_1} \exp -\left[w + pv_l + \left(\frac{N_2}{N_1+N_2}\right)^2 \Delta u\right]} \qquad (8)$$

or

$$\theta = \frac{1}{1 + \frac{N_1+N_2}{N_1} \cdot \frac{f_2}{f_1} \exp -z} \qquad (9)$$

By substituting the equation of Gibbs into the equ. (9) we derive

$$\Delta G = \frac{p_o RT \ln a}{1 + 1/x_1 \cdot f_2/f_1 \cdot \exp -z} \qquad (10)$$

We assume, that the partition function of the translation of molecules between interface and sublayer may be influenced by the "force" $K = \frac{du}{dx}$ of the concentration gradient.
By application of the law of force in its general form $\frac{mu^2}{2} + K_n x^n$ we have for the translation (n=1) between surface and sublayer

$$f_{1x} = \left(\frac{2\pi kT}{h}\right)^{1/2} \frac{kT}{K} \qquad (f_1 = f_a) \qquad (11)$$

The oscillation in the bulk phase (n=2)

$$f_{2x} = \frac{kT}{2h\nu} \qquad (f_2 = f_1) \qquad (12)$$

Therefore we have:

$$\frac{f_{2x}}{f_{1x}} = \frac{K_1 \text{ equilibr.} + K_1 \text{ unequilibr.}}{2\nu \, (2\pi \, mkT)^{1/2}} \qquad (13)$$

or

$$\frac{f_{2x}}{f_{1x}} = A + BK_{1\text{unequilibr.}} \qquad (14)$$

Therefore:

$$\frac{f_2}{f_1} = \frac{f_{2y} f_{2z}}{f_{1y} f_{1z}} \left(A + BK_{1\text{unequilibr.}}\right) = A' + B' K_{1\text{unequil.}} \qquad (15)$$

According to (8-15) we have:

$$\Delta G = \frac{\Gamma_0 RT \ln a_1}{1 + 1/x_1 (A' + B' K_{1\,un.}) \exp -2} \qquad (16)$$

$$\Delta G = \frac{\Gamma_0 RT \ln a_1}{1 + 1/x_1 (A'' + B'' K_{1\,un.})} \qquad (17)$$

$$\frac{\Gamma}{\Gamma_0} \quad \frac{1}{1 + 1/x_1 (A'' + B'' K_{1\,un.})} \qquad (18)$$

The constant A'' may be obtained by evaluation of the static adsorption, if $K_{1\,uneqilibr.}=0$, whereas the constant B'' results by approximation using the dynamics experiments. In tab.1 we can see with $A''=4{,}26 \cdot 10^{-8}$ and $B''=7{,}4 \cdot 10^{3}\,dyn^{-1}$ the difference between static and dynamic $C_{x=0}$-values for α-dodecyl-ω-hydroxy-hexa(oxyethylene).

Table 1

adsorption time (sec)	$\Delta V_{dyn.}$ (mV)	$c_{x=0} \cdot 10^7$ stat.	$c_{x=0} \cdot 10^7$ corr.
0,9	- 30	5,90	37,30
0,8	32	5,85	35,52
0,6	44	4,45	32,48
0,5	62	4,90	29,76
0,4	98	4,15	27,14
0,3	168	2,95	25,58
0,2	280	1,30	24,65
0,15	344	0,65	18,40

On comparing the $c_{x=0}$ values, we find that in dynamic and static systems the lapse of concentration is different. The straight line in fig.3 is calculated by using the data of tab.1.

References

|1| Addison,C.C.: J.Chem.Soc.1946,579

|2| Rideal,E.K.,and K.L.Sutherland: Trans.Faraday Soc.48, 1109(1952)

|3| Posner,A.M.,and A.E.Alexander: Trans.Faraday Soc.45, 651(1949)

|4| Defay,R.,and J.R.Hommelen: J.Colloid Sci.14,401(1959)

|5| Netzel,D.A.,G.Hoch and T.J.Marx: J.Colloid Sci.19,774 (1964)

[6] Lange,H.: J.Colloid Sci. 20,50 (1965)
[7] Lange,H.: Kolloid Z.Z.Polymere 201,131 (1965)
[8] Fordham,S.: Trans.Faraday Soc. 50,593 (1954)
[9] Hansen,R.S.: J.Colloid Sci. 16,549 (1961)
[10] Hansen,R.S.,and T.C.Wallace: J.Phys.Chem. 63,1085(1959)
[11] Kretzschmar,G.,and D.Vollhardt: Ber.Bunsenges.phys.Chem. 71,410 (1967)
[12] Kretzschmar,G.: Tenside 9,267 (1972)
[13] Kretzschmar,G.: Kolloid Z.Z.Polymere 206,60 (1965)
[14] Ward,A.F.H.,and L.Tordai: J.chem.Physics 14,453 (1946
[15] Hückel,E.: Trans.Faraday Soc. 28,442 (1932)
[16] Cassel,H.J.: J.physic.Chem. 48,195 (1944)
[17] Sutherland,K.: Australian J.Sci.Research A5,683 (1952)

Figures

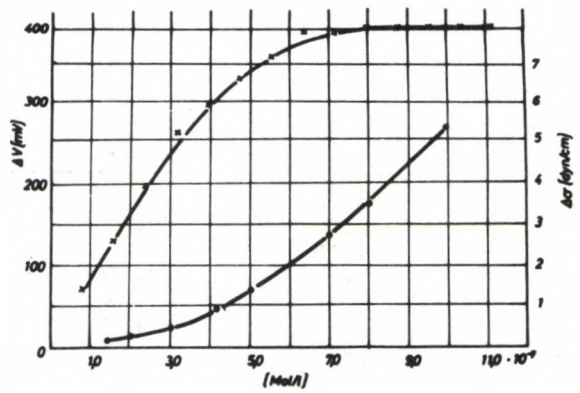

fig.1: Surface potential and surface tension of ω-dodecyl-ω-hydroxy-hexa(oxyethylene) as a function of concentration
X =surface potential, ● =surface tension

fig.2

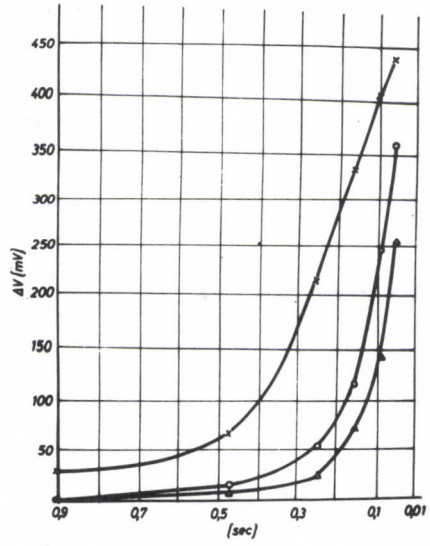

Dynamic surface potential of α -dodecyl-ω-hydroxy-hexa(oxy-ethylene) as a function of adsorption time.
$\times$ =0,4 · 10^{-4}m, O =1 · 10^{-4}m, Δ =2 · 10^{-4}m

fig.3

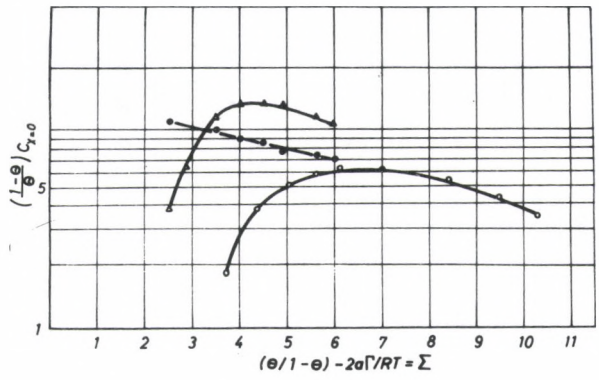

$\left(\frac{1-\theta}{\theta}\right) C_{x=0} = f(\Sigma)$ of α -dodecyl-ω-hydroxy-hexa(oxy-ethylene). Δ =0,4 · 10^{-4}m, O =1 · 10^{-4}m
● = corrected with the aid of equ. (17) and (18) for the concentration of 0,4 · 10^{-4}m

KINETICS OF THE SURFACTANT ADSORPTION ON THE SOLUTION SURFACE

J. Kloubek

The J. Heyrovský Institute of Physical Chemistry and Electrochemistry, Czechoslovak Academy of Sciences, Prague, Czechoslovakia

Kinetics of surfactant adsorption at the air-solution interface is most often studied by means of the dynamic surface tension measurements, γ_t. The respective dynamic surface pressure, $\pi_t = \gamma_o - \gamma_t$, ($\gamma_o$ is the surface tension of the solution at the zero surface age, t = 0, considered to be equal to the surface tension of the pure solvent) appears to be a useful quantity for an evaluation of the surface excess of solute, Γ_t. A direct relation between π_t and Γ_t is often assumed; this is based on the surface equation of state and the Gibbs adsorption equation in spite of the fact that they refer to equilibrium conditions.

Three main concepts concerning the limiting factor of the rate of adsorption were suggested: namely diffusion[1], energy barrier of the electrical double layer[2], and slow reorientation of molecules in the surface[3]. An important study of the diffusion process[4] is based on a model according to which the solute concentration in the so called sublayer decreases to zero immediately upon the new surface formation, i.e. $c_s = 0$ at $t = 0$. Thereafter, c_s is continuously enhanced by the diffusion from the bulk solution, until at equilibrium the bulk concentration, c_b, is reached. A back diffusion was considered in this process, too. However, for $c_b \gg c_s$, i.e. for small π_t and t, this back diffusion may be neglected and, in case the rate of adsorption is only diffusion controlled, in accordance with Langmuir and Schaefer[1] as well as with Ward and Tordai[4], the relation between Γ_t and t holds approximately

$$\Gamma_t = c_b(Dt)^{1/2} \qquad (1)$$

in which D is the diffusion coefficient. Bartholomé and Schäfer[5,6] found the empirical relation (2),

$$\pi_t = \pi_e/((b/t^{1/2}) + 1) , \qquad (2)$$

where π_e is the equilibrium surface pressure and b is a constant. Eq.(2) conforms with a simplified model of Ward and Tordai and, therefore, the dependence of $(\pi_e - \pi_t)/\pi_t$ on $1/t^{1/2}$ should be a straight line passing through the origin in case of the diffusion limited adsorption.

Glass[7] suggested another empirical relation (3),

$$\pi_t = \pi_e \exp(-k/t) , \qquad (3)$$

in which k is a constant. He estimated D from eq.(1) using t_e calculated by eq.(3) and Γ_e. Accordingly, eq.(3) should conform with the diffusion limited adsorption, and a linear dependence of log π_t on 1/t should indicate that this mechanism holds. However, there are two serious errors in the paper of Glass. He calculated Γ_e from a linear dependence of π_e on log c_b and uncorrectly applied the Gibbs adsorption equation; then Γ_e was independent of c_b. Further, he determined π_t by the drop weight method and used the Harkins and Brown's correction factors which are valid only for equilibrium conditions. Therefore, his π_t and also the dependence of π_t on t should deviate considerably from the actual values.

Netzel et al.[8] evaluated the course of adsorption by an equation of the first order kinetics

$$-d(\gamma_t - \gamma_e)/dt = k'(\gamma_t - \gamma_e) \qquad (4a)$$

from which they received after integration

$$\log((\pi_e - \pi_t)/\pi_e) = -kt . \qquad (4b)$$

Eq.(4b) was also applied by Kofanov et al.[9] who found that it conforms with the experimental results in the range measured by the vibrating jet (4 - 10 msec) and by the du Nouy tensiometer (5 - 200 min). According to eq.(4b), the rate of adsorption is directly proportional to the area of surface unoccupied by solute molecules, provided that π_t is directly proportional to Γ_t. However, Fordham[10] calls an attention to the fact that calculated Γ_t may be in serious error when based on the assumption that π_t corresponds to the same surface excess of solute as the equilibrium quantity π_e. The

reason is supposed to be a different concentration in the sublayer in comparison with that one in the bulk.

The values of π_t given in literature relate to different compounds, different ranges of t, and different methods of measurement. Therefore, they may be expected to be disparate and, accordingly, their interpretation may differ. However, diverse explanations were offered also for similar data: Defay and Hommelen[11] interpreted the linear dependence of π_t on $t^{1/2}$ as a diffusion limited process according to eq.(1). However, they neglected that at low surface ages π_t is rather proportional to t than to $t^{1/2}$. This fact lead Hansen and Wallace[12] to the suggestion that the rate of adsorption is energy-barrier limited. Later, Hansen[13] agreed with the course of diffusion and explained the deviation at the beginning either by an oriented structure of solvent molecules in the surface which creates a barrier before it melts or, in accordance with Fordham[10], by a change of the relation between Γ_t and π_t. According to him, π_t should be proportional to t at low surface ages, while Γ_t remains proportional to $t^{1/2}$. Deviation from the diffusion limited process at small t was also found by Kretzschmar[14,15] who measured the dynamic surface potential.

To avoid the problem of the relation between π_t and Γ_t, microtome measurements of hydrocinnamic acid in the surface of its aqueous solutions according to McBain et al.[16] are evaluated in this paper using eqs.(2) - (4) in which the surface pressure is substituted by the surface excess (Γ_t in g/cm^2, t in min). In Fig.1, line 1 relates to eq.(2). The scatter of experimental points from the linear dependence is rather high and there seems to be a significant deviation to higher Γ_t values at low t which contradicts the explanation given by Hansen[13]. Lines 2a and 2b in Fig.1 relate to eq.(3) and are plotted for the $10^{-3}x$ and $10^{-2}x$ scale of 1/t, respectively. There is a good linear dependence at higher t but an obvious change of slope for small Γ_t and t. These two above mentioned dependencies give little evidence of a diffusion limited rate of adsorption.

In Fig.2, lines 1a and 1b relate to eq.(4) and belong to

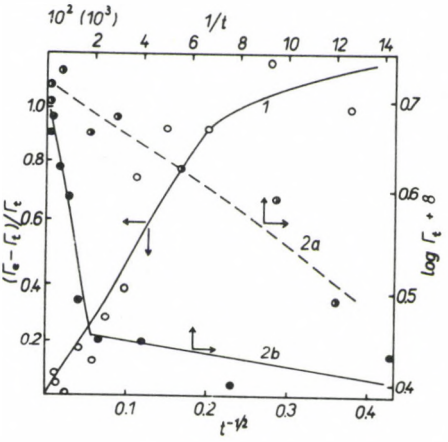

Figure 1

Graphic check of eqs.(2) and (3) for hydrocinnamic acid

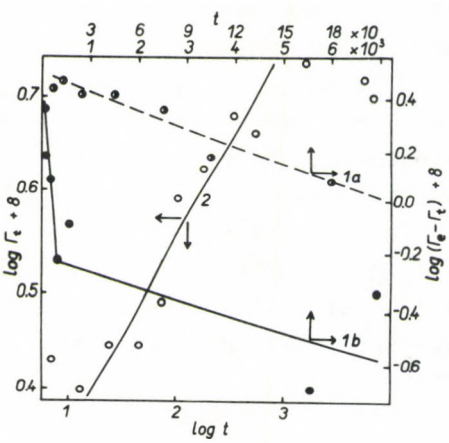

Figure 2

Graphic check of eqs.(4) and (5) for hydrocinnamic acid

the scale for the lower (10x) and the higher (10^3x) t values, respectively. There is a good linear dependence indicating the kinetics of the first order. Deviation of the two points at the highest t may be attributed to the state of surface saturation (the point at t = 1620 min. is not plotted because of $\Gamma_e = \Gamma_t$). The next relation in Fig.2 given by line 2 shows, with an exception of the first and two last points, also a good linear dependence which is given by eqs.(5a) and (5b),

$$\log \Gamma_t = 0.2 \log t - 7.85 \ , \qquad (5a)$$

$$t = 1.78\times10^{39}\Gamma_t^{5} \ . \qquad (5b)$$

The rate of adsorption is, according to the two above mentioned eqs.,

$$d\Gamma_t/dt = 0.2\,\Gamma_t/t = 1.124\times10^{-40}/\Gamma_t^{4} \ (g/cm^2min) = 1.25\times10^{-44}/\Gamma_t^{4} \ (mol/cm^2sec) \ . \qquad (6)$$

This is an interesting result which may be interpreted in the way that adsorbed molecules of hydrocinnamic acid form a double layer which creates an energy barrier limiting the rate of adsorption proportionally to the fourth power of their surface excess. However, there is not enough evidence to decide which one of the two last relations is more authentic.
When evaluating the kinetics of adsorption from π_t a special

care should be paid to obtaining correct values. There seems to be a lack of reproducible and reliable data in the literature. It was shown[17] that fundamentally divergent values could result if different methods of γ_t estimation were used. Therefore, corrections were introduced for maximum bubble pressure and drop weighing methods[18,19] to obtain values relating to the effective surface age. Both above mentioned methods were used for sodium dodecyl sulfate solutions[19,20] and γ_t in dependence on t was estimated. Evaluation of the equilibrium values, π_e, gave a linear relation[21],

$$\log \pi_e = 0.901 \log a + 3.582 \ , \qquad (7)$$

in which a is the activity of dodecyl sulfate. Inserting eq. (7) into the Gibbs adsorption equation results in

$$\Gamma_e = \pi_e / 2.22RT \qquad (8)$$

and

$$\Gamma_e = 7.06 \times 10^{-8} a^{0.901} \ . \qquad (9)$$

Eq.(9) represents a Freundlich adsorption isotherm and indicates that with an increase of Γ_e a simultaneous decrease of the adsorption energy occurs.

With respect to the validity of eq.(8) in the whole range of measured concentrations, no abrupt change in surface structure may be assumed. Therefore, no restructuring can be expected at non-equilibrium conditions which could limit the rate of adsorption. Furthermore, because of the above mentioned influence of ionized surfactant molecules in the surface on the energy of adsorption (cf.eq.(9)) as well as the results with hydrocinnamic acid (cf.eq.(6)), no sublayer with $c_s < c_b$ is assumed and similarly to eq.(8) relation (10) is anticipated for the dynamic conditions,

$$\Gamma_t = \pi_t / 2.22RT \ . \qquad (10)$$

Nevertheless, eqs.(2) and (3) are also used in this paper to examine the process of adsorption.

In Fig.3 the dependence according to Bartholomé and Schäfer[5,6] is plotted (open circles - line 1) for aqueous solution of sodium dodecyl sulfate, $c_b = 3.3 \times 10^{-3}$ mol/l at 25°C. With some scatter the data show a linear dependence in the range of smaller t. However, the straight line does not point to the origin as required by eq.(2). The dependence according

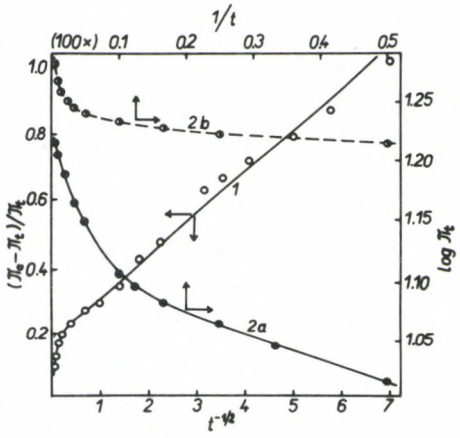

Figure 3

Graphic check of eqs.(2) and (3) for dodecyl sulfate

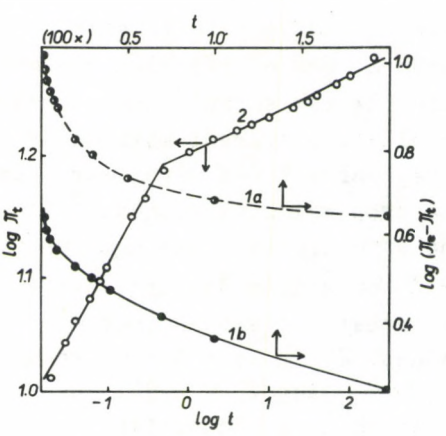

Figure 4

Graphic check of eqs.(4) and (5) for dodecyl sulfate

to Glass[7] is also given in Fig.3 (full points - curve 2a, scale for 1/t up to 50, semi-open circles - curve 2b, scale for 1/t up to 0.5 sec^{-1}). The respective curved lines do not fit eq.(3). Thus, Fig.3 shows that in the case of dodecyl sulfate diffusion does not control the rate of adsorption.

In Fig.4, the same experimental data are plotted in the functional dependence given by eq.(4) (semi-open circles - curve 1a for the scale up to 2, and full points - curve 1b for the scale up to 200 sec). The curvature clearly shows that the first order kinetics does not apply. The dependence between log π_t and log t is given by open circles (line 2). It breaks in two straight lines described by the general formula

$$\log \pi_t = x_1 \log t + y_1 \,. \qquad (11)$$

Taking into account eq.(10), the rate of adsorption is given by

$$d\Gamma_t/dt = x_2/\Gamma_t^{y_2} \ (mol/cm^2 sec) \,. \qquad (12)$$

The constants in eqs.(11) and (12) are the following:

	x_1	y_1	x_2	y_2
first (steeper) part,	0.125	1.23	1.25×10^{-77}	7
second part	0.034	1.20	1.41×10^{-282}	28.4

Examples of the calculated values are given in Tab.I.

Table I

Calculated rates of adsorption of dodecyl sulfate

π_t (dyn/cm)	t (sec)	Γ_t (mol/cm^2)	$d\Gamma_t/dt$ (mol/cm^{2}sec)
13	0.10	2.40×10^{-10}	2.7×10^{-10}
15	0.35	2.77×10^{-10}	9.7×10^{-11}
16	1.31	2.96×10^{-10}	5.7×10^{-12}
18	41.4	3.33×10^{-10}	2.0×10^{-13}

Similar results were obtained also for other concentrations of sodium dodecyl sulfate. There are quantitative alterations of constants in eqs.(11) and (12) dependent on t, c_b, temperature, solute species, and possibly also on other conditions. However, the rate of surfactant adsorption seems to be governed by eq.(12) in an extensive range of validity. Water molecules in the vicinity of hydrocarbon chains of the solute have an iceberg structure[22]. Ice has a larger surface free energy, but a smaller polar part of it than water[23]. Therefore, a restructuring of water in bulk sets free an energy which is a constant driving force of surfactant adsorption. At the equilibrium, the energy of adsorption decreases with the increasing of the surface excess, as indicated by eq.(9). A similar relation may be assumed to hold also for dynamic conditions. π_t may be considered as a retarding force increasing with t. Moreover, an energy barrier created by the electrostatical repulsion of the double layer should be also proportional to Γ_t and should increase with t. Thus, the product of all these factors is a power function of Γ_t, or π_t, and it determines the rate of adsorption as given by eq. (12).

Relation between π_t and π_e is a further interesting problem. For dodecyl sulfate of $c_b = 3.3\times10^{-3}$ mol/l, $\log \pi_e = 1.318$ was found[21]. Using this value in eq.(11), e.g. for the steeper part of the straight line in Fig.4, the relation

$$\pi_t = t^{0.125}\pi_e^{0.93} \qquad (13)$$

can be obtained. Derivative of eq.(13) writes

$$d\pi_t/dt = 0.125\pi_e^{0.93}/t^{0.875} \; . \qquad (14)$$

Inserting the relation between π_e and a from the previous paper[21],

$$\pi_e = 3.82 \times 10^3 a^{0.901} , \qquad (15)$$

into eq.(14),

$$d\pi_t/dt = 2.78 \times 10^2 a^{0.84}/t^{0.875} \qquad (16)$$

results. Unfortunately, eqs.(13), (14), and (16) are valid only in a limited range of t, π_t, and a.

References

1. I.Langmuir and V.J.Schaefer, J.Amer.Chem.Soc. 59,2400 (1937).
2. K.S.G.Doss, Kolloid Z. 86,205(1939).
3. A.E.Alexander, Trans.Faraday Soc. 37,15(1941).
4. A.F.H.Ward and L.Tordai, J.Chem.Phys. 14,453(1946).
5. E.Bartholomé and K.Schäfer, Melliand Textilber. 31,487 (1950).
6. K.Schäfer, Z.Elektrochemie 59,273(1955).
7. J.E.Glass, J.Phys.Chem. 72,4450(1968).
8. D.A.Netzel, G.Hoch and T.I.Marx, J.Colloid Sci. 19,774 (1964).
9. V.I.Kofanov, S.V.Rudenko and S.M.Levi, Kolloidnyj zhurnal 37,172(1975).
10. S.Fordham, Trans.Faraday Soc. 50,593(1954).
11. R.Defay and J.R.Hommelen, J.Colloid Sci. 14,411(1959).
12. R.S.Hansen and T.C.Wallace, J.Phys.Chem. 63,1085(1959).
13. R.S.Hansen, J.Colloid Sci. 16,549(1961).
14. G.Kretzschmar, Kolloid Z.-Z.Polymere 206,60(1965).
15. G.Kretzschmar, Tenside Detergents 76,267(1972).
16. J.W.McBain, T.F.Ford and G.F.Mills, J.Amer.Chem.Soc. 62, 1319(1940).
17. J.Kloubek and P.Kondelík, J.prakt.Chem. 22,77(1963).
18. J.Kloubek, J.Colloid Interface Sci. 41,1,7(1972).
19. J.Kloubek, Colloid & Polymer Sci., in print.
20. J.Kloubek, J.Colloid Interface Sci. 41,17(1972).
21. J.Kloubek, Proceedings 2nd Czechoslovak Conference on Physical Adsorption, Liblice 1975, p.178.
22. H.S.Frank and M.J.Evans, J.Chem.Phys. 13,507(1945).
23. J.Kloubek, J.Colloid Interface Sci. 46,185(1974).

Mixed Adsorption of Ionic and Nonionic Surfactants on Active Carbon

M. J. Schwuger and H. G. Smolka

Laboratories of Henkel & Cie GmbH, Düsseldorf

1. INTRODUCTION

In most of the areas in which surfactants find application, they are to be found as mixtures. Whereas the behaviour of pure surfactants during adsorption has been intensively studied, there are only insufficient examinations made with mixed-systems, in spite of their undoubted importance. Mixtures of ionic and nonionic surfactants are of especial importance, as these are basically different from each other, as regards the nature of the hydrophilic groups.

2. RESULTS AND DISCUSSION

2.1. Nonionic surfactants

Model substances used as nonionic surfactants were p-n-octylphenol-polyglycol ethers (OP_m) possessing from 7-12 oxyethyl groups and being of defined chain-length.

The measurements of equilibrium adsorption indicate monomolecular adsorption of the Langmuir type (Fig. 1). They are not altered in the presence of high concentrations of sodium chloride.

The adsorption decreases with an increasing number of oxyethyl groups. Fig. 2 demonstrates that this reduction is a linear function of $\sqrt{m}$, m being the number of oxyethyl groups. The same observation has been made for liquid/liquid interfaces. This shows that for a model whereby the hydrated polyglycol ether coils pro-

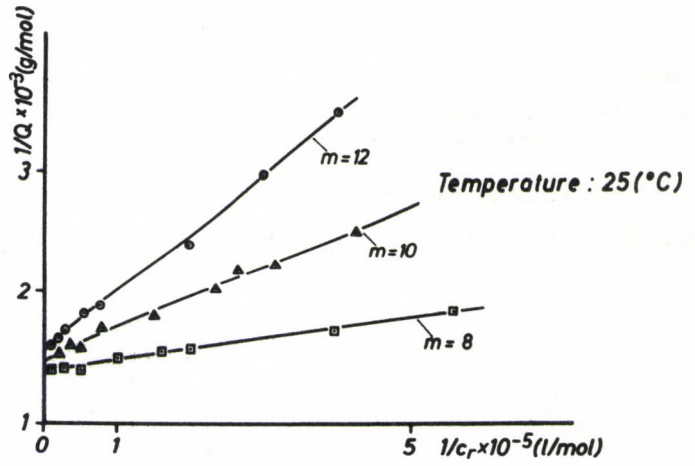

Fig. 1. Adsorption of OP_m on activated Carbon M

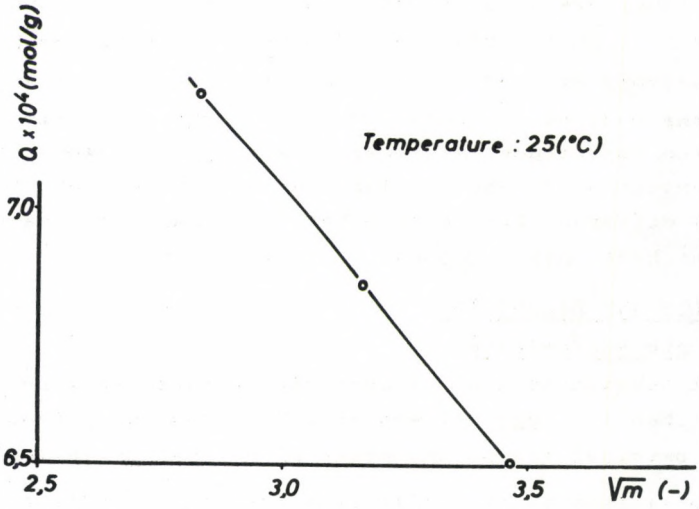

Fig. 2. Influence of oxyethyl groups on adsorption in the monomolecular layer

ject into the water phase, that the saturation adsorption changes with a change in $\sqrt{m}$ (1).

If, as in the case of monomolecular coverage, the amount of adsorbed substances is sterically determined because of the differing volumes of the hydrated hydrophilic groups, then

the product of the area occupied by a single molecule when the interface solid/liquid is heavily occupied (A), multiplied by the amount of substance in the monomolecular layer (Q_m), should be constant within an homologous series.

$$A \cdot Q_m = \text{constant}$$

For this to be true, it is necessary to assume that the whole surface of the activated carbon is equally accessible to the surfactant molecules. If the literature value for A, determined for the area occupied at the water/air interface (2), is used, which may be considered, to a first approximation, to be accurate for the carbon/water interface, together with Q_m, experimentally determined, then a value, constant to 2 %, of 4,63 Å^2 mol/g is obtained.

The corresponding accessible active charcoals have a surface area which also varies between 272 and 283 (m^2/g), i,e. with the same limits of error. This result indicates that only a fraction of the BET-area, -1400 m^2/g determined by nitrogen adsorption-, is available for the surfactant. Indications of multimolecular adsorption were not found, even at higher surfactant concentrations.

The above results suggest that the changes in the equilibrium adsorption with changes in the number of oxyethyl groups are caused sterically, and are therefore dependent upon the size of the oxyethyl-chain. However, they do not say anything about the free energy of adsorption. The various slopes of the straight-line plots shown in Fig. 1, indicate that the adsorption energies decrease with an increasing number of oxyethyl groups. To this extent, the result for the adsorption at the water/active carbon interface differs from the result obtained for the water/air interface, as far as the adsorption energy is concerned. This conclusion follows from a consideration of the meaning of the constants in the Langmuir-equation.

$$b_o = \text{const} \cdot \exp \frac{\Delta E}{R\,T}$$

The constant before the exponent has the same value for all OP_m, if it is assumed that the residence time of the indivi-

dual molecules on the surface is the same. Therefore, the variations in b_o must be caused by variations in the adsorption energies of the individual polyglycol ethers.

It is noteworthy that the adsorption on activated carbon can be described by a very simple equation, which is derived on the assumption of localised adsorption on an uniform surface. However, this does not allow one to conclude that the physical model corresponding to the Langmuir-equation applies to this specific case.

2.2. Sodium-n-dodecyl sulfate (SDS)

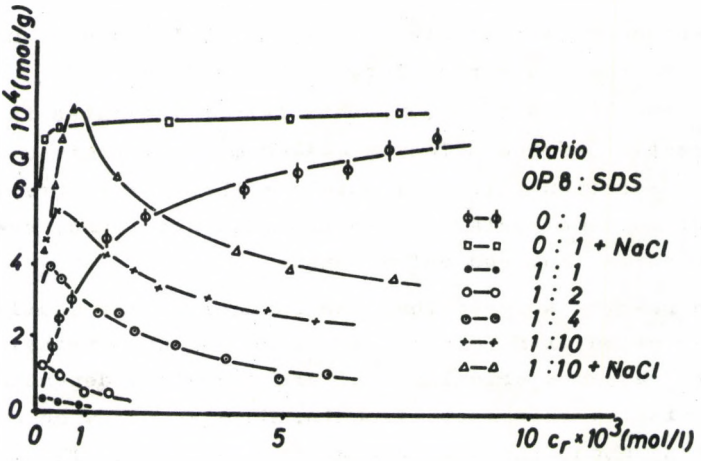

Fig. 3. Adsorption of SDS from mixtures

Fig. 3 (upper curves) shows a plot of the adsorption of SDS as a function of surfactant concentration with and without NaCl. As in the case of the nonionic surfactants, the adsorption is of the Langmuir type. Due to the strong electrical repulsion of the similarly charged hydrophilic surfactant groups with each other and with the also negatively charged adsorbent surface, the adsorption, when compared to nonionic surfactants with the same hydrophobic groups, only occurs at significantly higher concentrations. For the same reasons, the

electrolyte effect in the case of SDS is very evident. The electrical repulsion, reduced by addition of salt, results in an increased surfactant adsorption. The surfactant concentration, at which a steep increase in the adsorption commences, is however less than with OP_m, even in the presence of added electrolytes.

On the other hand, the saturation adsorption in the case of SDS is higher than that found for the nonionic surfactants examined. This phenomenon can be explained by noting the smaller space-requirements and the resulting higher packing density of the anionic surfactant.

2.3. Mixed adsorption of SDS and OP_8

If both surfactants are mixed in a 1:1 molar ratio, then the equilibrium adsorption of the nonionic surfactant in comparison to that of the pure surfactant, remains largely unaltered. In contrast, the ionic surfactant is scarcely adsorbed. The amount adsorbed are so small that a satisfactory, quantitative surfactant analysis is no longer possible. This means that the attraction of the nonionic surfactant to that activated carbon surface is very large in comparison of that of the ionic surfactant, and an almost complete displacement of the anionic surfactant results.

Analogous relations are observed at the water/air interface. n-Alcohols, which possess a molecular structure similar to that of the OP_m have a higher surface activity than do ionic surfactants of the same number of carbon atoms in the hydrophobic residue. For example, a concentration ratio of only 1:100 of n-dodecyl alcohol: SDS in water results in a 1:1 mixture as determined in the mixed film at the water/air interface (3). This is a demonstration of the marked selectivity of the adsorption. If the molar concentration of SDS in the solution, is raised in comparison to that of OP_8 then the adsorption of the anionic surfactant increases. As shown in Fig. 3 however, the shape of the ad-

sorption curve is very special. The amount of adsorbed SDS increases with increasing surfactant concentration, only in the region of lower concentration. Increasing the concentration of the nonionic surfactant in the solution, results in an expulsion of the ionic one from the active charcoal surface. It is especially noteworthy that the adsorption of SDS under these experimental conditions, in the area of low surfactant concentrations, is higher than it is in the case of the pure anionic surfactant.

Basically, two different effects and two different concentration regions can be discerned, when considering the adsorption of mixtures of ionic and nonionic surfactants on carbon.

a) The region of very low surfactant concentrations, where the adsorption of anionic surfactants in the mixture is increased, in comparison to the pure SDS solution. The limit of this region depend on the ratio of nonionic to anionic surfactant. The larger this ratio, the smaller is the surfactant concentration at which this effect appears. This is illustrated in the following example:

In the case of relatively low total-concentrations, which however can be relatively accurately determined, and with a ratio of OP_8 to SDS in the solution of 1:10 a ratio of approximately 1:1 was found in the adsorbed surfactant film. The mixed film is formed from equal amounts of both surfactant types. The inclusion of nonionic surfactant molecules in the adsorption film results in a reduction of electrical repulsion between the negatively charged groups of the anionic surfactant. It can be suggested that this is the reason for the basis of the observed stronger adsorption of the anionic surfactant from the mixture, than that observed in the case of adsorption from the solution without the addition of nonionic surfactant.

If, in the mixture, the ionic surfactant is only present in slight excess, then the surfactant concentration in the solution out of which the adsorbed film consists of equal

proportions of both surfactants, is so low that a satisfactory concentration determination is impossible. In this connection the result that in the case of a 1:1 concentration in the solution, no appreciable adsorption of SDS is present should be mentioned.

b) In the region of higher surfactant concentration, the ionic surfactant is displaced by the nonionic. The limits of this region follow from those limits set in a. The displacement is greater, the larger the total surfactant concentration in the solution and the larger the ratio of nonionic surfactant to ionic surfactant.

The influence of electrolytes in mixtures proceeds analogous to that of the pure surfactants. The reduction of the electrical repulsion by electrolytes causes an increased adsorption of SDS, so that the displacement by the nonionic surfactant from the solid surface is not so large. However, the basic adsorption curve remains unchanged, as shown in Fig. 3.

The kinetics of mixed-adsorption are dependent upon the magnitudes of the diffusion coefficients of the components in the mixture. As anionic surfactants, in general, diffuse more rapidly than nonionic surfactants, more anionic- than nonionic surfactants will be at the surface in the region of short adsorption times or low adsorption values. Only with increasing coverage of the surface and longer adsorption-times will the anionic surfactant be displaced by the ionic surfactant. This means that the adsorption of an anionic surfactant as a function of time should pass through a maximum. This could be verified for a few substance pairs. The principal change of adsorption with time is shown in Fig. 4.

ACKNOWLEDGMENT

We express our gratitude to Mr. H.M. Rostek for his conscientious execution of the experiments.

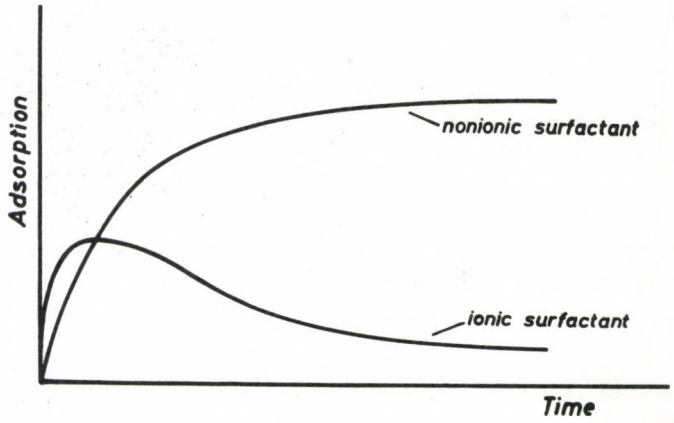

Fig. 4. Principle progress of the kinetics of the simultaneous adsorption from mixtures

Literature

1. van Voorst Vader F., Trans. Faraday Soc. 56, 1078 (1960)

2. Crook E.H., D.b. Fordyce, G.B. Trebbi, J. Phys. Chemie 67, 1987 (1963)

3. Tajima K., M. Muramatsu, T. Sasaki, Bull. Chem. Soc. Japan 42, 2471 (1969)

Group II/1
Formation of disperse systems

THE INFLUENCE OF CONSTITUTIVE AND NONCONSTITUTIVE COMPONENTS ON COLLOIDS "IN STATU NASCENDI"

B. Subotić

"Ruder Bošković" lnstitute, 41001 Zagreb, P.O.Box 1016
Croatia (Yugoslavia)

INTRODUCTION

The results of radiometric and X-ray studies of the negative stable silver iodide sols prepared "in statu nascendi" have shown that AgI sols are complex systems composed of several subsystems with respect to dispersity and structure of the dispersed phase (1,2,3,4,5). The heterogeneous exchange experiments have shown that a part of colloidal AgI exchanges very rapidly with constituent ions in the liquid phase, if a coagulating electrolyte is added to the system (2,3). By analysing the obtained results, it has been concluded that the negative stable silver iodide sols consist of two kinds of silver iodide: solid, crystallographically defined silver iodide and metaphasic, crystallographically amorphous modification (2,3). The X-ray analysis of the sol indicates the absence of the clear diffraction maxima characteristic for crystalline AgI and appearence of the diffractions corresponding to the metaphasic silver iodide (6). The iodide and silver ions within the metaphase are still solvated and very mobile, and the dynamic equilibrium of iodide ions between the metaphase and the liquid phase in the presence of coagulation electrolyte is reached quickly compared to the system with no electrolyte added. The experiments have shown that the metaphase transforms into solid AgI during the time of ageing, t_A (4,5). The purpose of this work is to investigate the kinetics of the metaphase-phase transition and the effect of constitutive and nonconstitutive components.

PREPARATION OF SOLS

Analar grade BDH sodium iodide, silver nitrate and sodium nitrate were used for the preparation of standard solutions. The silver iodide sols were prepared by adding 5 ml of $AgNO_3$ solutions of 0.1, 0.02, 0.004 and 0.0004 M to 5 ml of NaI solutions of 0.2, 0.04, 0.008 and 0.0008 M containing or not

$NaNO_3$. The sols used for sedimentation analysis were prepared from NaI solutions labelled with $^{131}I^-$. After precipitation the ratio of molar concentrations of I^- ions in the solid (n^S) and liquid phase (n^L) were 1:1 , so that $n^S/n^L = \alpha = 1$. All aged and mesaured systems were thermostated at 293.0 ± 0.2° K by a Haake ultrathermostate.

THE RADIOMETRIC INVESTIGATION OF THE KINETICS OF THE METAPHASE-PHASE TRANSITION

The method is based on the fact, that in the absence of a potential barrier around the particles (i.e. during coagulation) the dynamic equilibrium of I^- ions between the metaphase and liquid phase is reached more rapidly than the equilibrium between the metaphase and liquid phase or solid and liquid phase (2,3,4). If the sol is labelled by $^{131}I^-$, the equilibrium of radioactivity between the metaphase and liquid phase is defined as: $\gamma^L = \gamma^m = A^L_{eq}/n^L = A^m_{eq}/n^m = (A_o - A^L_{eq})/n^m$ [1] , where γ^L and γ^m are equilibrium specific radioactivities of the liquid phase and metaphase respectively, A^L_{eq} and A^m_{eq} are the total radioactivities, n^L and n^m are the corresponding molar concentrations of I^- ions, and A_o is the total radioactivity of the whole system. From eq. [1] , $n^m/n^L = \alpha_m =$ $= (A_o - A^L_{eq})/A^L_{eq}$ [2] . If $n^S = n^s + n^m$ where n^S and n^s are the concentrations of total AgI and crystallographically defined AgI respectively, then $\alpha_S = (n^s + n^m)/n^L = n^S/n^L$. By dividing eq. [2] with α_S , $\alpha_m/\alpha_S = n^m/n^S = (A_o - A^L_{eq})/\alpha_S A^L_{eq} =$ $= f_m$ [3] is obtained, where f_m is the fraction of metaphasic AgI relative to the total amount of AgI in the system. The experimental procedure was as follows: the silver iodide sols aged for t_A minutes were prepared essentially in the same maner as described above; 15 secondes before a given t_A value has been reached the systems were stregly shaken and labelled with 0.05 ml of $^{131}I^-$, and the sol has been coagulated at t_A by adding 0.05 ml saturated $Mg(NO_3)_2$ solution. After coagulation, the systems were stirred for five minutes and then centrifugated. The clear supernatant was used for determining

the radioactivity of the liquid phase A^L . The experimental determination of the total radioactivities A_o and α_S has been described previously (4). The experimentally determined radioactivities A^L are higher than A^L_{eq} if the exchange equilibrium is not reached and $(f_m) = (A_o - A^L)/\alpha_S A^L_{eq} < f_m = (A_o - A^L_{eq})/\alpha_S A^L_{eq}$ In principle, equilibrium radioactivity A^L_{eq} may be reached for each system if the time of exchange is rather long ($t_E = t_{eq}$) but as it is shown in Fig. 1 this is not needed, because the differences between f_m (crosslet in Fig. 1) and (f_m) are constant for each t_A , if t_E and $C_{sol} = C_o$ (concentration of sol) are constant too. Even, for sols of lower concentrations of AgI , the equilibrium is reached within the time of experiment t_E (Fig. 1-B). Thus we can write for sols of a given concentration of AgI : $(f_m) = f_m - \Delta f_m = f_m - c$ [4] , where c is a constant depending on C_o and t_E and independent of t_A . Than: $d(f_m)/dt_A = df_m/dt_A$ [5] . The experimental values of f_m as a function of t_A and the concentration of Na^+ ionsin the systems are presented in Fig. 2 . The broken curves in Fig. 2-A and 2-B are real values of the fraction of metaphase f_m , which has been calculated from the experimental values (f_m). The way of the computation will be discussed later. Generally, as it is shown in Fig. 2, the changes of (f_m) and f_m are faster if the concentrations of sols, C_o , and Na^+ ions for the same C_o are higher. In systems with $C_o = 0.002$ and 0.0002 M (Fig. 2-C and 2-D respectively) the f_m and (f_m) values are identical. After sufficient time of ageing, f_m and (f_m) tend to constant values different from zero. We can write: $f_m \longrightarrow a \neq 0$ and from eq. [4] $(f_m) \longrightarrow a - c \neq 0$ if $t_A \longrightarrow t_{A(eq)}$, where $t_{A(eq)}$ is ageing time in which df_m/dt_A and $d(f_m)/dt_A \longrightarrow 0$.

What is the mechanism of the metaphase-phase transition? Let us assume, that at $t_A = 0$, all AgI exists in the metaphasic form.The original number of particles (n^o_e) is taken to be proportional to the concentration of sol: $n^o_e = k_2 C_o$ [6]. Since the primary particles do not consist of crystallographically defined AgI , we call them embria (4,5). The collision of two embria can result in the formation of the solid phase (crystallographically defined AgI) at the site of collision, if the

sum of kinetic energies of particles in collision is larger than the critical activation energy E_a . The critical activation energy includes barrier the potential energy and energy of dehydration of I^- and Ag^+ ions that build the metaphase. The particles resulting from effective collisions are called nuclei, because they are the carriers of the first crystallographically defined solid phase. If the reaction rate J_e between embria is greater than the others, i.e. nuclei-embria, J_{e-nu} , and nuclei-nuclei, J_{nu} , reaction rate then we can write:

$J_e = -dn_e/dt_A = k_1 n_e^2$ if $J_{e-nu} \ll J_e \gg J_{nu}$ [7] , and

$n_e = 1/(k_1 t_A + 1/n_e^o)$ [8] . From eq. [6] and [8] ,

$f_e = n_e/n_e^o = 1/(C_o k_\pi t_A + 1)$ [9] , where $k_\pi = k_1 k_2$. If b is the fraction of solid phase in each of the nuclei (part of metaphase transformed into solid AgI when two embria collide), and a = 1 - b is the fraction of the metaphase, then the fraction of metaphase in the system aged for t_A minutes is:

$f_m = f_e + a(1 - f_e)$ [10] . By combining eq. [9] and [10] we have: $f_m = (1 - a)/(C_o k_\pi t_A + 1) + a$ [11] and in accordance with eq. [4] $(f_m) = (1 - a)/(C_o k_\pi t_A + 1) + a - c$ [12] . By using the first derivative of eq. [12] and values obtained by graphic differentiation of experimental curves in Fig. 2 the constantes k_π and a for a given sol can be calculated.

If $(df_m)/dt_A = (1 - a)C_o k_\pi / (C_o k_\pi t_A + 1)^2 = f'_m = (f_m)'$ [13] ,

then $\sqrt{f'_{m_1}/f'_{m_2}} = \mu = (C_o k_\pi t_{A_2} + 1)/(C_o k_\pi t_{A_1} + 1)$ and

$k_\pi(\mu t_{A_1} - t_{A_2}) = 1/C_o - \mu/C_o$ [14] . The constant k_π is the slope of the straight line obtained by plotting $1/\mu$ vs. $\mu(t_{A_1} - t_{A_2})$; $k_\pi = \Delta(\mu/C_o)/\Delta(\mu t_{A_1} - t_{A_2})$

From eq. [13] $a = 1 - \left[f'_m(C_o k_\pi t_A + 1)^2\right]/C_o k_\pi t_A$. By introducing the constants k_π and a into eq. [11] , the real f_m values are obtained (broken curves in Fig. 2-A, 2-B and 2-D). As it was shown, the mesaured data (Fig. 2) confirm the proposed model. The eq. [11] is valid from $t_A = 0$ to $t_A = t_{A(eq)}$, where $t_{A(eq)}$ can be experimentally defined as: $t_{A(eq)} \approx 1/C_o$ to $3/C_o$. If C_o is expresed in mol dm^{-3}, then $t_{A(eq)}$ is in minu-

tes. After this time other processes are predominated. The invariance of the constants k_π and a at observed ageing and validity of eq. [7] and [8] indicate the existance of monodisperse embria as a resonable posibility. This means that at $t_A = 0$ monodisperse embria exist, at the time $0 < t_A < t_{A(eq)}$ a mixture of embria and nuclei is present in the sols and at $t_A \approx t_{A(eq)}$ the largest part of AgI exists in the form of monodisperse nuclei. In the aim of bearing above assumption out or its deposition, the sedimentation analysis of sols has been done.

SEDIMENTATION ANALYSIS OF THE SOLS

The change of particle concentration, C_i , at distance x from the centre of effective force, as a function of the relative centrifugal force (RCF=F) may be presented by equation: $C_i = C_o \exp(-sFt_c x)$ [15] , where C_o and C_i are the concentrations of the particles in a small volume v at the distance x from the axis of rotation before and after centrifuging respectively, t_c is the duration of centrifuging and s is the sedimentation coefficient characteristic for a given kind of particles disperged in any medium. Eq. [15] is applicable for the case which the effect of diffusion may be ignored in comparison with the effect caused by centrifugal force, e.i. for highly polymeric substances and colloids (7). Equation [15] may be writen as: $f_i = C_i/C_o = \exp(-sFt_c x)$ [16] . t_c and x are experimentally determined and if they are constant (x will be constant under experimental condition if samples for analysis are always taken at the same position in the tube and if the volumes of samples are small in comparison to the volume of the centrifuged sol), it follows: $f_i = \exp(-K'F)$ [17] , where $K = st_c x$, and $\log f_i = -K \cdot F$ [18] . From eq. [18] , for a monodisperse system, $\log f_i$ is a linear function of F . For a polydisperse system, $\log \Sigma f_i = \log \Sigma \exp(-K_i F)$ [19] , where $\log \Sigma f_i$ is not in a linear relationship with F . On the basis of eq. [18] and [19] , by analysis of f_i and Σf_i respectively as a function of relative centrifugal force F , monodispersity or polydispersity of the systems can be verified. In our case the radiometric analysis has been used for the evaluation of f_i

and Σf_i . For this purpose an $AgNO_3$ solution (0.004M) was added to the labelled solution of NaI (0.008M). After precipitation the systems were 0.002M in AgI ($=n^S$) and 0.002M in NaI ($=n^L$) ; $n^S/n^L = \alpha_S = 1$, and corresponding equilibrium radioactivities of NaI in the liquid phase (A_∞) and AgI (A^S) were reached. If only a part of AgI is dispersed in the liquid phase. then $A^{L(s)} = A_\infty + f_i A^S$, where f_i is the fraction of dispersed AgI in relation to the total amount of AgI in the system.Then: f_i or $\Sigma f_i = \left[A^{L(s)} - A_\infty\right]/A^S = \left[A^{L(s)} - A_\infty\right]/(A_c - A_\infty)$ [20] where $A_o = A^S + A_\infty$ is the total radioactivity of the system. 2 ml of the suspensions aged for 5, 100 and 1450 minutes was centrifuged for 5 min by the Sorvall RC2-B centrifuge. After centrifuging, 0.2 ml of the suspensions were used for measuring the radioactivities $A^{L(s)}$. For the systems aged 5 and 1450 minutes linear relationships of "$\log f_i$ vs. RCF" were obtained; for the sol aged 100 minutes two slopes "$\log \Sigma f_i$ vs. RCF" resulted (Fig. 3). From eq. [9] and value of the k_π for the 0.002M sol ($k_\pi = 5.18$), the fraction of embria for the 5 minutes aged sol is 0.95 which means that embria are predominant, after $t_A = 100$ minutes a mixture of 50% AgI in the form of embria and 50% in the form of nuclei ($f_e = f_{nu} = 0.5$) is present and for the 1450 minutes aged sol $f_e = 0.065$ and $f_{nu} = 0.935$. The linear relationships between $\log f_i$ and RCF for sols in which one form of AgI particles is predominant indicate that embria and nuclei are predominantly monodisperse in accordance with eq. [18] . The above conclusions enable the direct measurement of f_e as a function of t_A . If differently aged sols are centrifuged with equal RCF the fraction of AgI , f_Σ , which after the spining, remains in a small volume at a constant distance x from the centre of rotation according to eq. [9] and [17] will be given by $f_\Sigma = f_e \exp(-K_e F) + f_{nu} \exp(-K_{nu} F) =$
$= m f_e + n f_{nu} = m f_e + n(1 - f_e)$ and

$$1/f_e = (m - n)/(f_\Sigma - n) = C_o k_\pi t_A + 1 \quad [21] .$$

The quantities $m = \exp(-K_e F)$ and $n = \exp(-K_{nu} F)$ according to eq. [17] represent the fractions f_i for the embrio and nucleus respectively at a given RCF value. Thus, for RCF = 14500 , m = 0.43 and n = 0.031 for the analysed 0.002M sol which can

be seen in Fig. 3. The fractions f_{Σ} were calculated by eq. [20] from the radioactivities, $A^{L(s)}$, of samples taken after centrifuging. The obtained experimental values for f_{Σ} and the from eq. [21] derived values f_e and $1/f_e$ are presented as functions of the ageing time in Fig. 4-A and 4-B . The linear dependence of $1/f_e$ confirms the assumption that AgI nucleation is second order reaction. Both k_{π} values obtained by sedimentation ($k_{\pi} = 6$) and by metaphase analysis ($k_{\pi} = 5.18$) methods were approximately equal. Very good agreement between the data calculated from eq. [9] and the data obtained by sedimentation analysis Fig. 4-A confirms the supposed model as reasonable for the system under examination.

REFERENCES

1. R. Despotović, Z. Despotović, M. Mirnik and B. Subotić, Croat. Chem. Acta, 42, 557 (1970) .
2. B. Subotić, M.Sc. Thesis, Zagreb University (1972).
3. R. Despotović and B. Subotić, Croat. Chem. Acta, 43, 153 (1971) .
4. R. Despotović and B. Subotić, Croat. Chem. Acta, 45, 377 (1973).
5. Proc. Symposium on "Particle Growth in Suspensions" , Auxbridge-London, 1972, Ed. A.L. Smith, Academic Press, London and New York (1973), p. 121 .
6. I. Šmit, private communication.
7. H. Fujita, Mathematical Theory of Sedimentation Analysis, Academic Press, New York and London (1962).

Acknowledgement. This work has been financially supported by Research Fund of Croatia.

Figure 1.

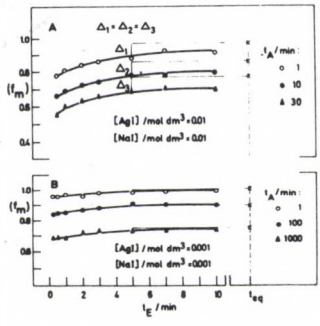

Figure 2.

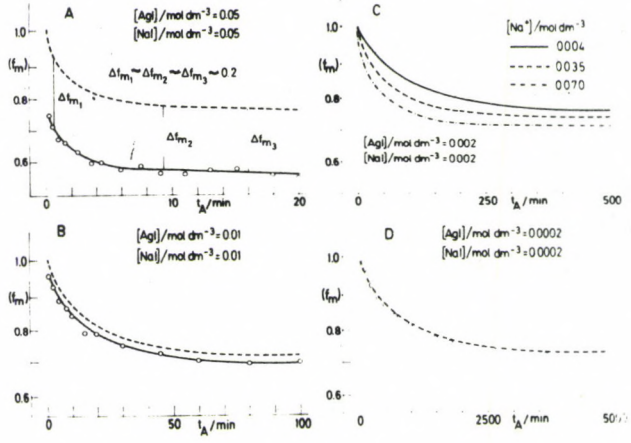

Figure 3.

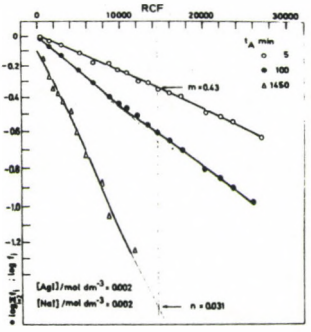

Figure 4.

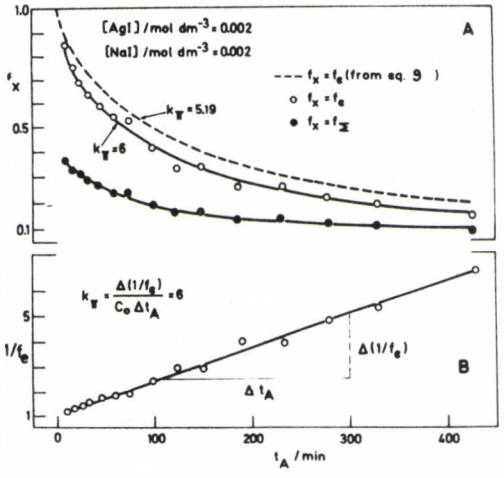

THE INFLUENCE OF SURFACTANTS ON THE FORMATION AND PROPERTIES OF SOME INORGANIC COLLOIDS

R. Despotović, N. Filipović-Vinceković, D. Mayer, S. Popović, and M. Szvoboda

"Ruder Bošković" Institute, 41001 Zagreb, P.O.Box 1016, Croatia (Yugoslavia)

INTRODUCTION

Ionic surfactants interact very strongly with stable silver iodide colloids in aqueous media causing various changes of colloid properties in the system; the results show a complex dependences of colloid stability, crystall growth, electrophoretic mobility, and "adsorption capacity" of silver iodide on the surfactant concentrations (1-3). The investigations of the surfactant/surfactant systems in aqueous media show complex mutual phenomena, indicating, as a reasonable possibility, the formation of submicellar colloid surfactant species, below the critical micellar concentration (4), and at concentrations at which the surfactants cause significant colloid interactions in silver iodide sols (1). The comparison of the obtained "adsorption capacity" data and the surfactant/surfactant measurements indicate the formation of complex colloid systems characterised by properties dependent on the surfactant concentrations (2,4) and on the association properties of the surfactant in aqueous solutions (5). In order to explain a correlation between the observed phenomena, that is, the mode of interactions between ionic surfactant n-dodecylammonium nitrate, DDA-NO_3 , and negative silver iodide sols in statu nascendi throughout the experiments optical (turbidity, electron microscopy, spectrophotometry, X-ray diffraction), electrochemical (microelectrophoresis, conductometry), radiochemical and tensometric techniques were applied. The obtained results show adsorption and flocculation processes and induced crystallization to occur as characteristic

phenomena in the observed systems.

EXPERIMENTAL

Analar grade BDH sodium iodide and silver nitrate were used for the preparation of standard solutions. n-Dodecylammonium nitrate DDA-NO_3 was prepared using puriss. grade FLUKA n-dodecylamine, by neutralization with dil. HNO_3 and further purification by five recrystallizations from hot 1:1 ethanol solution containing active carbon. Doubly distilled fresh water was used in all experiments. The silver iodide sols were prepared by adding a 0.002 M $AgNO_3$ solution to an equal volume of 0.004 M NaI solution containing various concentrations of DDA-NO_3 so that a AgI sol was obtained with AgI 0.001 mol/l , NaI 0.001 mol/l and 0.000001 M to 0.010 M DDA-NO_3 . Before measuring the systems were left to age for 100 minutes. (i) The electrophoretic mobility w of the suspensions was determined by ultramicroscopic electrophoresis, and the average results of 7 measurements are presented in figure 1. (ii) Radiometry was applied in order to determine the fraction F of heterogeneous $(AgI)_{solid} \rightleftharpoons (I^-)_{electrolyte}$ exchange and fraction f_s of sedimented AgI . The applied radiometric techniques were same as was described previously (1,8). (iii) The measurements of turbidity τ values were done by a Pulfrich photometer with a turbidimetric extension. (iv) Electron microscopy was carried out using a Trüb-Tauber Co. KM-4 electron microscope. Mowital films were used for supporting the specimens under examination. The results are schematically drawn in figure 2. Critical concentration for DDA-NO_3 micelle formation, c_M , was determined (v) by the ring method and (vi) from resistivity R (Ωcm) by means of a high frequency conductometer. By the Philips diffractometer (vii) the cubic/hexagonal ratio and the crystallite sizes were determined on silver iodide sols in contact with the original supernatant liquid. (viii) The adsorption of DDA-NO_3 at the silver iodide was determined by means of

spectrophotometric analysis (1) by determining the difference of concentrations for both DDA-NO_3 solutions without and with silver iodide sol present.

RESULTS and DISCUSSION

Turbidity of silver iodide sols measured as a function of DDA-NO_3 concentration shows the formation of twinned Tyndall maxima like in the systems AgI/Rhodamine 6G (2) indicating a complex dependence of colloid properties of sol on the concentration of surfactant. Following the concept of colloid surfactant association (4) and assuming the possibility of the Karaoglanov induced crystallization (6) of DDA-NO_3 at silver iodide/electrolyte interface the " τ vs. log c(M) DDA-NO_3 " curve (Fig. 1) can be explained. The first maximum at 0.00006 M DDA-NO_3 corresponds to electrical charge compensation of negative AgI particles with positive cationic surfactant. The result is the flocculation of sol. By increasing the surfactant concentration in the system DDA-NO_3 binds by adsorption at the crystal surface according to the Tamamushi model (7). The electrophoretic data indicate that the zero point of charge lies at 0.00006 M DDA-NO_3 confirming electrostatic interactions to be relevant in the formation of the first τ maximum. A decrease of the iodide exchange rate indicates that the AgI crystallites are surrounded by DDA-NO_3 . The result is a sedimentation of surfactant at the surface of flocculated silver iodide particles. Sedimentation measurements show total sedimentation, since the sedimentation factor f_s reaches unity, $f_s = 1$. Electronmicrographs support such an interpretation (Fig. 2); the obtained silver iodide particles are sourrunded by surfactant. Determination of critical micellar concentration indicates that c_M lies between 0.0074 M and 0.0092 M DDA-NO_3 at observed conditions confirming the deposit of surfactant at the sol particle surface as a consequence of supposed colloid interaction i.e. Karaoglanov induced crystallization. The dependence of the crystallite sizes, D , on

TABLE 1.

System; AgI sol 0.001 mol/l , NaI 0.001 mol/l , T = 293 K, t_A = 100 minutes, concentration of n-dodecylammonium nitrate c(M) = var. The dependence of the crystallite sizes (μm) , D , and the fraction of the cubic modification, C(%) , of silver iodide sols on the concentration of DDA-NO_3 , c(M) .

c(M):	$D_{C(111)}$:	$D_{H(100)}$:	$D_{H(101)}$:	C(%):
0.001	0.145	0.145	0.075	43
0.0001	0.145	0.145	0.075	46
0.00003	0.100	0.075	0.027	48
0.00001	0.075	0.075	0.037	41
0.000001	0.075	0.066	0.027	44
0.0000001	0.085	0.074	0.027	48

the DDA-NO_3 concentration (Table 1.) determined by X-ray diffractometry shows that $D_{H(100)}$ is always very similar to $D_{C(111)}$. This means that **a** dimension of hexagonal crystallites is similar to the average size of the cubic ones (these being usually observed as octahedrons). On the other hand, the **c** axis of the hexagonal crystallites is for a factor of two shorter than the **a** axis. All crystallite sizes increase abruptly as the concentration of DDA-NO_3 changes from 0.00003 to 0.0001 mol dm^{-3} , at the concentration region at which f_s reaches maximum changes. From the electronmicrograph picture the value of ca 0.8 μm is obtained as an average size of silver iodide particles at z.p.c., and from X-ray analysis about 0.145 μm . The differences between **c** and **a** hexagonal axes indicates the preferential adsorption of surfactant at the hexagonal plane with open prismatic planes to crystall growth. Two

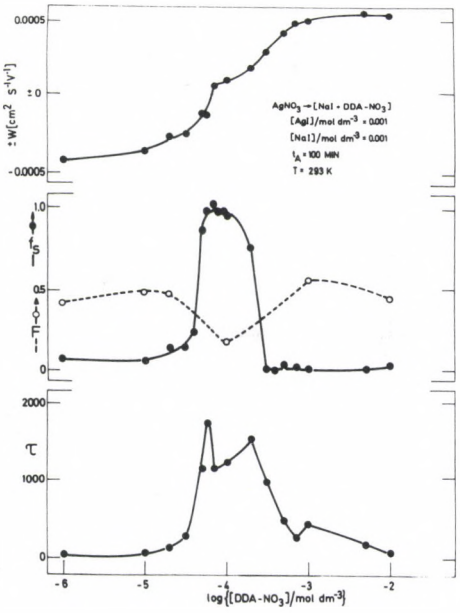

Figure 1. Electrophoretic mobility w ($cm^2 s^{-1} V^{-1}$), fraction exchange F, sedimentation fraction f_s and turbidity τ values for negative silver iodide sols plotted versus DDA-NO_3 surfactant concentration (log scale).

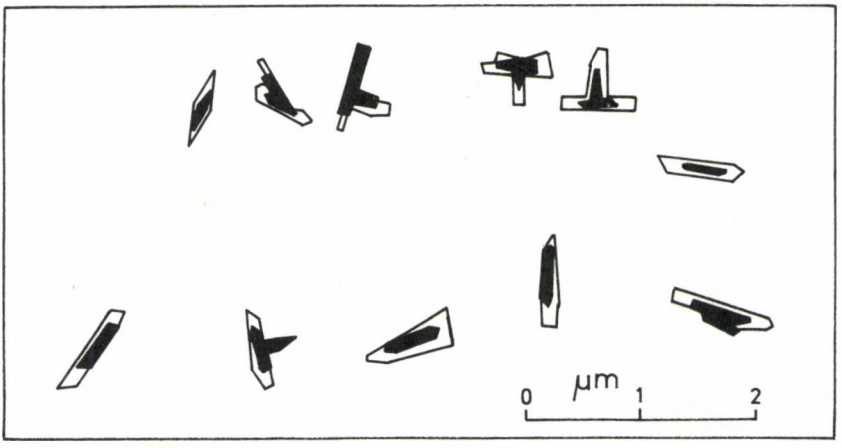

Figure 2. 100 minutes aged negative silver iodide sol 0.001 mol/l in 0.001 M NaI and 0.0001 M DDA-NO_3 . Schematic drawing of electronmicrograph; AgI crystallites surrounded by DDA-NO_3 .

consequences can be drawn from such considerations. One is the possibility of "adsorption" of surfactant associates at the crystal/electrolyte interface in which the surfactant associates cover the crystal surface following its hexagonal geometry. The radiometrically determined adsorption capacity of equally prepared silver iodide sol in the presence of $DDA\text{-}NO_3$ corresponds to ca $g = 2.7$ milli equivalent of inorganic ions per mole of sol (8) while our spectrophotometrical data for surfactant adsorption give ca $G = 16.6$ milli equivalent of surfactant ions per mole of sol. The G/g ratio corresponds to the association number of ca $A = 6.1$ which is in agreement with a possible hexagonal distribution of surfactant at the crystal/electrolyte interfaces. The second consequence of such "adsorption" are the van der Waals interactions among similar planes (9) which results in the formation of silver iodide crystallites with the **c** axis of a virtually greater **c** dimension as observed by electronmicroscopy. In this way the particle size (electronmicroscopy data) and crystallite size (X-ray data) can be understood, explaining at same time, the interactions in the systems up to the second Tyndall maximum, the more so because the fraction of the cubic modifications does not change significantly with the concentration of $DDA\text{-}NO_3$ (Table 1.). The results are also of interest from another point of view, that is in the explanation of "crystal growth" via oriented agglomeration as it was shown for the silver iodide sols prepared by dillution of $(AgI)_x \cdot (KI)_y$ complex in sodium n-dodecyl sulphate solution (10). The minimum F value, corresponding to the system in which silver iodide particles are surrounded by $DDA\text{-}NO_3$, increases with increasing surfactant concentration reaching a maximum value for the overcharged positive AgI particles and at conditions under which c_M is exceeded, and f_s value for silver iodide particles is approximately zero. The appearance of the second Tyndall maximum in this case is a consequence of

the stabilization (f_s = 0) and micellization processes including surfactant sedimentation caused via the Karaoglanov induction process. The good agreements of optical, electrochemical, radiochemical, and tensometric results indicate that our consideration of successive adsorption, flocculation, induced binding, stabilization and sedimentation processes at the $(AgI)_{solid}/(electrolyte + surfactant)_{liquid}$ interface is a possible explanation of observed phenomena.

REFERENCES

1. R. Despotović, N. Filipović and N. Peček, J. Colloid & Polymer Sci., in press.
2. R. Despotović, N. Filipović and J. Katanec, Ibid, in press
3. R. Despotović, Tenside, 10, 297 (1973).
4. R. Despotović et al., Lecture at "IV. Internationale Tagung über Grenzflächenaktive Stoffe Berlin 1974".
5. R. Despotović et al., Ibid.
6. Z. Karaoglanow, Z. analyt. Chem., 106, 129, 267, 309 (1937).
7. B. Tamamushi, Kolloid Z., 150, 44 (1957); B. Tamamushi and K. Tamaki, Trans. Faraday Soc., 55, 1007, 1013 (1959).
8. R. Despotović et al., Tenside, 7, 245 (1970).
9. R. W. Horne, E. Matijević, R. H. Ottewill, and J. W. Weymouth, Kolloid Z. 161, 50 (1958).
10. R. Despotović and V. Karaivanova, Proc. 6th International Congress on Surface Active Substances, Zürich 1972., Carl Hanser Verlag, München (1973) Vol. II/2. p. 697.

Acknowledgement. This work has been financially supported by Research Fund of Croatia. The authors wish to thank Mrs. M. Jutrović for the electronmicrographs.

THE KINETICS OF PRECIPITATION OF DICALCIUM PHOSPHATE DIHYDRATE

B. Purgarić and H. Füredi-Milhofer

Department of Physical Chemistry, Rudjer Bošković Institute, Zagreb, Yugoslavia

Introduction

Dicalcium phosphate dihydrate ($CaHPO_4 \cdot 2H_2O$, DCPD) is extensively used in industrial procedures such as the production of calcium halophosphate phosphors (1) and the production of tooth paste (2). It is known as the initial reaction product in soils, when phosphate fertilizers are applied (3). Besides, DCPD is mentioned as a possible intermediate in the mineralization of biological hard tissue (4) and has been found as a component in urinary calculi (5). It is also believed to play an important role during dental caries formation (6). Clearly then, the precipitation of dicalcium phosphate dihydrate is of considerable theoretical and practical interest. It has been found that DCPD nucleates from solutions of low supersaturations at $pH < 6.3$ (7-9). The conditions (reactant concentrations, pH, temperature) under which this salt is reasonably stable have been defined (9-11). Previous kinetic studies were concerned with the growth of well defined DCPD seed crystals from solutions supersaturated to this salt (12). The subject of this paper is the kinetics of spontaneous precipitation of dicalcium phosphate dihydrate as initiated by rapid mixing of the reactant solutions. The precipitation conditions were maintained such, that simultaneous or subsequent precipitation of other calcium phosphates did not occur during the reaction. It is shown, that pure crystal growth dominates in a limited region of low supersaturations.

Methods and treatment of data

Analytical grade chemicals and bidistilled water were used. Equimolar solutions of calcium chloride and sodium phosphate were preadjusted to pH 5 * and the sodium phosphate solution was made 0.3M with respect to sodium chloride. Equal volumes of these solutions were mixed to obtained zero time reactant concentrations 2×10^{-2}M - 4×10^{-2}M. For short induction periods rapid mixing device, constructed after similar devices used in stop-flow techniques (13,14) was employed. The reaction was carried out at constant temperature (25 $\pm$ 0.1°C), the slurry being constantly stirred by a magnetic stirrer. The pH was kept constant (pH=5) by adding carbonate free sodium hydroxide solution by means of a pH-stat device; the consumption of sodium hydroxide was automatically recorded. The precipitates were identified as DCPD by chemical analysis and IR and X-ray spectroscopy (10). Particle counts were obtained from micrographs taken at constant time intervals during the kinetic experiments. The number of particles within agglomerates was estimated. A computer program (B. Purgarić and Z. Tutek, in preparation) was used to simulate precipitation, i.e. to calculate the concentrations of all ionic species including the amount of hydrogen ions liberated during precipitation from known initial reactant concentrations and pH. From the amount of hydroxide added in a pH-stat experiment it was then possible to calculate at any given time the amount of DCPD (X moles) precipitated from one liter of the precipitation system and the degree of the reaction as defined by equation 1 :

$$\mathcal{L} = (\left[HPO_4^{2-}\right]_0 - \left[HPO_4^{2-}\right]_t)/(\left[HPO_4^{2-}\right]_0 - \left[HPO_4^{2-}\right]_s) \qquad (1)$$

where $\left[HPO_4^{2-}\right]_0$ and $\left[HPO_4^{2-}\right]_t$ are the concentrations of HPO_4^{2-} ions at zero time and time t and $\left[HPO_4^{2-}\right]_s$ is the solubility as calculated from the 25°C solubility product of DCPD (12).

---

* The pH was slightly higher to compensate for complex formation after mixing. It was intended, that the pH at zero time after mixing should be as close as possible to pH=5.

From the $\mathcal{L}$ values determined at different reaction times the corresponding values for the chronomals I_D and I_p as defined and tabulated by Nielsen (15) were obtained. The following definitions for the supersaturation were used :

$$S = ([Ca^{2+}]\cdot[HPO_4^{2-}]\cdot f_1\cdot f_2)^{1/2} / K_{sp}^{1/2} \qquad \text{(ref. 17)} \qquad (2)$$

$$S' = ([Ca^{2+}]\cdot[HPO_4^{2-}])^{1/2} - (K_{sp}/f_1\cdot f_2)^{1/2} \qquad \text{(ref. 16)} \qquad (3)$$

$$S'' = [Ca^{2+}]\cdot[HPO_4^{2-}] - K_{sp}/f_1\cdot f_2 \qquad \text{(ref. 12)} \qquad (4)$$

where f_1 and f_2 are activity coefficients and K_{sp} is the solubility product of DCPD. All ionic concentrations and activity coefficients were obtained by the above mentioned computer program.

Results

The precipitates were heterogeneous in size and shape. The average particle length did not exceed 40 µm and the average particle number was not higher than 5×10^8 particles/ml. Particles formed at higher initial reactant concentrations ($> 2.7\times10^{-2}$M) appeared smaller in size and more agglomerated than those formed in the lower concentration range. Typical X vs. time curves are shown in figure 1, while in figure 2 a rate curve (lower diagram) is compared to the corresponding X vs. time curve (upper diagram). The precipitation rate dX/dt is represented according to equation 5

$$dX/dt = k \cdot X^{2/3} \cdot (S')^n \qquad (5)$$

where $X^{2/3}$ is the available crystal surface area. All X vs. time curves are S shaped indicating autocatalytic reaction mechanisms. Consequently, the corresponding rate curves have maxima as shown in figure 2. The precipitates appeared after induction periods (t_i) which were determined from the corresponding $\mathcal{L}^{1/3}$ vs. time curves. The initial slopes of the rate curves (section A in fig. 2) are so steep that the time corresponding to the maximum rate (t_{max}) almost coincides with the respective induction period. The following relation was found:

$$t_{max} \cong t_i = (10^{5.17\pm0.07})/(S_0^{13.1\pm0.2}) \qquad (6)$$

where the initial supersaturation S_0 is defined according to Eq. 2. The maximum of the rate curve shown in figure 2 (initial reactant concentrations $P_T^0=Ca_T^0=2.7\times10^{-2}M$) is followed by a straight line (section B) with subsequent deviation from linearity towards higher supersaturations (section C). In all systems with initial reactant concentrations lower then $2.7\times10^{-2}M$ the maximum rate was followed by a linear part with no subsequent deviation. The number of particles in samples corresponding to the linear parts of the rate curves was between 10^7 and 3×10^8 particles/ml ; changes during each one experiment were within the experimental error. At initial reactant concentrations higher than $2.7\times10^{-2}M$ no linear dependence, but deviations towards higher supersaturations were observed. In figure 3 different kinetic experiments are compared by plotting the maximum rate (curve 2) and the corresponding crystal surface area available for growth (curve 1) as a function of the initial supersaturation. Throughout these experimental points, the number of particles was constant within the experimental error.

Discussion

The above results may be analysed in terms of several consecutive and/or simultaneous processes : nucleation, crystal growth and agglomeration. In the investigated concentration range nucleation was predominantly heterogeneous as indicated by the number of particles (relatively low and independent on initial supersaturation) and by the dependence of the induction period on the initial supersaturation (Eq. 6). Nucleation and initial crystal growth are very fast processes which are represented by a steep rise of the initial rate curve (section A in fig. 2 and Eq. 6). A similar observation was made by Khamskij (18) for the crystallization of barium nitrate. A comparison of different rate curves at conditions of maximum rate shows a linear increase of the crystal surface area with increasing initial supersaturation, while the particle number is approx. constant. Apparently under these conditions nucleation has ceased to be rate determinant and crystal growth is the dominant process. The rate of crystal growth is an exponential function of the initial supersaturation (curve 2 in fig. 3). In a single experiment the crystal growth process is represented by a straight

line on the rate curve (section B in fig. 2). At initial reactant concentrations higher than 2.7×10^{-2}M agglomeration sets in simultaneously causing a decrease of the surface area available for growth and consequently deviation from linearity (section C in fig. 2).

An analysis of the linear part of the rate curve of one of the systems ($P_T^0 = Ca_T^0 = 2.5 \times 10^{-2}$M) according to Nancollas (16) and Marshall and Nancollas (12) gave the following results :

$$(dX/dt) \cdot X^{-2/3} = 10^{9.33 \pm 0.06} \cdot (S')^{3.57 \pm 0.02} \qquad (7)$$

$$(dX/dt) \cdot X^{-2/3} = 10^{15.33 \pm 0.09} \cdot (S')^{3.07 \pm 0.02} \qquad (8)$$

In order to decide which of the two equations describes the crystal growth process more accurately the analysis after Nielsen (15) was also employed, although the theory is not quite applicable to low supersaturations*. The results are shown in fig. 4, where the chronomals I_D and I_p obtained from the corresponding $\mathcal{L}$ values are plotted as a function of time. According to definition the chronomal which defines the rate controlling mechanism should give a straight line. This requirement is best satisfied for the chronomal I_4 in fig. 4. The order of the reaction is comparable to the one obtained in equation 7. Consequently, this equation is most likely to represent the crystal growth process of DCPD in our system, indicating that the process is surface reaction controlled. This result is in accordance with those of other authors who investigated crystal growth in spontaneously precipitating systems. Thus Doremus (19) found the order of crystal growth for barium sulfate between 3 and 4, while Nielsen obtained 3 and/or 4 for barium sulfate, strontium sulfate, silver chromate and calcium oxalate (20). However, the growth of DCPD seed crystals was reported to be

---

* In the Christiansen-Nielsen theory the approximation $(c-s) \sim c$ (where c is the concentration and s the solubility) is used, which cannot be applied to low supersaturations.

second order with respect to concentration (12). It was also shown earlier (21) that at comparable supersaturations crystal growth is much faster in a spontaneously precipitating system than in seeded crystal growth experiments.

In conclusion it may be said that it is possible to analyse crystal growth in spontaneously precipitating systams, but only in a very limited range of low supersaturations.

Acknowledgement : This work was supported in part by the National Institutes of Health, DHEW, Bethesda, Md. and the US-Yugoslav Joint Board for Scientific and Technological Cooperation (Grand No 02-002-1, Amendment 3) and partly by the Croation National Research Fund.

References

1. Aia, M.A., Goldsmith, R.L. and Mooney, R.W., Ind. Eng. Chem. 53, 55 (1961).
2. Van Wazer, J.R., Phosphorus and its Compounds, Vol. II, p. 1645, Interscience Publ., New York, London, 1961.
3. Brown, W.E. and Lehr, J.R., Soil Sci. Soc. Am. Proc. 23, 7 (1959) ; Lehr, J.R. and Brown, W.E., ibid. 22, 29 (1958).
4. Francis, M.D. and Webb, N.C., Calc. Tiss. Res. 6,335(1971).
5. Morriss, R.H. and Beeler, M.F., Am. J. Clin. Pathol. 48, 413 (1967) ; Otto, H. and Ihmann, E., Frankfurt Z. Pathol. 77, 262 (1967).
6. Francis, M.D., Ann. New York Acad. Sci. 131, 694 (1965) ; Gray, J.A. and Francis, M.D. in Mechanisms of Hard Tissue Destruction, Publ. No. 75, Am. Ass. Adv. Sci. Washington D.C. 1963, p. 213-260.
7. Hlabse, T. and Walton, A.G., Anal. Chim. Acta 33, 373(1965).
8. Walton, A.G., Bodin, W.J., Füredi, H. and Schwartz A., Can. J. Chem. 45, 2695 (1967).
9. Newesely, H., Monatsh. Chem. 97, 468 (1966).
10. Füredi-Milhofer, H., Purgarić, B., Brečević, Lj. and Pavković, N., Calc. Tiss. Res. 8, 142 (1971).
11. Füredi-Milhofer, H., Oljica-Žabčić, E., Purgarić, B., Kosar-Grašić, B. and Pavković, N., J. Inorg. Nucl. Chem. in press.

12. Marshall, R.W. and Nancollas, G.H., J. Phys. Chem. 73, 3838 (1969).
13. Chance, B., Gibson, Q.H., Eisenhardt, R.H. and Lonberg-Holm, K.K. eds.: Rapid Mixing and Sampling Techniques in Biochemistry, p. 121, Acad.Press, New York, London 1964.
14. Gibson, Q.H. and Milnes, L. Biochem.J. 91, 161 (1964).
15. Nielsen, A.E.: Kinetics of Precipitation, Pergamon Press, Oxford 1964. · Croat. Chem. Acta 42, 319 (1970).
16. Nancollas, G.H., J. Cryst. Growth 3, 4, 335 (1968).
17. Turnbull, D., Acta Met. 1, 684 (1953).
18. Khamskij, E.V., Kristall und Technik 8, 107 (1973).
19. Doremus, R.H., J. Phys. Chem. 62, 1068 (1958).
20. Nielsen, A.E., J. Colloid Sci., 10, 576 (1955).
21. Purgarić, B. and Füredi-Milhofer, H., Croat. Chem. Acta 45, 233 (1973).

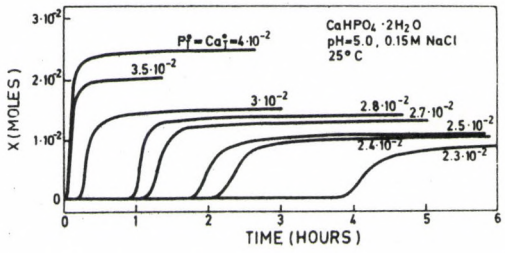

Figure 1. Kinetic curves showing the amount of DCPD (X moles) precipitated per liter of the precipitating system as a function of time.

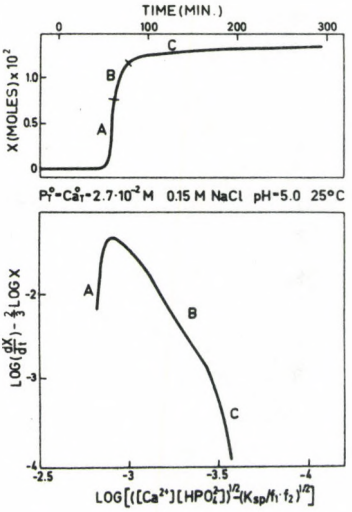

Figure 2. Lower diagram. The reaction rate (dX/dt) devided by the surface area ($X^{2/3}$) as a function of the supersaturation (S´) (log scale) (Eq. 3). Section A, B and C correspond in time to the same sections marked in the X vs. time curve (upper diagram).

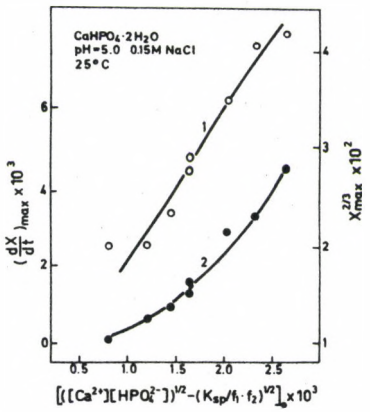

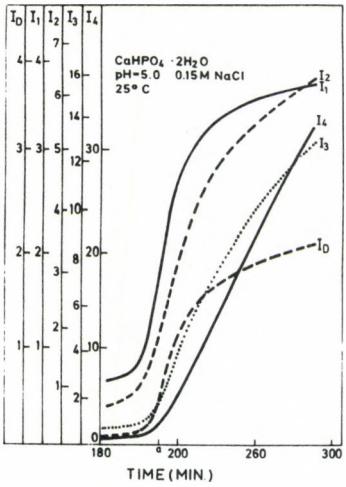

Figure 3. The maximum rate (curve 2) and corresponding crystal surface area (curve 1) as a function of the initial supersaturation S´.

Figure 4. The chronomals I_D and I_p (15) as a function of time. On the time scale "a" is the time of the maximum rate.

Group II/2

Stability and structure of disperse systems

STABILISATION OF HYDROPHOBIC SOLS BY WATER-SOLUBLE POLYMERS

A.A.Baran, O.D.Kurilenko, I.M.Solomentseva, I.I.Kocherga

Institute of Colloid Science and Water Pollution Control of the Ukranian Academy of Sciences, 252142, Kiev, Vernadsky street 42, USSR

Adsorbed high-molecular substances are known to stabilize or destabilize dispersions. Usually the first effect is observed at high coverage of the surface by polymers, the second-at low one. This work deals with the mechanism of stabilization of hydrophobic sols by water-soluble polymer additions; the preliminary results of these investigations have been described recently /1,2/ and reported at IV International conference on surface -active agents (Berlin, 1974).

The theoretical interpretation of stabilization is complex; in case of adsorbed polymer sheats one can take into consideration not only the van der Waals attraction and electric double layer repulsion between particles but the additional repulsive terms due to macromolecular chains interaction as well /3,4/. In the paper an attempt is made to calculate these contributions to the total energy of interactions between colloid particles of silver iodide and anthimony sulphide with different amount of adsorbed water-soluble polymers -polyethylene oxide (PEO) or polyvynil alcohol (PVA). The relults of the calculations are compared with the experimental data on the effect of PEO or PVA additions on the stability of AgJ and Sb_2S_3 hydrosols. For the measure of the stability we use the counterion coagulation value. The parameters necessary for evaluations were found by determination of: (1) macromolecular chain parameters in solution (from viscosity measurements); (2) adsorption of polymers mentioned by colloid precipitate of Sb_2S_3 and by particles of AgJ sol (interferometrically);

(3) surface charge density in polymer solutions(by radiometric determinations of counterion adsorption /5/) ; (4)effect of polymer additions on the electrokinetic potential of the particles (by macroelectrophoresis) and assessing on this basis the adsorbed layer thickness.Only some typical results of our experiments will be given.

The adsorption isotherms of polymers investigated are of the high affinity type without reaching a definite platform in case of PVA (fig.1,see also /6/) whereas the isotherms of PEO give real plateau /7/.The adsorbed amount increases with molecular weight and (for PVA) with the acetate groups content in molecule.Without dwelling on the adsorption data in detail it should be underlined that with increasing of electrolyte concentration the adsorbed amount of polymers decreases (fig.1). It is of importance for correct interpretation of stabilization experiments.With the assumption that PVA and PEO adsorb with their strongly bonded molecules of water the surface areas of hydrated monomeric units $(CH_2\text{-}CHOH)\cdot 2H_2O$ and $(CH_2\text{-}O\text{-}CH_2)\cdot 3H_2O$ /8/ were found to be 30 and 33 $\mathring{A}^2$.From the above one can see that the amount of PVA or PEO in a close-packed monolayer won't be higher than 0.24 or 0.22 $mg/m^2$and the maximum adsorption of these polymers (fig.1,see also/6,7/) is equivalent to the amount in several monolayers.

In order to determine the polymer sheat thickness we have measured the electrophoretic mobility of colloid particles containing different adsorbed amount of PVA or PEO.The conditions of these experiments were such (the mean radius of Sb_2S_3 and AgJ particles 230 and 530 $\mathring{A}$,the reciprocal Debye length 44 and 34 $\mathring{A}$, $\varkappa a \sim 5$ and ~ 16 ,the value of dimensionless relaxation criterium $Re \sim \exp(\psi_\delta/2-1)/\varkappa a$ /9/ $\sim 0,3$ and ~ 0.1 ,i.e.smaller than one) that in a first approximation the contribution of the polarization of the double layer may be neglected /9/;therefore the values of ζ -potential were calculated according to Smoluchovsky formula.An example of the dependence of ζ -potential on the amount of adsorbed polymer is given in fig.2.It was found that polymer additions either don't change the surface charge density (PVA on Sb_2S_3 or PEO on AgJ)at all or change it not strongly (up to 15% in case

of PEO adsorption on Sb_2S_3). Hence, the decrease of ζ-potential in the presence of rising addition of PVA or PEO should be caused by the shift of shear plane into the solution which is the result of forming of polymer layers with increasing thickness round the particles. The plateau of the curves ζ-a corresponds to completion of this process. Provided the polymer sheat doesn't change the charge distribution in the diffuse double layer /6/ for each value of ζ-potential one can calculate the distance of the shear plane from the surface characterising the polymer layer thickness (Δ) by using the formula /10/:

$$\tanh\left(\frac{e\zeta}{4kT}\right) = \tanh\left(\frac{e\Psi_\delta}{4kT}\right) e^{-\varkappa(\Delta-\delta)} \qquad (1)$$

where Ψ_δ is the Stern potential (for Ψ_δ the values of ζ-potential of non-protected sols were taken), δ the thickness of the Stern layer (~ 4 Å), e, κ, T have their usual meaning. The values of Δ on the adsorbed amount of PVA on Sb_2S_3 calculated in a similar way are shown in fig.2.

To evaluate the polymer layer contribution to the energy of interactions of covered particles we have to know the number of adsorbed loops per unit area (ν) and their length, i.e. the average number of segments per loop ($\bar{l}$). The values of $\bar{l}$ were estimated from the dependence of layer thickness on the adsorbed amount of polymer by the method described in detail by Fleer and Lyklema /6/. Using the expression for polymer segment density distribution near the interface and taking into account the Loop size distribution for adsorbed homopolymer the relationship between $\bar{l}$ and l_s was obtained /6/:

$$\bar{l} = 2b\sqrt{6} / l_s p_H \qquad (2)$$

where l_s is the length of the segment, b is a numerical constant $\sim 0{,}7$, the parameter p_H is the function of the fraction of units adsorbed (θ) and of the dimensionless constant (K_H) depending on the flexibility of the polymer chain. The value of θ is calculated from adsorption data as the ratio of number of units in the first (flat) layer (the latter a_0 was found from the surface area of PVA and PEO units with the assumption of 70 % coverage of the surface by polymer /6/) to their total amount per unit area (a_∞). The value of K_H was chosen empirically in such way that the

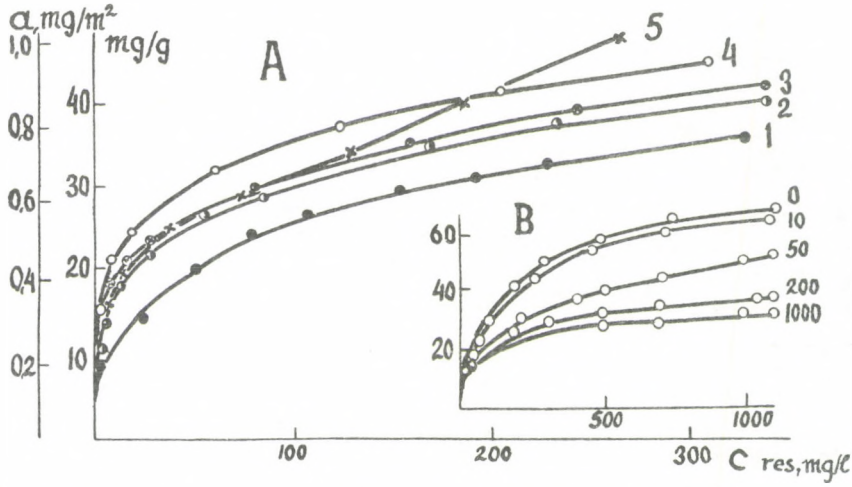

Fig.1.(A) Adsorption of PVA on the Sb_2S_3;1-PVA-12 (with 12 % of acetate groups and M=22000);2-PVA-2 (41000);3-PVA-2(63000); 4-PVA-12 (59000);5-PVA-18 (65000)

(B) Effect of KNO_3 additions (mmoles/l) on the adsorption of PVA-18 (65000) on the Sb_2S_3 particles.

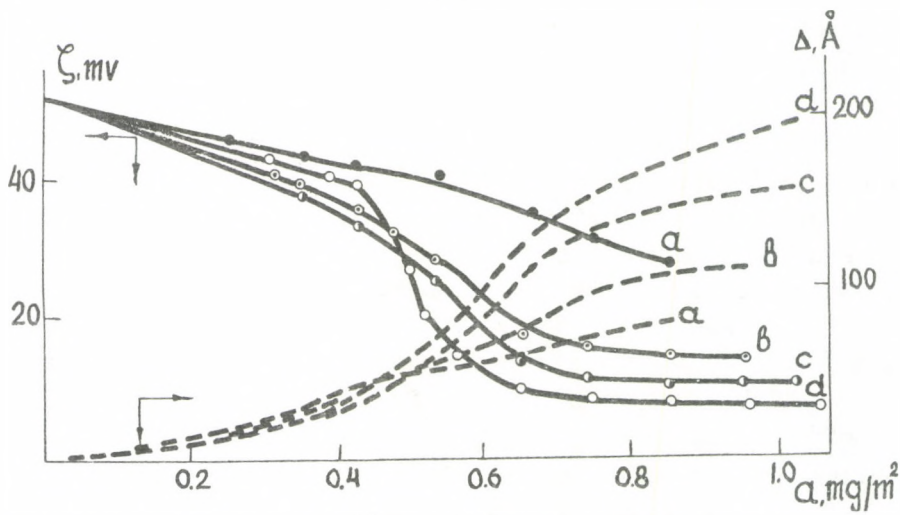

Fig.2. The dependence of ζ -potential and adsorbed layer thickness (Δ) of Sb_2S_3 particles on the adsorbed PVA amount: a-PVA-12(22000); b-PVA-2(41000); c-PVA-12(59000); d-PVA-18(65000).

theoretical dependence of the layer thickness on the adsorbed amount calculated from /6/

$$\Delta - \delta' = \frac{a_\infty - a_0}{K_H \rho_0} \ln K_H \rho_0 / \rho_{eff} \qquad (3)$$

would maximally coincide with the experimental curve $\Delta - a$ (fig.2). In expression (3) δ' is the thickness of monomeric units in the first layer, $\rho_0 \delta' = a_0$ and ρ_{eff} is calculated according to the theory of polymer solutions as the density of polymer chain with radius equivalent to the hydrodynamic radius in a free coil.

Starting from the results obtained we have evaluated the various contributions, i.e. the energy of van der Waals attraction (ΔF_A), the energy of double layer repulsion (ΔF_R)- and the repulsion energy due to polymer chains (ΔF_p) to the total energy of interactions between polymer covered particles for different values of ionic strength.

The ΔF_A for two flat plates is given by /10/:

$$\Delta F_A = - \frac{A_{12}}{12 \pi d^2} \qquad (4)$$

where d is the distance between the surfaces; for Hamaker constant A_{12} of particles Sb_2S_3 and AgJ we have adopted 2×10^{-12} ergs /11/ and 2.5×10^{-13} ergs /6/. Since the polymer investigeted are strongly hydrated in aqueous solution /8/ the Hamaker constant of the adsorbed layer was put equal to that of water /12/.

The electric double layer repulsion energy was found according to the expression which is true provided the potential is constant during the interaction and $\varkappa d > 1$ /10/:

$$\Delta F_R = \frac{\varkappa}{Z^2} f(Z) , \quad Z = \frac{ze\Psi_0}{KT} \qquad (5)$$

where z is the valency of counterion, Ψ_0 the surface potential; the values of $f(Z)$ were taken from exact tables in /10/, Ψ_0 was estimated from the charge density σ_0 on the surface determined by direct radiometric measurements of counterion adsorption/5/. For AgJ and Sb_2S_3 particles the values of σ_0 are 2.4×10^{17} and 5.0×10^{17} charges/m^2 and these values don't depend on the valency of counterions. For calculation of Ψ_0 we have used the Gouy-Chapman theory taking into account the practical constancy of σ_0 in the presence of

adsorbed polymer (see above).

To evaluate the rise in free energy due to the interaction of adsorbed polymer chains (ΔF_p) we made use of the theory of Hesselink, Vrij and Overbeek (HVO) developed for flat plates /4/ which includes the exponential density distribution for adsorbed homopolymer. In general ΔF_p consists of two terms: the volume restriction effect (ΔF_{VR}) due to decrease of configurational entropy of adsorbed loops on the approach of a second particle and the osmotic effect (ΔF_M) caused by polymer-solvent interaction changes when the interpenetration and mixing of adsorbed macromolecules occurs. The HVO theory gives the following expressions for calculations of ΔF_{VR} and ΔF_M /4/:

$$\Delta F_{VR} = 2\nu KT\, V(\bar{\imath},d) \qquad (6)$$

$$\Delta F_M = 2(2\pi/9)^{3/2}(\alpha^2-1)\,KT\nu^2\langle r^2\rangle\, M(\bar{\imath},d) \qquad (7)$$

where ν is the total number of loos per unit area; the root mean square end-to-end distance of polymer chain in solution $\langle r^2\rangle^{1/2}$ and the linear expansion factor α were estimated from viscosity measurements. $V(\bar{\imath},d)$ and $M(\bar{\imath},d)$ give the increase in free energy per average loop as a function of interparticle distance d . The numerical evaluation of ΔF_{VR} and ΔF_M , was performed on "Mir-2" computer for three modes of attachment of macromolecules to the surface starting from expressions for $V(\bar{\imath},d)$ and $M(\bar{\imath},d)$ obtained in /4/: (a) with the assumption, as it was suggested in /4/, that the polymer chain dimensions on the surface and in the solution are equal, i.e. $\langle r^2\rangle = i l_s^2$; this model indicates the existence of the energetic barrier at unlikely large (400–600 Å and more) d ; (b) for equal loops the barrier exists at distances somewhat smaller than the thickness of the polymer sheats (fig.3 b) ; (c) for homopolymer adsorption with exponential loop size distribution the increase of ΔF_{VR} and ΔF_M takes place at the most probable distances which are approximately equal to the double thickness of the polymer layer (fig.2,3). It is due to the fact that in this case the contribution of long loops is taken into account. For models (b) and (c) the value of ν was found as $n/\bar{\imath}$, where n is the number of monomeric units in loops calculated as the difference

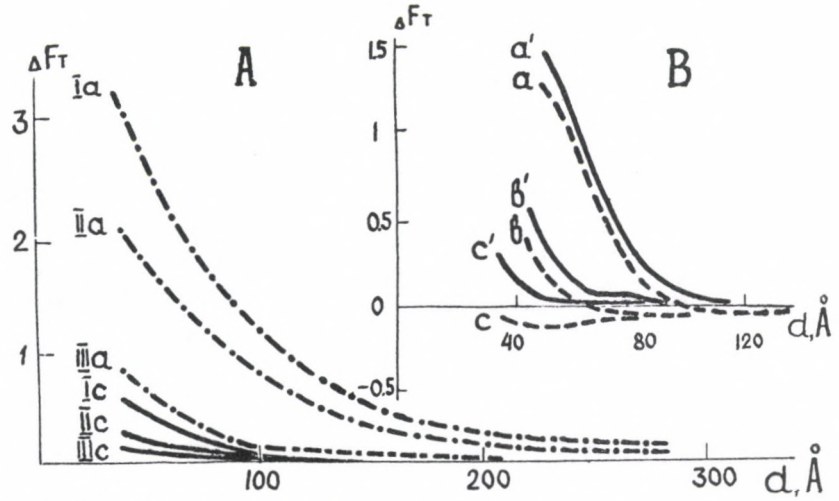

Fig.3. The free energy of interaction of Sb_2S_3 particles with different adsorbed amount of PVA-12: 1.0 mg/m^2, $\bar{\iota}$ =15.5 (a); 0.7 mg/m^2, $\bar{\iota}$ =9.7 (b); 0.5 mg/m^2, $\bar{\iota}$ =6.2 (c) in the presence of 1 mmol/l (a'b'c') and 1 mol/l (abc) KNO_3 in sol; (A) for exponential loop size distribution model: I- $\Delta F_p = \Delta F_{VR} + \Delta F_M$ II- $\Delta F_p = \Delta F_M$, III- $\Delta F_p = \Delta F_{VR}$ and (B) for equal loops model

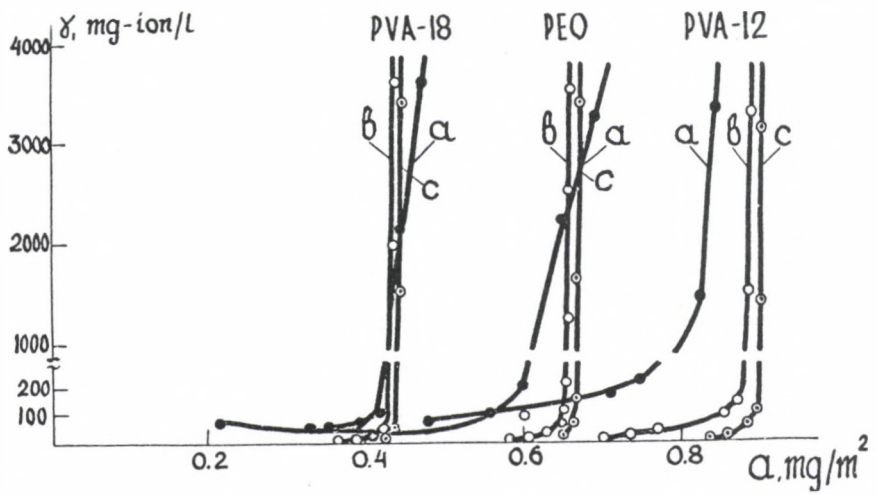

Fig.4. The coagulation values γ of the cations Na^+(a), Ca^{2+}(b) and La^{3+}(c) for Sb_2S_3 sol with different adsorbed amount of PVA or PEO

between the total adsorbed amount and the amount in the first layer; the value of $\langle r^2 \rangle$ was estimated from $\langle r^2 \rangle = \alpha^2 \bar{i} l_s^2$ The values of l_s for PVA-2 and PVA-12 are 16,9 Å and 17,1 Å (see /6/);for PEO it was found to be 8,1 Å. It is hard to imagine that the volume restriction and mixing effects operate at any interparticle distances simultaneously.Therefore,the contribution of each of these effects to the total energy of interaction ($\Delta F = \Delta F_A + \Delta F_R + \Delta F_{VR}$ or $\Delta F = \Delta F_A + \Delta F_R + \Delta F_M$) was calculated separately.In accordance with the predictions of the HVO theory the contribution of ΔF_M to the stabilization is higher than that for ΔF_{VR} (fig.3).The maximum height of curves $\Delta F(d)$ with lowering of the surface coverage diminishes or even vanishes,i.e. at coverages below the "critical" value the adsorbed polymer can't stabilize sols.This prediction of the theory is in good agreement with the results of stabilization experiments (an example is given in fig.4) provided one takes into consideration: 1) the polymer desorption in the presence of electrolytes ; 2) the loop size distribution of adsorbed homopolymer and 3) the contribution to the polymer chains interaction either of the mixing effect or of the volume restriction effect.

REFERENCES

1.A.A.Baran et al.,Kolloidni Zhurn.,35, 699 (1973)

2.A.A.Baran,I.M.Solomentseva,Kolloidni Zhurn.,36, 1035 (1974)

3.B.Vincent,Advances in Colloid @ Interf.Sci.,4, 196 (1974)

4. F.Th.Hesselink,A.Vrij, J.Th.G.Overbeek, J.Phys.Chem.,75 , 2094 (1971)

5. A.A.Baran et al.,Dokladi Akademii nauk SSSR,163, 125 (1965)

6. G.J.Fleer,L.K.Koopal,J.Lyklema,Koll.Z.u.Z.Polymere,250, 689 (1972); G.J.Fleer,Thesis,Agricult.Univ.Wageningen,1971

7.B.V.Eremenko,B.Platonov,A.Baran,Kolloidni Zhurn.37, (1975)

8.V.V.Mank,A.A.Baran,I.M.Solomentseva,O.D.Kurilenko,Kolloidni Zhurn. 36,1096 (1974);Ukrainsky Chim.Zhurn. 40, 28 (1974)

9.B.V.Derjaguin,S.S.Dukhin ,Kolloidni Zhurn. 31, 350 (1969)

10.E.J.W.Vwerwey,J.Th.G.Overbeek,Theory of the stability of Lyophobic Colloids, Elsevier,Amsterdam,1948

11.B.Visser,Advances in Colloid @ Intref.Sci.,3, 331 (1972)

12.H.Sonntag,Tenside, 5 ,188 (1968)

AN INVESTIGATION OF GOLD AND SILVER IODIDE HYDROSOLS FLOCCULATION BY POLYETHYLENOXIDE ADDITIONS BY FLOW ULTRAMICROSCOPY METHOD

Θ.D.Kurilenko, A.A.Baran, Ya.Ya.Vasko

Institute of Colloid Chemistry and Water Pollution Control of the Ukrainian Academy of Sciences, 252142, Kiev, Vernadsky Street, 42, USSR

It is known that with increasing of surface coverage by high molecular sustances the stabilization of disperse system often precedes its flocculation. The flocculation of suspensions by polyelectrolytes were first studied in detail by V.K. La Mer /1/; for its interpretation he proposed the "bridging" mechanism. The majority of investigations on flocculation has been carried out with systems practically important but difficult to characterize in view of shape and sizes of particles, double layer properties, electrolyte concentration in solution, etc. It makes it hard to interprete theoretically the results obtained. In addition, the processes of flocculation were studied, in the main, by means of indirect methods, i.e. the rate of filtration or sedimentation, the volume of precipitates etc. It is, therefore, desirable to investigate the model colloid systems taking advantage of the direct methods of particle concentration counting. The first attempt to interprete flocculation (on the silver iodide-polyvinyl alcohol system) on the basis of DLVO theory was made by Fleer and Lyklema /2/.

In the paper the flocculation of monodisperse sols of gold and silver iodide by polyethylenoxide (PEO) additions has been studied by means of particles number counting in a flow ultramicroscope designed by Vlasenko-Derjaguin-Koudryavtseva /3/. The sols of Au and AgJ were prepared as in /4/, the average radius of particles (electron microscopy) was 350 Å or 800 Å, respectively. All solutions were prepared

on twice-distilled water; the number of dust particles was less than 5×10^5 cm^{-3}, it is two orders lower of the smallest measured concentrations of particles. Three samples of PEO with molecular weights $\bar{M}$ of 6×10^3, 2.3×10^5 and 1.3×10^6 were used as flocculants.

The method. The effectiveness of flocculation depends strongly on the way of mixing of polymer solution with dispersion /2,5/; therefore, all experimental conditions were strictly standardized. The samples were prepared by "two-step" method /2/: the solution of PEO was added to the sol of volume V_1, the mixture was allowed to stay with periodical shaking for an hour and then the electrolyte solution and the second portion of sol V_2 was added, the system was allowed to stay again for an hour and after this time an aliquot part was diluted 20-100 times and the concentration of particles (N) was measured in a flow ultramicroscope as described in /3,4/.

Results and discussion. The effectiveness of flocculation characterized in the paper by decreasing of the number of particles per unit volume N depends on a variety of factors (see below); therefore, the effect of each of them on flocculation has been studied at the constancy of others.

The increasing of contact time between PEO and sol particles in the first portion leads to lowering of N only during the first 30 minutes; with further growth of time up to a day the flocculating effect of polymer doesn't change (see also /2/). At the same time with increasing of contact time of protected and unprotected portions of sol, i.e. the flocculation time , unbroken decreasing of N is observed. It shows the strong influence of the kinetic factor on the effectiveness of flocculation.

Effect of the way of mixing is illustrated by fig.1. One can see that at optimal polymer and electrolytes concentrations in sol (see below) the dependence of N on the ratio V_1/V_2 gives a minimum at $V_1/V_2 = 1$ as was noted firstly in /2/. In other words, the flocculation is maximum at the equal number of covered and uncovered particles in the system. This result may be easily explained on the basis of Hoeve model of adsorbed polymer layer /6/ and concept of "bridging" /1/.

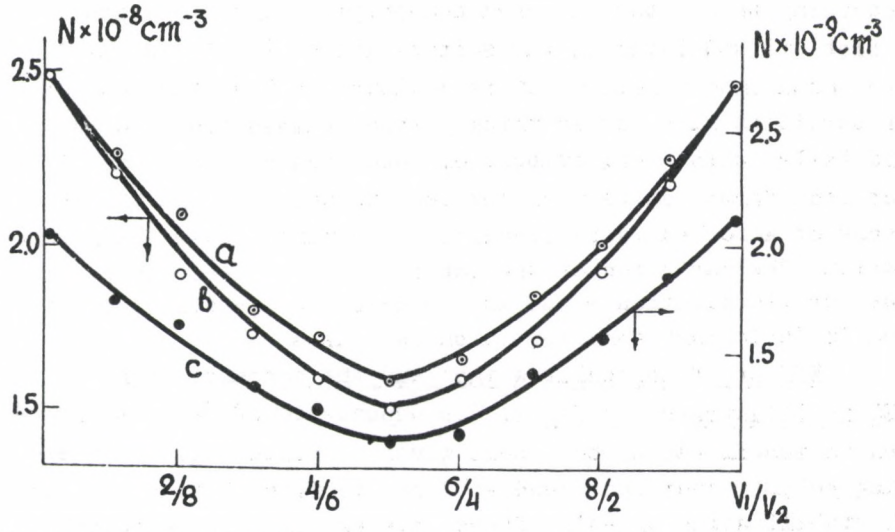

Fig.1. The flocculation as a function of V_1/V_2 for gold(a,b) and silver iodide (c) sols at conc.of KNO_3 30 mmol/l, PEO dosage 0,01 mg/l with M-$2{,}3\times10^5$(a,c) and $1{,}3\times10^6$ (b)

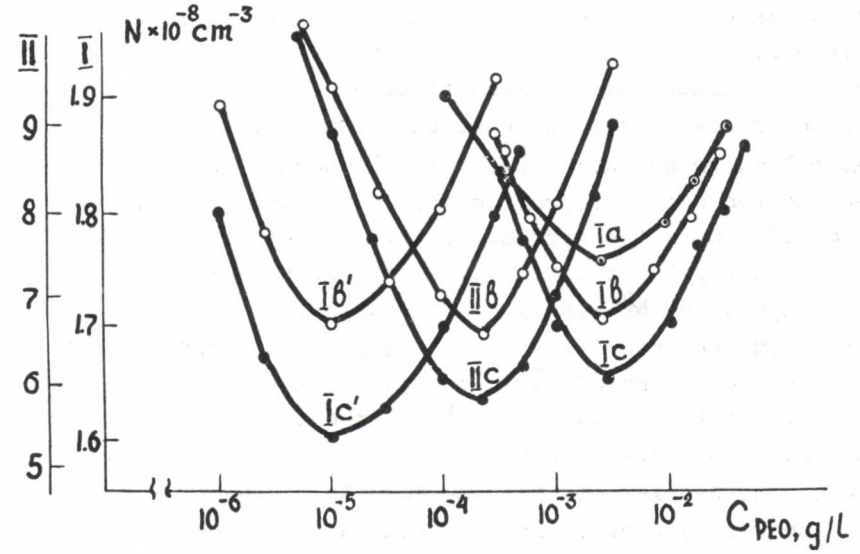

Fig.2.The flocculation of gold (I)and silver iodide (II) sols as a function of PEO dosage with M-6×10^3(a); $2{.}3\times10^5$(b) and $1{.}3\times10^6$(c) at sol conc. 0,24 mg/l (I b',c');4 8 mg/l (Ia,b,c); 12 mg/l (IIb,c)and conc. of KNO_3 30 mmol/l ; V_1/V_2 =1

According to /6/ the adsorbed homopolymer layer consists of a flat (first) layer on the surface and of loops and tails protruded into solution. It is obvious, that at the contact of particles with rather thick polymer sheats (long loops and tails) with equal numbers of bare ones optimal conditions for bond formation between covered and uncovered particles by means of adsorbed macromolecules exist which cause the flocculation. The variation of the ratio V_1/V_2 makes the conditions for flocculation worse as the number of particles involved in "bridging" bond formation decreases.

Effect of molecular weight and the concentration of PEO is illustrated in fig.2. The dependence of N on the concentration of PEO of both sols gives a minimum, i.e. increasing polymer additions lead at first to flocculation and then to stabilization of sols. These data are also in agreement with the discussed mechanism; at the low contents of PEO the adsorbed layer thickness of the particles of the first portion is not enough for the beginning of flocculation whereas at high concentration a part of polymer remains non-adsorbed and it will cover the surface of particles in the second portion which causes the sol stabilization (see also /2/). It was also observed that the effectiveness of PEO depends weakly on molecular weight: the maximum flocculation for all three samples occurs approximately at the same weight concentration of PEO in the system. It is, probably, due to the fact that the polymer layer thickness, at the given adsorbed amount, depends on $\bar{M}$ weakly. This conclusion is in good agreement with the results obtained earlier /8/, according to which the decreasing of ζ-potential of anthimony sulphide particles for PEO of different $\bar{M}$ on the adsorbed amount is described by the same curve. It is also evident from fig. 2 that for the samples of the same sol the proportionality exists between disperse phase content and the amount of PEO which causes maximum flocculation. It follows that (a) the polymer adsorption in the flocculation region is complete and (b) the flocculation occurs at the same "critical" surface coverage.

The dependence of flocculation effectiveness on the concentration and the valency of counterions is shown in fig. 3. The changes of N are given for optimal content of PEO in sol and $v_1/v_2 = 1$; These results qualitatively coincide with such obtained for AgI sol - PVA system /2/ and they show that: 1) for flocculation the given concentration of electrolyte in solution is needed below which no changes of N reveal; 2) this concentration is lower the valency of counterion is higher; 3) for the given counterion the electrolyte concentration at which the flocculation is effective depends on molecular weight of PEO weakly and is close to the rapid coagulation values of these ions /4/. The effect of electrolytes on flocculation may be interpreted by the fact that at low concentrations the double layer repulsive forces are considerable at distances much exceeding the thickness of polymer sheats; they lead to the existance of the barrier which prevents the approaching of particles to such distances where the attractive forces of "bridging" reveal. With increasing of electrolyte concentration the height of this barrier diminishes or even vanishes as the result of double layer compression or (for polyvalent counterions) reduction of surface potential; in this case the approaching of particles and their interaction by means of adsorbed polymer is possible, which causes flocculation. Further increasing of electrolyte concentration does not affect this process as the number of effective collisions will be determined only by the Brownien movement and the flocculation rate - by the rate of adsorbed bond formation.

To examine the considerations mentioned the potential curves of interactions of gold and silver iodide particles in different electrolyte solutions were calculated. Let's assume, as the first approximation, that adsorbed polymer does not affect the charge distribution in diffuse double layer /2/, i.e. the electric repulsive forces of covered and uncovered particles may be equalized to that of uncovered ones. The energy of van der Waals attraction ΔF_A for spherical particles was found according to /7/:

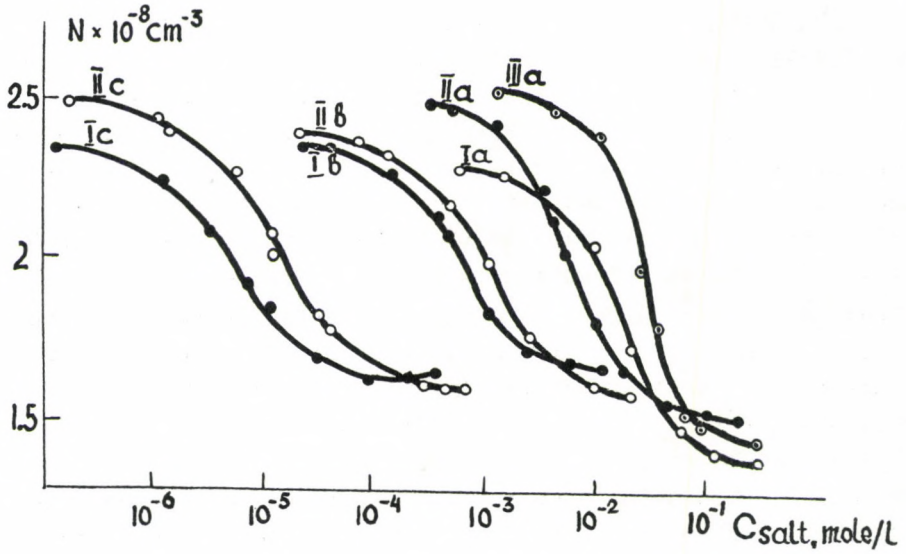

Fig.3. The flocculation of gold sol as a function of KNO_3 (a), $Ca(NO_3)_2$ (b) and $La(NO_3)_3$ (c) concentration at PEO dosage 0.01 mg/l with M-1.3x10^6 (I) ; 2.3x10^5 (II);6x10^3(III); V_1/V_2 =1

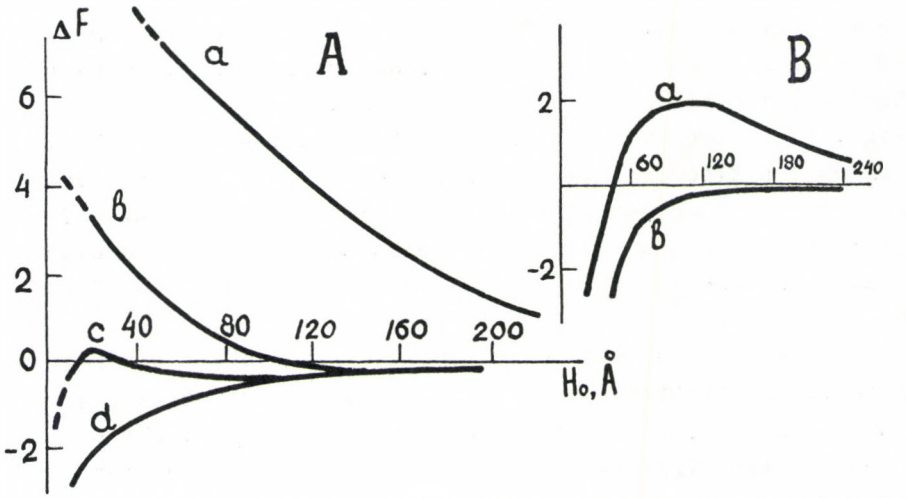

Fig.4. The energy of interaction between gold (A) an silver iodide (B) particles in (A) KNO_3 anb (B) $Ca(NO_3)_2$ solutions; conc.of KNO_3 -1 mmol/l (a),10 mmoles/l (b), 30 mmoles/l (c); 100 mmoles/l (d) ; conc.of $Ca(NO_3)_2$-0.1 mmol/l (a);1 mmol/l(b)

$$\Delta F_A = -\frac{A_{12}}{6}\left[\frac{2}{S^2-4} + \frac{2}{S^2} + \ln\frac{S^2-4}{S^2}\right]$$

for the Hamaker constant A_{12} of gold and silver iodide is adopted 4.1×10^{-12} /9/ and 2.5×10^{-13} ergs /2/, respectively; $S = R/a$, here R is the distance between the centres of spheres, a - their radius.

The double layer repulsion energy ΔF_R was calculated according to the expression true for large surface potentials ($\Psi_0 z > 25$ mv) and $\varkappa a > 3$ /7/:

$$\Delta F_R = \frac{a}{z^2} L(Z, \varkappa H_0)$$

where $\varkappa$ is the reciprocal Debye length, z - the valency of counterions, H_0 - the distance between the surfaces of the spheres, $Z = ze\Psi_0/KT$, where Ψ_0 is the surface potential. The values of function L were taken from tables given in /7/. The values of Ψ_0 were estimated from the data on the surface charge density σ_0 founded by radiometric determinations of the counterion adsorption /10/; for gold and silver iodide particles the σ_0 are 3×10^{14} and 2.4×10^{13} charges/cm^2 and don't depend on the valency of counterion. The diffuse double layer theory gives the relation between Ψ_0 and σ_0 /7/:

$$\sigma_0 = \left(\frac{2\varepsilon n_s KT}{\pi}\right)^{1/2} \sinh\frac{ze\Psi_0}{2KT}$$

here n_s is the number of counterions per unit volume, $\varepsilon, \pi, z, e, K, T$ have their usual meaning.

Some examples of potential curves calculated are given in fig.4. The comparison of them with the data of fig. 3 shows that the sol doesn't reveal flocculation just at such electrolyte concentrations in the system where a sufficient energetic barrier exists at the considerable (100-200 Å) distances between particles. It was shown earlier /11,8,12/ that the thickness of adsorbed layer of PEO on particles investigated is, probably, within these limits. All these data confirm the correctness of the ideas expressed concerning the mechanism of electrolyte effect on the flocculation processes. According to these considerations it may easily be exp-

lained why gold sol is flocculated in 10^{-2} M solution of KNO_3 in spite of the fact that the marked barrier between particles yet exists (fig. 4). It is obvious, that this barrier is located at the distances less than the polymer sheats thickness; therefore it doesn't prevent the aggregation between covered and uncovered particles.

In conclusion we note that the quantitative description of adsorbed layer contribution to the energy of interaction between particles will be possible after getting detail information about the structure of polymer sheat on the surface of sol particles and adsorption energy of monomeric units (see /2/).

REFERENCES

1. V.K.La Mer, Disc.Farad.Soc., 42, 248 (1966)
2. G.J.Fleer, J.Lyklema, J.Colloid @ Interf.Sci., 46, 1 (1974); G.J.Fleer, Thesis, Agricultural University Wageningen, 1971
3. B.V.Derjaguin, G.J.Vlasenko, Dokladi Akademii nauk SSSR, 63, 155 (1948); N.M.Koudravtseva, B.V.Derjaguin, Kolloidni Zhurn., 25, 739 (1963)
4. B.V.Derjaguin, N.M.Koudravtseva, Kolloidni Zhurn. 26, 61 (1964)
5. I.M.Solomentseva, A.A.Baran, O.D.Kurilenko, Ukrainski Chim.Zhurn., 39, 785 (1973)
6. C.A.J.Hoeve, J.Chem.Phys., 43, 3007 (1965); J.Polym.Sci. (C), 30, 361 (1970)
7. E.J.W.Verwey, J.Th.G.Overbeek, Theory of the Stability of Lyophobic Colloids, Elsevier, Amsterdam, 1948.
8. B.V.Eremenko, B.E.Platonov, A.A.Baran, Kolloidni Zhurn., 37 (1975)
9. B.V.Derjaguin, V.M.Muller, Ya.I.Rabinowitsch, Kolloidni Zhurn., 31, 304 (1969)
10. A.A.Baran et al. Dokladi Akademii nauk SSSR, 163, 125 (1965); Kolloidni Zhurn., 32, 167 (1970)
11. A.G.Savkin, I.M.Solomentseva, A.A.Baran, O.D.Kurilenko, Ukrainski Chim.Zhurn., 39, 1238 (1973)
12. A.A.Baran et al. (paper for present conference).

SURFACE PROPERTIES OF SOL PARTICLES

S.Rohrsetzer, M.Kabai-Faix and F.Csempesz

Department of Colloid Science, L.Eötvös University, Budapest
Hungary

Introduction

Sols of different chemical nature are significantly different in its colloid stability. According to Zsigmondy's earlier investigations as well as to the latest study of Benitez and MacRitchie /1/ the peptizability of the flocculated sols is different, too. In the opinion of Frens and Overbeek /2/ one of the reasons for this behaviour is the surface recrystallization of the sol particles. In a previous work of Rohrsetzer, Kabai-Faix and Wolfram the interaction of various sols with both polymers /3/ and ionic surfactants /4/, has been found to depend to a great extent on the nature of the sols.

From the results correlations between the repeptizability and the interaction with polymers and surfactants of the same sol are expected to exist. Investigating these correlations has been the subject of the present study.

Experimental

Prussian blue sol was prepared by adding $FeCl_3$ solution to $K_4Fe/CN/_6$ solution.

Tin hydroxide sol was obtained by peptizing $Sn/OH/_4$ suspension with NaOH.

Aluminium hydroxide sol was prepared by peptizing $Al/OH/_3$ suspension with $AlCl_3$ solution at 60°C.

Iron/III/hydroxide sol was obtained by using Graham's method.

Arsenic trisulphide sol was prepared by leading H_2S gas into saturated As_2O_3 solution.

Silver iodide sol: $AgNO_3$ solution 10^{-2} mole/l was added to the same concentration of KI by quickly pouring the solutions into each other.

The sols were dialysed except silver iodide.

TABLE 1

Some characteristics of the sols

Sols	Conc. of sols %	Stabilizing electrolyte	Flocculating electrolyte	Flocc. value mmole/l	Particle radius /Å/ from sediment const.	from spec. surf.area
Prussian blue	0,44	$K_4Fe/CN/_6$	$FeCl_3$	1,00	45	57
Tin hydroxide	0,28	Na_2SnO_3	HCl	2,45	47	-
Aluminium hydroxide	0,22	$AlCl_3$	NH_4OH	6,95	130	160
Iron hydroxide	0,30	$FeCl_3$	NH_4OH	3,35	35	32
Silver iodide	0,12	KI	$AgNO_3$	0,45	240	4100
Arsenic trisulfide	0,21	H_3AsO_3	$CaCl_2$	3,90	74	960

Surfactants and Polymers were used is listed below: sodium dodecyl sulfate /SDS/, sodium tetradecyl sulfate /STS/, dodecyl pyridinium bromide /DPB/, tetradecyl piridinium bromide /TPB/, fractionated polyvinyl alcohol /PVA/ with $\overline{M}_{visc.} = 34.10^3$; 115.10^3; 160.10^3 and 196.10^3; polyvinyl pyrrolidone /PVP/:$M \sim 22.10^3$, polyethylene glycol /PEG/:$M \sim 10^3$ and methylcellulose /MC/:$\overline{M}_{visc.} = 135.10^3$.

Peptizability of the sols

The sols were flocculated by electrolytes. The flocculate was aged for different times and then peptized by the same electrolyte that stabilizes the sol /see Table 1./. The peptizator was added in increasing amount to the flocculate that was then shaken for an hour and centrifugated /20 min., 2.10^6 cm sec^{-2}/. Finally the concentration of the sol obtained as well as the concentration of the peptizing agent has been determined at which 50% of the flocculate has been peptized.

Adsorption of surfactants and polymers on the sols

24 hours after mixing the sol with surfactant or polymer solutions of various concentration, the system was ultrafiltered and flocculated respectively and the equilibrium concentration was determined.

Stability of the sols

The flocculation value of the sols and the sol-surfactant mixtures was determined by NaCl. In order to investigate the stability the sol-polymer mixture was sensitized by an electrolyte. To accelerate flocculation the mixture was shaken for an hour and then centrifugated. Finally, the degree of coagulation was established.

Experimental results

The order of peptizability is shown in Table 2. The same result has been found from either the critical concentration of the peptizating agent, that results in 50% peptizability, or its change with aging time, but not from the solubility of the sols. On the other hand, the ability for peptization is in connection with the stability of the sols. The properties of the first four sols may remain constant even for years, but the particle size of the last two sols increases with a considerable rate.

TABLE 2

Concentration of the peptizating agents /in mmole/l/ at a given degree of peptization /50%/

Sols	Aging times /min./				
	10^0	10^1	10^2	10^3	10^4
Prussian blue	-	0,15	0,17	0,15	0,10
Tin hydroxide	-	0,4	0,5	0,7	1,4
Aluminium hydroxide	-	0,5	0,5	1,0	3,0
Iron hydroxide	-	0,8	1,0	2,5	11,0
Silver iodide	1,0	15,0	unattainable		
Arsenic trisulfide	unattainable				

The first three sols do not adsorb anyone of the polymers. The iron hydroxide sol is in the middle. Neither the PEG nor the PVP are adsorbed on it. But the MC does adsorb, giving adsorption isotherm of the Langmuir type, while the PVA samples are adsorbed giving so-called "high affinity" type adsorption isotherms. /Fig.1/ Each of the polymers are adsorbed on both the arsenic trisulfide and the silver iodide sol according to "high affinity" type isotherms.

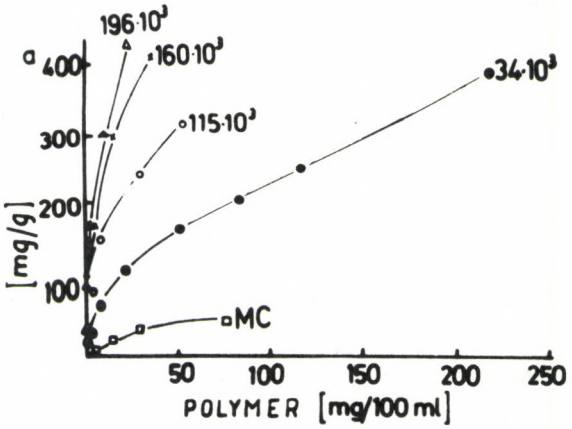

Fig. 1.: Adsorption isotherms of PVA various molecular weight and MC on $Fe(OH)_3$ sol.

As to the sensitization of the sols by polymers, only those polymers are effective in this respect, which are adsorbed according to the "high affinity" type isotherms. As it is known, the degree of flocculation gives a maximum type curve with increasing the concentration of the polymer. In contrary, the polymers cause an unexpected effect on arsenic trisulfide sol, having the greatest resistance against peptization. Both the PVA and PVP stabilize the sol at a low concentration /Fig.2/. The same type stability-curves are obtained on increase of PEG and MC concentration, but the sensitivity is not only relative in the maximum. This unexpected behaviour can be attributed the great surface energy of sol particles of arsenic trisulfid. In this case the polymer molecules lie close to the surface,

thus forming no long chain section for the formation of bridge--bounds among particles.

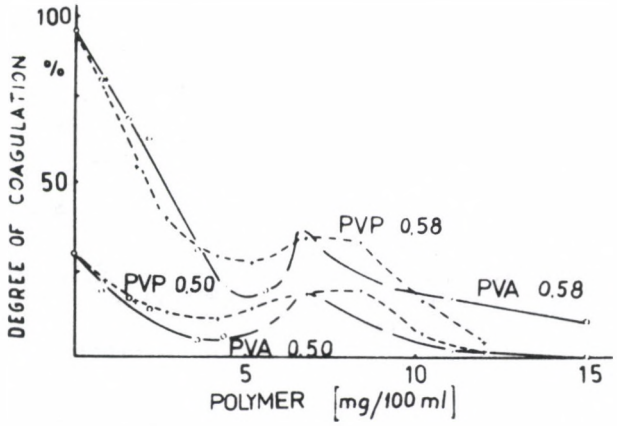

Fig.2.: Influence of PVA $\overline{M}_{visc.} = 115.10^3$ and PVP on the coagulation of As_2S_3 sol. Concentration of K_2SO_4 : 0,50 and 0,58 mmole/1. Concentration of As_2S_3 sol : 0,12%

The sols studied may be classyfied into two groups on the basis of their interaction with surfactants. The adsorption of SDS on aluminium hydroxide sol gives a Langmuir-type isotherm /Fig.3, curve I/. Neutralizing the surface charge of this sol it does not adsorb the surfactant /curve II/. The same has been found for the adsorption of DPB on Prussian blue sol.

The adsorption isotherm of SDS on iron hydroxide sol is of a "high affinity" type /Fig.4, curve I/. The SDS is adsorbed on this sol even after neutralizing the surface charge /curve II/. The arsenic trisulfide sol also has such properties with DPB surfactant.

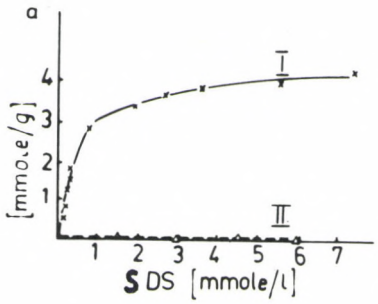

Fig.3.: Adsorption isotherms of SDS on $Al(OH)_3$ sol. I: charged surface II: neutralized surface

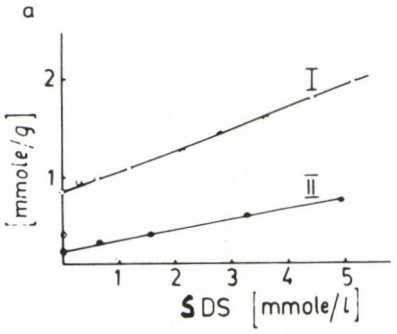

Fig.4.: Adsorption isotherms of SDS on $Fe(OH)_3$ sol. I: charged surface II: neutralized surface

The different behaviour of these sols is apparent in their flocculation values, measured by NaCl /Table 3/.

TABLE 3

The influence of surfactants on the electrolyte sensitivity of various sols

Sols	Conc. of sols %	Surfact	Conc. of surfact. mmole/l	Flocc. conc. of NaCl mole/l
Prussian blue	0,11	-	-	0,45
		DPB	100	0,15
		TPB	60	0,30
		TPB	100	0,35
Aluminium hydroxide	0,03	-	-	0,35
		SDS	80	0,12
		STS	20	0,08
Iron hydroxide	0,11	-	-	0,10
		SDS	80	2,00
		STS	20	1,50
Arsenic trisulfide	0,13	-	-	0,30
		DPB	2,0	3,00
		TPB	0,8	3,00

For those sols which can be easily peptized, the flocculation value is decreased by addition of surfactants even at high concentration. Contrary, an increase of about an order of the flocculation value has been detected only in concentrated solution of surfactants for sols having greater resistance against peptization.

Flocculating sols by the homologous series of ionic surfactant the arsenic trisulfide sol shows an unexpected behaviour, too. Namely, in this case the flocculation value is independent of the chain length of the alkyl pyridinium salts.

It is seen from these results that the higher the resistance against peptization, the stronger is the interaction of the sols with both polymers and ionic surfactants.

The differences in the peptizability are primarily connected with the ability of the particles to recrystalize among their surfaces. After drying the sols at room temperature solely the Prussian blue powder will be peptized in distilled water. Its peptizability vanishes only if the adsorbed water is removed by concentrated sulfuric acid in an exiccator. From the BET specific surface area of powders calculated equivalent radii are in a good agreement with the corresponding values obtained from the sedimentation constant except for the silver iodide and the arsenic trisulfide sol /Table 1/. The increase of about an order of magnitude in radii of the particles can be explained by the drying induced surface recrystalization.

On the basis of the results obtained, it has been concluded that the interfacial energy /S/L/ may play an important role in all types of interactions investigated.

References

/1/ R.Benitez, F.MacRitchie J.Colloid Interface Sci. 40, 310 /1972/

/2/ G.Frens, J.Th.Overbeek J.Colloid Interface Sci. 38, 376 /1972/

/3/ S.Rohrsetzer Kémiai Közl. 28 33 /1967/

/4/ M.Kabai-Faix, S.Rohrsetzer, E.Wolfram Annales Univ. Sci. Budapestin., Sec. Chim. 11 89 /1969/

RADIAL DISTRIBUTION FUNCTIONS FOR CONCENTRATED COLLOIDAL DISPERSIONS

P. RICHMOND and R. P. KEAVEY

UNILEVER RESEARCH
PORT SUNLIGHT LABORATORY
PORT SUNLIGHT
WIRRAL
MERSEYSIDE L62 4XN
ENGLAND

INTRODUCTION

Recent developments in both experimental techniques and specimen preparation have meant that basic studies of concentrated dispersions can be done with confidence.[1]

In this paper we present theoretical results for the radial distribution function of a concentrated colloid using the Percus-Yevick equations.

FORMULARY

These integral equations take the form:[2]

$$h(\underset{\sim}{r}) = f(\underset{\sim}{r}) + \rho \int d\underset{\sim}{r}' \, f(\underset{\sim}{r}') \, h(\underset{\sim}{r}-\underset{\sim}{r}') \qquad (1)$$

and

$$f(\underset{\sim}{r}) = (1 + h(\underset{\sim}{r})(1 - \exp(\beta\phi(\underset{\sim}{r}) \quad) \qquad (2)$$

Equation (1), commonly referred to as the Ornstein-Zernike equation is essentially an identity relating the indirect correlation function $h(\underset{\sim}{r})$ and the direct correlation function $f(\underset{\sim}{r})$. ρ is the particle number density. Equation (2) is the approximate relation used by Percus and Yevick for the closure of equation (1) which contains the pair potential, $\phi(\underset{\sim}{r})$. The radial distribution function $g(\underset{\sim}{r})$ is related to the indirect correlation function by

$$h(\underset{\sim}{r}) = g(\underset{\sim}{r}) - 1 \qquad (3)$$

It is convenient to re-express the Ornstein-Zernike equation (1) in terms of biopolar coordinates and a scaled distance $x = |\underset{\sim}{r}|/a$

where a is the radius of the spherical particles. Thus for a central force $\phi(\underset{\sim}{r}) = \phi(|\underset{\sim}{r}|)$ we obtain:

$$H(x) = F(x) + 2\pi \rho a^3 \int_0^\infty dx \; F(x) \int_{|x - x'|}^{|x + x'|} dy \; H(y) \qquad (4)$$

where $H(x) = \frac{|\underset{\sim}{r}|}{a} h(r)$ and $F(x) = \frac{r}{a} f(r)$ (5)

Now if we introduce a function:

$$p(x) = g(r) \; e^{\beta\phi(r)} = \frac{f(r)}{e^{-\beta\phi(r)} - 1} \qquad (6)$$

such that equation (2) is satisfied identically we obtain a non linear integral equation for the function p. i.e.,

$$p(x) = 1 + \frac{2\pi\rho a^3}{x} \int_0^\infty dx' x' \rho(x') \left[e^{\psi(x')} - 1 \right] \cdot$$

$$\int_{|x - x'|}^{x + x'} dy \; y \left[p(y) \; e^{-\psi(y)} - 1 \right] \qquad (7)$$

We may integrate the second term in the second integral to obtain

$$p(x) = 1 + \frac{2\pi\rho a^3}{x} \int_0^\infty dx' \, x' \, p(x') \left[e^{-\psi(x')} - 1 \right] \cdot \qquad (8)$$

$$\left[\int_{|x - x'|}^{x + x'} dy \; y \; p(y) e^{-\psi(y)} - 2xx' \right]$$

The dimensionless potential $\psi(x) = \beta\phi(r)$. In order to model the interaction between colloid particles we represent ϕ as a sum of three components. One an electrostatic repulsion; two, a van der Waals attraction and three, a term simulating the hard core born repulsion

i.e. $\psi = \psi_{es} + \psi_{vw} + \psi_{\beta}$ (9)

For the electrostatic term we use an expression due to McCartney and Levine [3]:

$$\psi_{es}(x) = \beta \varepsilon_s a V_\cdot^2 \left(1 - \frac{1}{x}\right) \ln \left\{ 1 + \frac{\exp\left[-\kappa a (x-2) \right]}{(x-1)} \right\} \qquad (10)$$

where ε_s is the static dielectric constant of the dispersion medium. V is the particle surface potential, κ is the usual Debye-Huckel inverse screening length and a is the radius. For the van der Waals component, we have chosen a simple functional form given essentially by Hamaker theory:

$$\psi_{vw}(x) = -\frac{2H}{3}\left\{\frac{(x^2-1)}{x^2(x^2-4)} + \frac{1}{4}\ln\left(1-\frac{4}{x^2}\right)\right\} \qquad (11)$$

For the Born repulsion we simply put in a hard core, i.e.

$$\psi_B = \begin{cases} \infty & r < 2a \quad x < 2 \\ \\ o & r > 2a \quad x > 1 \end{cases}$$

This does not permit particles to penetrate one another.

The potential was then substituted into equation (7) which was solved, as mentioned above, by an iteration method. To start the iteration we choose $p(x) = p^{(1)} = 1$. A "better" approximation $p^{(2)}$ is then obtained. To obtain convergence it was necessary to adopt a mixing procedure.[4] Thus

$$p(i+1) = (1-\alpha)\, p^{(i)} + \alpha p^{(i-1)} \qquad (12)$$

The parameter α is then chosen to obtain convergence. Typically for $\rho \sim 6.10^{11}$ or $c \sim 10^{-4}$, $\alpha \sim 0.25$.

RESULTS AND DISCUSSIONS

We consider the particular case of polystyrene like particles. We have studied in some detail the case where the particles have radius a = 5000Å and surface potential V = 75 mV. The Hamaker constant H = 1.5 kT. Sophisticated features such as retardation and electrolyte screening have not been considered here[5]. These effects we expect will affect the large distance behaviour of the radial distribution and intend to study them in detail later. The effect of particle number is qualitatively similar to that in simple liquids; the effect of electrolyte concentration is peculiar to colloidal systems. A qualitative insight into the effect of electrolyte concentration may be seen as follows. If the electrolyte concentration is low the interparticle potential is dominated by the

Born repulsion and the radial distribution function will fall to zero rapidly as $r \to 2a$ or $x \to 2$. The dominent first peak will also appear around $r \gtrsim 2a$. Now as the electrolyte concentration is reduced the primary maximum will appear in the interparticle potential peaking around $r \sim 2a + \kappa^{-1}$. This repulsive primary maximum will when it is greater than kT then take over from the Born repulsion in controlling the closest distance of approach of the particles and also the position of the dominent peak in the radial distribution function. This latter function now peaks at a distance $r \sim 2a + \kappa^{-1}$. We see this feature in the detailed calculations below.

In figure 1 we illustrate the results obtained. Consider first the case of high electrolyte concentration C=0.1m. For low particle numbers, $10^{11}/cm^3$ which corresponds for our 5000Å radius particles to a volume fraction $\pi/60 \simeq 0.05$, there is only one very sharp peak at $r \gtrsim 2a$. For higher particle number densities, secondary and even tertiary peaks appear characteristic of long range order which exists in the liquid state. In these colloid system this long range order typifies the region just before gelation. We also illustrate the result for $\rho = 6.10^{11}/cm^3$ i.e. a volume fraction $\pi/10 = 0.31$. As the electrolyte strength decreased it became increasingly more difficult to obtain results for higher particle number. This as we have explained above is due to the appearance of the primary maximum which increases the effective size of the particle and hence the effective volume fraction. For example, if the electrolyte concentration is 10^{-4}m, the Debye screening length is 335Å. The effective radius of the particles as far as binary collisions are concerned is then $\gtrsim$ 5335Å. The effective volume fraction for $\rho = 6.10^{11}/cm^3$ is then 0.38 which is very close to the gell transition point given by the Kirkwood-Alder molecular dynamic technique[6,7]. Figures (2-4) illustrate the results obtained for various particle number densities at these lower electrolyte strengths. It is clear from these curves how the position of the dominant peak in the radial distribution function shifts outwards as the electrolyte concentration is reduced. The peak is clearly shifting quite rapidly at low ionic strengths where the primary maximum in the interaction potential is large.

One feature of monodisperse latices is the observation of irridescent flecks. Kose and Hachisu[8] comment that these are characteristic of the presence of local spacial order characteristic of the liquid structure[7]. Our radial distribution functions clearly illustrate this type of order. Now in figure 5 we have plotted the position, d of the dominant peak in the radial distribution function as a function of electrolyte concentration. If this distance which separates nearest neighbours really does control irridescence then we expect that the maximum wavelength which may be observed will be $\lambda_{max} \sim d$. Thus figure 5 may be interpreted as a plot of the maximum wavelength which will be observed as a function of electrolyte concentration. Furthermore, although we are not here considering the gell or quasi-solid regime we expect that the colours observed in this phase where the radial distribution functions exhibits infinite long range order will behave similarly as a function of electrolyte strength.

REFERENCES

1. J. Brown, J.W. Goodwin, R.H. Ottewill and P. Pusey, J. Phys.A, May/June 1975.
2. For a recent review of such integral equation approaches see R.O. Watts, Specialist Periodical Reports : Statistical Mechanics Volume 1, K.Singer, Editor, Chemical Society (London) 1974.
3. L.N. McCartney and S. Levine, J. Coll. Int. Sci. 30, 345, 1969.
4. A.A. Broyles, J. Chem. Phys, 35, 493, 1961.
5. See for example P. Richmond, Specialist Periodical Reports : Colloid Science Volume 2, D.H. Everett, Editor, 1975.
6. J.G. Kirkwood, J. Chem. Phys. 7, 919, 1939.
7. B.J. Alder, W.G. Hoover and D.A. Young, J. Chem. Phys. 99 3688, 1968.
8. A. Kose and S. Hachisu, J. Colloid Interface Sci., 46, 460, 1974.

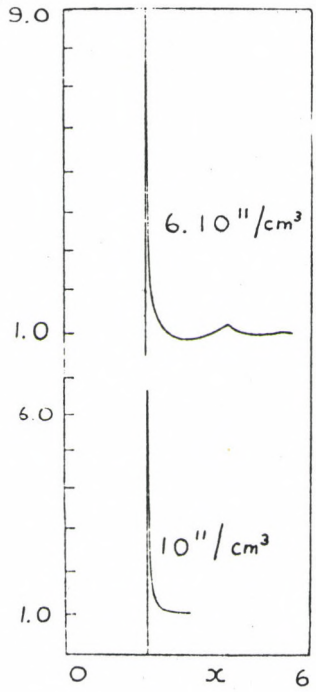

Figure 1

This illustrates radial distribution functions for colloid particles of radius 5000Å in an electrolyte solution of ionic strength 10^{-1}m. (κ^{-1} = 10.6 Å). The different curves correspond to different particle number densities as shown.

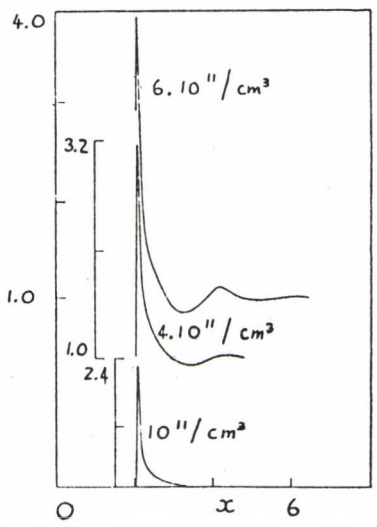

Figure 2

Radial distribution functions for colloid particles of radius 5000Å in an electrolyte solution of ionic strength 10^{-2}m (κ^{-1} = 33.6Å). The different curves correspond to different particle number densities as shown.

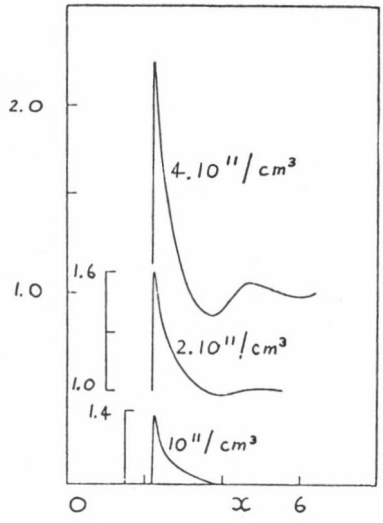

Figure 3

Radial distribution functions for colloid particles of radius 5000Å in an electrolyte solution of ionic strength 10^{-3}m (κ^{-1} = 106Å). The different curves correspond to different particle number densities as shown.

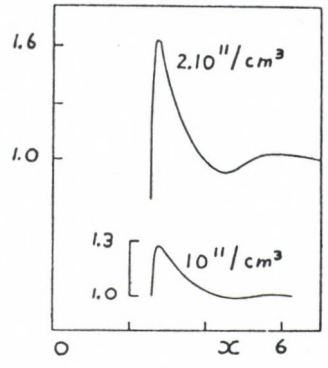

Figure 4

Radial distribution functions for colloid particles of radius 5000Å in an electrolyte solution of ionic strength 10^{-4}m (κ^{-1} = 336Å). The different curves correspond to different particle number densities as shown.

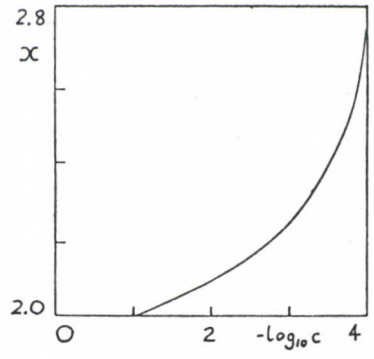

Figure 5

A plot of the position of the maximum of the dominant peak in the radial distribution function as a function of ionic strength.

STUDY OF THE HETEROADAGULATION OF LYOPHOBIC SOLS BY A RADIOACTIVE TRACER METHOD

I.Mádi

Isotope Laboratory, Kossuth Lajos University, Debrecen, Hungary

In the anisotropic field at the boundary of phases in contact, colloid particles undergoing Brownian movement -sols, association colloids and macromolecules - may be adsorbed. The term "adsorption" is not accurate fundamentally for the accumulation of lyophobic sols at a solid/liquid boundary layer, since it is a question of interaction between surfaces. Adagulation is an expedient term to be used to distinguish the adhesion of Brownian particles to macrosurfaces or macroscopic particles whose Brownian motion may be neglected owing to their large mass[1-3]. If the material properties of the sol and macroscopic particles are not the same, the correct term is heteroadagulation. The studies of Buzágh[4-6] indicated that the heteroadagulation of lyophobic sols is affected by those factors which determine the adhesion interaction between the sol particles and the solid surfaces; the material properties, the solvation of the colloid particles and macroscopic surface, the surface charge conditions, the adsorption properties of the ions, molecules and macromolecules in the dispersion medium. The rate and overall result of the heteroadagulation are determined by the maximum of the potential which is the resultant of the attractive and repulsive potentials between the sol particles and the macroscopic surface[7].

The present paper gives an account of the results obtained in a study of the rate of heteroadagulation of lyophobic

sols (gold sol, lead chromate sol, potassium hexacyanocobalt ferrate sol) labelled with the suitable radioactive indicators (^{198}Au, ^{212}Pb, ^{60}Co) on coarse disperse lead chromate, barium sulphate, aluminium oxide, hydrogen bentonite. Since the particles undergoing Brownian motion in the studied systems adhere to the surface of the coarse particles, the phenomena are typical examples of hetero-adagulation.

1. Materials

a/ Preparation and characterisation of sols.

The gold sol was prepared by reduction with hydrogen peroxide. The degree of dispersion of the sols was determined with a Tesla 513-A electron-microscope. The average diameter of the sol particles was 210 Å.

As regards the interaction of sols and coarse disperse systems, a knowledge of the surface charges and the electro-kinetic potentials of the sols is essential. The electro-kinetic potentials of the sol particles were determined in a Nernst-Buzágh apparatus[8] by the moving boundary method. The value found was - 120 mV.

The potassium hexacyanocobalt ferrate sol was prepared by mixing dilute solutions of $Co(NO_3)_2$ (labelled with ^{60}Co) and $K_4[Fe(CN)_6]$, using the method described by Srilev and Mokrusin[9]. The lead chromate sol was prepared by mixing of 0.0005 M $Pb(NO_3)_2$ (labelled with ^{212}Pb) and 0.002 M K_2CrO_4. The average diameter of the sol particles was 620 Å.

b/ Preparation and characterisation of coarse disperse adsorbents.

The coarse disperse lead chromate was prepared from 0.05 M lead nitrate by precipitation with 0.05 M potassium chromate. The reagents were mixed slowly, so that the degree of supersaturation was low. The precipitate was purified over a period of 4 months by daily decantation with doubly distilled water at 80-90 °C, and it was dried at 105 °C. Another adsorbent was a coarse disperse barium sulphate, prepared from 0.05 M barium chloride by precipitation with

0.05 M sulphuric acid. The precipitate was purified over a period of 3 months by daily decantation with doubly distilled water at 80-90 °C, and it was dried at 105 °C.
The surface area of the coarse disperse lead chromate and barium sulphate was determined by a radioactive tracer method, on the basis of the Paneth equation. ^{212}Pb was used in the case of lead chromate, and ^{140}Ba for barium sulphate. The following data were found:

$$A_{PbCrO_4} = 4400 \text{ cm}^2/\text{g}; \quad A_{BaSO_4} = 2160 \text{ cm}^2/\text{g}.$$

In addition, aluminium oxide and hydrogen bentonite were also used as adsorbents.

2. Method and experimental results

The time profile of the heteroadagulation was determined from the radioactivity decrease of the sol solution. The kinetic measurements were carried as follows: a suitable amount of the "adsorbent" was placed into the reaction vessel, 20 cm^3 sol solution was added, and the system was stirred vigorously. The temperature of the solution was previously adjusted to the desired value, and for the complete investigation period the system was thermostated with an accuracy of $\pm$ 0.1 °C. After the predetermined time the adsorbent was separated from the sol solution by centrifugation (3500 r.p.m.; 1 min). The radioactivity of the sol separated was determined with a γ-scintillation counter. The radioactivity of the sol solution separated after time $\underline{t}$ was compared with the activity of the sol originally taken, and thus the relative amount of sol adhering during a time $\underline{t}$ could be determined (n/n_o). The rate of heteroadagulation was determined via similar measurements for different times. As examples, Figure 1 gives data for the rate of heteroadagulation of a gold sol on lead chromate and barium sulphate.
For the determination of the activation energy of heteroadagulation, the rate of heteroadagulation were investigated at 0, 20 and 40 °C.

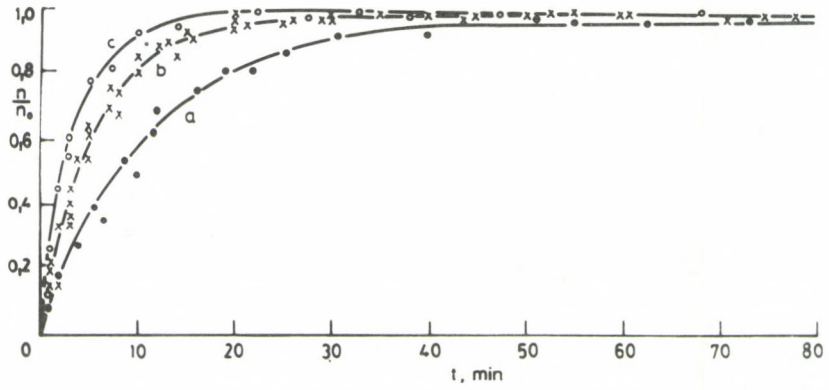

Fig. 1. Rate of heteroadagulation of gold sol on lead chromate. Amount of lead chromate: 0.05 g. Volume of sol solution: 20 cm^3. Sol concentration: $2.1x10^8$ particles cm^{-3}. Temperature: a 0 °C, b 20 °C, c 40 °C.

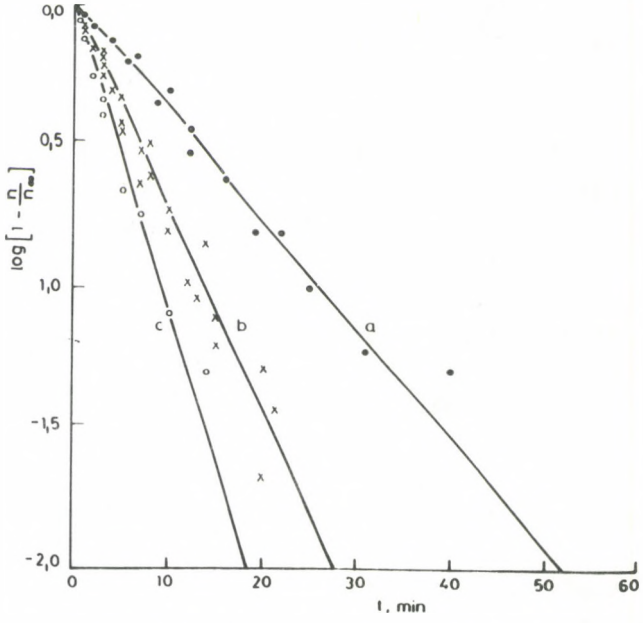

Fig. 2. Variation of log $1 - n/n_\infty$ as a function of time, based on the data of Fig.1. a 0 °C, b 20 °C, c 40 °C.

3. Discussion

The data of Figure 1 confirm that an equilibrium state develops between the amount of sol adhered and left in the solution in the interaction of sols and coarse disperse systems. The quantity of sol which reaches the surface of adsorbent in unit time can be given by Fick's Ist law:

$$\frac{dn}{dt} = \frac{DA}{\delta}(c_o - c_e) \qquad (1)$$

where dn/dt is the velocity of the heteroadagulation, D the diffusion constant of the sol particles, δ is the thickness of the Nernst adhesion layer, A is the surface area of the adsorbent, c_o is the concentration of the sol in the dispersion medium and c_e is that in the immediate vicinity of the adsorbent. Let n_o be the number of sol particles in the solution, at time $t = 0$ and n the number of particles adhered up to some time t. Then:

$$c_o = \frac{n_o - n}{V} \qquad c_e = \alpha n$$

where V is the volume of the sol solution, α is a proportionality factor. Substituting the values for c_o and c_e into equation (1) and taking into consideration that at equilibrium $dn/dt = 0$ and $n_o/n_\infty = 1 + \alpha V$, then the solution of the equation (1) for $n = 0$, when $t = 0$ is

$$\ln\left(1 - \frac{n}{n_\infty}\right) = -\frac{DA}{\delta V}\,\frac{n_o}{n_\infty}\,t \qquad (2)$$

Equation (2) is suitable for the evaluation of our experimental results, for if the log $(1 - n/n_\infty)$ values corresponding to the data in Fig.1 are plotted as functions of time, straight lines are obtained (Fig.2) and the rate constants of the heteroadagulation can be determined from the slopes of these lines. The rate constant

$$k = \frac{DA}{\delta V}$$

for the heteroadagulation of gold sol on lead chromate,

determined from the data of Fig. 2, is:

$$k_0\ ^oC = 1.6 \times 10^{-3}\ sec^{-1};\quad k_{20}\ ^oC = 2.7 \times 10^{-3}\ sec^{-1}$$

$$k_{40}\ ^oC = 4.1 \times 10^{-3}\ sec^{-1}$$

These data agree comparatively well with the values calculated from equation (2). The calculations require the knowledge of the diffusion constant. The diffusion measurements were carried out with a diffusion meter adapted to an ultracentrifuge (Phywe U-77). The diffusion constant of the sol particles was determined from the rate of shift of the inflection point of the Gaussian curves characteristic for the concentration distribution at various times. The following value was found:

$$D = 2.1 \times 10^{-7}\ cm^2\ sec^{-1}$$

The size of the surface of 0.05 g lead chromate, determined by a radioactive tracer method, is 220 cm^2. The following value was accepted for the thickness of the Nernst adhesion layer: $\delta = 1.0 \times 10^{-3}$ cm. If these data are substituted into equation (2), then the rate constant for the heteroadagulation is obtained:

$$k_{20}\ ^oC = 2.3 \times 10^{-3}\ sec^{-1}$$

This confirms that the rate of heteroadagulation in the system examined is determined by the rate of diffusion of the sol particles. For the determination of the activation energy of heteroadagulation, the rates of heteroadagulation were investigated at 0, 20 and 40 °C. The value of the activation energy (E_a = 3.4 kcal) was determined from the temperature dependence of the rate constant on the basis of the Arrhenius equation.

The time profile of the heteroadagulation of sols was investigated at various concentrations of the electrolyte. It was found that the rate constant, the maximum amount adhered and the activation energy of the heteroadagulation depend on the concentration of the electrolyte. For example table 1 and Figure 3 show some kinetic factors at different electrolyte concentrations.

Table 1. Variations of the rate constant, the maximum amount adhered for the heteroadagulation of lead chromate sol with the concentration of $La(NO_3)_3$

$La(NO_3)_3$ concentration $cx10^{-6}$ M	Rate constant $kx10^{4}$ sec^{-1}	Maximum adhered relative amount n_∞/n_o
0	15.0	0.97
8	3.3	0.85
12	1.8	0.81
16	1.2	0.50
32	0.8	0.25

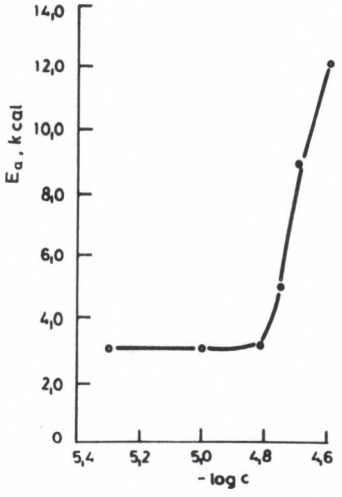

Fig. 3. Activation energy of the heteroadagulation of potassium hexacyanocobalt ferrate sol as a function of the concentration of $K_4[Fe(CN)_6]$

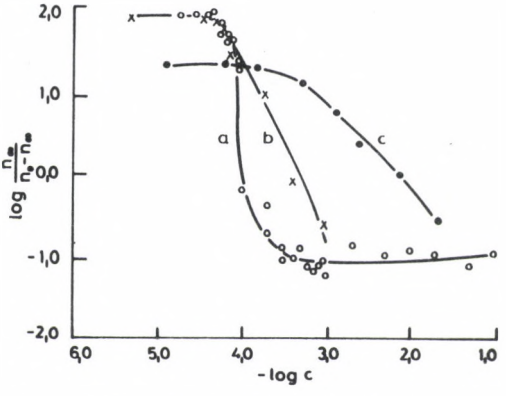

Fig. 4. Variation of the equilibrium distribution coefficient for the heteroadagulation of gold sol as a function of the gelatin concentration.
(a) barium sulphate, (b) aluminium oxide, (c) hydrogen bentonite

The time profile of the heteroadagulation of gold sol was investigated at various concentrations of gelatine. It was found that the rate constant and activation energy of heteroadagulation depend on the concentration of the protective colloid. Corresponding values are contained in Table 2.

Table 2. Variations of the rate constant and the activation energy for the heteroadagulation of gold sol with the concentration of the gelatine

Gelatine concentration %	Temperature °C	Rate constant $kx10^3$ sec^{-1}	Activation energy E_a kcal
0	20	2.21	5.1
	40	4.10	
$2.0x10^{-5}$	0	2.52	3.5
	20	4.03	
	40	5.72	
$4.0x10^{-5}$	0	2.81	3.4
	20	4.12	
	40	5.53	
$8.0x10^{-5}$	0	0.64	4.0
	20	1.06	
	40	1.60	
$20.0x10^{-5}$	0	0.045	7.1
	20	0.11	
	40	0.24	

Figure 4 shows the equilibrium distribution coefficient as a function of the concentration of gelatine. In these measurements stirring was always continued for 60 min, before the adsorbent was separated from the sol solution by centrifugation.

References

1 M. Smoluchowski, Physik. Z. 17, 557 (1916).

2 M. Smoluchowski, Z. physik. Chem. 92, 129 (1918).

3 B. V. Derjaguin, Discuss. Faraday Soc. 18, 85 (1954).

4 A. Buzágh and E.Kneppo, Kolloid-Z. 82, 150 (1938).

5 A.Buzágh and K. Dux, Kolloid-Z. 83, 279 (1938).

6 A. Buzágh, Kolloid-Z. 125, 14 (1952).

7 M. Hull and J. A. Kitchener, Trans. Faraday Soc. 65, 3093 (1969).

8 A. Buzágh, Colloid Practice (in Hungarian). Tankönyvkiadó, Budapest, 1962, p. 275.

9 L. D. Skrilev and S.G. Mokrusin, Kolloid Zh (SSSR) 22, 3 (1960).

MECHANISM BY WHICH DISPERSANT ADDITIVES STABILISE CARBON DISPERSIONS IN NON-POLAR MEDIA

R.J.R. Cairns and E.L. Neustadter

The British Petroleum Company Limited, BP Research Centre, Chertsey Road, Sunbury-on-Thames, Middlesex, England.

A. INTRODUCTION

The mode of action of detergent/dispersant additives in lubricating oils is not fully understood. It has been suggested (1) that these additives function by a micellar solubilisation mechanism. Whilst this mechanism may hold for the removal of polar species, carbon particles could not be stabilised in this way. Furthermore, the existence of micelles in lubricating oils has been disputed (2).

We have carried out model experiments using two different carbons (Table 1) and two quite different dispersant polymers (Fig 1) in heptane to attempt to elucidate the mechanism. One of the polymers (BP45) is a poly(meth-acrylic ester/amide) and the other (PV30 TEPA) is a polyisobutenyl succinimide.

B. EXPERIMENTAL

Dispersion of the carbons was effected ultrasonically. Adsorption was measured using a gravimetric technique to follow concentration changes in solution. Twenty hours in an end-over-end shaker were allowed for equilibrium attainment.

Microelectrophoresis, using a rectangular cell as described by Parfitt (3), was used to measure the zeta potential of the dispersed particles.

The turbidimetric method (4) was used to find theta solvent compositions(12) using ethanol (azeo dried) as non-solvent. In a theta solvent, a polymer shows pseudo-ideal behaviour. The critical flocculation volume(cfv) of ethanol was taken to be the minimum concentration required to cause flocculation of a heptane dispersion. This was assessed visually six

hours after mixing.

C. RESULTS

Electrophoretic mobilities and the corresponding zeta potential are given in Table 2. The zeta potential, ζ was calculated from the equation:-

$$\zeta = 6\pi\eta\mu\epsilon$$

in which η is the viscosity of the system, μ is the mobility of the particle (its velocity under unit potential gradient), ϵ is the dielectric constant. With appropriate values for η and ϵ, the equation becomes:-

$\zeta = 196\mu$ for 85 per cent heptane/15 per cent ethanol, and

$\zeta = 361\mu$ for heptane, with ζ in millivolts and μ in microns per second per volt per centimetre.

Theta solvent compositions are given in Table 3 and critical flocculation volumes in Table 4.

Adsorption of BP45 on to Kosmos BB from heptane at ambient temperature gave a high affinity isotherm with a plateau level of 55 ± 5 mgm gm^{-1}.

Deflocculation was effected by addition of heptane to a system flocculated by ethanol addition.

A poly(methacrylic ester), similar to BP45 but containing no basic nitrogen groups, was found not to adsorb on Kosmos BB and to confer no stability on the system.

Water was not excluded from the system but the materials used had a constant water content. In some experiments the water content of the ethanol was deliberately increased to 0.6 per cent. This reduced both the percentage of ethanol required in a theta solvent and the cfv so that it did not alter our conclusions.

D. DISCUSSION

The results obtained with the systems stabilised by BP45 are taken to mean that this additive acts as a steric stabiliser. It can be seen from Table 2 that charge stabilisation plays some part in Fiat Sludge dispersions stabilised by PV30-TEPA. The magnitude of the charge contribution is shown in Figure 3.

Napper and co-workers (5 - 9) have reported a marked similarity between theta conditions and the conditions required to effect flocculation of a sterically stabilised dispersion. Recently, however, his group have

published discordant results (10).

In Table 4, the ratio of the cfv of ethanol to its concentration in the corresponding theta solvent is given. It can be seen that this ratio is significantly greater than unity for the BP45 systems.

We wish to propose that flocculation of a sterically stabilised system occurs under conditions which lead to phase separation of the stabilising polymer in free solution at the same concentration as that of the adsorbed polymer. This means that there will be a concentration dependence of cfv (cf turbidity plot, Figure 2) and that, in general, the flocculating conditions will not correspond to theta conditions.

In the case of a high surface density of adsorbed polymer, there will be apparent agreement between flocculation conditions and theta conditions because of the logarithmic relationship between precipitation volume of non-solvent and polymer volume fraction (Figure 2). Such high surface densities seem to be the rule in aqueous sterically stabilised systems. In non-aqueous systems, however, it is possible to confer stability with adsorbed polymer layers of quite low density, as the present work shows. If the stabilising polymer is specially anchored to the surface then low surface density, sterically stabilised dispersions can be made in aqueous systems (10). Knowing the particle radius (a) and amount of polymer adsorbed (w), the concentration of polymer in the adsorbed layer (ϕ) can be expressed as a function of adsorbed layer thickness (t) using the equation:-

$$\phi = \frac{w\,\rho_s}{\left[\left(\frac{a+t}{a}\right)^3 - 1\;\;\rho_p\right]}$$

; ρ_s, ρ_p are densities of particle and polymer respectively.

A graph of log ϕ versus t is given for BP45 (Figure 4). Making suitable assumptions, based on random coil considerations, a likely range of values of t can be calculated. This is shown in Figure 4. Finally, corresponding precipitation volumes can be derived from Figure 2. It can be seen that the observed cfv falls within the range of predicted values thus supporting our proposition.

In the case of dispersions stabilised by PV3O-TEPA, the polymer is strongly adsorbed via its basic headgroup as shown by micro flow calorimetry (13) and the polyisobutene (pib) tail wags in solution. The question arises, therefore, as to whether solutions of the complete polymer or of just the

pib tail should be used in assessing the relationship between cfv and "precipitation volumes". In view of this, turbidity plots were made for each solution. Agreement was found (Table 4) between the concentration of ethanol in theta solvent composition for pib and cfv of ethanol for Kosmos BB dispersions in which charge effects are absent. This may, of course, be fortuitous but, in this system the adsorbed layer is quite dense (>10 per cent) so that the result could have been expected. The increased amount of ethanol required to flocculate Fiat Sludge dispersions is explained on the basis of a 'steric attraction' (polymer chains in worse than theta solvents attract one another) being required to overcome the charge stabilisation in this system.

Examples of bridging flocculation in non-polar media are comparatively rare. It is worth recording, therefore, that at low concentration (2×10^{-3} gm dm^{-3}), BP45 was found to give enhanced flocculation of a Kosmos BB dispersion. This is interpreted as being due to adsorption of polymer on more than one particle (bridging flocculation) taking place more rapidly than the enveloping of a single particle in polymer (protection ie steric stabilisation).

E. REFERENCES

(1) Vipper, A.B. et al, Neftekhimiya, 8, 922 (1968).

(2) Forbes, E.S. and Neustadter, E.L., Tribology 5, 72 (1972).

(3) Parfitt, G.D., J Oil and Colour Chemists Association, 51, 137 (1968).

(4) Cornett, C.F. and Ballegooijen, H. van, Polymer, 7, 293 (1966).

(5) Napper, D.H., Trans Farad Soc, 64, 1701 (1968).

(6) Napper, D.H., J Coll Intf Sci, 32, 106 (1970).

(7) Napper, D.H., J Coll Intf Sci, 33, 384 (1970).

(8) Napper, D.H. and Netschey, A., J Coll Intf Sci, 37, 528 (1971).

(9) Evans, D.B., Davison, J.B. and Napper, D.H., J Polym Sci, B10, 449 (1972).

(10) Napper, D.H. et al, J Coll Intf Sci, 45, 557 (1973).

(11) McGown, D.N.L., Parfitt, G.D. and Willis, E., J Coll Sci, 20, 650 (1965).

(12) Flory, P.J., "Principles of Polymer Chemistry", p 576, Cornell University Press Ithaca, New York 1953.

(13) Forbes, E.S., Groszek, A.J. and Neustadter, E.L., J Coll Intf Sci, 33, 629 (1970).

F. ACKNOWLEDGEMENT

The authors gratefully acknowledge permission from The British Petroleum Company Limited to publish this paper.

TABLE 1

DATA ON SOLIDS USED

Carbon	Particle Dia (μm)	% Polar Area	Water Extract	Source
Kosmos BB	0.025	18	Acidic	Chance and Hunt Ltd
Fiat Sludge	0.075	99	Acidic	Extracted from engine oil

TABLE 2

ELECTROPHORESIS OF CARBON SUSPENSIONS

	Solid Phase			
	Kosmos BB		Fiat Sludge	
	Mobility[1]	Zeta Potential[2]	Mobility[1]	Zeta Potential[2]
n-Heptane	not observable	-	not observable	-
n-Heptane + PV 30-TEPA	0.14	-49	0.097	+35
n-Heptane + 15% ethanol + PV 30-TEPA	very slight movement	small and negative	0.13	+25
n-Heptane + 25% ethanol + PV 30-TEPA	-	-	0.18	+27
n-Heptane + BP45	not observable	-	not observable	-
n-Heptane + 15% ethanol + BP45	not observable	-	not observable	-
n-Heptane + 34% ethanol + BP45	-	-	not observable	-

[1] mobility in microns per second per volt per centimetre.

[2] zeta potential in millivolts.

TABLE 3

COMPOSITION OF THETA SOLVENTS COMPRISING HEPTANE AND ETHANOL

Polymer	Temp (°C)	Ethanol (% volume) (θ)
PV30 (pib)	21	20
PV30-TEPA	21	27
BP45	21	38

TABLE 4

CRITICAL FLOCCULATION VOLUMES (cfv) OF ETHANOL FOR CARBON DISPERSIONS IN HEPTANE

Polymer	Carbon Type	Temp (°C)	cfv (% ethanol)	cfv/θ
PV30-TEPA	Kosmos BB	21	20	1
	Fiat Sludge	21	27	1.35
BP45	Kosmos BB	21	43	1.13
	Fiat Sludge	21	43	1.13

BP45

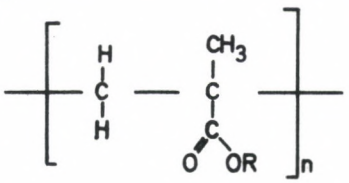

R = C_4 OR C_{8-12} ALKYL
OR $CH_2\ CH_2\ NH_2$

$M_W = 5 \times 10^5$; $M_W/M_N = 3$

N CONTENT ca 1%wt

PV30-TEPA

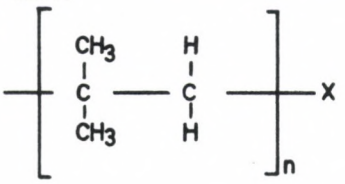

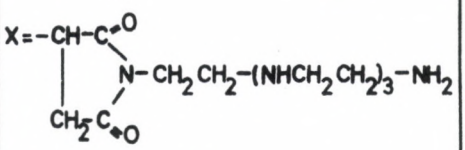

M_W OF pib = 2350

M_W/M_N = 1·5

FIG 1

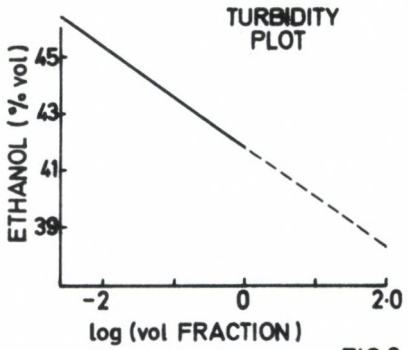

FIG 2

$V_R = \psi_0^2 \varepsilon a^2/(H_0+2a)$ (11)

a = PARTICLE RADIUS

ψ_0 = SURFACE POTENTIAL

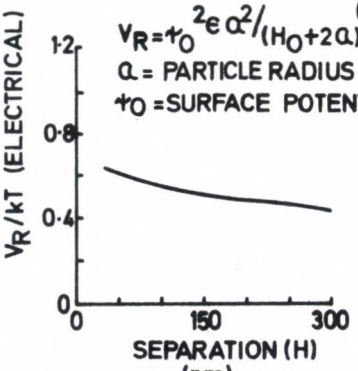

FIG 3

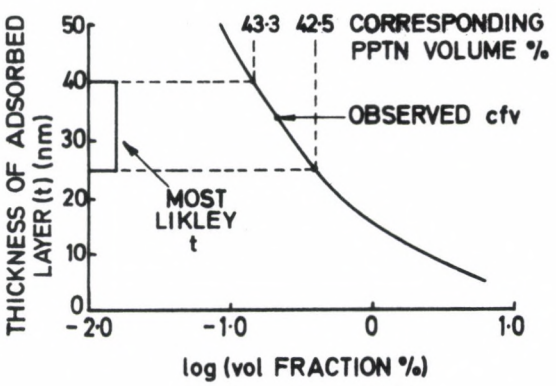

FIG 4

THE ROLE OF DEMULSIFIERS IN WATER/CRUDE OIL EMULSIONS

E.L. Neustadter, K.P. Whittingham and D.M. Grist

The British Petroleum Company Limited, BP Research Centre,
Chertsey Road, Sunbury-on-Thames, Middlesex, England.

Water-in-crude oil emulsions occur at many stages in the processing of crude oil. The breaking of these emulsions, frequently by the addition of chemical demulsifiers, is an essential step. In the desalting operation, for example, wash water is deliberately added to the crude oil stream, and the factors affecting the stability of the resulting emulsions and the role played by the demulsifier in destabilising them are therefore of paramount importance.

Stability in such cases, although dynamic in part due to the high viscosity of the thinning oil film, has often been attributed to adsorption phenomena of natural surfactants in crude oil (1) and the properties of the resulting interfacial film (eg its viscosity and elasticity) (2, 3).

Although little information exists for the complex crude oil systems, recent work (4) has suggested that the resistance to coalescence of the water drops in the final stage of breaking is associated with the structural-mechanical properties of the interfacial layer of the natural emulsifiers surrounding the drops. The addition of a demulsifier is thought to cause a disintegration of this layer at the interface. Further information revealed by our work supports this conclusion.

Several properties of the oil-water interface were measured. Iranian Heavy crude oil (difficult to desalt and with consequent stable emulsions), Kuwait and Nigerian Light crude oils (more easily desalted and with less stable emulsions) were chosen for study. Two commercially available demulsifiers, designated here as A and B, were used throughout. Refinery and laboratory scale experience had shown that the former performed successfully as a destabilising demulsifier with these crude oils whilst

the latter was noticeably less successful.

A. INTERFACIAL TENSION LOWERING

Measurements were made using a du Noüy tensiometer. A 40 mm perimeter PTFE-coated ring was lowered through the interface following the method of Krunitsky and Garrett (5) and the Zuidema and Waters correction equation (6) was applied. It is generally recognised that the importance of the measurement resides in the adsorption processes that accompany such changes. However, previous work had indicated that a rapid initial fall in interfacial tension for a crude oil-water system assists in emulsion stability (2). Surveys of the effects of crude type, salt and pH variation of the aqueous phase and of the demulsifier were carried out. Some of these results are shown in Table 1. They indicate that the measurement gives little guide to the understanding of the stability of the emulsion or of the role of a demulsifier in destabilising them.

TABLE 1

INTERFACIAL TENSION MEASUREMENTS

Crude type	Aqueous phase/pH	Demulsifier/ Level	γ_i (mN m^{-1})		
			3 min	30 min	Equilibrium
Iranian Heavy	Distilled/5.9	-	27.8	25.8	23.5
"	Distilled/8.4	-	25.9	25.2	23.9
"	5% w/v NaCl/5.9	-	27.3	25.9	23.3
"	5% w/v NaCl/8.4	-	27.3	25.7	23.3
Kuwait	Distilled/5.9	-	29.1	28.2	25.3
"	Distilled/5.9	A/30 ppm	30.0	23.5	15.6
"	Distilled/8.4	A/30 ppm	12.2	4.7	5.4
"	Distilled/5.9	B/30 ppm	29.1	25.1	22.0
"	Distilled/8.4	B/30 ppm	28.5	25.9	23.4

B. INTERFACIAL SHEAR VISCOSITY - η_i

Oil-water interfacial shear viscosities were measured as described previously (2). A stainless steel biconical bob was used to avoid slip of this surface with the interface (7). High interfacial viscosities present

a strictly mechanical barrier to coalescence and even moderate values will hinder the displacement of adsorbed molecules required for coalescence. The results, given in Table 2, show no rapid rise with time in η_i for either crude oil. The presence of either demulsifier gave a reduced value with no significant difference between them. Thus the role of a demulsifier in reducing η_i would appear to be subsidiary and η_i for the crude oil-water systems gives little guide as to their differing stabilities.

TABLE 2

INTERFACIAL SHEAR VISCOSITIES

Crude type	Aqueous phase/pH	Demulsifier/ Level	η_i (mNs m^{-1})		
			10 min	1 hour	4 hours
Iranian Heavy	Distilled/5.9	-	0.13	0.28	0.78
"	5% w/v NaCl/8.4	-	0.16	0.28	0.74
Kuwait	Distilled/5.9	-	0.12	0.31	2.0
Iranian Heavy	Distilled/5.9	A/5 ppm	-	0.10	-
"	Distilled/5.9	A/30 ppm	-	0.09	-
"	Distilled/5.9	B/5 ppm	-	0.15	-
"	Distilled/5.9	B/30 ppm	-	0.12	-

C. INTERFACIAL FILM PROPERTIES

An oil-water interfacial Langmuir trough of the type described by Brookes et al (8) was used. The relative film pressure of the crude oil-water interface was obtained during its compression and expansion, using a Wilhelmy platinum plate made hydrophobic with dichlorodimethyl silane (9). A microforce balance and pen recorder were used.

The method of Kimbler et al (10) was used to identify the phase state (and elasticity) of the various crude oil-water interfaces under compression. Figure 1, shows such results for Iranian Heavy, Nigerian Light and Kuwait crude oil-distilled water interfaces, aged for two hours.

Thus, solid film formation results with Iranian Heavy and accounts for the very stable water-in-oil emulsions that result with this crude oil. For Kuwait, only the well-defined condensation transition (X in Figure 1) to a condensed liquid film occurs. When held under compression the film

pressure falls slowly showing that the interfacially active material is being forced back out into bulk phase (10). This weaker film is consistent with the lower stability of its water-in-oil emulsions. For Nigerian Light crude oil only a liquid expanded film results, with no tendency towards strong film formation. This would explain why such crude oil emulsions were found to be particularly unstable.

Ageing effects of such interfaces are well-known (10, 1). The effect of interface age on the film properties of the Iranian Heavy-distilled water system are shown in Figure 2. The trend is towards a less compressible, more rigid, interfacial film.

The effect of 5 per cent weight/volume sodium chloride in the aqueous phase was investigated with Iranian Heavy and resulted in a weaker, less stable film. Similar behaviour was demonstrated by Kimbler et al (10). Laboratory experiments confirmed the much lower stability of Iranian Heavy/5 per cent weight/volume salt emulsions, compared with those formed with distilled water.

These two systems show similar interfacial tension and viscosity behaviour. Thus other than differences in the densities of the aqueous phase (slight increase in Stoke's law settling), change in aqueous phase bulk viscosity or charge effects of the interface (generally of less importance with water-in-oil emulsions (3)), the emulsion stability behaviour is only understandable, and indeed aptly described, by changes in the interfacial film properties.

The results show the importance of the film properties. One can therefore envisage the role of a demulsifier as breaking down, or displacing, these films. Figure 3, shows the results of the addition of the two demulsifiers to an aged Kuwait-distilled water interface. The demulsifier, A, displaces the strong interfacial film, resulting in an expanded liquid film that will present little barrier to coalescence. The other demulsifier, B, does not displace the film although a slightly weaker film results. The observed differences in emulsion destabilising effects are therefore explicable. Similar conclusions were reached when these demulsifiers were added to an Iranian Heavy crude oil.

Under certain circumstances, for example, in crude oil desalting, the demulsifier is conventionally added to the crude oil prior to forming the emulsion. Here, the effect of a demulsifier in inhibiting or modifying

the normal film forming tendencies will be important. Figure 4 shows the addition of A and B to Iranian Heavy crude oil prior to formation of the interface. Both substantially modify the film properties. In both cases, given sufficient time, the ageing trends were then towards the analogous 'displacement' experiment.

D. CONCLUSIONS

Previous workers (3, 4, 11) have indicated, for simpler systems than the crude oils dealt with here, that the strength compactness and elasticity of the interfacial film may be the most important factor favouring emulsion stability and that others are subsidiary insofar as they affect the properties of the film. This work strengthens that viewpoint.

The role of a successful demulsifier in displacing strong films and hence destabilising the emulsion also seems clearer. In some practical situations, for example the crude oil desalting operation cited, where the demulsifier is added prior to forming the emulsion the emphasis is mainly on their film modifying properties. The complexity of crude oils, which frequently still contain naturally present water (the so-called connate water) in emulsion form with associated strong interfacial films indicates that most of the poor film displacing demulsifier's problems are associated with this water. Thus, its ability only to modify film formation whilst not displacing strong films would therefore explain its poorer and more variable efficiency as a desalting chemical.

As further evidence of the weakening of the oil/water interfacial film by the demulsifier resulting in subsequent easier coalescence, some droplet coalescence measurements were made for oil and water drops at a plane water-oil interface. Although the technique is sensitive to vibration and measurements on drops at a plane interface are difficult to relate to real emulsion situations, the A demulsifier gave marked reductions in the droplet lifetime whilst the B one only made slight improvements.

E. REFERENCES

(1) Reisberg, J. and Doscher, T.M., Producers Monthly, 1956, 21, 43.

(2) Cairns, R.J.R., Grist, D.M. and Neustadter, E.L. Theory and Practice of Emulsion Technology Symposium, Brunel University, 16th-18th September, 1974.

(3) EMULSIONS, THEORY AND PRACTICE Becher, P., ACS Monograph No 162, Reinhold Publishing Corp, New York.

(4) Petrov, A.A. and Blatova, S.A., Khimiya i Tekhnologiya Topliv i Masel, 1974, 7, 32-35.

(5) Krynitsky, J.A. and Garrett, W.D., J Colloid and Interface Sci, 1963, 18, 893.

(6) Zuidema, H.H. and Waters, G.W., Ind Eng Chem Anal Ed, 1941, 13, 312.

(7) Cherkasov, R.I., Kurbanaev, U.Sh. and Babalyos, G.A., in Uses of Surfactants in the Petroleum Industry, edited by Rebinder, P.A., Consultants Bureau, New York, 1965, 224.

(8) Brookes, J.H. and Pethica, B.A., Trans Farad Soc, 1964, 60, 208.

(9) Cheesman, Ark Kemi Min Geol B, 1946, 22, 1.

(10) Kimbler, U.K., Reed, R.L. and Silberberg, I.H., Society of Petroleum Eng Journal, 1966, 153.

(11) King, A., Trans Farad Soc, 1941, 37, 168.

F. ACKNOWLEDGEMENT

The British Petroleum Company Limited is thanked for permission to publish this paper.

π - FILM PRESSURE ($mN.m^{-1}$)
A_D - RESIDUAL AREA RATIO
I - IRANIAN HEAVY
II - KUWAIT
III - NIGERIAN LIGHT

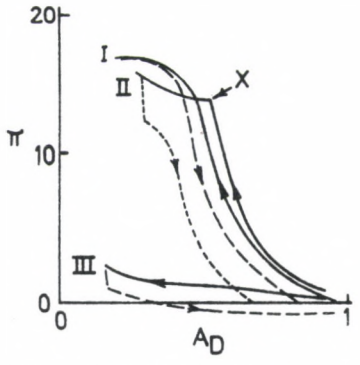

FIG 1 INTERFACIAL FILM PROPERTIES, FOR CRUDE OIL - DISTILLED WATER

I - INTERFACE AGE 40 MINUTES
II - INTERFACE AGE 2 HOURS
III - INTERFACE AGE 3¼ HOURS

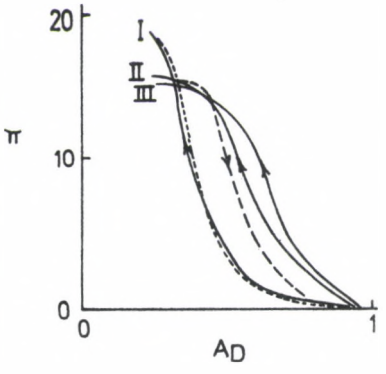

FIG 2 EFFECT OF FILM AGE, FOR IRANIAN HEAVY - DISTILLED WATER

I - KUWAIT - DISTILLED WATER
II - 30 ppm B ADDED
III - 100 ppm B ADDED
IV - 5 ppm A ADDED
V - 10 ppm A ADDED

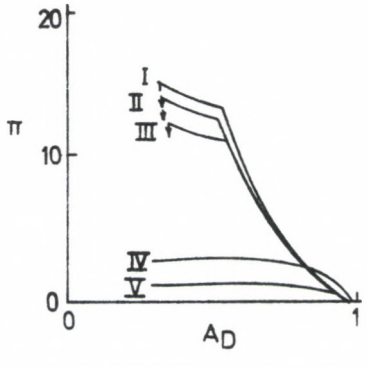

FIG 3 DISPLACING EFFECT OF DEMULSIFIERS : KUWAIT - DISTILLED WATER

I - IRANIAN HEAVY - DISTILLED WATER
II - 30 ppm B PREADDED (AFTER 20 MINUTES).
III - 5 ppm A PREADDED (AFTER 20 MINUTES).

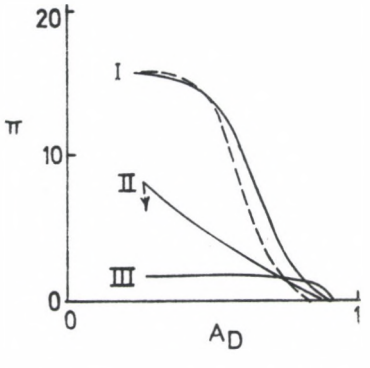

FIG 4 INHIBITING EFFECT OF DEMULSIFIERS: IRANIAN HEAVY - DISTILLED WATER

THE ROLE OF STRUCTURAL-MECHANICAL BARRIER IN WATER-IN-OIL EMULSIONS STABILITY

L.Mukhin, S.Shalyt, L.Ognyeva, E.Fedorova, I.Kazakova

The Gubkin Institute of Petrochemical and Gas Industry, Moscow, Leninski Prospekt 65, USSR

The large extent oil drilling activity is associated with drilling wells to great depths. This activity requires availability of highly stable drilling muds which are complex multicomponent and multiphase systems composed of hydrocarbon and aqueous liquids, various finely dispersed materials (clay, barite, calcite) as well as surface-active substances of different nature. Water-in-oil concentrated emulsions are widely used as drilling muds.

According to P.A.Rehbinder and his coworkers (I-6) high-stability concentrated emulsions result only when a structural-mechanical barrier appears at the interface in the form of a colloid-adsorption-diffusion film which prevents aggregation and coalescence of droplets. Resort to this stabilizing factor when preparing high-stability concentrated emulsions is inevitable due to its universal nature.

In view of the complex composition of drilling muds, the study of the mechanism of action of different components upon the drilling mud stability was carried out on a water-decane model system into which suitable surface-active and finely dispersed solid emulsifiers were added. As seen from our publications (5) 0.5% solutions of disubstituted aluminium soaps of synthetic fatty acids (SFA), C_{17}-C_{20}, in decane produce stable networks in the interfacial layer at the interface with water.

Stability characteristics of interfacial adsorption

layers were investigated by the technique suggested by P.A.Rehbinder and A.A.Trapeznikov (7,8), viz. by twisting a disk suspended on an elastic wire and placed at the interface.

The purpose of the work presented here was to study mechanical characteristics of mixed interfacial adsorption layers formed by aluminium disubstituted soap of SFA of various degree of hydrophobization at the decane-water interface in the presence of solid emulsifiers (barite, calcite) with an addition into water phase of low-molecular surface-active substance, sulfonol NP-I. Introduction into the system of low-molecular water-soluble surface-active substances such as sulfonol (which is used as a hydrophobic and peptising agent of the solid dispersion phase) considerably lowers the critical shearing strength of the layer composed of soap oil gel. We investigated stability characteristics of interfacial layers formed by 0.5% aluminium soap of SFA at water-decane interface with sulfonol added to the water phase. Sulfonol concentrations were: 0.05; 0.1; 0.2; 0.4 g/l. The results obtained are shown in Fig.1.

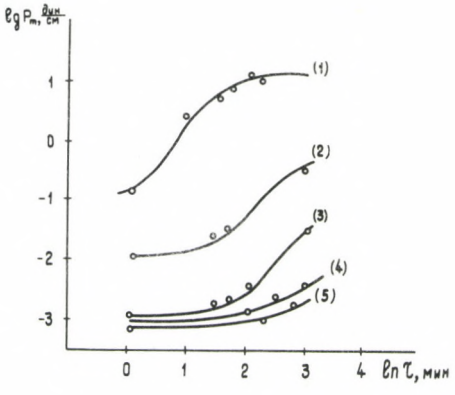

Fig.1. Effects of sulfonol NP-I additions on the critical shearing strength of the interface layer formed by 0.5% aluminium disubstituted soap of SFA at water-decane interface. 1.C_{NP-I}=0; 2.-0.05; 3.-0.1; 4.-0.2; 5.-0.4 g/l

The nature of curve (I) corresponds to high critical shearing strength of the interfacial layer (P_m 30 din/cm) formed by 0.5% aluminium disubstituted soap of SFA in the absence of low molecular surface- active substance. The high

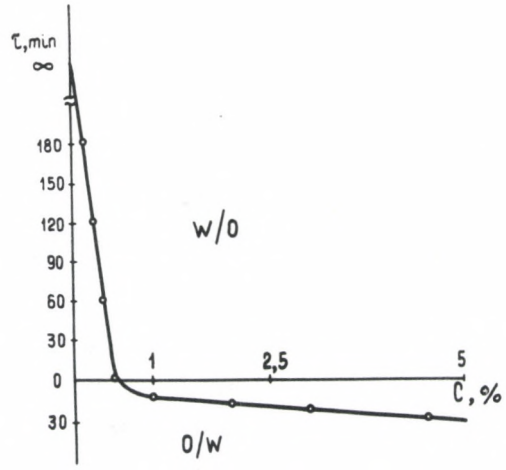

Fig.2. Dependence of water-decane emulsion stability (τ, min) stabilized by 1% aluminium disubstituted soap of SFA upon sulfonol content.

high as I% leads to inversion of the phases and a slight increase of oil-in-water emulsion stability. Water-in-oil emulsions that were not broken within 24 hr of centrifuging were referred to as infinitely stable. Maximum stability of direct water-in-oil emulsions was 30 min. These results were verified by us by the changes in electric stability of emulsions during their preparation (9).

As was said above, stable emulsions available commercially are multicomponent and contain large amounts of solid finely-dispersed phase, sulfonol being used as a hydrophobic and peptising agent. Sulfonol forms oriented adsorption layers on the surfaces of finely dispersed hydrophobic solid particles. Hydrophobization of solid particle surfaces prevents aggregation of particles and formation of networks within the decane volume. Besides, the solid dispersion phase converts into an active solid emulsifier "armouring" the reversible water-in-oil emulsions. This allows to emulsify large quantities of water. To achieve this, we utilized finely dispersed barium sulfate, calcium carbonate, and clay dispersed by means of a vibropulverizer. Specific surfaces of the samples determined by the BET method were 2.2; 2.0 and 29 sq. m. per g., respectively. It was previously shown (5) that adding small amounts of partially hydrophobic clay as a

value of the critical shearing strength can apparently be explained by chain-like arrangements of molecules with hydroxyl groups between them, followed by the formation of a stable network (8) due to Van-der-Vaals forces and hydrogen bonds. Such network are capable of thixotropic reversibility. Addition of sulfonol to the water phase and increase of its concentrations (curves 2,3,4,5) lead to progressively lower values of the interfacial layer critical shearing strength.

Reaction between low molecular surface-active substance-NP-I and aluminium soap of SFA results in the breaking of soap oil gel. It should be noted (curves 2 and 3) that sulfonol concentrations of up to 0.I g/l partially restore the interfacial layer critical shearing strength after 24 hr. With sulfonol concentrations (curve 5) approaching the critical concentration of mycel- formation (0.4 g/l), complete destruction of the interfacial layer network is observed, which is likely to be due to sulfonol adsorption at the interface resulting from its higher surface activity compared to that of aluminium soap of SFA.

Displacement of soap from the interphase and formation of an adsorption layer by sulfonol molecules, incapable of forming a network, results in a sharp lowering of the system critical shearing strength by more than three orders. Based on the data obtained in studying stability characteristics of interfacial layers, model water-decane emulsions stabilized by aluminium disubstituted soap of SFA in the presence of sulfonol were prepared. Emulsion phase ratios I:I; I% soap concentration; 0.I to 5 wt % sulfonol concentrations in water were used. Fig.2 shows the results obtained.

To evaluate emulsion stabilities, half-lives, $\tau_{\frac{1}{2}}$, of emulsions were determined. To accelerate the determinations, the emulsions were broken by a field of centrifugal forces of a centrifuge ($2 \cdot 10^3$ revolutions per minute). As seen from Fig.2 higher concentrations of sulfonol in water considerably decrease stabilities of water-in-oil emulsions stabilized by aluminium disubstituted soap. The 0.5% sulfonol concentration practically breaks the emulsion. Sulfonol concentration as

solid emulsifier (0.05%) to water-decane systems stabilized by a 0.5% solution of aluminium disubstituted soap of SFA makes the interfacial layer critical shearing strength more than twice as large. Moreover, clay additions brought about a sharp increase of the model emulsion dispersity and stability.

It was of interest to study the dependence of the interfacial layer stability characteristics upon the degree of barium sulfate and calcium sulfate hydrophobization with sulfonol. For this purpose we studied the dependence of the interfacial layer critical shearing strength formed at the interface of a 0.5% solid-emulsifier water suspension (solid phase particle size corresponded to $5 \cdot 10^{-6}$m) and of a 2% solution of aluminium disubstituted soap of SFA in decane upon solid particle hydrophobization. In this case solid powders were pretreated with various sulfonol concentrations and adsorption isotherms were obtained spectrophotometrically at λ=225nm. It has been shown by experiments that 0.5 g/l sulfonol concentration leads to the formation of a mono-adsorption layer. Further increase of sulfonol concentration results in polylayer adsorption.

Fig.3 illustrates dependence of interfacial layer stability characteristics upon the extent of hydrophobization.

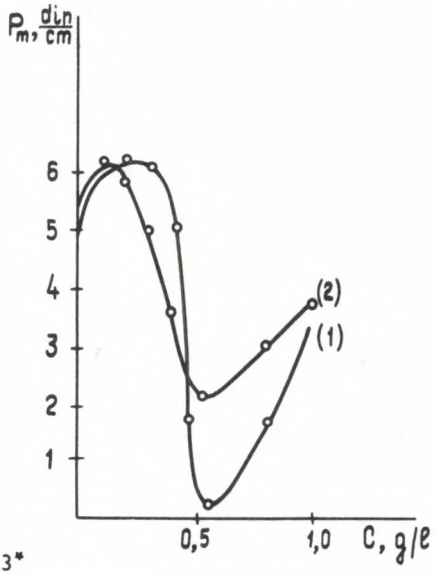

Fig.3. Dependence of the critical shearing strength of the interfacial layer formed by 0.2% aluminium disubstituted soap of SFA upon the extent of $CaCO_3$ and $BaSO_4$ hydrophobization at water-decane interphase. I.-$CaCO_3$; 2.-$BaSO_4$

Adding a solid sulfonol-treated emulsifier (concentrations not exceeding 0.3 g/l) gives two-to-three-times increase of the interfacial layer critical shearing strength. Further calcium carbonate hydrophobization results in lower critical strength values. At 0.5 g/l sulfonol concentration (on the adsorption isotherm, it corresponds to complete packing of the surface with monolayer) a sharp decrease (35 to 40 times) of the critical shearing strength compared to the maximum one is observed. Higher sulfonol concentrations, up to I g/l, produce another rise of the interfacial critical shearing strength; 0.5% barium sulfate-in-water suspension treated with a sulfonol solution containing not more than 0.3 g/l yields curves of a similar type.

Having in mind the results obtained, one may maintain that hydrophobization should not reach its critical value and should correspond to intermediate contact-angle values of selective wetting. Only due to such incomplete hydrophobization and consequently incomplete stabilization of solid dispersion-phase particles in hydrocarbon medium can these particles adhere to emulsified water droplets by their surface areas which remain hydrophobic. At the same time aggregating by these more hydrophobic areas with one another they will form coagulation space networks within interfacial layers. It is this effect that forms the structural-mechanical barrier preventing coalescence of water droplets in reversible emulsions (I0).

References.

I. P.A.Rehbinder, Izd. Akad. Nauk, Ser. Khim., No.5, 639, (I939)

2. P.A.Rehbinder, Coll.J., No.8, I57, (I957)

3. P.A.Rehbinder, J.Vsesoyusn. Khim. Ob. im. D.I.Mendeleyeva, V.XI, No.4, 362, (I962)

4. P.A.Rehbinder, A.B.Taubman, Coll.J., 30, 359, (I96I)

5. L.K.Mukhin, S.Y.Shalyt, L.G.Ognyeva, I.I.Kazakova, Papers presented at the IVth International Congress on Surface-Active Substances, I974, Berlin.

6. V.N.Ismaylova, P.A.Rehbinder, Structure formation in protein systems. Nauka, M. 1974
7. P.A.Rehbinder, Sborn. Nov. Metody Phys.- Chem. Issled. Poverkh. Yavl., Trudy Inst. Phys. Khim. AN USSR, I, 5, (1950)
8. A.A.Trapeznikov, V.A.Fedotova, Trudy III Vsesoyusn. konf. coll. khim., Izd. Akad. Nauk USSR, p.65 (1956)
9. A.G.Rosengaft, cand. thesis, 1974, Moscow.
10. L.K.Mukhin, S.Y.Shalyt, Papers presented at the VIth International Congress on Surface-Active Substances, 1972, Zürich.

Group II/3
Electrical phenomena

INDUCED DIPOLE MOMENTS OF COLLOID PARTICLES

S.S.Dukhin, V.N.Shilov, Yu.Ya.Yeremova

Institute of Colloid Chemistry and Water Pollution Control, Academy of Sciences of the Ukrainian SSR, 252142, Kiev, Vernadsky street 42, USSR

Induced dipole moment is an important electrophysical characteristic of disperse particle (macroion) which causes a variety of effects the significance of which for electrotechnology of disperse systems and investigation of electrycal structure of particle grows steadily. For a long period of time the idea of induced dipole moment has been associated only with processes occuring in particle volumes and adjacent medium. Although double layer (DL) polarization effect on induced dipole moment of particle has been subjected not only to detail theoretical analysis /1,2/ but acknowledged by various experimental techniques /3-6/ the determinations of electrosurface properties of particles (ζ -potential, specific surface conductivity $\varkappa^{\sigma}$) on the basis of induced dipole moments are not numerous yet /5,6/. The development of investigations in this direction is impeded by insufficient elaboration of quantitative theory permitting on the basis of measurement of induced moments to calculate the specific surface conductivity $\varkappa^{\sigma}$. The given paper is aimed at formulation of the problem of this theory in the more general possible form and discussion of the latest results in this sphere.

The idea of induced dipole moments d of disperse particles has first appeared in connection with development of the theory of electric conductivity and dielectric properties of disperse systems /7/. Induced dipole moment (side with constant one) is the basis of electrooptical phenomena

/4/, because the effect of electric field on anisometric particle gives rise to torgue moment proportional to dipole moment and, respectively, preferable orientation of particles with long axis parallel to field /8/. In spite of the fact that dipole is electroneutral system, in space-inhomogeneous electric field uncharged particle begins to move. The motion was called dielectrophoresis /9/ as dipole poles are under the influence of field of different magnitude.

After a long period of underestimation of the role of DL in formation of induced dipole moments the question has been rised by O'Konski /10/. For the first time the correct formulation of the problem of induced dipole moment as about manifestation of concentration polarization of diffuse part of DL was given by Overbeek. However, he regarded concentration polarization only as a phenomenon which makes it difficult to calculate electrokinetic potential ζ . Underestimation of induced dipole moment significance lies in the fact that having made huge work in calculation the reduction of electrophoresis velocity /11/ under the effect of DL polarization Overbeek did not seize the opportunity on considering electric conductivity /12/ in order to develop its theory on the basis of dipole moments.

A new appreciation of induced dipole moment as the most important electrophysical characteristic of colloid particles the measurement of which is specifically independent trend in DL investigation has been outlined at the XX Congress of IUPAC in the lectures of Dukhin /13/ and Stoilov /14/. Subsequently, Derjaguin and Dukhin /2/ have indicated the variety of effects caused by induced moment and suggested to undertake complex inves tigations including electrokinetic and induced dipole moment measurements in order to overcome difficulties connected with complexity of DL structure.

Induced moments cause dipole-dipole attraction forces and under certain conditions - coagulation and structure formation in electric field /15/. These effects are the basis of electrorheology /16/, they make sufficient contribution to the mechanism of electrophoretic coatings formation /17/,

and are widely uzed for the development of new methods of electrofiltration of dispersions /18/. The derivation of formulae for d is a first step in the development of quantitative theory of electrotechnology of disperse systems.

If potential φ at a great distance R from polarized particle has asymptoty

$$\varphi = \frac{d}{\varepsilon R^2}\cos\theta - E_0 R\cos\theta \qquad (1)$$

where ε is dielectric constant of disperse medium, θ - the angle with external field direction, then d is induced dipole moment. In the simpliest case when the field affects non-conducting particle in a non-conducting medium induced dipole moment appears owing to distribution of bonded polarization charges on the boundary of two mediums with different dielectric constants ε_1 and ε_2. The distribution of φ_1 potential outside the particle and φ_2 potential inside of it is described, in this case, by Laplace equations

$$div\,grad\,\varphi_1 = 0\,, \quad div\,grad\,\varphi_2 = 0 \qquad (2),(3)$$

with conditions that the normal component of dielectric-induction vector $\varepsilon\,grad\,\varphi$ and potential should not undergo change on passing throigh the interphase boundary

$$\varepsilon_1 grad_n\varphi_1 = \varepsilon_2 grad_n\varphi_2\,, \quad \varphi_1 = \varphi_2 \qquad (4),(5)$$

When the field affects the conducting particle in conducting medium the important role in formation of induced dipole moment is belonged to free charges which are redistributed when current passes through the boundary of two mediums with different conductivities K_1 and K_2 and dielectric constants ε_1 and ε_2. Let the external field E change versus time according to the law $E = E_0 exp(i\Omega t)$ where Ω is circular frequency, i - imaginary unit. Then according to Maxwell and Wagner /17/ the problem of determination of d for the system "conductor in conductor" will be equivalent to the problem for the system "dielectric in dielectric", if in the boundary condition (4) dielectric constant ε is replaced by complex dielectric constant $\varepsilon^* = \varepsilon - \frac{4\pi i}{\Omega}K$, then

$$\varepsilon_1^* grad_n\varphi_1 = \varepsilon_2^* grad_n\varphi_2 \qquad (6)$$

Owing to thermal motion, however, free charges are distributed not directly at the interface but are located in the layer with the thickness of the order of the reciprocal Debye length χ^{-1} and , what is important for henceforth, the equations (2,3) are not valid within the limits of the layer where space charge is different from zero. Therefore, in the conditions (5,6), strictly speaking, values of induction and potential must appear on the boundary of volume charge layer but not on external or internal sides of the interface. Hence, the analogy mentioned of cases "dielectric in dielectric" and "conductor in conductor" is unappropriate if at least one of the discribed below restrictions is not fullfilled: a) the Debye length χ^{-1} is much smaller than the linear dimension of each of conducting phases, b) the change of potential jump across the interface layer may be neglected in comparison with that within the limits of each phase as otherwise the condition (5) is not fulfilled, c) tangential flow carriers through the surface layer cross-section may be neglected as in the other case the condition (6) appears not to be valid.

Further development of Maxwell-Wagner's theory of induced dipole moments is connected with the refusal of one of the items a), b) or c).

In collaboration with I.N.Simonov /19/ we have calculated d for conducting spherical particles with non-conducting shell in conducting medium - a model of aqueous suspensions of biological cells. As distinct from the work of Pauly and Shwan who discussed this model on the basis of system of equations (2,3,6,5), our theory is not restricted by the rigid condition that χ^{-1} is less than the thickness of shell (membrane). It permits to determine more exactly the membrane thickness from dielectric measurements and obtain additional information on mobility of carriers inside the cell.

The condition (c) is not fullfilled when the surface of particle is charged and the excess of counterions is diffuse part of DL causes the appearance of surface conductivity $\varkappa^{\delta}$. To take into account the surface current instead of the condition (6) it should be written

$$\varepsilon_1^* \operatorname{grad}_n \varphi_1 - \varepsilon_2^* \operatorname{grad}_n \varphi_2 = \frac{4\pi i}{\Omega} \operatorname{div}_s I_s \qquad (7)$$

where $I_s = -\varkappa^s \operatorname{grad}_\theta \varphi_1$ is the surface current, $\operatorname{grad}_\theta \varphi_1$ - the tangential component of potential gradient, the symbol div_s corresponds to surface divergence. With such formulation the problem was solved by O'Konski /10/. The precise solution obtained in /10/ for spherical particle permits to take into account the contribution of surface conductivity as equivalent increasing of particle conductivity K_2 by the value of $\Delta K_2 = 2\varkappa^s / a$. a is the radius of a particle.

The formulation of the problem according to O'Konski on the effect of DL polarization on induced dipole moment is not quite general for the reason that with existing of a few types of carriers (for instance, anions and cations) one should require unchangeability of currents of each kind of ions separately but not only of the electric current as a whole. It leads to a conclusion about the appearance of a drop of electrolyte concentration beyond the DL. The appearing drop of electrolyte concentration along the surface of particle causes the potential jump change within the limits of double layer (concentration polarization of double layer) due to which the condition "b" is not fulfilled.

The problem of induced dipole moment of non-conducting spherical particle of a including the concentration polarization of DL lies in solution of equations of continuity of flows of anions and cations separately. Under the condition $\varkappa a \gg 1$ the problem has been brought /20/ to the solution of equations

$$\operatorname{div}\operatorname{grad}\varphi = 0 \,, \quad \operatorname{div}\operatorname{grad} C = \frac{1}{D}\frac{\partial C}{\partial t} \qquad (8),(9)$$

$$\operatorname{grad}\varphi\big|_\infty = -E_0 \exp(i\Omega t), \quad \operatorname{grad} C\big|_\infty = 0 \qquad (10),(11)$$

where C is electrolyte concentration beyond the double layer D is the coefficient of diffusion of ions. The boundary conditions express unchangeability of both flows of cations and anions at the surface.

$$-D \operatorname{grad}_n C \mp \frac{F}{RT} D C_0 \operatorname{grad}_n \varphi = -\operatorname{div}_s I_s^{\pm} \qquad (12)$$

here, C_0 is the electrolyte concentration far from a pafticle,

$I_s^{\pm}$ - the excess tangential flow of ions in diffused part of DL. On the condition of $\varkappa a \gg 1$ neglecting for the sake of simplicity the convected flows of ions (the more general case was discussed in /20/ for $I_s^{\pm}$ it might be written

$$I_s^{\pm} = -\frac{\Gamma_0^{\pm}}{C_0} \operatorname{grad}_\theta C \mp \frac{F}{RT} D \Gamma_0^{\pm} \operatorname{grad}_\theta \varphi \qquad (13)$$

where $\Gamma_0^{\pm} = \frac{2C_0}{\varkappa}\left(\exp(-F\Psi/RT) - 1\right)$ in the adsorption of cations and anions in diffuse part of DL, Ψ - is the Stern potential.

For spherocal particle the analytical solution of φ and C has been obtained.

On the basis of this solution it was shown /20/ that lowfrequency dielectric dispersion of suspensions is the manifestation of concentration polarization of DL.

The magnitude and direction of induced dipole moment for a spheroidal particle is readily expressed by two values $d_\parallel$ and $d_\perp$ - dipole moments at orientation of particle axis paralled or perpendicular to the field, respectively. When polarization of particles is described according to Maxwell-Wagner were obtained the exat expressions for $d_\parallel$ and $d_\perp$

$$d_\parallel = \frac{V}{4\pi}\varepsilon_1 \frac{\varepsilon_2^* - \varepsilon_1^*}{\varepsilon_1^* + (\varepsilon_2^* - \varepsilon_1^*)A_\parallel}, \quad d_\perp = \frac{\varepsilon_2^* - \varepsilon_1^*}{\varepsilon_1^* + (\varepsilon_2^* - \varepsilon_1^*)A_\perp}\cdot\frac{V}{4\pi}\varepsilon_1 \qquad (14),(15)$$

where $V = \frac{4}{3}\pi a b^2$, $A_\perp = \int_0^\infty \frac{a b^2 \, ds}{2(b^2+s)(a^2+s)^{1/2}}$, $A_\parallel = 1 - 2A_\perp$

a and b - long and short prticle axis, respectively. We have investigated the effect of surface conductivity and concentration polarization of DL on $d_\parallel$ and $d_\perp$ on the basis of Fourier method which in this case leads to infinite system of algebraic equations. The system obtained has been solved approximately /21/. For concentration polarization the result /21/ appears to be rather bulky that does not permit it to be involved here because of lacking of space. At frequences $\Omega \gg 2D/b^2$ when concentration polarization is absent and DL affects induced dipole moment only by the surface conductivity, it seems to be possible to reflect surface conductivity effect by formulae (14,15) by equivalent increasing of volume conductivity of particle

$$\Delta k_{2\parallel} = -B_\parallel \operatorname{ch}\omega_0 \frac{\varkappa a}{b}, \quad \Delta k_{2\perp} = -B_\perp \frac{\varkappa a}{b} \qquad (16),(17)$$

where

$$B_{\parallel} = -\frac{3}{2}\int_{-1}^{1}\frac{(1-x^2)\,dx}{\sqrt{ch^2\omega_0 - x^2}}\,, \qquad B_{\perp} = -\frac{3}{4}\int_{-1}^{1}\frac{(1-x^2)(ch2\omega_0 - x^2)\,dx}{(ch^2\omega_0 - x^2)^{3/2}}$$

where $th\omega_0 = b/a$. These expressions raise the accuracy of corresponding formulae of the paper /10/ in which they were derived less strictly. For spherical particle, when $ch\omega_0 \gg 1$ from (16,17) it appears that $\Delta K_{2\parallel} = \Delta K_{2\perp} = 2\varkappa_2^b/a$. For rather elongated particle, when $sh\omega_0 \ll 1$, from (16,17) it is derived that $\Delta K_{2\parallel} = 3\pi/4 \cdot \varkappa_2^b/a$ and $\Delta K_{2\perp} = 3\pi/8 \cdot \varkappa_2^b/a$ instead of $\Delta K_{2\parallel} = 2\varkappa_2^b/a$ and $\Delta K_{2\perp} = \pi/4 \cdot \varkappa_2^b/a$ obtained in /10/. It is not difficult to show that the torque moment which orients the long axis of the particle along the field is

$$M = (\gamma_{\parallel} - \gamma_{\perp}) E_0^2 \sin\theta_1 \cos\theta_1$$

where $\gamma_{\parallel} = d_{\parallel}/E_0$, $\gamma_{\perp} = d_{\perp}/E_0$, θ_1 – is the angle between field directions and long axes. When $\varkappa_2^b = 0$, from the simple analysis of expressions (14) and (15) at $\Omega \to 0$ it follows that the value of $\gamma_{\parallel} - \gamma_{\perp}$ will be positive at any value of K_2. Thus, the total torque moment alwys orients the lonf axes of the particle along the field. At $K_2 < K_1$ the sign of M is determined by the sign of $\gamma_{\perp}$, at $K_2 > K_1$ – by the sign $\gamma_{\parallel}$, at $K_1 = K_2$ the torque moment turns to zero.

For non-conducting particle with DL the equivalent volume conductivity is $\Delta K_{2\parallel}$ or $\Delta K_{2\perp}$ depending on orientation. In this case $M(\varkappa_2^b)$ will give minimum at $\varkappa_2^b = \varkappa_{2\,min}^b$ as well as $M(K_2)$ at $K_2 = K_1$. As $\Delta K_{2\parallel} \neq \Delta K_{2\perp}$, thus $M(\varkappa_{2\,min}^b)$ won't be zero, but will be a finite positive value.

Such kind of torque moment dependence on surface conductivity is confirmed in experiment /5/.

Literature

1. S.S.Dukhin, V.N.Shilov, Kolloin.Zh., 31, 706 (1969); S.S. Dukhin, Surface and Colloid Science, vol.3, Ed.Wiley, New-York, 1972.
2. B.V.Derjaguin, S.S.Dukhin, Surface and Colloid Science, vol.7, Egon Matijevic, Ed.Wiley Interscience, New-York, 1974.

3. T.L.Chelidze, V.N.Shilov, Kolloidn.Zh.,35,105 (1973).
4. S.P.Stoilov, Advan.Colloid Interface Sci.,3,45 (1973).
5. F.D.Ovcharenko et a Dokl. AN SSSR, 216,2,105 (1973).
6. T.L.Ghelidze, V.N.Shilov, A.A.Baran, Kolloidn.Zh.,34,791 (1972).
7. J.C.Maxwell, A Treatise on Electricity and Magnetism, Vol 2, Clarendon Press, Oxford, 1892.
8. V.N.Shilov et al, Kolloidn.Zh., 36,97 (1974).
9. H.A.Pohl, J.Appl.Phys., 22,869 (1951).
10. C.T.O'Konski, J.Phys.Chem., 64,605 (1960).
11. Th.G.Overbeek, Koll.Beihefte, 54,287 (1943).
12. H.R.Kroyt, ed.Colloid Science, Vol 1, Elsevier, 1962, Chapter 5.
13. S.S.Dukhin, XX-th International Congress IUPAC,Moscow (1965), A 72; Research in Surface Forces, vol 3, New-York, Consultant Bureau, 1971.
14. S.P.Stoilov, ibid., A 68.
15. V.R.Estrela, S.S.Dukhin, V.N.Shilov, Kolloidn.Zh.,36,(1974)
16. Z.P.Shulman et al, Electroreologichesky effect, Nauka i Tekhnika, Minsk, 1972.
17. Yu.F.Deinega, Z,R.Ulberg, V.R.Estrela-Ljopis, Electrophoretigheskoje osazhdeniye metallopolimerov,Naukova Dumka, Kiev, 1975.
18. S.S,Dukhin,O.D.Kurilenko,V.D.Grebenyjuk,Kolloidn.Zh.,37, 5 (1975).
19. V.N.Shilov, S.S.Dukhin, I.N.Simonov, Y-th International Biophisical Congress, Moscow, Vol.4, 293 (1972).
20. V.N.Shilov, S.S.Dukhin, Kolloidn.Zh.,32,114 (1970).
21. Yu.Ya.Yeremova, V.N.Shilov, Kolloidn.Zh. 37, 3, 5 (1975)

ELECTROKINETIC STUDIES OF SOME MODEL SYSTEMS: QUARTZ - ELECTROLYTE SOLUTIONS

M.P.Sidorova, M.Fazylova, D.A.Fridrikhsberg

Leningrad State University, Chemical Faculty,
Leningrad 199004, Sredni 41, USSR

The experimental study of electrokinetic properties on model systems offers the best opportunities to prove the classical theories under the simplest conditions ensuring the elimination of some complicating effects: non-uniformity of porous space, overlapping of diffuse layers, influence of curvature, etc./1,2/. These conditions are met by uniform straight capillaries and, to a great extent, in systems formed by strictly parallel packing of uniform fibers.

We measured the streaming potential (E), the streaming current ($\mathcal{J}_s$) and conductance ($\varkappa$) in such a diaphragm constructed from non-swelling fibers of quartz with radius r=50 μm. The volume porosity determined from water content as well as by the conductance method was 0,195. The mean effective pore radius of the diaphragm 6,7 cm in lenght and 0,65 cm^2 in cross-section was 19 μm. Filtration and porosity data corresponded to compact packing with θ =90° between fiber axes /3/. Such a system is equal to a set of parallel oriented capillaries of different cross-sections and the values of the electrokinetic ζ-potential, calculated from the Helmholtz-Smoluchowski formula are identical with the true ones /4/. Electrometer EDE-05M (resistance $10^{15}\Omega$) and low-resistance galvanometer were used to measure E and $\mathcal{J}_s$ correspondingly; measuring $Ag/AgCl$ disc electrodes were fitted to the ends of the diaphragm. Alternative current (a.c.) measurements of resistance ($\widetilde{R}$) were made with conductivity bridge E8-2, direct current re-

sistance ($\bar{R}$) was obtained either from E/J_s ratio, or ($\bar{\bar{R}}$) from the external voltage drop at a given value of current (10^{-7}– 10^{-9} A). The cell constant value was measured in HCl solution at the isoelectric point (pH=2.0) and in 0,1 M KCl, both sets giving C_d =51,5±0,2 cm^{-1}.

Values of ζ and $\varkappa$ were measured in solutions of HCl, LiCl, KCl and CsCl (prepared on bidistillate) over a range of concentrations (C) 10^{-1}– 10^{-5}M. The diaphragms were pretreated by 3 M HNO_3, washed and brought into equilibrium with the solutions under investigation.

The values of ζ were calculated from

$$\zeta_E = \frac{4\pi\eta}{\varepsilon} \varkappa \frac{\bar{E}}{P} , \qquad (1)$$

where $\varkappa$ - conductivity in pores - is connected with the specific conductivity in bulk, $\varkappa_V$, by means of effectivity coefficient $\alpha = \varkappa/\varkappa_V$. By analogy with $\varkappa_V$ for the measurements of $\varkappa$ in pores a.c. is usually employed to eliminate electrode polarization. But in this case it is not so evident due to possible frequence variations of $\varkappa$ (dispersion) /2/. In electrokinetic phenomena the direct field either appeares or is applied and so in equation (1) $\varkappa$ is to be $\bar{\varkappa}$. Introduction of $\tilde{\varkappa}$ is possible only in the absence of dispersion. For this reason the method of streaming current seems more preferable, because the equation

$$\zeta_J = \frac{4\pi\eta}{\varepsilon} C_d \frac{J_s}{P} \qquad (2)$$

does not include $\varkappa$.

The data in coordinates $\zeta - lgC$ are presented in Figs. 1 and 2. The values ζ for metallic univalent cations do not differ sufficiently from each other which agrees with the notions /5/ of non-specific adsorption of these ions on SiO_2 in neutral region. Comparing Figs. 1 and 2 we see, that ζ_E and ζ_J values are identical in the range of $C \geq 10^{-3}$M, whereas in more dilute solutions ζ_E in all the cases are greater than ζ_J. From (1),(2) it follows (since $\tilde{C}_d = \bar{C}_d$) that

$$\zeta_E/\zeta_J = \tilde{\varkappa}/\bar{\varkappa} \qquad (3)$$

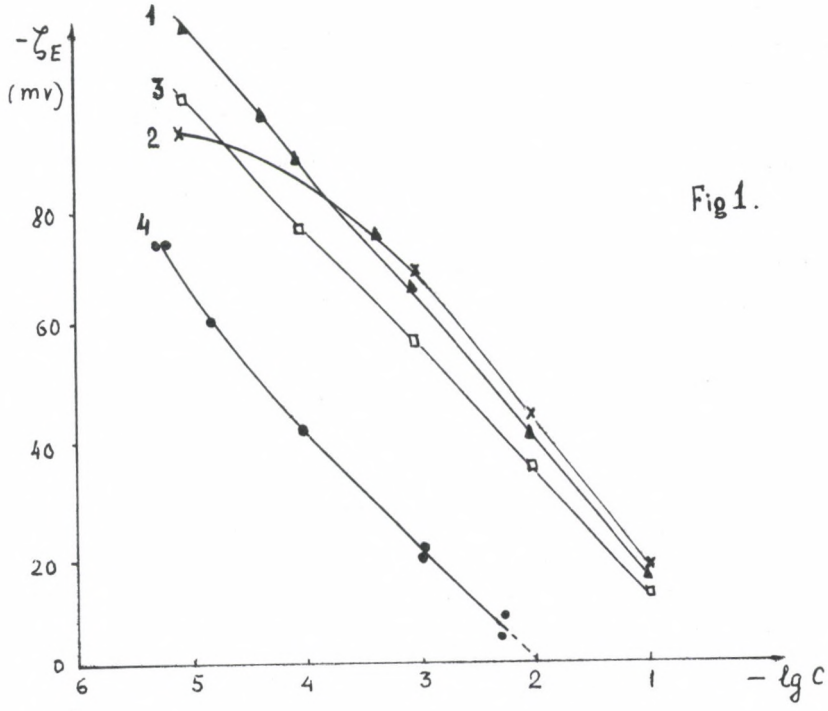

Fig 1.

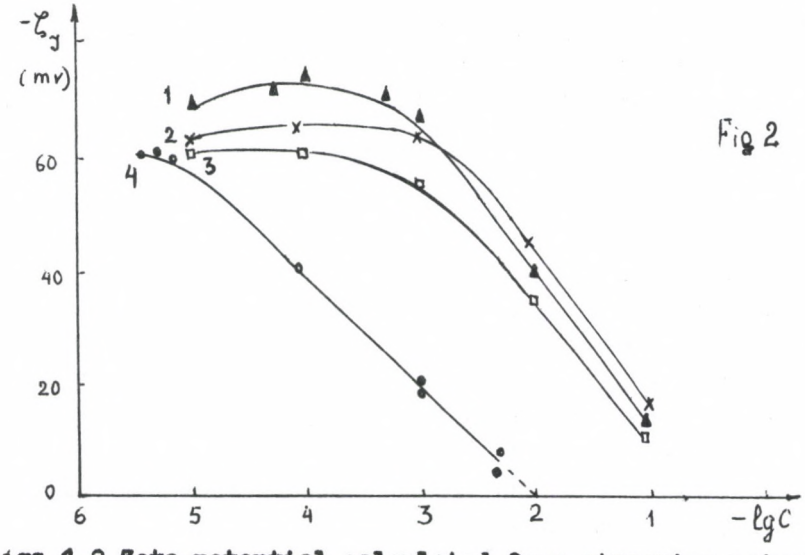

Fig 2

Figs.1,2.Zeta-potential,calculated from streaming potential (Fig.1- ζ_E) and streaming current (Fig.2-ζ_y) as a function of electrolyte concentration:1 - KCl,2- LiCl,3- CsCl,4- HCl

It is apparent that the discrepancy of ζ_E and ζ_γ depend on the difference between $\bar{\varkappa}$ and $\tilde{\varkappa}$ *).In fact,the experimental study of frequence dependence of $\tilde{\varkappa}$ has shown that $\tilde{\varkappa}$ increased about twice from 200 to 20000 cpc,the usual measurements by 1000 cpc being quite arbitrary.The checking of $\bar{\varkappa}$ values obtained from E/J_S ratio was fulfilled in experiments with the external field.These data ($\bar{\bar{\varkappa}}$) coincide practically with $\bar{\varkappa}$ (Table 1).To estimate the influence of electrode polarization we have measured $\bar{R}$ in the loose cell (without fibers) filled with solution.It was found that the difference between $\bar{R}$ and $\tilde{R}$ does not exceed 2 p.c. and lies in the limits of errors.

From Table 1 it is seen,that $\tilde{\varkappa}$ and $\bar{\varkappa}$ values differ from each other more distinctly with the dilution of solutions.It seems,that such a discrepancy is caused by the polarization effects in diaphragm.

From these data the values of $\varkappa_s = \varkappa - \varkappa_v$ and the specific surface conductance (for model with $\theta = 90°$)

$$K = \frac{4-\pi}{2\pi} \cdot \varkappa_s r \qquad (4)$$

were calculated.These values given in Table 2,were compared with those,calculated from Bikerman's equation (for ζ) including the electroosmotic component

$$K = \frac{1}{F}\sqrt{\frac{\varepsilon RTc}{2\pi}}\left[\left(e^{-\frac{zF\zeta}{2RT}}-1\right)\left(\lambda_+ + \frac{\varepsilon RT}{2\pi\eta}\right)+\left(e^{\frac{zF\zeta}{2RT}}-1\right)\left(\lambda_- + \frac{\varepsilon RT}{2\pi\eta}\right)\right], \qquad (5)$$

where λ_i - are ionic mobilities and F,R and T have their common sense.From Table 2 it is appearent that $\bar{K}$ values obtained from d.c.measurements are of the same order of magnitude as those calculated from equation (5) but are sufficiently smaller than $\tilde{K}$ values recieved from $\tilde{\varkappa}$.

So the use of a.c. conductivity of pore solution ($\tilde{\varkappa}$), generally employed in Helmholtz-Smoluchowski equation seems to be a matter of discussion.

---

*)Equation (1) gives ζ_E by $\varkappa = \tilde{\varkappa}$ and ζ_γ by $\varkappa = \bar{\varkappa}$

Table 1

Solution	Concentration M	$\varkappa_v \cdot 10^6$	$\bar{\varkappa} \cdot 10^6$	$\bar{\bar{\varkappa}} \cdot 10^6$	$\tilde{\varkappa} \cdot 10^6$	$\bar{\alpha}$	$\tilde{\alpha}$
		ohm^{-1}cm^{-1}					
LiCl	10^{-3}	127	127,5	—	130	1,00	1,02
	10^{-4}	13,7	13,9	14,3	15,7	1,02	1,15
	10^{-5}	2,50	2,90	3,0	4,27	1,16	1,71
KCl	10^{-3}	138	144	—	142	1,03	1,04
	10^{-4}	10,8	11,2	—	12,8	1,04	1,19
	10^{-5}	2,07	2,32	3,12	3,64	1,12	1,75
CsCl	10^{-3}	138	125	—	144	0,91	1,04
	10^{-4}	15,4	15,9	15,9	19,9	1,03	1,29
	10^{-5}	2,84	3,24	3,24	5,35	1,14	1,87
HCl	10^{-3}	380	—	—	392	—	1,03
	10^{-4}	43,1	—	—	49	—	1,14
	10^{-5}	3,50	3,98	3,98	5,96	1,08	1,70

Table 2*)

Solution	Concentration, M	$K \cdot 10^{10}$ (ohm^{-1})			
		from $\varkappa_s$ by (4)		Calculated from ζ by (5)	
		$\bar{K}$	$\tilde{K}$	from ζ_J	from ζ_E
LiCl	10^{-4}	1,4	13,7	0,7	1,0
	10^{-5}	2,7	12,2	0,3	0,8
KCl	10^{-4}	2,7	13,5	1,7	2,0
	10^{-5}	1,7	10,8	0,6	2,2
CsCl	10^{-4}	3,4	15,4	1,2	1,9
	10^{-5}	2,3	15,4	0,5	1,4
HCl	10^{-4}	—	25,5	—	2,5
	10^{-5}	3,3	16,9	2,1	5,1

*) In table the mean values are presented the error being in limits 18 p.c.

References

1. O.N.Grigorov,Z.P.Kozmina,A.V.Markovich and D.A.Fridrikhsberg Elektrokineticheskie Svoistva Kapillyarnich System,Izdatelstvo Akademii Nauk SSSR,Moskow,1956.
2. S.S.Dukhin,B.V.Derjaguin,Electrokinetic Phenomena,in Surface and Colloid Science,ed.E.Matijević,John Wiley a.Sons, N.Y.,1974.
3. C.S.Slichter,Ann.Rep.U.S.Geol.Surv.,19,295 (1898)
4. J.Th.G.Overbeek,P.W.O.Wijga,Rec.Trav.Chim.Pays-Bas,65,556 (1946)
5. J.Lyklema,J.Electroanal.Chem.,18,341 (1968).

ELECTROKINETIC POTENTIAL OF COLLOID PRECIPITATIONS IN AQUEOUS (POLY)ETHYLENOXIDE SOLUTIONS

B.V.Eremenko and B.E.Platonov

Schevchenko State University, 252017 Kiev-17, Vladimirskaya 62, Soviet Union

This paper deals with the effect of water soluble nonionic polymer additions on some colloid particles' double electric layer parameters - electrokinetic potential and disperse phase surface charge density. Colloid precipitations of antimony sulphide and silver iodide with specific surface 64 and 0,6 m^2/g and one of the simplest as to its structure water soluble polymer - (poly)ethyleneoxide (PEO) with molecular weight from 400 to $2{,}8 \cdot 10^6$ - were the subject of research. The electrokinetic potential of particles in PEO water solutions has been measured with the method of streaming potential. The effect of PEO on disperse phase particles' surface charge density (σ_0) has been studied with the help of direct radiometric estimation of counterion total adsorption (for Sb_2S_3) or on the change in AgI suspension intermicellar liquid radioactivity (AgI was labeled by isotope I^{131}). Increasing of PEO additions results in regular decrease of Sb_2S_3 particles' ζ -potential negative values (Fig.1), its the sharpest dip being observed, as simultaneous conducted adsorption measurements showed, in concentration region where the full polymer extraction from the solution takes place. At PEO contents relevant to adsorption saturation the region of electrokinetic potential values independence from polymer addition equilibrium concentration is observed. The maximum ζ -potential decrease depends on PEO molecular weight; high-molecular ($M > 10^6$) specimens descrease ζ -potential to zero. Rather different regularities are observed in the case of silver iodide suspension. ζ -potential descent here is preceded by its growth in the region of low PEO additions (Fig.2, curves 1,2). PEO introduction into positive AgI suspension (the charge is positive in this case

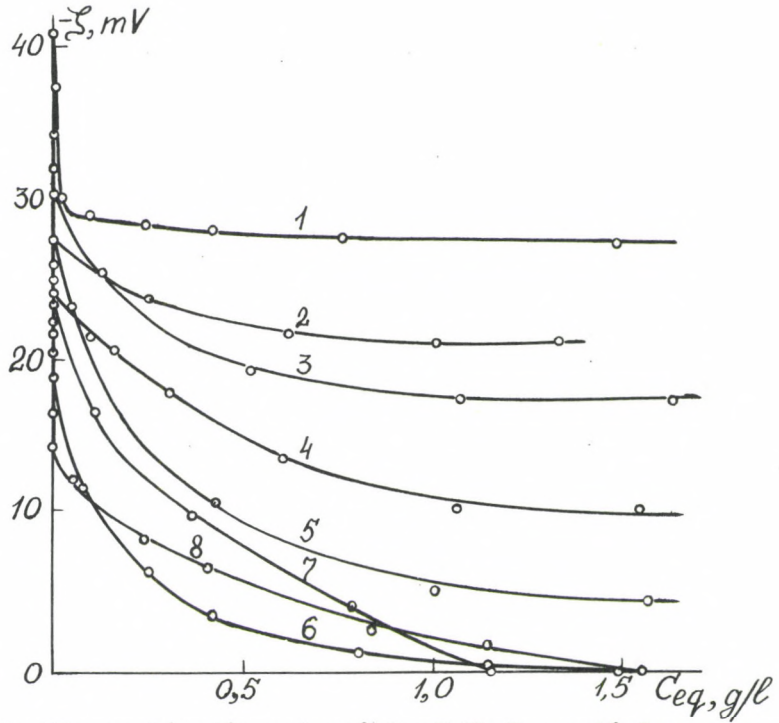

Fig.1. Electrokinetic potential of Sb_2S_3 particles as a function of PEO equilibrium concentration.
PEO molecular weight: 1- 1000, 2- 6000, 3- 20000, 4- $1{,}13 \cdot 10^5$, 5- $2{,}8 \cdot 10^5$, 6- $9{,}9 \cdot 10^5$, 7- $1{,}76 \cdot 10^6$, 8- $1{,}89 \cdot 10^6$.

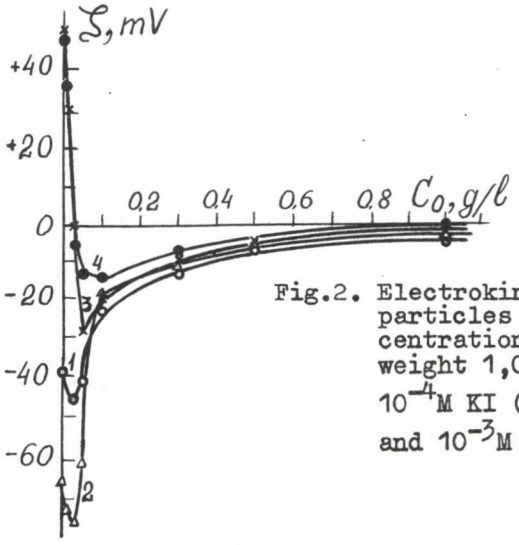

Fig.2. Electrokinetic potential of AgI particles as a function of concentration of PEO with molecular weight $1{,}05 \cdot 10^6$ in water (1), 10^{-4}M KI (2), $5 \cdot 10^{-4}$M $AgNO_3$ (3) and 10^{-3}M $AgNO_3$ (4).

due to $AgNO_3$ excess in intermicellar liquid) resulted in change of electrokinetic potential's sign.

We consider that all detected regularities of PEO effect on Sb_2S_3 and AgI particles' electrokinetic potential can be explained from the common point of view taking into account not only the shear plane shift presentations but also the appearance of additional potential drop as the result of oriented adsorption on interface of some macromolecule's dipole segments. In this case the total potential drop on interface φ_0 will be equal a sum of ionic (φ_i) and adsorption (φ_d) drops. Due to the fact that at invariable potential determining ions activity in silutions φ_0 is constant [1] the appearance of φ_d changes the value of φ_i and respectively the value of ζ -potential. Suppose that dipole segments $-CH_2-CH_2-O-$ are oriented to AgI hydrophobic surface irrespectively of its charge sign by their positive ends [2]. Then a sign of φ_d coincides with surface potential sign for positive AgI particles and will be opposite to φ_0 sign for negative ones. The potential adsorption drop in the case of silver iodide positive particles will surely cause ionic drop absolute value reduction (at $\varphi_d < \varphi_0$) or even its sign change (at $\varphi_d > \varphi_0$) that is showed by ζ -potential positive particles decrease and change of its sign (Fig. 2, curves 3,4).

PEO adsorption on AgI negative particles must, according to this point of view, result in φ_i negative values and, respectively, ζ -potential values increasing, that is confirmed by the experiment (Fig.2, curves 1,2).

From the point of view of developing presentations PEO segments' orientation, being under consideration, on Sb_2S_3 negative particles surface schould lead, as in the case of negative AgI, to the initial ζ -potential increasing; however even at low degrees of Sb_2S_3 surface coating when it is hardly to expect thick adsorption layer forming negative ζ -potential decreasing is observed. This experimental fact permits to suppose the opposite in comparison with AgI PEO segments orientation - by oxygen atom to the surface.

This can be explained by the originating of hydrogen bonds of oxyethylene group oxygen with acidic groups hydrogen on the surface of Sb_2S_3.

Depending on such orientation φ_i negative values decrease must be followed by decreasing of Sb_2S_3 particles surface charge (σ_0) density, that was confirmed by the experiment (Table 1). At the same time the detected absence of potential determining I^- ions desorption from AgI negative particles' surface (Table 2) confirmed said φ_d and φ_0 sign variance. The decreasing of ζ -potential (after its sharp initial descent) when adsorption of PEO increases, being observed, is impossible to connect with σ_0 change as far as beginning from a=0,08 mg PEO/m^2 Sb_2S_3 surface charge remains constant (look table 1). In this region of polymer coated surface area ζ -potential decrease obviously depends on shear plane shift into liguid phase as the result of forming of the polymer layer with increasing thickness on the solid surface. Such layers generation may be connected with transition on surface either individual macromolecules (layer thickening in this case can be explaned by polymer chain adsorbed "tails" and "loops" length increasing) or associates of macromolecules which are present in solution. Transition probability of said formations to the surface increases with polymer molecular weight and concentration rise.

It is necessary to bear in mind that both discussed factors - "potential adsorption drop" effect and shear plane shift - can act simultaneously; and observed ζ -potential variation in nonionic polymer additions presence will be determined by relative contribution of each of them. The first of them dominetes in region of low coating degrees of surface; this is confirmed by coincidence of PEO adsorption values at which both the initial sharp ζ -potential descent and decrease of Sb_2S_3 surface charge density are finished (Fig. 3 and Table 1) and also by the fact of AgI ζ -potential negative values increase (Fig. 1).

If we suppose that adsorbed polymer does not effect counter-

Table 1.

The influence of PEO on Sb_2S_3 surface charge density.

Adsorption of		$\Delta\sigma_0$	Number of PEO segments which are in the contact with the surface by		Portion of PEO segmens which are in the contact with surface in % by one molecule of polymer
PEO mg/m^2	Ca^{++} $\frac{g\text{-equiv.} \times 10^6}{m^2}$	$\frac{\mu Cul}{cm^2}$	$1cm^2 \times 10^{-13}$	1 molecule of polymer	
0	0,84	-	-	-	-
		Molecular weight 6000			
0,08	0,78	0,59	4,04	40,4	29,6
0,23	0,72	1,16	7,95	26,5	19,4
-	0,70	1,35	9,25	-	-
0,58	0,70	1,35	9,25	12,5	9,1
		Molecular weight $1,26 \times 10^6$			
0,08	0,77	0,70	4,80	$10,0 \times 10^3$	35,0
0,23	0,73	1,06	7,25	$5,06 \times 10^3$	17,7
0,59	0,73	1,06	7,25	$2,0 \times 10^3$	7,0
0,71	0,73	1,06	7,26	$1,67 \times 10^3$	5,9

Table 2.

Radioactivity of PEO solutions after their contact with AgI precipitation which was labeled by isotope I^{131}, imp./min.ml.

Initial PEO concentration, g/l	Radioactivity of PEO solutions		
	Molecular weight		
	1000	$1,05 \times 10^6$	$1,8 \times 10^6$
0	12	2	7
0,01	7	7	5
0,02	16	3	4
0,05	3	11	3
0,10	12	5	6
0,60	4	12	2

ion distribution in double electric layer diffusion part and shear plane distance from solid phase coincides with polymer adsorbed layer effective thickness then the latter can be estimated using the well-known ratio from diffusion ionic layer theory

$$th\left(\frac{ez\zeta}{4kT}\right) = th\left(\frac{ez\varphi_\delta}{4kT}\right) e^{-\varkappa(h-\delta)}$$

where h, polymer adsorption layer thickness,
δ, Stern layer thickness (≈ 4 Å [3]),
and e, z, k, T have their usual meanings.

For h estimation we supposed that $\varphi_\delta = \zeta_0$, where ζ_0 is Sb_2S_3 electrokinetic potential at PEO concentration where potential adsorption drop action apparantly finishes and transition sharp lowering of curve ζ - c into smooth (30 mV) is observed.

It turned out that calculation h values were much lower than statistic coil parameters estimated according to Flory theory from the values of characteristic viscosity. So transition on the surface of polymer kinetic units, existing in solution, is accompanied by their considerable deformation. Said Sb_2S_3 particles surface charge decrease ($\Delta\sigma_0$) as the result of PEO adsorption is connected, we consider, with emerging of oriented dipole segments $-CH_2-CH_2-O-$ on the surface of disperse phase. Disposing the information about PEO adsorption quality and surface charge density decrease we tried to value greatly significant for polymer adsorption theory characteristic - number of adsprbed macromolecular chain contacts with solid surface. As far as the main particles surface potential drop portion, at medium values of solution ionic force, falls on the double layer dense part [4], than our further considerations will be based on double electric layer structure in a form of plane capacitor. As Stern layer thickness (δ) usually is taken equal to ~ 4 Å [3] and PEO segment length is 4-5 Å [5] then at a supposition of normal PEO segments orientation to the surface ionic capacitor thickness can be without greyt mistake equaled to molecular capacitor thickness.

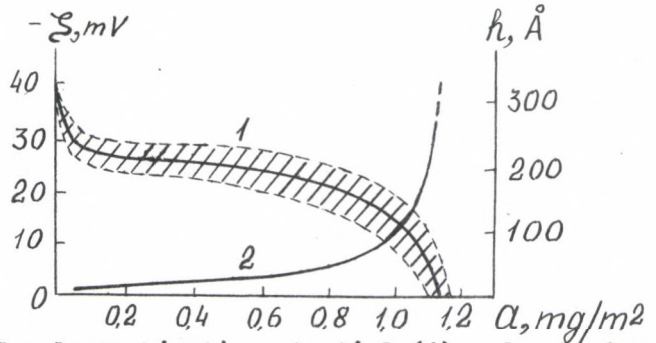

Fig.3. Sb_2S_3 electrokinetic potential (1) and calculated PEO adsorption layer thickness on this surface (2) as a function of PEO adsorption values. Solid curve 1 correspondes to averaged electrokinetic potential values for PEO specimens with different molecular weights; the experimental points are keeped within shaded area between two dotted lines.

Suppose then, that dipole arm (l) approximately corresponds to segment lenght; it follows from this that at equal dielectric constant values in ionic and molecular layers the capacity of ionic (C_i) and molecular (C_d) capacitor is equal ($C_i = C_d$). From the condition of plane capacitor plates charge proportionality to potential difference between them it follows that,for considered particular case, surface potential constancy condition $\varphi_o = \text{Const} = \varphi_i + \varphi_d$ can be substituted for surface charge constancy condition $\sigma_o = \text{Const} = \sigma_i + \sigma_d$, where σ_i - surface charge ionic component and σ_d - total charge of adsorbed dipole ends oriented to surface.

Therefore surface charge density change $\Delta\sigma_o$, estimated by radiometric method, can be equal to σ_d value. This gives us a possibility of estimating the number of dipole ends, oriented in polymer adsorption layer (n) from a ratio

$$\Delta\sigma_o = \sigma_d = \frac{D\,n}{l},$$

where D - dipole moment of seqment taken equal to 1,88 D [6]; l - dipole arm. The ratio of calculated n value to

experimentally determined total polymer adsorbed segments number gives portion of adsorbed macromolecular chain contacts with surface.

From the results given in the table 1 it follows that:

1) at given PEO adsorption value number of polymer contacts with surface practically does not depend on molecular weight of polymer specimens;

2) the portion of segments contacting with surface decreases when degree of surface coating by PEO increases;

and 3) the portion of segments, directly binded with surface, even at low surface coating degrees, makes up no more than 1/3 of adsorbed segments total amount.

References.

1. H.R.Kruyt, M.A.M.Klompe, Kolloidchem. Biehefte, 54,484(1943).
2. R.J.Hillson, J.Photographic Sci., 11,225(1963).
3. G.Fleer, L.Koopal, J.Lyklema, Koll.-Z. u. Z.Polym., 250,689(1972).
4. B.V.Eremenko, B.E.Platonov, A.A.Baran, V.V.Lukachina, Dokladi Akademii Nauk Ukrainskoy SSR, 428(1975).
5. P.J.Flory, Statistical Mechanics of Chain Molecules, N.-Y.-London-Sydney-Toronto,1969.
6. I.T.Goronovsky, Yu.P.Nazarenko, E.F.Nekrjach, Kratky spravochnik po chimii, Kiev, 1974.

INVESTIGATION OF LIQUID MOVEMENT IN ELECTRIC FIELDS THROUGH MULTILAYER DIAPHRAGMS

K.P.Tikhomolova

Leningrad State University,Chemical Faculty, Leningrad
Sredny pr. 41/43, Soviet Union

The laws of movement of liquids in real capillary-porous systems under the action of the electric field ("electroosmose") are based on the interaction of a great number of fac - tors and forces. The change of any state parameter during a test may lead to a change of any other one.

Of any reasons leading to changes in behaviour of complicated systems,as compare to the classic one (Helmholtz-Smoluchowsky formula),this report deals with only one of them , viz. the development of internal pressure differences.The basic aim is to demonstrate that the examination of this complicating factor would be not only particular,but of a fairly general interest and , besides, to analyse relations of motion parameters to structural and electric properties of some complicated systems.

For all cases it's assumed that the mobile phase is a truly viscous incompressible liquid;temperature,viscosity and dielectric permeability are constant over the whole volume of a given phase.

The report is devoted to results obtained when investigating the diaphragms,the pores space of which is filled with solutions of the same solvent.The complexity of systems is defined as follows.A diaphragm consists of many separate parts or layers differing in the electric field,active cross-section,the structure of pores space or in the thickness. Layers are arranged in series.Throughout a layer all the above-mentioned parameters are constant,in other words, any layer is

uniform.The difference in the electric field means the difference between ζ-potentials and axial components of total electric field intensity /E/.Change of axial components may be caused by that of the concentrations or ions nature in the layers (owing to simultaneous action of electroosmose and electrodialysis,to the exchange- and chemical reactions), or by the condition of external field connection (fig.1). When the active cross-sections are different,practically there may exist two opposite cases: the cross-section of diaphragm is constant -the porosity is changed; the porosity is constant - the cross-section is changed (Fig.1).The same Fig 1 shows a rough scheme of a case, when the layers are distinguished by the structure of porous space - mean radius of the pore and by the thickness.

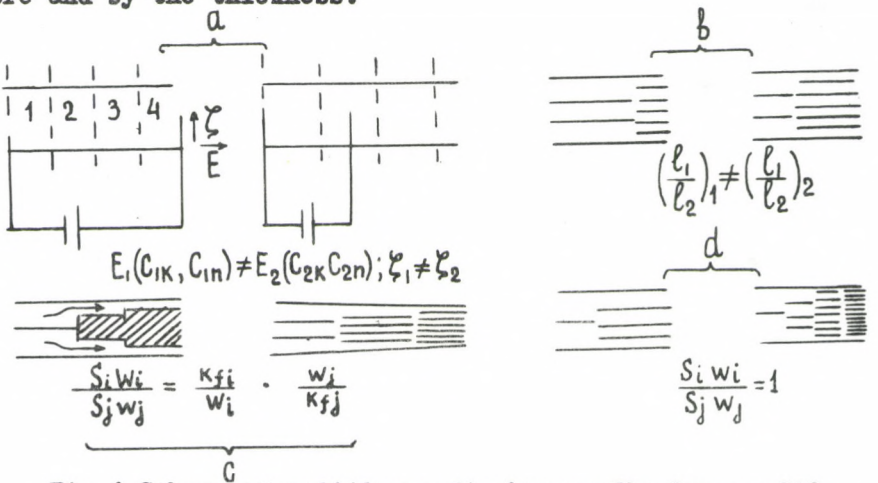

Fig.1.Scheme of multilayer diaphragms.The layers differ in a) electric field characteristics;b) thickness; c)active cross-section; d) mean radius.(C -concentration)

The specificity of all systems is based on the development within them of the internal pressure differences,being the result of system response to the difference of layers mass forces (electric and viscous friction)(Fig.2).The pressure gradient,caused by the action of the layer in question mass forces,is directed against the flow in this layer and along the flow in all other layers / 1 /. Its value depends

on the mass forces of this layer and on braking forces of other layers. The total pressure difference is the algebraic sum of all layers. The pressure distribution depends on the structural parameters of all layers in accordance with the filtration laws and power of the electroosmotic flow.

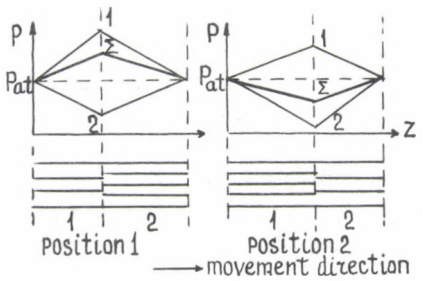

Fig.2 Pressure change in two-layer diaphragm.The broken line 1 correspond to action of mass forces of layer 1; the line 2-to action of mass forces of layer 2; $\sum$-the sum of action of mass forces of both layers.

It should be emphasized that according to the views developed here the flow velocity doesn't depend on the position of the diaphragm to the poles of the power source (the positions 1 and 2 of Fig 2 are equivalent).

When deducing formulae, a serious limitation was taken into consideration, viz.the sufficient thickness of layers /1/. The formulae obtained describe electroosmose only through multilayer diaphragms in a whole,and they can't be used a'priori for deriving any laws of flow through diaphragm, as they would be based on the analysis of the position of one elementary pore taken out of the porous space /2/. The development of internal pressures in the scheme is the result of the change along the diaphragm, and that should be emphasized specially,of hydraulic and electric resistances averaged over all active cross-section.

Let us mainly consider the cases,when either the flow is stationary or, when the change of the system during the test take place,the results of the analysis represent only the beginning of the test.In both cases the time is absent.

The set of initial equations is used for integration. It is derived from the total law of the quantity of motion for the case of stationary processes with the mechanism taken into consideration. The number of initial equations is equal

to that of layers. Of the boundary conditions only one is mentioned: the sum of differences pressures is 0. The rest of the conditions are trivial.

The integration gives some formulae describing the system behaviour. For example, the volume velocity may be represented by:

$$q_{cd} = -\frac{\varepsilon\, \zeta_1\, I}{4\pi\eta\, \varkappa_{p1}} \cdot \frac{\sum_1^m l_i\, \zeta_i\, \alpha_1 / k_{fi} S_i\, \alpha_i\, \zeta_1}{\sum_1^m l_i / k_{fi} S_i} \qquad (1)$$

where : q_{cd}- volume velocity through complicated diaphragm; ε, η - dielectric permeability, solution viscosity; $\varkappa_{pI}$ -electroconductivity in pores of layer i; l_i, k_{fi}, S_i, ζ_i, α_i - thickness, filtration coefficient, cross-section, ζ-potential and coefficient of efficiency, all relating to layer i; $\alpha_i = \varkappa_{pi} / \varkappa_o$, $\varkappa_o$ - electroconductivity of free solution; I- strength of the electric current ; m - number of layers.

For all complicated systems described above, there were set some experiments, using powder diaphragms. In all cases the formulae were satisfactorily confirmed by the results / 3-6 /.

We shall deal further with one of the particular problems - the behaviour of active diaphragms. Of all electrochemically active diaphragms let us consider those, the layers ζ-potentials of which are equal and the efficiency coefficients are different. It is interesting to emphasize one of the results, viz. the volume velocity through electrochemically active multilayer diaphragm is less than through the inactive one, having the same chemical nature, not only because of the increase of average electroconductivity in pores, but also because of the change of electroconductivity when passing from layer to layer.

As it is known, when calculating ζ-potential, the influence of changing average conductivity in pores is taken into account by use of the correction for the surface conductivity. This correction is cofactor-the efficiency coefficient, introduced in Helmholtz-Smoluchowsky formula /7/:

$\zeta = -\frac{4\pi\eta\varkappa_0 q}{\varepsilon I}\cdot\alpha$ (2). For being short, I shall define thus calculated value ζ as ζ_{cd}; and corresponding efficiency coefficient - α_{cd}. All stated above means there should be a difference between true value of ζ, which has to be calculated by: $\zeta = -\frac{4\pi\eta\varkappa_0}{\varepsilon I}\alpha_{cd}^{*}$ (3) , and ζ_{cd}. This inequality is characterized quantitatively by the deviation of the ratio (4) from 1:

$$\frac{\zeta_{cd}}{\zeta} = \frac{\alpha_{cd}}{\alpha_{cd}^{*}} = \frac{\sum_1^m l_i / S_i w_i}{\sum_1^m l_i / S_i w_i i} \cdot \frac{\sum_1^m l_i / i\, k_{fi} S_i}{\sum_1^m l_i / k_{fi} S_i} \quad (4)$$

where α_{cd} and α_{cd}^{*} are coefficients, correlating the Helmholtz -Smoluchowsky formula: the first - the correlation for the increase of electroconductivity on the average of diaphragm; the second - the correlation for the local changes. The relation ζ_{cd}/ζ is complex, not monotonous; under extremely unfavourable conditions there may be a minimum, the depth and position of which depend on specific values of the system parameter / 6 /. The above-said is illustrated by Fig. 3.

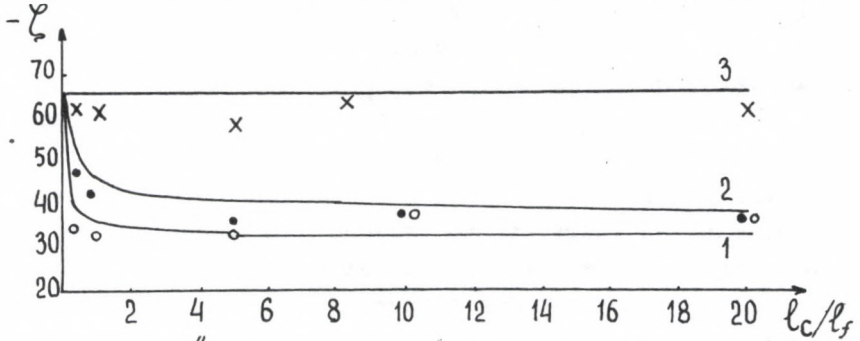

Fig. 3 The ζ-potential values calculated from the experimental data with quartz powder diaphragms in KCl -solution (fractions equivalent diameter: 200–300 μ and 8 - 16 μ ; $\varkappa_0$ = $1{,}5 \cdot 10^{-5}$ $om^{-1}cm^{-1}$). The curve 1 and points o ~ are calculated by formula Helmholtz-Smoluchowsky; the curve 2 and points • - by formula (2); points x -by formula (3); straight line 3 is a result of experiment with inactive diaphragms. (index „c" → coarse fraction, „f" → fine).

However, there are some cases, when the demand of the sufficient thickness of the layers is not satisfied. For examp-

le, this is the case with diaphragms, the characteristics of which are gradually changed along, or with diaphragms, which are active and uniform along the thickness, but have complex porous space (powder diaphragm composed of narrow fractions) The result is obtained either by deducing the limits ($l_i \to 0$, $m \to \infty$),or by logical consideration. Both methods gave some interesting results, though the calculation here can't be considered as strict.

The limit kinds of formulae differ depending on the type of diaphragms. Here is a formula for the type represented in Fig. 1 - d:

$$\frac{\varphi_{cd}}{\varphi} = \frac{R_{max} R_{min} \ln \frac{R_{max}(a + R_{min})}{R_{min}(a + R_{max})}}{a\left(R_{max} - R_{min} - \ln\left[\frac{a + R_{max}}{a + R_{min}}\right]\right)} \qquad (5)$$

where $a = (\alpha_{R_{min}} - 1) R_{min}$.

According to the analysis of formula (5) ,transition to more and more multilayer systems (the diaphragm thickness, the largest and the least active cross-sections are constant) leads to ever growing deviation of φ_{cd} from the true one.The limit of deviation depends on the relations of the radii and of the corresponding α_i.Thus , 4-5 layer diaphragm give the velocity which is very near to the limit one.

For getting an answer to the second question, the reality of arising the internal pressure differences in the net of transversally combining pores of powder diaphragm has been estimated.

Let us consider two schemes of Fig.4,where systems of 2 elementary pores,linked to each other by transversal pores-bridges M and N, are represented. The number of pores is of no importance for the case. It is necessary to satisfy the requirements of the proper ratio of the active cross-sections and of the presence/absence of transversal pores.

The scheme a). The cross-sections of wide and narrow portions of the first and second pores are equal; distribution

of pores by the dimensions along the diaphragm is not changed.

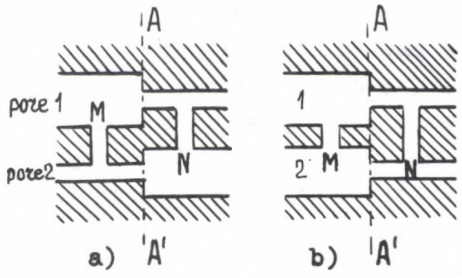

Fig.4 The scheme for estimation of pressure drops development in powder diaphragm.

According to above-said a high pressure zone must appear in the pore 1, and a low pressure one- in the pore 2. The influence of the pressure drop on the motion in any pore is equivalent.The presence of pores-bridges decrease both pressure drops. If pores N and M are far from each other,the pressure drop is nevertheless present.If M and N are arranged very close to each other,the formation of any substantial pressure drop is not expected.This is especially true of the porous space of powder diaphragms,which are composed of narrow fractions and have the constant cross - section.

The scheme b). The pores distribution by their dimensions along the diaphragm is changed: the ratio of active cross-sections can be any you like. The internal pressure drops will be present,because to the left of the line AA' the pressure in all capillars has to increase along the axis, and to the right it has to drop. Presence or absence of the transversal channels is of no importance.For example, this scheme represents the diaphragms formed by sedimentation from the powder suspensions with the particles of different dimensions In these cases the calculation of the correcting co-factor , with allowance for local changes, is obligatory, but it is not difficult(by dividing the diaphragm into 5-6 layers).

The last which we should like to touch on is the approach to the solution of problems,when the pores solution and the surface nature are changed during the test. Change of nature and concentration of pores solution is in the direct relation to the pressure change. Thus,the problem here is considered also in the terms of internal pressure,being the time function.It was contemplated, that the change of the soluti-

on in any section occurs at once from the initial to the final state. A new boundary condition is the relationship of the coordinate of property change and the mean value of the flow velocity along the cross-section of diaphragm.

For the range of the systems studied our experimental data show a good conformity with the results calculated by the corresponding formulae.In some cases one can observe the appreciable deviations being the result of not keeping the demand of a sharp drop / 8 /.Some attempts have been made to find a correlation with the theoretical formulae empirically.In some cases it was a success ,the "empirical " formulae being true for the not very narrow range of systems.In other cases we cauld only find a correlation between the picture anticipated according to the formula, experimental data and logical conclusions about the reasons of the discrepancy.

References

/1 / K.P.Tikhomolova , Kolloidn.Zh. 36 ,N4,715-721,(1974).
/2/J.Th.G.Overbeek,P.W.O.Wijga ,Recueil Trav.Chim. 65, 556,(1946).
/3/.K.P.Tikhomolova, Kolloidn.Zh. 30 ,N1, 144-149,(1968).
/4/.K.P.Tikhomolova,N.G.Sharova, Ingenern-physich.Zh, 20, N 1,56-62,(1971).
/5/.L.P.Kusenkova, K.P.Tikhomolova,N.G.Sharova,Kolloidn.Zh. 35 ,N 2,367-369,(1973).
/6/ K.P.Tikhomolova,L.A.Boikova, Kolloidn.Zh. 36 ,N 4, 722 - 729,(1974).
/ 7 /.P.A.Rebinder (editor),Electrokinetitscheskiye svoystva capillarnykh sistem (Electrokinetic properties of capillary systems), collection,Moskva-Leningrad,Izd.AN SSSR,Ch.8,9,(1956).
/8/.K.P.Tikhomolova,E.A.Judincev, Electropoverkhnostnye javlenija v disprsnykh sistemakh (Electrosurface phenomena in disperse systems),collection,Moskva,Izd Nauka,144 - 149,(1972).

ELECTROOPTIC STUDY OF THE COLLOID STABILITY OF ANISODIAMETRIC PARTICLES

S.P.Stoylov

Institute of Physical Chemistry, Bulgarian Academy of Sciences 1113 SOFIA, Bulgaria.

The electrooptic and dielectric studies of aqueous disperse systems in the last 20 years gave for the first time many convincing proofs for the unespected considerable importance of the interfacial electric dipole moments of various types of anisodiametric and isodiametric disperse particles [1-3, 4-5]. Biside this electrooptic methods provide, through the determination of the rotational diffusion constant of the particles, a simple and reliable tool for following the particles'dimensions and their variations.

Colloid stability is well known to depend strongly on the particles'electric properties (after Derjaguin-Landau-Verwey-Overbeek - DLVO theory) [6,7]. This is electric surface potential (or surface charge) which is closely related to changes in stability which is connected in many cases with the aggregation of the disperse particles. As for as electrooptic methods are connected with both important characteristics of colloid stability - electric properties and aggregation it is rather natural to use electrooptic studies for the characterization of colloid stability. The purpose of this

paper is to make a short review of recent development in the field of electrooptic study of colloid stability.

Before using electrooptics for the study of the colloid stability currently electrophoretic measurements were used for the electrical characterization of the colloid particles. Of greatest interest for our problem are the cases where zero ζ-potential (the isoelectric point) do not correspond to minimum stability of the disperse systems. Typical in this direction are AgBr and other solutions to which surface active substances are added [8,9]. The deviations of the minimum colloid stability from the isoelectric point in these studies were explained with dipolar interactions.

Starting from 1968 [10] a serries of publications described the effect of the addition of the cation active surface active substance cetyl pyridinium chloride (CPC) to the aqueous suspensions of the clays: palygorskite [10-13], bentonite [13], illite [13], caolonite [14], and the effect of the addition of $Th(NO_3)_4$ to the aqueous solution of palygorskite [15]. In all of the cases which were studied a clear correlation was found between the stability of the solutions and the electric polarizability of the disperse particles. At that the minimum stability corresponded in the most of the cases quite clearly with the minimum value of the electric polarizability. The stability of the colloid systems studied was followed in three ways. Most roughly this have been done visually and this gave the possibility only the state of minimum stability to be detected surely where after several hours sedimentation in the solutions occured which could be

interpreted as a result of slow coagulation. The second method is connected with the callibration of the electrooptic measurements by which it is necessary the exess light scattering of the solutions in comparison with the solvent (in our case water) to be measured. At constant volume concentrations of the dispersed clays which is assured by all reported cases [10-15], the change in the intensity of the scattered light from one solution to another and in one and the same solution with the time is connected before all with changes of particles'dimensions. The change of particles'dimensions or the rate of this change are closely connected with the stability of the respective disperse systems. The third method is directly connected with the electrooptic measurements. Through the relaxation times of the decrease in the intensity of the scattered ~~of~~ light after the switching off of the electric field the rotational diffusion coefficients of the clay disperse particles could be determined for the different solutions or for any of the solutions as a function of time. By this way independent information is gained only for the changes in the dimensions and form of the particles. In all the cases [10-15] the changes in the stability of the disperse systems with the adition of coagulating agent deduced by the three ways were in good mutual agreement. The supplementary study of the initial stages of coagulation at the concentrations of coagulating agents at which minimum stability was observed could for some of the cases give new valuable information which however can not change substantially the observed variation of the colloid stability in all the cases studied [10-15].

More complicated is the question with the study of the value of the electric polarizability of the disperse particles and especially in the points of minimum stability where the dispersity of the solutions changes with the time. Ordinarly the value of the electric polarizability and of rotational diffusion coefficient in this case are taken between the 15th and 30th minutes after the preparation of the solutions. Since the variations of the rotational diffusion coefficients are rather slight it could be accepted that the times of the measurement of the electric polarizability after the preparation of the solutions, the solutions are sufficiently unperturbed to make doubtful the deep minimum of the electric polarizability measured in all cases. A rigorous evaluation of the effect of the dimensions on the values of the electric polarizability was made quite recently using a computer. The results showed that in these cases the sharp minimum in the electric polarizability could become less sharp but it could not dissapear [16,17]. Supplemantary studies could be made on the dependence of the value of the electric polarizability on the time after the preparation of the solution and surch its extrapolation value for time zero.

Another possible complication at the determination of the value of the electric polarizability for the unstable solutions is the danger from aggregation in the electric field applied. Evidence for such coagulation of spherical particles in an electric field followed electrooptically exist [18,19]. For the cases studied, the electric pulses applied were sufficiently short to make quite unprobable such

electroaggregation. However future studies in this field are necessary to obtain exact prooves that electrocoagulation does not change the value of the electric polarizability determined. The best way is to study the dependence of the value of the electric polarizability determined on the electric field strength or on the electric pulse duration. The extrapolation of both dependences to zero electric field strength or to zero duration of the electric pulse applied has to give exact values of the electric polarizability, urperfurbed from electroaggregation.

When studying the changes of the electric polarizability with the concentration of the coagulating agent in many of the cases studied [10-15] a variation in the relaxion times of the electric polarizability (t.e. the time of its establishment) and of the permanent dipole moments of the disperse particles with the concentration were observed. A systematic study of these dependences could be of considerable interest. Variation of electrooptic effects of disperse systems with the addition of surface active and other substances interpreted as changes in the permanent dipole moments of the disperse articles have been communicated by several authors [20-23].

The studies reviewed here and especially these considering the correlation of the disperse particles'electric moments with colloid stability could be of considerable importance for the future development of the new concepts in the field of colloid stability. A further perfection of the DLVO theory in the direction of abandoning the assumption for

constant electric potential or electric charge distribution over the surface of the particle seems in connection with this quite reasonable. The importance of this phenomenon for the molecular biology where the role of colloid stability is replaced by the role of local molecular conformations seems to get some recognition in the last several years [24-27].

REFERENCES

1. C.T.O'Konski, A.J.Haltner, J.Am.Chem.Soc., 79,5634(1957).
2. S.P.Stoylov, Adv.Colloid Interface Sci., 3, 45 (1971).
3. N.A.Tolstoi, A.A.Spartakov, Kolloidn.Zh., 28, 580(1960).
4. H.P.Schwan, G.Schwarz, J.Maczuk, H.Pauly, J.Phys.Chem., 66, 2626 (1962).
5. T.L.Chelidze, Koll.Zh., 33, 327 (1971).
6. B.Derjaguin, J.Landau, Acta Physicochim. URSS, 14, 633 (1941).
7. W.E.J.Verwey, C.J.Th.Overbeek,"Theory of the stability of Lyophobic Colloids", Amsterdam, 1948.
8. R.Ottewil, A.Watanabe, Koll.Z., 170, 38, 132 (1960); ibid. 171, 32 (1961).
9. G.A.Johnson, J.Coldfarb, B.A.Pethica, Trans.Farad.Soc., 61, 2321 (1965).
10. S.P.Stoylov, I.Petkanchin, S.Sokerov, Proc. 5th Intern. Congress on Surface Activity, Barcelona, 1968, Ediciones Unidas, S.A., v.2, p.163.
11. S.P.Stoylov, I.Petkanchin, Dokladi BAN, 24, 487 (1971).

12. S.P.Stoylov, I.Petkanchin, J.Coll.Interface Sci., 40, 159 (1972).
13. I.Petkanchin, S.Sokerov, S.Stoylov, 6th International Congress on Surface Activity, Zurich, 1972, Carl Henser Verlag, 1973, p.671
14. I.Petkanchin, R.Bruckner, in the press in Koll.Z. .
15. I.Petkanchin, S.Stoylov, S.Baykusheva, God.Sof.Univ., Khim.Fak., 66, 271 (1971/72).
16. S.Stoylov, I.Petkanchin, S.Sokerov, in the press in God.Sof.Univ.
17. I.Petkanchin, Thesis, Sofia, 1973.
18. S.Sokerov, T.Vorobyova, S.Stoylov, in the press in J.Polym.Sci., C.
19. S.Sokerov, T.Vorobyova, to be presented on this conference.
20. N.A.Tolstoi, E.Kitanina, E.Rudakova, A.Spartakov, A.Trusov, Koll.Zh., 36, 82 (1974).
21. Yu.Glazman, E.Kitanina, I.Sapon, A.Spartakov, A.Trusov, Koll.Zh., 35, 348 (1973).
22. Yu.Glazman, E.Kitanina, I.Sapon, A.Spartakov, N.A.Tolstoi, A.Trusov, Ukr.Khim.Zh., 38 (1972)
23. N.A.Tolstoi, Yu.Glazman, O.Baram, E.Kitanina,A.Spartakov, A.Trusov, Koll.Zh., 36, 405 (1974).
24. E.Neumann, A.Katchalsky, Proc.Nat.Acad.Sci.,69,993(1972).
25. E.Neumann, D.Nachmanson, A.Katchalsky, Ibid.,70,727(1973).
26. K.Kikuchi, K.Yoshioka, Biopolymers, 12, 2667 (1973).
27. A.Revzin, E.Neumann, Biophys.Chem., 2, 144 (1974).

ELECTROOPTICAL INVESTIGATIONS OF THE INTERACTION AMONG SPHERICAL PARTICLES

S.Sokerov and T.Vorobeva*

Institute of Physical Chemistry, Bulgarian Academy Sciences, III3 Sofia, BULGARIA.
*Institute of Physical Chemistry, Academy of Sciences of USSR, Moscow B-7I, USSR.

I n t r o d u c t i o n

Under the action of alternating electric fields on disperse systems the disperse particles interact among themselves forming linear aggregates oriented along the force field lines[I-5].Through microscopic observations the kinetics of the process in model suspensions of monodisperse particles is studied and some regularities of the phenomenon are found [6,7].Depending on the concentrations of floculating agents(FA) the formation of reversible and irreversible aggregates is observed.The former are obtained without the addition of FA and after the field is switched off they desintegrate.The latter are obtained with the addition of small quantities of FA and after the field is switched off the linear aggregates remain.Those results are obtained by the investigation of the process in a plane cell where the micron particles are situated in a thin layer[8].Theoretically the phenomenon is treated, the Brownian movement of the particles in the zones of their mutual attraction connected with the interaction of polarized particles as limitating stage of the process[9-II].Equations are derived describing the kinetics of variation of the average size of oriented aggregates[6,7].The results obtained were verified by the investigation of reversible aggregates in three dimensional cell making use of the method of electric light scattering[I2].

THEORY

At the initial moment the disperse system consists of single particles.The light scattering from such a system is determined by the number of particles and the light intensity scattered from one particle.Upon application of an electric field,linear aggregates are formed and the scattered light intensity changes.The effect of a relative change in the scattered light intensity is described in general by[13]:

$$\alpha = (I_E - I_0)/ I_0 \quad \ldots\ldots \quad (1)$$

where I_E and I_0 are the scattered light intensities respectively with and without an electric field.

Considering the linear aggregates as cylinders of diameter equal to the sphere's diameter,in the case of electric field applied perpendicularly to the plane of observation for the average number of the aggregates in the system one obtaines[12]:

$$\bar{N} = \frac{I}{I - \alpha (P - I)/[P^2 A(K) - P]} \quad \ldots \quad (2)$$

where $A(K) = 8K J_1^2(K)/9\pi J_{3/2}^2(K)$; $K = \frac{4\pi}{\lambda'} R.\sin \frac{\theta'}{2}$; λ' is the wavelenght of light in the suspension, θ' is the angle of observation, R is the radius of the spheres and J_1 and $J_{3/2}$ are Bessel functions, P is the axial ratio of aggregates. The expression (2) is valid in the Rayleigh-Debye-Gans approximation for reversible as well as for irreversible aggregates,when the latter are formed by a system consisting only of single spheres.When irreversible aggregates are formed in the system for the average number of the aggregates after the application of the field one obtains:

$$\bar{N} = \frac{(\alpha_\infty^\tau/\alpha - 1).F(K)/G^2(K) + 1}{(\alpha_\infty^\tau/\alpha - 1).F(K)/G^2(K) + 1/P} \quad \ldots \quad (3)$$

where $G^2(K) = 9\pi J_{3/2}^2(K)/2K^3$ is a function tabulated by van de Hulst[14]; $F(K) = \int_w \frac{J_1^2(K\sin\beta).J_{1/2}^2(PK\cos\beta)}{2K^3 \sin^2\beta\cos\beta} dw \equiv P_0(\theta')$ and α_∞^τ are functions calculated on computer[15]; $J_{1/2}$ is a Bessel function.

The expression (3) does not provides univalued connection between α and $\bar{N}$ because by the application of electric field α changes both because of the formation of new aggregates and of the increase in the linear dimensions of the aggregates existing in the system.The latter leads to the change in the quantities α_{∞}, F(K) and P,which makes difficult the quantitive interpretation of the results.Most generally it could be stated that the increase of the effect is a result of the increase in the average number of the aggregates in the system - $\bar{N}$.

The variation of the average number of the aggregates with the time can be described quantitatively by the expression[7,12]:

$$\bar{N} = 1 + K_V C_0 (t)^{1/2} \quad . . . . \quad (4)$$

where C_0 is the initial concentration of spheres and K_V is their interaction constant for the three dimensional case, where the latter is given by[7,12]:

$$K_V = 3(2\pi D)^{1/2}.(\varepsilon \gamma^2 E^2/kT)^{2/3} \quad . . . \quad (5)$$

where D is the diffusion constant of the spheres, ε is the dielectric permitivity of the system, E is the electric field applied, γ is the electric polarizability of the spheres and k , T are respectively the Boltzmann constant and the absolute temperature.

The expressions (2) , (4) and (5) provide a possibility to calculate the interaction constant K_V and the electric polarizability γ by the variation of the relative effect α with the time.

E X P E R I M E N T A L

The experimental studies were made with aqueous suspensions of monodisperse spherical melamin-formaldehyde particles with a diameter of 0,75 microns and a weight concentration of 0,03%.The relative change in the scattered light intensity was studied at 90° angle of observation, applying to the suspension an alternating electric field perpendicular to the plane of observation at a friquency of 1000 Hz.The method and apparatus of investigation are the

same described for the electrooptics of anisodiametric particles[16].

The kinetic curves are identical for reversible and irreversible aggregation when the electric field is applied on a system containing single particles.When the aggregates are destroyed after the switching off of the field (reversible aggregation) the system returns very quickly in the initial state.The intensity of the scattered light from such a system before the switching on of the field and after its switching off are one and the same.If one adds FA after switching off of the field,the irreversible aggregates will remain in the system,which will change the intensity of the scattered light in comparison with the initial intensity before the application of the field.

On fig.1 the oscillogrames of the electrooptic effect after the switching off of the electric field are shown for systems without FA (1) and with FA (2).As it could be expected curve 2 after the switching off of the field is higher than the initial one.The higher relaxation times compared with curve 1 could be interpreted as an indication of desorientation of the anisodiametric irreversible linear aggregates.

On fig.2 the influence of the electric field on the variation of the effect α is shown at a FA concentration about 10%.As it could be seen by the higher electric field the average number of the aggregates - $\bar{N}$,which is proportional to α is higher.A short pulse (about 20 msec.)of sufficiently high field is applied which excludes the formation of aggregates and leads only to full orientation of the aggregates already formed.The effect is zero when the system contains only spherical particles.On fig.2 with full points the values of the effect are given at the application of short pulses on the system after the application on the system of a field of 510 V/cm. for a long time.The lower values of the effect for the short pulse are due to the fact, that after the switching off of the long applied field a part of the aggregates have disintegrated or that separate spheres

have detached from the aggregates.

On fig.3 the influence of the concentration of the FA is shown on the effect α, respectively on the average number of the aggregates - $\bar{N}$. The linear dependences obtained in the initial stage of interaction (up to 15sec.) give a possibility the rate of variation of the effect with the concentration of FA shown on fig.4 to be calculated. The rate of the variation of the effect with the concentration is linear and cuts from the abcissa some limiting concentration (C_{FA}=1,75%) at which the formation of irreversible aggregates is sure.

C O N C L U S I O N

The application of the electric field leads to forces of attraction among the particles (increases the probability of their collision) and changes the coefficient characterizing the efficacity of mutual collision[17]. This coefficient makes the application of the Smoluchowski equations for fast coagulation obtained with the assumption that every collision is effective to the slow coagulation in electric field permissible[17]. The coefficient of effective collisions can be changed by lowering of the energetic barrier influencing the approach of the particles one to another by the addition of FA[10] or by the increase of the energy of interaction among the particles - e.g. by the application of electric field or mechanical action[18].

As for as the energy of interaction of the particles in an electric field strongly depends on the field strength[19] its action can be controlled and by this way the coefficient of effectivity of mutual collisions for one and the same system could be considerably influenced i.e. a model could be made of the process of slow coagulation.

R E F E R E N C E S

1. E.Muth, Kolloid Z., 41, 97 (1927).
2. H.Kruyt and J.Vogel, Kolloid Z., 95, 2 (1941).
3. L.Gindin and I.Putilova, Kolloid.Zh., 17, 325 (1954).
4. L.Gindin and A.Volpian, Uspechi Chimii, 17, 130 (1968).
5. O.Usiarov, I.Efremov and I.Lavrov, Kolloid.Zh., 28, 596 (1966).

6. T.Vorobeva and I.Vlodavetz, Kolloid.Zh.,36,1154 (1974).
7. T.Vorobeva and I.Vlodavetz, Kolloid.Zh.,37,23 (1975).
8. T.Vorobeva,I.Vlodavetz and I.Zubov, Kolloid.Zh.,31,668 (1969).
9. W.Krasny-Ergen, Ann.Phys.,27,459 (1936).
10. N.Fuks, Mechanics of Aerosols, Moscow, 1955.
11. M.Smoluchowski, Handbuch der Elektrizität und des Magnetismus, II,Leipzig, 1914.
12. S.Sokerov,T.Vorobeva and S.Stoylov, J.Polym.Sci.,N°44, 147 (1974).
13. S.Stoylov, Advan.Colloid Interface Sci.,3,45 (1968).
14. H.van de Hulst, Light Scattering by Small Particles, Moscow, 1961.
15. S.Stoylov and S.Sokerov, Europ.Polym.J.,6,1125 (1970).
16. S.Stoylov and S.Sokerov, J.Colloid Interface Sci.,24, 235 (1967).
17. M.Smoluchowski, Coagulation of Colloids, Moscow, 1936.
18. R.Neiman and A.Egorov, Kolloid.Zh.,31,629 (1969).
19. I.Vlodavetz,T.Vorobeva and A.Grivtzov, Kolloid.Zh.,36, 1046 (1974).

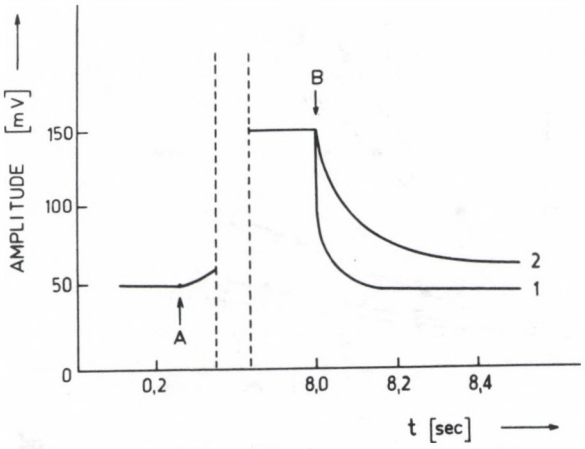

Fig.1. Oscillogram of the variation of the electrooptic effect with the time for reversible (1) and irreversible (2) aggregates. A - the moment of the field application, B -the moment of the field switching off.

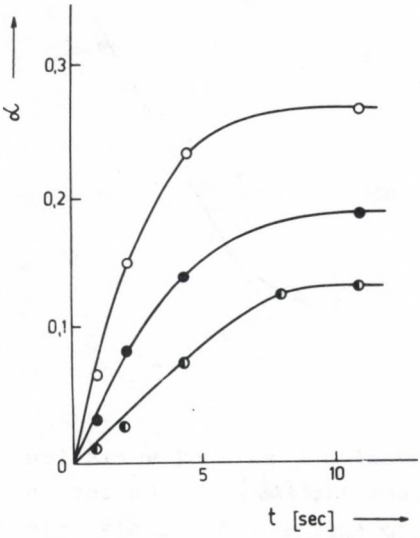

Fig.2. Variation of the electrooptic effect α with the time ○ - electric field 510 V/cm., ◐ - electric field 380 V/cm., ● - electric field 225 V/cm - controll pulse of duraction 20 msec.

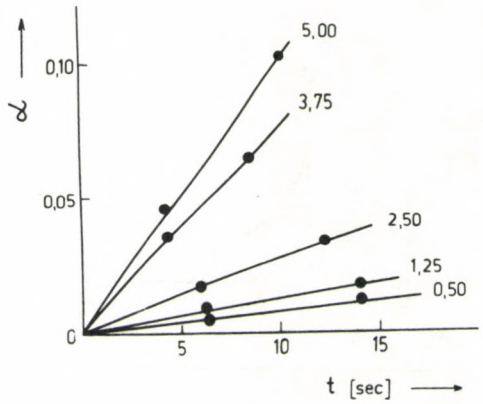

Fig.3. Time dependence of the electrooptic effect α at various concentrations of the flocculating agents - C_{FA} in % . Electric field 380 V/cm.

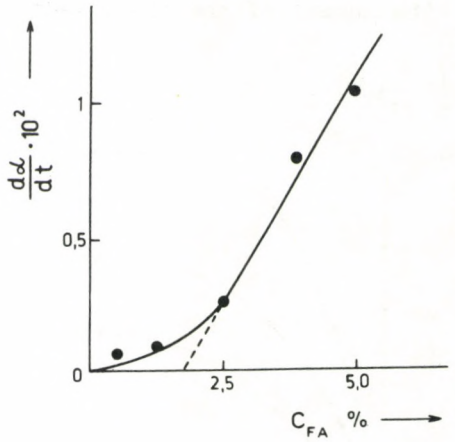

Fig.4. Dependence of the rate of variation of the electro-optic effect $d\alpha/dt$ on the concentration of the flocculating agents - C_{FA} . Electric field 380 V/cm of duration 8 sec.

Group II/4
Rheology

THE MODIFICATION OF THE ELASTIC BEHAVIOUR AND THE INTERPRETATION OF THE INTERPARTICULATE INTERACTION OF STRUCTURED SUSPENSIONS

K. Strenge and H. Sonntag

Zentralinstitut für physikalische Chemie,
Akademie der Wissenschaften der DDR,
DDR-1199 Berlin, Deutsche Demokratische Republik

A dispersion, which is sufficiently concentrated to build up a continuous structure throughout the complete volume under the action of attractive forces existing between the particles is called a structured dispersion, or coagulation structure.
There are various models possible in order to represent the nature of such a structure. For spherical particles three configurations are proposed:

a) all particles are arranged in a statistical network of chains

b) some dense floccs or clusters of particles are bonded by longer chains of particles

c) the spheres are surrounded by a thick, rigid layer of the solvent or of an adsorbed species in such a way that a dense packing of these "effective" particles fills the complete volume. (The apparent volume fraction of such a structure is appr. 0.7)

Fig. 1 shows the two-dimensional analoga of these three models for an area fraction of $\phi_a = 0.22$ (ϕ_a = area of all particles/total area). The number of particles is the same in all three cases.

Im a small constant stress (P < yield stress) acts upon such a structure, a small deformation (γ) will be measured. For

this purpose we used a very sensitive cone-plate arrangement with an air bearing for the main shaft and special knife edge bearings for the application of the momentum /1/. The disperse phase in our dispersions was Aerosil 200 /2/, an amorphous silica with spherical nonporous particles, diameter 12 nm. The volume fraction was $\Phi = 0.04$ (4 % by volume).

Fig. 2 is an idealized plot of γ as a function of time (t). From this creep-plot we may calculate both the moduli of fast and of slow elastic deformation ($E_0 = P/\ _0$; $E_R = P/\ _R$) and a term which describes the Newtonian part (called the creep viscosity). The elastic deformation is a reversible one, as we can see at the time t_E (withdrawal of stress). Some authors /3, 4, 5, 6/ tried to find a correlation between the elastic stress-strain relation and the energy of the interparticulate interaction. We /3/ chose a structural model like that of fig. 1a and yielded the following first order approximation:

$$G_o = \frac{3 \cdot \Phi \cdot (D+d_o)\ \Delta V}{\pi \cdot D^3 \cdot \Delta d} \qquad (1)$$

(Φ = volume fraction of the disperse phase; D = particle diameter; d_o = distance of equilibrium between the surfaces of two particles).

In our explanation of the elastic behaviour, the modells in fig. 1a and 1b are similar. Only the fraction of particles which participates in the deformation is smaller in 1b.
To verify equ. (1) we at first estimated the attraction force in two different liquids at constant Φ and D (considering dispersion forces only) and obtained good agreement for the two calculated Hamaker constants (A) of the particles in the two liquids /3/. For the modulus we used the following equation:

$$G_o = \frac{A \cdot \Phi \cdot (D+d_o)}{8 \cdot \pi \cdot D^2 \cdot d_o^2} \qquad (2)$$

Another proof of the validity of our derivation was the determination of the correlation between G_o and Φ. Fig. 3

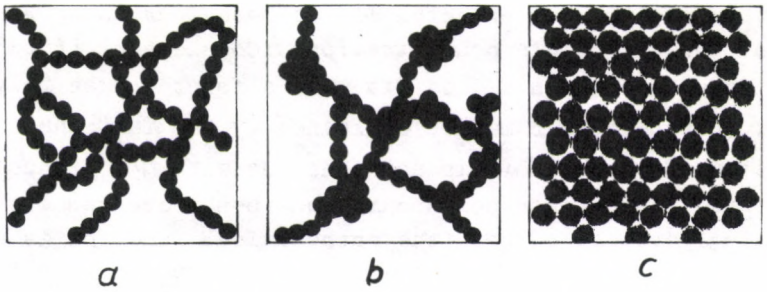

Fig. 1: two-dimensional analoga of the coagulation structure

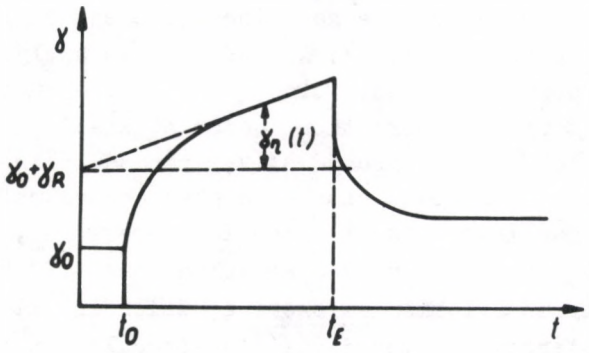

Fig. 2: idealized plot of γ as a function of time

shows the results. The expected linear behaviour is approximated at lower particle concentrations. Considering the whole set of data, we obtain a good fit with a fourth-order polynomial. This behaviour may be explained by the fact that the interaction force $\Delta V/\Delta d$ is not constant with ϕ, because the interaction between neighboured chaines increases with increasing particle number (the mathematical function is unknown).

In order to verify the dependence of G_o on the particle diameter D, we measured four different types of Aerosil with different particle sizes at constant ϕ. Assuming $D \gg d_o$ we obtain $G_o \sim 1/D^2$. Fig. 4 shows lg G_o as a function of lg D. A good fit for the four points is a straight with a slope of -3, that means, the experimental dependence is $G_o \sim 1/D^3$.

The dependence of G_o on $\Delta V/\Delta d$ has been explored by measuring dispersions in aqueous solutions of electrolytes and surface active agents /3, 7/. A quantitative analysis of the data is not possible at this time, because the theoretical derivations for the interaction forces at small distances are not available. An increase of V, induced by the decrease of the electrostatic repulsion at higher concentrations of electrolyte manifests itself by an increase in G_o, as was expected. The same is observed at an addition of the surfactant cetyl trimethylammonium bromide, which in diluted suspensions of Aerosil provoked visible flocculation (gelation) /7/. So we were able to proof that our model, based on energetic considerations, is in qualitative agreement with the experiments. Rehbinder and Ščukin /4/ used a pure entropic point of view for the interpretation of the elastic behaviour of bentonite suspensions. In the case of elastic deformations they postulated a rotation with simultanous drifting of one particle on another, and only considered the change of entropy of configuration. From these considerations they yielded:

$$G_E = 3 \cdot p \cdot k \cdot T \qquad (3)$$

$(G_E) = G_o \cdot G_R/(G_o+G_R)$; p = number of particles per cm^3;

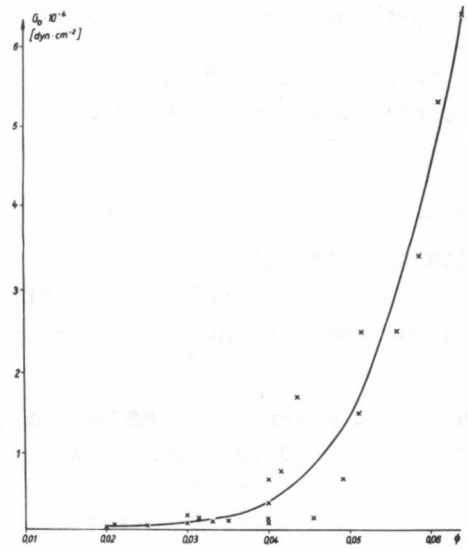

Fig. 3:
G_o-ϕ-relation,
experimental data
and fourth-order
polynomial fit

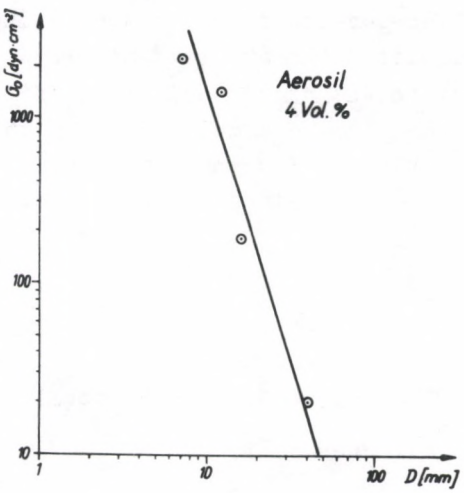

Fig. 4:
G_o-D-relation,
see text

k = constant of Boltzmann; temperature in degrees Kelvin).

This equ. (3) is in contrary to all experiences, because the elasticity of structured suspensions always depends on the environment, i.e., on the nature of the solvent, the concentration and nature of additives, the pH value. We can see that the entropic term of the deformation of structured dispersions must be small as compared with the energetic term. Part of the measured elastic deformation is, of course, of entropic origin. Later work should incorporate the entropic energy change as well.

An interesting paper concerning the interaction of particles in flocculated dispersions was published by Papenhuijzen /5/. For a dispersion of glycerol tristearate crystals in oil he supposed a structure similar to fig. 1b. For the case of small deformations he stated that the "deformation must be a result of possible rearrangements and reorientations in the chains of particles, without breakage of bonds, which is possible, when the chains are not completely stretched in the situation in rest". Assuming that only Van-der-Waals forces are acting between the particles, he calculated the apparent modulus "G" between two particles from the negative derivation of the V.-d.-W. force in respect to the distance, multiplied by the diameter of particles. By multiplying with the number of chains in the direction of shear he obtained a theoretical shear modulus of:

$$G_{th} = \frac{\Phi \cdot A}{6 \cdot \pi \cdot d_o^3} \qquad (4)$$

With $A = 2.10^{-13}$ erg; $\Phi = 0.07$ and $d_o = 10^{-7}$ cm he obtained

$$G_{th} = 7{,}5 \cdot 10^5 \text{ (dynes cm}^{-2}\text{)}$$

The experimental value for the dynamic storage modulus was:

$$G' = 2{,}5 \cdot 10^4$$

For a higher value of Φ ($\Phi = 0.2 - 0.3$) the differences bet-

ween theory and experiment are not as important. This behaviour is interesting, because we have experimentally verified that the volume fraction has no linear proportionality to G_o as assumed in equ. (2) and (4). Nevertheless with the parameters given by Papenhuijzen our equ. (2) permits a much better extimate of $G_o = 1{,}4 \cdot 10^4$.

A disadvantage of equ. (4) is the neglect of particle diameter, as the author himself states. The main value of the paper /5/ is in our opinion the attempt to interpret the flow part of the deformation-time plot.

Van den Tempel and coworker /6/ tried to calculate the stress-strain relation for a structured suspension under a load. They yielded for the modulus:

$$G_T = f_A \cdot 5 \cdot S^2 \frac{(1-\varepsilon_o)\cdot(1-\varepsilon)}{\varepsilon^3} \qquad (5)$$

with f_A = a constant describing the force between neighboured particles; S = surface of the particles per cm^3; ε_o and ε = porosity without load and with load. For very small loads $\varepsilon_o = \varepsilon$. With $\Phi = 1 - \varepsilon$ and $S = 6\,\Phi/D$, and if we substitute for f_A the V.-d.-W.-force

$$f_A = \frac{A \cdot D}{24 \cdot d_o^2} \qquad (6)$$

we obtain

$$G_T = \frac{15\,A \cdot \Phi^4}{2 \cdot D \cdot d_o\,(1-\Phi)^3} \qquad (5a)$$

Equ. (5) is derived for high values of Φ (porous sediment on a filter plate). Our results at much smaller Φ's cannot be interpreted by equ. (5).

To get an idea, if the structural model of fig. 1c is possible in our case (silica particles), we measured the relative viscosity (η_r) of diluted dispersions of Aerosil 200 /8/.

Despite some confused theories we obtained good experimental data for the $\Phi - \eta_r$ relation.

According to Arrhenius, Einstein and Happel /9, 10, 11/ we used the relation

$$\ln \eta_r = 5.5 \cdot \phi_{eff} \qquad (7)$$

From the apparent volume fraction (ϕ_{eff}) of the silica particles in water, and aqueous solutions of electrolytes (KCl, KOH, H_2SO_4) of concentrations up to 1 M we calculated a rigid layer with a thickness of approx. δ = 3 nm (with the Einstein coefficient = 2.5 we obtain δ = 5 nm). In this case the apparent volume fraction is appr. ϕ = 0.14, i.e., much below the value which is necessary for a structure like that of fig. 1c ($\phi \approx 0.7$).

Conclusion

At constant volume fraction the fast elastic behaviour of a structured dispersion of particles is beeing well described by our equ. (1) using the assumption of a three-dimensional network model of the structure. With this equation the experiments of /5/ also may be interpreted.

References

/1/ K. Strenge, Plaste und Kautschuk, in press

/2/ Aerosil, Degussa Druckschrift, Frankfurt/M., FRG

/3/ K. Strenge, H. Sonntag, Colloid & Polymer Sci. 252, 133 (1974)

/4/ E.D. Scukin, P.A. Rehbinder, Acta chimica Acad. Sci. Hung. 76, 381 (1973); Kolloid-Z. 33, 450 (1971)

/5/ J.M.P. Papenhuijzen, Rheol. Acta 11, 73 (1972)

/6/ E.M. Jager, M. Van den Tempel, P. De Bruyne, Proc. Koninkl. Nederl. Akad. Wetensch., Ser. B. 66, 17 (1963)

/7/ K. Strenge, H. Sonntag, Abh. Akad. der Wissensch. der DDR, Kl. Chemie, "IV. Intern. Tagung grenzflächenaktive Stoffe", 1974 Berlin, in press

/8/ S. Kophamel, Chemotechniker-Arbeit, Berlin 1975 (not otherwise published)

/9/ S. Arrhenius, Z. physikal. Chem. (Leipzig) 1, 285 (1887)

/10/ A. Einstein, Ann. Physik 19, 289 (1906); ibid. 34, 591 (1911)

/11/ J. Happel, J. Appl. Phys. 28, 1288 (1957)

DEFORMATION STRENGTHENING OF COLLOID AND POLYMER SOLUTIONS FILLED WITH AEROSIL

A.A. Trapeznikov and V.G. Taranenko

Institute of Physical Chemistry, USSR Academy of Sciences, Moscow

To study the composition and properties of greatly structured colloid and polymer systems, including those containing a filler, rheological methods have proved to be highly useful. They have found wide application in our laboratory when used at the stage of deformation we have termed pre-stationary /1,2/. This stage has proved to be of particular interest and importance since it is where the principal changes in the structure occur, which determine the further behaviour of the system in a stationary flow. In addition, the pre-stationary stage of deformation is of significance by itself in many technological processes.

Apart from the methods of unidirectional deformation employed previously, this research made use of the methods of periodic deformation and its superposition on unidirectional deformation by means of a device described in /3/. Such methods have recently been applied by other investigators as well /4,5,6/, but in our investigation we succeeded in establishing a number of new interesting properties of the structure of filled systems related to insufficiently studied phenomena of rheopexy in the case of thixotropic restoration and deformation strengthening. A study was made of the gels of aluminium naphthenate (AN) (corresponding approximately to disubstituted soap) in medical vaseline oil (MVO) and polyisobutylene (PIB), $M = 2.3 \cdot 10^6$) in tetradecane (TD) and of the same systems with aerosil of the trade mark 300 added to them.

The periodic deformation method was used to measure the dynamic shear modulus G' and viscosity η' (the real parts of the complex magnitudes), depending on the angular frequency ω and the magnitude of the amplitude. The resultant data for G' of 6% gel of AN in MVO at different temperatures are given in Fig. 1a, while Fig. 1b shows the dependence of reduced G'_{red} on reduced ω_{red}. The reduction was carried out after Ferry's method /7/ worked out for polymers. It comes to a shift of the curves in logarithmic coordinates along the axis of the abscissae by magnitude a_T. It is evident from Fig. 1b that all the data for the different temperatures (ignoring the change in the density of the system) can be plotted on one curve, which points to the possible application of such a method to a colloid system in which the thickener has a polymer structure which, however, may disintegrate in view of the comparatively weak coordination bonds in the main chain.

Addition of the filler (air-dry aerosil, dried at 120°C, together with the addition of hexyl alcohol, the surfactance) raises G' and η' as well as the viscosity of the stationary flow $\eta = P/\dot{\gamma}$, where P is the stress of the stationary flow and $\dot{\gamma}$ is the deformation rate. It was possible to ascertain for 6% gel of AN in MVO with addition of 8% aerosil that the magnitude of G' increases in the course of development of unidirectional deformation until the stationary flow is settled, which points to some strengthening of the system. In spite of the regular, though not very great, lowering of η with a rise in $\dot{\gamma}$ at a certain range of $\dot{\gamma}$ (Fig. 2, curve 2), the magnitude of G' increases with a rise in $\dot{\gamma}$ up to some $\dot{\gamma} = \dot{\gamma}_{P_{r_o}} \equiv \dot{\gamma}_{G'_{max}}$ above which, G' on passing over the maximum, it begins to decrease (Fig. 2, curve 3). It is worth noting that the maximum of strength P_r does not appear on the stress-deformation curve $P(\gamma)$ at each $\dot{\gamma} < \dot{\gamma}_{P_r}$. This is due to the fact that two processes occur simultaneously in the system: breaking of the structure, which brings about a general lowering of η, and a strengthening of the structure which raises G'. These processes come into equilibrium when the stationary flow is settled and consequently there emerges no maximum. When $\dot{\gamma}$ passes over $\dot{\gamma}_{P_{r_o}}$, the maximum P_r

appears on curve $P(\gamma)$, which indicates that despite the increase in G' and the strengthening of the structure at the pre-stationary stage, breaking of the structure begins to predominate, which results in the appearance of P_r. This relationship can be seen from Fig. 2, curve 4 which, in addition to dependences $G'(\dot{\gamma})$ and $\eta(\dot{\gamma})$, also shows the dependence $\Delta P = P_r - P_s = f(\dot{\gamma})$ appearing at $\dot{\gamma} > \dot{\gamma}_{P_{r_o}}$. Curve 1 defines the dependence $\eta(\dot{\gamma})$ for a 6% naphthenate gel. This result is important since it may account for the considerable preponderance of P_{r_o} over P_k, formerly observed in many filled systems, which corresponds to the beginning of breaking of the structure and the early lowering of viscosity.

One of the highly interesting properties of filled systems on the base of AN in MVO and PIB in TD is their capacity for accelerated rheopectic (after Freundlich) thixotropic restoration of the structure which changes over to strengthening and a capacity for a more or less quick relaxation of the strengthened condition. It has already been noted in the papers of our laboratory / 8/ that the term rheopexy, introduced by Freundlich and Juliusburger /9/ refers to thixotropic accelerated restoration of a broken structure under the influence of slight deformation (sign-changing rotation of a test tube between the palms of the hands, as described in Freundlich's works). This term was, however, later applied by many investigators to other phenomena, e.g. only to the rise of viscosity under the influence of deformation even in diluted polymer solutions, while the actual phenomenon of rheopexy, as defined by Freundlich, was not analysed and the quantitative methods for it were not described. Yet precisely such a property of the systems was demonstrated in /10/, proceeding from a study of the development of stress at the pre-stationary stage of deformation.

These experiments demonstrated, first of all, a similar phenomenon on other systems, and, secondly, a further transition of the system into a strengthened condition, the recording of the change in the properties being made after G'. Both systems under investigation, subjected to deformation at com-

paratively high $\dot{\gamma}$ =const, as for example 53 sec^{-1} or at a high rate of periodic deformation $\xi = \gamma\omega$, undergo an extensive breaking of the structure. This can be judged from the greatly lowered G' in the course of such deformation. If the latter is discontinued ($\dot{\gamma} \to 0$, $\xi \to 0$), there occurs a practically "instantaneous" (in two to three minutes required for measurement) thixotropic restoration of the structure to some limit. This is illustrated by the vertical sections of the lower curves 1 in Figs 3a and 3b. It is followed by slow thixotropic restoration of the structure along curves 1, which lasts many hours up to some limit. Thus, complete thixotropic restoration of the structure proceeds in both systems at a very slow speed. If, however, a system with a broken structure is subjected to unidirectional deformation at low $\dot{\gamma}$, restoration of the structure is greatly accelerated. This is evident from Figs 4a and 4b which pertain to PIB in TD containing aerosil. Curve 1 shows the growth of $P(\tau)$ at $\dot{\gamma}$ = 0.042 sec^{-1}, obtained for a system deformed both immediately after high $\dot{\gamma}$ = 53 sec^{-1} and after 20 minutes of rest or after a longer period. The coincidence of such curves for different periods of rest implies that the latter practically does not affect the intensity of growth of $P(\tau)$, i.e. when at rest, the system is practically not reduced. It follows from curve 1 which reflects the increase in P in the course of deformation, that complete restoration (up to equilibrium) continues for approximately 30 minutes, while the growth of P up to the same equilibrium P_s at repeated deformation (Fig. 4a, curve 2) takes only 12 seconds. This attests that, as a matter of fact, prolonged rest does not lead to a restoration of the structure. Hence, there is acceleration of thixotropic restoration of the structure upon careful deformation, and this manifests the true Freundlich rheopexy effect. However, the latter quantitatively relates not to the whole increment on G' on curve 1 of Fig. 4b. It should also include the initial part of the steep rise of G' on this curve up to a magnitude approximately equal to $4.8 \cdot 10^3$ dynes/cm^2, which corresponds to the extremity of the curve of thixotropic restoration for 15 hours (Fig. 3, curve 1). A further greater

increase in G' up to a magnitude of $8.4 \cdot 10^3$ dynes/cm^2 is related to deformation strengthening of a structure not envisaged by rheopexy.

This follows from a comparison between curves 3a and 3b which display a very considerable difference between the AN and PIB systems at the given degrees of filling with aerosil. It follows from curve 2, Fig. 3a that the strengthened condition of a system with AN is characterized by the magnitude $G' \approx 8 \cdot 10^3$ dyne/cm^2. However, this magnitude attained in a state of unidirectional deformation at $\dot{\gamma} = 0.035$ sec^{-1} rapidly diminishes at rest and gradually comes down to the ultimate value which was reached upon thixotropic restoration at rest. Consequently, this system comes spontaneously to an equilibrium non-strengthened state, which shows that the weakening proceeds in measurable time. In contradistinction, a system with filled PIB retains its strengthened condition (curve 2, Fig. 3b) for an indefinitely long time, without reverting to the equilibrium thixotropic-restoration state. A comparison between the two systems proves to be of considerable interest since it graphically corroborates their similarity in some properties and the difference in others. The phenomenon of strengthening, measured by viscosity upon deformation of greatly filled systems, is described in /11/.

The behaviour of the systems can be explained by the fact that the polar particles of aerosil in the initial system are in a state of some aggregation and that the entire system consists of sections of soap and aerosil aggregates with soap or polyisobutylene molecules adsorbed over their surface. The connection between the particles in the aggregate can be effected through hydrogen bonds between the surface hydroxyls or through adsorbed water molecules, as well as under the action of the van der Waals dispersion forces between the particles. Deformation is, on the one hand, accompanied by breaking of the bonds between the particles and the soap or polyisobutylene molecules, and on the other hand, by disintegration of the aerosil aggregates. A more uniform distribution of the aerosil particles may lead to a greater shear modulus. This more uniform distribution is equivalent

to an increase in the number of the finer aerosil chains in the lattice formed by the aerosil. The difference in the behaviour of the two systems is probably due to the fact that the soap molecules which contain polar groups are more surface-active in relation to aerosil. For this reason the blocking of the aerosil particle bonds proceeds more intensively and the connections between them in the new strengthened condition prove to be weaker. That is why the strengthened condition quickly relaxes at rest toward a non-strengthened one. In a system with PIB, which is non-polar, the blocking of the aerosil particles is weaker and therefore the strengthened condition is preserved for a long time. It is likely that in the course of unidirectional deformation the polymer molecules stretch and may break away from the aerosil particles which, when exposed, interact to a greater extent. As the polymer is non-polar, the polar lattice formed of the aerosil particles remains more stable. These processes of change in the structure are equivalent to some peptization of aerosil aggregates upon deformation and subsequent coagulation at rest, as well as to a change in the conformation of polymer molecules in deformation which is manifested in some stretching.

REFERENCES

1. A.A.Trapeznikov, Vestn. AN SSSR, 6, 70 (1960); Zh. fizich. khimii, 41, 1247 (1967) (Russ.).
2. A.A.Trapeznikov, T.G.Shalopalkina, Kolloidn. zh., 25, 703 (1963) (Russ.).
3. A.A.Trapeznikov, V.G.Taranenko, Kolloidn. zh., 36, 409 (1974); 36, 1002 (1974) (Russ.).
4. T.Kotaka, K.Osaki, J.Polym.Sci., c15, 453 (1966).
5. J.M.Papenhuijzen, Rheol. Acta, 10, 493 (1971).
6. M.G.Tsiprin, L.A.Faitelson, Mekh. polimerov, № 5, 913 (1970) (Russ.).
7. J.D.Ferry, Visco-elastic Properties of Polymers, N.Y.-London, Wiley a. Sons, Inc., 1961.

8. A.A.Trapeznikov, Report to IV International Conference on Surface-Active Substances, Berlin, December 2-5, 1974 (Russ.).
9. H.Freundlich, F.Juliusburger, Trans. Far. Soc., 31, 920 (1935).
10. T.G.Shalopalkina, A.A.Trapeznikov, Kolloidn. zh., 35, 715 (1973) (Russ.).
11. T.G.Shalopalkina, Kolloidn. zh. 35, 1017 (1973) (Russ.).

Fig. 1

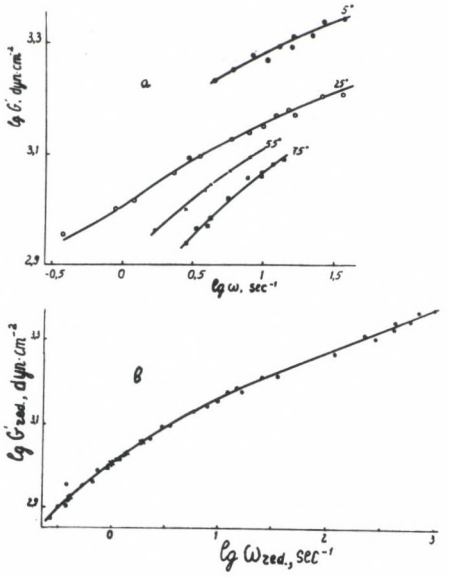

Fig. 2

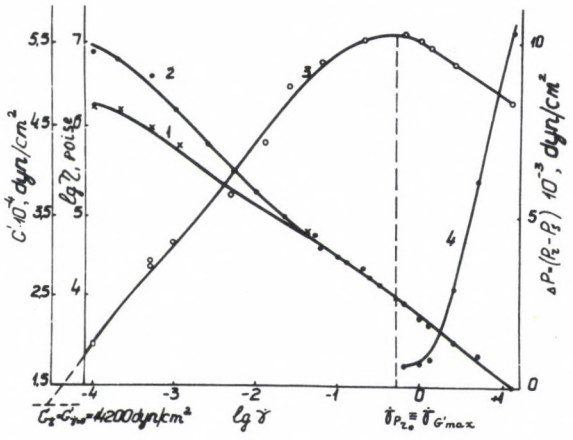

Fig. 3

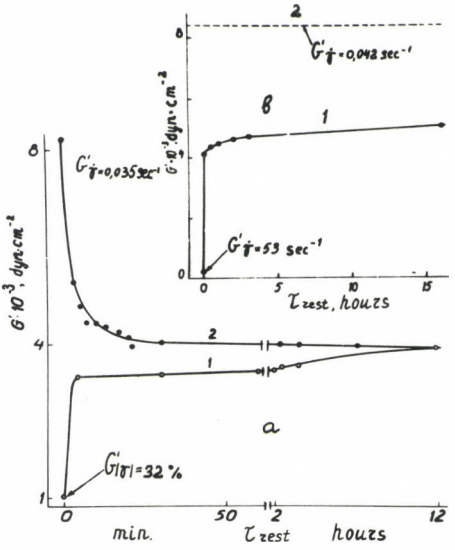

2
$G'_{\dot\gamma}=0{,}042\ sec^{-1}$
в
1
$G'_{\dot\gamma}=0{,}035\ sec^{-1}$
$G'_{\dot\gamma}=53\ sec^{-1}$
$G'\cdot10^{-3}$, dyn·cm^{-2}
τ_{rest}, hours
$G'_{|\gamma|}=32\ \%$
a
min.
τ_{rest}
hours

Fig. 4

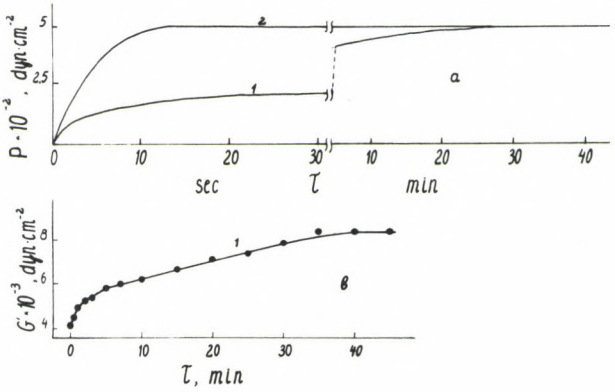

$P\cdot10^{-2}$, dyn·cm^{-2}
a
sec
τ
min
$G'\cdot10^{-3}$, dyn·cm^{-2}
в
τ, min

SEDIMENTATION AND RHEOLOGICAL PROPERTIES OF FLOCCULATED KAOLINITE SUSPENSIONS

M.Gilde, F. Szántó and B. Várkonyi

Department of Colloid Chemistry, József Attila University, 6720 Szeged, Hungary

Many research workers have recently dealt with the interaction of macromolecular flocculants and solid particles, and with the problem of the destabilization of the suspensions /see e.g. 5/. This topic is of great practical importance. The joint effect of electrolytes and flocculants is known, but few quantitative data are available with regard to the dimensions and structure of the flocs. The evaluation method of Michaels and Bolger /1/ was applied in our earlier work to kaolinite suspensions coagulated with electrolytes /3/. The aim of the present work was to extend these investigations to the effect of macromolecular flocculants, and to supplement them with the study of their effect on the rheological properties of concentrated suspensions.

The sodium kaolinite used contained particles smaller than 2 μm, and was obtained from Zettlitz kaolin /6/. Sedimentation was examined in calibrated tubes, and rheological measurements were made in a rotation viscometer. Flow curves were recorded in the rate of shear interval D=0.162...2 620 sec^{-1} . The temperature of measurement was 22 ± 1° C. The zeta potentials of the suspensions were determined with an electroosmosis measurement method.

A macromolecular compound based on acrylamide, Floconit-E / Nitrokémia, Hungary /, was used as flocculant. Ultracentrifugation examination gave a molecular weight of 420 000, while viscometric measurements led to an average end-to-end distance of 1 500 Å.

Results and Discussion

Without addition of electrolyte, the Na-kaolinite was a well-disaggregated, stable suspension, which sedimented out diffusely and slowly. Even 10 mmole/l NaCl led to a well - perceptible boundary in the suspension, the sedimentation of which could be followed. When the concentration of the suspension was varied in the volume fraction /Ø/ interval 0.0019...0.0077 sedimentation curves of various types were obtained /Fig. 1./:

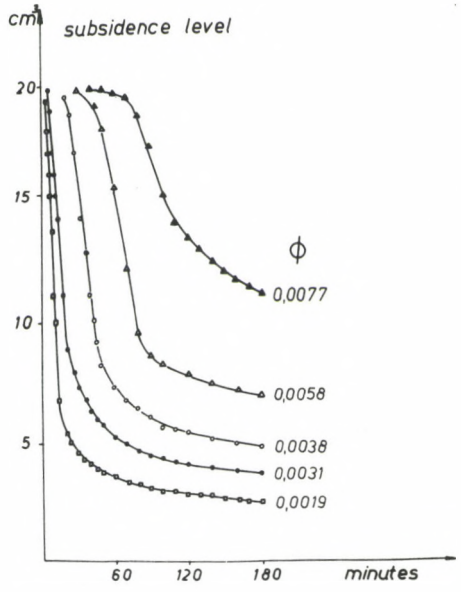

Fig. 1.

Sedimentation curves of Na-kaolinite suspensions with various concentrations Ø /NaCl concentration 20 mmole/l/

Rapid sedimentation began when aggregates developed in the system. The well-sedimenting aggregates appeared within a short time at low suspension concentration, but a longer time was necessary at higher concentration. The process was reproducible. The Michaels-Bolger relationship /1/ was used to characterize the aggregates, and the average size of the aggregates /$\bar{d}_A$/ and the water-solid ratio within the aggregates /C_A/ were calculated. $C_A \equiv Ø_A/Ø_K$, where $Ø_A$ is the volume of the aggregates, and $Ø_K$ the volume of the solid in the aggregates.

Table I.

Structural parameters obtained from settling rate data

NaCl mmole/l	c_A	$\bar{d}_A$ μm
10	55	110
20	66	140
50	70	170
100	87	190

Table II.

Value of the zeta potential at various NaCl concentrations

NaCl mmole/l	ζ mV
0	-31
10	-25
15	-21
20	-18
50	-12
100	- 4

It can be seen that with the increase of the NaCl concentration the aggregates which form are increasingly larger and more loosely packed /Table I./. The aggregation is correlated with the change in the zeta potential /Table II./. The results show that even at a NaCl concentration of 100 mmole/l there was no formation of a face-to-face card-pack structure, as was observed by Michaels and Bolger in a kaolin suspension at pH 9, coagulated with NaCl /1/.

Floconit-E itself did not bring about flocculation in the dilute suspension. Flocculation could be achieved only if the zeta potential of the particles, and thus the stability of the suspension, were first decreased. This effect was ensured with NaCl. Sedimentation was studied at NaCl concentrations of 10, 15 and 20 mmole/l, and Floconit-E concentrations of 2 and 6 mg/l. The suspension coagulated at all three electrolyte concentrations. The average end-to--end distance in the Floconit-E did not fall below 1 000 Å (at 10 mmole/l 1 200 Å, and at 20 mmole/l 1 050 Å). This is

of great significance from the aspect of the effectivity of the macromolecule /4/. As an example, the sedimentation curves obtained at NaCl and Floconit-E concentrations of 10 mmole/l and 2 mg/l, respectively, are shown in Fig. 2.

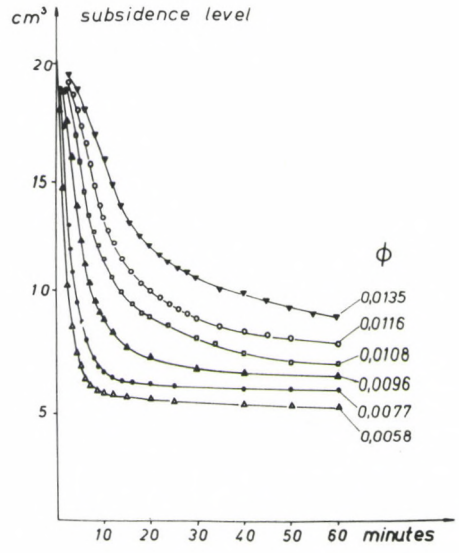

Fig. 2.

Sedimentation curves of flocculated Na-kaolinite suspensions with various concentrations Ø (10 mmole/l NaCl, 2 mg/l Floconit-E)

After addition of the macromolecule, the flocs developed during the period of homogenization. The calculated $\bar{d}_A$ and C_A values are listed in Table III.
More compact and larger flocs were thus formed in the presence of the macromolecule than merely on the action of NaCl. The optimum effect was found at NaCl and Floconit-E concentrations of 20 mmole/l and 2 mg/l, respectively.

Table III.

Structural parameters obtained from settling rate data

NaCl mmole/l	Floconit-E mg/l	C_A	$\bar{d}_A$ /µm/
10	2	41	380
15	2	40	320
20	2	22	490
10	6	44	390
15	6	24	300
20	6	17	180

Characteristic differences could be observed in the structures of the sediments formed on the action of NaCl, or the joint action of NaCl and macromolecule. In the former case the aggregates were stratified horizontally in the sediment and there were no interstices between them. In the latter case the sediment itself had a loose structure, and liquid was included in the space between the flocs. In spite of this, the volume of the sediment was smaller than that of a sample coagulated with NaCl alone. This is possible only if the flocs themselves are more compact than in the presence of NaCl alone.

The rheological examinations were made with suspensions of 0.155 volume concentration . A study was made of the flow curves of samples containing various amounts of NaCl, or Floconit, or NaCl and Floconit together. Besides the area of the hysteresis loops and the τ_B values, the "residual" yield stresses /τ_B'/ obtained by extrapolation from the descending branch of the flow curves were established.

The yield stress of the Na-kaolinite suspension is low. Even at NaCl concentration of 10 mmole/l the τ_B value increases significantly, and exhibits a tendency to rise with the increase of the electrolyte concentration /Table IV./.

Table IV.

Rheological parameters of concentrated suspensions coagulated with NaCl

NaCl mmole/l	τ_B dyne/cm^2	τ'_B dyne/cm^2	Hysteresis loop area cm^2
0	70	30	5
10	270	180	18
20	250	200	12
50	280	210	14
100	430	350	15
150	470	420	14

The area of the hysteresis loop is the greatest at the lowest electrolyte concentration; it then decreases and becomes nearly constant. The structure is thus readily reformed after shear. The τ'_B values show that this regeneration tendency increases with the rise of the electrolyte concentration.

In the concentrated suspensions the macromolecular flocculant proved effective itself /Table V./. This indicates that the Floconit-E is able to adsorb on even the kaolinite particles with maximum zeta potential. The flocculating effect was observed to increase with increase of the Floconit-E concentration up to 150 mg/l. At concentrations higher than this the effect decreases.The size of the hysteresis loop varies with the increase of the flocculant concentration according to a maximum curve. τ'_B is considerably smaller than τ_B.

Table V.

Rheological parameters of concentrated suspensions flocculated with Floconit-E

Floconit-E mg/l	τ_B dyne/cm^2	τ'_B dyne/cm^2	Hysteresis loop area cm^2
2	130	60	11
6	210	120	20
12	220	120	20
20	250	130	30
50	270	120	38
100	330	120	58
150	540	140	82
175	450	80	58
200	160	80	16
250	170	80	20
300	160	70	21

This suggests that as a result of the shear some of the bonds break, and the bulk of the macromolecules use their adsorption-active groups to bind to only one particle /2/. This is in agreement with the finding of Rohrsetzer /7/ that the adsorption may be irreversible as regards the whole macromolecule, but reversible as regards the individual segments. Study of the electrolyte-flocculant combinations showed that the presence of the electrolyte did not cause a significant flocculation increase in the case of the concentrated suspension.

References

1. A. S. Michaels, J. C. Bolger, Ind. Eng. Chem. Fund., 1, S 24 /1962/.
2. G. Y. Fleer, J. Lyklema, Proc. 5th Int. Congr. Surf. Activ. Sub. Barcelona B. S 247 /1968/.
3. M. Gilde, F. Szántó, Bull. Hung. Geol. Soc. 99, S 60 /1969/.
4. R. W. Slater, J. P. Clark, J. A. Kitchener "Proceedings of the British Ceramic Society" S 1 June 1969.
5. J. A. Kitchener, Polym. J. 4, S 217 /1972/.
6. F. Szántó, M. Gilde, Acta Phys. et Chem. Szeged, 19, S 183 /1973/.
7. S. Rohrsetzer, Dissertation, Budapest, S 86 /1973/.

STRONG ELECTRIC FIELD INFLUENCE ON RHEOLOGICAL PROPERTIES OF DISPERSE SYSTEMS

U. F. DEINEGA, N.YAK. KOVGANICH

INSTITUTE OF COLLOID CHEMISTRY AND CHEMISTRY OF WATER, ACADEMY OF SCIENCE OF THE UKRAINIAN SSR, KIEV, USSR

Strong electric fields permit to change cardinally the structure and properties of a disperse system. Depending on charge and polarizability of the particles the field strength in hydrocarbon disperse systems extraodinary various phenomena are observed. Orientation of anisodiametric particles, particle movement to one or two electrodes (electrophoresis, double electrophoresis), interelectrode reciprocal or rotational movement of the particles, particle interaction leading to the structural formation also can be observed in diluted systems.

The compression of structural frame at one electrode and separation of disperse medium at other one, interelectrode extending and compression of structural frame with the formation of near wall layers of disperse medium simultaneously at both electrodes, strengthening of structural frame can be possible in concentrated disperse systems/1/. All these changes of a structure substantially influence physical and mechanical properties of disperse systems.

Strong electric fields can either increase or decrease the strength of limit and effective viscosity of disperse systems. Any phase separation in electric field leads to decreasing of system resistence to deformation. This schematically is showed in the figure 1.

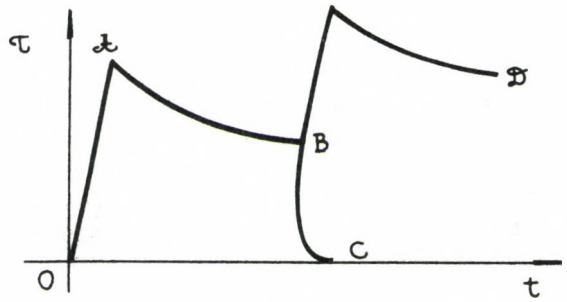

Fig. 1. The electric field influence on rheological properties of plastic disperse systems.

Here it is given the kinetics of the development of the shift strength (τ) under the constant rate of deformation for soap (plastic) lubrications in rotary plastoviscosimeter - condenser.

The curve OAB was received without electric field. After transition through the limit of strength at the A point the shift stress falls up to the established value. If there is more or less considerable potential jump in the system at the boundary of interface then electrokinetic phenomena appear. The shift stress falls sharply (curve BC) as a result of the phase separation and the formation of near wall layer of disperse medium.

Another picture is observed for the system in which polarization phenomena play an main role. In this case the shift stress sharply is growing (curve BD) as a result of polarization interaction of disperse phase particles. After the transition through the limit of strength the steady flowing conditions are established. Effective viscosity in the electric field for each system is considerably higher than initial one.

The phenomenon of rapidly reverse increasing of viscosity

under the influence of electric field gained the name of electrorheological effect(ERE) /2/. The possibility of considerable increasing of the viscosity (by 10^2 - 10^3 times) with the help of electric field determines both scientific and practical interest to this effect. At present the number of general rules of electrorheological effect development is established. Electrorheological effect dependence on electric field stress, deformation rate, disperse phase concentration, temperature are investigated. The search of new electrorheological systems is under way. The regions of practical use of electrorheological effect is being determined, namely in frictional clamps, locking and other devices.

Investigation of electrorheological effect nature is one of the most important questions of electrorheology of disperse systems. Viscosity increase of disperse systems in electric field can be connected with anisodiametric particle orientation /3/, double electric layer deformation /4/, interelectrode circulation /5/, particle interaction/6/

Structural formation in electric field is the most important cause of viscosity increase. Dielectric polarization that is induction of dipole moments within disperse phase particles is the base factor in particle interaction. Arising chain aggregates is usually connected with ionic polarization of the atmosphere in polar medium. In unpolar medium, namely in hydrocarbons in which the charge concentration is very small, film and macrostructural polarization plays an important role /7/.

Structure influence of disperse phase on the electrorheological effect was investigated on hydrocarbon dispersions of a soap, clay minerals, polymers. In case of use of higher fat acid salts - miristic, palmic, stearic, begenic acid the viscosity increase in electric field is not observed.

System behaviour in electric field is sharply changed when hydroxylic groups are introduced in hydrocarbon chain of an acid. In this case electrorheological effect develops, dispersion of dielectric constant (ε) in the radio frequency range and the change of during the shift(rheoelectric effect) are observed.

The formation of hydroxylic group chains, connected by hydrogen bonds, in volume or on the surface of disperse phas se plays an important role in the change of particle polarization of hydrocarbon medium. By such chains in electric field proton migration is possible. This migration stipulates high polarizability of the systems with cooperated hydrogen bonds /8/.

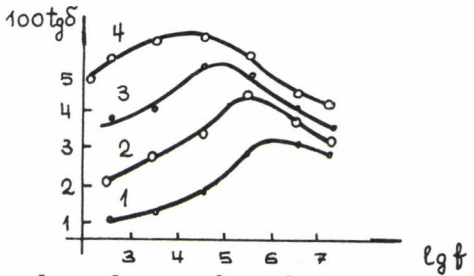

Fig. 2. Frequency dependance of angle tangent of dielectric loss for solid solutions of sodium recinolat and stearat 1-100% NaRi;2-75% NaRi;3-50% NaRi;4-25%NaRi

Figure 2 shows the influence of hydroxylic chain length on dielectric dispersion of solid solution of sodium recinolat and stearat. The curve of dispersion shifts to the region of high frequencies with the increase of the concentration of sodium stearat. This is stipulated by the decrease of chain lengthes of associated groups in soap crystallites the result from the "delution" of sodium recinolat by sodium stearat and consequently decreasing of relaxation time.

The role of water in polarization and structural formation of soap dispersions was studied on hydrated calcium salts of high fat acids. Water penetrates into the crystal stucture during its formation when calcium soaps are formed on mixtures of fat acids of different molecular weight. This stipulates high polarizability of such soaps. With the increase of difference in hydrocarbon radical length of soaps the dispersion curve shifts to the range of low frequencies (Fig. 3).

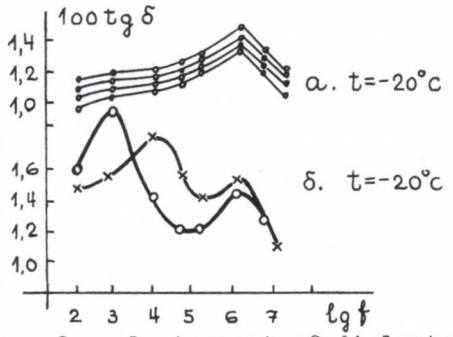

Fig. 3. Frequency dependance of angle tangent of dielectric loss for calcium soaps on the base of acid mixtures
1). $CaMi_2$;2). $CaPt_2$;3). $CaSt_2$;4) $CaBe_2$
5). $CaLa_2$+$CaMi_2$+$CaPt_2$+$CaSt_2$+$CaBe_2$.
6). $CaMi_2$+$CaPt_2$+$CaSt_2$.

This can be explained by growing of the chain length of water molecules, included in the crystal structure of soaps and by the increase of relaxation time of heat proton polarization. The more soap polarizability the stronger electrorheological effect develops in the systems with hydrated soaps on the base of acid mixtures.

Similar influence is shown on electrorheological and dielectric properties by hydration of hydroxylic contained disperse phases (silica, natural polymers, clays). Transition of water from free state to bonded one is accompanied by ordering of water structure at the expence of interaction of water molecules with the surface and also with each other on hydrogen bonds /9/. The formation of such

surface associates of water molecules stipulates the $\mathcal{E}$ curve shift of hydrated compounds to the region laying between 10^{10} and 10^{5}hz that is between water and ice /10/.

It is necessary to note that proton polarization and electrorheological effect are possible in the systems in which absorbed layers are formed by the molecules with polar groups, for example, aminogroups capable to form hydrogen bonds.

The influence of moisture of disperse phase on electrorheological effect is shown in Figure 4 for a starch suspension in hydrocarbon medium.

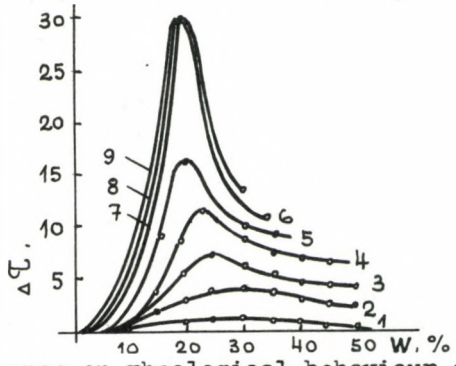

Fig. 4. Hydratation influence on rheological behaviour of starch suspension in electric field.
1-4kv/cm;2-8kv/cm;3-12kv/cm;4-16kv/cm; 5-20kv/cm;
6-24kv/cm;7-28kv/cm;8-32kv/cm;9-36kv/cm.

With the increase of starch hydratation the strength limit is increasing receiving maximum, and then falls. The higher field stress the maximum of strength limit is observed under smaller humidity. The fall of structure strength above critical values of humidity and electric field stress is connected with sharp growing of electric conductivity of the system and as a result of this with the decrease of polarization interaction of the particles.

So the investigation of the influence of disperse phase on electrorheological effect shows that proton polarization

and conductivity have an important significance for the particle polarization and structure formation in hydrocarbon media. This opens interesting possibilities for the creation of new highly effective electrorheological systems.

REFERENCES

1. Ю.Ф.Дейнега, Г.В.Виноградов, ДАН СССР, 174, 398(1967).
2. G.V.Vinogradov, Yu.F.Deinega, J. Inst. Petroleum, 52, 279 (1966).
3. З.П.Шульман, Ю.Ф.Дейнега, Р.Г.Городкин, А.Д.Мацепуро, "Электрореологический эффект", Изд. "Наука и техника", Минск, 1972.
4. C.E.Chaffey, S.G.Mason, J.Coll.Sci. 19, 525(1964); 20, 330 (1965); 27, 115(1968).
5. D.L.Klass, T.W.Martinek, J.Appl.Phys. 38, 67,75 (1967).
6. В.Н.Шилов, Ю.Ф.Дейнега, "Электронная обработка материалов", № 2, (1974).
7. W.M.Winslow, J. Appl. Phys. 20, 1137 (1949).
8. С.С.Духин, В.Н.Шилов "Диэлектрические явления и двойной слой в дисперсных системах и полиэлектролитах", Изд. "Наукова думка", Киев, 1972.
9. Дж.Пиментел, О.Ма-Клеман "Водородная связь", М..1964.
10. А.В.Думанский "Лиофильность дисперсных систем", Изд. АН УССР, Киев, 1960.
11. B.Jacobson, J.Amer.Chem.Soc. 77, 2919 (1955).

ELECTRO-RHEOLOGICAL INVESTIGATION OF SUSPENSIONS

Dárdai, Z. - Ms. Magyarits, A.

Research Laboratory of Applied Chemistry and Colouristics, 1390 Budapest, P.O.B. 182, Hungary

Aqueous suspensions are widely used in industrial practice. In many instances application takes place in electric field. The electrophoretic painting process is one of the most popular field of application. Although the appropriate rheological state is a substantial precondition of usability, many problems have to be solved in regard of the electrorheological investigation of aqueous suspensions

Experimental

In the course of our work the dependence of the viscosity of aqueous suspensions upon the electric field and pH-value of the medium have been investigated. Considering the complexity of systems applied in the industry /broad spectrum of particles size distribution, application of various auxiliary agents, etc/ we made use of model systems comprising the essential components determining the rheological character, however, at the same time secondary processes affecting the results of measurements have been eliminated within the bounds of possibility.

Aqueous suspensions of Rutile TiO_2 have been studied. The pigment consisted 99,3 per cent of Rutile TiO_2, particle size varied between 1 to 3/um. The starting suspension medium had a conductivity of 3/uS. Suspensions have been prepared on a ball--mill; pH-values of the suspensions have been adjusted immediately before application with hydrochlorid acid and sodium hydroxide of analytical grade.

Stability of the suspensions was determined by measuring of settling volumina. Glass settling tubes have been used with metal bottom, a perforated electrode with dimensions corresponding to the surface of the bottom plate was attached to the upper part of the tube.

We employed the following field intensities: 0; 1.5; 4.5; 6.0 V/cm.

The dependence of electrophoretic migration speed of the pigment investigated upon the pH-value was measured in order to evaluate rheological changes. The measurements based upon the well-known "U" tube process. Platine electrodes were employed to prevent ion dissolution. An overlayered fluid the conductivity of which is identical with that of the suspension medium is a precondition of accurate measuring; this was obtained by centrifuging of one part of the suspension.

A modified rotation viscosimeter of Rheotest Type was employed to our electrorheological measurements. Rotor and cuvette were electrically isolated, an electric field was formed between them by means of an external supply unit. Rotor was the cathode in all instances. Field intensity was continuously varied from 0 to 10 V/cm.

Experimental results

In the course of our measurements in order to determine settling volumina practically no changes of settling volumina could be observed in the acidic and neutral pH domains.

A sudden change of the settling volumen occurs in alkaline pH domains. Above pH = 12 measurements became uncertain due to heavy peptization. Decrease of settling volumina occured when systems have been affected by the electric field as well. The extent of decrease was nearly the same in the acidic and alka-

line domains. Increase of the settling volume was lesser above pH = 7 as in a state free of electric field. /Fig. 1./

Fig.1

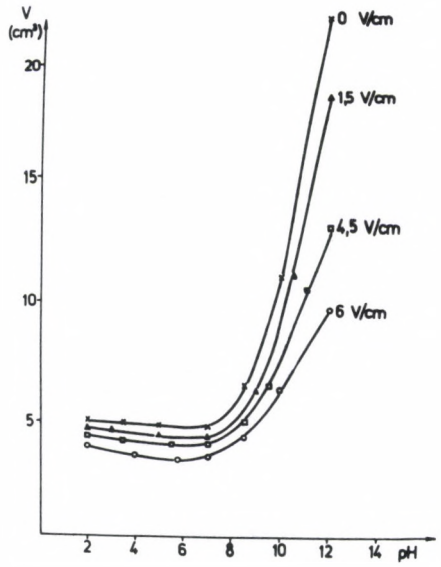

Investigations of electrophoretic migration speeds indicated a rapid decrease in the mobility of dispersed particles as the pH-value rises. /Fig. 2./ Above pH = 12 accurate measurements were similarly hindered by the diffuse character of the surface. Remarkably in both measurements a critical pH-value can be observed. These two critical pH-values have nearly been identical in our measurements.

Relationship between viscosity of the suspensions and pH-value thereof may characterized by a maximum curve. The lesser the speed gradient, the higher the maximum of the curves. It could unanimously settled that, deviation of the pH-value from a critical value where viscosity is at maximum irrespective of the decrease or increase of pH, caused a rapid decrease of

Fig. 2

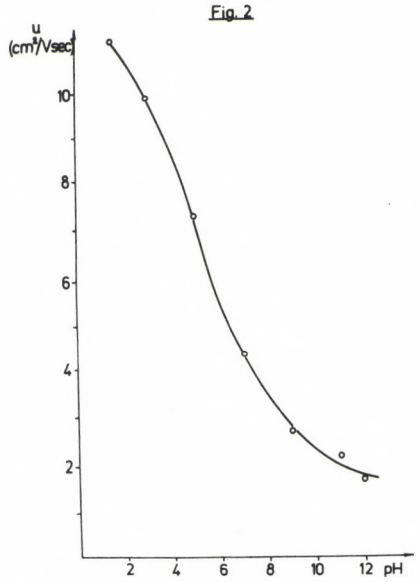

viscosity in all instances. We have found this critical pH value beeing lower than those observed during determination of the electrophoretic migration speed and the settling volumina. /Fig. 3./

Fig. 3

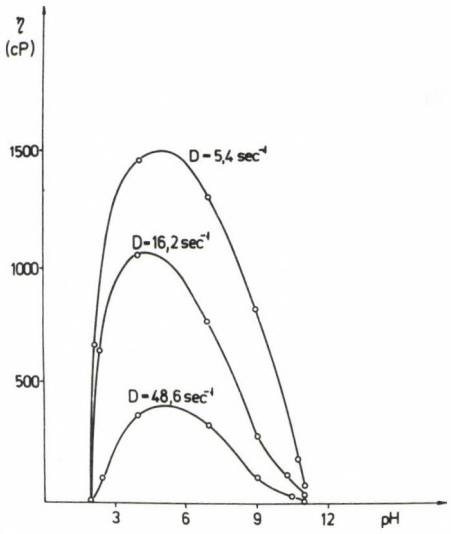

When additionally electric field affects on the system the relationship between viscosity and pH-value differs from that described above. Maximum of the curves characterizing the phenomenon decreases when field intensity is rising - among otherwise identical circumstances.

Maximum of viscosity is shifted as compared to the conditions free of electric field, with other words critical pH-value increased in this particular case. /Fig. 4./

Fig. 4

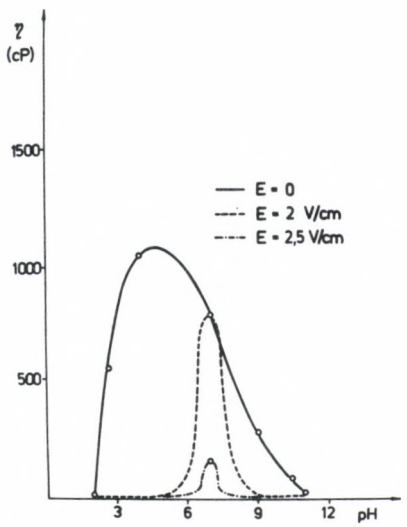

Discussion

It is evident from the experimental results that suspensions having a neutral or slightly acidic medium may be considered as more stable systems. Thus being conversant with the critical pH-value is of capital importance in view of the stability of suspensions. As is well-known, electrokinetic potential - which determines the stability of a suspension - is affected by pH changes of the medium. Considering that cataphoresis occured

with all systems investigated /$\varepsilon_{\text{Rutile}} \sim 130$/, decrease of stability above the critical pH-value as well as sudden decrease of electrophoretic migration speed above a critical pH-value thus become understandable.

Maximum of the viscosity/pH relationship occurs in the domain of pH = 4.5 to pH = 5.5. The reason for this is that pH-value of the suspension depends also on the rate of CO_2 uptake of the pigment from the environment, apart from the superficial dissociation - which inevitably takes place to a certain extent - thus pH-value of the suspensions varied after preparation from 4.5 to 5.5

In an electric field two forces are acting on the particle. Viscosity of the suspension in affected in the same manner by increase of the electric field and alteration of the pH-value.

From viscosity/pH relationships measured at various field intensities a linear interconnection between the area enclosed by the curves and the field intensity could be established. Incidentally this is evident since interconnections between electrophoretic migration speed, field intensity and electrolyte concentration resp. aré also of a linear character.

Determination of relationship between viscosity and field intensity is a question of great importance. As far we couldn't set up a mathematical formula describing the phenomenon within the total pH domain, however, in the case of pH = 4 to 8 the following equation may be applied:

$$\sqrt{\frac{\eta_o}{\eta_{min.}}} = A \frac{\varepsilon}{\text{u. log D}}$$

where

η_o = static viscosity

$\eta_{min.}$ = viscosity formed on the action of electric field

ε = dielectric constant of the medium

D = speed gradient

u = electrophoretic migration speed

A = a constant characteristic of the substance suspended

Based on our experimental result it could be established that a close connection exists between the pH-value of aqueous suspensions and their electrorheological effects. Comprehensive investigations are required in order to explain in full all processes.

References

1./ H. Enneking, Erdöl u. Kohle 14, S 1005 /1961/

2./ R.S. Allan and S.G. Mason, Proc. of Royal Society, A, 267 S 45 /1962/

3./ R.S. Allan and S.G. Mason, Proc. of Royal Society, A, 267 S 62 /1962/

4./ C.E. Chaffey and S.G. Mason, J. of Coll. Sci. 19 S 525 /1964/

5./ C.E. Chaffey and S.G. Mason, J. of Coll. Sci. 20 S 330 /1965/

6./ C.E. Chaffey and S.G. Mason, J. of Coll. a. Interface Sci. 27 S 115 /1968/

7./ Z.P. Sulman, J.F. Dejnega, R.G. Gorodkin and A.D. Macepuro, Elektroreologicseszkij effekt, Izv. Nauk i Technika, Minszk, 1972.

8./ Z. Dárdai, Kolor. Ért. 11 S 130 /1969/

9./ Z. Dárdai, Kolor. Ért. 12 S 175 /1970/

Group II/5
Gels

THE GELATION OF IRON-OXIDE SOLS

D. Bargeman, E.J. van Emmerik and C.A. Smolders
Twente University of Technology, Enschede, The Netherlands

INTRODUCTION

In the present literature different models have been proposed to explain the structure of inorganic metal-oxide gels.

Some authors (1-3) state that metal hydroxydes can form polynuclear species, linear macromolecules as well as chains with side branches, due to an olation-oxolation process. The gels then are the final products of these hydrolytic reactions and they consist of a network of polynuclear complexes linked up by -O- and -OH bridges.

Other authors, however, consider the gels as flocculated colloids (4,5). Efremov et.al (6,7) suggest that the gelation of metal-oxide sols arises because the colloidal particles are fixed at distances corresponding to the secondary minimum in the interaction potential curves.

It is the purpose of this work to investigate the nature of the network structure, which causes the large increase in viscosity upon gelation of the sol.

EXPERIMENTAL

Sol preparation: Iron-oxide sols are prepared by slowly adding (1 drop per 3 seconds) of a 25 wt % NH_4OH solution to 500 ml of a molar solution of $Fe(NO_3)_3.9H_2O$ until a pH value of 7 is reached. The precipitate is centrifuged and washed thorougly with twice distilled water to a dilution of about 4000 times. A minor part of the precipitate peptizes spontaneously. The precipitate is decanted and diluted with water to a volume of

600 ml and 10 ml 65 wt % nitric acid is added. The solution is refluxed for 30 minutes under stirring. After cooling, water is added to a total volume of 800 ml. The pH value of the sol is about 1.8. Analysis gave an iron concentration of about 0.6 $Mol.L^{-1}$ and a nitrate concentration of about 0.21 $Mol.L^{-1}$. The sols are stable for more than one year.

Techniques: Electron micrographs are made by use of a Philips EM 200 electron microscope with a resolution of 0.7 nm. The samples for the electron micrographs are obtained by spraying a diluted (250x) solution of the sol or the gel onto a grid provided with a carbon membrane. The specimen then is dried at room temperature. When undiluted sols are used , recrystallization is observed in some cases and the particle layers are too thick to allow a proper observation with the electron microscope. The gels are diluted under stirring.

Surface-area determinations of the sol particles are obtained from N_2 adsorption at liquid N_2 temperature with the Perkin-Elmer 212 D sorptometer. The samples are degassed for 24 hrs at 80 ^{o}C; at higher temperatures sintering takes place.

Zeta-potential measurements are performed with a modified Burton moving-boundary apparatus. The iron-oxide sols are diluted before use with a nitric acid solution of the same pH. The dilution factor was about 30 x. The acid solution is also used as the colloid-free phase.

Viscosity is measured with an Ubbelohde viscosimeter.

RESULTS

Size and morphology of the iron-oxide sol particles are investigated with the electron microscope and from surface area determinations. Electron micrographs showed more or less spherical particles with a diameter of 4.5 nm. Surface areas of the sol particles obtained with the aid of the BET equation yielded values of 280-320 $m^2/gram$. With a density of 4.0 $g.cm^{-3}$ and assuming the particles to be completely spherical a particle diameter of 4.7 to 5.3 nm is found. The somewhat larger value of the particle size determined by the surface area method may be due to some sintering of the particles during degassing in the BET apparatus at 80 ^{o}C.

The gelation of the sol is brought about by a number of different procedures:

a. Titration with concentrated (25 wt %) ammonia: When the titration is rapidly performed (within a few minutes) a gelatinous precipitate forms. When the titration is done very slowly and under stirring a homogeneous gel is obtained at a pH value of about 3. The exact pH value at which the gelation takes place depends on the rate of addition of the ammonia solution. A jelly is obtained at a pH value of 3.1 when 0.38 ml ammonia is added to 20 ml of the sol at a rate of 1 drop per 20 min. When 0.3 ml of the ammonia solution is added under stirring within 5 min., followed by the slow addition of 1 drop per 20 min we also obtained a jelly at a pH value of 3.1. The addition of 3.8 ml of ammonia to the sol within 5 min., however, always yields a gelly precipitate.

b. Dialyzing the sol: A very slow change in the pH of the sol can be performed by a dialyzing process. A pH value of 5.0 was reached within two weeks when the dialyzing bath consisted of doubly distilled water recirculated through the bath. When this pH was reached no NO_3^- ions could be detected in the sol ($[NO_3^-] < 10^{-4}$ Mol.L^{-1}). Then NaOH was added to the bath up to a pH value of 10. After 1 day the sol gelled at a pH value of 5.9.

When sodium nitrate was present in the dialyzing liquid, however, the pH value at which gelation took place decreased: gelation occurred at a pH value of 4.6 with a nitrate concentration in the sol liquid of 0.02 Mol.L^{-1} and at a pH value of 3.1 with a nitrate concentration of 0.21 Mol.L^{-1}.

During dialysis 20 ml samples were taken from the sol after certain intervals. Zeta-potential and viscosity measurements were performed with these samples. The results of these measurements are given in Fig. 1 and Fig. 2 respectively.
Since the κa values (κ^{-1} is the double layer thickness and a the radius of the sol particles) are in the critical region of $0.1 < \kappa a < 100$, the zeta potentials are calculated using the Wiersema, Loeb, Overbeek method (8).

It is worth-while to note here that the sol-gel transition does not occur at a well defined pH value in the dialyzing procedure at constant salt concentration since after longer waiting times gelation occurs at lower pH values. Table I gives the results for the system with a constant nitrate conc. of 0.21 $Mol.L^{-1}$.

Table I

pH value	Gelation time
3.2	instantaneously
3.1	12 hours
2.8	1 week
2.7	1 month
2.5	no gelation (> 1 year)

c. Titration with Na_2SO_4: A 0.4 M Na_2SO_4 solution is added to 20 ml iron-oxide sol (pH = 1.8) at a rate of 1 ml per 3 hrs. The sol gelled after addition of 2.0 ml sulphate solution. We also investigated the change in viscosity of the sol when various amounts of sodium sulphate were rapidly added under vigorous stirring with an Ultra-Turrax mixing apparatus. Gelation of the sol occurred after 1 week upon addition of 1.6 ml Na_2SO_4, after 1 day upon addition of 1.8 ml Na_2SO_4 and after 15 min upon addition of 2.0 ml Na_2SO_4. The addition of 3.0 ml Na_2SO_4 to the sol yielded a gelatinous precipitate.

Electron microscopy is used to determine the internal structure of the sols and gels. No structure could be observed when a specimen was taken of the sol, but electron microscopic photographs of the gel show the presence of strings of flocculated particles. Examples of electron micrographs of two different gels are given in Fig. 3.

DISCUSSION

The data given above demonstrate, that the gelation of the sol arises, when the stability of the sol is decreased by the addition of potential determining ions and/or by the addition of indifferent electrolyte. A homogeneous gel, however, is obtained only when the zeta-potential is such that rapid flocculation cannot occur.

This indicates that an still existing energy barrier prevents the formation of a gelatinous precipitate. We therefore calculated the height of the energy barrier from the DLVO theory.

For the repulsive electrostatic energy V_R between the particles, the equation for somewhat higher potentials is used (9)

$$V_R = \frac{64\ \pi nakT}{\kappa^2}\ \gamma^2\ \exp\ (-\kappa H)$$

where H is the shortest distance between the two spheres, a is the particle radius, $\gamma = \left\{ \exp\left(\frac{ze\psi_\delta}{2kT}\right) - 1 \right\} / \left\{ \exp\left(\frac{ze\psi_\delta}{2kT}\right) + 1 \right\}$, ψ_δ is the Stern potential of the particle, $1/\kappa$ is the double layer thickness, k the Boltzmann constant and T the absolute temperature.

For the dispersion attractive energy, the unretarded sphere-sphere expression was used:

$$V_A = -\frac{A_{121}}{6}\left[\frac{2}{s^2-4} + \frac{2}{s^2} + \ln\frac{s^2-4}{s^2}\right]$$

where A_{121} is the Hamaker constant describing the attraction between two particles 1 in medium 2 and $s = \frac{2a+H}{a}$ is the reduced distance between the particles.

From the flocculation concentration of sulphate ions a Hamaker constant of 3×10^{-13} ergs is calculated, in good agreement with the value given for α-Fe_2O_3 (10). Substitution of this value and of the experimental values a = 2.5 nm, $\psi_\delta \approx \zeta$ = 70 mV and κa = 1.2 yields a potential barrier height of 8 kT under the conditions where the steep increase of the specific viscosity starts. The secondary minimum in the potential curve is small compared to kT, indicating that the Efremov concept (6,7) is not applicable.

Thomas and McCorkle (11) have shown that the interaction of spherical double layers can lead to anisotropic flocculation, if the thermal kinetic energy kT is small compared with the energy maximum. For flocs of two spherical particles these authors calculated a minimum in the repulsion energy barrier at the ends of the floc; this minimum was about half as high as the maximum lying between the two particles. Therefore, they infer that slow flocculation will favour the formation of a string of beads instead of spherical flocs.

This is in agreement with the results obtained from the electron microscopic investigations, which show the presence of flocs that are interconnected by chain-like flocs.

Hence we conclude that the network structure of the iron-oxide gel results from anisotropic flocculation, made possible if flocculation is slow.

REFERENCES

1. C.L. Rollinson in The Chemistry of the coordination compounds, Ed. J.C. Bailer and D.H. Busch, Reinhold Publ. Corp., N.Y., 1956, pg. 448.
2. J.J. Fripiat and M. Pennequin: Bull.Soc.Chim. France 1965, 1655.
3. G. Scibona, A. Bazan, A. Cabrini, R. Chairazza, P.D. Danesi, M. Magini, E. Mezi: Proceedings of Simposio Internazionale de Torino 1967, pg 27.
4. H.B. Weiser and W.O. Milligan: J.Phys.Chem. 44, 1081 (1940).
5. A.A. van der Giessen: Dissertation Eindhoven, The Netherlands, 1968.
6. I.F. Efremov and S.V. Nerpin: Colloid J. USSR 19, 759 (1957).
7. G.M. Lukashenko, M.V. Serebrovsaya, O.G. Us'yarov and I.F. Efremov: Colloid J. USSR 33, 88 (1971).
8. P.H. Wiersema, A.L. Loeb and J.Th.G. Overbeek: J. Colloid Interf. Sci. 22, 78 (1966).
9. J. Lijklema: Adv. in Colloid Interf. Sci. 2, 67 (1968).
10. F.M. Fowkes in J.J. Burke (ed.), Surfaces and Interfaces Vol 1, Syracuse Univ. Press, N.Y., 1967, pg 199.
11. I.L. Thomas and K.H. McCorkle: J. Colloid Interf. Sci. 36, 110 (1971).

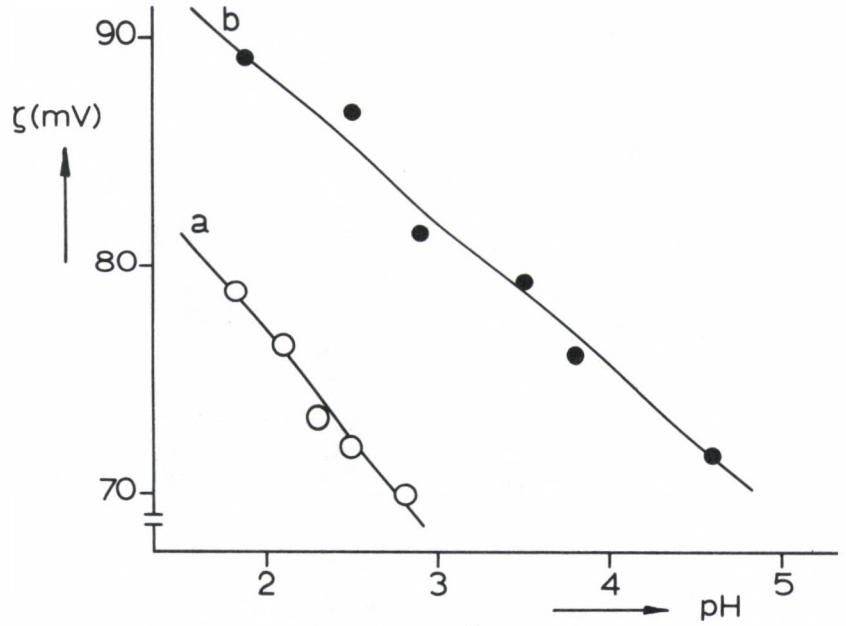

Fig. 1. Zeta-potential vs pH curves for nitrate concentrations of 0.21 Mol/L (curve a) and 0.02 Mol/L (curve b)

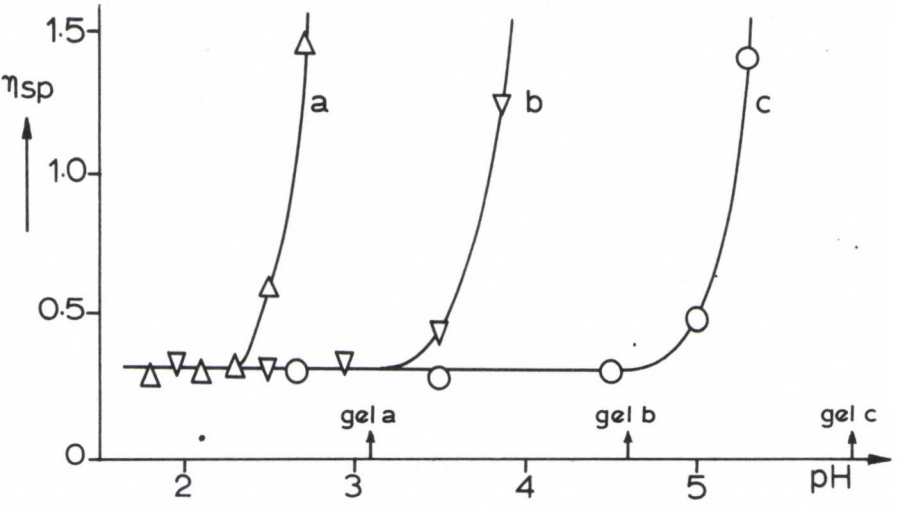

Fig. 2. The specific viscosity vs. pH curves for nitrate concentrations of 0.21 (curve a); 0.02 (curve b) and 0.00 (curve c) Mol/L.

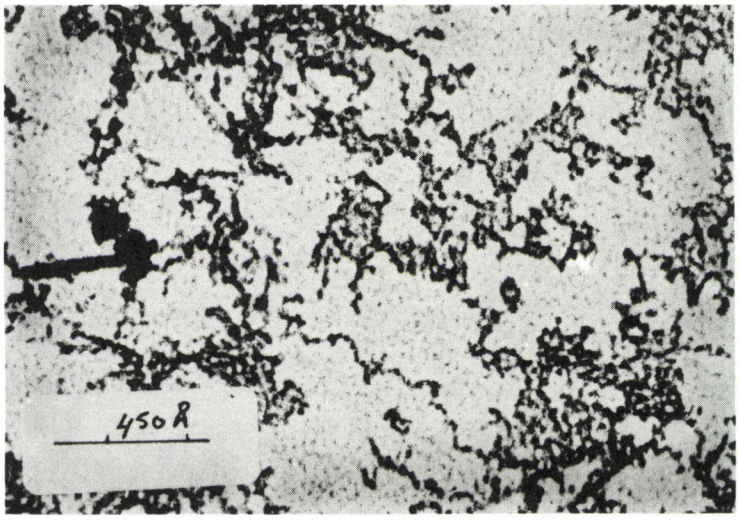

(a)

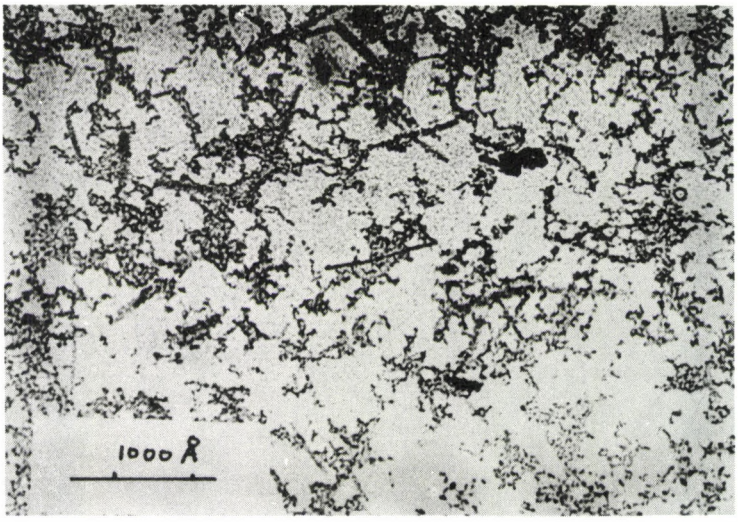

(b)

Fig. 3. Electron microscopic photographs of iron-oxide gels.

a. Gel formed by dialyzing the sol.

b. Gel obtained by titration with ammonia.

FORMATION OF DISPERSE STRUCTURES IN POLYMER GELS

M.Nagy, E.Wolfram, T.Váradi

Department of Colloid Science, Loránd Eötvös University
Budapest, Hungary

Introduction

The quantitative description of polymeric networks is based on models that are assumed to have an idealized structure involving primarily uniform distribution of Gaussan network chains throughout the system without any significant inhomogeneities. [1,2] Real networks, however, differ from these models in having defects either at molecular level, such as cyclic structures, entanglements, unreacted functionalities, or those at supermolecular level, resulting mainly in local chain element densities being significantly in excess over average values. Inhomogeneities of the latter kind are usually formed when the gelation process is accompanied by hindered phase separation. [3-5]

Clearly, the existence of such inhomogeneities permits, at least in principle, to synthesize materials of great structural variety, from molecular networks to porous sorbents. The biological importance as well is obvious. In spite of this neither the mechanism of formation of the structures mentioned nor the connection between structure and properties of such systems seem to have been so far studied satisfactorily.

It was shown in our previous work[6] that among factors affecting network structures that are formed by chemical cross-linking of a polymer, both the degree of cross-linking /DC/ and the initial polymer concentration are of primary importance. The DC is defined as the average number of monomeric units between crosslinks.

The main purpose of the present work has been to study the effect of an inert, non-reactive macromolecular component, poly /N-vinyl pyrrolidone/ /PVP/, on the gelling of poly /vinyl alcohol/ /PVA/. It was assumed that PVP, although taking no part in the chemical cross-linking, should cause changes in the spatial distribution of both the segments and the chains of the reactive polymer thus leading to structural characteristics that may be detected experimentally.

Experimental

After mixing of the aqueous solution of PVA /$\overline{M}$ =1.1 10^5/ containing various amount of PVP /PVP-1: $\overline{M}$ =4·10^4 and PVP-2: $\overline{M}$ =3,6 ·10^5/ with aqueous solution of glutaraldehyde the cross-linking process was initiated by adding HCl /pH=1/. Prior to the gelling one part of the mixture was filled into the spectrophotometric cell, the second part was cast to a glass plate /to obtain gel-membrane/ and the third one was poured into the gelation apparatus to get cylindrical gel pieces, with equal height and diameter, to be used for measuring of the unilateral compression by means of a modified analytical balance.

For turbidity measurements Spekol ZV type spectrophotometer was applied. The weight degree of swelling were determined in the usual way.

Results and discussion

Optical properties of the gels. Fig. 1 shows that both the concentration and the molecular weight of the PVP effect the turbidity of the gels. In those systems which contain PVP-2 the turbidity sharply increases with increasing amount of this additive. Similarly, quite different results were obtained for the two PVP samples when measuring the kinetics of the development of the turbidity. Already near the gel point the systems containing PVP-2 show a very high and rapidly increasing turbidity during the gelling process. This phenomenon is typical for the phase separation occuring in any type of polymer-solvent systems. On the other hand, the moderate increase

in turbidity with time and concentration of PVP-1 clearly indicates the structurization of the network controlled by the cross-linking reaction and the relatively slow relaxation of the continuously formed network. The formation of inhomogeneous gel structure showing high scattering power of the light are indicated by the high value of the turbidities.

The phenomena observed show the important role the cross-linking induced phase separation in the formation of inhomogeneous network structures. It is known that the thermodynamical stability of a ternary system containing two polymeric components is governed by the interaction parameters as well as by the overall concentration and the ratio of the molar volume of the macromolecular components. The higher the molecular weight, the less is the stability of a given component.

In the course of gelation of PVA the molecular weight increases up to infinity. Due to the relatively high compatibility of PVA with PVP-1, the component having higher molecular weight, i.e. the PVA will separate and will be simultaneously fixed by cross-linking resulting in a more or less inhomogeneous distribution of the PVA chains in the network. Evidently, because of its low concentration and high molecular weight, the separation of the PVP-2 solution starts already in the early stage of gelation. The fine droplets of this solution are then fixed in the network.

In order to estimate the mean size of the supermolecular elements the turbidity ratio method was used.[7] For systems containing PVP-2, practically independently of both the DC and the concentration of the polymers, the formation of droplets with rather uniform size could be detected / Table 1/. In presence of PVP-1 the particle size passes through a deep minimum and maximum with increasing amount of this component and it depends strongly on both the DC and the concentration of each of the polymers / Fig. 2/. In spite of some limitation in the application of the turbidity ratio method it is believed that at least the relative changes in the size of the structural elements may be considered to be relevant.

Stress-strain behaviour of the gels. For characterizing non-

-ideal networks, instead of the basic equation generally used in the statistical theory of rubber elasticity the so-called Mooney - Rivlin relation[2] is more suitable:

$$\sigma = C_1\left(\alpha - \frac{1}{\alpha^2}\right) + C_2\left(1 - \frac{1}{\alpha^3}\right)$$

where σ and α are the stress and the extension ratio, respectively. The constant C_1 is proportional to the concentration of the elastically active network chains /or to the modulus/, while C_2 indicates the deviation from the properties of the ideal network /for this latter, $C_2 = 0$/.

Except for the highest value of the DC in each of the C_1 vs. PVP curves a maximum and a minimum occur indicating serious change induced by PVP-1 in the structure of the gels /Fig. 3 and 4/. The position of the maximum in the above curves is approximately in the same PVP-1 concentration range where a change in the size of the supermolecular particles is observed. Likely, due to the relatively low concentration of the PVP-2, this polymer did not, or only to a slight extent alter the mechanical behaviour of the gels. The dependence of the elasticity of the networks on the concentration of PVP-1 can be probably explained by assuming changes in both the shape and the spatial arrangement of the supermolecular elements in the gels.

Swelling and syneresis. According to the thermodynamics of the swelling the weight degree of swelling of the gels has been found to vary the opposite direction as does C_1 /Fig. 5/. For the systems containing PVP-1 the extent of the syneresis decreases with increasing amount of this additive.

In conclusion two important points are emphasized:

1. The effect of the polymer additive depends strongly on which stage of the gelation the phase separation is induced.
2. In order to attain a good regulating ability with respect to the network structure, a relatively high compatibility of the two polymeric components is needed.

References

1. Flory, P.J.: Principles of polymer chemistry, Ithaca, Oxford Univ. Press, 1953
2. Dušek, K. and W.Prins: Adv. Polymer Sci., 6 1-102/1969/
3. Dušek, K.: J. Polymer Sci., 16 1289-1299/1967/
4. Dušek, K. and B.Sedláček: Collection of Czechoslovak Chem. Commun., 34 136-157 /1969/
5. Dušek, K.: Chem. zvesti 25 184-189 /1971/
6. Nagy, M. and E.Wolfram: 14th Prague Microsymp. on Macromolecules. Crosslinking and Networks. August 26-29, 1974 Prague Preprints D10
7. Sakurada, I., M.Hosono, S.Tamamura: Bull. Chem. Research Kyoto Univ., 42 145-152 /1964/

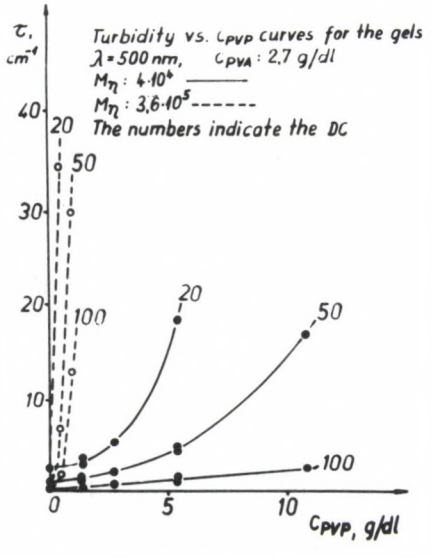

Fig. 1

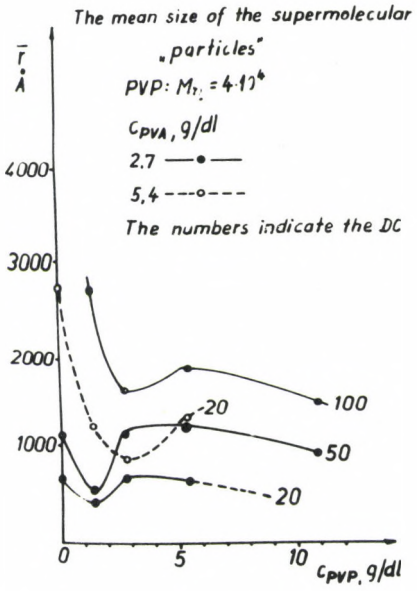

Fig. 2

Table 1

The mean size (in Å) of the droplets of PVP ($M_\eta = 3{,}6 \cdot 10^5$) solution

c_{PVA}, g/dl

DC \ c_{PVP}	2,7		5,4	
	0,45	0,90	0,45	0,90
100	2400	2600	2400	3700
50	1900	2000	2500	1800
20	2600	—	2400	—

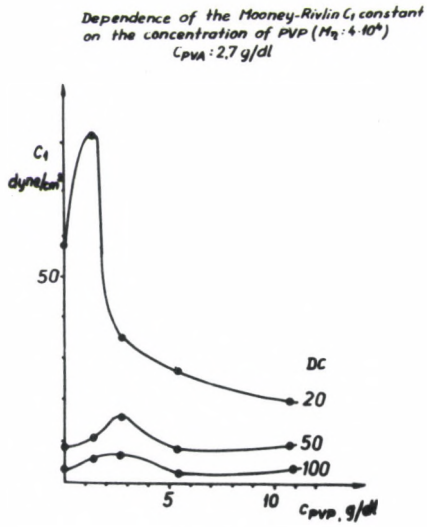

Fig. 3

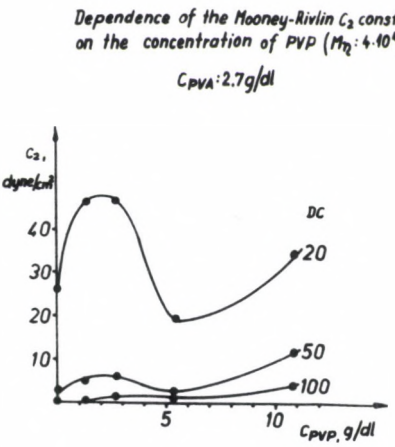

Fig. 4

Fig. 5

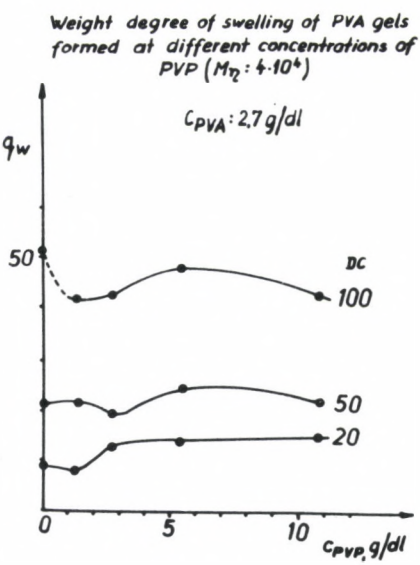

THE EFFECT OF CO-SOLVED SUBSTANCES ON THE GEL-SOL TRANSITION OF GELATIN

I.Tar and E.Wolfram

Department of Colloid Science, L. Eötvös University, Budapest, Hungary

An examination of the extensive literature shows that in spite of our knowledge concerning gelatin molecules which can exist independently in solution and some physical characteristics of the gel which they can form, little is known on the gel $\leftrightarrow$ sol transition. This must be attributed to the lack of methods to characterize transition phenomena.

The more promising field of gel $\rightarrow$ sol transition, that is the determination of the melting temperature of gelatin gels and calculating heat of gelation data (1) was practiced in the early seventieth by Bobrova and co-workers. Park and co-workers (2) developed a new method for obtaining melting point of synthetic polymers by the use of a micro capillary--viscometer and calculated ΔH values.

It is important to point to the lack of systematic studies concerning the effect of substances present in or added to the gelling system, the more so, as protein gels never exist in a laboratory-clean state in the living cell or in praxis. Those to be found mostly refer to gel characteristics modified by co-solved substances of rather diverse origin.

As a result of our own investigations (3) we could show the existence of interaction between gelatin in solution and co-solved nonionic surfactants. We extended our studies to the gel $\rightarrow$ sol transition, with the same group of added molecules. In order to reveal the mechanism of the possible interactions, we introduced polyethylene glycols with molecular weights similar to the nonionic surfactants used, as well as ionic sur-

factants and neutral salts with diverse anions.

EXPERIMENTAL

Materials

Rousselot No. 15100 photographic gelatin was used /IEP = 5.33, $\bar{M}_w$ = 72600/.
Co-solved substances were the following: REANAL salts of analytical grade and polyethylene glycols /PEG/ $\bar{M}$=550, and 2000, sodium dodecyl sulfate /NaDS/ M=288,38, Merck product. Sodium hexadecyl sulfate /NaHS/ Pinnow product M=344,44. Poly-oxyethylene ethers: BEROL 043, $C_{18}H_{37}EO_{10}OH$ M=711,0 and BEROL 08 $C_{18}H_{37}EO_{50}OH$ M=2473,2, Berol products, PEG-free.

Methods

Gel melting points /t_m/ were determined using a Harrison-Morgan-Park micro capillary-viscometer /H-M-P/ see Fig. 1/. When filled with gelatin solution in a way to produce a certain Δh at 10-15 °C, the viscometer was allowed to stand at the same temperature overnight. The temperature was increased with a constant rate of 0.2 °C per minute, while height difference in the two limbs were registered. Gel melting point was obtained from the intersection of the linear portions of the graph log Δh vs. t °C /see. Fig.2/.

Fig. 1.

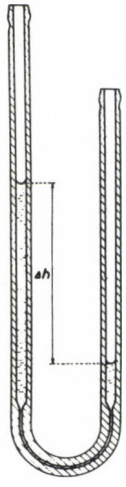

Fig. 2.

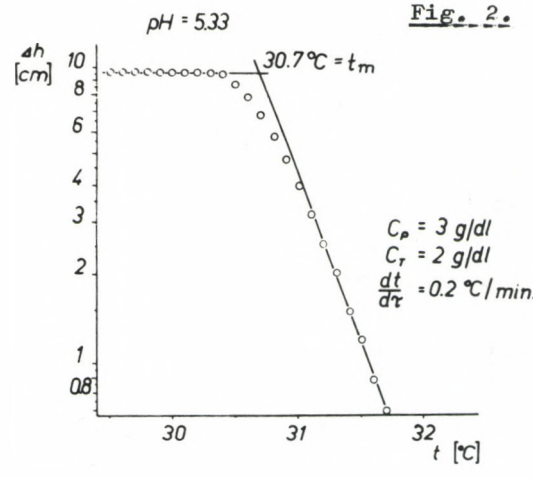

The values obtained for gels of different concentrations /$\underline{c}_p$/ were used to calculate the heat of gelation /$\underline{\Delta H}$/ after Eldridge and Ferry (4) /$\ln c_p = \Delta H/RT_m$/. In addition, both melting and setting points /$\underline{t}_s$/ were measured by a simple version of the falling sphere method, too /f-s/.

RESULTS AND DISCUSSION

In order to study the gel → sol transition we measured the melting points of gels with or without any co-solved substance. Their effect was studied in two ways: by the change of the melting point /$\underline{t}_m$/ and by checking changes of $\underline{\Delta H}$ that arise from the presence of substances added to the gelling system.

Experiments made by the simplified falling sphere method were carried out in order to confirm the direction and sign of changes with a second method, and with the aim of showing whether changes analogue to those in melting /$\underline{t}_m$ values/ might be produced by the same substances in the setting process /$\underline{t}_s$ values/.

The effect of all of the added substances was studied over a wide concentration range, the extent of which was dependent on the compatibility of gelatin molecules and the additive.

The following equation was found to fit our experimental results: $\log t_{m,s} = k\ c + b$, /1/ in which $\underline{c}$ is the concentration of the substance co-solved with gelatin, $\underline{b}$ is the log of the melting or setting temperature when $\underline{c} = 0$. This constant is a characteristic of the gelatin of given concentration at a given pH. In our case $\underline{c}_p$ was 5 g/dl and isoelectric state /pH = 5.33/ was obtained. The slope $\underline{k}$ of the lines was taken as a characteristic value for the various substances used.

The data in Table 1 /column 1/ show how the salting-out effect of the different chlorides manifests itself in negative slopes. The magnitude depends on the valency of the cation. By value $\underline{k}$ a quantitative data is given to the so-called specific effect of sulfate ions as well, having a rather high positive value.

Table 1. The effect of co-solved substances on the gel ⟷ sol transition of gelatin

Character and composition of the co-solved substance		Constant k in Eq. /1/ [°C.dl/g]. 10^3 Melting H-M-P	Melting f-s method	Setting f-s method	Conc. [M/l]	ΔH [kcal/mole] H-M-P method
Hydrophile						
Ionic	NaCl	-5.1	-5.4	-13.3	0.855	-68.4
	KCl	-3.9	-5.7	-10.3	0.855	-61.0
	$BaCl_2$	-9.9	-15.2	-29.4	0.205	-61.4
	Na_2SO_4	+6.1	+ 5.4	+ 6.2	0.155	-62.9
Nonionic	PEG $\overline{M}$=550	+1.6	-	-	0.036	-67.1
	PEG $\overline{M}$=2000	+2.4	-	-	0.005	-60.4
Amphiphile						
Ionic	NaDS	+220	-	-	0.002	-63.4
	NaHS	+180	-	-	-	-
Nonionic	BEROL 043	+ 2.2	-	-	0.014	-68.6
	M=711.0				0.028	-74.5
	BEROL 08	-	-	-	0.002	-74.5
	M=2473.2				0.004	-75.6
					Gelatin in dist. water	-67.4±2.4

The close analogy of Eq. /1/ with the equation valid for the solubility of proteins in salt solutions by Green and co-workers (5) should be pointed out, as both phenomena are governed by the same two effects, i.e. the decrease of the rate of dissociation and changes brought about by the salts in the structure and extent of the hydration layers around the gelatin molecules.

Special mention is due to the alkyl-sulfates (6). Fig.3 shows the changes of log $\underline{t}_m$ when the concentration of the ionic surfactants increases. The first part of the curve testifies that these molecules exert an increase in $\underline{t}_m$, but in a much higher extent than simple sulfates. When places capable for Coulomb-type interactions are occupied, no more changes arise. Earlier investigations (7) on the complex formation of gelatin molecules with ionic surfactants in solution led to similar conclusions. The great increase of $\underline{t}_m$ values could be derived from the fact that besides the so-called energetic interaction points formed between positively charged gelatin segments and the $[DS]^-$ or $[HS]^-$ anions, resp., hydrophobic bonding is built, too, as a result of interactions between the C_{12} or C_{16}-chain and non-polar portions /leucine, proline/ of gelatin /see Fig.4/a/ or with the alkyl chain of the surfactant anions fixed to another part of the network /see Fig.4/b/.

The results of the falling sphere method led to the same conclusions both with respect to the gel $\rightarrow$ sol transition /melting/ and the sol $\rightarrow$ gel transition /setting/ phenomena. /Table 1, columns 2 and 3./

Heat of gelation /$\Delta\underline{H}$/ data are summarized in the last column of Table 1. The most interesting features are as follows: The salting-out effect characteristic of neutral salts is reflected in reduced $\Delta\underline{H}$ values. The same was found with NaDS which, building a network with several hydrophobic bonds, hinders the development of cross-links of higher energy. Nonionic surfactants are able to interact with gelatin not only through their alkyl chains /hydrophobic bonds/ but also with their ethylene oxyde chains. These chains are protonized at pH = 5.33, thus giving rise to a highly structured water shell along the network-forming gelatin molecules to which their alkyl chains

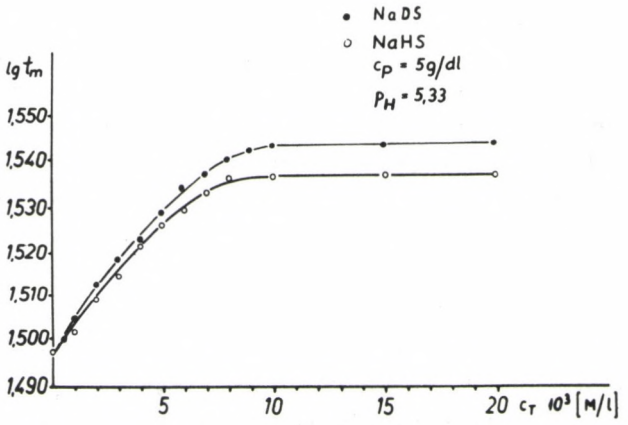

Fig. 3.

a/

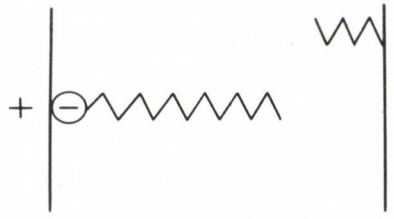

b/

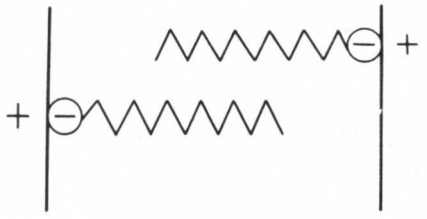

Fig. 4a-b.

are linked. On the other hand, H-bridges might form between these protonized chains and some polar segments of the protein. This is the possible reason of the considerable increase in the heat of gelation (8). Polyethylene glycols, on the contrary, reduce the heat required to disrupt gel structure, just as the other hydrophil substances used. This fact emphasizes the importance of alkyl chains in the interaction of gelatin with nonionic surfactant molecules. The results of other authors led to similar conclusions (9).

References

1. I.E.Bobrova, V.N.Ismailova, P.A.Rehbinder: Koll.J.USSR, 32, 662, /1970/, ibid. 34, 6 /1972/.
2. M.A. Harrison, P.H.Morgan, G.S.Park: Brit.Polymer J., 3, 154 /1971/, Europ.Polymer J., 8, 136 /1972/.
3. I.Tar, Zs.Fodor, E.Wolfram: Magy.Kém.Folyóirat, 79, 532 /1973/.
4. J.E.Eldridge, J.D.Ferry: J.Phys.Chem., 58, 992 /1954/.
5. A.A.Green: J.Biol.Chem., 93, 495, 517 /1931/; ibid., 95, 47 /1932/.
   E.J.Cohn: Chem.Rev., 28, 395 /1941/.
6. M.Kustos: B.Sc.- Thesis, 1974, Budapest.
7. K.G.A.Pankhurst, R.C.M.Smith: Trans.Faraday Soc., 40, 565 /1944/.
   W.J.Knox, J.F.Wright: J.Colloid Interface Sci., 20, 177 /1965/.
8. Zs.Fodor: Thesis, 1972, Budapest.
9. E.N.Ovchinnikova, I.F.Ponomarenko: Koll.J., USSR, 29, 377 /1967/;
   I.Michlik et al.: Košarštvi 19, 19 /1969/.

Group III/1
Micellization and related phenomena

MICELLE FORMATION IN AQUEOUS SOLUTIONS OF SURFACE-ACTIVE SUBSTANCES

Z.N.Markina, O.P.Bovkun, N.N.Tsikurina, A.V.Sinyova

Department of Colloid Chemistry, Lomonosov State University, Moscow, USSR

At the present time micellar theory is the foundation for investigations of solutions of soap-like surfactants, since the existance of micelles in such systems is proved /1/. Times of formation and destruction of micelles are usually several milliseconds (10^{-3} - 10^{-4} sec.) and this essentially differs them from regular fluctuations of concentration /2/. Unlike hydrophobic sols ultramicroheterogeneous systems of lyophilic surface-active substances in aqueous environment are thermodynamically stable, since they are spontaneously formed with high dispersity, e.g. by means of dispersion of macroscopic phase, i.e. soap crystals, or association of separate soap molecules. Such systems are characterised with equilibrium curves of size distribution of particles, the main motivity of association of soap molecules being the hydrophobic interaction of their hydrocarbon chains in the process of micro-(pseudo-)-phase nuclei formation. Separation of the surface-active agent as a macrophase is stopped with hydratation of hydrophilic groups, losses in entropy and - in case of ionogenic soaps - electrostatic repulsion of terminal groups.

The phase theory of micelle formation is testified with a number of experimental facts, in particular according to our data (fig.1) the efficiency of intramicellar dissolving compared to hydrotropic (when micelles don't present) one in solutions of sodium butyrate refered to benzene; this fact agrees also with negligible solubility of hydrocarbons below

CMC, which was found in our laboratory /3,4/.

Presence of micelles as a separate phase is proved and intramicellar character of solubilisation is directly confirmed with our early investigations /5/ of polymerisation of acrylonitrile, methyl methacrylate and styrene in soap solutions (sodium mersolates C_{12}-C_{18}) saturated with the initiator - benzoperoxide, not soluble in pure water, that is under conditions when polymerisation process occurs only in micelles of the emulgator and the oleophylic initiator is solubilised in quantities sufficient for agitation of polymerisation with considerable speed. It is established that the dependence of intramicellar polymerisation speed on emulgator concentration is determined with conditions of distribution of the monomer between soap micelles and molecular aqueous solution. These results, clearing some topochemical aspects of emulsion polymerisation, undoubtedly confirm the significance of solubilisation as an important elementary stage in this heterogeneous process of polymer production.

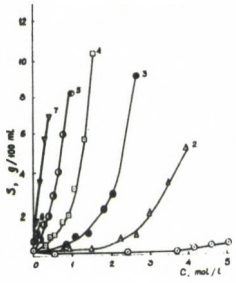

Fig.1. Dependence of benzene solubilisation (S) on concentration of sodium caproate (2), caprilate (3) caprate (4), laurate (5), myristate (6) and oleate (7) aqueous solutions as compared to its hydrotropic dissolving in aqueous solutions of sodium butyrate (1).

Micellar systems' consisting of two phases above CMC was confirmed with our investigations of structural peculiarities of aqueous soap solutions with the method of complex dielectric permeability

$$\varepsilon(\omega)=\varepsilon'-j\varepsilon''$$

at ultra-high frequences. Measurements at wave lengths 1.7sm and 3.2sm were conducted with modified method of cylindric rod in the wave conductor, and at 10sm wave length - with a method based upon separate determining of fading constant in

the liquid /6/. Dielectric losses of dipole origin are found with introduction of corrections covering losses caused by ionic conductivity. With the help of the common method of graphic analysis it was found /fig.2 and 3/ that in the investigated interval of frequences, unlike in diagrams usually observed for solutions with commensurable concentrations of components, the dependence of ε'' on ε' for solutions of sodium desoxycholate and oleate of concentrations from 5 to 20 g/100 ml and at temperatures from 20° to 60° can be presented (within the limits of measurement errors) as a semicircle with the centre at the axis of abscissas according to Debye equations. It is established that in the interval of frequencies studied there exists only one mechanism of electric polarisation in solutions of surface-active compounds.

According to Debye formulas we calculated times of dielectric relaxation which don't depend on concentration of soap /fig.4/ and practically coincide with corresponding values for pure water. It results in that thermodynamic values of dielectric relaxation process ($\Delta\Phi_\varepsilon^\ddagger$, $\Delta H_\varepsilon^\ddagger$, $\Delta S_\varepsilon^\ddagger$) don't differ from similar values for pure water too. This allowed to conclude that the interval of dispersion observed is connected with existance of considerable plots of original water structure as a separate phase in micellar soap solutions, presence of micelles not changing its relaxational characteristics. It testifies that micellar systems above CMC consist of two phases.

Using the pseudo-phase model of micelle formation one can consider the changes in CMC under influence of different factors as changing of real solubility of surface-active agents.

Influence of temperature on CMC in the interval 5-90° in aqueous systems for various soaps (pH = 11) according to our data is presented at table. Here the axis of ordinates placed average values of CMC obtained with 3 methods (conductometrically, with method of surface tension and interferometrically).

Temperature dependence of CMC being obtained, the evaluation of thermodynamic functions of micelle formation (7)

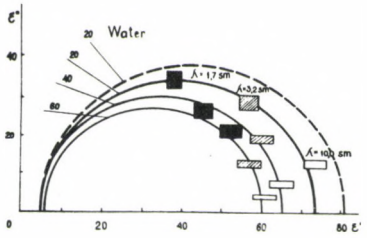

Fig.2. Dependence of ε'' on ε' for sodium desoxycholate aqueous solutions (5g/100ml) at various temperatures. Figures indicate wave lengths (sm), rectangles - the measurement errors. Dotted line is the diagram for water at 20°.

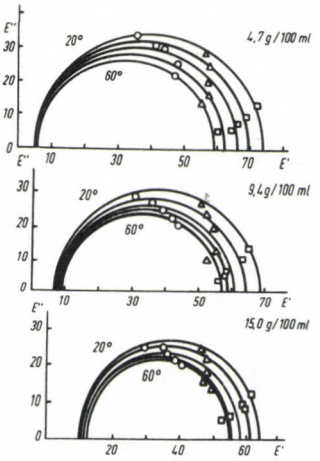

Fig.3. Dependence of ε'' on ε' for sodium oleate aqueous solutions, concentration being 4,7 g/100ml at temperatures 20-60°.
O - λ=1,7cm, Δ - λ=3,2cm, □ - λ= 10cm.

was carried out (see the table).

In all the cases studied there were found positive changes of the entropy member, values of ΔH in the investigated temperature interval being negative, zero (for ammonium oleate, higher homologues of aliphatic acids, cholic acids' salts) and positive (for sodium ricinoleate and non-ionogenic soaps). This fact points out the significant role of total entropy changes in spontaneous process of micelle formation, which are determined to a great extent with peculiarities of the structure of the solvent. Actually the analysis of existing data on structure of pure liquid water and aqueous solutions of hydrocarbons /8/ enab-

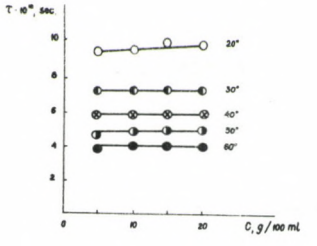

Fig.4. Dependence of dielectric relaxation time (τ) on concentration of sodium desoxycholate in aqueous solution at various temperatures.

Table

Thermodynamic functions of micelle formation of surface-active substances in aqueous environment

$C_k \cdot 10^3$, molar fraction	t°C	$-\Delta\Phi^\circ$ kcal/mol	$-\Delta H$ kcal/mol	$T\Delta S^\circ$ kcal/mol	$C_k \cdot 10^3$, molar fraction	t°C	$-\Delta\Phi^\circ$ kcal/mol	$-\Delta H$ kcal/mol	$T\Delta S^\circ$ kcal/mol
Sodium caproate					**Sodium dodecylsulphate**				
13,0	5	2,40	1,09	1,31	0,170	20	5,05	1,09	3,96
14,6	20	2,46	1,21	1,25	1,180	30	5,18	0,66	4,52
17,8	60	2,66	1,08	1,58	0,183	60	5,69	0,55	5,14
21,8	90	2,76	1,27	1,49	0,204	90	6,12	0,65	5,47
Sodium caprylate					**Sodium oleate**				
6,39	20	2,94	0,98	1,96	0,0148	5	6,13	3,48	2,65
7,23	40	3,06	1,10	1,96	0,0178	7	6,08	3,48	2,60
8,09	60	3,18	1,05	2,13	0,0196	25	6,41	3,45	2,96
Sodium pelargonate					0,0296	40	6,48	3,50	2,98
					0,0356	60	6,77	3,46	3,31
2,89	20	3,40	0,79	2,61	0,0623	90	6,98	3,60	3,38
2,87	40	3,64	0,55	3,09	**Sodium ricinoleate**				
3,12	60	3,81	0,50	3,31					
3,44	90	4,08	0,52	3,56	1,39	20	3,83	-9,05	12,88
Sodium caprate					0,816	30	4,28	-5,00	9,28
					0,798	40	4,43	-0,20	4,63
1,89	5-90	3,46-4,52	0	3,46-4,52	0,741	50	4,62	-0,40	5,02
					0,752	60	4,75	-0,20	4,95
Sodium laurate					**Ammonium oleate**				
0,430	30-90	4,67-5,56	0	4,67-5,56	0,00193	20-60	7,64-8,70	0	7,64-8,70
Sodium myristate					**Sodium cholate**				
0,0828	30-90	5,65-6,77	0	5,65-6,77	0,295	20-50	4,73-5,21	0	4,73-5,21
					Sodium desoxycholate				
					0,0901	20-50	5,42-5,97	0	5,42-5,97

les us to affirm that by uniting of non-polar parts of surface-active molecules into micelles the orientation of water molecules induced by real dissolving of a surface-active substance (the degree of hydrogen binding) decreases, and it leads to significant positive changes in entropy (besides the entropy of mixing) and, correspondingly, decrease in free energy of the system, increasing with the grow of the length of the hydrocarbon radical or with fall of general hydrophility of soap molecules.

For ionogenic surface-active agents a certain role in the negative change of the entalpy (in this case 1-3 kcal/mol) should be played by both changes of the structure of the solvent, which accompanies micelle formation, and electrostatic interactions in solutions of soap. According to Poland and Scheraga /9/ this effect can be explained qualitatively with the possibility of additional structurising of water by micelle formation in solutions of ionogenic soaps, accompanied with heat emission ($\Delta \bar{H}$), as the structure-breaking charged terminal groups of the monomers leave for the micelle. Besides that, a minimum, observed at curves CMC=f(t°) in solutions of ionic surfactants can find satisfactory explanation in overwhelming of hydrophobic share over the "dielectric" one at low temperatures (decrease of CMC with temperature) and opposite effect at high ones (if we take into consideration the lowering of dielectric constant of the environment with increase in temperature, leading to growing of repulsion forces between ionic groups of surface-active molecules, i.e. possible increase in CMC).

An interesting part of our investigations is devoted to promotion of micelle phase formation, that is decrease in CMC by introducing of truly dissolved hydrocarbons (or oleophilic alcohols) into aqueous phase at various temperatures. It was shown /1/ that in a triple system (e.g. soap-hydrocarbon-water) micelle formation starts at concentrations, lower than in double systems (soap-water), because in the first case during the process of mutual formation and stabilisation of greater micellar aggregates (saturated with hydrocarbon) there occurs additional breaking of the structure of water,

leading to greater gain in entropy of the system as compared to pure solution of the surfactant.

Introducing of organic additives decreasing the total polarity of the aqueous phase leads to an opposite effect. Thus adding of dioxan, methyl alcohol and ethylene glycol in a wide interval of temperatures and concentrations of the additives (up to 70 mol %) has shown for all the soaps investigated that CMC increases, this fact speaking for lowering of gain in energy by micelle formation in such systems. These investigations established that in solutions of biologically active steroid surface-active compound - sodium cholate, its molecules not posessing strongly pronounced asymmetry of structure, and also in solutions of a soap with short chain - sodium caproate, if concentration of additives exceeds 5-12mol% micelles in mixed solvents are not formed (degeneration of micelles). As regards solutions of long-chain soaps - sodium oleate and laurate - the tendency to form associates is kept up to 50-70 mol % of additives, though CMC can decrease in this case more than 50 times. Fall of concentration of micellar soap in solutions as a result of introducing additives is confirmed also with viscosity measurements. Dioxan appeared to be the most efficient demicellising agent among all investigated. Due to its low dielectric constant this substance notably increases the electric component of micelle formation energy (fig.5).

Additives being introduced to the solutions, the negative values of standard free energy of micelle formation ($\Delta\Phi^{\circ}$ = RTlnCMC) characterising to an extent the stability of micelles decrease for all soaps studied and for all temperatures (see examples at fig.6). Enthalpies of micelle formation, which we calculated for a number of temperature intervals, appeared to be negative, small in absolute value (1-4 kcal/mol) for all soaps investigated in mixed solvents, that is, were closed to above mentioned heats of micelle formation in aqueous solutions without additives. So it can be concluded that the fall of $-\Delta\Phi^{\circ}$ found, reflecting in a certain way the weakening of hydrophobic interactions of surface-active substances in mixed solvents, is mainly caused with decrease

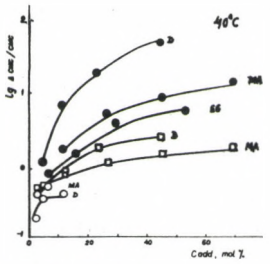

Fig.5. Relative increase in CMC in sodium caproate (○) laurate (□) and oleate(●) solutions in water with different additives (mol%): dioxan (D),methyl alcohol (MA) and ethylene glycol (EG) at 40°.

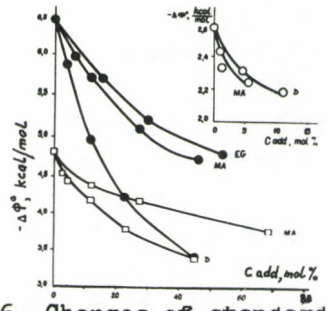

Fig.6. Changes of standard free energy of micelle formation ($\Delta\Phi^\circ$) for aqueous solutions of sodium oleate (●), laurate (□) and caproate(○) at 40° with D, MA and EG added

in positive entropy share (from 6-15 e.u. in pure water to 0-6 in presence of additives) in the free energy of micelle formation. Degeneration of micellar phase and weakening of hydrophobic interactions in mixed solvents is also confirmed with our data (fig.7)on falling of solubilising capacity of soap solutions studied relating to different hydrocarbons. This fact in its turn emphasises the intramicellar character of solubilisation as a process.

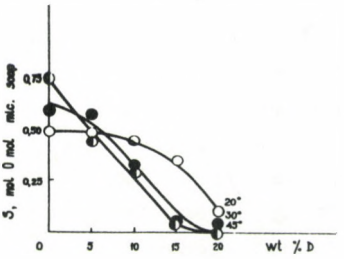

Fig.7. Solubilisation of octane (S)in water-dioxan solutions of sodium oleate(5g/100ml)at different temperatures.

References

1. P.A.Rebinder,Khimicheskaya nauka i promishlennost',4,554 (1959).
2. B.C.Bennion,L.K.J.Tong,J.Phys.Chem., 73, 3288 (1969).
3. Z.N.Markina,N.Z.Kostova,IV Intern.Congress on Surfactants, p.905, Barselona, 1969.
4. N.Z.Kostova,Z.N.Markina,Kolloidny Zhurnal, 33, 553 (1971).
5. Z.N.Markina,P.M.Khomicovskiy,S.S.Medvedev,DAN SSSR,75,243 (1950).
6. V.V.Levin,Vestnic MGU,chemistry,4,59 (1966).
7. D.G.Hall,B.A.Pethica,Nonionic Surfactants,516 (1967);M.F. Emerson,A.Holtzer,J.Phys.Chem., 69, 3718 (1965).
8. G.Nemethy,H.Scheraga,J.Chem.Phys.,36,3382 (1962).
9. D.C.Poland,H.A.Scheraga,J.Colloid.Interf.Sci.,21,273(1966).

A STUDY OF MIXED MICELLES OF CATIONIC AND NONIONIC SURFACTANTS BY MEMBRANE OSMOMETRY

K.S.Birdi

Fysisk-Kemisk Institut,Technical University,buildg. 206,Lyngby,Denmark

Mixed micelles of ionic and nonionic surfactants have been investigated by various workers (1-5). In these studies the following properties of the mixed micelles in aqueous medium were investigated , e.g., c.m.c. , electrophoresis,dye solubilization,cloud-point,spectral analysis (U.V., NMR) and micellar molecular weight (weight average). From these studies it was concluded that mixed micelles were formed when two (or more) surfactants were present. Recently we have reported on the determination of the number average micellar molecular weight, M_n , of various surfactants by using membrane osmometry (6 - 8). It was therefore considered of interest to determine the number average micellar molecular weight of mixed micelles by membrane osmometry . The purpose of this study is to report the M_n of mixed micelles of cationic (cetyltrimethylammonium bromide, CTAB) and nonionic (Triton X-100, OPE) surfactants in aqueous medium. These results are discussed in relation to the various forces responsible for the micelle formation.

Experimental : N-Cetyltrimethylammonium bromide (CTAB) ,99 % purity , was used as supplied by Theodor Schuchardt . Triton X-100 (OPE) was used as supplied by Rohm and Haas Co . The micellar molecular weights (number average, M_n) of mixed micelles in 0.025 N-KBr aqueous solutions were determined by membrane osmometry (at 30° C), as reported by us elsewhere in detail (6,7).

Results: As described elsewhere (6,7), the measured osmotic pressure, Π, existing between a sample solution of concentration c g/l (many times larger than c.m.c.) ,and a solution of concentration c' g/l (~ c.m.c.) is given by :

$$\Pi = RT\,(c - c')/M_n + RTB\,((c-c')^2 + 2\,(c-c')(c' - c.m.c.)) \qquad (1)$$

where B is the second virial coefficient. From the plots of $\Pi/(c-c')$ versus $(c-c')$, extrapolation to $c=c'$, M_n can be determined as given by:

$$\Pi/(c-c')_{c=c'} = RT/M_n + 2RTB(c - c.m.c.) \qquad (2)$$

The plots of $\Pi/(c - c')$ versus $(c-c')$ for various mixtures of CTAB and OPE, in 0.025 N-KBr aqueous solutions at 30° C, are given in figure I. The values of M_n and B calculated from figure I are given in table I. The variation of M_n with the composition is given in figure II. A maximum in M_n is observed around molar ratio of 2 OPE: 1 CTAB. The variation of the second virial coefficient, B, with composition is given in table I.

Discussion: It is well established that in a solution containing two (or more) species of surfactants, the components do not form micelles composed of single species, but rather form mixed micelles. The most direct evidence for this has been given by the presence of a single moving boundary in the electrophoretic measurements (2), besides the other methods of analysis of mixed systems (1-5). It has also been reported (9) that since the driving force for micellar association between amphiphile molecules is nonspecific, and because the micelles have a liquid like core, micelles containing mixtures of amphiphile molecules should be readily formed.

In order to be able to discuss the results, it is of interest to describe the various forces which are responsible for the micelle formation. The free energy of transfer of a single amphiphile molecule from aqueous solution to a micelle of size N, ΔG^o_m, can be written as follows (10,11):

for ionic amphiphiles:

$$_+\Delta G^o_m = {}_+\Delta G^o_\phi + {}_+\Delta G^o_w + {}_+\Delta G^o_e \qquad (+ \text{ as in } {}_+\Delta G^o \text{ refers to CTAB}) \qquad (3)$$

for nonionic amphiphiles:

$$_o\Delta G^o_m = {}_o\Delta G^o_\phi + {}_o\Delta G^o_w \qquad (o \text{ as in } {}_o\Delta G^o \text{ refers to OPE}) \qquad (4)$$

where $_+\Delta G^o_\phi$ or $_o\Delta G^o_\phi$ (which will be negative) is the free energy change associated with the transfer of the hydrophobic part of the molecule from the aqueous medium to the core of the micelle of size N, $_+\Delta G^o_w$ or $_o\Delta G^o_w$ (which will be positive) is the free energy associated with the hydration of the polar group, and $_+\Delta G^o_e$ (which will be positive) is related to the electrostatic charge repulsion.

At this stage the hydrophobic interactions can be estimated quantitativ-

ely, wheras the interactions arising from the polar group are not well defined (9,10,12). Therefore, a semi-quantitative treatment of these energy terms will be given in the following. The magnitudes of the terms $_{+}\Delta G^{o}_{\phi}$ and $_{o}\Delta G^{o}_{\phi}$ can be estimated in the following manner. It has recently been shown by various workers (13,14,15) that the free energy of transfer of hydrophobic groups from aqueous medium to the nonpolar phase (which is analogous to the interior of a micelle) is a function of the surface area of the hydrophobic group. From the surface area data given by these workers, we find that the surface area of $C_{16}H_{33}$- group in CTAB is ~ 596 $Å^2$,while the surface area of the $C_8H_{17}C_6H_4$- group in OPE is ~ 440 $Å^2$. Since the proportionality constant between surface area and energy is 25.5 cal/$Å^2$ (15),it is thus found that the $_{+}\Delta G^{o}_{\phi}$ and $_{o}\Delta G^{o}_{\phi}$ terms correspond to 15.2 kcal/mole and 11.2 kcal/mole, respectively.However,it is reasonable to expect that the CH_2 group closest to the polar group in CTAB is not hydrophobic at all (9).It is also found in literature (16) that in octylphenoxyethoxyethanols with ethylene oxide chain lengths of 1-10,the hydrophilic property shows nonlinearity when the number of ethylene oxide units is less than 3. It will thus be safe to conclude that the difference between $_{+}\Delta G^{o}_{\phi}$ and $_{o}\Delta G^{o}_{\phi}$ will be lesser than calculated,i.e. $_{+}\Delta G^{o}_{\phi} \sim {}_{o}\Delta G^{o}_{\phi}$ .In other words, we will expect negligible variation in the hydrophobic interactions in the mixed micelles as a function of the mixing ratio. Since the magnitude of $_{o}\Delta G^{o}_{w}$ will be much larger than that of the $_{+}\Delta G^{o}_{w}$, it will thus be safe to neglect the latter term in the present discussion. The value of $_{o}\Delta G^{o}_{w}$ will be related to the degree of hydration of the ethylene oxide units in the OPE micelle.As reported by us elsewhere (11), 3-5 moles water is bound per ethylene oxide unit in nonionic micelles.

For ionic micelles the term $_{+}\Delta G^{o}_{e}$ can be approximately determined from the following relationship (9,17):

$$_{+}\Delta G^{o}_{e} = \frac{A\ e^2\ N}{2\ D}\ (\ 1/R - k\ /(1+ka)) \qquad (5)$$

where R is the micelle radius for a micelle of average aggregation number N, a is the radial distance of closest approach of counterions, k is the Debye-Hückel reciprocal length (proportional to the square root of the ionic strength), e is the unit of electronic charge, D is the dielectric constant of the solvent (in the present case water),and A is the Avogadro's number.From the relation in equation 5,it is thus

seen that the magnitude of $_{+}\Delta G_{e}^{o}$ decreases in the mixed micelles as the charge per micelle decreases, when the concentration of OPE increases in the mixture.

The results given in figure II and table I show that in mixed micelles, M_n has a maximum around a molar ratio of 2 OPE : 1 CTAB. The variation in aggregation number, N, is given in figure III. These results thus indicate that the various forces responsible for the micelle formation, as given in equations 3 and 4, show nonideal behaviour in mixed micelles. In order to describe this nonideal behaviour, following interactions are of interest:

(a) since $_{+}\Delta G_{\phi}^{o} \sim {}_{o}\Delta G_{\phi}^{o}$, then negligible variation in aggregation number in mixed systems would be expected.

(b) the interactions related to the term $_{o}\Delta G_{w}^{o}$ would be expected to decrease rather linearly with decreasing concentration of OPE in the mixture. This would give rise to increase in N as OPE concentration decreases.

(c) the term related to the electrostatic interactions, $_{+}\Delta G_{e}^{o}$, would show large variation with the change in CTAB concentration in the mixture. However, it is reasonable to accept that since the expression for $_{+}\Delta G_{e}^{o}$, as given by equation 5, is dependent on the charge density of micelle, this term will not show linear variation in mixed micelles with CTAB concentration in the mixture. Especially when the concentration of CTAB is low, the term $_{+}\Delta G_{e}^{o}$ would be negligible. This would thus give rise to a nonlinear behaviour in the mixed micelles.

From the above discussion it can thus be concluded that mainly due to the nonlinear behaviour of $_{+}\Delta G_{e}^{o}$, a maximum in the aggregation number in mixed micelles of CTAB and OPE is observed, around 2 OPE :1CTAB molar ratio.

The value of second virial coefficient, B, varies in the mixed micelles with the composition, as given in table I. At this stage it is not possible to describe the variation of B quantitatively for these aqueous micellar solutions. It is worth mentioning that the value of B for a charged and comparatively less hydrated micelle (CTAB) is ~40 times larger than that of a highly hydrated nonionic OPE micelle. It is also of interest to notice that the values of B in the mixed micelles show comparatively weak dependence on the composition of the mixture. In any case, qualitatively one can conclude that the variation of B in mixed

micelles is not linearly related to the composition of the mixture. This observation agrees with the discussion given above in relation to the forces responsible for the micelle formation.

References:

1.P. Becher, in M.J.Schick,Ed.,Nonionic Surfactants,Vol.I,p.478, New York,1967

2.T. Nakagawa,in M.J.Schick,Ed.,Nonionic Surfactants,Vol.I,p.558,New York,1967

3.K.S.Birdi, Proceed. of the Vth Intern.Congress on Surface Active Substances,Vol.II,p.1055, 1968

4.F.Tokiwa,K.Tsujii,J.Phys.Chem.,75, 3560 (1971)

5.F.Tokiwa,K.Tsujii,J.Colloid Interface Sci.,41 ,343 (1972)

6.K.S.Birdi,H. Kyllingsbæk, J. Pharm. Pharmacol. 23, 900(1971)

7.K.S.Birdi, Kolloid-Z. u. Z. Polymere, 250, 731 (1972)

8.K.S.Birdi, in K.L. Mittal,Ed.,Colloidal Dispersions and Micellar Behavior, p. 233, 1975.

9.C. Tanford, in C. Tanford,Ed.,The Hydrophobic Effect,New York,1973

10.D. Attwood, A.T. Florence, Kolloid-Z. u. Z. Polymere,246 ,580(1971)

11.K.S.Birdi,Colloid and Polymer Sci.,252 ,551 (1974)

12.C. Tanford, J.Phys. Chem., 78, 2469 (1974)

13.R.B. Herman, J.Phys. Chem.,76 ,2754 (1972)

14.S.M.J. Harris, T. Higuchi,J.H. Rytting, J.Phys. Chem.,77 ,2694(1973)

15.G.L. Amidon, S.H.Yalkowsky, S. Leung, J. Pharm. Sci.,63 ,1858 (1974)

16.E.H.Crook,D.B. Fordyce, G.F.Trebbi, J. Colloid Sci.,20 ,191(1965)

17.A. Holtzer,M.F. Holtzer, J.Phys. Chem.,78 ,1442 (1974)

Table I. Number Average Micellar Molecular Weights and Second Virial Coefficients of Mixed Micelles of CTAB and OPE(in 0.025 KBr at 30° C)

Surfactant	M_n X 10^{-3}	Aggregation Number, (N)	B X 10^4 ml-mol- g^{-2}
OPE	154	238	0.14
2 OPE : 1 CTAB	179	324	1.27
1 OPE : 1 CTAB	157	311	1.06
1 OPE : 2 CTAB	140	307	1.45
CTAB	91	250	6.2

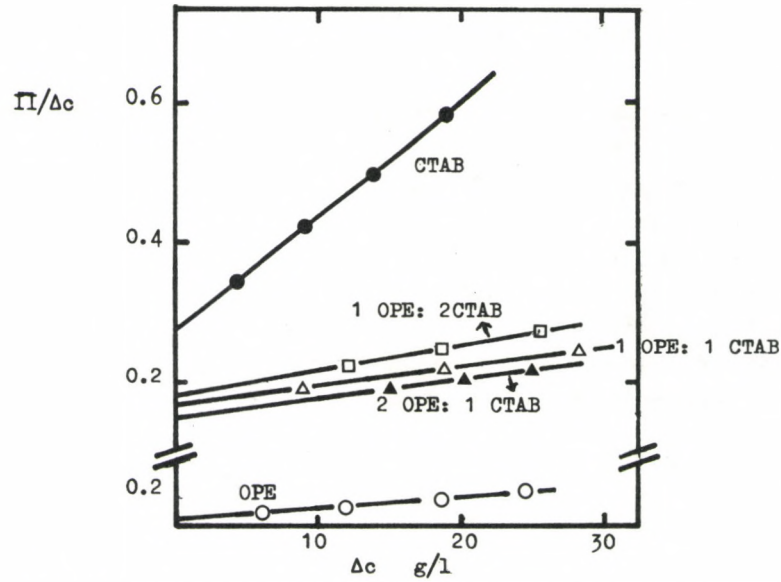

FIG. I. REDUCED OSMOTIC PRESSURE VERSUS CONCENTRATION OF CTAB AND OPE MIXED SYSTEMS IN 0.025 KBr AT 30° C.

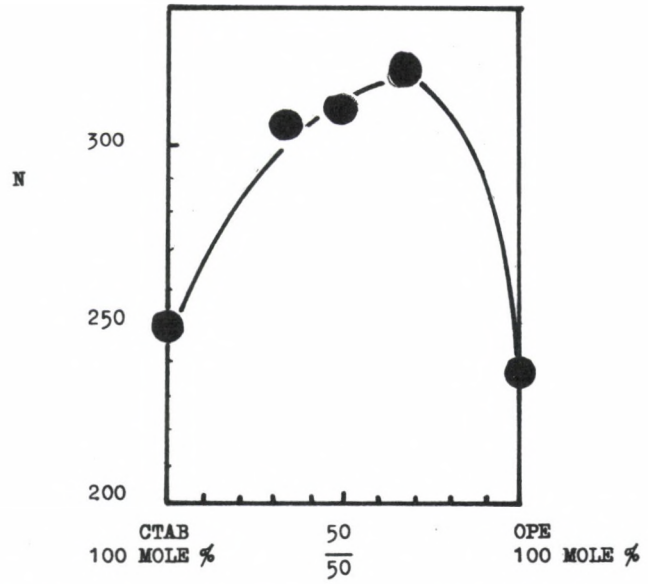

FIG. III. AGGREGATION NUMBER (N) OF MIXED MICELLES OF CTAB AND OPE AS A FUNCTION OF MIXING RATIO

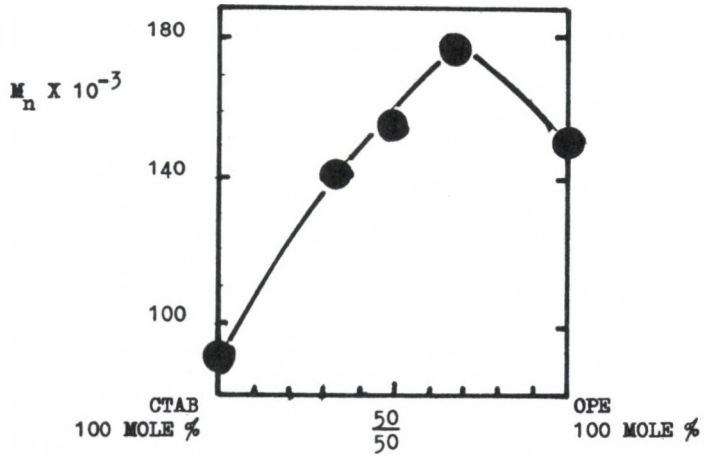

FIG. II. MICELLAR MOLECULAR WEIGHT (M_n) OF CTAB AND OPE MIXTURES IN 0.025 KBr AT 30°C, AS A FUNCTION OF MIXING RATIO

EQUILIBRIUM CONSIDERATIONS ON MICELLE FORMATION IN APOLAR MEDIA IN THE PRESENCE OF SOLUBILIZED WATER

Christen,H., Eicke,H.F. and Rehak,J.

Institute of Physical Chemistry, University of Basel
Klingelbergstrasse 80, CH-4056 Basel, Switzerland

Introduction: It is well known that in solutions of surfactants in apolar solvents considerable amounts of water or other polar substances can be solubilized [1]. For example a solution of Aerosol OT in isooctane solubilizes up to 50 M H_2O per Mol surfactant. Of considerable importance is in this respect the micelle stability which may be remarkably increased (indicated by a decrease of the cmc) at small amounts of the polar solubilisate. With increasing content of the polar substance the stability decreases [2].

In the present paper the ternary system - surfactant, apolar solvent, solubilisate - will be described by phenomenological equations with respect to an equilibrium thermodynamic treatment. Particulary the influence of the amount of the polar solubilisate on the proposed equilibrium is to be investigated. Measurements of the dielectric loss, of the viscosity and of the partial spec. volume of water were carried out as a function of the solubilized amount of water in AOT/isooctane and AOT/n-octane solutions, respectively.

Experimental: a) According to changes in the quality of an electrical circuit variations of the specific conductivity can be calculated. If C is the capacity of a sample cell ω the angular frequency and Q the quality factor of the circuit, the specific conductivity κ of a dielectric material without loss is given by $\kappa = \omega \cdot C/Z \cdot Q$ (Z = cell constant). With the help of a Feri-

sol Q-Meter, type M803A, variations of the quality factor Q were measured with continuous addition of water to a 0.1 M AOT/isooctane solution. The corresponding plot of the specific conductivity is shown in Fig. 1. The measuring frequency $f=\omega/2\pi$ was 55 and 300 kHZ respectively.

b) A KPG- Ubbelohde viscosimeter was used to determine the viscosity η at room temperature of a 0.1 M AOT/isooctane solution adding water up to 30 mol per mol surfactant. In Fig. 2 the specific viscosity $\eta_{sp} = (\eta/\eta_o)-1$ and the reduced viscosity $\eta_r = \eta_{sp}/c_{H_2O}$ were plotted, where η_o is the viscosity of the pure surfactant solution and c_{H_2O} the amount of H_2O in g/100ml solution. The same measurements were carried out for different amounts of surfactant and the maximum or the "break" of the viscosity curve appears always at the same mole ratio.

c) The density of a 0.1 M AOT/isooctane solution containing 0 to 5 moles H_2O was determined with a digital densitometer, type DMA02A (Anton Paar, KG). From these values the partial spec. volume v_{H_2O} of the solubilized water was calculated according to

$$v_{H_2O} = \frac{1}{\varrho_o}\left(1 - \frac{\varrho_1 - \varrho_o}{c}\right)$$

(ϱ_o and ϱ_1 density of the surfactant/isooctane solution without and with water, respectively, c = the added H_2O amount in g/ml solution). Fig. 3 shows a graph of these values.

Model of Solubilisation: Considering the formation of micelles it has become customary to distinguish two approximations: The multiple equilibrium- and the pseudo-phase-model. The first applies to stepwise self-association (sequential, chain-association) phenomena. Typical micelle forming systems exhibiting a high degree of association (n=15-20) show no evidence of micelle formation until the c.m.c. is reached which is the result of the high cooperativity of association in initial growth of micelles [3]. Due to recent investigations applying vapor-pressure-osmometric, conductivity, and dielectric increment measurements [4] together with theoretical considerations on the

formation and stability of typical micelle forming surfactants in apolar media, the second model has been preferred.

The satisfactory results which were obtained with the pseudo phase model applied to the transition monomer → micelle are taken to justify the attempt to base the solubilisation phenomena on the same model. Now, addition of water molecules to an apolar surfactant solution which is above the c.m.c. disturbs the equilibrium between monomers and micelles. The H_2O molecules interact with the polar groups of the monomers where it is assumed that the dissociable (hydrophilic) groups of the surfactant molecule will be hydrated. Therefore, the pure micelles decompose according to the equilibrium given in eq.1 (see below). Furthermore, it will be assumed analogous to the observations with pure surfactant solutions that the hydrated surfactant molecules also will form micelles. These are able to accept additional amounts of so-called "free" water due to their increased stability [2] (compared with pure micelles). The equations corresponding to these working hypotheses are

$$n\,S \overset{K_1}{\rightleftharpoons} S_n \quad , \qquad S_n = K_1 S^n \tag{1}$$

$$S + h\,W \overset{K_2}{\rightleftharpoons} S' \quad , \qquad S' = K_2 S W^h \tag{2}$$

$$\ell\,S' + z\,W \overset{K_3}{\rightleftharpoons} S_\ell \quad , \qquad S_\ell = K_3 S'^{\ell} W^z \tag{3}$$

Eq.2 describes the formation of hydrated monomers S' by attaching h water molecules to a monomer, eq.3 the building up of hydrated micelles with an association number ℓ with regard to an additional taking up of "free" water zW. A distinction between "free" and "bound" water (water of hydration) appears suitable with respect to various observations [5] on solubilized water in apolar surfactant solutions. The eq.1 to 3 are supplemented by two relations for the conservation of mass, namely

$$S_o = S + nS_n + S' + \ell S_\ell \tag{4}$$

and

$$W_o = W + hS' + (\ell h + z) S_\ell \tag{5}$$

As a further condition the dependence of the association number ℓ on the amount of solubilized water could be considered. With respect to the experimentally confirmed mono dispersity of pure and solubilizing micellar solutions of certain surfactants it is assumed that the (monomolecular) occupation of the micellar "surface" with surfactant molecules, i.e. the association number n and ℓ, respectively, is connected with the surfaces and volumes of the micelles according to the equation

$$\frac{\ell}{n} = \frac{F'}{F} = \left(\frac{V'}{V}\right)^{2/3} \qquad (6)$$

F and F' are the "surfaces", V and V' the corresponding volumes of pure and solubilizing micelles, respectively. Under the assumption that the volumes of the surfactants and water are additive one obtains $V = nV_T$, $V' = \ell V_T + (\ell h + z) V_w$ where V_T and V_w, respectively, are the volumes of a surfactnat and a water molecule. This yields together with the above eq.6

$$\frac{\ell}{n} = \left(\frac{\ell}{n} + \alpha \frac{\ell h + z}{n}\right)^{2/3} \qquad (7)$$

The number z of "free" water molecules per solubilizing micelle can be estimated: An upper limit of z is obtained if it is assumed that the total amount W_o of the added water is solubilized (to a first approximation). Consequently, the number S_ℓ of solubilizing micelles is large compared with pure surfactant components in the solution. Thus eqn.4 and 5 are reduced to

$$\frac{S_o}{W_o} = \frac{\ell}{\ell h + z} \quad \text{or} \quad z = \ell \left(W_o/S_o - h\right) \qquad (8)$$

Substituting this expression in eq.7 it follows

$$\ell = n\left(1 + \alpha \frac{W_o}{S_o}\right)^2 \quad \text{and} \quad z = n\left(\frac{W_o}{S_o} - h\right)\left(1 + \alpha \frac{W_o}{S_o}\right)^2 \qquad (9)$$

This limiting value of z (or ℓ) is applicable (in the frame of this approximation) to the validity range of the equn.1 to 3 as long as $W_o/S_o > h$. If $W_0/S_o \leq h$, z must be equal to zero.

The latter condition permits solving the system of the 5 equations (1) to (5) in order to obtain the five unknowns W, S, S_n, S', S_ℓ with respect to the initial concentrations S_o and W_o. The condition z=0 corresponds to the upper limit up to which the added water W_o is as water of hydration within the micelle. Above this limit "free" water is taken up by the micelles until they decompose.

Results and Discussion: The non-homogeneous system of equations 1 -5 could be solved implicitely ("dynamically") with the help of aPDP 11/45 computer and a Vector General Display System with analog-input and graphical output. Variations of the initial concentrations S_o and W_o, respectively, could be simulated with the help of potentiometers and the corresponding variations of the reaction participants were recorded. Fig.4 shows the dependence of the number S_ℓ of solubilizing micelles on the amount of solubilisate W_o at constant surfactant concentration S_o. The steep incresae of S_ℓ at the smallest amount of added water appears remarkably . The maximum is reached if the hydration is finished, i.e. $W_0/S_o=h$. This extreme value indicates that the uptake of additional ("free") water is accompanied by an increase of the volume and. therefore, the surface of the already formed micelles. The number of the hydrated micelles must decrease because of the mass conservation of the surfactant. The concentration of the non-hydrated micelles is negligible due to the considerable difference of the chemical potential of the monomers in the pure and hydrated micelles, respectively, [2]. Fig.5 shows the calculated transformation of the surfactant (in monomeric units) of the pure micelles into the hydrated species. The concentration dependence of the reaction participants derived from this model permits a satisfactory interpretation of the observed dielectric losses , the viscosities, and , to some extent, the partial spec. volume (Fig.1 to 3).

a.) Interpretation of conductivity measurements: The conductivity of an apolar surfactant solution is essentially determined by micelles sufficiently above the cmc [4]. The specific conduc

tivity is composed of ionic and dielectric contributions. The latter could be neglected as was shown by DC measurements. The dissociation equilibrium corresponding to the ionic contribution reads with respect to pure micelles S_n: $2S_n = S_n^+ + S_n^-$ from which the specific conductivity is calculated according to $\kappa = S_n^+ u^+ + S_n^- u^-$, where u^+ and u^- are the mobilities of the ionized micelles. Introduction of a mean mobility $\bar{u} = (u^+ + u^-)/2$ leads to $\kappa = 2\alpha \bar{u} S_n$, where $\alpha = \kappa/(1+\kappa)$ is the degree of dissociation. If validity of Stokes law is assumed the mean mobility is related to the solvent viscosity η and the micellar radius r_{mic} by $\bar{u} = ze/\eta r_{mic}$ (z=valence number, e=elementary charge). Assuming spherical micelles then $r_{mic} \; n^{1/2}$ may be introduced to give $\kappa = \text{const} \cdot \alpha \, S_n / n^{1/2}$. In the presence of water of hydration within the micelles (S_ℓ) the degree of dissociation is increased, i.e. α'. Introducing the same assumption as above for S_ℓ the total specific conductivity (neglecting the contribution by the monomers) may be expressed by

$$\kappa_{tot} = \text{const.} \left(\frac{S_n}{n^{1/2}} + \frac{\alpha'}{\alpha} \frac{S_\ell}{\ell^{1/2}} \right), \quad \frac{\alpha'}{\alpha} > 1 \qquad (11)$$

In Fig.6 a plot of eq.11 is given. A comparison between this plot and Fig.1 can be only of qualitative value since the added amount of water was not identical with the solubilized water.

b.) Interpretation of the viscosity data: Under ideal conditions the influence of dissolved spherical particles on the viscosity is given by Einsteins relation $\eta_{sp} = [\eta] \cdot \phi$ ($[\eta]$ = intrinsic viscosity and ϕ total volume of the dissolved substance). The value of $[\eta]$ which is according to Einstein 2.5 (ideal case) may be changed considerably by the "surface structure" of the particle, by solvation shells, and immobilized solvent molecules. In the present investigation the viscosity curve is determined essentially by the two types of micelles S_n and S_ℓ, i.e. by a change of the corresponding volume contributions $\Delta\varphi_n$ and $\Delta\varphi_\ell$, respectively. Thus $\eta_{sp} = [\eta]_n \Delta\varphi_n + [\eta]_\ell \Delta\varphi_\ell$. Assuming tentatively that both types of micelles have the same surface structure (which is probably true for a mean degree of solubilization (see Menger[51])), $[\eta]_n$ may be put equal to $[\eta]_\ell$. Furthermore, taking $\Delta\varphi_n \sim (S_n - S_n^o) n^{3/2}$ which describes

the decrease of the volume contribution of S_n (S_n^o=conc.with resp. to W_o=0) and $\Delta\phi_\ell \sim S_\ell \cdot \ell^{3/2}$ the specific viscosity reads η_{sp}=const$(n^{3/2}(S_n-S_n^o)+\ell^{3/2}S_\ell)$. Fig.7 shows a graph of this eq. against W_o which agrees satisfactoryly with Fig.2.

c.) Qualitative interpretation of the partial spec. volume: The dependence of v_{H_2O} on W_o (Fig.3) is determined evidently by two effects. The initial steep decrease of v_{H_2O} indicates a change of the over all surfactant volume within the micelles produced by the increased packing density. The slight increase above the minimum is probably due to the increased amount of solubilized free water.

Conclusions: The plots of κ, η_{sp}/c_{H_2O}, and v_{H_2O} are characterized by an extreme value for a definite amount of H_2O. The region below this peak value is marked by a successive disappearence of the original pure micelles while - at the same time - the hydrated micelles are beeing formed. This is, therefore, the true transformation region of the surfactant mononers from the pure to the hydrated micellar phase. The position of the extreme value indicates the end of this transformation, i.e. the surfactant is used up completely for the solubilization process (Fig.5). The region above this value is determined solely by the behavior of the hydrated micelles, i.e. the decrease of their number with the simultaneous (relative) increase of the association number of surfactant monomers.

Literature

[1] Poon, P.H. and Wells, M.A., Biochemistry 13, 4928 (1974)

[2] Eicke, H.F., J.Colloid Interf.Sci. (1975) in press

[3] Eicke, H.F. and Christen, H., J.Colloid Interf.Sci. 48, 281 (1974)

[4] Eicke, H.F. and Arnold, V., J.Colloid Interf.Sci. 46, 101 (1974)

[5] Menger, F.M., Donohue, J.A. and Williams, R.T., JACS 95, 286 (1973)

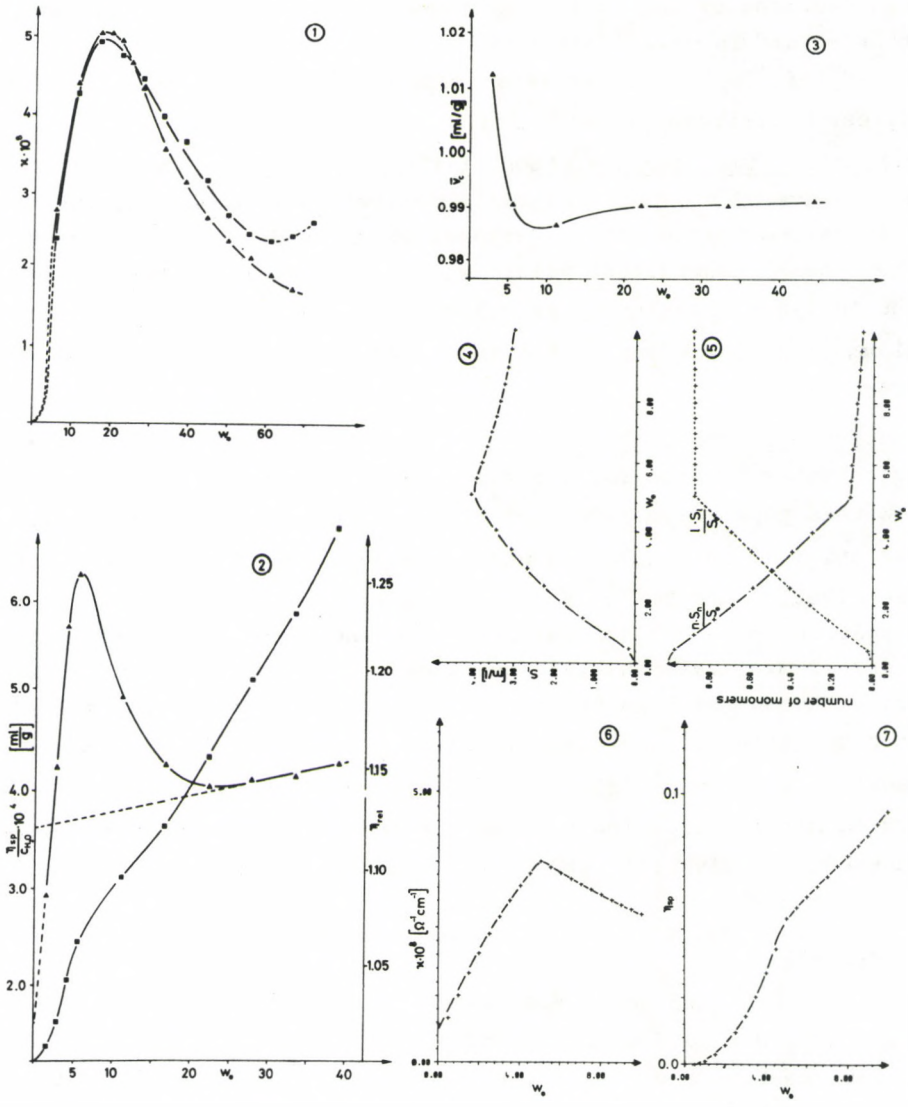

Fig. 1,2 and 3: Experimental values - ① of κ [■ 55kHz, ▲300kHz] ② of η_{sp}/c_{H_2O}[▲] and η_{rel}[■], ③ of v_{H_2O} - against W_o (Mol H_2O per Mol surfactant)

Fig. 4,5 6 and 7: Theoretical curves (see text).

STABILITY CONSIDERATIONS WITH RESPECT TO CONFORMATIONAL TRANSFORMATIONS DURING MICELLE FORMATION IN APOLAR MEDIA

H.F. Eicke , H. Christen and R.Hopmann

Institute of Physical Chemistry ,University of Basel
Klingelbergstrasse 80, CH-4056 Basel,Switzerland

Typical micelle forming systems in apolar media,for example,Aerosol OT are characterized by a high degree of association($N_n \simeq N_w \simeq 20$,number and weight averages,resp.),a considerable monodispersity indicated by the corresponding values of $N_n$and N_w, and the high cooperativity of association in the initial growth of micelles. With respect to the above mentioned properties the application of the pseudo-phase model seems to be appropiate.

Essential evidence for this model was the experimental verification by dielectric and conductivity measurements that certain premicellar subunits play the role of nuclei in the micellization process(1).For example,plots of the dipole moment contribution per monomer to the total moment of the aggregate revealed characteristic curves with a quasi sudden change in the slope which is taken to indicate a preferred type of premicellar subunit,i.e. a nucleus(Fig.1). The further slight decrease of the dipole moment after the nucleation step indicates a possible rearrangement of these subunits during the micellization process.

The concept of nucleation as a prerequisite for the micelle formation is supplemented by the findings of Ekwall et al. (2) with respect to X-ray investigations on Aerosol OT.General considerations on the stability of such micelles in apolar media(3) together with experimental evidence for their ellipsoi-

dal shape(4)demand an interpretation of the transition from a linear arrangement(which is to be expected with respect to the discussion on the nucleation process of micelle formation(2)) to a "closed" aggregate,i.e. to a stable micelle.

To verify this hypothesis kinetic experiments were made utilizing the dielectric field effect(5).The dielectric field method is based essentially on the differences in the overall reaction moments with and without an applied electric field. The selected anionic surfactant(Aerosol OT) in different solvents should be particularly suitable since the effective dipole moment of the surfactant monomers is reduced from about five to one Debye by compensation within the micelles.

Experimental

Aerosol OT(AEOT) and the solvents were commercial products of analytical grade quality which were purified and dried before use. The solutions were made up and could be transfered under N_2 into the dielectric sample cell.

A sensitive differential dielectric resonant bridge which covers the frequency range from 0.5 to 120 MHz is used to determine the dielectric losses of the solutions. It is possible to apply high static fields of the order up to $2.5 \cdot 10^7$ V m^{-1} to the sample cell. Details of the apparatus and sample cell are given elesewhere(6). The quality factor Q is a measure of the losses of the circuit and can be derived from bandwidth measurements. In order to determine the dielectric losses by the orientation of the dissolved substances(without field,subscript $_0$),the Q-factor was measured for several concentrations of the surfactant in various solvents and for the solvents themselves. Thus,$\tan\delta_o = (1/Q)_{solution} - (1/Q)_{solvent}$ have been plotted for each concentration as a function of frequency (see Fig.2:AEOT,0.018M and 0.0034M resp.in cyclohexane,open circles and squares).

Eigen and coworkers(5) have shown that chemical dielectric loss increments can be used to derive kinetic informations of reacting chemical systems if the chemical transformation is

accompanied by a finite change of the electrical moment of the system expressed as the molar moment of reaction ΔM.Due to the non-linear relationship between lnK, the loganthm of the equi= librium constant of the reacting system and the electric field strength(E),i.e. $\delta \ln K/\delta E = \Delta M/RT$(R= Gas constant and T=abs.Temp) high static fields modulated by an a.c. field of low amplitude must be used to observe finite shifts of the chemical equili= brium. Consequently,the dieletric excess loss is the quantity which has to be determined experimentally. The frequency de= pendence of these chemical loss increments and of the dielec= tric losses produced by the orientation of the dissolved sub= stances(without static field) correspond to a Debye-type ab= sorption curve. The corresponding amplitude factors contain the physical parameters of the aggregates and the reacting chemical system,respectively(5).

The applied high static field will cause a considerable alignment of the particles which is dependent on the dipole moment. Thus the dielectric losses produced by this effect will decrease(=loss decrements) in contrast to the losses de= scribed above. Now,both effects(with opposite sign) can occur in the same frequency region. Their superposition is shown in Fig.2(filled circles and squares)(for a more detailed discus= sion cf.(7)).

Results

Various concentrations of AEOT in benzene and dioxane were measured under the applied static field. The excess loss= es have been found to be always negative and to correspond to a Debye-type absorption(Fig.3). If it is assumed to a first approximation that the shape of the relaxing species is sphe= rical(radius a) the characteristic frequencies with respect to the two solvents can be related to the volumes of the species by means of the Debye equation $f_c = kT/(8\pi^2 \eta a^3)$ with k=Boltzmann constant and η the dynamical viscosity of the solvent. The ratio of f_c in dioxane (~120 MHz) and benzene(~23 MHz)yielded a volume(a^3) ratio close to the integers 1:5 which very satis=

factorily agrees with results from dielectric(1) and vapor pressure measurements(12). From the latter it was derived that aggregates in benzene contain most probably 15 monomers, in dioxane but 3 monomers. The aggregates in dioxane are to be viewed as premicellar subunits(nuclei) which are stabilized by the pseudo apolar dioxane.

Since the present investigations are mainly concerned with cyclohexane solutions of AEOT these results will now be treated seperately. Earlier chemical relaxation studies on homoassociative phenomena have demonstrated that the time constants of these bimolecular reactions are found in the same frequency region as for the orientational relaxations in the present study. Thus, superposition must occur. The results plotted in Fig.2(filled circles and squares) show a strange appearance. They cannot be described by a typical Debye absorption term. A separation into two relaxation processes can be achieved with the help of a computer procedure based on a least squares fit according to the steepest descent(8). Two relaxation processes could be assigned: one with negative sign in the vicinity of 20 MHz, another one with positive sign which was concentration dependent. The accuracy of the measurements did not allow to identify more than two relaxation processes. Thus, according to the above the data have been described by an orientational and a chemical contribution. By comparison of the concentration independent relaxation frequency in cyclohexane with that in benzene it is concluded that both processes are due to orientational relaxation by the micelle(details see(7)). The significance of the data points has been carefully checked by determining the standard deviation of each value.
The amplitudes of the orientational and chemical relaxation processes plotted in Fig.4 show a sigmoidal shape of the curve, thus indicating the cooperative features of micelle formation(cf.(9)),while the quasi sudden increase of the slope of the curves indicates the critical micelle concentration(c.m.c.). A particular interesting feature shows the plot of the calculated

chemical relaxation frequencies against the concentration(Fig. 5).This will be discussed in the next paragraph.

Discussion

The discussion of the results is based on the pseudo-phase model(10)(11)which proved to be appropiate in a number of investigations on AEOT(1)(3)(4).In this respect the present results represent a new and independent confirmation for the existence of trimeric subunits which are apparently the sole species in dioxane solutions but also exist in benzene and cylohexane solutions of AEOT(12).As has been fully discussed(1)the trimeric subunits can play the role of nuclei for the micellization process.The model to be devellopedbelow depends essentially on this fact.The most important result of this investigation is the concentration dependence of the chemical relaxation time(Fig.5):It rules out a linear aggregation as the dominant relaxation process which would not be compatible with a finite micelle size.Instead,the kinetic behav iour(with decreasing relaxation times in a particular concentration range)can be explained on the basis of Monods model(13)describing conformational changes induced by ligand-enzyme interactions.Since such a conformational change during micelle formation appears quite reasonable the following reaction scheme is proposed:

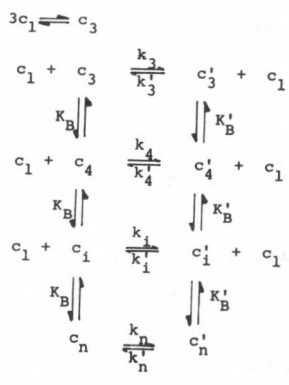

(c_1=concentration of monomers,c_3 and c_i concentration of nuclei and premicellar aggregates,resp.)Due to previous results (12)and chemical reasoning three different elementary steps for the micellization have to be considered:1.at very low concentration(c_o<<cmc)an equilibrium between monomers,di- and trimers 2. the growing of premicellar aggregates by binding surfactant monomers at medium concentration(aggregation of nuclei is unprobable(1)).Both processes are diffusion controlled, and3. conformational change of larger premicelles could alter them in such a way that-at a

certain stage-the binding of monomers will become too difficult or end:Micelles of a certain size then have been formed which determine the properties of the solution.

The general form of relaxation equations for concentration dependent homoassociation is $^1/\tau = \nu^2 k_R c_1^{\nu-1} + k_D$ (ν = stoichiom.factor, c_1=monomer equil.concentration, k_R and k_D= rate constants of association and dissociation). Since the initial concentration of the investigated surfactant solutions are about millimolar and the monomer concentration is only a fraction of it the reciprocal relaxation time ($1/\tau$) will be determined predominantly by k_D. It should be further noted that with increasing c_o the trimers adapt the role of nuclei, i.e. they grow quickly to larger premicellar aggregates. Thus, c_3 does not pass (to a first approximation) a certain value which is also true for c_1 This corresponds essentially to the pseudo-phase model. Since this situation is applicable in this investigation and the behavior of the experimental relaxation times suggests to be not primarily due to intermolecular association explanation was sought on the basis of intramolecular changes occuring in the premicelles or micelles. The contribution to the relaxation time of the micellization due to association processes yielding trimers is, therefore, negligible (i.e. the conformational equilibrium is adjusted at all times compared with the bimolecular reaction step) and c_1 is considered to be constant with respect to the conformational change, i.e. $\delta c_1 \approx 0$.

The computation of such a conformational change model according to the reaction scheme given above is related to Eigens(14) treatment of Monods model. With regard to the quantitative treatment one should refer to(7). The essential idea is as follows: Each association step may undergo a conformational change, $c_i \rightleftharpoons c_i'$ with an equil.constant K_i. Furthermore, the binding constant $K_B = \bar{c}_{i+1}/\bar{c}_i\bar{c}_1$ and $K_B' = \bar{c}_{i+1}'/\bar{c}_i'\bar{c}_1$ resp., is equal for each successive association step, i.e. it is assumed that a conformational change does not influence the binding energy of a monomer to the premicellar aggregate. The final equation for the reciprocal

relaxation time (see (7)) which will be compared with Fig.5 reads

$$1/\tau_{ch} = k_3 S_{\alpha,j}\{1/K_3 + \sum_{i=3}^{n} i(xK_B'/K_B)^{i-3} / \sum_{i=3}^{n} ix^{i-3}\} / \sum_{i=3}^{n} (xK_B'/K_B)^{i-3}$$

where $S_{\alpha,j}=1+x+\ldots+\alpha x^{j}+\ldots+x^{n-3}$, $(1<j<n-3)$, $x=K_B\bar{c}_3$, $x'=K_B'\bar{c}_3'$.
It expresses the fact that the rate constants k_i and k_i' at the beginning and the end of the micellization process must be smaller than for premicellar aggregates of a medium size: Thus, $k_i = k_3$ for all i except the j-th $(4 \leq j < n)$ would fulfill this requirement The j-th rate constant is, therefore, α times k_i $(k_j = \alpha k_i)$.

By fitting the theoretical curve to experimental data the parameters involved could be determined and their influence on the shape and position of the curve estimated. The factor α determines almost exclusively the height of the maximum of the theoretical curve and influences the slopes near to the maximum. The experimental data points are fitted suitably by the parameters: $\alpha=6.5$, $k_3=5\cdot10^{7}\,\mathrm{sec}^{-1}$, $K_B=K_B'=222\ \mathrm{l\cdot mole}^{-1}$, $K^*=1(\mathrm{l\cdot mole}^{-1})^{2}$, $j=6$ (K^*=equil.const. for premicellar association process) indicated by the solid line in Fig.5. The rather low value of K^* indicates a balance of enthalpic and entropic contributions of the primary association steps which comprises that small subunits are present in very low concentrations in accordance with its nature as nuclei.

The very satisfactory agreement between experimental and theoretical curves (Fig.5) strongly supports the underlying idea of a conformational change which is certainly not confined to the micellization process but should be given due consideration in discussing the termination of any linear association of subunits to obtain aggregates of limited size.

Literature

(1) Eicke, H.F. and Christen, H., J.Coll.Interf.Sci. 48, 281 (1974)
(2) Ekwall, P., Mandell, L., Fontell, K., J.Coll.Interf.Sci. 33, 215 (1970)
(3) Eicke, H.F. and Christen, H., J.Coll.Interf.Sci. 46, 417 (1974)
(4) Eicke, H.F. and Shepherd, J.C.W., Helv.Chim.Acta 57, 1951 (1974)
(5) Bergmann, K. Eigen, M., DeMaeyer, L. Ber.Bunsenges.Phys.Chem. 67,
(6) Hopmann, R., Rev.Sci.Instr. 46, 306 (1975) 819 (1963)
(7) Eicke, H.F., Hopmann, R., Christen, H. Ber.Bunsenges.Phys.Chem.
(8) Nelder, J.A. and Mead, R. The Computer J. 7, 308 (1965) (in prep.)
(9) Christen, H. and Eicke, H.F., J.Phys.Chem. 78, 1423 (1974)

Literature continued:

(10) Tanford,Ch.,The Hydrophobic Effect,J.Wiley New York 1973
(11) Hutchinson,E,Inaba,A.,Bailly,L.G.,Z.Phys.Chem.NF5,344(1955)
(12) Eicke,H.F.and Arnold,V.,J.Coll.Interf.Sci.46,101(1974)
(13) Monod,I.Wyman,J.and Changeaux,J.Mol.Biol.12,88(1965)
(14) Eigen,M.,Quaterly Rev.Biophys. 1,3 (1968)

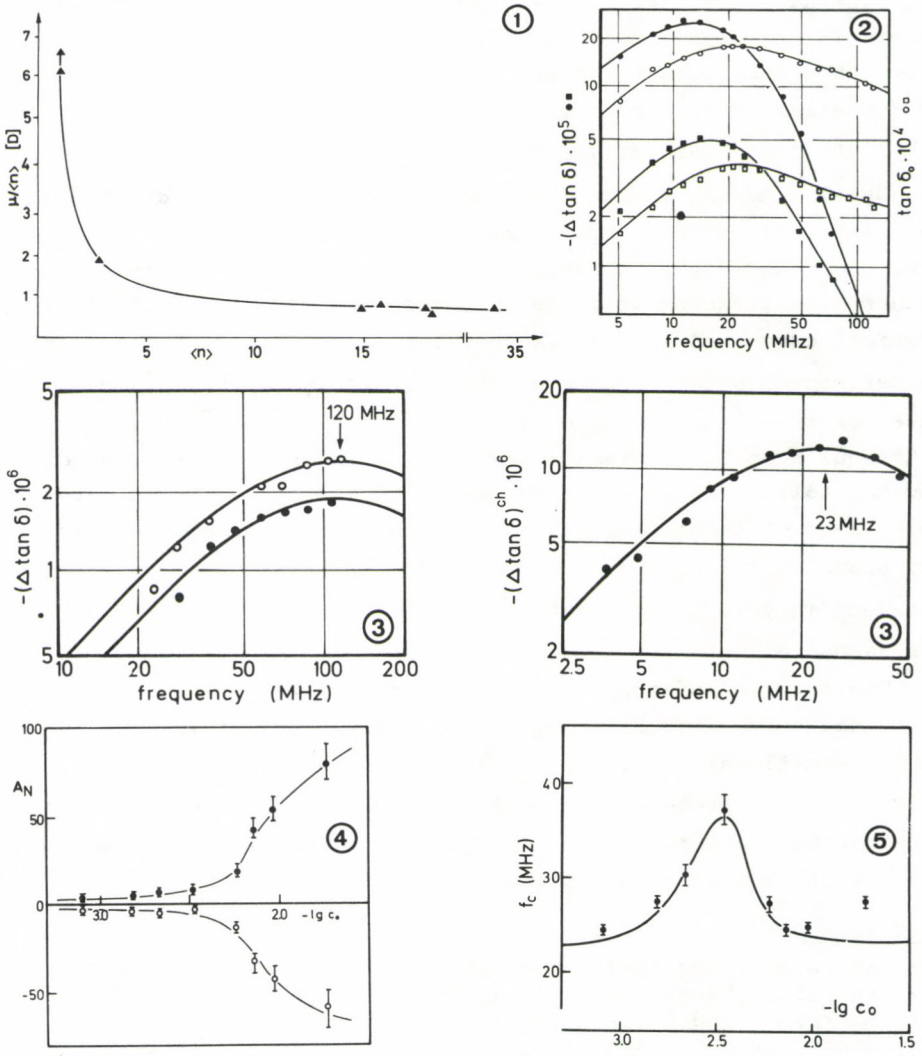

1.μ/⟨n⟩ against association number⟨n⟩(AEOT);2.Orientational relaxation(OR)(E=0(○)),Orientational field effect(OFE)(E=2·10⁷ Vm⁻¹(•))AEOT/C_6H_{12};3.OFE: AEOT/dioxane(2.66·10⁻³m(○),1.77·10⁻³m(●))left:AEOT/C_6H_6(4.55·10⁻²m)(E=2·10⁷ Vm⁻¹)right;4.Amplitude factors of FE(AEOT/C_6H_{12})chemical excess loss(●), OFE(○);5.Calc.relaxation frequency versus conc.(points=experimental)

AGGREGATION OF ALKYLAMMONIUM BISULFATE IN BENZENE

A.S. Kertes, Institute of Chemistry, The Hebrew University, Jerusalem, Israel

O. Levy and G.Y. Markovits, Practical Engineering College, Beer-Sheva, Israel

Our previous vapor pressure-lowering (1-3), conductance, viscosity (4) and dielectric constant (5) measurements on a large number of various cationic surfactants in hydrocarbon solvents indicate that there is a significant difference in the aggregation behavior of the amphiphiles when compared to that in their aqueous solutions. The characteristic features of hydrocarbon solutions are the presence of aggregates at low solute concentrations and the small number of molecules per micelle, both features in sharp contrast to the behavior of surfactants in aqueous solutions. It has been advocated (6) that the process of aggregation in hydrocarbon solvents can be presented in terms of mass-action law equilibria, implying the coexistence of monomers, dimers, trimers and higher oligomers in a dynamic equilibrium. As a result of such an aggregation process, a smooth continuity is observed in all conventional physical properties measured in these systems. This is again in contrast to the phenomenon in aqueous systems where a sharp transition is usually observed at the critical micelle concentration, due to the simple monomer $\rightleftarrows$ micelle equilibrium. The lack of firm evidence (6) to the existence of CMC in hydrocarbon solutions of surfactants makes it questionable whether the concept of critical micelle conentration, as known and defined for aqueous solutions, can be applied to surfactant-hydrocarbon systems.

Cationic surfactants of the alkylammonium bisulfate type in hydrocarbon solvents have been found to exhibit a higher tendency toward aggregation than the corresponding halides. At room temperature in benzene solutions tri-n-octylammonium bisulfate was found

to have an average aggregation number of $\tilde{\underline{n}}\approx 2$ by light scattering measurements (7) in the concentration range of 2-8 wt%, but $\tilde{\underline{n}}$ was found to vary between 2 and 3.8 by isopiestic vapor pressure measurements (8), and up to $\tilde{\underline{n}}=4.8$ at $\sim 5°C$ by cryoscopy (9) at comparable concentrations. Under similar experimental conditions trilaurylammonium bisulfate in benzene, as found by vapor pressure osmometry (1), has an average aggregation number ranging between $\tilde{\underline{n}}=1.8\text{-}3.4$.

We now report additional experimental data on the trilaurylammonium bisulfate-benzene system at 25°C as obtained by the dye-solubilization method (10) using Rhodamine B as the polar dye. The optical data are interpreted in terms of a stepwise aggregation of the surfactant using the concept and calculation procedure described previously (1).

Results and Discussion

The optical densities at 560 nm, of benzene solutions of the bisulfate in the concentration range between 2.5×10^{-4} and 5×10^{-3}M, and in the presence of a constant, 3×10^{-6}M, concentration of Rhodamine B yield a conventional S-shaped curve which levels off at about 1.2×10^{-3}M. Since the dye-solubilization method is based on the assumption (10) that the colored species in solution is due to one specific dye-micelle complex, the molar absorbence of the complex could be evaluated from the optical density measured at constant dye and high surfactant concentrations where the optical density has a constant value.

Previous osmometric measurements on the same system under similar experimental conditions (1) have shown that trilaurylammonium bisulfate undergoes aggregation with increasing concentration in benzene. It has been found that the predominating aggregated species in equilibrium are the dimer and the hexamer with the corresponding overall aggregation constants of $\log \beta_2 = 3.63$ and $\log \beta_6 = 13.66$ at 25°C. Using a similar concept (1), the optical density curves can be interpreted in terms of a set of mass-action law equilibria represented as

$$2M \rightleftarrows M_2 \qquad \beta_2 = [M_2]/[M]^2 \qquad (1)$$

$$\underline{n}M \rightleftarrows M_{\underline{n}} \qquad \beta_{\underline{n}} = [M_{\underline{n}}]/[M]^{\underline{n}} \qquad (2)$$

$$M_{\underline{n}} + R \rightleftarrows M_{\underline{n}}R \qquad \beta_{\underline{n}R} = [M_{\underline{n}}R]/[M_{\underline{n}}][R] \qquad (3)$$

where M, M_2 and $M_{\underline{n}}$ are the monomer, dimer and oligomer respectively; β_2 and $\beta_{\underline{n}}$ the corresponding dimerization and oligomerization constants; and R and $M_{\underline{n}}R$ the dye and the dye-oligomer complex, and $\beta_{\underline{n}R}$ the formation constant of the latter. The concentrations of the species at any given bisulfate concentration were expressed through the respective equilibrium constants of eqs. 1-3 in the material balance equation for the total bisulfate concentration

$$\underline{c}_M = \underline{n}[M_{\underline{n}}R] + \underline{n}[M_{\underline{n}}] + 2[M_2] + [M] \qquad (4)$$

in terms of the experimentally accessible [R] and $[M_{\underline{n}}R]$, and the resulting equation was solved by a linear least-squares program for values of $\underline{n}$ ranging from 2 to 10. The best fit was obtained for $\underline{n}$=6, in complete agreement with the previous osmometric data representing the aggregation equilibrium in the trilaurylammonium bisulfate-benzene system at 25°C in terms of monomer, dimer and hexamer formation. The preliminary value of the dimerization constant is $\log \beta_2 = 3.92$, and the product of the equilibrium constants for reations 2 and 3 is $\log \beta_6 \cdot \log \beta_{6R} = 23.85$. A refinement of the computer calculations is in progress and will be reported at the Conference.

References

1. A.S. Kertes and G.Y. Markovits, J. Phys. Chem. 72, 4202 (1968).
2. A.S. Kertes, O. Levy and G.Y. Markovits, J. Phys. Chem. 74, 3568 (1970).
3. A.S. Kertes, H. Gutmann, O. Levy and G.Y. Markovits, in "Chemie, physikalische Chemie und Anwendungstechnik der grenzflachenaktiven Stoffe", Proceedings VIth Inter'l Conf. Surface Activity, Zurich 1972, Carl Hanser Verlag, Munich 1973, p.1023.

4. G.Y. Markovits, O. Levy and A.S. Kertes, J. Coll. Interf. Sci. 47, 424 (1974).
5. O. Levy, G.Y. Markovits and A.S. Kertes, J. Phys. Chem. 75, 542, (1971).
6. A.S. Kertes and H. Gutmann, in "Surface and Colloid Science", Vol.8, E. Matijevic, Ed., Wiley-Interscience, New York 1975.
7. K.A. Allen, J. Phys. Chem. 62, 1119 (1958).
8. C.F. Coleman and J.W. Rody, in "Solvent Extraction Chemistry", D. Dyrssen, J.O. Liljenzin and J. Rydberg, Eds., North Holland, Amsterdam, 1967, p. 362.
9. V.V. Fomin and V.T. Potapova, Zhur. Neorg. Khim. 8, 990 (1963).
10. C.R. Singleterry and L.A. Weinberger, J. Amer. Chem. Soc. 73, 4574 (1951).

SOLUTIONS OF COBALT HEXAMMINE SOAPS IN ORGANIC SOLVENTS

Wahid U.Malik, Ajay K.Jain and (Miss) M.J.Siddiqui

Chemical Laboratories, University of Roorkee, Roorkee, U.P. India.

The importance of heavy metal soaps as catalyst, additives in lubricants and emulsifier in water-in-oil systems is well recognised. Since a knowledge of their micellar behaviour and solubility in non-aqueous solvent is important to assess their applied utility, investigations on these two aspects of the chemistry of heavy metal soaps are highly desirable. Literature survey shows that sufficient data is available on the solubility of these soaps and, to some extent, on their aggregation, micellisation etc.

Another aspect of the chemistry of heavy metal soaps worth investigation is to prepare modified metal soaps and study their physico-chemical properties. With this aim in view modified cobalt soaps were prepared by the metathesis of sodium salts of higher fatty acids with cobalt ammines in aqueous solutions. The modified soaps which can be appropriately designated as metal complex soaps, were subjected to solubility and aggregation studies in various non-aqueous solvents. In this paper we discuss the results of our studies on the solubility of cobalt-hexammine stearate, palmitate and myristate as determined by radio-tracer technique[1-3].

EXPERIMENTAL

Reagent and material

Sodium myristate, palmitate and stearate were reagent grade B.D.H. products and were used without further purification. All other reagents and solvent were of A.R. grade. Radio-

isotope Co^{58} in the form of cobalt chloride in HCl solution was obtained from Isotope Division, Bhabha Atomic Research Centre, Trombay, Bombay.

Preparation of labelled hexammine cobalt chloride:- Co^{58} in the form of $CoCl_2$ was added to inactive cobalt chloride aqueous solution and the resulting mixture was warmed up to bring about complete isotopic exchange. This solution was then used for the preparation of hexammine cobalt(III) chloride by the method listed in literature[4].

Preparation of labelled cobalt hexammine soaps:- The labelled cobalt hexammine stearate, palmitate and myristate were prepared by interacting aqueous solution (0.01M) of respective sodium soaps with aqueous solution (0.02M) of labelled hexammine cobalt(III) chloride. The precipitated cobalt hexammine soaps were filtered and washed with doubly-distilled water and then with alcohol and were dried in vacuum desicator. The labelled cobalt hexammine soaps were prepared and analysed for C, H and N. On analysis these soaps were found to conform to the following molecular formulae.

Soaps	% calculated			% found		
(i) Cobalt hexammine myristate	C	H	N	C	H	N
$Co(NH_3)_6(C_{13}H_{27}COO)_3$	59.92	11.77	9.98	59.46	11.42	9.55
(ii) Cobalt hexammine palmitate						
$Co(NH_3)_6(C_{15}H_{31}COO)_3$	62.12	12.09	9.13	62.14	12.14	9.34
(iii) Cobalt hexammine stearate						
$Co(NH_3)_6(C_{17}H_{35}COO)_3$	64.22	12.19	8.32	63.63	12.19	8.59

Preparation of standard solution:- Each standard solution of cobalt hexammine soap was prepared by dissolving a weighed amount of the soaps in known volume of methanol.

Preparation of saturated solution of cobalt hexammine soaps:- Each saturated solution was prepared by the agitation of an excess of cobalt hexammine soap in pyrex stoppered bottle about half full of solvents. Agitation was continued till true solubility equilibrium was established as indicated by the constancy of the counting rate (activity) on successive

measurements.

Analysis:- Sample withdrawn from the bottles at various time intervals were filtered through a fine paper. Five ml were taken for counting purposes. Specific activity of cobalt hexammine soaps was determined in terms of count rate by measuring the activity of 5 ml of soap standard solution in methanol on a gamma ray scintillation spectrometer(B. A. R. C., Bombay) employing NaI(Tl) crystal. All measurements were made under same geometrical conditions. Appropriate corrections were made for coincidence loss and the decay of the isotope.

RESULTS AND DISCUSSION

Solubility behaviour:- The solubility values of cobalt hexammine soaps are given in Table-1. The results indicate that the effect of decrease in carbon chain length of the soaps is to increase the solubility of the soaps. Further, it is obvious that these soaps are sparingly soluble in all solvents used but are relatively more soluble than corresponding simple metal soaps[1].

Effect of temperature on cobalt hexammine soaps solubility:- The effect of temperature on the solubility of these metal complex soaps in some solvents, viz., benzene, m-xylene, toluene, ethyl methyl ketone, nitrobenzene and chlorobenzene has also been investigated. The change in solubility as a function of temperature is shown in Figs.1-3 for three solvents(benzene, m-xylene and chlorobenzene) only. Exactly similar behaviour was also observed in case of other solvents already mentioned. It is evident from Fig.1-3, that at low temperatures the solubility increases slowly with increase in temperature. Then within a narrow temperature range, the solubility begins to increase enormously. The temperature at which the abrupt change occurs is known as the Krafft point[5] or critical solution temperature (C. S. T.) and the concentration at which it occurs is the critical micelle concentration(c.m.c.)of the soap. This behaviour is the characteristic of micelle-forming substances and is explained in terms of the low solubility of the soap molecule and the high solubility of the micelle. This type of solubility behaviour of cadmium, silver and chromium soaps has

already been observed by us[1,3]. The c.m.c. and C.S.T. values calculated from abrupt changes in Figs.1-3 are given in Table-2. Similar plots were also obtained in toluene, ethyl methyl ketone and nitrobenzene and c.m.c. and C.S.T. values of cobalt hexammine soaps determined from these plots are also given in Table-2. It is interesting to note that C.S.T. value decreases and c.m.c. value increases as we pass on from stearate to myristate. Since, cobalt hexammine myristate has highest solubility (Table-1), we may conclude that higher is the solubility of the soap, the lower is its C.S.T. and higher is its c.m.c. value as compared to other soaps.

Table-1

Solubility of cobalt hexammine soaps in different solvents at 30 ± 1°C.

Solvents	Stearate ($x10^{-5}$ M/L)	Palmitate ($x10^{-5}$ M/L)	Myristate ($x10^{-5}$ M/L)
Benzene	7.3	16.4	35
m-xylene	12.0	13.5	44
Toluene	8.1	12.7	115
Ethyl methyl ketone	6.1	6.7	89
Nitrobenzene	7.0	17.1	55.8
Chlorobenzene	10.1	13.8	64
Dimethyl sulphoxide.	10.7	16.4	62
Dioxane	15.7	16.9	50
Dimethylformide	5.5	8.7	76
Chloroform	12.8	18.7	100
Acetone	5.8	10.5	85
Water	4.8	17.0	79

Table-2

C.S.T. and c.m.c. values of cobalt hexammine soaps in different solvents

Solvents	Stearate		Palmitate		Myristate	
	C.S.T. (°C)	c.m.c. ($x10^{-5}$M/L)	C.S.T. (°C)	c.m.c. ($x10^{-5}$M/L)	C.S.T. (°C)	c.m.c. ($x10^{-5}$M/L)
Benzene	45	20	41	21	37.5	42
m-xylene	45	17	44	18	30.0	46
Chlorobenzene	45	15	39	26	28.5	34.0
Toluene	40	11	36	13	27.5	80
Ethyl methyl ketone.	45	23	44	34	35.0	60
Nitrobenzene	47	15	40	27	35.0	110

REFERENCES

1. Wahid U.Malik, Ajay K.Jain and O.P.Jhamb, J.Chem.Soc.(A),1514 (1971).
2. Wahid U.Malik, B.P.Singh and A.K.Jain, Experientia, 23,346(1947).
3. Wahid U.Malik and Ajay K.Jain, J.Colloid and Interface Sci., 31,460(1969).
4. Grt.G.Schlessinger, Inorganic Laboratory Preparation, Chemical Publishing Company, New York,175 (1962).
5. F.Krafft and H.Wiglow, Ber., 28,2566 (1895).

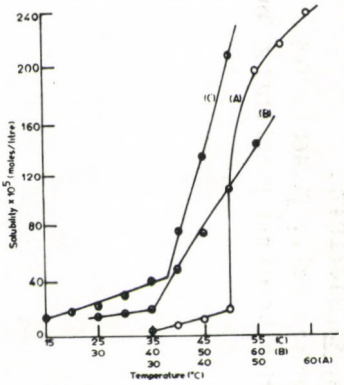

FIG.1- Solubility of Cobalt hexammine stearate (A), Palmitate (B), Myristate (C) in Benzene as a function of temperature.

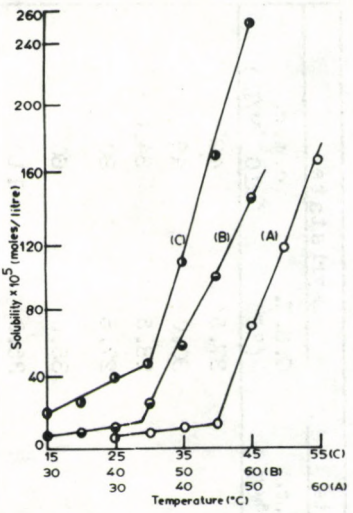

FIG.2- Solubility of Cobalt hexammine Stearate (A), Palmitate (B), Myristate (C) in m-xylene as a function of temperature.

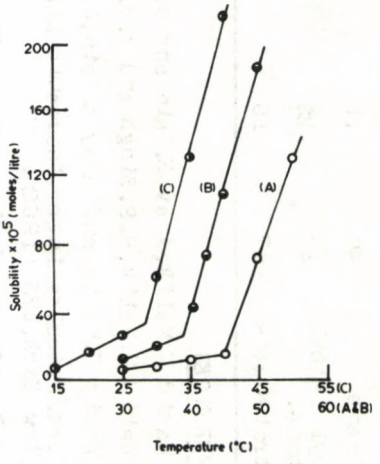

FIG.3- Solubility of Cobalt hexammine Stearate (A), Palmitate (B), Myristate (C) in chlorobenzene as a function of temperature.

MICROEMULSIONS USING NONIONIC EMULSIFIERS

J.B. Brown, Denison University, Granville, Ohio, USA,
I. Lapczynska and S. Friberg, The Swedish Institute for Surface Chemistry, Box 5607, S-114 86 Stockholm.

Introduction

The structure of microemulsions, transparent thermodynamically stable "emulsions", has been the subject of discussion for a long time. The generally held view has changed, from an acceptance of the original description of microemulsions as two-phase systems (1) with the interest centered on the interfacial properties (2-7) to the later realization that the microemulsions are micellar systems characterized by extremely high solubilization ratios (8-11).

Microemulsions which are stabilized by ionic surfactants combined with medium chain length alcohols (1-7) are characterized by comparatively high amounts of emulsifier (~15 % W/W) and large stability ranges versus temperature (10). Nonionic surfactants on the other hand cause extremely large solubilization with small amounts of emulsifier, but the temperature range for stability is extremely small (12-19). The solubilization maxima versus temperature, both of oil in the aqueous phase and of water in the oil phase, are related to the cloud point of the surfactant and the nature of the hydrocarbon.

In a small temperature range the solubility of the emulsifier shifts from water to oil with increasing temperature and the solubilization is simultaneously changed from O/W to W/O. The temperature in the middle of this range has been denoted the phase inversion temperature (PIT) or HLB-temperature by Shinoda, who originally (20) used these phenomena as an aid in emulsifier selection in order to obtain efficient emulsification.

Robbins (21) has recently published a theory for micro-

emulsions stabilized by nonionic emulsifiers assuming spherical aggregates, and calculated the chemical potential of solubilized water in the droplets from differences in surface pressure of the non-polar and polar parts of the surfactant molecules. Furthermore his postulate was that all the emulsifier molecules be at the interface.

A preliminary investigation (22) has displayed the connection between the surfactant phase (14) and the normal micellar solutions. The surfactant phase may in the lower temperature range of its existence be infinitely diluted with water simply being an isotropic solution and stable in a limited hydrocarbon/emulsifier range. In the middle of the PIT range the surfactant phase forms an isotropic solution region with no connections to the hydrocarbon solution on the aqueous part of the system. At higher temperatures the surfactant phase region coalesces with the area for the hydrocarbon solution.

At the PIT a minimum of emulsifier concentration was required in order to obtain a surfactant phase. Lower and higher temperatures both gave rise to similar solubilization regions but larger amounts of emulsifier were necessary. The solubility regions in the PIT were extremely sensitive to temperature changes; a variation in temperature of $2^{o}C$ gave regions with no overlap. On the other hand a mixture of emulsifiers with different polyoxyethylene chain lengths gave corresponding solubility regions but with less sensitivity to temperature. In the systems investigated the emulsifier concentrations were high and no minimum at PIT was observed (23).

With regard to the fact that microemulsions have a pronounced technical importance at present and that many questions concerning the structure of microemulsions still remain unanswered, we considered that an investigation on the structural changes occurring with changes in temperature in a system water, nonionic emulsifier and hydrocarbon would be of interest. The purpose of the investigation was

to evaluate the behavior of polyoxyethylene emulsifiers with a distribution of polar and non-polar chain lengths.

Experimental

Material. The hexadecane was Fluka p.a. used without further purification. The emulsifier was obtained by molecular distillation using a Leybold-Heraus distillation apparatus KDLT. The chain length distribution was determined by gas chromatography using pure monodisperse compounds from Nikkol (more than 98 % pure) as calibration compounds both for retention time and response of the detector for the individual compounds. The samples were silylated by Merk BSA (trimethyl silyl acetamide) after dehydration. The gas chromatograph was Perkin Elmer 881 with an OVI column with 3 % ABS Chromosorb W. The temperature was raised 8°C min^{-1} from 150°C to 330°C after an initial time of 2 min. Injection temperature was 300°C. The hydrocarbon chain length was a mixture of C_{12} and C_{14}; the distribution of oxyethylene groups is given in Fig. 1. About half the amount consists of molecules with 4 and 5 oxyethylene groups; the remaining molecules are mainly of longer chain length.

Determination of phase regions. The isotropic liquid regions were determined by titration in a thermostat using turbidity points as a sign of phase limits. Long-time storage ($\sim$ one month) of samples outside and inside the solubility limits served as a control to avoid inclusion of metastable solutions. Bacterial degradation was avoided by adding 10 ppm sodium azide to the emulsifier.

Results

Isotropic solutions. The regions of isotropic solutions in the system are shown by the diagrams in Fig. 2. At 20°C (Fig. 2A) the emulsifier was dissolved in water to a total of 41 per cent by weight. Hexadecane was solubilized to a

maximum of 10 per cent (W/W) in this solution. The emulsifier and the hydrocarbon were mutually completely miscible forming a solution region in which water dissolved approximately in proportion to the emulsifier content.

When the temperature was raised to 50°C (Fig. 2B) the water solubility of the emulsifier disappeared, the temperature being in excess of the cloud point. However, a considerable water solubility of a combination of emulsifier and hydrocarbon was observed, forming an isotropic liquid solution sector from the water corner and limited to a hydrocarbon/emulsifier range of 1.4-2.4. The water solubility in the hydrocarbon-emulsifier solution was modified only to a small extent.

At 70°C there was no connection to the water corner of the isotropic liquid aqueous solution, and the surfactant phase constituted an isolated region with about 20 % (W/W) of emulsifier: higher than the corresponding value at 50°C. The water solubility in the hydrocarbon/emulsifier solution now indicated a broad and low maximum in the hydrocarbon/surfactant ratio range 0.7-4.

At 75°C no separate surfactant phase was observed but the water solubility in the hydrocarbon/emulsifier solution now displayed a significant maximum containing 29 % W/W. About half this amount may be considered solubilized.

The results from the long-time storage of the samples confirmed the compositions of the solubility regions and demonstrated the presence of a liquid crystalline phase along the water/emulsifier axis which extended to high hexadecane contents. The structure of the phase was lamellar. To define the exact limits of its composition lies outside the aim of this article. A similar system with a monodisperse emulsifier has been reported earlier (24).

Discussion

The results illustrated the influence of temperature on the changes in the composition of the isotropic liquid phases in a system water, hydrocarbon, and a nonionic emulsifier of polyoxyethylene alkyl ethers.

The disappearance of emulsifier solubility in water with increasing temperature was observed and the surfactant phase appeared as an isolated solubility region without connections to the two solvent corners when the temperature was in the PIT range.

There was a marked distinction from systems with a monodisperse tetraoxyethylene dodecyl ether (22), but not in the extension of the PIT range. For the monodisperse emulsifier the PIT range has been determined to 16.5°C; the present emulsifier composition gave a range of about 20°C. The difference in a series of didisperse emulsifiers with increasing difference of oxyethylene chain length has earlier been shown to be small, varying between 15 and 20°C. Furthermore, no difference was observed when the liquid phase formed a sector from the aqueous corner (Fig. 2B); a comparison shows similar hydrocarbon/emulsifier ratio ranges 1.4-2.2 (monodisperse (22)) and 1.4-2.0 (this emulsifier).

For the isolated surfactant phase, on the other hand, the difference in emulsifier content is significant. The monodisperse emulsifier has given a surfactant phase containing only 8 % emulsifier (22); the present emulsifier required 15 % (Fig. 2). The increase is not due to the fact that the present emulsifier contains a mixture of tetra- and pentaoxyethylene compounds; a combination of tri- and pentaoxyethylene compounds has earlier (23) shown a distinct concentration minimum (5.9 %) for the isolated surfactant phase. Rather it would appear more reasonably connected with the "tail" of compounds with high oxyethylene numbers; it is instructive to compare with earlier results of samples containing decane and well defined emulsifier mixtures. Larger differences in

the oxyethylene chain length gave higher emulsifier contents in the surfactant phase (23).

The structure of the surfactant phase was not determined. From the reasonable postulate of normal spherical micelles with the polar groups outward towards the water medium in aqueous solution at lower temperatures than the PIT, and inverse micelles in the hydrocarbon solution at higher temperatures, Shinoda has earlier (loc. cit) concluded that the structure should be lamellar. Approximate estimations of the bending energy (24) of such a lamella indicated that the frequency of closed micellar figures in the solution should be low or non-existent. In the present investigation it was noticed that the solutions in the sector from the aqueous corner (Fig. 1B) showed an increasing turbidity with decreasing content of hydrocarbon and emulsifier, indicating a wide size-distribution of particles similar to the conditions prior to phase separation at critical points.

Conclusions

A special case of microemulsions is constituted by the surfactant phase which forms an isolated isotropic solution region in the phase diagrams of water, nonionic surfactant, and water.

The polydisperse commercial emulsifiers required higher percentages of emulsifier to give a microemulsion than the monodisperse emulsifiers did.

References

1. T.P. Hoar and H.H. Schulman, Nature 152, 102 (1943).
2. J.H. Schulman, R. Matalon and M. Cohen, Disc. Faraday Soc. 11, 117 (1951).
3. J.H. Schulman and J.A. Friend, Ibid. 4, 497 (1949).
4. J.E.L. Bowcott and J.H. Schulman, Z. Electrochem. 59, 283 (1955).
5. W. Stockenius, J.H. Schulman and L. Prince, Kolloid-Z. 169, 170 (1960).
6. L.M. Prince, J. Colloid Interface Sci. 23, 165 (1967).
7. C.E. Cooke and J.H. Schulman in "Surface Chemistry" p. 231, Munksgaard, Copenhagen (1965).
8. A.W. Adamson, J. Colloid Interface Sci., 29, 261 (1969).
9. G. Gillberg, H. Lehtinen and S. Friberg, J. Colloid Interface Sci. 33, 40 (1970).
10. K. Shinoda and H. Kunieda, J. Colloid and Interface Sci. 42, 381 (1973).
11. S. Friberg, J. Am. Oil Chem. Soc. 48, 578 (1971).
12. K. Shinoda and T. Ogawa, J. Colloid and Interface Sci. 24, 56 (1967).
13. H. Saito and K. Shinoda, Ibid. 35, 359 (1971).
14. K. Shinoda, Ibid. 24, 4 (1967).
15. K. Shinoda and H. Saito, Ibid. 26, 70 (1968).
16. A. Kitahara, T. Ishikawa and S. Taniusori, Ibid. 23, 243 (1967).
17. H. Saito and K. Shinoda, Ibid. 24, 10 (1967).
18. H. Saito and K. Shinoda, Ibid. 32, 649 (1970).
19. K. Shinoda, Ibid. 34, 278 (1970).
20. K. Shinoda and H. Arai, J. Phys. Chem. 68, 3485 (1964).
21. M. Robbins, "The Theory of Microemulsions", Nat. A.I.Ch.E. Meeting, Tulsa, Oklahoma, March 1974.
22. S. Friberg and I. Lapczynska, Progr. Colloid & Polymer Sci. 56, 16 (1975).
23. I. Lapczynska and S. Friberg, 48th National Colloid Symposium, Houston (1974). Preprints P.
24. S. Friberg, T. Doi and L. Rydhag, Advances in Chem. Series. In press.

LEGENDS TO THE FIGURES

Fig. 1

The distribution of number of oxyethylene groups of the emulsifier used in the investigation.

Fig. 2

The regions of isotropic liquid solutions (black) in the system water, hexadecane, and emulsifier at different temperatures. The shaded area approximately shows the extension of the area of a liquid crystalline phase.

A 20°C
B 50°C
C 70°C
D 75°C

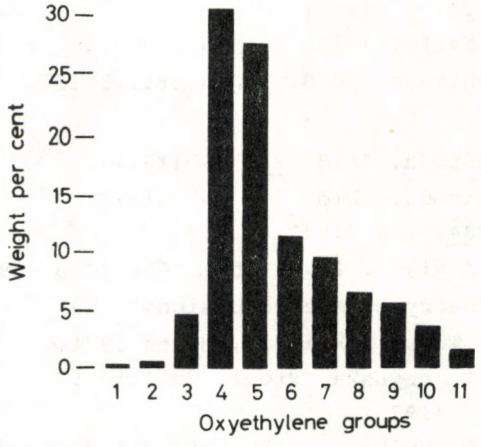

Fig. 1

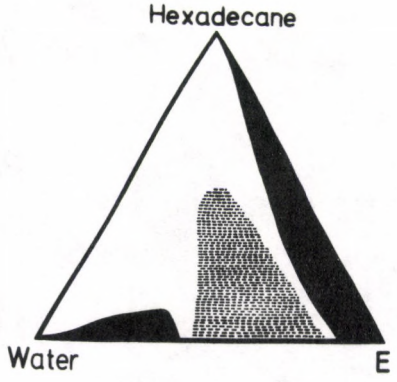
Hexadecane
Water
E

A

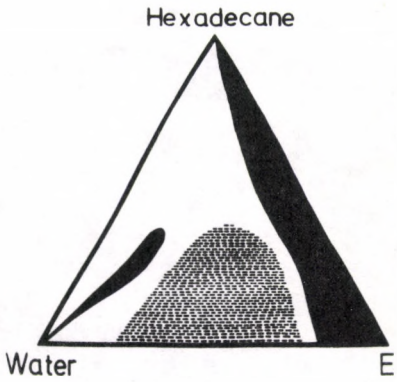
Hexadecane
Water
E

B

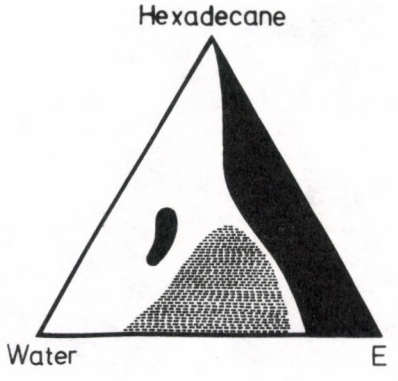
Hexadecane
Water
E

C

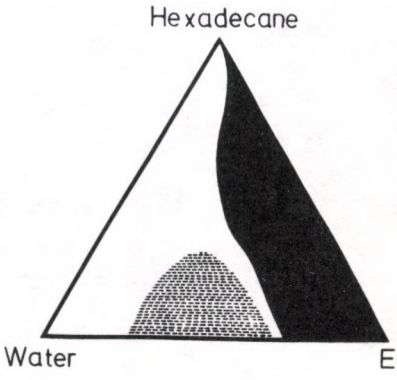
Hexadecane
Water
E

D

Fig. 2

INVESTIGATION OF MICELLAR SOLUTIONS /MICROEMULSIONS/

Zs.Bedő, E.Berecz and M.Szakszon

Department of General and Physical Chemistry,
Technical University of Heavy Industry,
Miskolc-Egyetemváros, Hungary

The micellar solutions or "microemulsions" differ from emulsions in many ways, the most considerable difference is that the former are thermodynamically stable including very small size of disperse particles /Ø = 8-80 nm/. Such systems normally are transparent and single phase ones, and perform as true solvents.

The Tyndall-effect of the micellar solutions can't be observed, and can be interpreted by the high dispersity [1-8]. The micellar dispersions are combined colloid systems, they are composed of organic solvent as an external dispersion medium, water or aqueous solution as an internally dispersed phase, surface-active substance, cosurfactant /mainly alcohols/, electrolyte, and sometimes cosolubilizer /mostly modified alcohols/ to insure the stability of the internal water phase so that in an expected range of temperature it should remain as a homogeneous fluid, as well as its miscibility should be kept to some extent both with the disperse phase and the dispersion medium.

The surfactant and cosurfactant act as coupling agents to create a single-phase solution from two otherwise immiscible fluids.

The type and amount of ingredients must be carefully selected to formulate a stable micellar solution.

We directed our studies toward finding a single micellar solution that would meet these criteria, focusing

particular attention on developing the surfactant and co-surfactant combinations that would produce the optimal properties in the micellar solutions.

According to the earlier publications, dealing with micellar solutions, the amount of cosurfactants can be reduced by the application of certain additives. The most frequently used additives /cosolubilizers/ are the different modified alcohols.

On the basis of our experimental tests the most suitable components of the microemulsions are the gasolyn as dispersion medium, the natural water, including 6000 ppm inorganic salts, as disperse phase, petroleum-sulphonate /"Hostapur OS"/ and "Turkey red oil" as surfactants, isopropil-alcohol as cosurfactant, some kind of etoxilated alcohols /"Intrasol FA"/ as cosolubilizer and sodium-hydroxide as electrolyte.

In the laboratory we have examined the properties of about 20 surfactants 10 cosurfactants and cosolubilizers, and we have found that the application of only the above listed components have guaranteed the single-phase in the expected range of temperature. The micellar solutions, prepared with these substances, have kept their temperature--stability to their boiling-points /70-80 °C/.

The micellar solutions, tested, should be characterized by the n_o/n_w ratios, where n_o is the volume of the organic phase, n_w is the volume of the aqueous phase.

The compositions of the micellar solutions prepared in the laboratory are given in Table 1.

In the case of the developed micellar solutions Newtonian-flow behaviour was observed /the viscosity measured by Höppler-rheoviscosimeter was independent from the gradient of velocity/.

The viscosity and density of the micellar solutions have been measured by the Höppler-viscosimeter and by method of picnometer respectively, as the function of the various added water contents and the temperature. The test-

Table 1. The compositions of the micellar solutions

Tenside	"Hostapur OS"	"Turkey red oil"
Hydrocarbon %	31,5	42,0
Water %	31,5	21,0
Surfactant %	3,0	3,0
Cosurfactant %	17,0	17,0
Cosolubilizer %	17,0	17,0
Electrolyte ppm	2000,0	2000,0

ed microemulsion was prepared with "Hostapur OS" surfactant, and the hydrocarbon-water ratio was equal to one. The experimental results for the values of the viscosity and of the density are given in Table 2 and in Figures 1-2.

As it appears from the tables and figures, the viscosity of the microemulsions have increased exponentially with increasing water content to a critical inversion point, then the viscosity have dropped exponentially to the viscosity of water and the solution have changed in appearance.

It turns from a transparent into a slightly hazy, but stable single-phase solution. This point probably denotes a change in the micelle structure and in the distribution of fluids, held inside and outside the micelles.

Above 40 vol% water content the viscosity of the micellar solutions increases with the increasing temperature remaining as a single phase. This irregular behaviour is probably a sign of some changes in the structure of the micellar solutions.

The viscosity of the different microemulsions, including less than 40 vol% added water content, decreases rapidly with increasing temperature. The change of the viscosity as a function of the temperature is shown in Figure 3. This decline, being more rapid than for water, resembles the viscosity-temperature relationship of some hydro-

Table 2. The viscosity and density of the micellar solutions

T [K]	added H_2O %	η [cP]	ρ [gcm^{-3}]	T [K]	added H_2O %	η [cP]	ρ [gcm^{-3}]
298	-	15,00	0,8800	318	50	5,55	0,9350
308		7,95	0,8730	328		9,40	0,9300
318		5,02	0,8650	298	58	4,00	0,9550
328		3,64	0,8580	308		3,22	0,9500
298	10	39,90	0,9000	318		3,22	0,9450
308		14,00	0,8900	328		5,80	0,9400
318		6,42	0,8800	298	66	2,77	0,9650
328		4,04	0,8700	308		2,27	0,9600
298	20	49,40	0,9100	318		2,11	0,9550
308		24,70	0,9050	328		2,88	0,9500
318		10,30	0,9000	298	75	2,00	0,9770
328		4,89	0,8900	308		1,66	0,9700
298	30	25,00	0,9250	318		1,55	0,9650
308		17,70	0,9150	328		2,65	0,9580
318		14,60	0,9080	298	80	1,75	0,9780
328		6,70	0,9000	308		1,44	0,9750
298	40	12,10	0,9350	318		1,33	0,9700
308		10,20	0,9300	328		2,65	0,9650
318		12,00	0,9200	298	87	1,41	0,9950
328		8,40	0,9150	308		1,26	0,9880
298	50	6,30	0,9500	318		1,09	0,9800
308		5,10	0,9400	328		1,15	0,9730

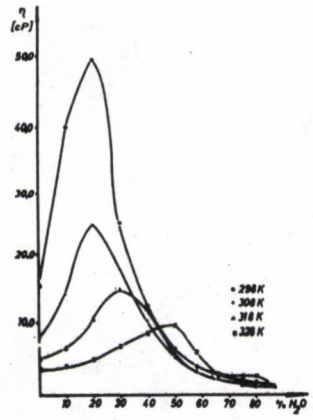

Figure 1. The viscosity of the micellar solution as a function of the added water content.

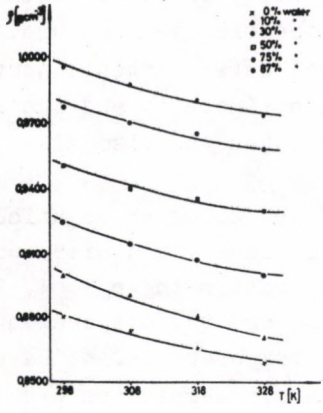

Figure 2. Connection between the density and the temperature of the micellar solution by adding different water contents.

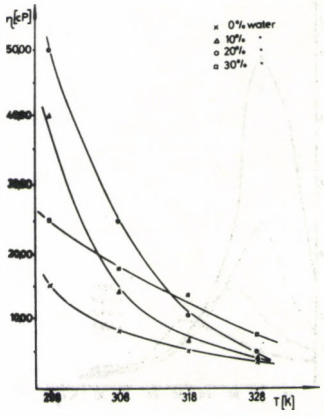

Figure 3. The viscosity of the micellar solutions as a function of the temperature.

carbon systems. The density of the micellar solutions declines also with increasing temperature, and increases by increasing the added water content. Above 80 vol% added water content the viscosity and the density of the microemulsions approximates the viscosity and the density of the water.

The miscibility of the micellar solutions preparing with "Hostapur OS" and "Turkey red oil" surfactants and having different n_o/n_w ratios /n_o/n_w = 1, 2, 3, 4/ both with the disperse phase and the dispersion medium was investigated at various temperatures. We have found that the miscibility of the microemulsions with the hydrocarbon component increases by increasing temperature, and decreases with the increasing n_o/n_w ratio. The miscibility of the micellar solutions with the disperse phase /water/ decreases with increasing hydrocarbon--water ratios, and it changes accordingly with a minimum--curve with increasing temperature. The existence of the minimum value at 40 °C involves some transformations in

the structure of the micellar solutions at this temperature. The water-miscibility will be total only in case if the hydrocarbon-water ratio is equal to one.

Our studies above have dealt with the preparation and some properties of the micellar solutions, but on the basis of our following investigations we should like to find some explanations for the structure and thermodynamic characteristics of the micellar solutions. The first step of this examinations was the determination of the critical--micelle-concentration /CMC/ of the aqueous solutions of the different surface-active agents as function of the temperature /293 K - 323 K/ [9].

From the temperature dependence of the CMC or the equilibrium constant of the micella formation process the change of enthalpy, entropy and free energy of the formation of micelles were determined [10, 11].
The temperature dependence of these thermodynamic parameters was interpreted by the interactions between the hydrophobic groups of surface-active substances and by their changes caused by that of the temperature [12, 13].

Our further plans: to study the changes of the thermodynamic properties of these solutions taking the presence of the other components of the micellar solutions /cosurfactants, cosolubilizers/ into consideration.

References

1. T.P. Hoar, J.H. Schulman, Nature. 152. 102. /1943/.
2. J.H. Schulman, T.S. McRoberts, Trans. Faraday Soc. 42 B. 165. /1946/.
3. J.H. Schulman, D.P. Riley, J. Coll. Sci. 3. 383. /1948/.
4. J.H. Schulman, J.A. Friend, J. Coll. Sci. 4. 497./1948/.
5. J.E. Bowcot, J.H. Schulman, Z. für Electrochem. 59. 283. /1955./
6. J.H. Schulman, J.B. Montagne, Ann. N.Y. Acad. of Sci. 92. 366. /1961/.

7. W. Strockenius, Koll. Zeitschrift, 169. 177. /1960/.
8. K. Suzuki, S. Natsumuto, T. Watanabe, Bull. Chem. Soc. 42. 2773. /1969/.
9. Bedő Zs., Berecz E., Magy. Kém. Folyóirat 81. 109./1975/
10. G. Stainsby, A.E. Alexander, Trans. Faraday Soc. 46. 587. /1950/.
11. N. Muller, F.E. Platko, J. Phys. Chem. 75. 547. /1971/.
12. G. Némethy, H.A. Scheraga, J. Phys. Chem. 66. 1773. /1962/.
13. A. Ray, G. Némethy, J. Phys. Chem. 75. 809. /1971/.

Group III/2
Monolayers and foams

INTERACTION LIPID-GRAMICIDIN S AT THE AIR-WATER INTERFACE

M. Landuyt-Caufriez, J. Caspers, J.M. Ruysschaert, J. Jaffé

Université Libre de Bruxelles, Laboratoire de Chimie Physique des Macromolécules aux Interfaces, Faculté des Sciences

INTRODUCTION

Antibiotics like Gramicidin S are thought to interact with the bacterial membrane. However, because of their insolubility in water, the physico-chemical properties were investigated in non aqueous solvents (1-3).
To obtain information about the antibiotic conformation in an aqueous environment, they can be spread at the air-water interface (4). This technique has already been used with success in the case of insoluble polypeptides (5-12). Moreover, the possible formation of antibiotic-lipid mixed films allows the study of the interaction with an essential constituent of the membrane : the lipid (13).

In the present work, the Gramicidin S - lipid interaction is investigated in mixed films spread at the air-water interface, at high and low concentrations.

MATERIALS AND METHODS

Gramicidin S (GrS), DL-α-lecithin dipalmitoyl (PC) and phosphatidyl serine (PS) were obtained from Mann Research Laboratories, England. The samples were dissolved in chloroform and spread at the air-water interface, with an Agla microsyringe. The ionic strength of the subphase is 0.5M KCl and the temperature of the aqueous phase was maintained at $23 \pm 0{,}1°C$.
At high surface concentrations (condensed films), surface

pressure was measured on a Cahn RG electrobalance using the Wilhelmy plate method. At low surface concentrations (dilute films), the instrument used was the Guastalla manometer (14, 15).

EXPERIMENTAL RESULTS AND DISCUSSION

1. Condensed films

The existence of an eventual antibiotic-lipid interaction can be demonstrated from surface pressure isotherms, obtained in mixed films of well defined composition.

Indeed, if a mixed monolayer behaves ideally (16) :

$$A_{1,2} = X_1A_1 + X_2A_2 \qquad [1]$$

where $A_{1,2}$ is the average molecular area in the two-component film, X_1 and X_2 are the molar fractions of the two components, and A_1 and A_2 are the molecular areas in the two single component films at the same pressure. Any deviation of mixed monolayer behavior from equation [1] provides evidence of an interaction between the two components of the binary system.
For the Gramicidin S - lipid system, fig. 1 and 2 show the existence of an interaction between the two components of the mixed films.

The interaction is stronger with a negatively charged lipid (phosphatidylserine) than with the neutral lipid (DL-α-lecithin dipalmitoyl) and allows us to imply the electrostatic nature of the interaction (17).

A more quantitative approach is to calculate the excess free energy of mixing in the films. Indeed, this excess free energy ΔG_m^e can be obtained from the surface pressure isotherms, using the equation (16, 18, 19) :

$$\Delta G_m^e = \int_0^{\Pi} (A_{1,2} - X_1A_1 - X_2A_2)\, d\Pi \qquad [2]$$

The value of ΔG_m^e was obtained graphically and the upper limit of equation [2] was set at Π = 20 dynes/cm.
A maximum energy of mixing of -840 cal./mole was obtained (fig. 3) for the phosphatidylcholine - Gramicidin S system and of -1170 cal./mole for the phosphatidylserine - Gramicidin S system.

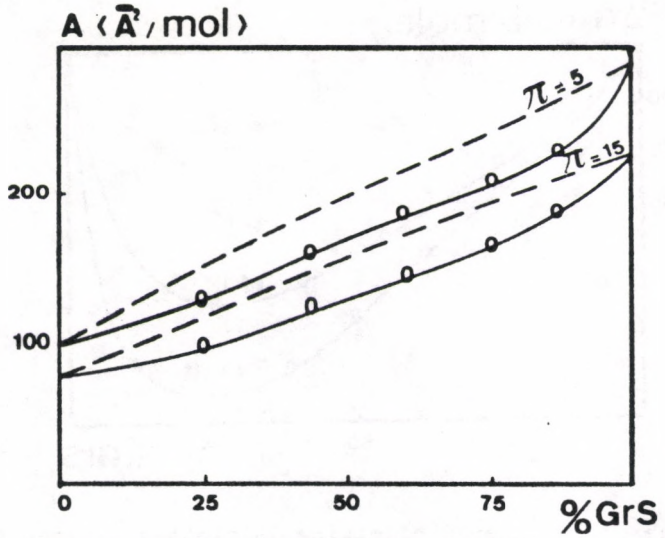

Fig. 1 : Molecular area of GrS - DL-α-lecithin dipalmitoyl mixed monolayers. The dotted line is predicted from surface pressure area curves of components measured alone. The solid line gives the experimental values.

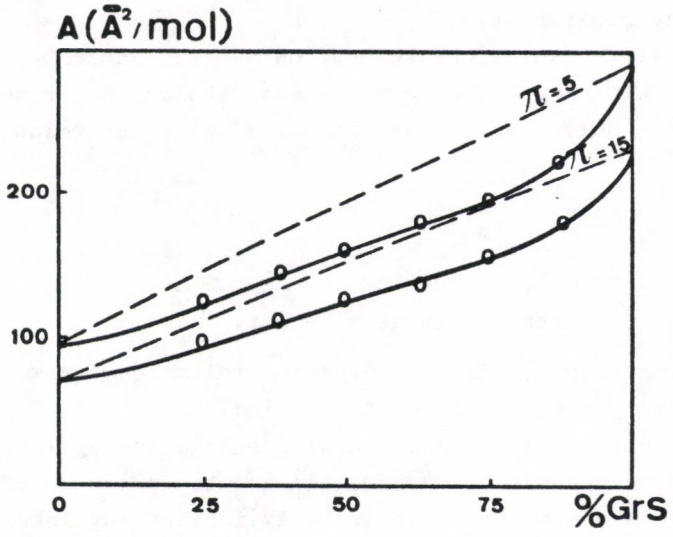

Fig. 2 : Molecular area of GrS - Phosphatidylserine mixed monolayers. The dotted line is predicted from surface pressure area curves of components measured alone. The solid line gives the experimental values.

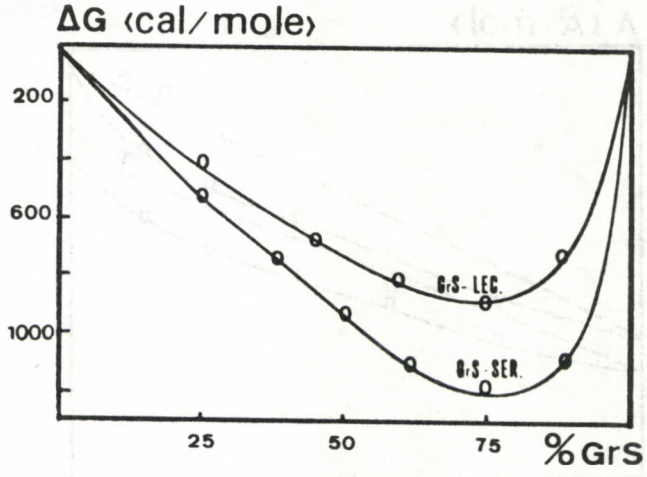

Fig. 3 : Excess free energy of mixing is plotted against the molar fraction of Gramicidin S.

2. Dilute films

Experimental facts suggest that Gramicidin S solubilizes the lipid aggregates (17).
This eventuality can be checked at low surface concentrations. Indeed, in this range of concentrations, the molecular weight of the spread molecules can be estimated using the relation (14) :

$$\lim_{C_S \to 0} \frac{\Pi}{C_S} = \frac{RT}{M} \qquad [3]$$

C_S is the surface concentration
M is the experimental molecular weight.

For the Gramicidin S film, the experimental molecular weight (1130) was very similar to the theoretical value (1141). The cyclic conformation of this antibiotic stabilized by intramolecular hydrogen bonds (3, 4, 20, 21) and the presence of positive charges on the molecule probably inhibit any intermolecular interaction.
The molecular weight obtained using the same technique for the lipids (M_{PS}=35,000, M_{PC}=97,000) is very different from

the theoretical molecular weight and demonstrates clearly the presence of aggregates at the air-water interface.
If we define the molecular weight $\overline{M}$ of the mixture, we can write :

$$\overline{M} = X_1' M_1 + X_2' M_2 \qquad [4]$$

X_1' : molar fraction of lipid aggregates
M_1 : molecular weight of one of these aggregates
X_2' : molar fraction of antibiotic
M_2 : molecular weight of antibiotic.

From the comparison of the molecular weight (Tables 1 and 2) obtained from the relation [4] and the molecular weight obtained experimentally (relation [3]), the hypothesis of a decreasing number of lipid aggregates due to an antibiotic - lipid interaction is suggested.

X_{PC}	X_{GrS}	$M_{(rel[3])}$	$M_{(rel[4])}$
1	0	97,000	97,000
0.91	0.09	50,000	8,600
0.82	0.18	18,000	5,000
0.72	0.28	7,000	3,000
0.55	0.45	4,500	2,000
0.38	0.62	2,900	1,600
0.25	0.75	2,250	1,400
0.15	0.85	1,750	1,250
0	1	1,130	1,130

Table 1 : Evolution of the molecular weight obtained from relations [3] and [4] for lecithin - Gramicidin S mixed films.

X_{PS}	X_{GrS}	$M_{(rel[3])}$	$M_{(rel[4])}$
1	0	35,000	35,000
0.78	0.22	13,000	3,750
0.71	0.29	7,000	2,950
0.63	0.37	5,500	2,400
0.50	0.50	4,000	1,850
0.43	0.57	3,400	1,700
0.29	0.71	2,600	1,450
0.13	0.87	1,650	1,250
0	1	1,130	1,130

Table 2 : Evolution of the molecular weight obtained from relations [3] and [4] for phosphatidylserine - Gramicidin S mixed films.

CONCLUSION

The existence of a strong interaction between Gramicidin S and the two lipids (DL-α-lecithin dipalmitoyl and phosphatidylserine) is clearly demonstrated through the evolution of the excess free energy of mixing and of the mean molecular area of the mixed films. This interaction is stronger with a negatively charged lipid; these results show the electrostatic nature of the interaction, probably between the two positive charges of the cyclic antibiotic and the negative charge on the hydrophylic group of the lipid.

About the evaluation of the molecular weight, if a correct value was obtained for the GrS films, the formation of aggregates was observed in the case of spread lipid monolayers. The molecular weight obtained for the mixed films suggests a diminution of the number of lipid aggregates due to a lipid-antibiotic interaction.

In conclusion, the monolayer approach allows to demonstrate clearly the existence of a strong GrS-lipid interaction.

REFERENCES

1. A.M. Liquori, F. Conti, Nature 217, 635 (1968).
2. A. Stern, W.A. Gibbons, L.C. Craig, Proc. Natl. Acad. Sci. 61, 735 (1968).
3. Yu.A. Ovchinnikov, V.T. Ivanov, V.F. Bystrov, A.I. Miroshnikov, E.N. Shepel, M.D. Abdullaev, E.S. Efremov, L.B. Senyavina, Biochim. Biophys. Res. Commun. 39, 217 (1970).
4. A.V. Few, Trans. Faraday Soc. 53, 848 (1957).
5. B.R. Malcolm, Progress in Surface and Membr. Sci. 7, 183 (1973).
6. K.S. Birdi, G.D. Fasman, J. Polymer Sci. Symposia 42(3), 1099 (1973)
7. Y. Deboeck, J. Jaffé, Berichte vom VI. Intern. Kongress für Grenzflächenaktive Stoffe, Zürich 1972, II, 1, 305, Carl Hanser Verlag, München (1973).
8. J. Caspers, C. Berliner, J.M. Ruysschaert, J. Jaffé, Berichte vom VI. Intern. Kongress für Grenzflächenaktive Stoffe, Zürich 1972, II, 1, 295, Carl Hanser Verlag, München (1973).
9. J. Kummer, J.M. Ruysschaert, J. Jaffé, Berichte vom VI. Intern. Kongress für Grenzflächenaktive Stoffe, Zürich 1972, II, 1, 285, Carl Hanser Verlag, München (1973).
10. J.P. Williot, J.M. Ruysschaert, J. Jaffé, J. Polymer Sci. A2, 10, 2125 (1972).
11. J. Caspers, C. Berliner, J.M. Ruysschaert, J. Jaffé, J. Coll. Interf. Sci. 49, 433 (1974).
12. J. Caspers, W. Hecq, A. Loffet, Biopolymer, to be published.
13. G. Kemp, C. Wenner, Biochim. Biophys. Acta 282, 1 (1972).
14. J. Guastalla, Mem. Serv. Chim. Etat, 30, 265 (1947).
15. J. Jaffé, J. Chim. Phys. 51, 243 (1954).
16. G.L. Gaines, Insoluble monolayers at liquid-gas interfaces, Interscience Publ., J. Wiley, N.Y. (1966).
17. W. Pasche, D. Chapman, R. Hillaby, Biochim. Biophys. Acta 255, 358 (1972).

18. F.C. Goodrich, Proc. of the Second Intern. Congress of Surf. Activity, I, 85, Butterworths Scientific Publ. London (1957).
19. F. Villalonga, R. Altschul, M.S. Fernandez, Biochim. Biophys. Acta 135, 557 (1967).
20. R. Schwyzer, U. Ludescher, Biochemistry 7, 2519 (1968).
21. D.C. Hodgkin, B.M. Oughton, Biochem. J. 65, 752 (1957).

THE PENETRATION OF HOMOLOGOUS SODIUM ALKYL SULFATES INTO LIPID MONOLAYERS

W. Rettig, H.-D.Dörfler and H.Sackmann

Martin- Luther- Universität, Sektion Chemie,
402 Halle (Saale), Mühlpforte 1

I. Introduction

SCHULMAN and co- workers (1,2) have firstly studied the penetration of n-alkyl sulfates into monomolecular layers of lipids. The penetration of homologous ionic and nonionic surfactants into monomolecular layers of fatty acids, cholesterol, glycerides and phospholipids was carried out by PANKHURST (3), CRISP (4), MATSURBARA (5) and VILLALONGA et al.(6). The thermodynamic treatment of the penetration was made by PETHICA (7), FOWKES (8) and MILLER and NANIS (9).

The aim of the own studies is to examine the penetration of homologous n - alkyl sulfates ($C_8H_{17}SO_4Na$ = SOS, $C_{12}H_{25}SO_4Na$ = SDS, $C_{14}H_{29}SO_4Na$ = STDS and $C_{16}H_{33}SO_4Na$ = SCS) into cholesterol (Ch) monolayers.

The penetrationkinetics and the thermodynamic evaluation will be discussed.

2. Materials

The n- alkyl sulfates SDS, STDS and SCS were comercial products from Schuchardt (Munich). The purification was carried out according to KLOUBEK and NEUMANN (10) by recrystallization. All samples of alkyl sulfates gave no minima in the curves of surface tension against the logarithm of concentration. SOS was synthezisied by reaction of gaschromatographically pure octyl alcohol with chlorsulfonic acid and purified by recrystallization. Cholesterol (m.p. 149,5 - 150,5) was recrystallized with benzene. Benzene was fractionally redistilled over alkaline permanganate from a

glass apparatus.

3. Apparatur

The used apparatus for penetration experiments is shown in fig.1. It consists of a cylindrical trough of teflon (volume :425 ml; effective surface area of 130 cm^2). The spreading of the insoluble monolayer takes place between the two radially arranged barriers. In this way any point of the force- area isotherm of spread monolayer can be exactly given as a constant. Recording of surface pressure is done by means of measuring the surface tension by a roughened Wilhelmy platinum plate(22,5 x 11 x 0,1 mm) attached to an Cahn -RG - electro - balance. The trough is enclosed in a box and is movable with the aid of a fine coil to the platinum plate. To avoid air contaminants the box was rinsed by water saturated nitrogen during the measurement. Water evaporation was minimized by hanging strips of wet filter paper in the box.

fig.1

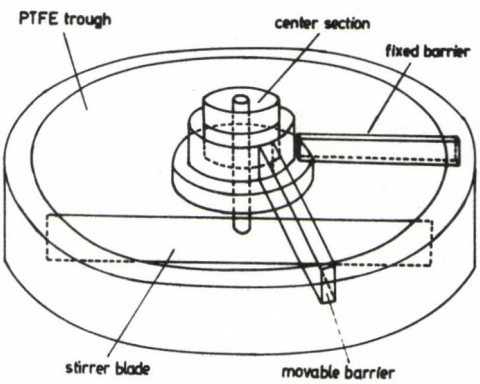

4. Procedure

Before spreading the cholesterol monolayer the water surface was cleaned by suction with a fine glass capillary. The cholesterol monolayer was adjusted to the initial surface pressure ($5 \pm 0{,}2$ dynes/cm) by changing of the position of the movable barrier. This value of surface

corresponds to a cholesterol monolayer at 22°C with a value of 38,4± 0,5 Å molecule. This value could be verified by check measurements with a Langmuir balance. The surfactants were injected as a concentrated solution with the aid of a metering installation trough the film free section between the barriers into the subphase. Simultaneously the stirring began. It was maintained for one minute and then stopped. Identical surface pressure increases were obtained by injecting a given amount of surfactant in one or several steps. This was taken as a criterion that the measured values represent equilibrium values. The concentration of the surfactant solution which was injected was kept below the CMC. All measurements were performed at 22± 1°C.

5. Results and Discussion

All the results of penetration equilibrium studies of SOS, SDS, STDS and SCS into cholesterol monolayers are diagrammed in fig.2. All measurements were performed at an initial surface pressure of 5 dynes per cm.

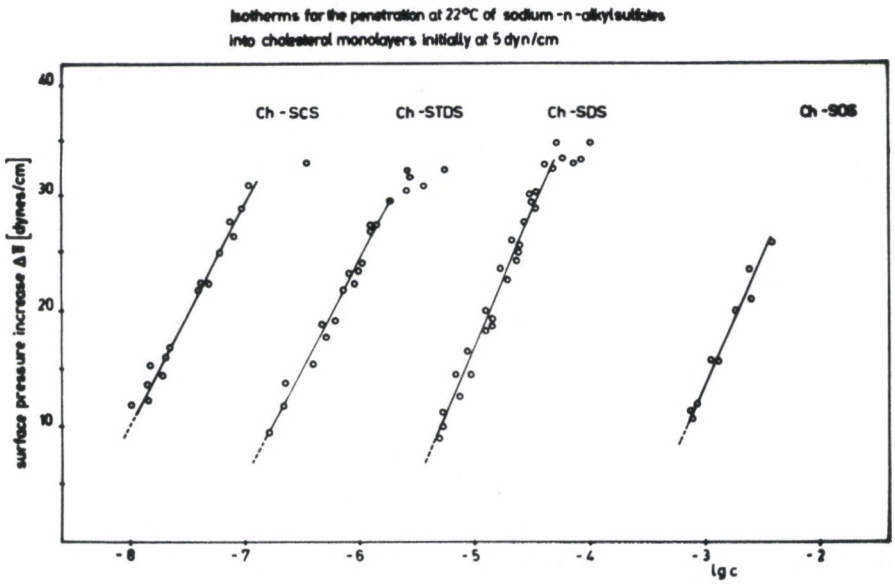

fig.2

The initial part of the penetration isotherms at low

concentrations was not studied till now because of the long time for setting equilibrium. From orientating measurements we can conclude that this part of the isotherm is not linear.

The analysis of the curvature of the penetration isotherm indicates the following compendencies :
The slopes of the isotherm differ not very much. Several π - values in the range of high surface pressure values cannot be assigned to the linear slope of the penetration isotherm. Further studies at high concentrations must show if this deviation from linearity coheres with saturation effects in the mixed film formed by penetration.
The penetration isotherms represented in fig.2 can be described in its middle part (full line) by a modified SZYSZKOWSKI- equation (9,11).

$$\Delta\pi = \pi_i - \pi_m = a \log \left(1 + \frac{c}{b} \right) \qquad (1)$$

The increase of the surface pressure $\Delta\pi$ results from π_i as the surface pressure at the beginning of the penetration (π_i=5 dynes/ cm) and from π_m as the surface pressure of mixed film formed by penetration. The constant a represents the slope of the penetration isotherms at high concentration values. The constant b expresses the penetration affinity. It makes it possible to calculate the free penetration enthalpie ΔG_p:

$$b = 55{,}56 \quad \exp \frac{\Delta G_p}{R \; T} \qquad (2)$$

These parameters a , b and ΔG_p resulting from the evaluation of equations (1) and (2) are listed in table 1.

The numerical calculation was made by non - linear regression.

Table 1

System	a	b [mol/ l^{-1}]	ΔG_p [Kcal/ mol]	ΔG_p/ CH_2
cholesterol-$C_8H_{17}SO_4Na$	25,5	$3{,}8 \cdot 10^{-3}$	6,9	
cholesterol-$C_{12}H_{25}SO_4Na$	26	$3{,}0 \cdot 10^{-6}$	9,8	0,72

table 1 continued

cholesterol-$C_{14}H_{29}SO_4Na$	22,5	$1,1 \cdot 10^{-7}$	11,7	0,95
cholesterol-$C_{16}H_{33}SO_4Na$	21,9	$4,96 \cdot 10^{-9}$	13,7	0,9

The a values reflect the figure recognizable in the slopes of the graph. The numerical values increase with increasing chain length of the alkyl sulfates. We can say that the penetration ability depends primarily on the carbon content of the nonpolar part of the surfactant. So there are paralelles between the surface activity (12) and penetration affinity of sodium alkyl sulfates. MATSUBARA (5) came to the same conclusion by studying the penetration affinity of alkyl sulfates into cholesterol monolayer initially at 15 dyn/ cm.

It was found that the increase of ΔG_p per CH_2-group has an average value of 0,9 Kcal/ mol. This result goes confirm with the Traube - rule . This rule reflects the nonpolar interaction of filmforming molecules. This indicates that the surfactant molecules are not adsorbed at the film but penetrate it. The difference of ΔG_p values between $C_8H_{17}SO_4Na$ and $C_{12}H_{25}SO_4Na$ was found to be smaller in relation to the other differences.

It is possible that adsorption of sodium ions takes place due to increasing bulk surfactant concentration of the shorter chain length alkyl sulfates ($C_8H_{17}SO_4Na$). This adsorption also influences the value of b.

Further penetration studies will be carried out on a subphase containing supporting electrolyte. Interesting aspects result by pursuing the penetrationkinetics.

The result of studies of penetration of STDS into cholesterol is obtained by successive injection of surfactant and is diagrammed in fig.3. Spreading of the cholesterol monolayer is started in point s . This spreading causes on the recorder an amplitude p. After evaporation of solvent the surface pressure approaches $\pi \approx 0$ dyn/ cm. Then the cholesterol monolayer is compressed to the initial surface pressure of 5 dyn/ cm. After injecting STDS (t = 0) and

following stirring for one minute the penetration process occurs.

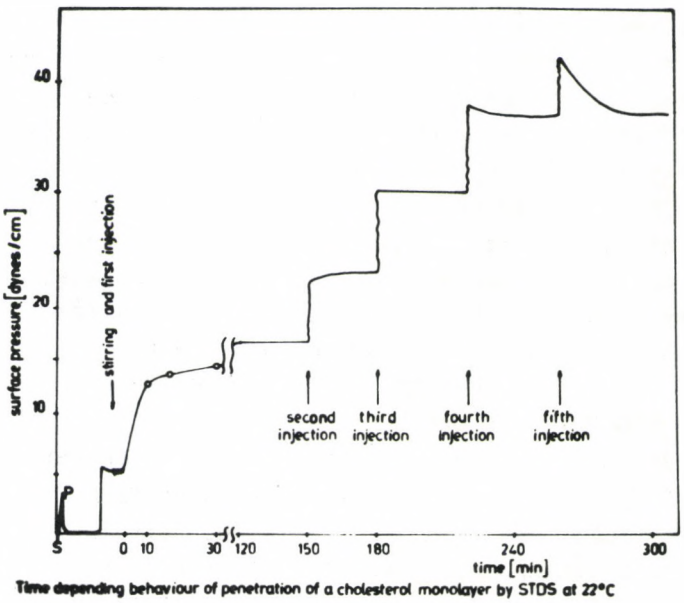

Time depending behaviour of penetration of a cholesterol monolayer by STDS at 22°C

fig.3

The penetration equilibrium is reached when the mixed monolayer formed by penetration shows no more temporal changing of the surface pressure. The surface pressure against time curves originating from the second and third injection must be interpreted in similar manner. The penetration-kinetics arising from the fourth and fifth injection shows another behaviour. After an abrupt increase due to injection and stirring the surface pressure approaches a limiting value. The surface pressure increases due to penetration and lead now to an unstable state which again is abolished. Further penetration studies in this concentration range are necessary to find out if the collapse of mixed film formed by penetration occurs after the fourth and fifth injection.

6.References

1.Schulman,J.H. and Rideal,E.K.,Proc.Roy.Soc.,B 122 (1937),29.

2.Schulman,J.H. and Stenhagen,E., Proc.Roy.Soc.,B126 (1939) 356.
3.Pankhurst,K.G.A., Proc.Roy.Soc., A179 (1942),26.
4.Crisp,D.J. in Surface Chemistry,p.65, Butterworths, London 1949.
5.Matsurbara,A.,Bull.Chem.Soc.Japan, 38 (1965), 1254.
6.Villalonga,F.A. and Garrett,E.R.,J.Pharm.Sci. 62 (1973), 1605.
7.Pethica,B.A. Trans.Farad.Soc.,51 (1955),1402.
8.Fowkes, F.M. Proc. III rd Intern.Congr.Surf.Act., Cologne, 1960, Vol.2, 161
9. Miller,I.R. and Nanis,L., Proc. IV.Intern.Congr. Surf. Act.,Brussels,1964, Vol.2,841.
10.Kloubek,J. and Neumann,A.W., Tenside 6 (1969),4.
11.Stauff,J., Z.Phys.Chem.,N.F. 10 (1957),24.
12.Köblel,H.,,Klamann,D. and Kurzendörfer,P.,Angew. Chem. 73 (1961),290.

PROPERTIES OF ANTAMANIDE AT THE AIR-WATER INTERFACE

A. Poss, C. Berliner, J.M. Ruysschaert, J. Jaffé

Université Libre de Bruxelles - Laboratoire de Chimie Physique des Macromolécules aux interfaces.

INTRODUCTION

Antamanide is a cyclic antibiotic that has been shown to complex the Na^+ ion selectively. The action of this kind of molecule is to modify the membrane cation permeability (1-5).

Because of its insolubility in water, the antamanide has been principally studied in organic solvents.

The spreading of antamanide at the air-water interface can however give interesting information about its properties in an aqueous environment.

In the present work, the interaction between alkaline monovalent cations dissolved in the aqueous phase and the antamanide monolayer was investigated with three experimental techniques : surface potential measurements, surface pressure measurements and tritium-hydrogen exchange between the spread tritiated molecule and the aqueous phase.

MATERIAL AND METHODS

Valinomycin was obtained from Sigma Chemical Co. The sample of antamanide was a gift from Dr. Birr (Max Planck Institut, Heidelberg).

The antibiotics were dissolved in chloroform and spread at the air-water interface with an Agla microsyringe. The temperature of the support was maintained at 23°C $\pm$ 0,1°C. Inorganic salts were analytical grade. Surface potentials were measured with the vibrating plate method. The apparatus was described in a preceeding paper (6). Surface pressures were measured on a Cahn RG electrobalance using the Wilhelmy plate method.

The method used to follow the tritium-hydrogen exchange between the tritiated monolayer and the aqueous phase was already described (7).

To facilitate the exchange, the antibiotics were dissolved in a mixture of

tritiated water (10 Curies/ml) and dichloroacetic acid (V/V = 1/99) to which a large excess of helicogenic solvent (chloroform) was added to decrease the exchange. The mixture is then spread with an Agla microsyringe on the aqueous support. The surface radioactivity proportional to the tritium concentration is recorded, in function of time, with a gas-flow counter (7).

EXPERIMENTAL RESULTS AND DISCUSSION

A) Surface potential

Surface potential was measured to show the existence of a complex between the antamanide monolayer and the alkaline ions (Na^+) dissolved in the aqueous phase. Such a complex was already described in bulk (8-10).

Fig. 1 shows the evolution of the surface potential in function of the ionic strength of the support.

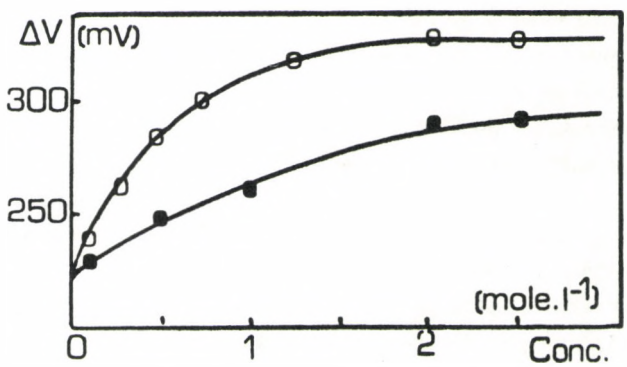

Fig. 1 : Surface potential vs the ionic concentration in the support
○ - Na^+, ● - K^+.

The surface potentials obtained with Na^+ ion being more elevated than those obtained with K^+ ion imply the existence of a selective Na^+ - antamanide interaction.

The complexation of cations at the air-water interface might be described by a simple equilibrium expression :

$$K_c = \frac{(\text{Antamanide} - Na^+)}{(\text{Antamanide})(Na^+)} \qquad [1]$$

The surface concentration of the Na^+ - antamanide complex and of the

uncomplexed fraction can be calculated from the surface potential measurements (12). Indeed :

$$(\text{Antamanide} - Na^+) = \frac{\Delta V_{Na^+} - \Delta V_{K^+}}{\Delta V^{max}_{Na^+} - \Delta V_{K^+}}$$

ΔV_{Na^+} : surface potential in the presence of Na^+ ion in the support

ΔV_{K^+} : surface potential in the presence of K^+ ion in the support

(The ΔV_{K^+} values are used as a measure of the surface potential of the uncomplexed form).

$\Delta V^{max}_{Na^+}$: maximum surface potential in the presence of Na^+ ion in the support

and $$(\text{Antamanide}) = \frac{\Delta V^{max}_{Na^+} - \Delta V_{Na^+}}{\Delta V^{max}_{Na^+} - \Delta V_{K^+}}$$

Thus, from equation [1] one can write :

$$K_c = \frac{\Delta V_{Na^+} - \Delta V_{K^+}}{\Delta V^{max}_{Na^+} - \Delta V_{Na^+}} \cdot \frac{1}{[Na^+]}$$

The surface potential used was always the value obtained at the minimum packing area. The K_c value calculated for the Na^+ - antamanide complex is 1.8 l/mole and doesn't depend on the ionic strength of the support.

Table 1 gives the constant of complexation obtained for other antibiotics at the air-water interface and in organic solvents.
The values obtained are in agreement with the results obtained by other authors at the air-water interface.

Experimental conditions / Antibiotic	C_2H_5OH	C_2H_5OH 42% H_2O 58%	Air - Water Interface
Valinomycin - $K^{(+)}$	$3.8.10^5$ (11)	~500 (12)	1 (13)
Antamanide - $Na^{(+)}$	2.10^3 (14)	-	1.8
Trinactin - $K^{(+)}$	-	-	2.15 (13)

Table 1

B) Surface pressure

In Table 2, the ratio of the collapse surface pressure for the complexed (Π_c) and uncomplexed form of antamanide (Π) is given in function of the ionic strength of the support.

	Valinomycin	Antamanide
Ionic concentration (M/l)	$\frac{\Pi_c(K^+)}{\Pi(Na^+)}$	$\frac{\Pi_c\ (Na^+)}{\Pi(K^+)}$
1	0.9	1.6
2	0.8	1.6
3	0.6	1.6

Table 2

The constant value of this ratio demonstrates that antamanide does not undergo a conformational change after cation binding.
This result is in agreement with the information obtained in bulk (10).
In the case of valinomycin monolayer however, the association with cations (K^+) from the subphase cannot be described by a simple equilibrium expression. Indeed, if the surface potential is plotted against the subphase cation concentration, a sigmoidal relationship is obtained suggesting a change of conformation of the valinomycin during the complex formation (15).

C) Tritium-hydrogen exchange at the air-water interface

Tritium hydrogen exchange between the tritiated antibiotic monolayer and the aqueous subphase allows us to study the conformation of the spread molecule. Indeed, if the tritium is involved in intramolecular bonds, the exchange with the support is very slow. But, if the molecular conformation is not stabilized with intramolecular bonds (hydrogen bonds) the tritium is immediately exchanged with the subphase and the decrease in surface radioactivity is very fast. The helical conformation of spread polypeptides was demonstrated with this technique (7).
Valinomycin and antamanide are stabilized with intramolecular hydrogen bonds and the technique of the tritium hydrogen exchange at the air-water interface can be used to study the stability of these bonds in the complexed and

non complexed forms.

The rate of exchange of the tritiated valinomycin monolayer with the support is slower in presence of K^+ ions than in presence of Na^+ ions dissolved in the aqueous phase (fig. 2).

This result demonstrates that the hydrogen bonds are stabilized during the complex formation. Moreover, the initial decrease in surface radioactivity shown in fig. 2 is described by a first order kinetic which allowed the calculation of the kinetic constant : $13.10^{-3}sec^{-1}$ is obtained for the complexed form and $7.3\ 10^{-3}sec^{-1}$ for the uncomplexed form.

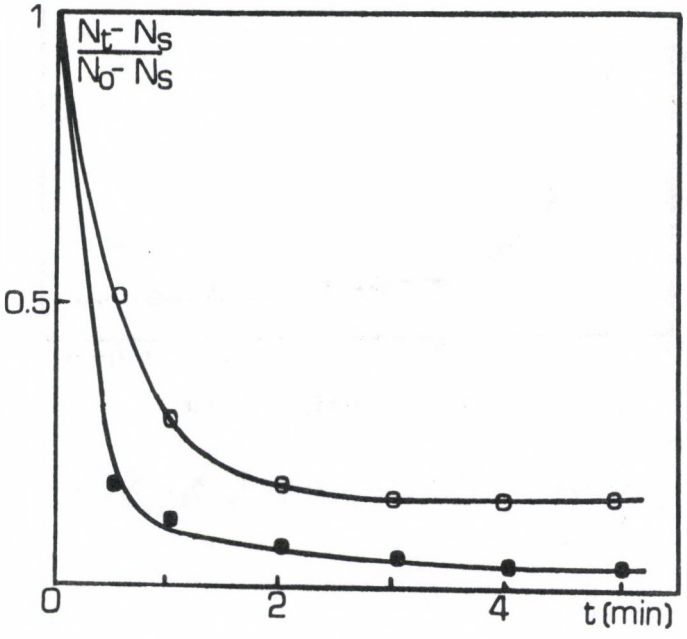

Fig. 2 : Evolution of the surface radioactivity in function of time - valinomycin.

N_t : surface radioactivity (cpm : counts per minute) at time t

N_0 : surface radioactivity (cpm : counts per minute) at time t=0

N_s : surface radioactivity (cpm : counts per minute) due to the spreading solvent

□ - K^+, ■ - Na^+.

Fig. 3, however, shows that the capacity of exchange of a tritiated antamanide monolayer doesn't depend on the nature of the ion (Na^+, K^+) dissolved in the aqueous phase. The same value of the kinetic constant (9.10^{-3} sec) obtained in the two cases shows that the conformation is not modified

after ion complexion. This result agrees with the experiments realized in organic solvents (10).

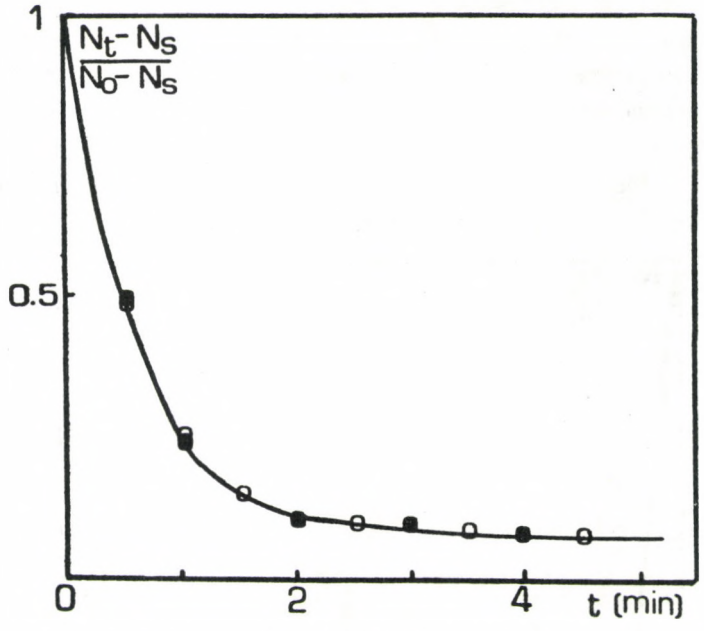

Fig. 3 : Evolution of the surface radioactivity in function of time - Antamanide.
For the explanation of the symbols N_t, N_o, N_s, see Fig. 2
o - K^+, ● - Na^+

CONCLUSION

The interaction antamanide - Na^+ was studied at the air-water interface. Surface potential measurements demonstrated the existence of an antibiotic - ion complex and allowed the calculation of the constant of complexion.

Surface pressure and tritium - hydrogen exchange measurements gave information about the conformation of the antibiotic and its complex with monovalent alkaline ions. If a stabilization of the hydrogen bonds is observed in the case of the K^+ - valinomycin complex, no modifications of this kind were noticed in the case of the Na^+ - antamanide complex.

In conclusion, the monolayer approach seems promising to investigate the conformation of antibiotic insoluble in aqueous phase and to obtain

information about their capacity to complex ions.

REFERENCES

1. H.A. Lardy, S.N. Graven, S. Estrada-O, Federation Proc. 26, 1355 (1967).
2. P. Mueller, D.O. Rudin, Biochem. Biophys. Res. Commun. 26, 398 (1967).
3. E.H. Harris, G. Catlin, B.C. Pressman, Biochemistry 6, 1360 (1967).
4. A.A. Lev, E.P. Buzhinsky, Tsytologia (U.S.S.R.) 9, 102 (1967).
5. B.C. Pressman, E.J. Harris, W.C. Jagger, I.H. Johnson, Proc. Nat. Acad. Sci. 58, 1949 (1967).
6. J. Jaffé, J.M. Ruysschaert, G. Bricman, J. Polymer Sci. 8, 817 (1970).
7. J. Kummer, J.M. Ruysschaert, J. Jaffé, Berichte vom VI. Intern. Kongress für Grenzflächenaktive Stoffe, Zürich 1972, II, 1, 285, Carl Hanser Verlag, München.
8. V.T. Ivanov, A.I. Miroshnikov, N.D. Abdullaev, L.B. Senyavina, S.F. Arkhipova, N.N. Uvarova, K.Kh. Khalilulina, V.F. Bystrov, Yu.A. Ovchinnikov, Biochem. Biophys. Res. Commun. 42, 4, 654 (1971).
9. Yu.A. Ovchinnikov, V.T. Ivanov, V.F. Bystrov, A.I. Miroshnikov, Chemistry and Biology of Peptides, Ann. Arbor Science Publ. 111 (1972).
10. D. Patel, Biochemistry 12, 4, 677 (1973).
11. Yu.A. Ovchinnikov, V.T. Ivanov, A.V. Evstratov, I.A. Laine, Peptides 1969, North-Holland Publ. Co., 266 (1971).
12. M.M. Shemyakin, Yu.A. Ovchinnikov, V.T. Ivanov, V.K. Antonov, E.I. Vinogradova, A.M. Shkrob, G.G. Malenkov, A.V. Evstratov, I.A. Laine, E.I. Melnik, I.D. Ryabova, J. Membr. Biol. 1, 402 (1969).
13. G. Kemp, Ch. Wenner, Biochim. Biophys. Acta 323, 161 (1973).
14. Th. Wieland, H. Faulstich, W. Burgemeister, Biochem. Biophys. Res. Commun. 47, 5, 984 (1972).
15. G. Kemp, E. Wenner, Biochim. Biophys. Acta, 282, 1 (1972).

ON THE ELECTROSORPTION BEHAVIOUR OF PHOSPHOLIPIDS : MEASUREMENTS OF DIFFERNTIAL CAPACITY AND INHIBITION

H.-D.Dörfler and E.Müller

Martin- Luther-Universität, Sektion Chemie,
402 Halle (Saale),Mühlpforte 1 , GDR

1.Introduction

First investigations into electrosorption behaviour of phospholipids were carried out by MILLER and BACH (1), SOHR and POP (2) and JEHRING and co-workers (3).

The aim of our own work was to study the concentration dependence of differential capacity curves with synthetic pure products to be able to calculate the thermodynamic adsorption parameters. Also the transport of metal ions across adsorbed phospholipid layers was studied, to get some informations about the properties of adsorbed layers as a barrier of charge transfer.

2. Methods and Materials

Synthetic DL-α- dipalmitoyllecithin (dpl) of purum grade from Fluka (Schweiz) was used without further purification. The measurements were carried out by use of a.c. polarography (BREYER), phase selective polarography and d.c. polarography.A.c. and d.c. polarograph GWP 563 produced by Akademiewerkstätten für Forschungsbedarf was used for registering a.c. and d.c. polarographic curves. This instrument for registering a.c. polarographic curves works with a frequency of 78 hz. The phase selective polarograph was similar to the instrument described in the literature by DE LEVIE and HUSOVSKY (4). In the case of a.c. and d.c. polarographic measurements dropping mercury electrodes were used (with automatic drop time control). The phase selective polarograph works with a hanging mercury drop electrode

from Methrom (Schweiz). The study of the ion permeability across the adsorbed layers was related to the transport of cadmium and tallium ions. The supporting electrolyte was prepared from KCl (analytical grade) with doubly destilled water. The potentials are related to the saturated calomel electrode. Unfortunately the dpl is only soluble in small amounts. Therefore mixed solvents were used which had been prepared from KCL 1 m and 10 % methanol, 10% ethanol and 2,5 % chloroform were added. But the solubility did not much increase. The most successful solvent was the mixture of 1 m KCl and chloroform.

3. Results

Fig.1 shows the concentration dependence of a.c. polarographic differential - capacity curves in 1 m KCl as solvent. In the potential range from E = 0 V to E = - 0,5 V (positive part of the electrocapillary curve) there appears one characteristic ad-/desorption wave (curve 4). In the potential range from E = - 0,5 V to E = - 2 V (negative part of the electrocapillary curve) there are to see two smaller capacity maxima. We get this shape of the curve only at a concentration of 10^{-3}m, at smaller concentrations the differential- capacity curves are unreproducible (fluctuations in fig.1 curves 2,3). It could be not excluded, that at potentials more negative than the electrocapillary maximum the capacity maxima are combined with a rearangement of the adsorbed film or with ad-/desorption of liposoms. We got references from the investigations of solutions prepared by ultrasonic. To improve the solubility 10 % methanol was added. The shape of these curves is similar to that discussed in fig.1. Different to the shape of the discussed a.c. polarographic curves are the curves registered by using the phase selective polarography. A hanging mercury drop electrode was used. The solutions of dpl was prepared in 1 m KCl with an addition of 2,5 % chloroform. The capacity- potential curves, which are presented in fig.2 show concentration dependent capacity maxima in the positive part of the electrocapillary curve. The ad-/ /desorption potential did not much vary with increasing concentration.

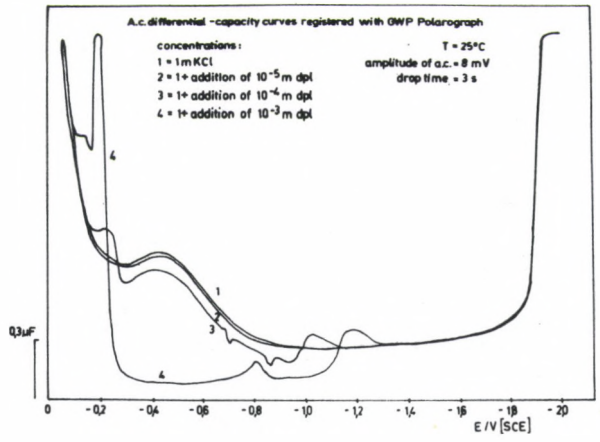

fig.1

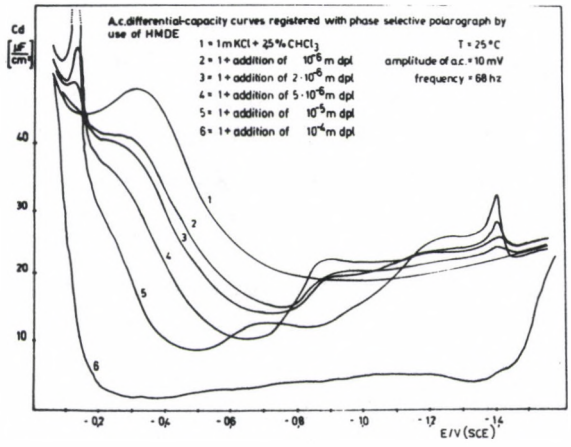

fig.2

In curve 6 there appears no capacity maximum, which may be due of the adsorption at potentials from E ≥ 0. In the potential range from E = - 0,2 V to E = - 0,6 V a systematic concentration dependent lowering of the electrode capacity takes place. In curve 6 the capacity is lowered to 1µF/cm^2, which was first found by MELIK-GAIKASJAN (5) in the case of adsorption of hexyl and octyl alcohol. This phenomenon indi-

cates, that polylayer formation takes place. For example, a 20 Å thick hydrocarbon layer of D = 2, fully impermeable to water and ions would cause a differential capacity of saturation of 1 $\mu F/cm^2$. The maxima in the negative branch different to the capacity maxima in the positive branch of the electrocapillary curve. These maxima are concentration dependent and are displaced with higher concentrations to more negative potentials. From a concentration of 10^{-5}m of dpl this capacity maximum does not exeed the curve of the supporting electrolyte. From this we can conclude, that this maximum is caused by a rearangement of the adsorbed layer. At more negative electrode potentials (E = - 1,3 V) curves 3 and 2 show only one maximum. In curves 4 and 5 two capacity shoulders appear. The splitting of the capacity shoulders indicates, that critical micelle concentration is attained, because the concentration of the stray electroyte is high. It is not impossible , that at concentration of 10^{-5}m of dpl concentration of critical micelle concentration is attained. Remarkable is, that the capacity in curve 6 did increase from 1 $\mu F/cm^2$ to 5 $\mu F/cm^2$ in the potential range from E= - 0,6 to E = - 0,8 V, what may be due to the rearangement of the adsorbed layer.

To get more information about the structure of the adsorbed layer the charge transport (inhibition investigations) was studied by measurement of current- potential curves. These measurements are related to the transport of metal ions across adsorbed lecithin layers. We selected cadmium and tallium ions, because this ions have redox potentials near the electrocapillary maximum, where maximum adsorption takes place. The redox potentials of such biological interesting ions like potassium, calcium and sodium ions lie in potential branches, where dpl is desorbed from the mercury surface. In fig. 3 there are registered the current potential curves of cadmium with and without dpl.
This fig. shows, that cadmium ions are only low impeded by dpl adsorption layers. We can conclude it from the small shift in the half wave potential and the displacement of

the diffusion current. We notice, that the current potential curves are quite reproducible from E = - 0,3 V to E = - 0,8 V. If the potential is larger than E = - 0,8 V the diffusion current will show fluctuations, which goes confirm with the concept of adsorbed clusters. The transport of tallium ions is faster than the transport of cadmium ions. Therefore it is not surprising, that tallium ions are not impeded. The tallium ion mobility is the same as for sodium ions.

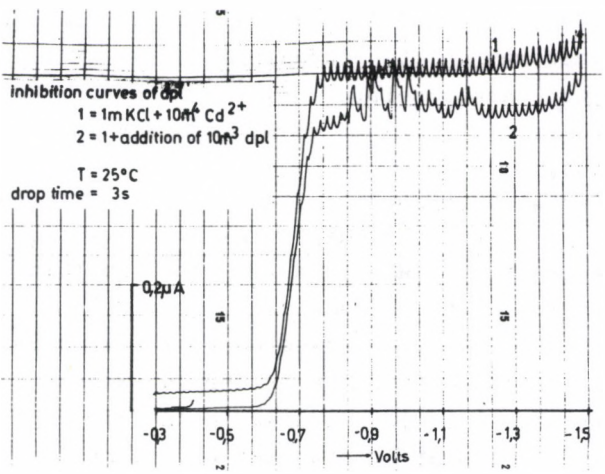

fig.3

4. Discussion

Basic difficulties are present for the interpretation of the experimental results in the case of a.c. polarographic measurements. During the study of the electrosorption behaviour of homologous n- alkylsulphates and n- alkylsulphonates we found, that in the concentration range of critical micelle formation the times for reaching adsorption equilibrium 100 times larger than for the adsorption of monomers. So it is obvious that we did not get any equilibrium value in the a.c.polarographic capacity curves. The drop time was only 3 s. It is reasonable to discuss the two branches of the capacity- potential curves:

- the range from E = 0 V to E = - 0,8 V
- the range from E = - 0,8 V to E = - 1,2 V.

For the potential range from E = - 0 V to E = - 0,8 V MILLER

and BACH (1) discuss a monolayer structure and from E =-0,8V the posibility of a clusterstructure. This was deduced from the value of the capacity at the potential of zero charge. MILLER and BACH (1) also used dropping mercury electrodes but an equilibrium is not secured. This disagrees also with the fact, that in fig.2, curve 6 the electrode capacity is lowered to 1 $\mu F/cm^2$. The decrease in the capacity of a fully covered electrode to 1 $\mu F/cm^2$ is characteristic før polylayer formation and was first found by MELIK- GAI - KASJAN (5) in the case of adsorption of hexyl and octyl alcohol near the concentration of saturation.

Two opposite conclusions are possible:

- In the potential range from E = 0 V to E = - 0,6 V a monolayer is present,
- polylayer formation takes place.

The adsorption takes place at only small negative potentials this means, that the negative charged part of the lecithin molecule may be adsorbed on the mercury surface (fig.2 curve 6). From reports of BARRADAS and co-workers (7) it is known, that such adsorption position is preferred, where the apolar part of the molecule is oriented to the mercury surface. So it is possible, that in the case of adsorption of the head group on the mercury surface a second layer is adsorbed to stabilize the nonpolar groups, which are oriented to the bulk phase. In the potential range from E=-0,5 V to E = - 0,8 V the value of the saturation capacity is increasing, which may be due to the rearangement of the adsorption layer. From E = - 0,8 V the presence of adsorbed clusters on the mercury surface is possible. This conception is supported by the investigation of ultrasonic solutions. As the obtained a.c. polarographic curves at small concentrations are unreproducible and are not equilibrium values, it was required to get some informations about the intermolecular forces in the electrosorption layer from the potential and concentration dependent maxima. From the shape of the capacity shoulders we can conclude qualitatively that only weak intermolecular forces in the electrosorption layer predominate. From the capacity- potential curves

obtained by use of phase selective polarograph the adsorption isotherm was calculated at constant potential, which is presented in fig.4. From further analysis according to FRUMKIN and DAMASKIN (8) we found, that the isotherm may be described with LANGMUIR isotherm, this means, that the attractive forces in the electrosorption layer only small. The calculation of the adsorption isotherm is not accurate, because not enough is known about monolayèr- polylayer formation.

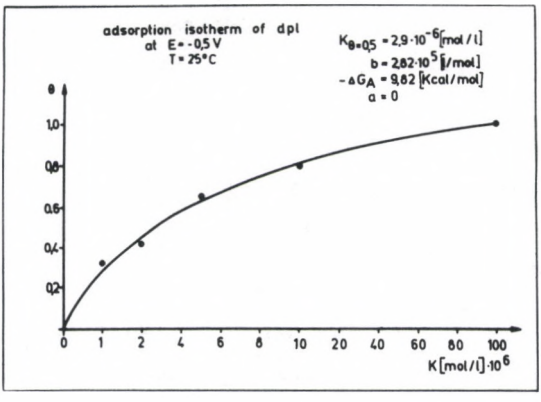

fig.4

The current - potential curves also give references, that the electrosorption layer is not compact. The transport of ions is only hardly impeded (fig. 3 curve 2).
Two conclusions are possible :
- the phospholipid layer is not compact
- dpl is strongly adsorbable, but the transport of ions is only a little impeded because dpl is an ionic substance.

The diffusion current is reproducible up to E = - 0,8 V (fig.3 curve 2). At more negative potentials fluctuations take place. This confirmed, that to E = - 0,8 V the presence of a homogenious mono- or bilayer is possible and the predomination of a clusterstructure from E = - 0,8 V. The fluctuations in the capacity values in fig.1 may be due to the disturbance of the structure of the electric double layer. At higher concentrations it is possible, that by the displacement of the solubility equilibrium there are enough molecules to built an electrosorption layer

and mechanical stabilisation of the double layer is possible. At concentrations of 10^{-3}m of dpl the solutions are **cloudy.** Only a small amount of dpl is really in solution.

It was impossible **carrying** out electrocapillary measurements because the solutions are cloudy.

Acknowledgement

The authors expresses here thanks to Doc.Dr. Kůta and Dr. L. Pospíšil for the helpful discussions and for carring out the measurements with the phase selective polarograph.

References

1. Miller, I.R. and D. Bach, J.Colloid.Sci. 29 (2),250 (1969)
2. Sohr,H. and L. Pop, Monatsber. der Akad.d.Wiss.d.DDR 12,504 (1970)
3. Jehring,H. and N.Huyen, Ber.Chem.Ges.d.DDR,20,147 (1973)
4. De Levie and L.Husovsky,J.Electroanal.Chem.,23,169 (1969)
5. Melik-Gaikasjan,W.J., J. Phys.Chem.(russ.) 26,560 (1952)
6. Müller,E.and H.-D.Dörfler, Abhandl.d. Akad.d.Wiss. DDR in press
7. Barradas,R.G. and P.G.Hamilton, Can.J.Chem. 43,2468 (1965)
8. Frumkin,A.N. and B.B. Damaskin, Modern Aspects in Electrochemistry, Vol.4 Butterworths 1964

BEHAVIOUR OF β-APO-8'-CAROTENAL AT THE OIL/WATER AND AIR/WATER INTERFACES

Maria Tomoaia, Anca Ioanette and E. Chifu

"Babeş-Bolyai" University, str. Arany János nr.11, Department of Physical Chemistry, Cluj-Napoca, Romania

Research on carotenoidic pigments in films is of great interest because these substances are components of biological membranes[1]; as well, the film state may be looked upon as a simplified model of the membrane[2].

The study of carotenoids in film state started only a few years ago[3,4,5]. In a previous work we have examined all-trans-canthaxanthin from this point of view[6].

The aim of the present work is to study the behaviour of all-trans-β-apo-8'-carotenal at the oil/water and air/water interfaces. The structure of this compound is shown in Fig. 1.

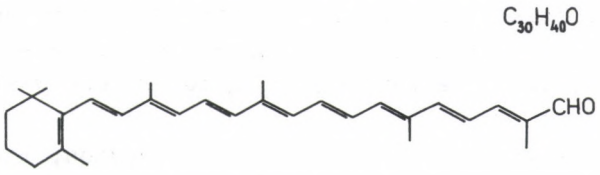

Fig.1. Structure of β-apo-8'-carotenal.

Experimental

β-apo-8'-carotenal used in our experiments was a BASF synthetic product. Its purity was verified in the course of the study by thin layer chromatography. Benzene pro-analysis "Reactivul"-Bucureşti and doubly distilled water were used as oil respectively aqueous phase. Benzene solutions of β-apo-8'-carotenal were kept at dark and measurements were made on freshly-prepared samples in order to prevent possible degra-

dation.

Two kinds of measurements have been performed :

- liquid-liquid interfacial tension at the interface benzene solution of β-apo-8'-carotenal/water,
- surface pressure of the monomolecular β-apo-8'-carotenal film at the air/water interface.

Interfacial tensions σ, dyn/cm, were measured by the du Noüy method using a Lauda Tensiometer type TE-1, equipped with a platinum-iridium ring. The accuracy of the measurements, performed at 25±0.1°C, was of ±0.1 dyn/cm. Surface pressures π, dyn/cm, of the monolayer were measured by Wilhelmy plate method[2], at ambient temperature (22±2°C) making use of doubly distilled water as subphase and of benzene as spreading liquid. The accuracy of the measurements was ±0.5 dyn/cm. The compression of the film was started immediately after the spreading, to avoid the compound degradation and to assure reproducibility of measurements.

Results and Discussion

The interfacial film at benzene/water interface. The interfacial tension σ (dyn/cm) at the interface benzene solution of β-apo-8'-carotenal/water, strongly varies with time t(min) as can be seen in Fig.2, for some systems having different concentrations c, mole/l, of β-apo-8'-carotenal. For the static value of the interfacial tension, when adsorption equilibrium was reached, that one corresponding to 200 min was taken into account.

Using the static values of interfacial tension, the isotherm interfacial tension- concentration logarithm was drawn, as seen in Fig.3. By means of the known Gibbs' equation,

$$\frac{\partial \sigma}{\partial \ln c} = - RT\Gamma \qquad (1)$$

Γ, mole/cm^2, being the adsorption, from the slope of the linear portion-corresponding to the small values of the interfacial tension, the maximum adsorption was calculated using the least squares method. Hence, the limiting area of the β-apo-8'-carotenal at the benzene/water interface was found to be:

$$A_o = 66 \pm 2 \text{ Å}^2/\text{molecule}$$

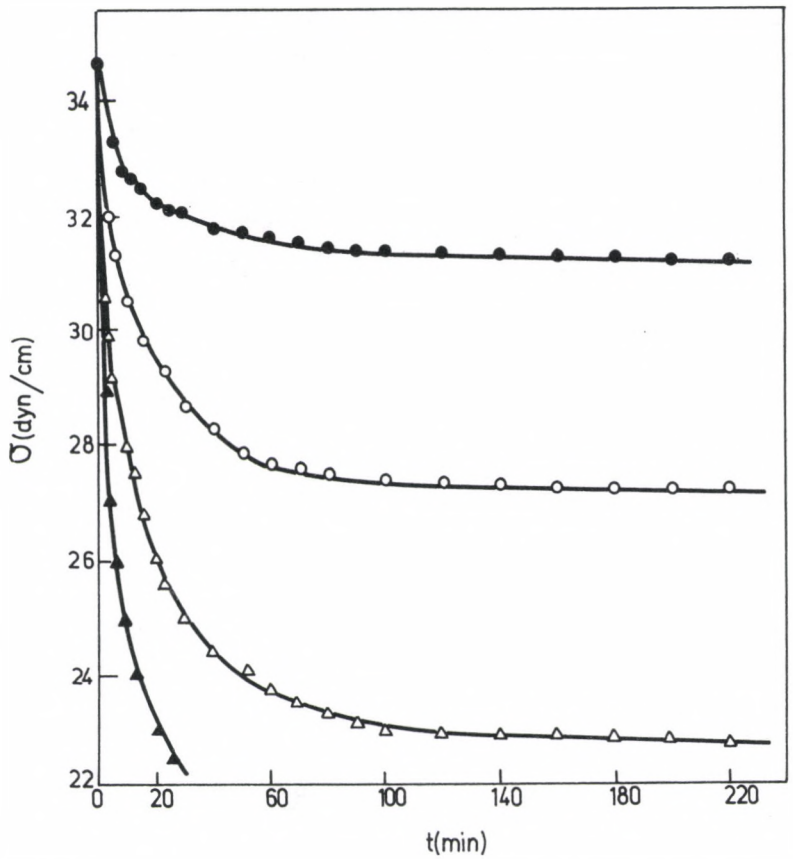

Fig.2. Interfacial tension (σ)-time (t) isotherms for benzene solutions of β -apo-8'-carotenal/water. The concentrations (c, mole/l) are : (●) 1.01×10^{-4}; (○) 2.97×10^{-4}; (△) 6.25×10^{-4}; (▲) 1.1×10^{-3}.

The experimental data concerning the static interfacial tension variation with concentration were processed by a Hewlett-Packard 9100 B Calculator.

We found that the interfacial tension - concentration dependence is expressed by the parabolic equation :

$$\sigma = 6.85329\ 10^{6}\ c^{2} - 2.05\ 10^{4}\ c + 33.0 \qquad (2)$$

Introduction of the derived $\frac{d\sigma}{dc}$ values in eq. (1) allowed the calculation of the adsorptions Γ , for different concentrati-

ons c, and using the adsorptions Γ, molecular areas A, were evaluated. On the other hand, interfacial pressure π, dyn/cm, is defined as:

$$\pi = \sigma_0 - \sigma \qquad (3)$$

where σ is the interfacial tension at the c concentration and σ_0 is its corresponding value at zero concentration.

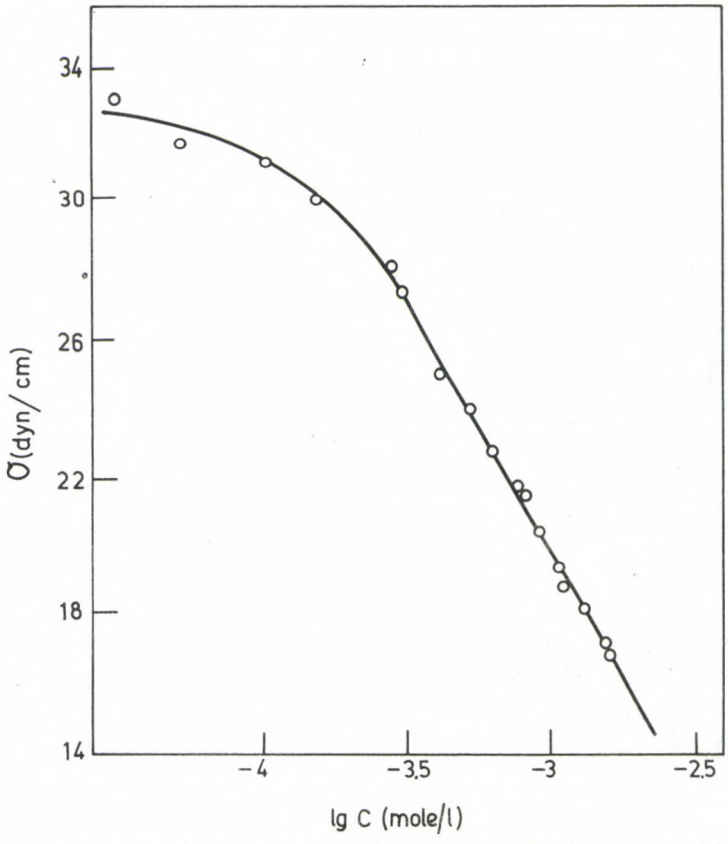

Fig.3. Static interfacial tension vs. logarithm of the concentration of β-apo-8'-carotenal.

Fig.4 renders the π-A isotherm, calculated in this manner for the interfacial film of β-apo-8'-carotenal at the benzene/water interface. $\pi = 0$ extrapolation of the linear portion of high pressures leaves to the limiting area :

$$A_0 = 64 \pm 2 \text{ Å}^2/\text{molecule},$$

in good agreement with the value obtained from the σ - log c isotherm in Fig. 3.

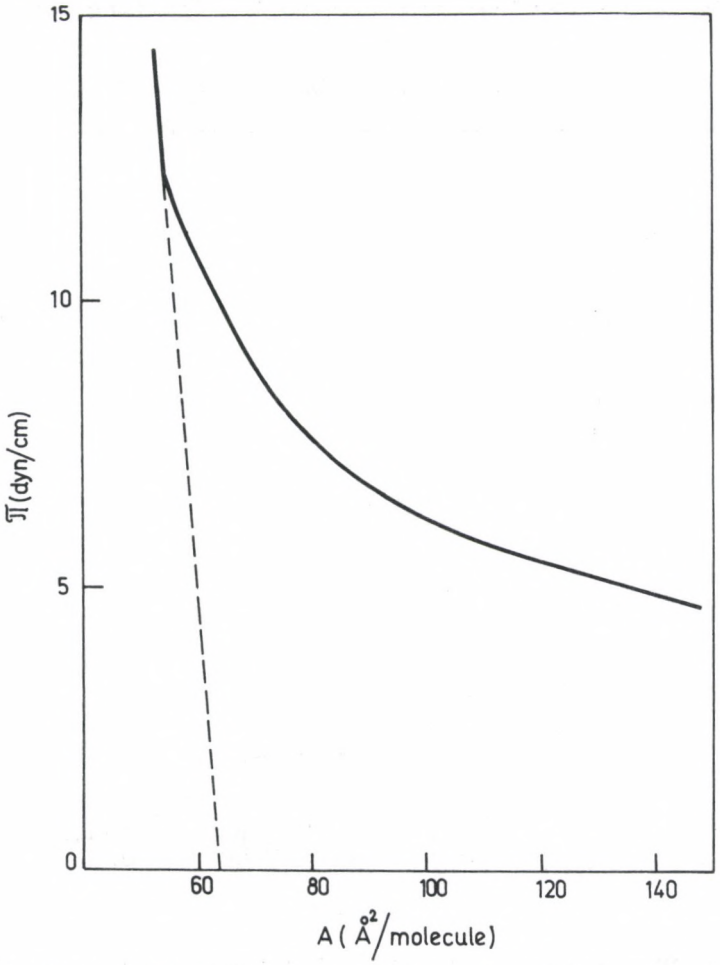

Fig. 4. Interfacial pressure (π) - area (A) isotherm for β-apo-8'-carotenal film at benzene/water interface.

The monomolecular film at the air/water interface was studied by means of the compression isotherms : surface pressure π - area A. In Fig.5 an exemple is shown from twenty isotherms. At the surface pressure of about 2 dyn/cm the isotherm presents a horizontal portion, which ought to be attributed to a bidimensional state transformation (probably expanded liquid

$\longrightarrow$ condensed liquid).

By extrapolating to $\pi = 0$ the linear portion, of high pressures, of the π - A isotherm one obtains the limiting area:

$$A_o = 54 \pm 2 \text{ Å}^2/\text{molecule},$$

independently on the quantity of spreaded substance.

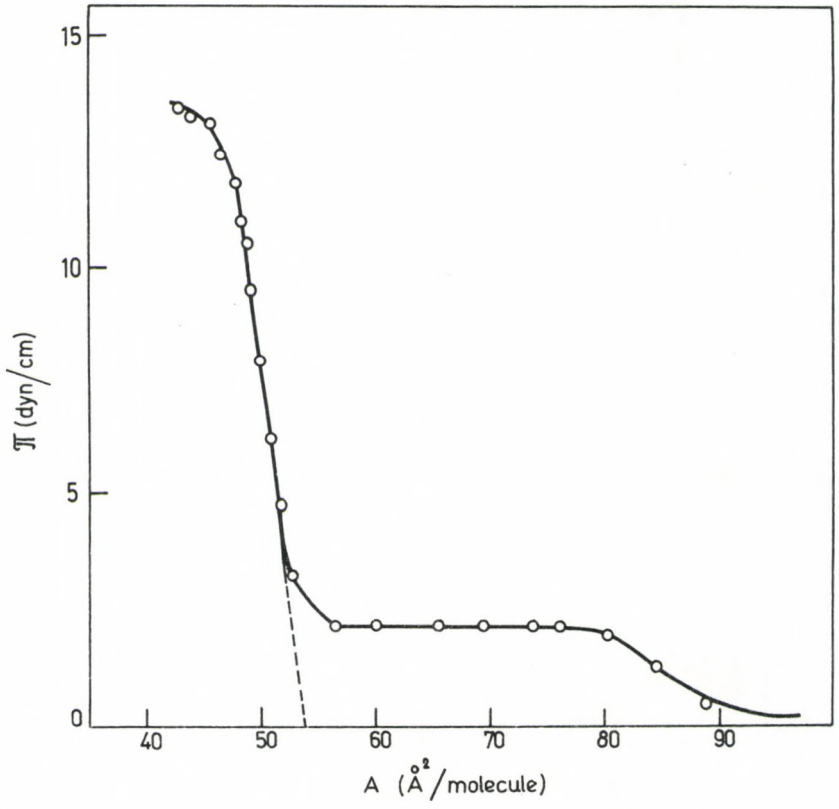

Fig.5. Surface pressure (π) - area (A) compression isotherm for β-apo-8'-carotenal film at air/water interface.

Surface compressional moduli. π - A compression isotherms, namely their linear region slopes at high pressures, were used to estimate surface compressional moduli, taking $A = A_o$.

$$C_s^{-1} = - A\left(\frac{\partial \pi}{\partial A}\right)_T \qquad (4)$$

One finds that, for the interfacial film (Fig.4), the compres-

sional modulus is

$$C_s^{-1} = 80 \text{ dyn/cm},$$

while for the monomolecular film at the air/water interface (Fig.5) it is

$$C_s^{-1} = 100 \text{ dyn/cm}.$$

Conclusions. The relative high values of the limiting areas obtained by us for β-apo-8'-carotenal, were also found in the case of other carotenoids[3,4,5,6]. The fact is to be correlated with the presence of the iononic nucleus and with that of the methyl side groups.

Comparison of the limiting area value obtained at the benzene/water interface (66 Å^2/molecule) to that obtained at the air/water interface (54 Å^2/molecule) results in the finding that the interfacial film is more expanded than the monolayer. The area increment is due to the penetration of the oil molecules among the hydrocarbon chains, causing the change of inter-chain attraction.

In what the values of the surface compressional moduli are concerned (80 dyn/cm for the interfacial film and 100 dyn/cm for the monomolecular air/water film), they are situated at the lower limit of the values admitted for the bidimensional state of the condensed liquid, 100-250 dyn/cm[7]. The value of the surface compressional modulus is however smaller at the benzene/water interface than at the air/water interface, in the first case the film being more expanded.

Appreciation is expressed to the Institute for Stable Isotopes, Cluj-Napoca, for the use of its facilities - the Lauda Tensiometer and the computer program.

References

1. O. Isler, Carotenoids, Birkhäuser Verlag, Basel und Stuttgart, 1971

2. G.L. Gaines, Jr., Insoluble monolayers at liquid-gas interfaces, Interscience Publishers, New York - London - Sydney, 1966

3. R.M. Leblanc and B.H. Orger, Biochim. Biophys. Acta, 275, 1o2 (1972)
4. V. Lejeune and C. Tric, J. Chim. Phys., 68, 1o5 (1971)
5. R.M. Leblanc, Vision Research, in press.
6. E. Chifu, M. Tomoaia, A. Ioanette, to be published.
7. J.T. Davies and E.K. Rideal, Interfacial Phenomena, Academic Press, New York - London, 1963.

SOME NEW RESULTS ON THE SURFACE DIFFUSION IN SPREAD MONOLAYERS AT THE GAS/LIQUID INTERFACE USING THE RADIOTRACER TECHNIQUE

D. Vollhardt and L. Zastrow

Central Institute of Organic Chemistry, Academy of Science of the GDR, 1199 Berlin Rudower Chaussee 5, German Democratic Republic

The direct experimental determination of surface concentration is of fundamental importance for the characterization of adsorption layers at liquid interfaces. The radiotracer technique is the only method allowing a direct determination of distibution of surface active substances at liquid interfaces. The radiotracer technique is most suitable for the investigation of properties of spread monolayers because the measured activity is not influenced by the activity of molecules dissolved in the bulk.

On this basis we studied the dynamic behavior of insoluble monolayers, in particular the distribution hysteresis of the spread substance by compression and following dilatation of the monolayer, the desorption from spread monolayers and the problem of surface self-diffusion, which will be discussed here.

Until the early sixties scientists held that the mass transport at fluid interfaces takes place exclusively by convection or bulk diffusion. Since then the significance of surface diffusion at fluid interfaces was recognized by hydrodynamic effects at kinetic investigations of monolayers and thin films [1,2]. Recently Sakata/Berg [3], Good/Schechter [4], and Chung/Berg [5] determined surface self-diffusion coefficients by partial tagging with radioactive isotopes.

The measuring device developed by us is based on the following principle. At constant film pressure the change of surface distribution of a tagged substance is determined as function of time. Before the measurements begin the surface area is divided into two equal regions by a barrier separating a radioactive monolayer from a nonradioactive one. The changes of distribution of radioactive materials can be measured after the removal of the barrier. The fundamental conditions

important for an adequate accuracy and reproduceability are the following: the apparatus must be free from vibrations, air currents being eliminated, evaporation from the surface of the trough being minimized by water vapour saturation, and temperature being constant. The Geiger-Müller counting tube is moved from outside the experimental enclosure by using a special coupling device along the surface area of the trough. A surface diffusion trough with simple separation using barriers differently shaped could not be applied because of disturbances in form of leakages of the boundary and turbulences occuring by opening the barrier.
Therefore the trough shown in the scheme (Figure 1) was developed for the measurement of surface self-diffusion. A 0.01 mm thin platinum plate (e) fixed in a lowering device divides the trough into two equal parts. The lowering of the barrier without disturbances was obtained by insignificant inclination of the platinum edge. Smallest pressure differences of surface and bulk between the two regions must be adjusted inorder to secure perfect initial conditions, before the barrier is removed. This problem was solved by the connecting canal (b), closed for the surface, but not for the bulk during spreading at position (c). After that the barrier at (c) is removed to obtain precisely the same film pressure on either side of the barrier at (e). Finally the diffusion path is blocked up by the stable barriers at positions (d) before the surface self-diffusion process is started.
The measurement of the distribution along the surface is carried out in direction from nontagged to tagged substance. The distance between every test point is 2 mm.

Theoretical fundamentals of the measuring system are the following. According to Levich 6 the initial point is the law of conservation of surface active material.

$$\frac{\partial \Gamma}{\partial t} + \operatorname{div} (j_{surf} + j_{diff}) + j_n = 0 \qquad (1)$$

The convective flux j_{surf} of the surface active substance along the liquid surface is given by $j_{surf} = \Gamma v_t$

where v_t is tangential liquid velocity at the surface.
The diffusion mass flux arising on the surface is given by

$$j_{diff} = -D_s \operatorname{grad} \Gamma$$

and j_n designate the mass flux from the surface to the bulk.
Now the result is the following

$$\frac{\partial \Gamma}{\partial t} + \operatorname{div} (\Gamma v_t - D_s \operatorname{grad} \Gamma) + j_n = 0 \qquad (2)$$

In the case of insoluble monolayer $j_n \approx 0$

and $y = 0$

in the case of a plane liquid surface.
All quantities occuring are independant of z, and $w \equiv 0$,
wherew is the velocity component in z-direction.
Then we obtain

$$\frac{\partial \Gamma}{\partial t} + u_s \frac{\partial \Gamma}{\partial x} + \Gamma \frac{\partial u_s}{\partial x} = D_s \frac{\partial^2 \Gamma}{\partial x^2} \qquad (3)$$

For the condition $u_s = 0$ where u_s is the velocity component in x-direction we have finally a differential equation analogous to the bulk

$$\frac{\partial \Gamma}{\partial t} = D_s \frac{\partial^2 \Gamma}{\partial x^2} \qquad (4)$$

With the initial conditions for $\Gamma(x,t)$

$$\Gamma(0,x) = \Gamma_o \qquad 0 < x \leq L$$
$$\Gamma(0,x) = 0 \qquad -L \leq x < 0 \quad (L = \text{length of diffusion trough})$$

and the boundary conditions

$$\Gamma(t,L) = \Gamma_o$$
$$\Gamma(t,-L) = 0 \qquad \text{for } L \gg \sqrt{4 D_s t}$$

we get the fundamental equation

$$\Gamma(x,t) = \frac{\Gamma_o}{2} \left[1 + \operatorname{erf} \left(\frac{x}{\sqrt{4 D_s t}} \right) \right] \qquad (5)$$

for the surface concentration Γ as function of x and t.
Instead of real surface concentration $\Gamma(x,t)$ we measured an average weighed concentration $\overline{\Gamma}(x,t)$ because of the counting tube geometry where 2Δ can be considered to be the recording width.

With the equation of Gauss

$$\bar{\Gamma}(x,t) = \frac{1}{\sqrt{\pi}\cdot\Delta}\int_{-\infty}^{+\infty}\Gamma(x',t)\, e^{-(x-x')^2/\Delta^2}\, dx \qquad (6)$$

by substitution of expression (5) it follows

$$\Gamma(x,t) = \frac{\Gamma_o}{2}\left[1 + \operatorname{erf}\left(\frac{x}{\sqrt{4\, D_s\, t + \Delta^2}}\right)\right] \qquad (7)$$

This expression permits to calculate the surface self-diffusion coefficient D_s by differentiation

$$\frac{\partial \bar{\Gamma}(x,t)}{\partial x} = \frac{\Gamma_o}{\sqrt{\pi(4D_s t + \Delta^2)}}\, \exp -x^2/4D_s t + \Delta^2 \qquad (8)$$

It follows for the tangent of the inflexion point ($x = 0$, $\bar{\Gamma} = \Gamma_o/2$) at any time t

$$\frac{\partial \bar{\Gamma}(0,t)}{\partial x} = \frac{\Gamma_o}{2x_o} = \frac{\Gamma_o}{\sqrt{\pi(4D_s t + \Delta^2)}}$$

$$D_s = \frac{x_o^2}{\pi t} - \frac{\Delta^2}{4t} \quad \text{or} \quad x_o^2 = \pi D_s t + \frac{\pi}{4}\Delta^2 \qquad (9)$$

and at the time $t = 0$

$$\frac{\partial \bar{\Gamma}(0,0)}{\partial x} = \frac{\Gamma_o}{2x_{oo}} = \frac{\Gamma_o}{\sqrt{\pi}\,\Delta}$$

$$\Delta^2 = \frac{4}{\pi} x_{oo}^2 \qquad (10)$$

These conditions yield the simple equation for D_s

$$D_s = \frac{x_o^2 - x_{oo}^2}{\pi t} \qquad (11)$$

where x_{oo} is the intersection point of the tangent with the abscissa at the measured initial distribution and x_o at the measured distribution at the time t respectively.
Moreover D_s can be calculated from the straight line of the x_o^2 - t diagram according to equation (9).

The experiments with palmitic acid show in Figure 2 how a surface concentrations profile depends on x, determined by the measurements for the time $t = 0$ and the time $t = 142$ min

selected at random. On the right side of Figure 2 we transferred the results on a probability paper and obtained straight lines both for the initial distribution and for distributions at $t > 0$. D_s can be calculated from the slope according to equation (11). Besides, the straight line justifies the representation of the recording curve as Gauss distribution in conformity with our theoretical model.

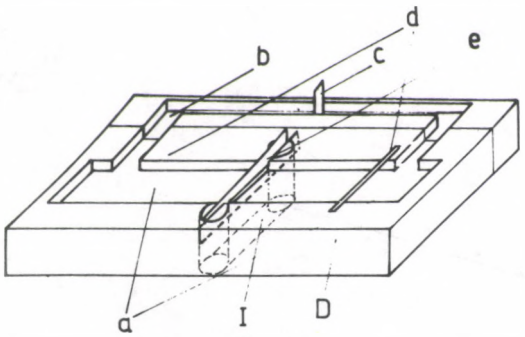

Fig. 1. Surface diffusion trough
a = diffusion path, b = connecting canal, c = teflon lamella, d = stable teflon barrier, e = platinum plate, D = trough, I = lowering device .

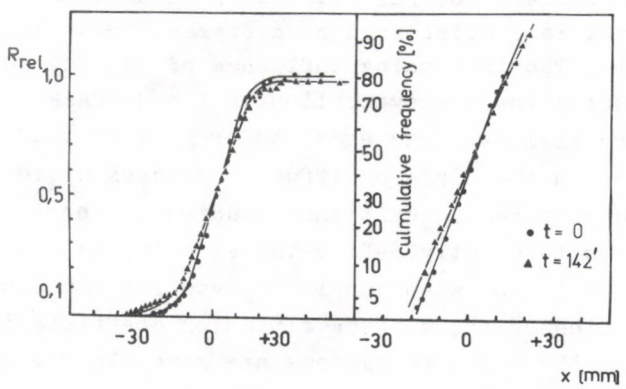

Fig. 2. Surface concentration profile of the system palmitic acid 33 A^2/molecule.

The computation of D_s from successive measurements of the surface concentration profile is shown in Figure 3 by the x_o^2 - t diagram of the same system palmitic acid 33 A^2/ molecule. D_s follows according to equation (9) from the slope of the least square fitted straight line obtained from the experimental data.

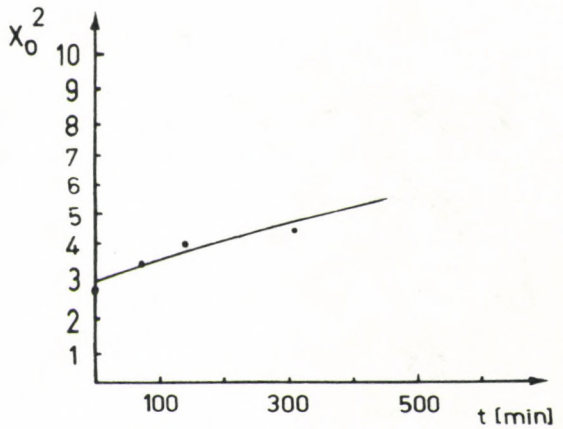

Fig. 3. x_o^2 - t diagram of system palmitic acid 33 A^2/molecule for calculation of D_s according to equation (9).

Using these two methods (Figures 2 and 3) the surface self-diffusion coefficients of palmitic acid, stearic acid, and stearyl alcohol were determined at different areas up to 75 A^2/molecule. The increasing influence of density convection did not allow the evaluation of the surface concentration profiles at areas equal to or greater than 100 A^2/ molecule, whereas the surface diffusion process up to 75 A^2/ molecule is undisturbed. Additional studies not presented here enabled us to exactly define the experimental and theoretical conditions when density convection can disturb the determination of the surface diffusion coefficient. The results of the measured systems are given in Figure 4 which shows how the values of D_s depend on the area. It can be seen that all values of D_s have the same order of

magnitude (greater than $10^{-5}cm^2/sec$) and lie one power of ten higher than in the bulk, there is no doubt about it because only two degrees of freedom of movement exist at the interface, and the hindrance from the adjacent bulk possesses asymmetric character.

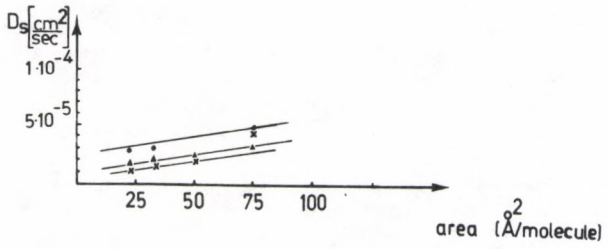

Fig. 4. D_s in dependence of area
• palmitic acid, ▲ stearic acid, × stearyl alcohol

Moreover, Figure 4 shows unambiguously that D_s decreases nearly with the same slope at the diminishing area of the molecules for all three compounds. It has to be like that because of the dispersion interactions of the alkyl chains and the decrease of the mean free path of the monolayer molecules. The dispersion Interactions also cause the decrease of D_s with increasing alkyl chain length. Finally D_s depends on the nature of the polar groups. This can be explained by the differences of the dipol/dipol interactions of the monolayer molecules and the interaction between the monolayer and the adjacent water molecules of the bulk.

References

[1] J.C. Berg and A. Acrivos Chem. Engng. Sci. 20,737 (1965)
[2] S. Withaker Ind. Engng. Chem. Fundamentals 3,132 (1964)
[3] E.K. Sakata and J.C. Berg Ind. Engng. Chem. Fundamentals 8,570 (1969)
[4] P.A. Good and Schechter, R.S. J. Colloid Interface Sci. 40,1 (1972)
[5] S.T. Chung and J.C. Berg J. KIChE 10,4 (1972)

INVESTIGATION OF BLACK FILMS BY α-PARTICLES

D.Exerowa, I.Penev and Chr.Christov

Institute of Physical Chemistry, Bulgarian Academy of Sciences, Sofia 13 Bulgaria

The black films (common and Newtonian) have been a subject of detailed investigations [e.g.1,2,3,4,5]. Never theless, the problems of their structure and properties as well as the factors determining the conditions of their stability (especially of Newton black films), are far from being cleared. Introduction of new methods of investigation would help to perceive the nature and, respectively, the stability of black films.

We have developed a method based on the forced destruction of foams and foam films by dosed external action. As an destructive agent the α-irradiation of foam films (or foams) has been employed. It is to be expected that such relatively unstable systems as the thin black films and the built out of them foams will be destoyed by sufficiently strong disturbances. The α-particles flux is a well defined and easily controlled disturbing agent.

The destructive action of α-particles upon foams has been observed long ago [6,7,8] but the observations were of thoroughly qualitative nature and reffered to foams obtained out of complex mixtures. The methods for destruction of foams and foam films by α-bombardment which we have developed allow to observe the behaviour of common and Newton black films very distinctly.

The irradiation of a single black film is carried out in a measurement cell, analogous to that that we have used in

other investigations of foam films [2,9,10,11]. The microscopic foam film (1) is formed in the middle of a double-concave drop (fig.1). The space in the cell is saturated by the vapours of the investigated solution and thermostated. On a special holder above the film the α-ray source is mounted (4). The latter can be moved freely in vertical direction. The radiation can be performed with variably collimated (by the collimator (3)) α-beam. The α-ray flux is measured separately by special counting device. The irradiation is switched on in a definite moment by means of the screen (2) with the aid of a D.C.electromagnet. Thus conditions of dosed action of α-rays on the microscopic film are realized. As a parameter characterizing the destructive action of the α-particles, the life-time τ_α of the black film under irradiation is assumed. It turned out that the rise of the electrolyte concentration decreased the stability of common black films (τ_α decreases) while with Newton films it increased (τ_α increases). Thus in the curve $\tau_\alpha(C_{el})$ a clearly expressed minimum appears, corresponding to the transition common/Newton black film. Fig.2 shows the dependence τ_α vs. C_{el} obtained with films (of radius $2{,}5.10^{-2}$ cm) stabilized by sodium layryl sulphate, NaLS (5.10^{-4} mol/l) at 23°C. The films are irradiated by Am^{241} ($1{,}48.10^{7}s^{-1}$). The minimum of the curve is at 0,331 mol/l NaCl. This value of $C_{el,cr}$ for NaLS coincides with the values obtained with microscopic films by other methods [4,11,12]. Since the minimum is very sharp, the determination of the transition common/Newton black film is very sensitive and accurate ($\pm$ 0,003 mol/l). The method has been employed to establish the transition with films stabilized by several surfactants of different types [12] under identical conditions. In all cases under investigation the values found for $C_{el,cr}$ are substantially higher than those calculated from DLVO-theory. Moreover, a difference in $C_{el,cr}$ between ionic and nonionic surfactants has been established. For ionic surfactants (with higher φ_0-potential of the diffuse electric layer [13]) $C_{el,cr}$ are higher than those for non-ionic surfactants. The results are pre-

sented and discussed in details in [12].

A method for destruction of a foam by α-irradiation is also developed [12,14]. The time $\tau_{R/2}$ of destruction of a foam column to a distance R from the α-source (R equals half the free-path of the α-particles in air) is introduced as a characterizing parameter. The curve $\tau_{R/2}$ (C_{el}) also possesses a pronounced minimum, corresponding to $C_{el,cr}$. In this manner the transitions with the mentioned above surfactants have also been established [12]. $C_{el,cr}$ determined with microscopic films proved to be higher than those with foams. For example, in the case of NaLS $C_{el,cr}$ at the same temperature and composition of the solution is 0,320 mol/l. This difference, which is discussed in details in [11,15] will be explained further on. Comparing the time of forced ($\tau_{R/2}$) and spontaneous (τ) destruction for a number of diverse surfactants one notices that they follow the same order [12, 16]. The forced distruction of foams by α-particles yields the possibility (through comparison of $\tau_{R/2}$ at equal conditions) of characterization of the stability of the diverse foams and to estimate the effectivity of the foamers. The results reffering to the stability of the foams are considered in [12,14,16].

The forced destruction of black films by α-radiation proved to be an important way for studying Newton films and the transitions to them. In a free of external disturbances system the Newton films ought to appear at electrolyte concentration providing a value of Π at the maximum of Π (h) dependence (Π is disjoining pressure, h is film thickness) equal to or lower than the external capillary pressure P_σ . If, however, the film is subjected to external disturbances or is simply larger, the Newton film will be formed at lower electrolyte concentration at which the maximum of Π (higher than P_σ) will be overcome. This is apparently the case of local heating of the film in Mysels'experiments [1] as well as in other macroscopic investigations [e.g.1,17]. In such a way, when approaching $C_{el,cr}$ defined by the condition $\Pi_{max} = P$, a metastable region is passed where the energy barrier is of

the order of kT and is more exactly reached with microscopic black film which is very clearly demonstrated by the divergence in the curves θ (C_{el}) (θ is contact angle film/bulk liquid) for microscopic [4] and macroscopic [17] films in the neighbourhood of $C_{el,cr}$ and is directly confirmed by the measurements of θ in [15]. More rigorous experiments by α -particles method, analogous to Mysels'heating have been carried out, in which Newton black spots are generated in the common black film at $C_{el} < C_{el,cr}$. At that, for given irradiation at each C_{el} and temperature, the expectation time $\bar{t}$ of the transition is well reproducible and can be used in the investigation of the metastable black films. Fig.3 represents the dependence $\bar{t}$ (C_{el}) for a spontaneous transition (curve 1) in the metastable region (C_{el} = 0,28-0,334 mol/l NaCl) and for the transition in the case of α -particles irradiation (curve 2). The investigations have been carried out with microscopic films (r = 10^{-2} cm), stabilized by NaLS (5.10^{-4} mol/l) at 23°C. Each point on the curve is obtained from about 50 measurements. The deviations from t for series of 10 measurements are 1%. Curve 1 shows that the expectant time of the transition diminishes with the rise of C_{el} until $C_{el,cr}$ is reached (0,334 mol/l in the case) in a very good agreement with the value established with microscopic films by other methods [4,11,15]. At lower concentrations (e.g. 0,22 mol/l) the transition is observed at times after waiting 1 to $1^1/2$ hours. This transition can be induced by α -particles, at suitable for each case irradiation, within 12-15 sec. In fig.3, curve 2, it can be seen that the expectant time of the transition substantially diminishes (on the average, 4-5 times for the studied interval of C_{el}) and $C_{el,cr}$=0,331 mol/l is identical with that found from the dependence τ_{α} (C_{el}) and concurs within the limits of accuracy with the value reported above. The lower values of $C_{el,cr}$ (about 0,2 mol/l) obtained with macroscopic films and foams could be explained with the relative stability metastable common black films which can be realized in the concentration interval 0,2 - 0,33 mol/l (with microfilms) but are omitted with larger films.

The mechanism of action of the α-particles upon the foam films has not been considered up to now. Numerous results of our experiments point to the following. Only the nuclear processes during the transit of α-particles through the film can be rejected because of the relatively low energy of the used radiation (about 5 MeV). It could be expected that under the action of the radiation a change in the film composition takes place e.g. because of ionization, radiolysis or warming up of the film at which the films should noticeably change during the experiment. In order to check this assumption the life-time τ_α of Newton films at continuous α-irradiation from the formation up to their rupture has been measured as well as the time τ_α^N when the radiation is switched on by means of the screen (2) (fig.1) at the moment when the Newton film is formed. Mean values from about 60 measurements have been obtained for τ_α and τ_α^N . Their comparison reveals that within the limits of statistical scattering of the data $\bar{\tau}_\alpha$ and $\bar{\tau}_\alpha^N$ coincide i.e. the time of destruction is the same whether the film is only irradiated during the final stage (Newton film, life time τ_α^N) or from the very instant of its formation and during the subsequent stages of thick film, common and Newton black film (life time τ_α). This result indicates that the destruction of the film is not connected with a change in the composition because of the irradiation, at least during the experiment. We have also determined the time of destruction of Newton films at irradiation at given intervals of T sec, the time between the intervals being also T sec. The total time of destruction has been compared to τ_α^N . Practically no difference has been established when varing T from 1,5 to 8 sec. These results show that no total warming up of the film or any accumulation of energy practically occurs. The above experiments give us the grounds to reject the mechanism of accumulative action of the α-particles. Some other facts support them as well. For example, no change of the longitudinal conductivity $\partial\ell_f$ (measured by the method described in [18]) has been noticed with powerful α-irradiation of Newton film stabilized by NaLS (ionic surfactant)

and sucrose dodecyl urethane (non-ionic surfactant). It is worth noting that the mean life-times at irradiation which are very sensitive to minute changes in composition of the solution remain constant at continuous irradiation of the film. The experiments on $C_{el,cr}$ lead to analogous conclusions. The fact that $C_{el,cr}$ coincides with the values obtained by ahother method proves that the solution from which the film is made corresponds to the defined composition and temperature. All this leads us to the thought that the distruction by α-particles occurs as a statistically fortuitous act in the process of film irradiation i.e. the results are in favour of a statistical mechanism, not of a accumulative mechanism. The described transitions in the metastable region are of analogous character and the fact that the irradiation can only reduce the mean time of the transition correborates the above hypothesis.

With a view to understand the process of destruction we have studied the dependence of $\bar{\tau}^N_\alpha(n)$ (n-is the number of passing through the film α-particles per second). Newton films ($r=5.10^{-2}$ cm) obtained from solutions of diverse surfactants are subjected to irradiation of definite intensity and the time τ^N_α to the rupture is measured. The mean life-times τ_α are determined from 50-100 measurements; sufficient to determine τ^N_α with satisfactory small statistical error. In fig.4 the dependences $\tau^N_\alpha(n)$ for films stabilized by NaLS (curve 1), hexadecyltrimethylamonium bromide (curve 2) and sodium octyl sulfate (curve 3) are presented. The continuous lines in the same figure are calculated from the formula:

$$\tau^N_\alpha = \frac{\pi r^2}{(a+bn)n}$$

with suitably chosen values of the parameters a and b. The expression is obtained on the grounds of the hypothesis of the statistical mechanism of film destruction at α-irradiation. These investigations are not yet completed. The good agreement of the theoretical curves in fig.4 with the experimental points is unambiguously in favour of the statistical mechanism. It appears that the effect of the α-particles

consists in artificial provoked external disturbances in the films which, otherwise, can spontaneously arise on account of thermal fluctuations and lead to the film rupture [e.g.19, 20,21]. Thus the action of the α-particles leads, in fact, to a manyfold increase of the number of disturbances in the film, respectively of the probability of rupture and, as a result, reduces the life-time. The forced destruction yields richer possibilities for studying the processes of rupture of the black films which undoubtly is way to understanding the origin of their stability.

R E F E R E N C E S

1.M.Jones, K.Mysels and P.Sholten, Trans.Farad.Soc., 62, 1336 (1966).
2.A.Scheludko, Adv.Kolloid Interface Sci., 1, 391 (1967).
3.J.Clunie, J.Goodman and B.Ingram, Surface and Colloid Sci., 3, 167 (1971).
4.T.Kolarov, A.Scheludko and D.Exerowa, Trans.Farad.Soc., 64, 2864 (1968).
5.D.Engelsen and G.Frens, Farad.Trans.I, 70, 237 (1974).
6.R.Chaminade, Compt.Rend., 228, 480 (1949).
7.Ader, J.Phys.Radimn., 11, 198 (1950).
8.R.Kato and T.Kono, J.Appl.Phys., 34, 708 (1963).
9.A.Scheludko and D.Exerowa, Kolloid-Z., 24, 168 (1960).
10.D.Exerowa, Thesis Akad.Bulg.Sci., Sofia (1969).
11.D.Exerowa and D.Platikanov, Ann.Univ.Sofia, Fac.Chim., 65, 237 (1970/71).
12.D.Exerowa, I.Penev and S.Awgarska - to be published.
13.D.Exerowa, Kolloid-Z., 232, 703 (1969).
14.D.Exerowa and D.Ivanov, Compt.Rend.Bulg.Sci.,23,547(1970).
15.D.Exerowa and Ch.Christov - to be published.
16.D.Exerowa, Ch.Christov and I.Penev-paper presented on the Simposium on Foams, Brunel Univ., London (1975).
17.F.Huisman and K.Mysels, J.Phys.Chem., 73, 489 (1969).
18.D.Platikanov, N.Rangelova,Compt.Rend.Bulg.Sci.,21,913(1968)
19.A.Scheludko, Proc.Koninkl.Ned.Akad.Wet., B65, 76 (1962).
20.A.Vrij, Disc.Faraday Soc., 42, 23 (1966).
21.B.Deryaguin and Yu.Gutop, Kolloid-Z., 24, 431 (1962).

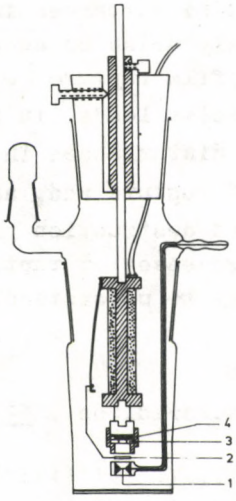

Fig.1

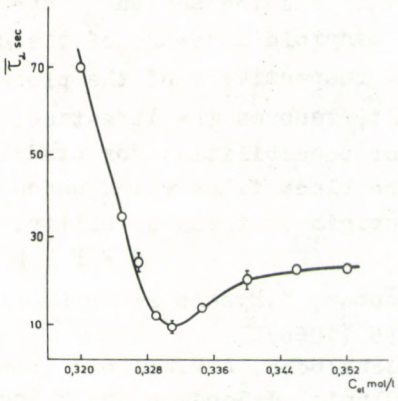

Fig.2

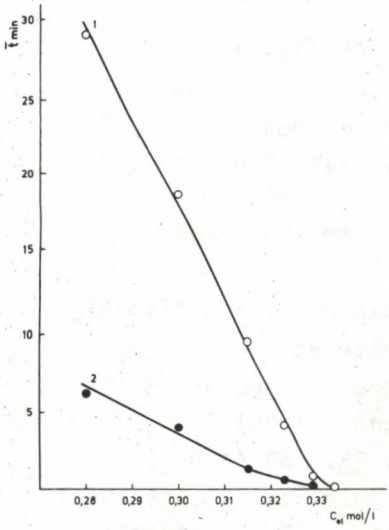

Fig.3

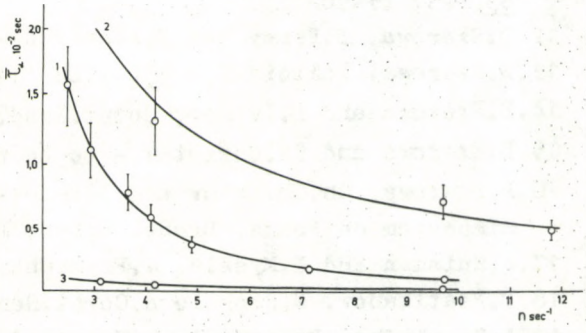

Fig.4

HYDRODYNAMICS OF FOAM AND EMULSION FILMS

I.B.Ivanov, B.P.Radoev, T.Tr.Traykov, D.St.Dimitrov, E.D.Manev and Chr.St.Vassilieff
Department of Physical Chemistry, Faculty of Chemistry, University of Sofia, Sofia 26, Bulgaria

The main stages of formation and evolution of a thin liquid film originated between two foam bubbles are (fig. 1 a - f):

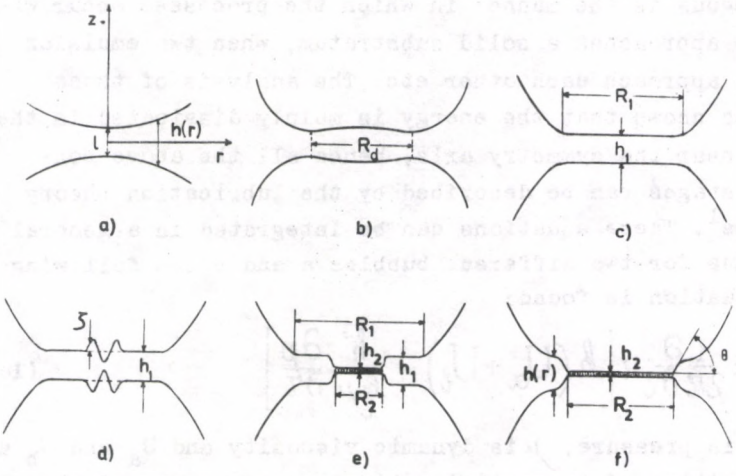

a) mutual approaching of two slightly deformed bubbles under the action of an external driving force F; b) at a given value l_1 of the distance l=h(0) the curvature at r=0 changes its sign and a cupped-shaped formation (dimple) of radius R_d arises; c) the dimple height initially increases then decreases and eventually a quasiplane parallel first film of

radius R_1 forms; d) because of thermal fluctuations (or other disturbances) corrugations appear on the film surface. Due to the disjoining pressure Π their amplitude ζ can spontaneously grow up and at a thickness $h_{cr}=2\zeta$ either rupture of the film or formation of second (black) spot occurs; e) under the action of the tension difference $\Delta_1 - \Delta_2$ of the first and the second films the spot of radius R_2 and thickness h_2 expands with velocity $V_r=dR_2/dt$ (t is time) until the whole first film turns into a second one; f) in this moment the contact angle between the film and the bubble sharply increases up to its equilibrium value Θ (contact angle between a second film and a bubble); at this the mechanical equilibrium of the bubble is violated and expansion of the second film begins. This leads to deformation of the bubble surface. Finally an equilibrium second film, the lifetime of which can be unlimited, forms.

Analogous is the manner in which the processes occur when a bubble approaches a solid substratum, when two emulsion droplets approach each other etc. The analysis of those processes shows that the energy is mainly dissipated in the regions near the symmetry axis, hence all the above considered stages can be described by the lubrication theory equations[1]. These equations can be integrated in a general form. Thus for two different bubbles a and b the following basic equation is found:

$$\frac{\partial h}{\partial t} = \frac{1}{2r}\frac{\partial}{\partial r} r\left[h\left(U_a+U_b\right) - \frac{h^3}{6\mu}\frac{\partial p}{\partial r}\right] \quad , \qquad (1a)$$

where p is pressure, μ is dynamic viscosity and U_a and U_b are the velocities of tangential motion on the upper and the lower surfaces. With deformable surfaces we shall admit that h depends on t through $l=h(0)$ only, so that $\partial h/\partial t=-V\partial h/\partial l$ where $V=-\partial l/\partial t$. The pressure is determined by Laplace's equation

$$-\frac{\partial p}{\partial r} = \sigma_a \frac{\partial}{\partial r}\Delta_r h_a = -\sigma_b \frac{\partial}{\partial r}\Delta_r h_b \quad , \qquad (1b)$$

where σ_a and σ_b are the respective surface tensions and Δ_r

is the radial part of the surface laplacian. Thus from (1) the dependence of h on r, l and V can be found. With non-deformable surfaces the velocity $\partial h/\partial t=-V$ does not depend on r and if U_a and U_b are known, the pressure can be obtained from (1). The dependence of V on F can be calculated from the balance of forces:

$$F = \int_{(S)} (p-p_\infty)\, dS \quad , \tag{2}$$

where p_∞ is the pressure in the liquid at $r\to\infty$ and the integration is carried out over the surface S upon which the pressure is applied.

Let us first consider the case when the surfaces of the two bubbles do not perform any tangential motion ($U_a=U_b=0$). If the bubbles (of radius R_a and R_b) are non-deformable, from (1a) and (2) we obtain the generalization of Taylor's equation for the velocity of approaching of two solid spheres[2], and at $h=h_1=\text{const}$ - Reynolds' equation for the velocity of thinning of a film between two solid circular plates of radius R_1:

$$\text{a)}\ V_T = \frac{2Fl}{3\pi\mu\bar{R}^2}\ ;\ \bar{R}=2R_aR_b/(R_a+R_b)\quad \text{b)}\ V_{Re} = \frac{2h_1^3F}{3\pi\mu R_1^4} \tag{3}$$

Reynolds' equation (3b) is also applicable for a thin film of nematic liquid crystal formed between two solid plates but then $\mu_\perp$ must be substituted for μ and the condition $\mu_\perp VR_1/d\ll 1$ must be satisfied (d is the modulus of elasticity)[4].

With deformable bubbles the system (1)-(2) can be solved for the stages a) and b) from fig.1 either by parametric expansion in series with respect to the small parameter[2] $\beta=F/4\pi\sigma_aR_a$ or by matching the coordinate expansions at small and great values[5] of r. At that, in first approximation, again Taylor's equation (3a) is obtained for the velocity of approaching of the two bubbles (at r=0) and the dependence of the distance between the two surfaces on r is described by the equation

$$h = l + r^2/\bar{R} - \beta(2\sigma_aR_a/\bar{\sigma})\ln(1+r^2/\bar{R}l)\ ;\ \bar{\sigma}=2\sigma_a\sigma_b/(\sigma_a+\sigma_b)\ . \tag{4}$$

From here, for the radius R_d of the dimple and for the thickness l_1 at which it forms we have

$$a)\quad R_d^2 = R_1^2(1-\ell/\ell_i)\ ; \qquad b)\quad \ell_i = F/4\pi\bar{\sigma}\ , \tag{5}$$

where

$$R_1^2 = F\bar{R}/2\pi\bar{\sigma} \tag{6}$$

is the radius of the equilibrium film which would appear between the two bubbles (at $l \ll l_1$) in the presence of long range (electrostatic) disjoining pressure. With various limiting values of $\bar{R}$ and $\bar{\sigma}$ equation (6) gives as particular cases all the known expressions for the radius of the equilibrium film: a) bubble-solid surface ($R_a=\infty$, $\sigma_a=\infty$ - Derjaguin and Kussakov), b) solid sphere-plane liquid surface ($R_a=\infty$, $\sigma_b=\infty$ - Allan, Charles and Mason), c) two identical bubbles ($R_a=R_b=R$, $\sigma_a=\sigma_b=\sigma$ - Princen; Lee and Hodgson) and d) bubble-plane liquid surface ($R_a=\infty$, $\sigma_a=\sigma_b=\sigma$ - Chappelear). Eqs. (4)-(6) are in qualitative and semi-quantitative agreement with the experimental results of Roberts and of McKay and Mason.

The method of matching of the coordinate expansions[5] was also applied at $l \ll l_1$. At that the deformation of the bubbles has been taken into account in a general form without assuming the presence of a thin film of definite radius. In the final results only, the radius of the equilibrium film R_1 has been introduced through (6). The numerical analysis of the obtained equation for the surface of the bubbles shows that at $0 \leqslant r \leqslant R_1$ the thickness h does not depend practically on r, i.e. a film of almost uniform thickness forms. This thickness diminishes at the rate $V=h_1^3F/2\pi\mu R_1^4$. This expression differs from Reynolds' equation (3b) very little (by the numerical coefficient only) which justifies the application of eq.(3b) for calculating the rate of thinning of plane parallel foam films (stage c).

The shape of the film surface corrugated by thermal fluctuations (stage d) can be represented as a result of the superposition of waves, one of which, with wave number k and equation $\zeta(r,h)$ (we assume cylindrical symmetry) is determinant for the rupture of the film. For the velocity of deepe-

ning of this wave $v_\zeta^o = \partial\zeta/\partial t$ from (1) (in the right hand side of (1b) in this case a term $-2(d\Pi/dh_1)(d\zeta/dr)$ must be added) we obtain $v_\zeta^o = -(k^2/24\mu)(\sigma k^2 - 2d\Pi/dh_1)h_1^3\zeta$. Since $v_\zeta^o = d\zeta/dt = (d\zeta/dh)(dh/dt)$, the wave amplitude ζ and respectively the critical thickness of film rupture h_{cr}, will depend on the ratio v_ζ^o/V_{Re}:

$$\zeta = \text{const}\ \exp\left[-\int \frac{v_\zeta^o}{V_{Re}}\, dh_1\right] . \qquad (7)$$

Hence the final expression for h_{cr} depends[6,13] on F, Π and σ but not on μ.

In the analysis of the stage e) the black spot is considered as a piston expanding in radial direction with velocity V_r. The velocity of thinning V of the first film is also allowed for. Complicated expressions have been obtained for V_r and V which give[8] $V_r = h_1(\Delta_1 - \Delta_2)/12\mu R_2 \ln(R_1/R_2)$ in the particular case of V=0. This result is in agreement with the established by Kolarov, Scheludko and Exerowa proportionality between V_r and $\Delta_1 - \Delta_2$. The problem for the expansion of a second film (stage f) has been solved by the method of parametric expansion[9]. The expression obtained for the velocity of expansion of the film $V_r = \Theta^2 F\left[6\pi n\mu R_2 \ln(R\Theta^2/12, 2h_2)\right]^{-1}$ (n=1 for a film on a substratum and n=4 for a symmetrical film) satisfactory agrees with the experimental results of Tchalyovska and Kolarov in the cases when the second film is thick enough to assume that the viscosity has its bulk value .

In fact, never are the interfaces in foam and emulsion systems immobile. The velocities of tangential motion $U_a = U_b = U$ (for identical droplets or bubbles) are determined by the balance of forces acting tangentially on the interface:

$$\mu(\partial v_r/\partial z) = \mu^*(\partial v_r^*/\partial z) + (\partial\tilde{\sigma}/\partial r) + \mu_s \partial(\nabla_r v_r)/\partial r \quad , \qquad (8)$$

where v_r is the radial component of the velocity, ∇_r is the radial part of the surface gradient and μ_s is surface viscosity. The asterisk denotes that the respective quantities refer to the droplet. The local value of the surface tension is expressed as a sum of the equilibrium value σ and

the small perturbation $\tilde{\sigma}$. Analogous approximations are also used for the bulk and the surface surfactant concentrations c and Γ . The velocity v_r is found by solving Navier-Stokes' equations for the drop and $\tilde{\sigma}$ is found from the adsorption isotherm, the diffusion equation (which for the dispersion medium has the form $\partial^2\tilde{c}/\partial z^2 + \Delta_r\tilde{c}=0$) and the condition of conservation of the surfactant:

$$\Gamma v_\eta U - D_s \Delta_\eta \tilde{\Gamma} = -D(\partial\tilde{c}/\partial z) + D'(\partial\tilde{c}'/\partial z) \quad .$$

Here D and D_s are the bulk and surface diffusion coefficients respectively.

The application of the above presented method (with $\mu_s=0$) to the stages a)-d) of the film evolution[2,3,6,10,11] led to the equations

$$V/V_{immob} = v_\zeta/v_\zeta^\circ = 1+\alpha \; ; \; \alpha = -\left(1+\frac{2D_s}{Dh_1}\frac{d\Gamma}{dc}\Big/\frac{3D\mu}{\Gamma(\partial\sigma/\partial c)}\right) \quad (9)$$

where V_{immob} is V_T for the stages a) and b) and V_{Re} for the stage c). Equation (9) has been experimentally confirmed by measuring the velocity of thinning of films of aqueous solutions of three fatty acids[12]. The value of D_s thus obtained is of the order of magnitude 10^{-4} cm/s. The amplitude ζ of the fluctuational waves and the critical thickness of rupture in this case depend on v_ζ/V and according to (7) and (9) must have the same values as with immobile surfaces i.e. h_{cr} should not depend on the surfactant concentration[6]. The term allowing for the effect of μ_s on the velocity of thinning V (stage c) is proportional to h_1/R^2 and on v_ζ (stage d) to $h_1k^2/6$. Since $kR_1 \approx 10$, it is possible that[13], with $\mu_s \approx 10^{-3}$ s.p., the effect of μ_s on V to be negligeably small, being, at the same time, so great with respect to v_ζ that $v_\zeta = v_\zeta^\circ$. Then h_{cr} will depend not on v_ζ°/V_{Re} but on v_ζ°/V and its value will be smaller than that with immobile surfaces (or with $\mu_s=0$). At sufficiently low surfactant concentrations the surface viscosity μ_s vanishes and the velocity of wave motion becomes equal to $v_\zeta = v_\zeta^\circ(1+\alpha)$ which results in increasing of h_{cr}. This is a possible explanation for the

experimentally observed increase of h_{cr} when c diminishes[6].

The case of mutual approaching of two identical emulsion non-deformable droplets of radius R in the absence of surfactant (stage a) was also considered[14]. From the obtained general equation, analogous to the equation derived by Haber, Hetsroni and Golan the following more important limiting cases result: 1) at $l/R \gg 1$ one obtaines

$$F = 6\pi\mu R \frac{2/3+\mu^*/\mu}{1+\mu^*/\mu}\left[1+\frac{1+11(\mu^*/\mu)+45(\mu^*/2\mu)^2}{15(2/3+\mu^*/\mu)(1+\mu^*/\mu)}\right], \quad (10)$$

which is a generalization of the well-known formulae of Stokes, Rybczynski-Hadamard and Lorentz; 2) at $l/R \ll 1$ we have

$$F = (3\pi^2/8\sqrt{2})\mu^* V R\sqrt{R/l} \quad . \quad (11)$$

Note that in (11) and (13) (see below) F does not depend on the viscosity μ of the dispersion phase; 3) at $l/R \ll 1$ and $\mu^*=0$ (non-deformable bubbles) $F = 2\pi\mu V R \ln(R/l)$.

When the distance between the emulsion droplets is sufficiently small a plane parallel film appears between them (stage c). In the case of soluble only in the dispersion medium surfactant and $\mu_s=0$, the velocity of thinning of the film[15] is

$$V/V_{Re} = 1+\alpha/(1+\alpha\varepsilon) \quad ; \quad \varepsilon = \frac{2}{3B}\left(\frac{\rho^*\mu^* h_1^4 F}{\pi\mu^3 R_1^4}\right), \quad (12)$$

where ρ is density and $B \approx 3$ is dimensionless quantity depending very little on h_1. For systems of practical interest $\varepsilon \ll 1$ and (12) turns into (9) i.e. V is chiefly determined by the effect of the surfactant. In this case the velocity V is greater but still of the order of magnitude of Reynolds' velocity V_{Re}. In the case, when only soluble in the dispersion phase, the surfactant is evenly distributed over the film surface ($\partial\tilde{\sigma}/\partial r=0$ in (8)) and the system behaves as in the absence of surfactant. Then (put $\alpha \to \infty$)

$$V = V_{Re}(1+1/\varepsilon) \approx B\left(h_1^5 F^2/\pi^2\rho^*\mu^* R_1^8\right)^{1/3} \quad (13)$$

so that $V \gg V_{Re}$ (note that $\xi \ll 1$)[16,17]. These results show that the droplets formed by the liquid in which the surfactant is soluble will coalesce much faster then those formed by the other liquid and, according to Bancroft's rule, this emulsion will be stable in which the surfactant is soluble in the dispersion medium. On the other hand, these results indicate that the disregard of the hydrodynamic factor in Davies' theory of HLB is not grounded, at least in the case of low stable emulsions[15].

References:

1. B.P.Radoev,Annuaire Univ.Sofia,Fac.Chim.,66 (1971/72) (in press).
2. B.P.Radoev and I.B.Ivanov,Annuaire Univ.Sofia,Fac.Chim., 65, 441 (1970/71).
3. B.P.Radoev and I.B.Ivanov,Annuaire Univ.Sofia,Fac.Chim., 66, (1971/72) (in press).
4. D.St.Dimitrov and I.B.Ivanov,Doklady BAN (in press).
5. D.St.Dimitrov and I.B.Ivanov - to be published.
6. I.B.Ivanov,B.P.Radoev,E.D.Manev and A.Scheludko,Trans. Faraday Soc.,66, 1262 (1970).
7. I.B.Ivanov,B.P.Radoev,E.D.Manev and A.Scheludko,Annuaire Univ.Sofia,Fac.Chim.,64, 363 (1969/70).
8. T.Traykov,B.P.Radoev and I.B.Ivanov,Annuaire Univ.Sofia, Fac.Chim.,65, 421 (1970/71).
9. I.B.Ivanov,D.St.Dimitrov and B.P.Radoev - to be published.
10. B.P.Radoev,E.D.Manev and I.B.Ivanov,Koll-Z.234,1037 (1969).
11. B.P.Radoev,D.St.Dimitrov and I.B.Ivanov,Coll.Polym.Sci., 252, 50 (1974).
12. E.D.Manev,Chr.St.Vassilieff and I.B.Ivanov,Coll.Polym. Sci. (in press).
13. I.B.Ivanov and D.St.Dimitrov,Coll.Polym.Sci.252,982 (1974).
14. V.N.Beshkov,B.P.Radoev and I.B.Ivanov - to be published.
15. T.Traykov and I.B.Ivanov - to be published.
16. I.B.Ivanov and T.Traykov,Annuaire Univ.Sofia,Fac.Chim., 66, 641 (1971/72).
17. I.B.Ivanov and T.Traykov - to be published.

INVESTIGATION OF BLACK FOAM FILMS WITH DIFFERENT STRUCTURE BY ELECTRIC IMPULSES

D. Platikanov and N. Rangelova

Department of Physical Chemistry, University of Sofia, Sofia 26, Bulgaria

Many investigations, for instance [1 - 9], are already devoted to the black soap films. Using a lot of experimental techniques, the main film properties - film thickness, film tension, contact angle film/bulk, electric conductance, surfactant concentration etc. - for both common black and Newton black films are studied (formerly "first black" and "second black" films respectively). The data, communicated or reviewed in the above and many other papers, allow the so called "sandwich model" to be applied to the common black films and to explain their stability mainly on the ground of the D.L.V.O.- theory. The available data, however, are unsufficient to understand the nature of the Newton black films.

The main method for film thickness measurement - the light reflection method - is not very reliable for the Newton black films: on one hand, the light reflected by these thinnest lammelae is very small and on the other hand the calculation of the thickness depends on the film model. Consequently, the values obtained by different authors are scattered. For instance, values between 36 and 51 Å are reported for one and the same system: sodium dodecylsulphate (NaDS) + NaCl + water [4 - 8]. There are also different opinions about the water content of the Newton black films: from the relatively thick (about 27 Å) "water core" of the threelayer sandwich model [4] to the bilayer model without any water in it [2, 7]. The different authors make also different conclusions about the salt content in the Newton black films:

some assume that only the ions of the surfactant and no additional electrolyte are available in the film [7], others think that an adsorption excess of salt must take place in the Newton black films [4, 5].

All these discrepances make it very difficult to build up the model of the structure of the Newton black films and therefrom to explain the forces, responsible for their stability. Although the sandwich model is commonly accepted, there are many indications, that it can not be simply treated as an aqueous solution layer between two adsorption layers. Our electric conductance measurements showed that the ions mobility in the Newton black films is smaller than in the bulk solution of the same system [9]. A well-defined organisation capable of accomodating only certain ions is suggested in [4] and a square lattice with the surfactant ions of different sign at the opposing surfaces facing each other is spoken about in [8]. On the ground of a complete analogy between the temperature dependences of the black film conductance and the conductance of surfactant/water gels and neat phases, we assumed similar structure of both these systems [10].

Obviously more information is needed for the final solution of the problem about the structure of the Newton black films. One of the possibilities to get it is to observe the film behaviour when applying electrical impulses on it.

The experimental cell, together with the block-scheme of the electric circuit is shown on fig.1. The hollow cylindric silver electrodes E are set coaxial one above the other. Two porrous glass rings P are put on the ends of both silver cylinders - their role is to guarantee always complete wetting of the electrodes by the solution. The lower cylinder is fitted in the middle of the teflon dish A, containing the solution. The level of the solution surface is somewhat under the end of the porrous ring, but always in contact with it. The upper cylinder can be moved vertically by a fine mechanical device. So a soap film F can be pulled out between the two wetted rings. The cell is put in a small vessel with sa-

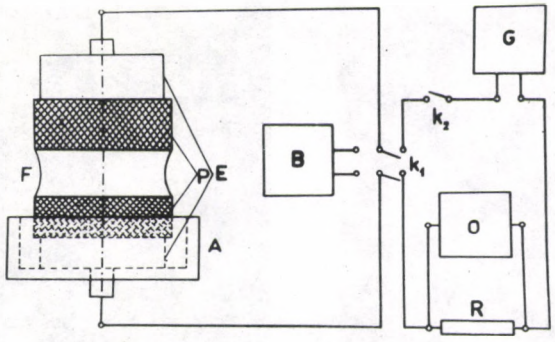

Fig. 1

turated water vapour in it and the whole system is put in an air thermostate. After pulling out a film, one must wait some time, during which the film grows thinner and the equilibrium black film is obtained. The electric resistance of the film is controlled by the RLC-bridge B with frequency 800 Hz. After the equilibrium resistance is reached, a Π-shaped electric impulse of 100 - 300 volts is applied at the electrodes, using the pulse-generator G and the commutators K_1 and K_2. The electric current I through the film is measured and the current/time curves are observed and photographed by the oscilloscope O. Depending on the applied voltage and the duration of the impulse, the films either rupture or do not. In both cases I(t) - curves with characteristic shape for each type of soap films are obtained.

The films investigated were obtained from 0,05% sodium dodecylsulphate aqueous solutions with different NaCl concentrations C_{el} in the range 0,005-0,7 mol/l. This system was chosen, because it is widely investigated [3 - 10] and much data about it are available. The regions of stability (temperature and C_{el}) of both common black and Newton black films are well known for this system [4].

The pictures of the I(t)- curves for the common black films

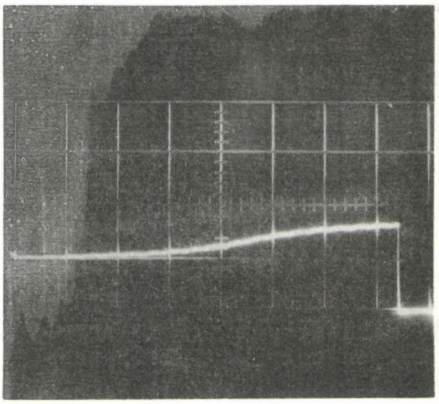

Fig. 2

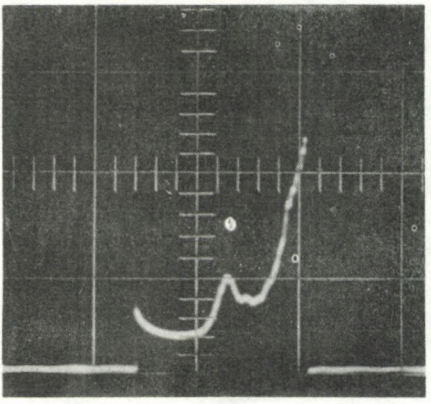

Fig. 3

are somewhat different for the different electrolyte concentrations. This is explicable taking into account that the film thickness depends on C_{el}. Fig. 2 presents a I(t)-curve for a film from a 0,006 mol/l NaCl NaDS-solution at 30,8°C and fig.3 - a I(t) curve for a film from 0,2 mol/l NaCl NaDS -solution at 30°; on both figures the time scale is 50 msec/cm. Although the shapes of the two curves considerably differ, it is characteristic for both, that the current increases (the resistence decreases), reaching a maximal value before the film ruptures. The current increase is steeper for the thinner black film (fig. 3). The decrease of the film resistence can be explained by increasing the film thickness because of electroosmotic flow. Microscopical observation of the film during the process confirms this assumption. This effect is interesting and it shall be studied separately.

The Newton black films show another picture (fig. 4 - film from 0,7 mol/l NaCl NaDS-solution, at 35,8°C, impulse 300 V, time-scale 100 msec/cm). After applying the impulse, a sharp peak occurs, immediately after which the current remains constant until the film rupture. A statistics, including the data about 50 Newton black films, shows that the current-value of the peak corresponds to a resistance almost equal or somewhat greater than that, measured by the RLC-bridge

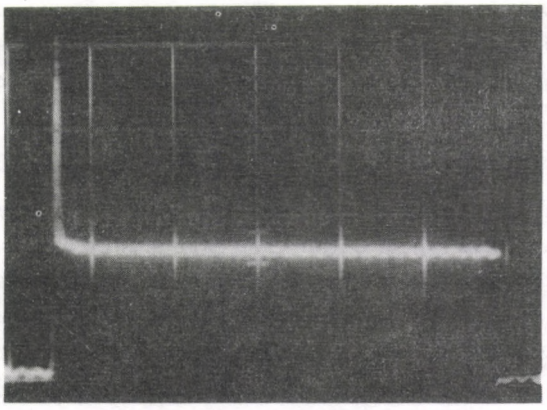

Fig. 4

(800Hz) - about 2 - $5.10^6\Omega$ for films with diameter c. 1,2cm and length c. 0,12cm. The resistence, corresponding to the constant current is about 2-3 times greater. A check for the reliability of the peak was made by registrating the I(t) curve for a thick (coloured) film of the same solution, immediately after its pulling out (fig. 5). It is seen that in this case the current is constant from the beginning until the rupture of the film. Hence the sharp peaks occur only with the Newton black films.

Using the current and time values from the I(t)-curves for the Newton black films, the energy, necessary to rupture the

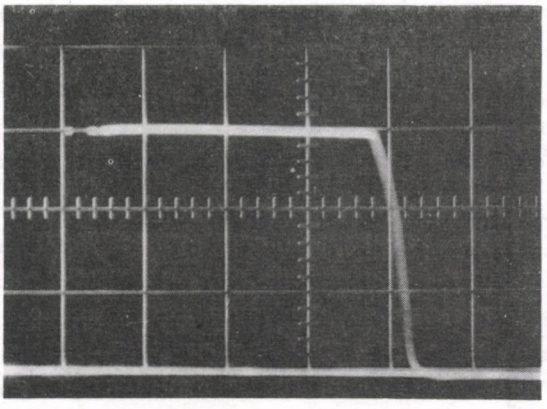

Fig. 5

film is calculated. The values obtained are statistically scattered, the average being about 4.10^{-4}cal/cm^2. Assuming that the Newton black films are 44Å thick [4], that means about 900 cal/cm^3. This is a very big value, which can be compared with the heat of sublimation.

Both the peaks in the I(t)-curves and the large energy-values speak in favour of a well organised structure of the Newton black films. The ions change their positions in the structure under the action of the electric field and the whole film is polarised. That causes the sharp peak in the I(t)- curve. The large heat-effect shows, that although the films are very thin, they are considerably stable, which is possible only when the film has well defined structure with strong forces acting between its elements.

Another interesting fact in favour of the above consideration was found recently by us together with Sidorova and Nedyalkov [11]. We used the cell of fig. 1 to make a concentration galvanic cell, wetting the upper and the lower porrous rings by solutions with different NaCl-activity. The electrodes are the silver cylinders, covered by AgCl and the electrolyte bridge is the Newton black film stretched between the rings. Measuring the electromotive force of this cell, we obtained values about the transport numbers of the Na^+, $t^+ = 0,83$ and the negative ions (Cl^- and $C_{12}H_{25}SO_4^-$), $t^- = 0,17$. That means there is almost no additional salt in the Newton black film and mainly the ions of NaDS are present. The Na^+ is the main carrier of the current, the $C_{12}H_{25}SO_4^-$ being bound in the film structure. The same has been found for the ionic conductance of the ionic crystals: for instance, in the alkali halides the transport numbers of the alkali ions are approximately a unit [12].

In favour of a crystal-like structure of the Newton black films is also the established analogy between the transition common/ Newton black films and a phase transition in the concentrated surfactant/water system [10]. The X-ray diffraction measurements [13] of NaDS/water gels in the temperature

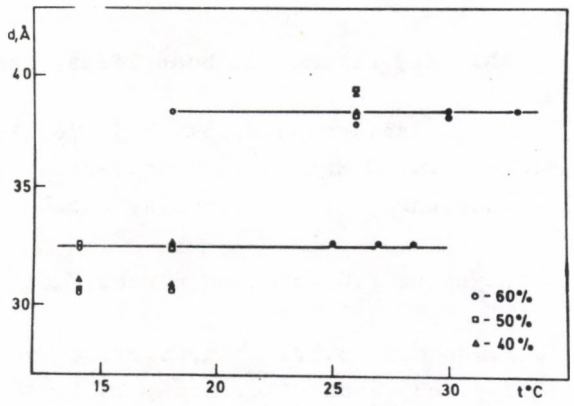

Fig. 6

range of this transition showed a considerable change in the main spacing d , the low temperature phase giving much more orders of reflection (fig. 6 - the filled points are values measured at increasing temperature, the open points - at decreasing temperature; there is a hysteresis in the transition temperature). Taking into account the structure of the NaDS/ water gel, in which the hydrocarbon chains of two adjacent layers are fitted parallel one between the others [13] , the main spacings of about 32Å correspond to the thickness of the Newton black films. Of course this analogy is not complete - there are many points in which the analogy between the films and the gel can not be extended.

It is impossible on the ground of these results to establish the complete structure of the Newton black films and especially the crystal-like one. In any case, however, these results are in favour of a well organised structure. It is also evident, that the investigation of the black soap films by electrical impulses promises some new information about them and we hope, that a detailed study of the peaks in the current/ time-curves by a more precise device will give us interesting data about the structure and the forces in the Newton black films.

REFERENCES

1. K.J.Mysels, K.Shinoda, S.Frankel, Soap Films, Pergamon Press, (1959).
2. A.Sheludko, Proc.Konikl.Ned.Acad.Wet. B65, 76 (1962).
3. T.Kolarov, A.Sheludko, D.Exerova, Trans.Faraday Soc. 64, 2864 (1968); A.Sheludko, Ann.Univ.Sofia, Fac.Chimie 62, 47 (1967/68).
4. M.N.Jones, K.J.Mysels, P.C.Scholten, Trans.Faraday Soc. 62, 1336 (1966).
5. J.S.Clunie, J.F.Goodman, B.T.Ingram, Surface and Colloid Science, Vol.3, p.168, John Wiley Sons, 1971.
6. J.Lyklema and H.G.Bruil in the thesis of H.G. Bruil, Landbouwhogeschool Wageningen, 1970.
7. D.den Engelsen, G.Frens, J.Chem.Soc.Faraday Trans.I 70, 237 (1974).
8. J.Vrij and J.A.de Feijter in the thesis of J.A.de Feijter, Univ.Utrecht, 1973.
9. D.Platikanov, N.Rangelova, A.Sheludko, Ann.Univ.Sofia, Fac.Chimie 60, 293 (1965/66); D.Platikanov, N.Rangelova, Compt.Rend.Acad.Bulgare Sci. 21, 913 (1968).
10. M.Sidorova, M.Nedyalkov, D.Platikanov, Colloid Polymere Sci. (1975) in press.
11. M.Sidorova, N.Rangelova, M.Nedyalkov, D.Platikanov, Ann. Univ.Sofia, Fac.Chimie 68 (1973/74).
12. A.Lidiard, Ionic Conductivity, Handbuch der Physik, Band XX, Teil II, Berlin, 1957.
13. D.Platikanov and A.Weiss, to be published.
14. A.Skoulios, Advan. Colloid Interface Sci. 1 , 79 (1967).

Group III/3
Molecular interactions

THE MECHANISM OF CHARGE TRANSFER SOLUBILIZATION OF 7,7,8,8-TETRACYANOQUINODIMETHANE IN SURFACTANT SOLUTION

K.Meguro, S.Muto, K.Deguchi and M.Ueno

Department of Chemistry, Science University of Tokyo, Kagurazaka, Shinjuku-ku, Tokyo, Japan

INTRODUCTION

7,7,8,8-Tetracyanoquinodimethane(TCNQ) is only slightly soluble in water and has usually an absorption maximum of spectrum at 405 nm in benzene solution, which is assigned to the neutral molecule. However, when TCNQ was solubilized in aqueous solution of several surfactants, a remarkable color was found in the region above the critical micelle concentration (CMC) of surfactants. In this article we will report the mechanism of color appearance of TCNQ in surfactant solution and related phenomena.

RESULTS AND DISCUSSION

Mechanism of color appearance of TCNQ in surfactant solution

The absorption spectra of TCNQ solubilized in aqueous solution of some typical surfactant such as heptaethyleneglycol n-dodecylether($C_{12}E_7$) and dodecylpyridinium chloride(DPCl) are shown in Figs. 1 and 2, and the the characteristic absorption bands of TCNQ are listed in Table 1(1,2).

The bands at 420,680,750 and 850 nm were already attributed to the TCNQ anion radical by several authors(3,4) in the study of TCNQ-alkali metal complexes. Recently we have confirmed that the band at 480 nm depended on the charge transfer interaction by the comparison with the spectra of 2,5-dichloroquinone being solubilized in aqueous dodecylpyridinium chloride solution(5).

The appearance of charge transfer bands and anion radical

bands of TCNQ was characterized to be restricted in the region above the CMC of surfactants.

According to the ordinary concept of charge transfer complexes of Mulliken's theory, the wave function of the

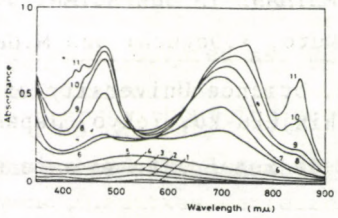

FIG. 1. Absorption spectra of TCNQ solubilized in aqueous solutions of $C_{12}E_7$. $C_{12}E_7$ concentration in moles/liter: 2.5×10^{-5} (1); 5.0×10^{-5} (2); 6.5×10^{-5} (3); 8.3×10^{-5} (4); 1.0×10^{-4} (5); 2.5×10^{-4} (6); 5.0×10^{-4} (7); 1.0×10^{-3} (8); 2.5×10^{-3} (9); 5.0×10^{-3} (10); 1.0×10^{-2} (11); cell thickness = 1.0 cm.

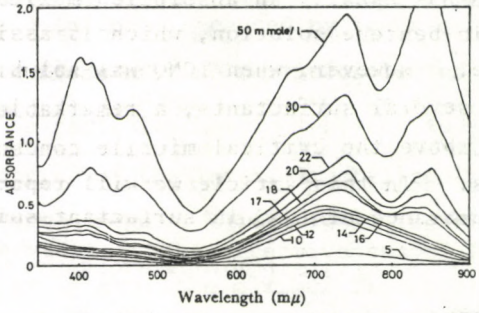

Fig. 2. Visible absorption spectra of TCNQ solubilized in DPCl solutions in the presence of the light.
Figures show concentration of surfactant solutions.

Table 1. Absorption spectra bands of TCNQ solubilized in aqueous solutions of DPCl and C_{12} E_7.

surfactants	absorption bands (nm)						
	λ_1	λ_2	λ_3	λ_4	λ_5	λ_6	λ_7
DPCl	395-400	420	440	480-485	680	750	850
C_{12} E_7	-	-	440	480	-	700-750	850

DPCl : dodecylpyridinium chloride, C_{12} E_7 : heptaethyleneglycol n-dodecylether, λ_1 : neutral TCNQ molecular band, λ_2,λ_5,λ_6,and λ_7 : TCNQ anion radical bands, λ_4 : TCNQ-surfactant micelle charge transfer band

ground state of charge transfer complex is described as ;

$$\psi_N(AD) = a\psi_0\ (A,D) + b\psi_1\ (A^- - D^+) \text{ ----------(1)}$$

and that of the excited state as ;

$$\psi_E(AD) = a^\dagger\psi_1(A^- - D^+) - b^\dagger\psi_0\ (A,D) \text{ ----------(2)}$$

where ψ_0 and ψ_1 are the "no-bond" and "dative bond" wave function, respectively. Where $S_{01} = \int\psi_0\psi_1 d\tau$. As ψ_N, ψ_E, ψ_0, and ψ_1 are all normalized, the coefficients a and b, $a^\dagger$ and $b^\dagger$ are related by the expression(3) and (4), respectively.

$$a^2 + 2abS_{01} + b^2 = 1 \text{ ----------(3)}$$

$$a^{\dagger 2} + 2a^\dagger b^\dagger S_{01} + b^{\dagger 2} = 1 \text{ ----------(4)}$$

For weak interaction, the ground state energy(W_N) will be obtained second order pertubation theory as follows;

$$W_N = \int\psi_N H\psi_N d\tau \simeq W_0 - \frac{(H_{01} - S_{01}W_0)^2}{(W_1 - W_0)} \text{ --------(5)}$$

where $W_0 = \int\psi_0 H\psi_0 d\tau$; $W_1 = \int\psi_1 H\psi_1 d\tau$ is the energy of the dative structure A^-D^+; $H_{01} = \int\psi_0 H\psi_1 d\tau$; and H is the exact Hamiltonian for the entire set of nuclei and electrons, and the energy of excited state (W_E) will be represented by the same way as follows ;

$$W_E = W_1 + \frac{(H_{01} - S_{01}W_1)^2}{(W_1 - W_0)} \text{ ----------(6)}$$

For an interaction of electron donor-electron acceptor molecule pairs, the theoretical process $\psi_0 \rightarrow \psi_1$ involves the jump of one of a pair of electrons, initially occupying a molecular orbital in donor,say ψ_D, to an unoccupied molecular orbital in acceptor, say ψ_A. This must occur in such a way that the excited electron still remains paired to its original electron partner. It may be shown that ;

$$S = \sqrt{2}S_{AD}(1 + S_{AD}^2)^{1/2} \text{ ----------(7)}$$

where $S_{AD} = \int\psi_A\psi_D d\tau$. This is the overlap integral between the highest-filled molecular orbital of the donor and the lowest-unfilled molecular orbital of the acceptor(in the case of atom donors or acceptors, then the corresponding atomic orbitals are involved). For the usually small values of S_{AD}, S_{01} will vary linearly with S_{AD}. H_{01} will also vary linearly with S_{AD} for small values of S_{AD}. The electron donor and acceptor

species will tend to orientate themselves relative to one another in such a way as to make S_{01}, or S_{AD}, a maximum(the overlap and orientation principle).

This principle can be used to predict the interaction between TCNQ and surfactant micelle. In the region at the concentration above critical micelle concentration, the surfactant molecules or ions exist in their micelles as orientated state corresponding to a lquid or solid states.

When the TCNQ is solubilized in micelle of surfactant solutions, the maximum overlapping of molecular orbital of TCNQ and molecular orbital of donor part of surfactant molecule may be achieved more easily and more probably due to the orientation of surfactant in micelles. The sudden appearance of charge transfer band at 480 nm of TCNQ being solubilized in DPC1 solution above CMC will be explained by the above principle. Conversely speaking, this principle can be also used to predict the degree of orientation in micelle from the intensity of charge transfer band.

Cloud points and charge transfer interaction

It is well known that the cloud points of nonionic surfactants were affected by the addition of inorganic salt and urea(6). Fig. 3 shows the effect of several inorganic salts and urea on the cloud point of $C_{12}E_7$ aqueous solution($5X10^{-3}M$)(7).

Figs. 4 and 5 show the absorption spectra of TCNQ solubilized in aqueous solution of $C_{12}E_7$ containing K_2SO_4 and KSCN, respectively. As shown in Fig. 4 the absorbance at each band due to the charge transfer interaction of $C_{12}E_7$ micelles with TCNQ increased with the increase of K_2SO_4 concentration. On the other hand, the reversed tendency was observed in the case of KSCN addition. The spectral changes observed in the case of other additives are also similar to either of those in the case of K_2SO_4 or KSCN. The plots of absorbance at 480 nm band against additive concentration were shown in Fig. 6. It indicates that the effects of additives on the charge transfer interaction can be classified two categories. One is the case that the charge transfer interaction enhances by the addition

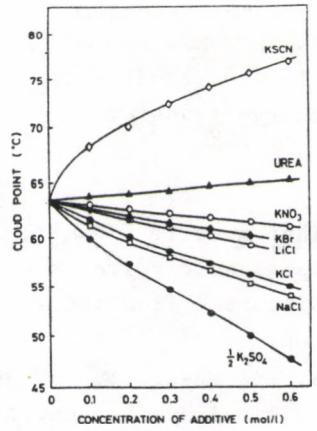

FIG. 3. The effects of additives on the cloud point of $C_{12}E_7$ (5.0×10^{-2} *M*).

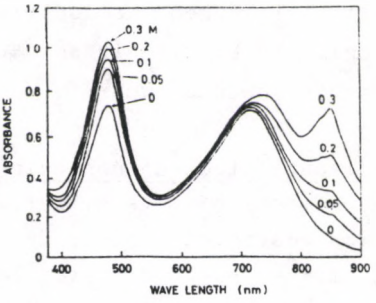

FIG. 4. Absorption spectra of TCNQ solubilized in aqueous solutions of $C_{12}E_7$ containing K_2SO_4. Figures show K_2SO_4 concentration. $C_{12}E_7$ concentration: 5.0×10^{-2} *M*. TCNQ concentration: 1.0×10^{-4} *M*.

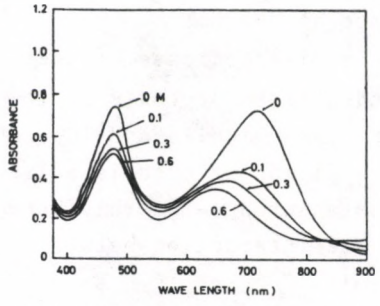

FIG. 5. Absorption spectra of TCNQ solubilized in aqueous solutions of $C_{12}E_7$ containing KSCN. Figures show KSCN concentration. $C_{12}E_7$ concentration: 5.0×10^{-2} *M*. TCNQ concentration: 1.0×10^{-4} *M*.

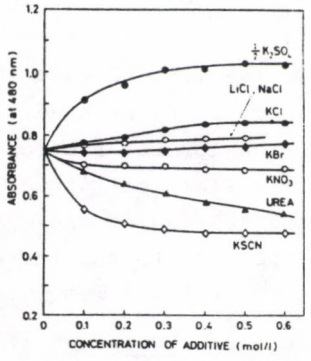

FIG. 6. Relationship between absorbance at α-band and additive concentration.

of salts, such as LiCl, NaCl, KBr and K_2SO_4, and the other is the case that the reduction occurs by the addition of salts such as, KNO_3, KSCN and urea.

By the comparison of Figs. 3 and 6, it is recognized that the additives which increase the charge transfer interaction have the depressing effect in the cloud point, and vice versa. The salts which enhance the cloud point have the power to make the salting out of $C_{12}E_7$, and also have the power to make the micelle of $C_{12}E_7$ more compact state. When the state of micelle became more compact, the enhance of interaction between TCNQ and donor part of surfactant will be more enhanced, and

the intensity of charge transfer band becomes stronger.

On the other hand, the salt, such as KSCN has the effect of salting in, then the addition of such a salt makes the state of micelle to be more loose, and the charge transfer interaction becomes weaker.

The solvent effect on nonionic surfactant micelle

The effects of several water-soluble organic solvents on micellar destruction of $C_{12}E_7$ can be discussed from the view point of the charge transfer interaction.

In the presence of organic solvents, the absorption at 480 nm decreased with the increase of organic solvent concentration up to a certain concentration as shown in Fig.7. However, further addition of organic solvent from this certain concentration gave an increase in absorbance at 480 nm.

These results indicate that the initial decrease of the absorbance at 480 nm band corresponds to the decrease of the charge transfer interaction between $C_{12}E_7$ micelle and TCNQ due to the micellar destruction by the addition of organic solvent, while the subsequent increase of the absorbance at this band may be ascribed to the increase of the interaction between organic solvent and TCNQ. This detail is shown in Fig. 8.

The effect of counterion of surfactant

The CMC of surfactant is influenced usually by the kinds of

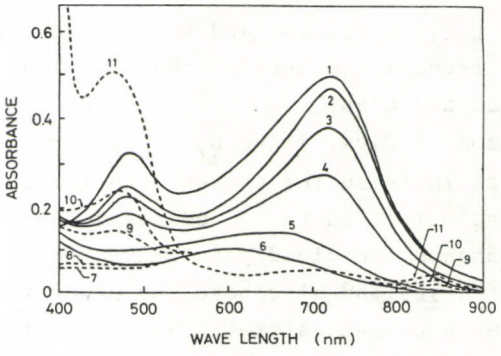

FIG. 7. Absorption spectra of TCNQ solubilized in aqueous solutions of $C_{12}E_7$ mixed with methanol at 25°C. $C_{12}E_7$ concentration: 1.0×10^{-3} *M*. TCNQ concentration: 7.5×10^{-6} *M*. Methanol concentration: (1) 0; (2) 15; (3) 25; (4) 30; (5) 35; (6) 40; (7) 45; (8) 55; (9) 70; (10) 85; (11) 100 vol %.

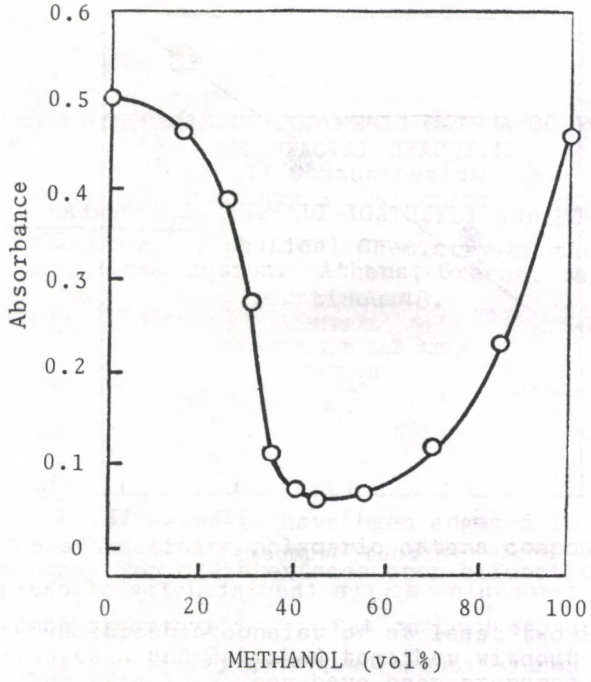

Fig. 8. Effect of the addition of methanol on the absorbance of TCNQ at 480 nm appearing in Fig. 7.

counterions of surfactant, because the fixation of counterion on micelle surface differs with the defference of hydration to counterion. When the fixation of counterion is stronger, the value of CMC becomes lower by the increase of neutralization degree of surface charge of micelle.

By the same reason, when the fixation of counterion of micelle surface is stronger, it is expected that the packing degree of surfactant molecules or ions in micelle will becomes closer, then the chance of overlapping molecular orbital of TCNQ with molecular orbital of donor part in surfactant molecule will be enhanced and it is predicted that the surfactant which has the counterion having stronger hydrating power shows weaker charge transfer absorption of solubilized TCNQ. This estimation was confirmed by the comparison of the intensity of the charge transfer band of solubilized TCNQ in the aqueous

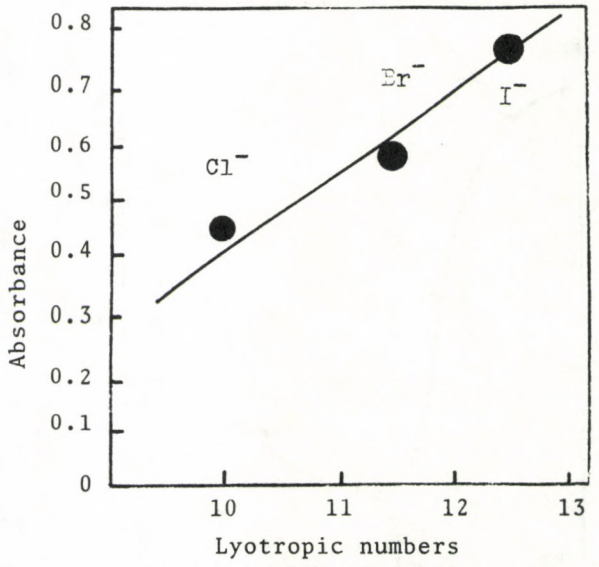

Fig. 9. Relationship between the intensity of charge transfer band at 480 nm and lyotropic numbers of counterions of surfactants.

solutions of dodecyl pyridinium chloride, bromide and iodide as shown in Fig. 9. It shows that the strongest absorption was found in dodecyl pyridinium iodide in which iodide ion has the weakest hydrating power, and on the other hand, the least absorption is obtained with the dodecyl pyridinium chloride having the heavily hydrated Cl ion.

REFERENCES

1). K.Deguchi and K.Meguro, J. Colloid Interface Sci., 38, 596 (1972).

2). S.Muto,K.Deguchi,Y.Shimazaki,Y.Aono and K.Meguro, Bull. Chem. Soc. Japan, 44, 2087(1971).

3). L.R.Melby,R.J.Harder,W.R.Hertler,W.Mahler,R.E.Benson and W. E.Mochel, J. Amer. Chem. Soc., 84, 3374(1962).

4). A.Rembaum,A.M..Hermann,F.E.Stewart and F.Gutmann, J. Phys. Chem., 73, 513(1969).

5). S.Muto and K.Meguro, J. Colloid Interface Sci.,49,422(1974).

6). M.J.Schick, J. Colloid Sci., 17, 801(1962).

7). K.Deguchi and K.Meguro, J. Colloid Interface Sci., 50,223 (1975).

DISTRIBUTION OF DYE IN SURFACTANT MICELLE SYSTEMS

Shigeo HAYANO and Masamichi FUJIHIRA

The Institute of Industrial Science, The University of Tokyo

In the previous papers,[1-5] the polarographic studies of solubilized dyes in several surfactant solutions have been described. The first four papers dealt with the masstransfer of the micelles tagged with dispersed dye and the last with the electron transfer kinetics of the solubilized Orange OT. The solubilized dispersed dyes used in these experiments (aminoanthraquinone derivatives and Orange OT) showed well-defined diffusion controlled polarographic waves. The diffusion coefficients calculated from the polarographic data were found to be practically equal to those of the surfactant micelles. In other words, the solubilized dyes diffuse to the electrode with the micelles.

If all the tracer dye molecules are solubilized into the micelles, the observed diffusion coefficient of solubilized dyes D_{ob} is equal to that of micelles D_m. However, a finite fraction of total dye molecules always exists in the aqueous part of the system as free molecules, because of the water-solubility of the dye. The diffusion coefficient of free dye molecules in water D_f is relatively large. This may leads to a high value of D_{ob},[6] if a dye, used as a tracer, is appreciably soluble in water. On the other hand, this effect may be neglected, if a dye such as Orange OT, almost insoluble in water, is used as a solubilizate.[7]

In the present paper, we shall report the polarographic results of 1,4-diaminoanthraquinone (DAA) in tetradecyldimethylbenzylammonium chloride (TDMBAC) solutions and sodium 2-anthraquinone sulfonate (SAQS) in decaoxyethylene nonylphenyl ether

(NP-10) solutions. DAA is a dispersed dye slightly soluble in water, while SAQS is an ionic compound appreciably soluble in water. These results have implications to the existence of the appreciable partition of the dyes between the aqueous and micellar phases. For the purpose of comparison, the results obtained by spectrophotometry and conductometry will be discussed. On the assumption that the true partition equilibrium constant K is obtained by spectrophotometry, the apparent K values obtained by conductometry and polarography will be discussed.

Experimental

DAA was recrystallized from ethanol. G.R.-grade SAQS purchased from Tokyo Kasei Chemical Co. and G.R.-grade HDMBAC from Dojindo Co. Research Laboratories were used without furtner purification. NP-10 was received through the courtesy of Meisei Chemical Co., and was purified by three times extraction by water saturated n-buthanol from its aqueous solution according to Nagase and Sakaguchi.[8] DAA was solubilized in TDMBAC solutions containing a Kolthoff's buffer solution, a mixture of a 0.1 M KH_2PO_4 and a 0.05 M borax aqueous solution in the volume ratio 9:11 (pH=8.1) as a supporting electrolyte. The solutions containing a constant concentration of DAA 2×10^{-6} M and various concentrations of TDMBAC were stored for a week at 40°C with occasional shaking, and then measured by polarography and spectrophotometry at 40°C. SAQS was dissolved in NP-10 solutions containing a Britton-Robinson buffer solution (pH=5.03). The solutions were used for the measurements of polarography and spectrophotometry at 25°C. For the purpose of comparison, SAQS was also dissolved in NP-10 aqueous solution without electrolyte for the other couple of measurements,i.e., conductometry and spectrophotometry at 25°C. In these solutions, the concentration of SAQS was kept constant 1×10^{-4} M and that of NP-10 was varied.

The polarographic measurements were carried out by using a PAR Electrochemistry System Model 170 (Princeton Applied Research Co.). UV and visible absorption spectra were measured with a Union High Sensitivity Spectrophotometer Model SM-401. The conductivity was measured with a Toa Electronics Conduct

Meter Model CM-2A. The critical micelle concetration (CMC) was determined by surface tension measurements with a Shimadzu Wilhelmy's Surface Balance Model ST-1.

Results and Discussion

DAA in the TDMBAC Solution

The visible absorption spectra of DAA in the various concentration of TDMBAC solutions are shown in Fig. 1. Below the CMC, the spectra were independent of the concentration of TDMBAC.

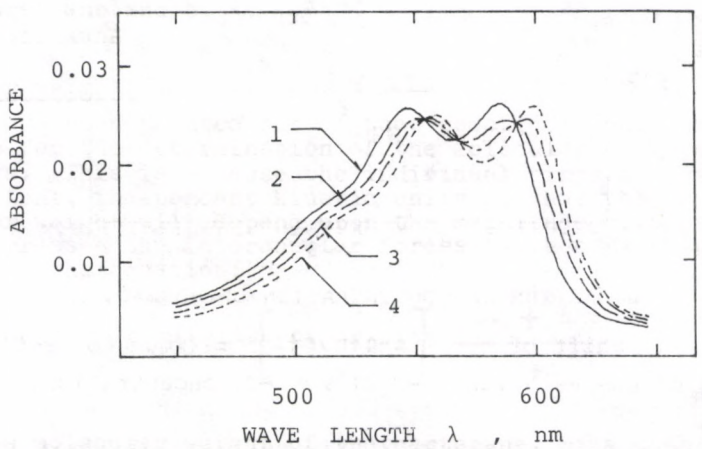

Fig. 1. Shift of the absorption spectrum of DAA as a function of TDMBAC concentration. Concentration of surfactant: (1) 0 M; (2) 4×10^{-4}M; (3) 8×10^{-4}M; (4) 1×10^{-2}M. Dye concentration 2×10^{-6}M.

The change in spectra above the CMC can be attributed to the partition equilibrium of DAA between the aqueous and micellar phases.

$$\text{Dye} + \text{micelle} \rightleftharpoons \text{Dye}_{\text{in micelle}} \quad (1)$$

Since the concentration of DAA was kept constant for all solutions, appearance of the isosbestic points at 553 nm, 567 nm, and 592 nm also supports the existence of the simple partition equilibrium such as is described by eq. (1).

With increase in concentration of TDMBAC, the wavelengths of maximum absorption λ_{max}'s of DAA shift toward the longer wave length. The change in the λ_{max} around at 590 nm against

the concentration of TDMBAC below and above the CMC is shown in Fig. 2. There appears a sudden change in the λ_{max} at the concentration of TDMBAC, 3×10^{-4}M, which agrees with the CMC, $2\text{-}3\times10^{-4}$M determined by the surface tension measurements for the same solutions.

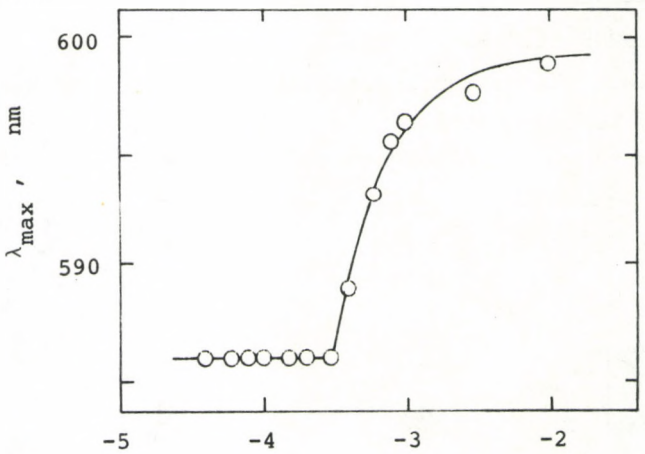

Fig. 2. Shift of the wavelength of maximum absorption λ_{max} of DAA as a function of TDMBAC concentration.

The partition equilibrium constant K for the present system is described simply by

$$K = \frac{x}{1-x} \frac{C_w}{C_s - CMC} \qquad (2)$$

where x is the fraction of the dye present in the micellar phase of all the dye, and C_s and C_w are the concentration of surfactant and water in the solution. The fraction x can be obtained from the absorption spectra shown in Fig. 1 and thus the constant K will be calculated, if we know the spectrum which is expected when all the dye molecules are solubilized. This may be realized if the surfactant is added in the solution in great excess. However, the extrapolation was applied in this work instead, to determine the difference of absorbance at infinite and zero surfactant concentration $\Delta A_\infty(\lambda)$. If ΔA is the difference in absorbance between the spectrum of a surfactant solution and that of the aqueous solution at the same wavelength for ΔA_∞,

the fraction x is expressed by the ratio $\Delta A/\Delta A_\infty$. If the ratio $\Delta A/\Delta A_\infty$ is introduced into eq. (2) instead of the fraction x, the following equation will be derived.

$$\frac{1}{\Delta A} = \frac{C_w}{K \cdot \Delta A_\infty} \frac{1}{C_s - CMC} + \frac{1}{\Delta A_\infty} \qquad (3)$$

Since the partition equilibrium constant K is independent of the surfactant concentration and C_w is regarded as constant, $1/\Delta A - 1/(C_s - CMC)$ plots will show a straight line. Thus, ΔA_∞ is obtained from the intercept of $1/\Delta A - 1/(C_s - CMC)$ plots. The partition equilibrium constant K and the fraction x, thus obtained from the change in absorbance of DAA at 606 nm, are shown in Table 1.

In the analysis of the polarographic data, the same extrapolation procedure was used to determine the diffusion current difference for the infinite surfactant concentration, Δi_∞. For the calculations of the polarographic partition equilibrium constant K, it is assumed that the fraction x is also equal to the ratio $\Delta i/\Delta i_\infty$. This assumption leads to the following equation,

$$i = (1-x) i_0 + x i_\infty \qquad (4)$$

where i_0 and i_∞ are the diffusion current at zero and infinite surfactant concentration.

Since the free dye molecules diffuse to the electrode more rapidly than the solubilized dye molecules, the concentration of the free dye molecules becomes lower than the concentration under the partition equilibrium in the diffusion layer. However, if the rate of dissociation of the dye molecule from the micelle is sufficiently slow compared with the rate of diffusion, the increase in the diffusion current due to the change in the form from the slowly diffusing solubilized dye to the more rapidly diffusing free dye may be neglected. In other words, the dyes in each state diffuse to the electrode independently. The diffusion current for such a system is given by

$$i = \text{const} \cdot C_0 \{(1-x) D_f^{1/2} + x D_m^{1/2}\} \qquad (5)$$

from the modification of the Ilkovic equation. In addition to the above assumption, if it is assumed further that the diffusion coefficient of the micelle D_m is independent of the surfactant concentration, eq. (5) is simplified to eq. (4). There-

fore, if the partition equilibrium constant K and the fraction x obtained from the polarographic data agree with those obtained from the absorbance change, two assumptions made in the analysis of the polarographic data, i.e., 1) slow dissociation of the solubilized dye molecule from the micelle, and 2) independence of the micellar diffusion coefficient D_m of the surfactant concentraion, holds for the system. We cannot conclude, however, whether these assumption are correct or not, from the comparison of the results obtained by two methods for DAA in the TDMBAC solutions. This is because the uncertainty is present in the polarographic data due to the low concentration of DAA, 2×10^{-6}M. However, the difference in the fraction x seems to be appreciable in the concentration range slightly above the CMC. In an attemt to ascertain the reliability of these two assumptions, the similar experiments for SAQS in the NP-10 solutions were carried out.

Table 1. The fraction of DAA present in the micellar phase of TDMBAC solutions x, and the partition equilibrium constant K obtained from the spectrophotometric data.

Concentration of TDMBAC (M)	x	$K\times10^{-5}$
4×10^{-4}	0.432	3.35
6×10^{-4}	0.670	3.46
8×10^{-4}	0.765	3.44
1×10^{-3}	0.819	3.46
3×10^{-3}	0.941	3.25
1×10^{-2}	0.984	3.50

SAQS in the NP-10 Solutions

Second assumption described above may be expressed in another way as the size of the micelle is independent of the surfactant concentration. Since no concentration gradient results in the solution for the conductivity measurements, the fraction x can be calculated from the conductometric data provided that the second assumption holds. Thus, the adaptation of the second assumption may be confirmed by the comparison of the results obtained from the conductometry and spectrophotometry. The conductivity of the NP-10 solutions containing a constant concentration of SAQS 1×10^{-4}M decreased with increase in the NP-10 con-

centration. This is because the more anthraquinone sulfonate anion is incorporated into the micelles when the NP-10 concentration increases. The fraction x obtained from the conductivity change $\Delta C/\Delta C_\infty$, and the partition equilibrium constant K calculated therefrom are compared in Table 2 with those obtained from the ratio of the absorbance changes $\Delta A/\Delta A_\infty$ at 355 nm. Agreement of these values within the experimental errors suggests that the second assumption holds for the NP-10 solutions approximately.

Table 2. Comparison of the fraction of SAQS present in the micellar phase of NP-10 solutions and the partition equilibrium constant K obtained from three different methods.

i) aqueous solution

Concentration of NP-10 (M)	Spectrophotometry x	Spectrophotometry $K\times10^{-3}$	Conductivity x	Conductivity $K\times10^{-3}$
1×10^{-3}	0.088	5.67	-	-
2×10^{-3}	0.158	5.37	0.111	3.55
3×10^{-3}	0.221	5.34	0.237	5.87
6×10^{-3}	0.362	5.27	0.475	8.42
1×10^{-2}	0.487	5.27	0.556	6.96
2×10^{-2}	0.672	5.64	0.691	6.13
4×10^{-2}	-	-	0.756	4.19
1×10^{-1}	-	-	0.886	4.04

ii) Britton Robinson buffer (pH=5.03)

Concentration of NP-10 (M)	Spectrophotometry x	Spectrophotometry $K\times10^{-3}$	Polarography x	Polarography $K\times10^{-3}$
1×10^{-3}	0.084	5.35	0.039	2.37
2×10^{-3}	0.199	7.08	0.095	3.00
3×10^{-3}	0.275	7.12	0.141	3.09
4×10^{-3}	0.355	7.73	-	-
6×10^{-3}	0.437	7.23	0.328	4.53
1×10^{-2}	0.559	7.04	0.451	4.56
2×10^{-2}	0.711	6.77	0.571	3.65
4×10^{-2}	0.834	6.80	0.751	4.07

The fraction x and the partition equilibrium constant K obtained from the polarographic and spectrophotometric data for SAQS in the solution containing a Britton-Robinson buffer (pH= 5.03) as a suporting electrolyte for the polarographic measure-

ments are also listed in Table 2. From the comparison of the spectrophotometric results for both solutions, it is clear that those values in the buffer solutions are slightly greater than those in the aqueous system. This difference may be interpreted in terms of 'salting out' effect on the partition equilibrium. If the electrolyte is added into the surfactant solution, the partition of the dye becomes favorable to the micellar phase. The effect of the addition of electrolyte on the CMC should be also taken into account. However, this effect is not only small for a nonionic surfactant such as NP-10, but also influences the fraction x negligibly because of the very low CMC. Furthermore, this effect was reflected already in the calculation of the K values through using of eq. (2).

As is evident from Table 2, the results obtained from the polarographic data are apparently lower than the true values obtained from the spectrophotometric data of the same solutions. This implies that the effect of the dissociation of the solubilized dye from the micelles on the diffusion of the whole dyes in the micellar solution cannot be neglected.

Work is now in progress to estimate the rate constant of the dissociation from the deviations of the polarographic partition equilibrium constant K from the true value by using a digital simulation.

References

1) S.Hayano and N.Shinozuka, Bull.Chem.Soc.Japan,42,1469(1969).
2) S.Hayano and N.Shinozuka, Bull.Chem.Soc.Japan,43,2083(1970).
3) S.Hayano and N.Shinozuka, Bull.Chem.Soc.Japan,44,1503(1971).
4) S.Hayano,N.Shinozuka,H.Suzuki, and T.Asahara,Proc. VI International Congress on Surface Active Substances (1973),p.899.
5) H.Suzuki,N.Shinozuka, and S.Hayano, Bull.Chem.Soc.Japan,47, 1093(1974).
6) K.J.Mysels and D.Stigter, J.Phys.Chem.,57,104(1953).
7) D.Stigter,R.J.Williams, and K.J.Mysels, J.Phys.Chem.,59,330 (1955).
8) K.Nagase and K.Sakaguchi, Kogyo Kagaku Zasshi,64,635(1961).

INTERACTION OF SURFACE-ACTIVE MACROMOLECULES WITH NON-POLAR SUBSTANCES IN AQUEOUS SOLUTIONS

V.N.Izmailova, G.P.Yampol'skaya, V.K.Mazo

Chair of Colloid Chemistry, Moscow Lomonosov State University, Moscow, 117234, Leninskiye gory, Chemical Department

A special peculiarity of soaps and proteins from the point of view of structure of their primary particles (molecules and macromolecules respectively) is that in both there present non-polar oleophilic groups, located asymmetrically with respect to polar hydrophilic groups. This asymmetry leads in its turn to their strongly pronounced surface activity.

At present it is shown that the stability of compact structure of globular proteins is determined with the same forces, which lead to micelle formation in solutions. As a result of hydrophobic interactions in protein globulas and micelles of surfactants there appear non-polar regions, responsible for solubilisation.

Studies of hydrocarbons interaction with proteins (solubilisation of hydrocarbons) is of interest from different points of view. First, solubilisation of hydrocarbons can be used as a method of detection of hydrophobic interactions in protein macromolecules and supply new data on their structure. Second, studies of solubilisation of hydrocarbons in solutions of biologically active proteins makex possible to clear out the role of hydrophobic interactions in biocatalytic processes. Finally, studies of solubilisation of hydrocarbons in solutions of proteins can be interesting for clarification of pro-

cesses of lipide type substances transfer and exchange.

In the work being reported we present investigations of interaction of high molecular surface-active substances with different conformations of macromolecules in aqueous solutions with hydrocarbons /2/ and low molecular surface-active compounds /3/.

A qualitative estimation of bounding of hydrocarbons and surfactants was carried out with methods of refractometry and equilibrium dialysis. Changes in ligand concentration in aqueous solution were determined with differential refractometry method and spectrophotometrically.

Let us try to understand the mechanism of solubilisation of hydrocarbons in protein aqueous solutions on the basis of energetic estimations of this process. Let us consider the results of determining of hydrocarbons and low molecular surfactants bounding with proteins at different temperatures.

The process of solubilisation of hydrocarbons may be analysed like a process of distribution of a third component between two non-mixing phases. This approach allows to calculate the constant of distribution ($K = C_p/C_w$) of the hydrocarbon between water and protein, and estimate the change in free energy $F = -RT\ln K$ by bounding of hydrocarbon with protein, and data on temperature dependance of the distribution constant enable us to estimate changes in enthalpy (ΔH) and entropy (ΔS) of bounding. So calculated thermodynamical parametres for some proteins are presented in tables 1, 2, 3.

TABLE 1. Thermodynamic parametres (ΔF and ΔH, kcal/mol, ΔS, cal/mol. degree) of solubilisation of hydrocarbons in solutions of proteins

Hydrocarbon	Serum albumin			Gamma-globulin			Lysozime		
	ΔF	ΔH	ΔS	ΔF	ΔH	ΔS	ΔF	ΔH	ΔS
Heptane	-2,7	0	9	-2,8	0	9	-2,3	0	8
Decane	-2,9	0	10	-3,0	0	10	-2,9	0	10
Tetradecane	-2,9	0	10	-3,0	0	10	-3,2	0	11
Benzene	-2,4	0	8	-2,1	0	7	-1,7	0	6
Toluene	-2,6	0	5	-2,4	0	8	-1,8	0	6
p-Xylene	-3,0	0	10	-2,7	0	9	-2,1	0	7

TABLE 2. Thermodynamic parametres of solubilisation of hydrocarbons in solutions of alfa-chimotrypsin (ΔF and ΔH kcal/mol, ΔS cal/mol.degree)

Hydrocarbons	ΔF	ΔH	ΔS
Benzene	-3,0	0,8	10
Toluene	-3,1	0	8
Ethyl benzene	-4,1	2,3	22

TABLE 3. Thermodynamic parametres of sodium oleate and linoleate bounding with bovine serum albumin BSA and alfa-chimotrypsin in aqueous solutions

System	Balance between surfactant and protein, g/g	ΔF kcal/mol	ΔH kcal/mol	ΔS cal/mol degree
α-Chimotrypsin - sodium oleate	0,12	-4,8	0,7	18,4
α-Chimotrypsin - sodium linoleate	0,08	-3,3	0	11,0
BSA - sodium oleate	0,12	-4,9	-1,8	10,3
BSA - sodium linoleate	0,08	-3,5	0	11,7

Thus the presented data on bounding show, that solubilisation of hydrocarbons and small quantities of surfactants is determined to a considerable extent with entropy. growth. It corresponds with the statistico-thermodynamic model of hydrophobic bounding and confirms the model we had chosen for distribution of hydrocarbons by solubilisation between two phases.

Small negative values of free energy from -3 to -5 kcal/mol by bounding of hydrocarbons and surfactants indicate that the bounding process is spontaneous and thermodynamically advantageous. In the systems studied changes in enthalpy of the process are closed to zero, so the main share in the change of free energy belongs to the entropy member.

Hydrophobic character of solubilisation mechanism, following from estimations of thermodynamic parametres, and also connection of protein structural changes with the change in the solubilisation value, noted in our former works, show that investigations of hydrocarbons may become a method of characterising of hydrophobic structure of proteins. Studying of bounding of hydrocarbons with proteins allows to obtain an approximate estimation of number and capacity of hydrophobic regions /2/.

As it could be seen from table 3, in case of bounding of a low molecular surface-active substance - sodium oleate- with bovine serum albumin the values of enthalpy changes by solubilisation were negative and different from zero, this fact meaning that the presence of a charge on both components becomes significant. Stabilisation of BSA - sodium oleate complex is provided besides hydrophobic interactions also with electrostatic interaction of a negatively charged ligand with positive charges of the globule, which are located mostly in the outer envelope (4). But it should be taken into consideration that the character of interaction and structure of the proteinlipide complex

depends apparently on the balance between protein and surfactant concentration in the solution as well as on phase state of the surfactant in the solution of micellar or molecular dispersity. An investigation was carried out in this work of the isotherm of sodium octylbenzosulphonate bounding with α-chimotrypsin from molecular solutions (surfactant below CMC) and micellar systems of the surface-active substance. The results are presented at fig. 1.

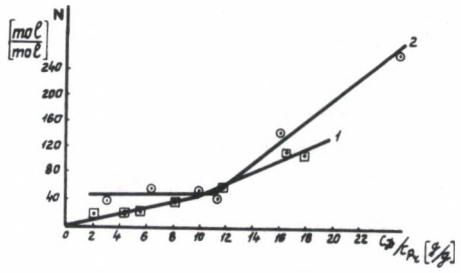

Fig. 1. Dependance of reduced solubilisation (N) of sodium octylbenzoluphonate with alfachimotrypsin on balance between surfactant/protein concentrations 1 - molecular, 2 - micellar degree of dispersity of the surfactant.

Dispersity being molecular (curve 1), one can separate two fields of bounding, which are characterized with different constants of interaction. If the initial balance between surfactant and protein concentrations is relatively low, bounding is characterized with constant K equal to 8000; when this balance becomes more than 10, bounding increases, the constant of bounding, however, falling to 7200.

Bounding of the surfactant with protein grows as a result of emerging of new bounding centres in the macromolecule of alfa-chimotrypsin and apparently testifies to conformative changes in the protein.

As it is seen at fig. 1 (curve 2), saturation of the protein globule with molecules of surfactant when

the surfactant/protein balance is relatively low is reached much earlier if the state of the surfactant is micellar than in molecular solution. In the interval of surfactant/protein balances under 10 the composition of proteinlipide complex does not change. If the concentration balance surfactant/protein exceeds 10, the degree of bounding of the surfactant with the protein component sharply increases. This process is characterized with K equal to 2600.

Since the micelle of a surfactant and the globule of protein both represent hydratated particles of lyophilic disperse systems and are approximately equal in size, one should speak here about process of micelles and protein globules association. The principal role at the first stage of this process should be payed apparently by electrostatic interactions. Due to high flexibility of surfactant micelles the micellar structures can be expected to decompose. Localization of a great number of surfactant molecules near the macromolecule of protein in course of association provides quick and the most thermodynamically advantageous interaction of these molecules with the protein. Cooperative emerging of bounding places provides the conformation change of the polypeptide chain and formation of mixed micelles, composed of a polypeptide chain with more loose tangle-like random coil spatial structure and surface-active molecules connected with it.

The conclusion on dependance of proteins conformation on degree of bounding of the surfactant, obtained for the system sodium octylbenzosulphonate - α-chimotrypsin, agrees with results of kynetic investigations on influence of surfactants on enzymatic activity of alfa-chimotrypsin.

Besides that, when great concentrations of surfact-

ants interacted with alfa-chimotrypsin and bovine serum albumin, there was observed (with method of differential spectroscopy) a shift to the blue part of the spectrum, this phenomenon being a consequence of changes in surrounding of chromophoric groups (tyrosin and tryptophan). In all the cases the hypochromic effect was observed and minimums at 287 and 294-299 nm. Effect of great quantities of surfactants in micellar form is analogous tc denaturating effect of the pH.

So the composition and structure of protein-surfactant complexes are determined with initial balance of concentrations between surfactant and protein as well as with phase state of the surfactant in the solution.

The degrees of bounding of a diphilic component with the protein being small, stabilisation of the tertiary structure of the protein is observed, and the resistance of the complex to denaturating influences increases. The data on dispersion of optical rotation obtained in our work confirm this statement. Actually the constancy of Moffit - Young equation parametres in the region of smooth dispersion and absence of changes of characteristical parametres in the region of Cotton effect for alfa-chimotrypsin and bovine serum albumin and their complexes with sodium oleate and linoleate, the degrees of surfactant bounding with protein being low, testifies to that under these conditions the secondary and tertiary structure of the proteins do not undergo any appreciable changes.

When concentrations of surfactants are high, conformation changes of protein macromolecules are observed and mixed micelles surfactant-protein appear.

REFERENCES

1. Scheraga H.A. Protein Structure, New York-London, Acad. Press, XVI (1961).
2. V.N.Izmailova, P.A.Rebinder. Structure Formation in Protein Systems, "Nauka", Moscow (1974).
3. V.K.Mazo, G.P.Yampol'skaya, A.V.Elenskiy, V.N.Izmailova. Vestnik MGU, N 6, 715 (1974).
4. G.P.Yampol'skaya, V.N.Izmailova, V.K.Mazo, E.D.Manev. Vestnik MGU, N 2, 93 (1975).

ALKALI AND HALIDE ION NUCLEAR MAGNETIC RELAXATION AND SHIELDING IN SURFACTANT SYSTEMS

Hans Gustavsson and Björn Lindman

Division of Physical Chemistry 2, The Lund Institute of Technology, Chemical Center, Lund, Sweden

INTRODUCTION

For the elucidation of ionic interactions in surfactant systems, several different nuclear magnetic resonance principles can be envisaged to be useful but, as yet, few of them have been systematically tested. Quadrupole relaxation studies have been applied for some time to provide qualitative ion binding information in soap-water systems[1] but, using the results of a recent theoretical study,[2] a more quantitative analysis of the data should be feasible. While the type of information provided from counterion quadrupole relaxation depends on the system under study, it appears that in many cases the relaxation rate may be interpreted in terms of the counterion-polar head separation distance and the mobility of the counterion at the amphiphile aggregate surface.[2] The shielding of alkali and halide nuclei in aqueous solutions is generally considered to be dominated by the paramagnetic term,[3] and the observation[4] of changes in the counterion chemical shift at surfactant self-association opened the way for the use of such shifts to probe the overlap between the electron cloud of the counterion and the electron clouds of other species in the system. The counterion shielding may, therefore, be expected to provide direct information on the mechanism of ion binding. The NMR spin-echo method for diffusion studies has the disadvantage of requiring that spin relaxation should not be too rapid but the significant advantage of being applicable irrespective of the macroscopic rheological properties of the sample. It can be foreseen that NMR diffusion studies of counterion binding should be of particular interest in liquid crystal and model membrane systems, but no such experiments have so far been reported.

In addition to these methods, based on the NMR signal of the counterion itself, information on counterion binding may also be obtained indi-

rectly. Thus studies of the NMR signal of the amphiphile and of water in the presence of different counterions should give information on counterion-surfactant and counterion-water interactions, respectively. Studies of this type, based on static quadrupole effects in ^{2}H NMR, have been performed[5] and it should be possible to use, for example, ^{1}H and ^{13}C chemical shifts and relaxation times analogously. A further possibility to elucidate ion-water interactions would be to make use of the considerable water isotope effect in ion chemical shifts.[6]

Work along the lines described are in progress in our laboratory and the present report describes some observations on alkali and halide ion quadrupole relaxation and shielding. We have previously described in some detail aqueous surfactant solutions[7,8]. Here we will also consider the behaviour of solutions of surfactants and water in non-aqueous solvent. In particular, we consider changes in the ^{23}Na NMR properties at the transition from normal micelles to micelles of the reversed type and the applicability of the water isotope effect in an ion's chemical shift to probe into hydration properties.

SHIELDING

Whereas below the critical micelle concentration (cmc) the counterion chemical shift of an aqueous surfactant solution is only weakly concentration dependent, rather large changes are obtained in the micellar region.[4] ^{35}Cl chemical shifts for aqueous solutions of octylammonium chloride and octyltrimethylammonium chloride are given in Fig. 1 as a function of the inverse amphiphile concentration. From a plot of this type it is, as described in Ref. 8, possible to obtain δ_m, the chemical shift characterizing the micellarly bound counterions. (This procedure, assuming the validity of the phase-separation model of micelle formation, is a convenient way of estimating from different types of NMR data, the properties of the bound counterions. In view of the approximate nature of the model it would be more appropriate to base the analysis on aggregate formation constants as provided in the pioneering work of Danielsson and Stenius[9,10] but information on more systems is needed before this possibility may be realised.) Values of δ_m for a number of systems are listed in Table I together with cmc values obtained from the intersection points.[8] (Chemical shifts towards higher field are throughout taken as positive.)

The markedly different behaviour of sodium octanoate and sodium octyl sulphate solutions is of particular interest and suggests that the mode of

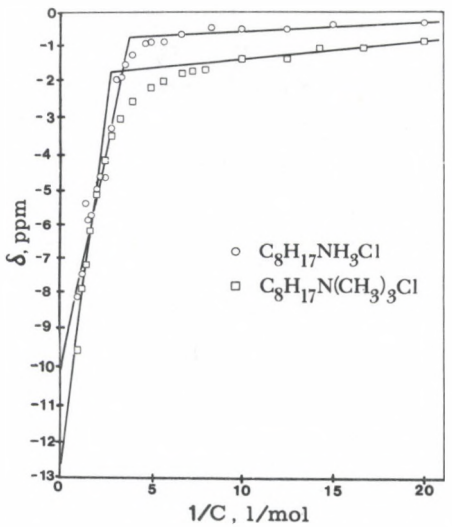

Fig. 1. ^{35}Cl chemical shifts, δ (in ppm), as a function of the inverse concentration of octylammonium chloride (○) and octyltrimethylammonium chloride (□).

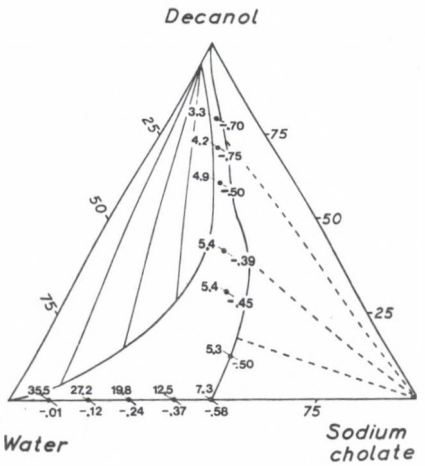

Fig. 2. ^{23}Na chemical shifts (in ppm; lower right figure) and longitudinal relaxation times (in seconds; upper left figure) for solutions composed of sodium cholate, decanol and water. Phase diagram from Ref. 12. Compositions in percent by weight.

counterion binding may be quite different in the two cases. One possible explanation is that, in the case of octanoate, hydrogen-bond interactions (which should be enhanced by the presence of the counterion) between surfactant end-group and water of counterion hydration are significant. The low basicity of the sulphate end-group would tend to make such an effect unimportant in the case of sodium octyl sulphate. According to the δ_m values, the mode of counterion binding should be similar for octylammonium and octyltrimethylammonium micelles. The approximately equal δ_m values in the two cases is consistent with the counterions remaining hydrated when bound to the micelles. According to the plots of Fig. 1 no change in counterion binding with increasing surfactant concentration above the cmc has to be invoked to explain the data. This is in contrast to the findings for other surfactants[8] but consistent with what was deduced for hexadecyltrimethylammonium chloride from ^{35}Cl quadrupole relaxation data.[11] Unfortuna-

Table I

Chemical shifts, δ_m, of micellarly bound counterions relative to the ion at infinite dilution in water. δ_m and cmc values were obtained from the concentration dependence of the ion's chemical shift as described in Ref. 8. The ratio of counterions to surfactant ions in a micelle was assumed to be 0.6.

Surfactant	δ_m, ppm*	cmc, mol/l
$C_8H_{17}NH_3Cl$	-16 (^{35}Cl)	0.27
$C_8H_{17}N(CH_3)_3Cl$	-20 (^{35}Cl)	0.37
$C_7H_{15}COONa$ (Ref. 8)	-0.95(^{23}Na)	0.37
$C_8H_{17}SO_4Na$ (Ref. 8)	+0.93(^{23}Na)	0.14
$C_7H_{15}COOCs$ (Ref. 4)	-13.5(^{133}Cs)	0.40

* Nucleus studied is given in parentheses.

tely, details are not obtainable from ^{35}Cl shielding measurements since the accuracy of the chemical shifts are greatly reduced by the strong line-broadening on micelle formation. ^{19}F NMR studies on the fluoride ion, which are now in progress, should offer considerable advantages in this respect.

Investigations of the counterion chemical shifts in reversed micellar and liquid crystalline solutions have been initiated with two three-component systems where continuous transitions from normal to reversed micelles have been inferred, i.e. the systems sodium cholate-decanol-water[12] and sodium octanoate-octanoic acid-water.[13] Experimental ^{23}Na chemical shifts for these systems are summarized in Figs. 2 and 3. It is not possible here to discuss these data in detail but it is interesting to note especially that no drastic changes in ^{23}Na chemical shift at the transition from normal to reversed micelles can be inferred for the two systems. This suggests that the counterion binding remains approximately unaffected by the change in the nature of the micelles. Over wide concentration regions, increasing the content of octanoic acid for the sodium octanoate-octanoic acid-water system leads to an upfield shift of the ^{23}Na NMR signal. This effect is consistent with the low electron-donating ability of the acid (cf. Ref. 3). The extensive broadening of the ^{23}Na signal[14] precludes detailed studies of the ionic interactions in the water-poor region of the solution phase. These problems are presently being studied by experiments using ^{133}Cs NMR.

WATER ISOTOPE EFFECT IN SHIELDING

The change in ion chemical shift on substitution of D_2O for H_2O has so

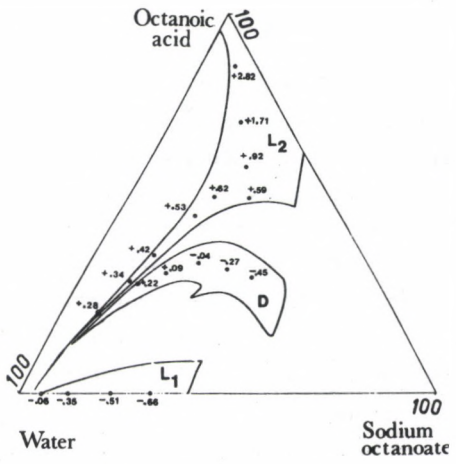

Fig. 3. ^{23}Na chemical shifts (in ppm) for samples composed of sodium octanoate, octanoic acid and water. Phase diagram from Ref. 13. L_1 and L_2 denote isotropic solution phases and D lamellar liquid crystalline phase. Compositions in percent by weight.

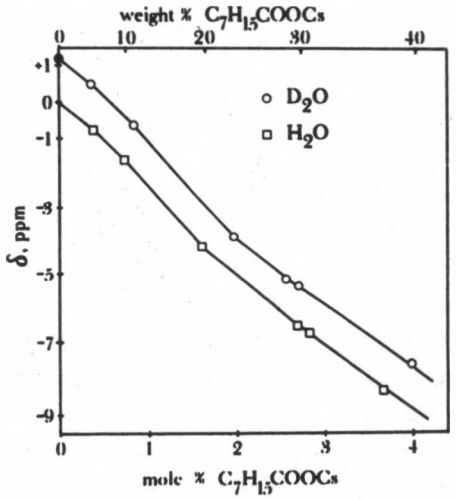

Fig. 4. ^{133}Cs chemical shifts (in ppm) of H_2O (□) and D_2O (○) solutions of cesium octanoate as a function of amphiphile concentration. The water isotope effect for CsCl solutions extrapolated to infinite dilution is denoted ●.

far only been reported for aqueous alkali halide solutions. Even if the full explanation of this phenomenon has still to be found, the water isotope effect in the chemical shift of ions is expected to be helpful for probing into ion hydration in a large number of systems. For example, for studies of preferential solvation in mixed solvent systems, the effect should be useful. We are presently exploring the application of this principle to surfactant systems. It would, for example, be of considerable interest to establish to what extent different ions retain their hydration sheaths on attachment to various types of amphiphile aggregates.

According to the ^{133}Cs chemical shift data given in Fig. 4 for H_2O and D_2O solutions of cesium octanoate, there is no significant reduction of the water isotope effect even at quite high surfactant concentrations. Consequently, no detectable elimination of the counterion-water contact on attachment of the ion to a micellar aggregate can be inferred for this system. With other surfactants as well as with reversed micellar solutions reductions in the water isotope effect have been observed. These results will be

presented elsewhere.

RELAXATION

The nuclear magnetic relaxation of alkali and halide ions (except fluoride) is generally dominated by time-modulated interactions between the nuclear electric quadrupole moment and electric field gradients from the surroundings. The rate of relaxation is determined by two factors, i.e. the magnitude of the interaction which is modulated and the correlation time characterizing the rate of change of the field gradients. For surfactant systems containing large aggregates the time-variation of the quadrupole interaction may be a complex process. In a recent analysis[2] of this problem, it was found useful to consider the averaging of the quadrupole interaction as a two-step process in which part of the interaction is varied due to a fast local motion while the rest is affected by a slow motion over the dimensions of the aggregates. For the interpretation of quadrupole relaxation data, a distinction between these two contributions to quadrupole relaxation is essential. It can be postulated that the contribution from the slow motion should be strongly dependent on aggregate size and shape whereas the contribution from the rapid local motion should be relatively independent of these factors. Studies of changes in relaxation rate at phase transitions are important in this respect. However, another possibility is to investigate systems where, within a single phase region, marked changes in aggregation take place.

For the two three-component systems represented in Figs. 2 and 3, changes from normal to reversed micelles within a one-phase region have, as mentioned above, been suggested.[12,13] ^{23}Na relaxation data shown in Fig. 2 for the sodium cholate-decanol-water system and data presented in Ref. 14 for the sodium octanoate-octanoic acid-water system give no indication of a change in relaxation rate in the concentration regions where changes in the nature of the aggregates have been proposed. According to these data it appears that the dominant mechanism of relaxation may be referred to a fast local motion while the slow motion over larger distances should be relatively unimportant. It seems not unreasonable to assume that this conclusion should apply also to other similar surfactant systems where tests of the type described are not possible.

A general observation for the two systems considered is that it is only at quite low water contents that the ^{23}Na relaxation rate becomes appreciably dependent on sample composition. The drastically enhanced

relaxation with decreasing water content in the water-poor solution region can probably be referred to the appearance of direct ion-ion interactions as the reversed micelles cease to exist. The $^{85}Rb^{+}$ quadrupole relaxation rate in solutions composed of rubidium cholate, decanol and water changes relatively much more with composition than the $^{23}Na^{+}$ relaxation rate. This is consistent with the more extensive hydration of Na^{+} ions compared to Rb^{+} ions.

From the magnitude of the counterion quadrupole relaxation rates it is possible to obtain quite detailed information on interactions and microdynamic properties of the system.[7,8] Of particular interest is the finding that the intrinsic relaxation rates of micellarly bound Na^{+} ions are quite different for octanoate and octyl sulphate micelles. These results are consistent with the model for counterion binding mentioned above.

EXPERIMENTAL

Part of the ^{23}Na chemical shift measurements were performed using a Varian V-4200 wide-line NMR spectrometer as described in Ref. 8. The wide-line spectrometer was also used to obtain ^{35}Cl and ^{133}Cs chemical shifts and ^{85}Rb relaxation rates. In order to improve precision and sensitivity most of the ^{23}Na chemical shifts were, however, obtained using a modified Varian XL-100-15 spectrometer employing the Fourier transform technique. ^{23}Na spin-lattice relaxation times were measured on a Bruker Bk-322s spectrometer as described in Ref. 8. All experiments were performed at $27\pm2^{\circ}C$. All chemical shifts are given relative to the ion at infinite dilution in water and with a positive chemical shift denoting a shift to higher field.

REFERENCES

1. G. Lindblom and B. Lindman, in "Chemie, Physikalische Chemie und Anwendungstechnik der grenzflächenaktiven Stoffe," Carl Hanser Verlag, München, 1973, Vol II, p. 925.
2. H. Wennerström, G. Lindblom and B. Lindman, Chem.Scr. 6, 97 (1974).
3. E.G. Bloor and R.G. Kidd, Can.J.Chem. 46, 3425 (1968).
4. H. Gustavsson and B. Lindman, J.Chem.Soc., Chem.Commun. 1973, 93. (The reference solution given in this paper for ^{133}Cs should be 1.0 M, and not 0.5 M, CsCl.)

5. H. Wennerström, N.-O. Persson and B. Lindman, Amer.Chem.Soc. Symposium Series, in press.

6. A. Lowenstein, M. Shporer, P.C. Lauterbur and J.E. Ramirez, Chem. Commun. 1968, 214.

7. G. Lindblom and B. Lindman, J.Phys.Chem. 77, 2531 (1973).

8. H. Gustavsson and B. Lindman, J.Amer.Chem.Soc., in press.

9. I. Danielsson and P. Stenius, J. Colloid Interface Sci. 37, 264 (1971).

10. P. Stenius, Thesis, Åbo, Finland, 1973.

11. G. Lindblom, B. Lindman and L. Mandell, J. Colloid Interface Sci. 42, 400 (1973).

12. K. Fontell, Kolloid-Z.Z.Polym. 250, 825 (1972).

13. P. Ekwall, J. Colloid Interface Sci. 29, 16 (1969).

14. B. Lindman and P. Ekwall, Kolloid-Z.Z.Polym. 234, 1115 (1969).

INTERACTION OF POLYMERS WITH SURFACTANTS IN AQUEOUS SOLUTION

T.Gilányi and E.Wolfram

Department of Colloid Science, Loránd Eötvös University, Budapest, Hungary

Introduction

When ionic surfactants are dissolved in aqueous solutions of polymers interactions occur leading to the formation of a polymer-surfactant complex, or to the surfactant "adsorption" onto the polymer.

Most of the studies confirm that the adsorption of the surfactant ion increases with decreasing hydrophilic character of the polymer, from which the conclusion may be drawn that hydrophobic bonding is likely to be the principal binding mechanism involved in these interactions.[1]

In order to understand the properties of polymers in surfactant solutions a quantitative study seems to be most important. This work aims to present first approximation to a quantitative treatment of polymer-surfactant complex formation and some preliminary results obtained for poly(vinyl alcohol) (PVA) - sodium dodecyl sulfate (NaDS) system.

Thermodynamic formulation

In order to obtain quantitative information on complex formation the first step, generally, is to construct a binding isotherm, i.e. a curve representing the amount of bound, or complexed, surfactant as a function of concentration, or activity, of free surfactant ions in equilibrium. From the isotherm an attempt is made to deduce a model for binding process.

Such an isotherm is shown in Fig. 1 calculated from dia-

lysis equilibrium data without Donnan-correction. The amount of bound surfactant increases suddenly in a narrow concentration range below the critical micelle concentration (c_M). This type of isotherm is characteristic throughout for polymer-surfactant systems studied in the literature.[2]

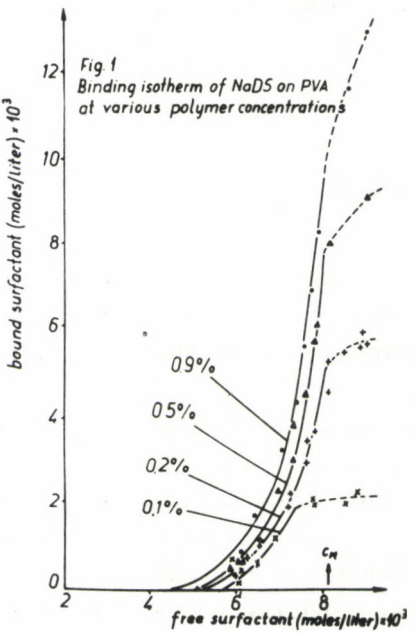

The existence of a critical concentration (c_{cr}) for the surfactant to interact with the polymer is an indirect experimental evidence that the surfactants in complex are not uniformly distributed as single ions along the polymer chains but they are present in form of aggregates. Apparently, there are two possibilities for interpretation: the active sites of the polymer serve as nucleus for micelle formation and the c_M of this type of micellization is lower than that for ordinary free micelles, or else the c_M is decreased in presence of the polymer and the micelles formed solubilize the polymer sites. If it is recognized that the structure, shape, symmetry,

aggregation number, etc. of the free and the polymer-bounded micelles differ from each other the two interpretations seem to be equivalent because the free micelle-complex equilibrium exists through the monomer - free micelle and monomer-complex equilibria.

Model calculations suggest that the concentration of free micelles at the beginning of complex formation may be neglected, so in this concentration range it is sufficient to consider merely the complex formation.

Assuming the equilibrium

$$P + m\ A^{\ominus} + n\ K^{\oplus} \rightleftharpoons \left(PA_mK_n\right)^{\ominus(m-n)} \equiv (\text{compl.}) \qquad 1$$

the equilibrium constant is given as

$$K_{m,n} = \frac{[\text{compl.}]}{[P]\,[A^{\ominus}]^m\,[K^{\oplus}]^n} \qquad 2$$

where P is the active site of the polymer, $A^{\ominus}$ is the surfactant anion, $K^{\oplus}$ is the counter ion, $\underline{m}$ is the aggregation number and the meaning of $\underline{n}$ is discussed below.

Although in a rigorous treatment a series of $\underline{m}$ and $\underline{n}$ values should be considered, only a single value of $\underline{m}$ is considered here. Using this simplification, however, will not result in serious errors because the size distribution of aggregates is probably limited to a very narrow range, as it is generally accepted in the thermodynamics of micelle formation. The polymer geometry itself is likely to be the predominant factor for the aggregation number, and there are no many possibilities for polymer-surfactant structurization being similar in energetics.

Obviously, the above treatment is a formal one. The assumption of thermodynamic ideality in derivation of eq. 2 would be a serious limitation. Next we shall discuss the relation of $[P]$ and $\underline{n}$ to experimentally observable parameters.

The activity coefficient of polymer sites can be taken to be unity at infinite polymer dilution. The fact, however, that these sites are involved in a polymer chain that cannot

be diluted, is omitted. Insofar, the activity of polymer sites may depend on the degree of polymerization even at infinite dilution. Experimentally we have not found any significant dependence of the interaction on the polymer molecular weight in the interval from 6.10^4 to 3.10^5 for the PVA-NaDS system. On the other hand, a great effect was found for polyethylene oxide - NaDS systems below a very low degree of polymerization,[3] which may be due to the influence of the molecular weight itself, or to the appearance of a different complex structure for short polymer chains. It is supposed, therefore, that up from a certain degree of polymerization the molecular weight does not influence the value of $[P]$.

Surfactant ions aggregated in a small space around the polymer chain represent a high electric charge density and electric double layer and ion-pair formation must be allowed for. The separation of electric and non-electric contributions to the free energy of complex formation would give difficulties in a first approximation. To avoid this $\underline{n}$ is defined as the apparent number of bound counterions, irrespectively, whether they are really bound or else, their movement is merely restricted in the ionatmosphere. The aggregation number n is readily related to measurable quantities as

$$\frac{m-n}{m} = \alpha = \left(\frac{\partial [K^{\oplus}]}{\partial [\text{compl.}]} \right) \qquad 3$$

where α is the apparent degree of dissociation.

If $m \gg 1$ (pseudo phase-separation) and using concentrations instead of the activities the following formula can be derived:

$$\log c_{cr} = K' - \frac{1}{m(1-\alpha)} \log c_p \qquad 4$$

where c_{cr} is the critical concentration for complex formation which is defined analogly as the c_M is and c_p is the polymer concentration. The same experimental methods may be used to determine both c_{cr} and c_M.

Eqs. 1 - 4 are applied to get information about the complex subunits. The equations are valid only for infinite dilution of aggregates, i.e. for c_{cr}, because the repulsion

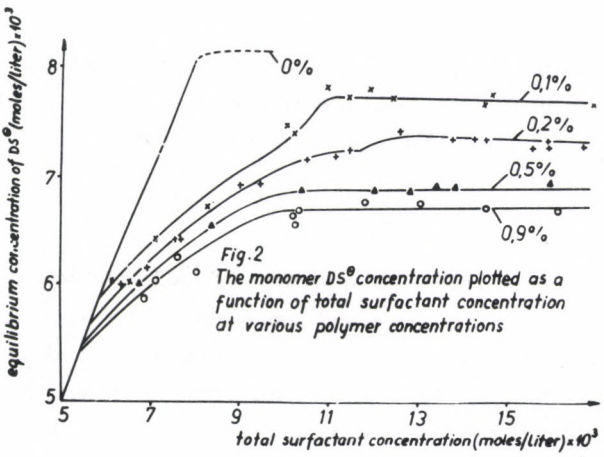

Fig. 2
The monomer $DS^{\ominus}$ concentration plotted as a function of total surfactant concentration at various polymer concentrations

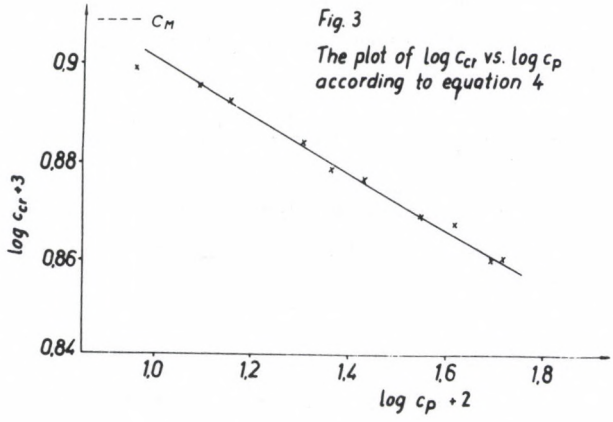

Fig. 3
The plot of log c_{cr} vs. log c_P according to equation 4

between the aggregates in the same polymer chain, and consequently, any conformational change of the polymer has been neglected. Considering the entire polymer molecule as being complexed with surfactant Eq. 2 may be rearranged as

$$\frac{\theta}{1-\theta} = K'' e^{\frac{f}{RT}} a^m \qquad 5$$

where θ is the relative saturation of polymer with surfactant aggregates, $\frac{f(\theta)}{RT}$ is an energy term accounting for the contributions from aggregate-aggregate interaction and from polymer conformation change. By definition $f(\theta) = 0$ when θ tends to 0, and $a^m = [A^{\ominus}]^m [K^{\oplus}]^{m(1-\alpha)}$ is the ionic product of the aggregate.

Essentially, Eq. 5 is a modified Langmuir isotherm deduced from the Mass Action Law. The same equation can be obtained in one step using the adsorption model for complex formation with the same suppositions.

From Eq. 4 or 5 the free energy of transfer of a single surfactant ion from monomer state to an aggregate of size m, is as follows:

$$\Delta G_m^o = RT(1-\alpha)\ln x_{cr} + \frac{RT}{m}\ln\frac{x_p}{k} \quad \left(\text{if } \frac{x_p}{k} \ll x_{H_2O}\right) \qquad 6$$

here x represents the concentrations expressed in mole fraction units, x_p refers to segments and k is the number of segments in the active site.

Results and discussion

Fig. 2 shows the monomer $DS^{\ominus}$ concentration vs. total $DS^{\ominus}$ concentration curve as calculated from dialysis equilibrium data with Donnan-correction. The value of α used to the calculations was obtained from emf measurements made with sodium-responsive glass electrode.[4]

The significant curvature near c_{cr} suggests that the aggregates in the polymer chain are considerably smaller than the free micelles and thus the phase separation model is a rough approximation.

The c_{cr} data used in Fig. 3 were determined from specific conductivity *vs* concentration curves. The relation of log c_{cr} to log c_p is linear as predicted by Eq. 4 . From the tangent the value of *m* was found to be 10±2. A plot of dialysis data according to Eq. 5 gives a value of 9 for *m* (Fig.4) in excellent agreement with the former one.

The procedure used in this work does predict a positive energy contribution from aggregate-aggregate interaction which should cause a downward curvature in Fig. 4. The absence of deviation from linearity means that the conformation changes of polymer in fact do not contribute significantly to the free energy of complex formation even at high saturations or other compensating effects are misleading, i.e. the number of polymer sites itself depends on the bound surfactant concentration.

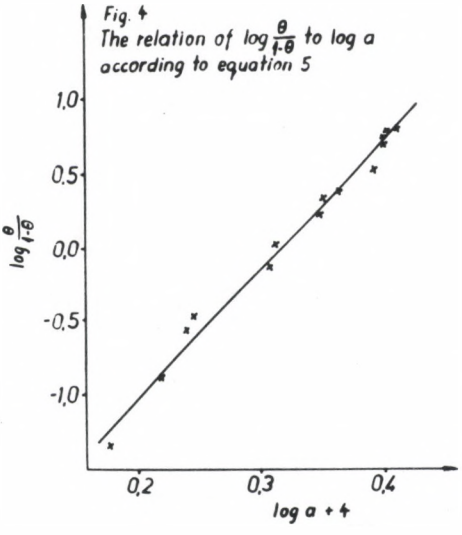

Fig. 4
The relation of $\log \frac{\theta}{1-\theta}$ to log a according to equation 5

The Gibbs free energy of transfer of the DS ion was found to be -9,76 kcal/mole, using k=50 (estimated from saturation data) in Eq. 6. The value of $\underline{k}$ is uncertain but fortunately ΔG_m^o is insensitive to $\underline{k}$. An error of three order of magnitudes in $\underline{k}$ (1 and 10^3) makes only 4% difference in ΔG_m^o. From the temperature dependence of c_{cr} the value of ΔS_m^o has been found to be 19,8 cal/mole. degree. This energetics is very close to that of micelle formation and supports the idea that the driving force, mainly of entropic origin, is due to hydrophobic interaction.

References

1. Saito,S.: J. Colloid Interface Sci. 24,227 1967 .
2. Breuer,M.M., Robb,I.D.: Chem. and Ind. 13,530 1972 .
3. Jones,M.N.: J. Colloid Interface Sci. 23,36 1967 .
4. Gilányi,T.: Acta Chem. Scand. 27,729 1973 .

THE STABILITY OF BOVINE CASEIN MICELLES

C. Holt

Hannah Research Institute, Ayr, Scotland KA6 5HL, UK.

The main protein fraction of milk consists of three proteins known as α_s-, β- and κ-casein. Nearly all of this protein occurs in the form of relatively large particles known as casein micelles and the ease or otherwise with which these particles aggregate is an important characteristic in processing milk. Factors which have been found to be important in destabilising micelles include the binding of calcium ions and calcium phosphate, complex formation between the serum protein β-lactoglobulin and κ-casein and the development of acidity in milk. Casein micelles can be precipitated by proteolytic enzymes, particularly rennin. The primary phase of this enzyme's action is the cleavage of κ-casein into para-κ-casein and a glycomacropeptide.

There has been a recent increase in interest in the physico-chemical characterisation of micelles[1,2,3,4] using both electron microscopy and light scattering techniques. With one exception[4,5], average particle radii measured by electron microscopy are smaller than corresponding averages measured by light scattering techniques. The discrepancy has been ascribed to sample preparation techniques[1] or counting methods[3] in electron microscopy. It has also been suggested[3] that micelles have an outer, water-rich envelope which is not seen by electron microscopy. If this suggestion is correct, there should be a discrepancy between the hydrodynamic radius and radius of gyration obtained from calculations based on homogeneous sphere models. Such a discrepancy has not been observed[4]. However, the uncertainty in the size distributions of micelles is sufficiently large for a water layer of 10 - 20 nm to be undetectable. Work designed to establish with more precision the distribution of sizes and also a comparison of results of electron microscopy with those of elastic and quasi-elastic light scattering techniques will be presented and discussed.

The suggestion that casein micelles may have an outer hydrophilic region is relevant to an understanding of micelle stability. Earlier attempts have been made to discuss stability in terms of the hydrophobic colloid theory[6,7,8], but the high water content of micelles

argues against long range dispersion forces being important[4]. In some cases, only 10% of the volume of the micelle may be protein.

A coat-core model of the casein micelle has been developed in order to obtain a semi-quantitative understanding of the free energy change on the approach of two particles. For the long range repulsive force, the theory of Ninham and Parsegian[9] has been adapted to allow for:

(a) Diffuse spherical particles

(b) Two potential-determining ions: H^+ and Ca^{2+}

(c) Two types of ionising groups: phosphate and carboxyl

A typical example of the long range free energy changes using the parameters in Table 1 is given in Fig. 1.

Table 1

Micelle Properties	
(COO^-)	$= 5 \times 10^{19}$ ions/ml
(PO_4R^{2-})	$= 5 \times 10^{18}$ ions/ml
radius	= 100 nm
$K_{Ca}(COO^-)$	= 10 mM
$pK_H(COO^-)$	= 3.5
$K_{Ca}(RPO_4^{2-})$	= 3 mM
$pK_H(RPO_4^{2-})$	= 5
Aqueous Phase Properties	
pH_r	= 6.8
n	$= 1 \times 10^{20}$ ions/ml
η	= 0.05

At close approach, the free energy change on mixing the outer diffuse layers was calculated from an adaption of the Fischer theory[10] for the stabilisation of hydrophobic colloids by polymer chains. An example of the free energy changes using the parameters of Table 2 is given in Fig. 2.

Fig. 1

Double Layer Repulsion Between Casein Micelles

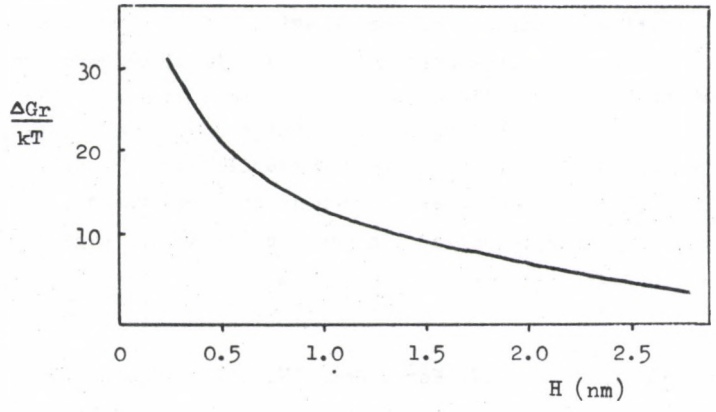

Table 2

Overlap Free Energy Parameters

B(coat)	=	$+10^{-3}$ mole ml g^{-2}
B(core)	=	-10^{-3} mole ml g^{-2}
B(coat/core)	=	0
radius	=	100 nm

Fig. 2

Overlap Free Energy Changes

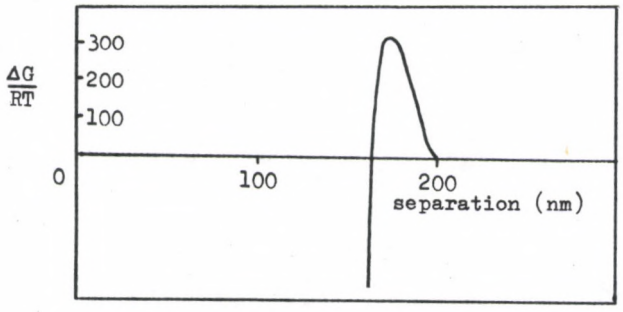

The properties of the coat were taken to be those of κ-casein macropeptide, one third of which was placed in a surface layer of 10 nm thickness and the rest distributed throughout the micelle.

A qualitative comparison of the behaviour of this model with that of micelles will be presented and its usefulness in understanding the problems of casein micelle stability will be discussed. The stabilisation of micelles by hydrophilic chains such as κ-casein macropeptide may have its parallel in the stabilisation of cells by glycoproteins. These proteins are common in cell membranes (e.g. glycophorin in erythrocyte cells) and can provide a high degree of stability against aggregation.

References

(1) V.A. Bloomfield and C.V. Morr, Neth. Milk Dairy J. 27, 103, (1973).

(2) W. Bucheim and U. Welsch, Neth. Milk Dairy J. 27, 163, (1973).

(3) D.G. Schmidt, P. Both, B.W. Van Markwijk and W. Bucheim, Biochim. Biophys. Acta 365, 72, (1974).

(4) C. Holt, Biochim. Biophys. Acta (1975). To be published.

(5) R.J. Carrol, M.P. Thompson and G.C. Nutting, J. Dairy Sci. 50, 1903, (1968).

(6) T.A.J. Payens, J. Dairy Sci. 49, 1317, (1966).

(7) M.L. Green and G. Crutchfield, J. Dairy Res. 38, 151, (1971).

(8) O. Kirchmeier, Neth. Milk Dairy J. 27, 191, (1973).

(9) B.N. Ninham and V.A. Parsegian, J. Theor. Biol. 31, 405, (1971).

(10) E.W. Fischer, Kolloid Z. 160, 120, (1958).

STUDIES ON MOLECULAR PROCESSES IN POLY/VINYL-ALCOHOL/ - WATER SYSTEMS

Gy. Inzelt and P.Gróf

Department of Physical Chemistry and Radiology, Loránd Eötvös University, Budapest, Hungary

The hydration of macromolecules has significant influence on the behaviour of their aqueous systems. This phenomenon has been studied by numerous authors using several methods of investigation [1]. Especially the systems containing proteins and nucleic acids have been investigated because of their vital importance. On the basis of these studies however, no answer can be given to the quantity of water bound by different groups for several reasons such as their variety e.g. in a protein molecule, uncertainity in our knowledge on the structure of substances, the presence of other components, etc. If information is wanted about the hydration of the individual groups, and at present this seems to be the most important question of this theme macromolecules are to be studied with identical sites of interaction and known chemical nature of their active binding sites.

As model substance for studying the hydration of OH-groups we chose poly/vinyl-alcohol/ /abbreviated PVA/. Our experimental method involved measurements of self-diffusion of water, microwave dielectric investigations as well as determination of viscosities and densities of the solutions. All measurements were made in the range of 0 to 10 wt.-% of concentration for PVA and at temperatures 25 and 35 ^{o}C in aqueous solutions of PVA.

1. EXPERIMENTAL SECTION

Self-diffusion measurements

The self-diffusion coefficient of water was determined by the open-end capillary mathod without stirring as described previously [2] at 25 and 35± 0.01 °C. Water was labelled with ^{18}O. Our preliminary investigation showed that there is no exchange of oxygen between water and alcoholic OH-group. The isotope content of samples was analyzed by mass-spectrometer determining the ratios of the $H_2{}^{18}O$/ $H_2{}^{16}O$ ion intensities.

Microwave dielectric measurements

The microwave dielectric parameters were determined by measurements of microwave refractivity and damping factor. The experimental method and the relations used for the calculations are described in detail in ref.[3] The low-frequency conductivity was measured at 20 kHz with an RC-bridge method. The investigations were carried out at 25, 30 and 35± 0.01 °C.

Density determinations

The densities of the solutions were measured with a pycnometer at temperatures of 25 and 35± 0.01 °C.

Viscosity determinations

were effected at temperatures: 25, 30 and 35 °C ±0.05 °C using Höppler viscometer.

Materials and sample preparations

PVA Rhodoviol 16/20 was used. In order to eliminate the low molecular weight constituents, it was partially fractionated by n-propanol. After fractionation the molecular weight was 110,000± 10%, the degree of hydrolysis 98%.

2. RESULTS AND DISCUSSION

1. Self-diffusion and density

The results of the self-diffusion measurements are listed in Table 1. The self-diffusion of water decreases linearly with the weight fraction of PVA. The activation energy of the self-diffusion process is approximately equal to that of pure water /4.5±1.0 kcal/mol/. In order to estimate the hydration number on the basis of the method that Wang [4] proposes the partial specific volume and the shape of the macromolecule are to be determined. Specific volumes were calculated from the density measurements and are also listed in Table 1. The partial specific volumes of PVA are equal to 0.7344 and 0.7628 cm^3/g at 25 and 35°C, respectively. To estimate the shape factor / $\bar{\alpha}$ / no exact model is available for PVA. We calculated, therefore, the hydration number taking $\bar{\alpha}$ = 1.500 and 1.667 as extreme cases for sphere and rod shape, respectively. The values of hydration numbers are tabulated in Table 4. The hydration numbers calculated from the results of the self-diffusion measurements are in good accordance with the results of Sponsler and his co-workers [5].

2, Dielectric measurements

The characteristic dielectric parameters are summarized in Tables 2 and 3. The microwave conductivity increases linearly with the square of the frequency. The dielectric permittivity of the solutions decreases proportional to concentration. The activation energy for the dipole rotation of water was 4.0± 1.0 kcal/mol. The estimated wavelength of relaxation for bound water was found to be two orders of magnitude higher /80-140 cm/ than that for pure water. The hydration number was calculated on the basis of two methods of analysis [6,7], and the results are summarized in Table 5. The values of hydration numbers calculated applying the method of Haggis et al.[6] are very sensitive to the shape factor. It is possible that the very low values for the hydration number compared with values obtained by other experimental

methods results from the inadequacy of the model in the case of PVA. When applying the Pottel-Kaatze method[7] similar value is obtained for the hydration number as to that from the self-diffusion measurements where Wang's method is used.

3. Viscosity measurements and investigation of $D'\eta$ products

The results of viscosity measurements are listed in Table 6. The viscosity $/\eta/$ of the solutions increased considerably with the concentration but the activation energy for viscous flow was found to be constant and the value obtained was $7,4 \pm 0,4$ kcal/mol. The constant value of activation energy in the range of concentration at issue indicates that the degree of intra- and intermolecular association existing in aqueous solutions of PVA are unchanging.

In consequence of the considerable increase of viscosity $D'\eta$ product increases with the concentration. The change in the internal frictional coefficient or microviscosity $/\eta_{micro}/$ determined from the dielectric relaxation frequency is less and the product $D'\eta_{micro}$ slightly decreases with the concentration. The similar molecular mechanism for the self-diffusion and the dielectric relaxation of water is indicated in similar values of activation energies for these processes and appeared in the behaviour of the $D'\eta$ products.

SUMMARY

Our results are compatible with the idea of water binding to macromolecules though it is pointed out that the value of the hydration number depends on the model of calculation. In the case of PVA it is the hydrogen bonding that is responsible for hydration phenomenon instead of ion-dipole interaction as in the solutions of polyelectrolytes. It should be mentioned that the lengthening of the relaxation time of water indicates the existence of distant hydration in these solutions i.e. PVA molecules plays a structure-forming role.

Table 1

Self-diffusion coefficients of water and specific volumes of solutions at 25 and 35°C

wt. -% PVA	$D'_{25}.10^5$ /cm²/s/	$D'_{35}.10^5$	V_{m25} /cm³/g/	V_{m35}
0,00	2,57±0,024 [a/]	3,49±0,15	1,004 [b/]	1,006
3,93	1,95±0,103	2,48±0,15	0,9932	0,9960
6,01	1,69±0,051	-	0,9884	0,9919
7,69	1,54±0,077	1,99±0,10	0,9831	0,9878
9,20	1,25±0,078	-	0,9795	0,9831
9,56	1,30±0,104	-	0,9785	-

a/ All data are average of 5 to 11 measurements. The spread of the measurements is given by the average error of the mean value.

b/ The accuracy of the specific volume ±0,5%

Table 2

Specific conductivity of PVA solutions in function of concentration and temperature

°C \ wt.-% PVA		2,83	4,55	6,23	10,00
25	σ [a/]	34,93	35,69	36,61	38,27
	σ_o [c/]	0,025	0,035	0,041	0,054
	σ_{ohm}	0,800	1,38	1,98	2,41
30	σ	28,51	30,60	32,48	35,29
	σ_o	0,028	0,039	0,045	0,056
	σ_{ohm}	1,08	1,70	2,14	2,61
35	σ	25,36	27,66	29,48	31,43
	σ_o	0,031	0,044	0,051	0,061
	σ_{ohm}	1,01	1,17	1,42	2,92

a/ Conductivity at 4 GHz in $10^{-3}\ \Omega^{-1}cm^{-1}$ units. Experimental error in ±1%

b/ Conductivity at 20 kHz in the same units as a/

c/ Conductivity occurring in processes of relaxation at lower frequences - in the same units as a/.

Table 3

Characteristic dielectric parameters in function of concentration and temperature

wt.-% PVA / °C		0,00 [a]	2,83	4,55	6,23	10,00
25	ε' [b]	75,6	72,6	70,6	68,9	65,0
	ε_s [c]	78,5	76,1	74,3	72,8	69,4
	λ_s [d]	1,53	1,71	1,77	1,84	2,02
30	ε'	74,5	71,2	69,5	67,8	64,0
	ε_s	76,8	73,8	72,0	70,7	67,3
	λ_s	1,37	1,48	1,53	1,61	1,77
35	ε'	73,1	70,2	68,6	66,9	63,3
	ε_s	74,9	72,3	70,9	69,4	65,8
	λ_s	1,25	1,33	1,43	1,51	1,56

a/ Ref. 8.

b/ Dielectric permittivities at 4 GHz. Experimental error in $\varepsilon \pm 2\%$

c/ Static dielectric constant of the solutions at dispersion corresponding to the relaxation of water

d/ Wavelengths of relaxation of the solutions in cm.

Table 4

Hydration number of OH-group of PVA in H_2O molecules/OH-groups units

Techniques	Methods of analysis	Shape factor 1,500	Shape factor 1,667
Self-diffusion of Water	Wang [4]	4,0±0,3	3,7±0,3
Dielectric dispersion	Haggis et al. [6]	0,2±0,1	0 ±0,1
	Pottel and Kaatze [7]	3,5±0,5	

There is no change in the value of the hydration number between 25 and 35°C.

Table 5

Viscosity of aqueous solutions of PVA in function of concentration and temperature

wt.-% PVA	η_{25} [a/]	η_{30}	η_{35}
0.00	0.8941	0.8019	0.7250
3.93	21.9±0.2	17.9±0.2	14.6±0.1
6.01	82.5±0.8	-	54.8±0.5
7.69	223.0±2.2	176.0±2.0	149.7±1.0
9.20	479.5±5.0	-	316.2±3.0

a/ Viscosity of the solutions in cP units.

Table 6

D"η and D'ηmicro products in function of concentration and temperature

	D'$\eta \cdot 10^7$ / dyn /				
wt.-% PVA / °C	0.00	3.93	6.01	7.69	9.20
25	2.297	42.7	139	343	598
35	2.53	36.2	-	296	-
	D'η micro$\cdot 10^7$ / dyn /				
wt.-% PVA / °C	0.00	2.83	4.55	6.23	10.0
25	2.3	2.1	2.0	1.8	1.4
35	2.4	2.1	2.0	1.8	1.3

ACKNOWLEDGEMENTS

We would like to express our gratitude to Dr. G.Masszi for his help in the dielectric measurements, to Dr. O.Kaposi for the mass-spectrometry analyses and to Dr.M.Nagy for the discussions and for all his useful advice.

REFERENCES

1. G.N.Ling, in Water and Aqueous Solutions, ed.R.A.Horne, Wiley-Interscience,N.Y. 1972. p.663.
2. T.Erdey-Gruz, Gy.Inzelt and P.Fodor-Csányi, Acta Chimica Acad.Sci.Hung., 77,173 /1973/
3. G.Masszi, Acta Biochim.Biophys.Acad.Sci.Hung.,7,349/1972/
4. J.H.Wang, J.Amer.Chem.Soc., 76,4755 /1954/
5. O.L.Sponsler,J.D.Bath and J.W.Ellis, J.Phys.Chem., 44,996 /1940/
6. G.H.Haggis,T.J.Buchanan and J.B.Hasted, Nature, 167,607 /1951/
7. R.Pottel and U.Kaatze,Ber.Bunsenges.Phys.Chem., 73,437 /1969/
8. J.B.Hasted, in Water a Comprehensive Treatise,ed.F.Franks, Vol.1. Plenum Press, N.Y. 1972. p.255.

IV. APPLICATIONS AND METHODS

Group IV/1
Applications

SIMULTANEOUS ELECTRODEPOSITION OF POLYMER DISPERSIONS AND METALS

Z.R.Ulberg, U.F.Deinega

INSTITUTE OF COLLOID CHEMISTRY AND CHEMISTRY OF WATER, ACADEMY OF SCIENCE OF THE UKRAINIAN SSR, KIEV, USSR

The use of electric field for the formation of disperse structures gains more and more significance. Particle orientation on their geometric and molecular axes, directed particle movement, interaction of polirized particles leading to the structural formation can be exercised in electric fields. These effects are used in electrodeposition processes for material production which have anizotropic properties for the control of mechanical properties of disperse systems (electrorheological effect).

Application of electric fields for simultaneous deposition and particle orientation of different nature in order to receive compositional and especially the metal and polymer coatings gains a special interest. This process includes the following stages: charging of polymer particles, movement of them to an electrode and coagulation at near electrode zone, electrochemical metal separation. The formation of metal and polymer deposit, its composition and structure are determined by the character of polarization chemisorption interaction between the polymer and metal particles.

We shall consider three moments in the deposition process of polymer dispersions with metals : the influence ofelectrolytes on electric properties of the dispersions, electrodeposition of polymers on metal separation and polarization interaction of polymer , metal and polymer particles. At

the presence of electrolytes the ζ- potential decrease takes place at the expence of compression of diffuse part of double layer when ionic force of a solution increases.

The presence of surfactant electrolyte and charged polymer particles substantially influeces the formation of high disperse cathode deposit of metals and permits to regulate their structure. Separation potential increases up to 2.5v and effective energy of activation of ion discharge is sharply growing with the concentration increase of disperse phase and electrokinetic potential of polymer particles. With the growth of polymer concentration the particle size of metal in deposit decreases from 2-3 to 0.2-0.5 micron. The conditions , when deposition rate of polymer exceeds the separation rate of metal and the main mass of metal ions is delivered to the electrode surface through the polymer layer, correspond to the formation of metal and polymer deposit. Herewith the deposit thickness and weight is limitted by its substantial conductance.

In this case the equation of nonstationary diffusion is acceptable for the flow of metal ions which changes in time The boundary conditions for the solution of the equation reflect the fact that after a certain time the ion concentration on electrode surface is equal to zero in consequence of impossibility of a diffusion through the film of l thickness. The beginning of polymer and metal deposition corresponds to the conditions under which ion concentration of a metal at near electrode layer and in volume is equal to: $x=o, \tau \geq o,\ c=o;\ x=\infty,\ \tau > o, c=c_o\ ;\ \tau=o,\ c=c_o, o > x \geq l$ (1)

The growth rate of film thickness is determined from the conditions:

$$\frac{dl}{d\tau} = \frac{D}{M} \cdot \frac{d^2C}{dx^2} \qquad (2)$$

where D-effective coefficient of diffusion; c_o-Me^{2+}ion con-

centration; x- a distance from electrode; M-coefficient determined by ion concentration of the metal inside the film. In case of the thin films and great times of deposition under the condition $1/2\sqrt{\tau D} \ll 1$ of the solution of the equation /3/ with the boundary conditions /2/ the connection between the film thickness and the deposition time is expressed:

$$l = \sqrt{\frac{2 \mathfrak{D} C_0 \tau}{M}} \qquad (3)$$

Actually during the disperse codeposition of epoxy oligomer with lead it is established that the thickness dependance of metal and polymer film on deposition time corresponds to the equation /3/. We shall introduce the criterion α in order to evaluate the relation between polymer and metal fraction in deposit:

$$\alpha = 4\pi \frac{\eta}{\varepsilon} \frac{\sigma k}{C_n C_n}, \qquad (4)$$

where η -viscosity of a suspension; σ -conductance; k - electrochemical equivalent; C_n - concentration of disperse phase. The formula is true for the condition of complete polymer and metal deposotion.

Mutual separation of polymer and metal on electrode leads to the considerable reaction braking of metal deposition . This effect is intensified with the increase of polymer particle charge and disperse phase concentration. As it is seen from the figure the yield of metal and polymer deposit is sharply increase with the charge increasing of polymer particles(concentration of surfactant) and disperse phase concentration. However, the content of metalic fraction decreases in it. Maximum values of deposition rate of polymer and metal components is reached in different regions of field intensity and cathode current density. In connection with this calculated and experimentally determined values of the criterion coinside only in a certain interval of studied magnitudes (Table 1).

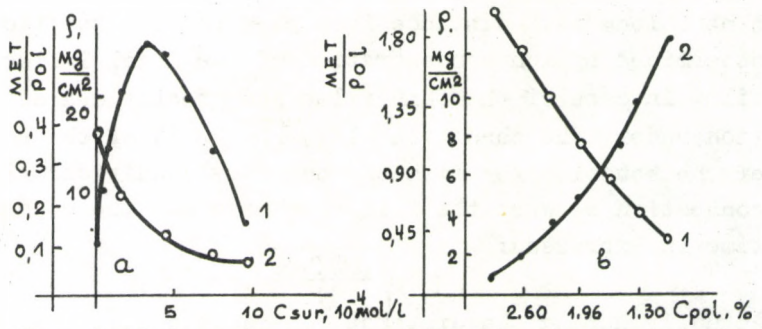

Fig. 1. The yield dependance of metal and polymer deposit / 1 / and the metal content in it / 2 / on the concentration: a - surfactant;
b - polymer.

TABLE 1.

Dependance of lead and epoxy oligomer relation in deposit on electrokinetic potential value and cathode current density.

ζ-poten. (mv)	calculated α	experimental α	current density on cathode (a/cm^2)	calculated α	experimental α
0	1.0	0.93	2	1.14	0.35
-40	1.0	0.98	4	0.93	0.52
+24	0.82	0.78	6	0.67	0.62
+35	0.70	0.65	8	0.62	0.70
+45	0.64	0.42	15	0.83	0.50

The formation of metal and polymer deposits, uniformity of distribution of conducting and unconducting particles, effectiveness of polymer particle influence on metal electrocrystallization are determined by the processes of polymer particle interaction among each other and with metal parcles. Herewith dipole phoretic and electrophoretic forces acting on a particle near electrode play an important role. The electrophoretic force (Fef) acting on a positively charged particle is equal to the product of electrophoresis

rate $\mathcal{E}$ef and viscosity resistance:

$$Fef = \mathcal{E}ef \cdot E \cdot \eta \cdot \pi \cdot a, \qquad (5)$$

where E- field intensity; η -viscosity.

Maximum value E is reached at particle surface of metal, and therefore Fef helps to the deposition of a polymer particle on metal one. Thanks to field non-uniformity near metal dendrite the dipolephoretic force Fd (2) acts on deposit particle:

$$Fd = \gamma \cdot \nabla (E^2), \qquad (6)$$

where γ - particle polarizability. In case of charged spheric particle the expression for γ can be written as

$$\gamma = -\varepsilon a^3 \left(\frac{1}{2} - \frac{3Rel}{4Rel+1}\right), \qquad (7)$$

where Rel - polarization criterion (3)

$$Rel = \frac{e^{0.5\varkappa} - 1}{\varkappa a},$$

where $\varkappa$ - a value, reverse to the thickness of double layer, a - particle size. According to the expression (7) when

$$Rel > 1 \qquad (8)$$

particle polarizability is positive, that is the direction of induced dipole moment coincides with the field direction and dipole phoretic force, this corresponds to the polymer particle streching to the region of stronger fields that is to the metal particle approach. Under the condition (8) the dipole phoretic force direction and electrophoretic force direction coincide, this helps to polymer particle deposition.

When a polymer particle has negative polarizability

$$Rel \ll 1 \qquad (9)$$

the induced dipole moment is directed against field and dipole phoretic force pushes out a polymer particle to the region of weak fields. Herewith dipole phoretic force different from electrophoretic one will prevent the deposition of polymer particle on metal particle and coat structure will be different from the dependance of the relation of two forces.

In order to find out the influence of two mantioned forces on deposition process the evaluation of them was made for the case of particle deposition of plymer on the end of dendrite - like metal particle. For the particle, which is in close approach to dendrite

$$Fef = \frac{2}{3}\ \varepsilon\ \ell\ a\ \varphi_0\ \frac{\delta}{(a+\delta)^2}\ , \qquad (10)$$

where φ_0 - cathode potential; δ - dendrite radius.

$$Fd = -\frac{\varepsilon \cdot a^3 \cdot \delta^2}{(a+\delta)^5}\ \varphi_0^2 \qquad (11)$$

The conditions of polymer and metal particle deposition, analogous expressins (8) and (9) are true under the conditions respectively:

$$\mathcal{F}_d / \mathcal{F}_{ef} > 1 \quad (12) \ ; \qquad \mathcal{F}_d / \mathcal{F}_{ef} < 1 \quad (13)$$

The table 2 gives the main characteristics of electrodepositional systems for which Rel and ration $\frac{Fd}{Fef}$ have meaning more or less of a unit. For the particle deposition of epoxy oligomers and lead from dispersions in the solution of lead formiate inqualities (8) and (12) are true with small electrolyte concentrations and with high values of electrokinetic potential. Expansion of concentration region of used electrolyte is possible at the expence of decreasing of size of polymer particles(table 2, Rel = 1.45 - 10).

TABLE 2.

The main electrodeposition characteristics of metal and polymer deposits.

concentr.of electrolyte mole/l	concentr.of surfactant 10^4 mole/l	particle size of polymer, cm	φ_δ	$\varkappa a$	Rel
6×10^{-4}	3.2	3×10^{-6}	6	2	10
6×10^{-4}	3.2	2.5×10^{-5}	6	13.7	1.0
10^{-3}-:-10^{-2}	3.2	3×10^{-6}	6	15	1.45
6×10^{-4}	3.2	1.25×10^{-5}	6	43	0.58
10^{-2}	3.2	2.5×10^{-5}	6	130	0.18
6×10^{-4}	3.2	1×10^{-4}	1-2	17	0.1

This corresponds to the deposition conditions when unconducting polymer particles are deposed on metal particles and block their growth. A metal of fine particles (0.1 -

0.3 micron) of uneven form is distributed in the polymer medium. The lead concentration in a deposit does not exceed 10 - 25 %, coat thickness is 40 - 50 micron.

Under electrodeposition conditions corresponding to the values Rel $\ll$ 1 and $\frac{Fd}{Fef} < 1$, the structure of deposits changes (Table 2).

Depositting polymer brakes in smaller degree the growth of metal particles. Lead particles have needle - like form and size up to 2 micron. In this case it is possible to receive the coat thickness up to 1 mm as the growth of long metal dendrites ensure their conductance.

On the base of made evaluation of electrophoretic and dipole phoretic forces (equations 10 and 11) the character of structural dependence of deposit on field intensity and partical charge, which is confirmed experimentally, was established. So with the increase of field intensity the transfer from dendrite - like (Rel > 1) to fine-crystalline (Rel $\ll$ 1) structure is observed. The increase of ζ - potential leads to the same effect.

On the base of above mentioned investigations electrophoretic methodes for the production of metal and polymer coatings are proposed.

SOME ASPECTS OF SEMICONTINUOUS EMULSION POLYMERIZATION PARTICLE SIZE AND WATER ABSORPTION OF LATEX FILMS

J.Šňupárek, Jr.

Research Institute for Synthetic Resins and Lacquers,
532 07 Pardubice, Czechoslovakia

In practical emulsion polymerizations, the monomers are usualy continuously added into the polymerization reactor. There are several modes in carrying out such semicontinuous polymerizations. In case of a monomer feed, when all the emulsifier is charged into the reactor, the particles form during the preparation of the seed latex and no new particles appear during the monomer addition /1/. When the polymerization is run without the seed latex formation, a great number of small particles are produced in its early stage, and they flocculate during the following polymerization /2/. When monomers are fed in the form of a water emulsion, the emulsifier is added into the reactor simultaneously with the monomers. It was found, that the particle nucleation during the feeding of monomer emulsion is affected by the preperiod as well as by the feeding rate /1/.

During the emulsion polymerization of acrylic monomers the flocculation of particles may occur /3/. It was found that the flocculation of particles, in the case of the monomer emulsion feed and without the seed latex, depends on

the distribution of the emulsifier between the initial reactor charge and the monomer emulsion /4/. The distribution ratio of the emulsifier affects the surface tension development during the addition of the monomer emulsion /Fig. 1/ and the final particle size /Fig. 2/. The surface tension development, the final particle size, the initial polymerization rate and the particle size distribution indicate, that particle flocculation occurs at reactor/emulsion emulsifier ratio higher than about 20/80. The flocculation is controlled by the total amount of emulsifier. It is clear, that the mechanical stability of the particles which underwent the flocculation, is low. The colloid system lies practically at the limit of flocculation, so the secondary stabilization has to be applied. The usage of combinations with nonionic emulsifiers in monomer emulsion added into the reactor, however, led to the formation of a great amount of coagulum in the latex, when R/E ratio of anionic emulsifier was greater than 20/80. When nonionic emulsifier was not used, no coagulum appeared.

In a previous study /5/, the water absorption in the films from latices prepared at R/E emulsifier distribution within the range of controlled flocculation, was studied. It was found, that the amount of absorbed water in the film depends on the latex stability. Other authors found /6,7/, that the water absorption of films depends also on the particle size of the latex. On prolonged immersion the water uptake of films based on fine-particle latex increased continuously, while for corresponding films based on coarse-particle latices a maximum or a limit was reached in an early stage. We suggest, that this

may be ascribed to the undersaturation of the particle surface by emulsifier in the case of small particles.

Latices with particle size 0.11 μm and 0.56 μm were prepared by the semicontinuous copolymerization of butyl methacrylate, butyl acrylate and acrylic acid / wt. ratio 82 : 15 : 3 / at the emulsifier distribution between the initial reactor charge and the monomer emulsion R/E = 25/75 and 0/100 respectively. Anionic emulsifier Etoxon AF 5 / $C_9H_{19}C_6H_4/OCH_2CH_2/_5OSO_3Na$ - ČSSR, Spolek Boletice / was used for polymerization, Lutensol AP 9 / $C_9H_{19}C_6H_4/OCH_2CH_2/_9OH$ - BASF / was used for secondary stabilization. The water absorption was measured during 10 days of immersion of films 300 - 350 μm thick.

The product with coarse particles was mechanically stable, while the fine particle latex was unstable. Its mechanical stability was achieved by post-addition of nonionic emulsifier. The effect of secondary stabilization as well as the effect of dissociation of carboxylic groups / pH of the latices adjusted to 8 / on surface tension is demonstrated in figure 3. In case when latices without post-stabilization were used, the typical developments of water absorption in the films were found /Fig. 4 /. The water uptake of films based on latex with particles 0.11 μm continuously increased, while for the corresponding films based on latex particles 0.56 μm a limited absorption was found. Stabilizing effect of dissociated carboxylic groups is evident from figure 5, in which the amount of secondary emulsifier, necessary for decreasing water absorption of films from acid and alcaline latices, is shown. Water absorption of films from the latex with particle size 0.56 μm,, which was stable

even without post-stabilization, was found practically independent of the amount of post-added nonionic emulsifier.

Conclusions

In the case of semicontinuous emulsion polymerization with monomer emulsion feed and without the seed latex preparation, the final particle size and the latex stability depends on the distribution ratio of the emulsifier between the initial reactor charge and the monomer emulsion. The stability of the latex greatly affects the water uptake of polymeric films. It may be suggested, that the great water absorption of films from fine-particle sized latices is caused by lower stability of the particles. The surface of fine particles is less covered by emulsifier and the particles have a tendency to premature flocculation during drying of the latex. Immobilized particles are not allowed to form a regular structure in the film. This results in higher water absorption of the films.

References

1. H.Gerrens, J.Polymer Sci. C 27, 77 /1969/
2. V.I.Eliseeva and others, Vysokomol.Soedin.Ser.A XI, 1005 / 1969 /
3. N.Sütterlin, G.Markert and H.-J.Kurth, Angew.Chem. 13 /6/, 418 /1974/
4. J.Šňupárek, Jr., Angew.Makromol.Chem. 37, 1 /1974/
5. J.Šňupárek, Jr., J.Oil Col.Chem.Assoc. 55, 1007 /1972/
6. H.A.Oosterhof, J.Oil Col.Chem.Assoc. 48, 256 /1965/
7. I.Anžur, V.Osredkar, I.Vizovšek, J.Oil Col.Chem.Assoc. 57, 170 /1974/

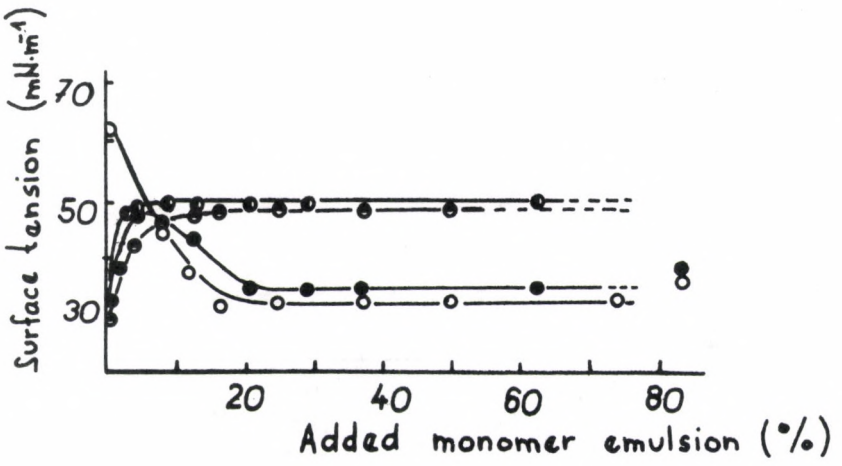

Fig. 1 : Change of surface tension during the feeding of monomer emulsion in relation to the distribution of emulsifier Etoxon EPA / sodium alkylpolyoxyethylene sulfate, Spolek Boletice ČSSR /between the initial reactor charge and monomer emulsion. Total amount of emulsifier - 1% wt.act.matter related to monomers, feeding time 120 min. Monomer emulsion : 800 g monomers, 500 g water, 4 g ammonium persulfate, 25 g ammonia /25 % / and portion of emulsifier. Initial reactor charge : 200 g water, 4 g sodium metabisulfite, 5 g ammonia and portion of emulsifier.
R/E ratios : ○ 0/100, ● 1/99, ◐ 25/75, ◓ 50/50.

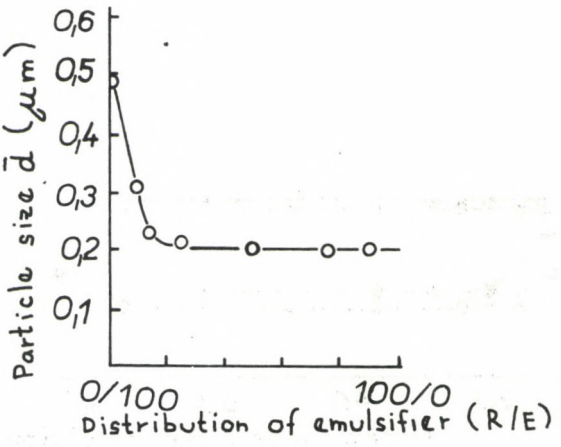

Fig. 2 : Average particle size in relation to the distribution of emulsifier between the initial rector charge and monomer emulsion. Reaction conditions as described in figure 1.

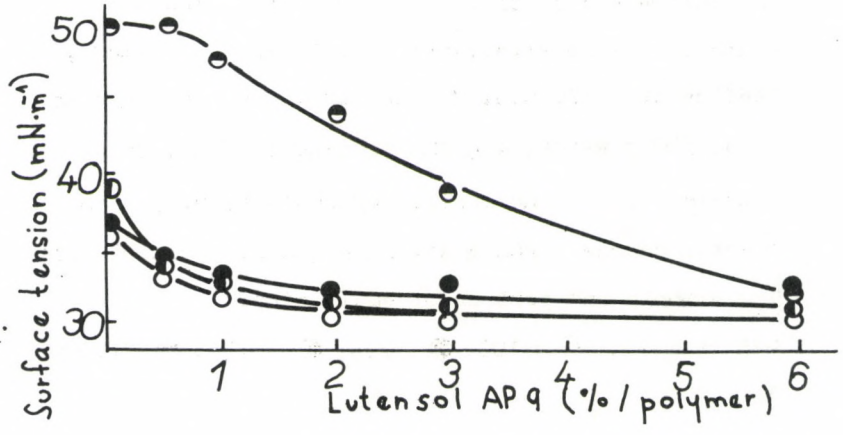

Fig 3 : Surface tension of latices in relation to the amount of post-added Lutensol AP 9. ◓● $\bar{d}$ = 0.11 µm, ◐ ○ $\bar{d}$ = 0.56 µm, ◓ ◐ pH = 3,5, ● ○ pH = 8.

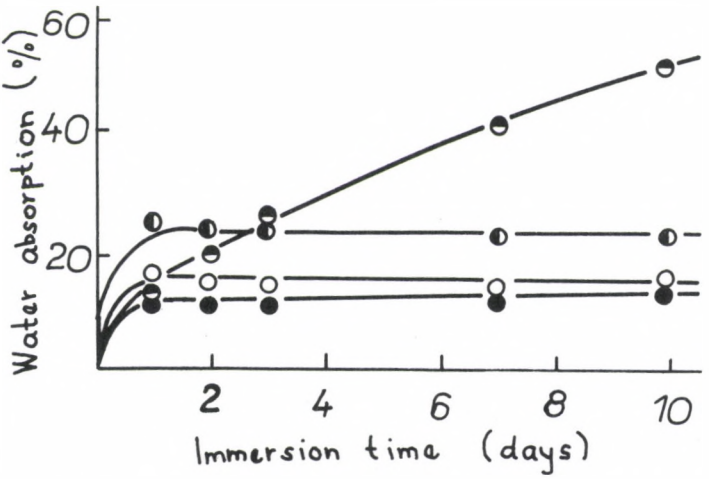

Fig. 4 : Absorption of water in relation to immersion time.
○● $\bar{d}$ = 0.56 µm, ◒◐ $\bar{d}$ = 0.11 µm, ◒○ without post-stabilization, ◐● post-stabilized by 6% of Lutensol AP 9 / polymer.

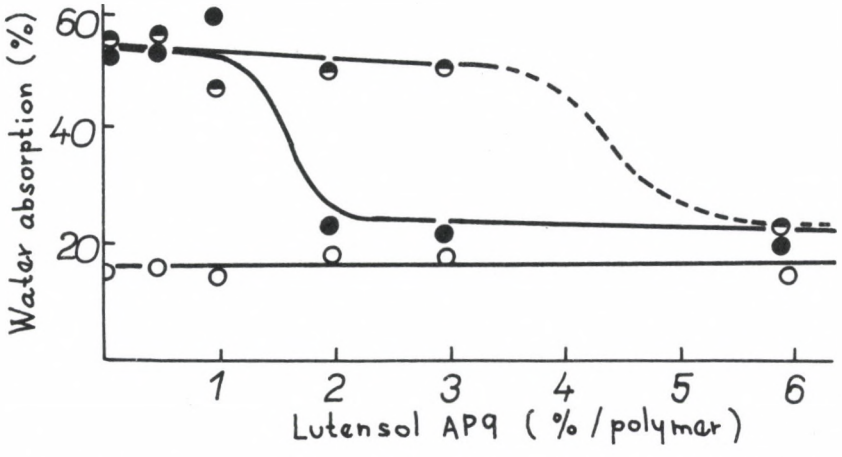

Fig. 5 : Absorption of water after 10 days in relation to the amount of post-added Lutensol AP 9. ○ $\bar{d}$ = 0.56 µm ●◒ $\bar{d}$ = 0.11 µm, ◒ pH = 3.5, ●○ pH = 8.

THE SYNTHESIS OF POLYMERIC CATENA COMPOUNDS BY INTERFACIAL REACTIONS
VI Communication

G. KARAGOUNIS, I.PANDI-AGATHOKLI AND E. KONTARAKI
Laboratory of physical Chemistry of the National Research Foundation. Athens, Greece, Bas. Constantinou 48.

Introduction.

For several years we have been engaged in developing a method for synthetising polymeric catena compounds using the orientating action of interfaces upon bifunctional bipolar molecules.

Catena compounds consist of at least two interlocking ring molecules A and B linked together without a chemical bond between them (Fig.1). They have been prepared by E.Wasserman[1], Lüttringhaus, G.Schill and coworkers[2] in a step by step organic synthesis.[3]

Fig.1.

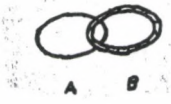

The method we have developed[4-10] leads directly to polymeric catena compounds, that is to a chain of catena molecules consisting of a great number of rings, as shown in Fig.2 for a simplified one dimentional case of two individual rings A and B.

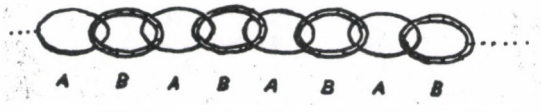

Fig. 2.

The method, is described in detail in the publications mentioned above. It bases upon a threading of aligned long chain bifunctional molecules through a high membered ring compound of at least 18 members and linking the ends of the chainmolecule by a chemical reaction in order to close the ring. Compare the preparation of stable rotaxanes by I.T. Harrison[11-12]

Proofs for the catena constitution of the product

The evidence for a mutual interlocking of the ring molecules by the proposed method of preparation is given by the following observations of the synthetised products:

1) The observed IR spectra of the polymeric products consist of the sum of the IR-spectra of the two constituent interlocked rings. This is proof that the linking between the two ring constituents does not imply a covalent chemical bond.

2) The IR bands of the catena compounds show small shifts (from 4 up to 24 cm^{-1}) in both directions, compared with the IR spectra of the pure rings in the non-interlocked state. These shifts are ascribed to interannular van der Waals forces exerted due to the mutial penetration of the rings.

3) Thorough extractions with various solvents in which at least one of the two rings in the pure state is easily soluble, do not change the intensity ratios of the bands. This proves that the rings are not adsorbates or even mixtures.

4) If the formation of the polymer takes place in the presence of two preformed ring molecules than the IR bands of both rings appear in the IR spectra of the reaction product with varying intensities. This indicates an interlocking of both rings to a different degree.

5) The Debey-Scherrer diagrams of the polymers built up in the presence of a preformed ring molecule show a distingly different pattern compared with that of the polymers prepared in the absence of these rings. Many of the interference lines are absent in the catena compounds while the rest have exactly the same spacing as the pure polymers.

6) The paper chromatograms of the polymers formed show uniform but somewhat broad spots. A great number of chromatograms of the same product have been unified, extracted with solvents and their IR-spectrum taken. It is a superposition of the IR spectra of the two pure ring molecules with the above mentioned small shifts.

7) The gas chromatograms of the catenanes of low molecular weight show a retention time different to that of its constituent ring molecules. Catenanes of high molecular weight do not give gas chromatograms because they are not volatile. On the other hand, as shown by their IR-spectra they contain both ring molecules which in the pure state they give air chromatograms with distinct retention times. This observation excludes the possibility that the two rings are in an absorbed state or exist as mixtures.

8) The molecular surfaces of the monolayer of the catananes, as determined with the aid of the Langmuir balance, are higher than the sum of the molecular surfaces of the ring constituents by a factor 2 up to 3. This is a consequence of the interlooking of the rings. By this interlocking the hy-

drophilic groups, which lie under the water surface in the pure state of the rings, are forced to the surface.

9) In the case one of the rings to be threaded has a center of symmetry we observe that in the catenane the rule of mutual exclusion of infrared and Raman lines does not hold, as all frequences are active. We explain this by the destruction of the center of symmetry by the chain threaded.

A soluble catenane of low molecular weight.

By the present communication we wish to report on the preparation of a catenane built up by the reaction of 1-18-octadecandiol $HO(CH_2)_{18}OH$ with trimethylhexamethylendiisocyanate

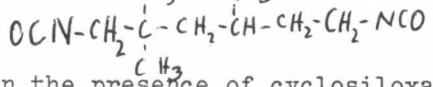

in the presence of cyclosiloxane (mean molecular weight 1144). During the reaction a strong magnetic field (18.000 gauss) is applied. The reaction, which takes place at room temperature, consists in the formation of linear and cyclic polyurethane of various molecular sizes. As the reacting substances are aligned in the magnetic field their exists a definite chance that they be threaded by the present, cyclosiloxane ring. After rigorous extraction with CCl_4, to constant weight, the cyclosiloxane not embodied is removed. From the CCl_4 -solution a small amount (300 mg) of a crystalline substants is isolated. The melting point after recrystallisation from hexane is 83°-95°. Its IR-spectrum consists in a summation of the IR-bands of the urethane and the cyclosiloxane (Fig. 3) and it is similar to the IR spectrum of the high polymer, which was insoluble in CCl_4. The only difference is in the relative intensity of the bands of the two constituents.

The gas chromatographic behaviour.

Table 1 contains the gas chromatographic data of the soluble recrystallized catenane (4), the polyurethane (2), the cyclosiloxane (1) having the mean molecular weight of 1140, and a mixture of the two last substances (1+2). It is evident that by the formation of the catenane compound heavier species having a higher retention time appear. This does not happen with the mechanical mixture of the two substances.

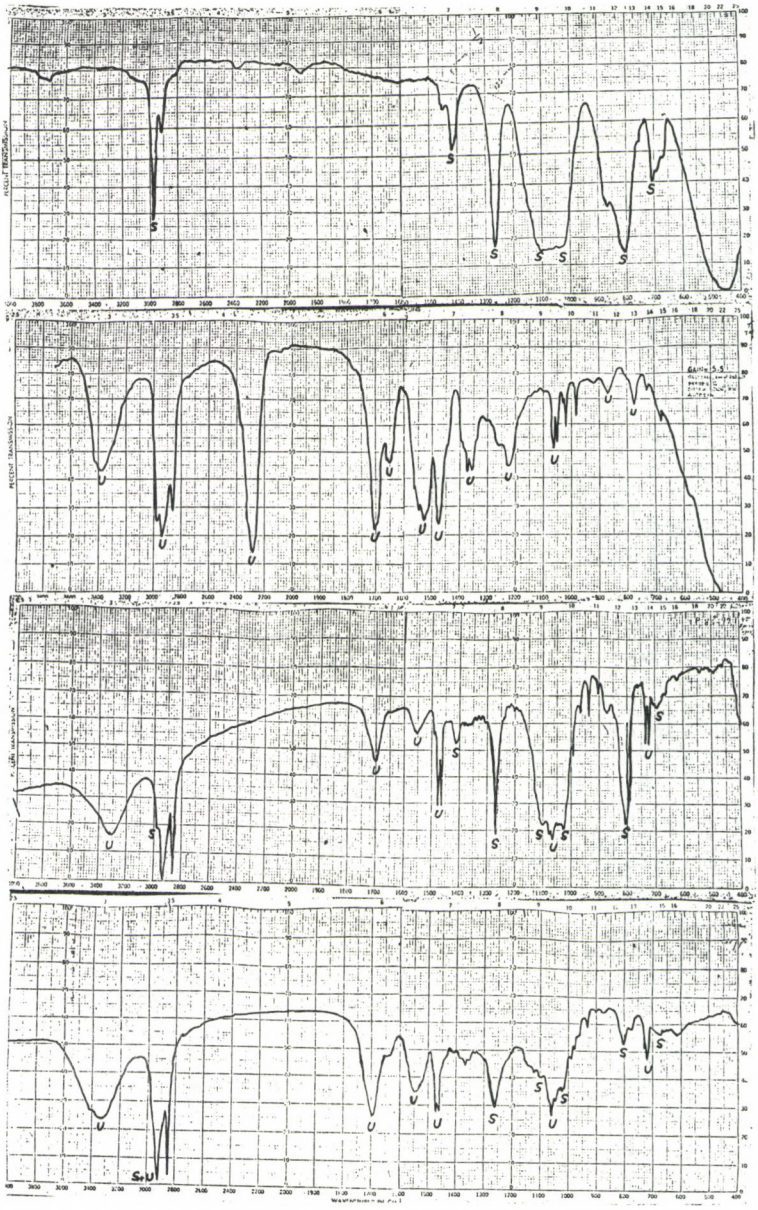

Fig 3. IR-spectra of: I cyclosiloxane, II polyurethane, III catenane of I and II, soluble in hot hexane, IV catene insoluble in hot hexane. S= bands of siloxanrings U= bands of urethanrings.

Table I

Substance	Retention time of the gas chromatographic peaks in minutes			
1. Cyclosiloxane mean Molecular weight 1140	0,60	0,75	1,30	
2. Polyurethane	0,68	0,75	1,06	1,60
3. Mixture of (1) and (2)	0,68	0,75	-	1,60
4. Catenane from Polyurethane and Cyclosiloxane	0,80	1,45	2,50	

Molecular weights

It has been pointed out[10] that osmotic methods are not suitable for the determination of the molecular weights of catenanes. This is because the individual rings are, to a great extent, independant kinetic units so that the resulting molecular weight will depend upon the magnitude of a parameter α which expresses the interannular forces between two rings according to the equation:

$$M_C = \left[1+a(m+n-1)\right] \frac{mM_A + nM_B}{m+n}$$

M_C is the molecular weight of the cantenane, M_A and M_B the molecular weights of the individual ring A and B resp. m and n the number of the rings A and B resp. in the chain. On the contrary the mass spectrographic investigation of the above mentioned microcrystalline product reveals the real molecular weights as the declination of the mass particles in the magnetic field is macroscopic, compared to the molecular motion of the individual rings. The mass spectrogram of the crystalline product contains masses up to 1330 mass units. In the region between 1000 and 1330 five groups appear which differ from one another by 74 mass units (Table II). We assign these peaks, to a mixture of catenanes built up by the interpenetration of the simplest diurethane 30-membered ring.

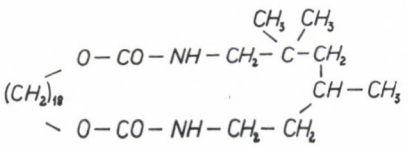

Table II

(1) Group number	(2) Region of masses	(3) Number of lines	(4) Number of isotope combinations
I	1006-1018	6	11
II	1078-1096	9	15
III	1149-1165	9	15
IV	1221-1243	15	17
V	1302-1325 (1335)	10	19

of the mass 496, with cyclosiloxane rings of varying members 14, 16, 18, 20 and 22. The difference between members corresponds to multiples of the group $\cdots Si(CH_3)_2 O \cdots$ which has a mass of 74. This assumption is consistent with the IR-spectra (Fig. 3.)

Each of these mass groups consists of many lines which are due to the possible combinations of the three Si isotopes 28, 29 and 30 in the Siloxane ring. Table II contains the mass regions of these groups (2), the observed number of lines which they contain (3) and the number of the theoretically possible isotope combinations (4). The intensities could be calculated on the ground of the natural abundance of the Si isotopes and they are, in agreement with the observation, statistically distributed round the most probable combination.

We could not obtain a mass spectrum of the high polymer catenane (i.e. of that part which was insoluble in hot hexane) because of its very low vapour pressure. We are engaged in experiments in order to determine its molecular weight by the use of the ultracentifuge.

NMR and Raman Spectra of Catenanes.

The most interesting feature of the NMR-spectra of catenanes containing cyclosiloxan as constituent ring is the appearance of the Siloxan peak circa 80 Herz to higher field compared to cyclohexane as reference. Its exact position varies depending probably on the number of members of the siloxane i.e. of the size of the ring.

The Raman spectrum of the soluble catenane obtained shows not only the Raman bands of the siloxane ring but also its infrared bands. This is most remarcable because the siloxane ring, having a center of symmetry, follows, in the pure state, the rule of mutual exclusion, th.i. transitions that are allowed in the infrared are forbidden in the Raman spectrum and conversely, transitions that are allowed in the Raman are forbidden in the infrared. However by the interlocking of the rings the center of symmetry is to a great extend cancelled so that all bands appear. This is notable because the center

of symmetry is not destroyed by a chemical bond but only by the interannular forces between the rings, which decrease the symmetry of vibrations.

The hydrolytic decomposition of this substance, brought about by heating with 70% HCl for several hours, sets free the siloxane ring (identified by its IR-Spectrum after CCl_4 extraction) with the formation of diaminodimethylhexane. The latter compound was identified by its colour reaction with $CuSO_4$ which is almost identical with that obtained after the HCl hydrolysis of the diisocyanate, with the same salt.

The combustion analysis of the catenanes which contain siloxane rings does not give a real picture of their composition because SiO_2 aerosol is formed which adulterates the carbon and hydrogen values.

LITERATURE

1. E.Wassermann J. Amer. Chem. Soc. Vol. 82, p.4433, (1960).
2. A. Lüttringhaus and G.Isele Ang. Chem. Vol. 79, p.945, (1967).
   G. Schill and A.Lüttringhaus Ang. Chem. Vol. 76, p.567, (1964).
   W. Vetter and G.Schill Tetraedron (London) Vol. 23, 9. 3079, (1967).
3. G.Schill. Catenanes, Rotaxanes, and Knots. Academic Press (1971).
4. G. Karagounis and J. Pandi-Agathokli: Practica of the Athenian Academy of Sciences, Vol. 45, p. 118, (1970).
5. G. Karagounis and J. Pandi-Agathokli: Fourth Conference of the Greek Chemists Association. Athens May 1970.
6. J. Pandi-Agathokli, Doctoral Thesis, Athens 1972.
7. G. Karagounis, J. Pandi-Agathokli and E. Kontaraki: Chem. Chronika Vol. 1, p. 130-147, (1972).
8. G. Karagounis, E. Kontaraki and E. Petassis: Practica of the Athenian Academy of Sciences Vol. 48, p. 197 (1973).
9. G. Karagounis, J. Pandi-Agathokli, E. Petassis and A. Alexakis Folia Biochim et Biol. Graeca 10: 31-41 (1973).

10. G. Karagounis, J. Pandi-Agathokli, E. Kontaraki and D. Nikolelis: Practica of the Athenian Academy Dec.1974(in press).

11. I.T. Harrison and S. Harrison, J. Amer. Chem. Soc. 89, 5723 (1967).

12. I.T. Harrison J.C.S. Chem. Comm. 1972, p. 231. J.C.S Perkin I 301 (1974).

TRIBOLOGY AS A BRANCH OF SURFACE CHEMISTRY

E. Vámos

NAKI, High Pressure Research Institute,
1368 Budapest, Pf. 208., Hungary

A substantial feature of friction, wear and lubrication processes occuring in machine-parts is, that they proceed at the surface layers or in their vicinity.

In mechanical engineering practice metallic surfaces are considered to be perfectly smooth and homogenous. Real surfaces however are neither smooth nor homogenous but rough, porous and varying in physical and chemical properties. In consequence the real surface of metallic parts, even if machined with utmost care, is larger than its geometrical surface and their behaviour is influenced by their morphology /1/.

The free energy of the ions, atoms or molecules at the surfaces, but especially at the surface peaks is known to be larger than that of particles in the bulk. This presents itself with liquids and solid surfaces e.g. in the form of surface tension and with ionic materials as surface electric charge too. One manifestation of the effect of the surface energy at boundaries is sorption /chemisorption or adsorption/. Through sorption secondary surfaces e.g. oriented or diffused sorption layers arise. Thus the surfaces differ not only by the energetic condition but often also from the point of view of the chemical composition from the bulk of the phases, between which they form a boundary. The same phenomenon occurs when reaction layers are formed at solid surfaces, e.g. by oxidation. These basic facts are often

neglected in lubrication engineering practice. The deviations observed in the chemical composition of the surfaces as compared to the bulk, are traceable to other phenomena too. Due to processes in the course of cooling, the surfaces of the alloys may be richer or poorer in certain components, than the bulk of the alloy. The chemical composition of heat-treated surfaces always differs from the bulk composition of the metal, e.g. carbon content of steels is usually lower due to surface oxidation.
Also physical properties of the surfaces differ from the bulk of the material /1,2,3/. Crystallographic and rheologic properties, for instance hardness of solid surfaces are substantially different from the properties of the bulk.
Becaues of the higher free energy of virgin metallic surfaces reaction rates are greater at the boundary than in the phases surrounding them.

Effect of the relative motion of contacting surfaces

According to lubrication-engineering experiences the processes occuring at the surface are greatly influenced by friction and wear. Temperature of the surfaces changes as a consequence of heat of friction. Temperature differences in time and space will increase as compared to the state of rest. As an example the temperature flashes and hot spots appearing in the course of dry friction and boundary lubrication may be mentioned. The temperature of these hot spots may reach 500 to 1000 ^{o}C, while the bulk of the metal is as cool as 30-60 ^{o}C. However the duration of such temperature flashes is of the order of magnitude of 10^{-3} sec. Thus the surface under friction is not only subjected to great temperature differences but also to the quick time fluctuations of the temperature distribution /4,5/. Figure No 1 shows a typical spatial temperature distribution diagram at a given time, figure No 2 a time distribution diagram at a given point of the surface.
The morphology of the surface is modified during friction

processes. Due to frictional processes, the surface peaks are deformed to an extent depending from the kinetic energy of the impact. Deformation may be elastic or plastic. Following an impact of appropriate speed and kinetic energy, rigid breakage of surface peaks may occur too. In the course of these deformations the crystal structure of the surface changes. The successive elastic deformation vibrations may lead to the growth of the surface crystals /recrystallization/.

Plastic deformation causes cold hardening. Because of deformation, policrystals containing numerous lattice defects and even amorphous layers may arise at the surface. Typical phenomena of this type are the formation of Beilby layers during the running in of piston engines and gears. Due to these phenomena physical properties of the surface layer, e.g. its hardness, elasticity, crystal structure etc. are changed. Simultaneously the free energy and potential catalytic effect of the surface layer, containing numerous lattice defect spots or even being amorphous, will increase as compared to the static state. This effect of impacts on surface layer structure has been demonstrated by Heinicke /6/.

The rate of physical and chemical processes occuring at the surface increases with friction. For the sake of distinction from the frictionfree surface processes these surface-chemical and physical processes are called tribosorption, tribodiffusion, tribocorrosion, tribocatalysis, etc. respectively /7,8,9,10/.

Potential causes of increasing reaction rates at surfaces in contact and relative motion, are among others the above mentioned hot spots by which reaction chains in the fluid phases surrounding the rubbing surfaces are initiated.

Another possible source of increase of reaction rates may be explained by considering the structure of technical metallic surfaces. /Figure 3/. As may be seen technical metallic surfaces are practically never really metallic. They are covered usually by an oxide layer and an adsorbed layer, consist-

ing of the substances of the environment, e.g. water and CO_2 in the case of dry friction, or lubricant or additive components in the case of liquid or boundary lubrication. However if rupture of sorbed layers occurs due to friction and wear or adsorbed and oxide films are carried off by abrasion, the true virgin metallic surfaces appear. These have substantially higher surface energies than technical surfaces. As a consequence e.g. friction factor of technical copper, being about 0,3-0,5 increases, if protective layers are broken through and if high vacuum is produced /e.g. under space conditions/ to 8,0 that is, by one order of magnitude /1/. It is interesting to note that catalytic activity of metallic surfaces, if surface layers are broken through by tribological effects /e.g. shake-impacts or high friction/, increases usually also by approximately one order of magnitude, as shown in Table 1. Some of the detrimental consequences of this tribocatalytical activity in lubrication is increased rate of oxidation of metals, due to vibration, called fretting corrosion, and causing special difficulties in transport activities. Another phenomenon is lubricant degradation due to increased oxidation rate of oil, or decomposition rate of additives due to tribocatalytic effects.

Table 1

Examples of apparent activation energies of tribochemically activated reactions as compared to unactivated processes /11/

Reaction	Apparent activation energy $E^{\ddagger}$ kcal/mol tribologically activated	unactivated
$Ni+4CO \rightarrow Ni/CO/_4$	2,1	10,2
$Fe+O_2 \rightarrow$ iron-oxides	0,32	13
$C+2H_2 \rightarrow CH_4$	2	30
$CH_3OH \rightarrow CO+2H_2$	3-5	35
$C_6H_6+3H_2 \rightarrow C_6H_{12}$	6	10,6

Another detrimental effect of tribological phenomena during lubrication is tribodesorption of adsorbed layers. This occurs when oriented adsorption layers of semipolar oiliness

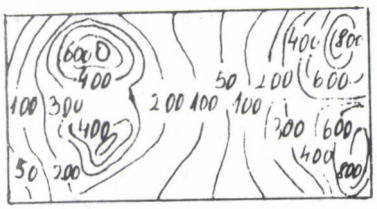

Fig.1 Spatial temperature distribution /in °C/ at a rubbing surface

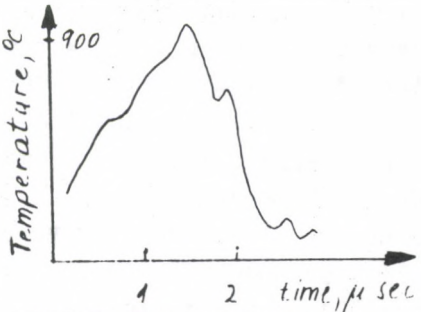

Fig.2 Temperature change with time at a hot spot

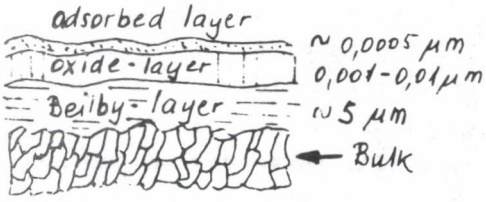

Fig.3 Layer structure at metallic surfaces

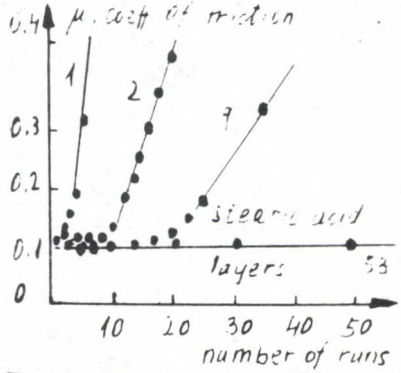

Fig.4 Tribodesorption of stearic acid at a steel surface

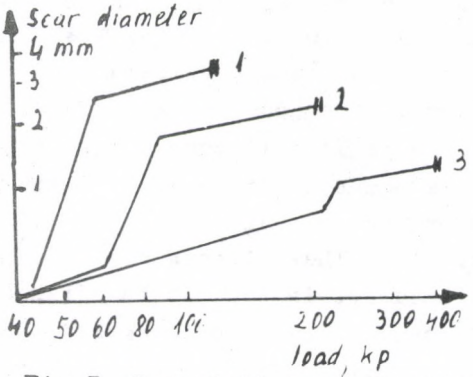

Fig.5 Four-ball test of spindle oil with and without additives 1./ oil; 2./ 1wt% chlorinated paraffin; 3./ 1,8wt% chlorinated and sulphurized oleic acid

Table 2
Temperatures of acid formation determined by derivatography

H_2S	~ 230 °C	starting temperat.
HCl	~ 260 °C	"
HCl+H_2S	~ 330 °C	end of acid formation

improving additives /alkylamines, fatty acids, fatty alcohols/ are used in boundary lubrication. These form oriented polymolecular adsorption layers on metallic surfaces, thus protecting them from wear at high loads. With increasing load and shearing stress the number of molecular layers decreases even if no change of temperature occurs, as shown in Figure 4, based on the experiments of Bowden and Tabor /5/. At sufficiently high load the adsorption layer is fully carried off and metallic contact, leading to wear by scuffing occurs. If the load is extremely high, organic lubricating films become unefficient and abrasive wear will give place to the highly detrimental phenomenon of scuffing. Scuffing consists in welding of contacting peaks of the metallic parts. The welded micro-joints are ruptured by the motion of the surfaces, causing quick degradation of the surfaces. If load is sufficiently high, extensive areas will be welded and motion has to stop. If the energy of the motor is sufficiently high, this resistance of the welded surfaces to motion will result in breakage of the machine part /1,2/.

A solution of this problem is, to produce nonweldable surfaces e.g. by chemisorbed layers. To this end Cl, S and P containing organic additives are added to lubricants. When load rises and lubricants film rupture occurs, temperature flashes and hot spots will appear at the contacting surfaces. Due to this, the above mentioned organic compounds decompose, to yield HCl, H_2S or H_3PO_4 or analogous acids, reacting with the virgin metallic surface to produce a chemisorbed chloride, sulphide or phosphate layer /12/. These layers are unweldable, and thus scuffing will cease. As soon as this takes place, number of temperature flashes /and surface temperature/ will diminish and therefore further development of acids will cease, as long as a uniform chemisorbed layer exists. If however the chemisorbed layer is carried off by abrasion, number of temperature flashes will rise again, and the virgin metallic surface will again be covered by a protective layer. Thus these EP additives form a selfcontrolling system, which starts and ceases functioning at a limit-

ing temperature, being identical with the threshold temperature of decomposition of the EP additive.

Threshold temperatures of some characteristic EP additives were determined by us using the derivatographic method. Welding-loads of lubricants without additives, and containing the above additives respectively were determined by the four-ball apparatus. Figure 5 shows some of the results. /See Tab.2/

Summarizing, these and similar phenomena of friction, wear and lubrication lead to the concept, that a new branch of science has to be established, dealing with the friction, wear and lubrication in machines, and taking into consideration, that surface phenomena are changed if friction takes place. This new branch of science has been called by the Institute of Mechanical Engineers /London/ tribology, from τριβειν and λογοι /8,13/.

Now, considering that friction and wear is not limited to metallic surfaces and machine parts, it may be suggested, that the concept of tribology should be extended to all types of friction and wear, as it is certain, that special behaviour of contacting surfaces is not limited to metals and machine parts.

Some other potential applications of tribological concepts are: friction of tyres, brakes, finishing of precious stones, erosion of rocks and soil, behaviour of bone joints, agriculture, tribocatalysis in chemical industry, wear of textile fibers, leather, asphalt, wood, concrete; petroleum drilling, grinding of cereals, optical glass etc. This shows, that tribology is a general branch of surface science, not limited to lubrication.

Literature

1. E.Vámos: Elméleti kenéstechnika /Tribológia/ Vol.I-III. MTK Int., Budapest 1969-71.
2. G.H.Göttner: Einführung in die Schmierungstechnik. Karl Marklein Verlag, Düsseldorf 1961 and 1966.

3. R.Houwink: Elastizität, Plastizität und Struktur der Materie. Dresden 1950.
4. F.P.Bowden, D.Tabor: Reibung und Schmierung fester Körper. Springer Verlag Berlin, Göttingen, Heidelberg, 1959.
5. F.P.Bowden, D.Tabor: Friction and Lubrication. Methuen & Co. Ltd. London 1967.
6. G.Heinicke: Schmierungstechnik 3, 65 /1970/
7. R.W.Heinemann: Untersuchungen über tribomechanisch angeregte Festkörperreaktione. Hannover 1967.
8. E.Vámos: Ropa a Uhlie, 5, 257 /1971/
9. X.Liebl, E.Vámos: Kőolaj és Földgáz /Petroleum and Natural Gas/ 5,/105/, 3, 85 /1972/.
10. H.Hofmann: Wiss.Z. der Hochschule für Maschinenbau, Karl Marx Stadt 3, 259 /1960/.
11. P.A.Thiessen, K.Meyer, G.Heinicke: Grundlagen der Tribochemie, Akademie Verlag, Berlin, 1967.
12. E.Vámos, Z.Adonyi, G.Kőrösi, I.Valasek: Ropa a Uhlie, 16, 1, 46 /1974/.
13. Editor: Tribology in iron and steel works. Edit.Inst. of Mech.Engr. London, 1967.

EFFECT OF BEATING ON SORPTION CAPACITY OF BLEACHED SULPHATE PULP

H.Máttyus[x], I.Rusznák[x], L.Gy.Nagy[xx], P. Lengyel[xxx], J.Gajari[xxxx]

x Technical University , Budapest, Hungary

Organic Chemical Technology Department

xx Technical University Department of Physical Chemistry

xxx Pulp and Paper Research Institute Budapest

xxxx Technical University, Institute of Agriculture Chemical Technology

Introduction

Beating of pulp fibres in water produces in paper a higher tensile strength , density, somewhat lower tearing strength , opacity and a number of other changes in physical properties. These modifications are caused by changes in the surface characteristics of individual fibres/1,2/ , such as hydration, swelling, collapse, fibrillation and cutting. All these processes are in connection with the increased specific surface area of fibres measured by nitrogen adsorption. /3/

The aim of our work was to compare the sorption capacity in dry and wet conditions of the fibres before and after beating. We have also studied whether it was possible to characterise the quality and quantity of interactions between liquid and fibres measuring integral immersional heat or the kinetics of wetting respectively.

Experimental

Pulps

Commercial bleached sulphate pulp was investigated by different methods. The air dried pulp was partly slushed in water, partly beaten in Jokro mill. Both samples were dried by solvent exchange applying methanol-n-hexane succesively. The latter was removed in vacuum at room temperature.

Methods

Crystalline region was studied by X-ray diffractometry. /Mikrometa-2, Chirana/

B.E.T surface was measured by sorptometer./4/

Porosity of pulp was determined by applying a mercury porosimeter./Carlo Erba/

Surface excess isotherms were measured at 25°C from completely miscible non-electrolyte liquids. The solid-liquid ratio was about 1:10. The concentration change caused by the adsorption was determined by measuring the refractive index of solutions before and after adsorption process, that took place by agitating the system for 48 hours. Adsorption capacity of samples was calculated by the graphical method of Nagy and Schay /5/. About thirty points were enough to draw the isotherms.

Immersion heat measurements were carried out using a quasi adiabatic microcalorimeter, the dead time of which, measured by prompt neutralization of HCl and NaOH using magnetic stirrer, was not more than 30 seconds. The sensitivity of the calorimeter is better than 0,05 cal. The applied liquids were the following :water, methanol, n-butanol, n-propanol-, benzene and n-hexane.

Results and discussion

Characteristic parameters of fibres in dry condition are summarised in Table I. Data given in Table I. show that commercial beating process results no significant change in the amount of crystalline regions, but the B.E.T surface area increased considerably. Other authors'/6/ data were similar except those of Stone and Scallan. /7/, which were higher.

On account of fibrillation the pore diameter increased significantly too.

Table I. Characteristic parameters of fibres measured in dry condition of the pulp

Method	before beating /14 SR°/	after beating /73 SR°/
crystalline region %	54,5	52,4
B.E.T surface are m^2/g	0,99	4,58
porosity ml/g	0,92	0,98
volume of pores with radii greater than 1 μ m	2 %	4o %

For characterising pulp fibres in "wet" condition surface excess isotherms were measured from completely miscible non-electrolyte liquids. The applied systems were the following: methanol-benzene, benzene-n-propanol, n-hexane-benzene. The three surface excess isotherms can be seen on Fig. 1 .

Figure 1. shows, that selectivity of adsorption increases with increasing difference in polarity of the components. The type of isotherms changed from I to III in the classification of Schay and Nagy. Equivalent surface areas calculated from sorption capacity data and surface area requirement of adsorbed molecules are as follows : 14o6 m^2/g , 1oo8 m^2/g and 1o4o m^2/g , in due coarse of isotherms,1.2. and 3. / $a_{m,methanol}$ 94 m^2/millimole , $a_{m,benzene}$ 18o m^2/millimole, $a_{m,hexane}$ 13o m^2/millimole/ From these data it can be concluded that equivalent surface area is about the same measured by non swelling liquid pairs, curve 2 and 3. Equivalent surface area is a considerable higher value than B.E.T surface area. This is due to the better penetration of liquids into the "amorph" region of the fibres, the total covering and liquid bound with secondary forces. Both polar and non-polar molecules

are adsorbed on pulp fibres. It can be explained by the double character of cellulosic fibres, containing polar and non polar planes as well.

Data given in Figure 2. and Figure 3. show the effect of beating on the adsorption capacity of pulp measured from methanol-benzene and n-hexane-benzene system respectively. The ratio of the adsorption capacities were 1,37 and 1,21 respectively. No such significant change of adsorption capacity could be noticed in "wet" condition of the fibres due to the beating, as in the case of using the B.E.T method. For production purposes however the behaviour of pulp immersed in liquid is more interesting.

Exotherm heat effect accompanying wetting and swelling of the fibres using liquids of different polarities were characterised by the integral heat evolved for 15' and heat vs. time curves.Integral data are to be seen in Table II.

Table II. Immersion heat values of pulp fibres wetting with liquid of different polarity , before and after beating.

liquid	immersion heat in cal/g	
	14 SR^{o}	73 SR^{o}
water	12,8	12,7
methanol	1o,4	11,5
n-propanol	6,8	7,4
n-butanol	3,3	4,5
benzene	2,6	2,7
n-hexane	0,7	0,7

No significant difference was noticed either in strongly or weakly swelling agents,between fibres before beating and after it. Kinetic data given on Fig. 4,5,6 and 7 show however considerable differences depending on the degree of beating and drying applied before the measurement. Vacuum drying resulted in and increased degree of associations of

the fibres. Initial lower exotherm heat effect and shape of curves on Figure 5. and Figure 6. support the theory of new bonds.. Methanol as swelling agent easily breaks up these bonds while n-propanol and n-butanol did not. Data measured in the case of methanol were evaluated formal kinetically. Figure 7. shows the heterogenity of unbeaten pulp and the uniformity of fibres after beating.

Literature

1. S.Annus, Rostok fajlagos felületének vizsgálata, Papiripari Kutató Intézet Közleményei 6o-1o29, Budapest, 196o
2. H.W.Giertz, The effects of beating on individual fibres " Fundamental of papermaking fibres" Conference . Cambridge, 389-4o5 /1957/
3. Rennel,J. Svensk.Papperstidn. 72 1-8 /1969/
4. Heiszmann,J.; Petro,J. ; Tungler,M.; Csürös,Z. Magyar Kém.Foly. 8o 556 /1974/
5. Schay,G.; Nagy L.Gy. J.Colloid.Interface.Sci. 38 3o2 / /1972/
6. W.R. Haselton.; Tappi, 37 4o4 /1954/

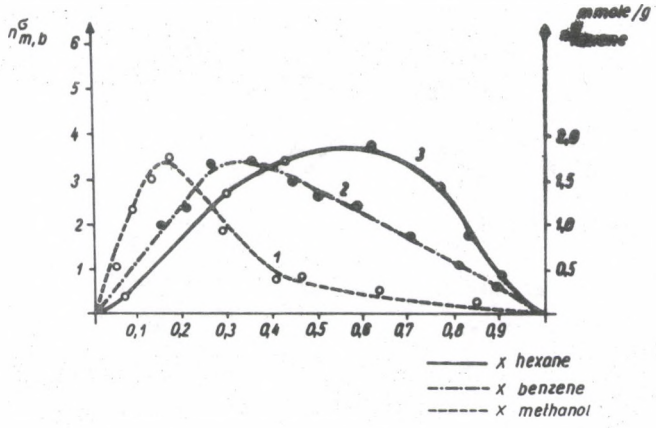

Fig.1 Surface excess isotherm of methanol-benzene /1/, benzene-npropanol /2/ and hexane-benzen system on pulp before beating. 25 °C

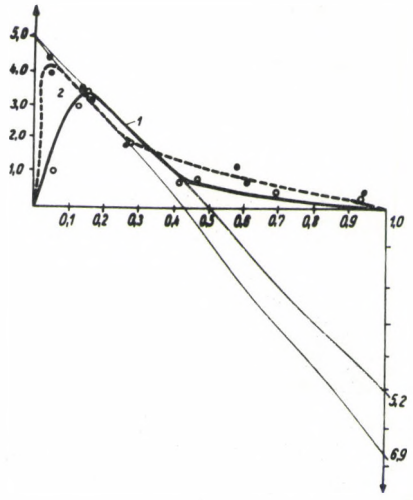

Fig.2. Surface excess isotherm of methanol-benzene system on unbeaten /1/ and beaten pulp /2/ at 25°C.

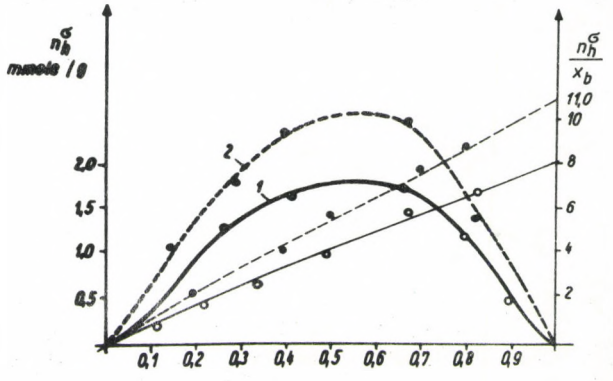

Fig.3. Surface excess isotherm of n-hexane -benzene system on unbeaten /1/ and on beaten pulp/2/ at 25 °C.

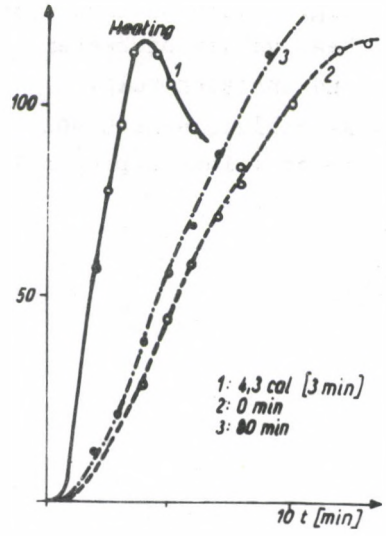

Fig.4. Heat of immersion process in cellulose-n-butanol system. Cellulose was dried in N_2 stream.

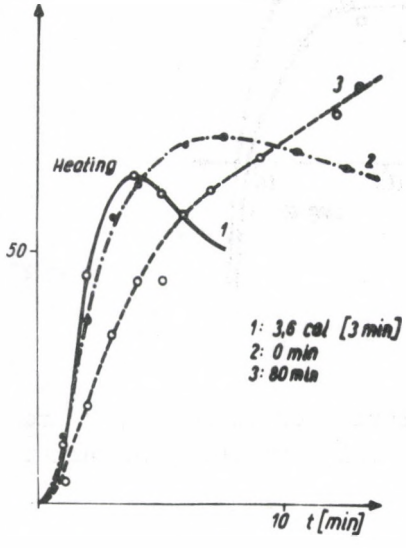

Fig.5. Heat of immersion process in cellulose-n-propanol system. Cellulose was dried in vacuum at 25° C.

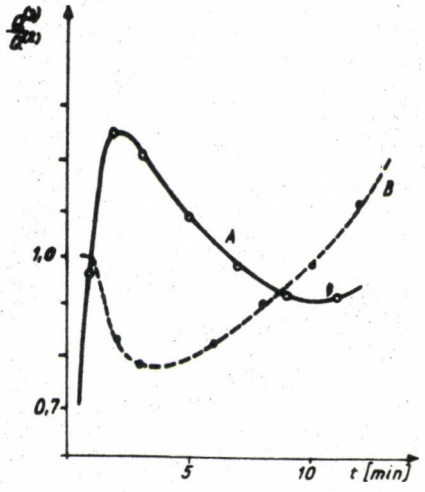

Fig.6 Ratio of immersion heat values of beaten and unbeaten pulp.
A- cellulose-methanol
B- cellulose-n-propanol

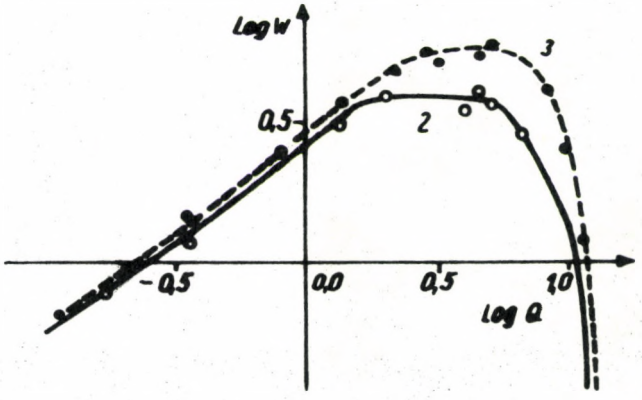

Fig.7 $\log \frac{\Delta Q}{\Delta t}$ - log Q function of unbeaten /2/ and beaten /3/ pulp in methanol. Pulp was dried in vacuum at 25° C

THE ROLE OF ADHERENCE IN THE PREPARATION OF PHOSPHOR COATING OF FLUORESCENT LAMPS

V. Fraknóy-Kőrös and K. Lutter

TUNGSRAM Research Institute, 1340 Budapest, Váci ut 77, Hungary

The luminescent layer of low-pressure mercury discharge lamps is prepared generally by applying an organic suspension of the phosphor containing a binder to the walls of the glass bulb. The most often used solvent is butylacetate and binder nitrocellulose. The suspension is prepared by milling in a ball mill in order to secure the proper adherence of the luminescent coating. In the manufacture of fluorescent lamps the binder is removed from the coating by its burning out.[1] The required adherence of the coating has been achieved earlier by milling the phosphor for a prolonged time which resulted in the formation of large amount of fine particles. The larger is the quantity of the fine particles, the better is the adherence of the coating to the glass bulb. It is well known on the other hand that an increase of the percentage of fine particles affects adversely the optical properties of the luminescent powder: increases the light reflection and so reduces the light efficiency.[2] Thus at the preparation of coating a compromise is necessary between the good adhesive and optical properties.

Further improvement can be achieved by adhesion-increasing effects which are independent of the milling. There are 3 possibilities to improve the adhesion according to the previous consideration:

1/ to change the nature of the binder,

2/ to alter the properties of the glass surface,

3/ to mix an additive to the suspension.

In respect of practical implementation we were concerned with possibilities related to point 3/. The additives tested can be included in two groups:

1/ additives insoluble in the dispersion medium,

2/ additives soluble in the dispersion medium.

As solid additives silicon dioxide, aluminium oxide and barium metaphosphate were applied. The soluble additives include organic and semiorganic - oxygen and halogen containing - silicon compounds and silicon resins. The characteristic data of the additives are compiled in Table I.

Table I.

Additive: Chemical composition	Additive: Industrial name	Spec. surface area m^2/g	Mean value of particle size
SiO_2	Degussa Aerosil R972	120 ± 30	10-30 nm
Al_2O_3	Degussa Alox VGA	~10	< 1 /um
$Ba/PO_3/_2$	prepared by us	0.45	10.2 /um
$/C_2H_5/_2Cl_2Si$	SISS Primer	-	-
Silicone resins	SISS Resine	-	-
	SISS Vernis	-	-
$Si/OC_2H_4Cl/_4$	prepared by us	-	-

In the different phases of the preparation of coating the following types of adhesion are important:

"Wet adhesion" plays an essential role at the application of the coating to the surface. This is influenced by the composition of the suspension.

"Dry adhesion" is significant after burning out of the binder. This is affected both by the properties of the phosphor and the glass surface.

The additives both in solid phase and dissolved in a solvent can alter the extent of both types of adhesion. Here we report on our investigations concerning the influence of various types of additives on the wet and dry adhesion, respectively.

Wet adhesion was measured by two methods. The adhesion forces existing between the phosphor particles and the glass surface were measured by the rupture angle method of Buzágh; those existing between particles by measuring the sediment volume.[3]

The rupture angle was measured as follows: on a glass plate, corresponding to the glass composition of glass bulbs, a monodisperse monolayer was deposited and the glass plate inclined gradually. The rupture angle / α / is that angle at which the homogeneity of the layer just breaks, i.e. a certain proportion of the particles in the layer slips down. $\sin\alpha$ is proportional to the specific adhesion of the phosphor to the glass plate.

The sediment volume /V/ which was measured in graduated test tubes after 24 hours sedimentation is the larger the greater is the adhesion between the particles.

After burning out of the coating dry adhesion was measured in two ways.

In the "blow off" method through an orifice of 1 mm in diameter and inclined to 45° in respect to the surface of the coated luminescent tube, air is blown on the surface. At a certain air pressure the coating facing the orifice is blown off. This air pressure gives the characteristic adhesion value in torrs.[4]

The measurement of "peeling off" is an empirical method. In this method the diameter of decoated area occurring by the effect of a well-defined mechanical impact gives the characteristic value.

Results and discussion

The results are given in Figs. 1-6. On Figs. 1-3 the sediment volume, specific adhesion and adhesion value data are plotted against the concentration of the solid additives. Figs. 4-6 give similar plots, however, in respect of the additives dissolved in the dispersion medium.

From the measurement data it can be concluded that the adhesion-increasing effect of solid additives silicon

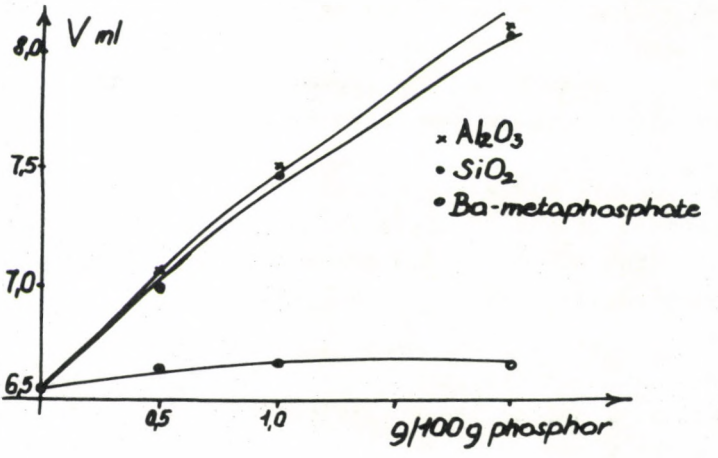
V ml
8,0
7,5
7,0
6,5
0,5
1,0
g/100g phosphor
× Al_2O_3
• SiO_2
• Ba-metaphosphate

Fig.1

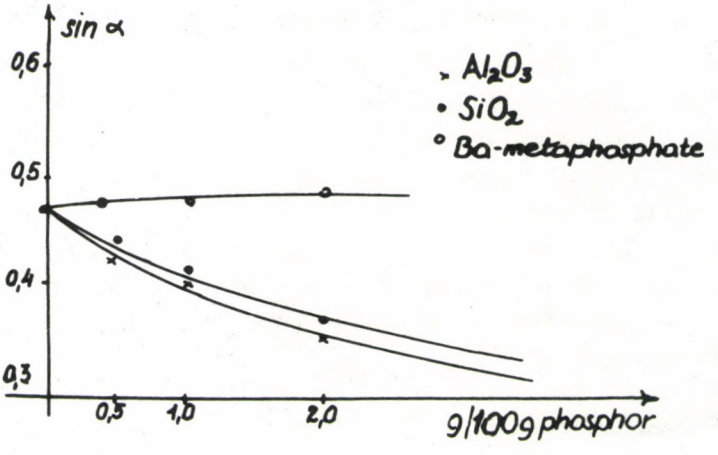
sin α
0,6
0,5
0,4
0,3
0,5
1,0
2,0
g/100g phosphor
× Al_2O_3
• SiO_2
° Ba-metaphosphate

Fig.2

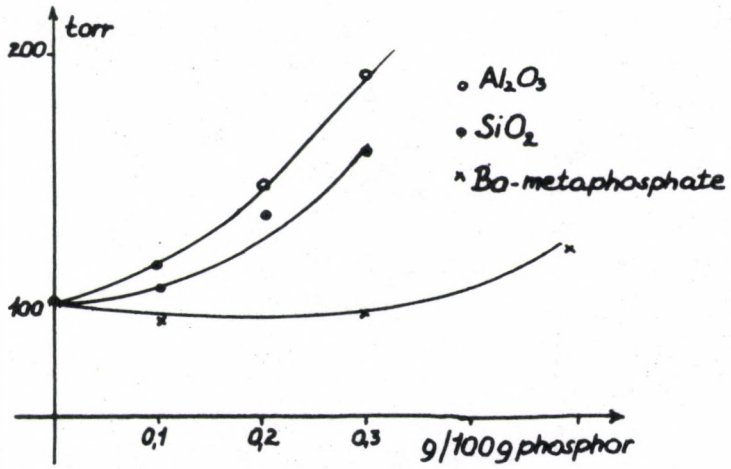
torr
200
100
0,1
0,2
0,3
g/100g phosphor
Al_2O_3
SiO_2
Ba-metaphosphate

Fig.3

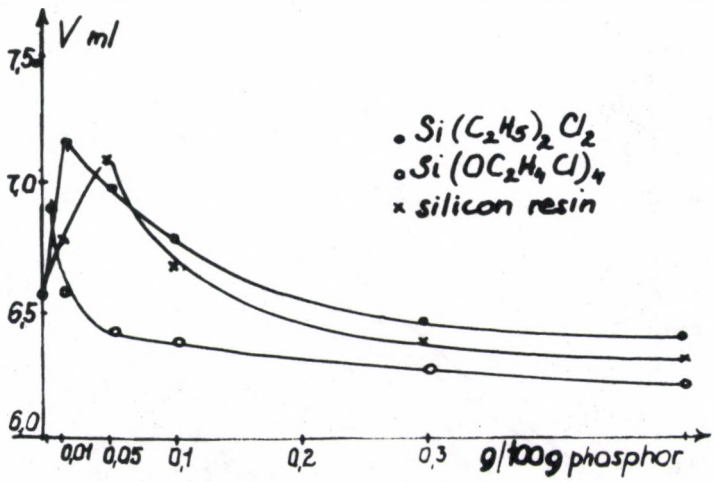
V ml
7,5
7,0
6,5
6,0
0,01
0,05
0,1
0,2
0,3
g/100g phosphor
$Si(C_2H_5)_2Cl_2$
$Si(OC_2H_4Cl)_4$
silicon resin

Fig.4

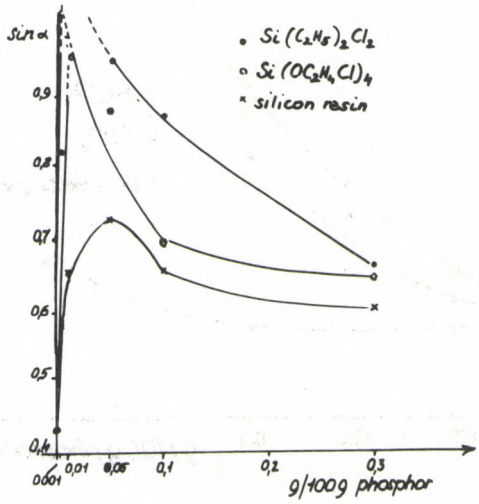
sin α
0,9
0,8
0,7
0,6
0,5
0,4
0,001
0,01
0,05
0,1
0,2
0,3
g/100g phosphor
Si (C2H5)2 Cl2
Si (OC2H4Cl)4
silicon resin

Fig.5

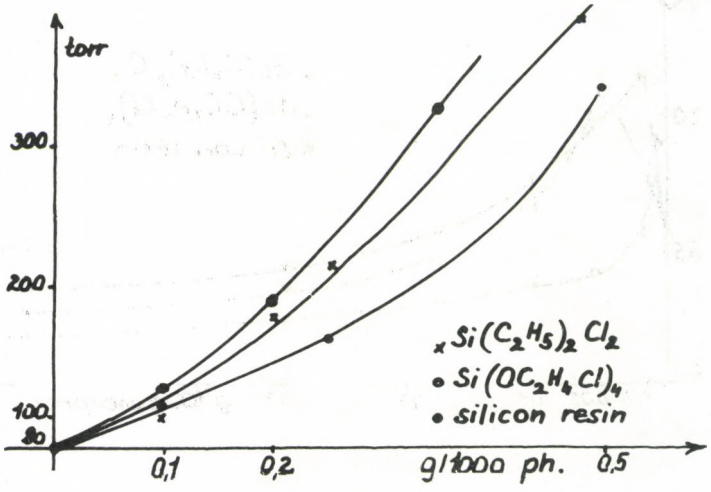
torr
300
200
100
80
0,1
0,2
0,5
g/1000 ph.
Si(C2H5)2 Cl2
Si(OC2H4Cl)4
silicon resin

Fig.6

dioxide and aluminium oxide appears only in the sediment volume data characteristic of the adhesion between the particles. The specific adhesion calculated from the rupture angles indicate a decrease in the adherence to the glass wall. Though the adhesion value of the luminescent coatings increases, the peeling off values remain unchanged indicating that from the practical point of view these solid additives are unfavourable.

The barium metaphosphate additive has no or very small influence on both wet and dry adhesion values.

By the increase of the amount of soluble additives both the rupture angle and the sediment volume show maximum curves. In both functions the maxima appear at the same concentrations of the individual compounds. After the maximum the sediment volume drops below the value measured without any additive. These additives increase considerably the adhesion value of the luminescent tubes and at the same time reduce the diameter of the peeling off area. This type of additives should be applied, however, only in definite concentration interval, their greater quantity has unfavourable effects.

The effect of the two types of additives - as it can be seen on the figures - differs from each other considerably.

Solid additives which are consisted of very small particles / < 1 /um/ compared with the phosphor grains greatly increase the adhesion between particles. In the same time, however, due to the great adhesion, aggregates are formed in the suspension and for this reason the adherence of the phosphor particles to the glass wall is reduced. This explanation is supported by the fact that barium metaphosphate grains in the same particle size interval as that of phosphor show no measurable effect.

In the case of soluble additives during the preparation of coating - due to hydrolysis and thermal effect - the compounds decompose. Between the phosphor and the glass surface - Si-O-Si - layer is formed and this assures the adherence between the glass surface and the phosphor grains. Adhesion

between grains increases also to a certain value, after the maximum, however, the function shows an abrupt decrease. It means that a desaggregation process occurs and seemingly the appearance of the coating is improved. This latter fact and the maxima on the curves indicate that the influence can be related to the adsorption of the additives on the phosphor grains. The extent of adsorption varies with the chemical composition of the additive molecules. The continuously improving adhesion and peeling off values indicate that the - Si-O-Si - layer formed on the glass surface by thermal treatment preserves its adhesive properties.

References

1/ W.Elenbaas, Fluorescent Lamps, MacMillan Press Ltd., 1972.

2/ A.H.McKeag, Trans.Ill.Eng. 25, 41 /1960/.

3/ A.Buzágh, Kolloid-Z., 52, 46, /1930/.
A.Buzágh, Kolloid-Z., 79, 156, /1937/.

4/ D.W.Jordan, Brit.J.Appl.Phys., Suppl.No. 3., 194, /1954/.

ION - EXCHANGE STUDIES IN SOIL COLUMNS

M. Rédly

Research Institute for Soil Science and Agricultural Chemistry of the Hungarian Academy of Sciences. Budapest, Hungary.

From the viewpoint of surface chemistry, soil can be considered as a polydisperse system, having solid, liquid and gaseous phases. Main soil properties determining the fertility, are affected by the surface conditions of the solid phase as well as by the equilibrium between the concentration and composition of ions in the soil solution, and those adsorbed on the surface of soil particles.
The study of surface phenomena have had an ever-growing importance in the development of soil science /7,8,9/.
Water soluble salts, especially sodium salts are responsible for the undesirable physical, chemical, biological properties and low fertility of salt affected /saline and alkali/ soils. These soils can be characterized by the accumulation of sodium ions in the soil solution and/or on the surface of soil colloid particles. Both general problems such as: evolution and genesis of salt affected soils, and practical problems - interactions between soil and water in the course of irrigation - or reclamation of alkali soils /i.e. the amelioration of soil properties by the exchange of adsorbed Na ions by Ca /require the description of an exchange process of heterovalent cations /Na^+ and Ca^{2+}/ taking place between the solid and liquid phases of the soil.
Soil salinization and alkalinization processes are always in connection with the movement of different sodium compounds in the soil profile /14./ The exchange of cations during the

flow of solutions, can be studied in soil columns. The laws found for ion-exchange chromatography in ionic separation processes of synthetic ion-exchanger resins, were applied with certain simplifications and approximations to study ion transport processes in soils. The model of de Vault /16/ was applied by Rible and Davis /13/ for studying ion-exchange reactions in soil profiles. Hiester and Vermeulen's /10, 17/ theoretical model, based on the kinetic theory of the reversible second-order reactions was used by Bower et al. /1/, for the description of ion-exchange processes in soil columns treated with electrolyte solutions. Several simplified analytical solutions of chromatographic models have been elaborated for calculating the amount of adsorbed sodium cations in the different depths of columns /5,6/.

Model experiments were carried out to study the vertical distribution of Na-ions in Ca saturated soil columns equilibrated with percolating NaCl solutions.

The vertical distribution of sodium ions was studied by using isotope technique.

Experimental

The 0,5-2 mm particle size fraction of the upper horizon of a Ca saturated chernozem soil was used in the model experiments.15 cm high soil columns were prepared by uniformly packing known weights of air-dried soil sample into plastic tubes with 2,2 cm internal diametre, and having an outlet tube and stopcock to control the flow. A plastic screen covered by filter paper was placed in the bottom of the tube before filling.

The concentration of equilibrating NaCl solutions was between 5.10^{-3} and 1.10^{-1}N. The flow rate was 0,4 cm/h. 3 cm high constant head of solution was set up on the top of the column. The percolation was carried out until reaching dynamic equilibrium i.e. reaching the same Na^+ concentration in the influent and effluent solution. The distribution of Na-ions in the different depths of the columns was studied in two ways:

1./ NaCl solutions labelled with Na-22 of the same concentration as the equilibrating solution, had been percolated through the column until the activity became measurable in the effluent.

The activity of each centimetre of the column was measured outside, without destroying the column itself, using a heavily shielded γ detector /EKCO N 618 type/. The activity of each layer was expressed as the percentage of the total activity added to the column.

2./ After equilibration with NaCl solutions, the soil columns were sectioned into 1 cm thick layers. The total amount of Na^+ and exchangeable Na^+, the total amount of Ca^{2+} and exchangeable Ca^{2+} was determined in each section with the isotope dilution method by the analysis of 1:10 soil-water suspension using Na-22 and Ca-45 /2,3,11/. The moisture content was determined with thermostat method.

One column equilibrated with 1.10^{-2} N NaCl solution was labelled with Cl-36. After sectioning the column, the activity of 1 cm thick layers was measured with liquid scintillation technique.

Results and discussion

The vertical distribution of Na-22 equilibrated with 1.10^{-2}N NaCl solution is demonstrated on Fig. 1.

The highest relative value of Na-22 activity /30-40 per cent of the total activity/ was found in the 2-3 cm thick top layer of the column. In the deeper layers the activity sharply decreased, it reached only 0,5-2 per cent in 7-15 cm depth.

The distribution pattern of Cl-36 in the soil column equilibrated with 1.10^{-2} N NaCl solution was similar to that of the moisture /Fig.2./.

Comparing the vertical distribution of Na-22 representing the changes in the total amount of sodium, and the distribution of Cl-36 representing the amount of sodium in the solution, we can see, that the maximum of sodium adsorption can be found on the top of the column being in direct connection with the solution.

Disregarding the concentration of equilibrating solution, Na^+ could not be removed from the soil column by treatment with distilled water. Water did not penetrate into the 2-3 cm top layer.

After percolating the columns with different volumes of $CaCl_2$ solutions, the maximum of sodium became less expressed and moved towards the deeper layers. That was also clear when the concentration of the leaching solution was lower than that of the equilibrating solution. /Fig. 1./.

In the vertical distribution of the total amount of sodium and exchangeable sodium, a sharp maximum was found in the top layer of the column, similarly to the radiochromatographic distribution pattern.

Data for the exchangeable Na^+ and sodium in the solution in each 1 cm thick layer of the columns determined with the Na-22 isotope dilution method, were compared with the data calculated with the chromatographic equation used by Filep /6/.

$$Na_x = \frac{1}{1 - K} \left[\sqrt{C_o KQr \frac{V - X f}{X}} - KQ \right] \qquad /1/$$

$$C_{Na} = \frac{1}{1-K} \left[C_o - \sqrt{C_o KQr \frac{X}{V - Xf}} \right] \qquad /2/$$

where: Na_x = exchangeable Na^+, me/g; C_{Na} = Na^+ concentration of the soil solution, me/ml; C_o = concentration of the equilibrating salt solution, me/ml; r = bulk density of soil, g/cm³; f = part of the column filled with water, dimensionless; K = Gapon's exchange constant; Q = cation exchange capacity of the soil, me/g; X = cepth of column, cm; V = volume of equilibrating solution /water column cm/.

The equation was elaborated on the Hiester-Vermeulen model, and simplified for the case of Na^+-Ca^{2+} ion-exchange. This theory assumes a laminar flow in a material with homogenous pores. Another assumption is, that during the experiment the ion-exchange constant and the cation exchange capacity of the adsorbent should not change, and the channel effect as

well as ion diffusion are neglibile.
The measured and calculated data corresponded to each other, small deviations were found only in the 2-3 cm top layers. /Table 1./ These differences can be explained by the simplified conditions of the chromatographic model and by experimental errors.
The amount of exchangeable Na^+ surpasses the amount of Na^+ in the solution, all over the column. The ratio of the two kinds of sodium ions is much higher on the top ot the column than in the deeper layers.
Assuming an apparent equilibrium between the cation in the solution phase and that adsorbed, the Vanselow selectivity coefficient was calculated from the measured data of each layers using the following equation /4,12/.

$$K_{Ca}^{Na} = \frac{N_{Na}^2 \quad C_{Ca} f^3 \quad /CaCl_2/}{N_{Ca} \quad C_{Na} f^4 \quad /NaCl/}$$

where: K_{Ca}^{Na} = Vanselow selectivity coefficient, N_{Na}, N_{Ca} = = the mole fraction of the exchangeable Na^+ and exchangeable Ca^{2+} respectively; C_{Na}, C_{Ca} = Na^+, and Ca^{2+} concentration in the equilibrium colution mole/l; f_{NaCl}, f_{CaCl_2} = activity coefficients of the salts in the solution.
Data related to the soil column equilibrated with $5{,}10^{-2}$N NaCl solution are presented in Fig. 3. In the deeper layers, where the mole fraction of exchangeable Na^+ was less than 0,5, the selectivity of the adsorbent for sodium changed only slightly. In 5 cm depth, the mole fraction of exchangeable Na^+ became higher than 0,5 and a sharp increase was found in the value of the selectivity coefficient, showing that an increase in sodium saturation in the upper layers of the columns is accompanied by certain changes in the colloid properties of the adsorbent /15/.
Generally the value of the Vanselow selectivity coefficient increases with the decreasing of ionic strength in the solution. Leaching the columns with $CaCl_2$ solutions the total amount of Na^+ considerably decreased and its maximum was found in the deeper layers of the column. /Table 1./

References

/1/ Bower,C.A., Gardner, W.H., Goertzen, J.O.: Soil Sci.Soc. Amer. Proc. 21. 20-24. /1957./

/2/ Darab, K.: Agrokémia és Talajtan 18. Suppl. 271-277. /1969./

/3/ Darab, K., Rédly, M.: Agrokémia és Talajtan 15. 465-466. /1966./

/4/ Darab, K., Rédly, M.: Agrokémia és Talajtan 16. 588-590. /1967./

/5/ Filep, Gy.: Agrokémia és Talajtan 18. 388-397. /1969./

/6/ Filep, Gy.: Agrokémia és Talajtan 23. Suppl. 69-76. /1974./

/7/ Fripiat, J.J.: Experimental Pedology. Ed.Hallsworth, E.G. Crawford, D.V. /3-13/ Butterworth, London. /1965./

/8/ Gapon, E.N.: Zhurn. Obsch. Chim. III. 2. 144-159./1933./

/9/ di Gléria, J., Klimes - Szmik, A., Dvoracsek M.: Talajfizika és Talajkolloidika. Akad.Kiadó. Bp. /1957./

/10/ Hiester, N.K., Vermeulen, T.: Chem.Eng.Prog. 48. 505-516. /1952./

/11/ Poelstra, P. Frissel, M.M.: "Isotopes and Radiation in Soil Plant Studies" IAEA. Vienna. 55-61. /1965./

/12/ Rédly, M., Szabolcs, I.: Trans. 10th Int. Cong. Soil Sci. X. 223-232 Moscow, /1974./

/13/ Rible, J.M., Davis, L.E.: Soil Sci 79. 41-47. /1955./

/14/ Szabolcs,I.: Trans. 10th Int. Cong. Soil Sci X. 49-55. Moscow, /1974./

/15/ Szabolcs, I., Darab, K.: Techn Rep. Ser. N° 48. 24-36. IAEA, Vienna /1965./

/16/ Vault, de D.: J. Amer. Chem. Soc. 65. 532-548. /1943./

/17/ Vermeulen, T. Hiester, N.K.: J.Chem. Phys. 32. 96-101. /1954./

Table 1.

Vertical distribution of Na-ions in soil columns equilibrated with 1.10^{-2}N NaCl solution and leached with $CaCl_2$ solutions of different concentration./Comparison of measured and calculated data/

Depth of column cm	Na^+ me/100 g soil				Ratio between exchangeable sodium and sodium in the solution	Na^+ me/100 g soil total amount	
	Total amount[x]		Exchangeable /adsorbed/			in column leached with 60 ml 5.10^{-3}N $CaCl_2$ solution /measured data/	in column leached with 60 ml 1.10^{-2}N $CaCl_2$ solution
	measured	calculated	measured	calculated			
0 - 1	4,56	6,85	4,05	6,37	8,19	0,43	0,23
1 - 2	3,76	4,84	3,31	4,42	7,29	0,87	0,67
2 - 3	3,43	3,93	3,00	3,54	7,04	1,94	1,88
3 - 4	3,14	3,39	2,73	3,01	6,45	3,28	2,01
4 - 5	2,84	2,82	2,48	2,50	6,84	3,38	2,06
5 - 6	2,74	2,69	2,33	2,34	6,71	2,33	2,71
6 - 7	2,59	2,53	2,20	2,18	5,55	2,18	2,81
7 - 8	2,36	2,30	1,95	1,96	4,72	1,99	2,26
8 - 9	2,42	2,21	2,01	1,86	4,85	1,95	2,25
9 -10	2,35	2,05	1,93	1,71	4,67	1,89	2,17
10 -11	2,15	1,96	1,96	1,65	5,05	1,94	2,03
11 -12	1,88	1,89	1,46	1,56	3,55	1,76	2,02
12 -13	1,81	1,78	1,48	1,47	3,54	1,66	1,81
13 -14	1,86	1,71	1,44	1,41	3,54	1,82	1,74
14 -15	1,80	1,73	1,42	1,38	3,62	1,75	1,73

[x] Determined in 1:10 soil-water suspension with Na-22 isotope dilution method

Figure 1.

Distribution of Na-22 in soil column equilibrated with 1.10^{-2} N NaCl solution and leached with $CaCl_2$ solutions of different concentrations

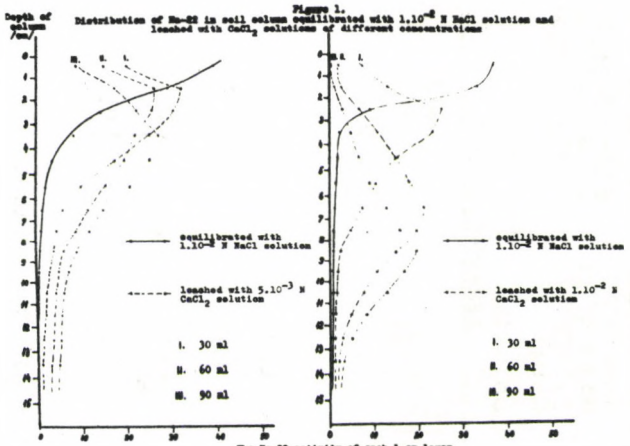

The Na-22 activity of each 1 cm layer expressed in the percentage of the total activity added to the column

Figure 2.

Distribution of soil moisture and Cl-36 on soil column equilibrated with 1.10^{-2} N NaCl solution

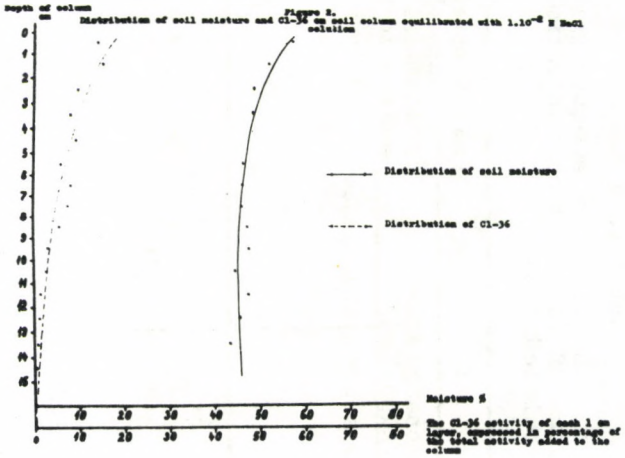

The Cl-36 activity of each 1 cm layer, expressed in percentage of the total activity added to the column

Figure 3.

Vanselow's selectivity coefficient as a function of the exchangeable Na^+ ion's mole fraction on soil column equilibrated with 5.10^{-3} N NaCl solution

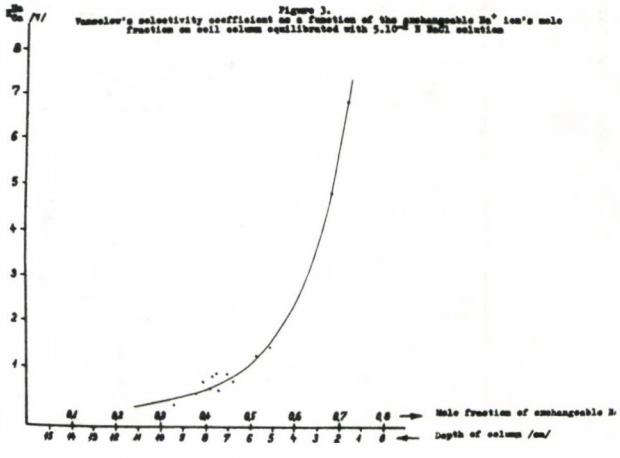

STUDY OF THE DISSOLUTION RATE OF PHARMACEUTICAL AGENTS SUSPENDED IN LIPOIDS OF VARYING COMPOSITION

József Bozzay[+], Zoltán Csűrös[+], Ágoston Dávid[‡], Rudolf Soós[+]

[+]Institute of Organic Chemical Technology, Technical University Budapest, 1111 Budapest, Müegyetem rkp.3.

[‡]Chinoin Pharmaceutical and Chemical Works,Ltd., 1077 Budapest, Rottenbiller u.26.

In order to promote oral therapy it has been an overall trend in pharmaceutical technology for the past decades to develop pharmaceutical agents with pharmacokinetic characteristics ensuring optimal and eventual prolonged biological activity to satisfy the therapeutic requirements.

The variation of the drug level in the organism can be influenced by the methods of pharmaceutical technology, for instance by the modification of the dissolution rate of the solid pharmacon at the first stage of the consecutive steps.

The dissolution rate of the active agent can be influenced by embedding the particles of the solid pharmaceutical in various matrixes by means of various technological processes,as described in a large number of papers and patents.

The composition, formed from various matrixes and incorporated particles of the active agent, represents a colloidal system of complex structure, wherefrom the active principle, depending on the structure of the system as well as on the properties of the applied matrixes, may generally have a limited dissolution rate.

In our previous communications /1/, in the course of the analysis of a simple, generalized pharmacokinetic model representing three steps of a process,it was demonstrated, that at identical initial doses, and presuming elementary steps to follow first order kinetics, the therapeutic period of a pharmacon of good solubility is longest and, from the point of view of retarding effect, optimal, when the dissolution rate is specified. This specified value of dissolution rate depends on the characteristics of the active agent /absorption, elimination, metabolism, etc./ which can not be influenced by means of pharmaceutical technology.

As the dissolution rate of an individual drug is a defined value at specified conditions, by the preparation of retard compositions this dissolution rate is to be modified to the desired optimal value by means of suitable processes of the pharmaceutical technology. Consequently the prerequisite of planning and biological optimation of oral pharmacons with prolonged activity consists in the correct knowledge at the dissolution-decreasing effect of an embedded matrix structure, e.g. and of the conditions of their regulation.

In order to enable planning, suitable relations were looked for, which could give a good approach to the description of dissolution rate conditions as a function of any relatively easily variable parameter. This paper describes some results of our studies concerning two-component, solubile, solid dispersions.

The study is limited to solid dispersions satisfying the following conditions: 1/ They consist solely of monodisperse pharmacons with a particle size surpassing the molecular one and of a matrix ensuring a continuous dispersion medium. 2/ They are highly solubile in the solvent without attaining the saturation level and without former swelling. 3/ The solubility of the dispersing medium is lower than that of the dispersed active agent. 4/ They do not exhibit any interaction either with one another or with the solvent. They are not form solid solution. 5/ They are compatible with one another and with the solvent.

As regarding the dissolution the following simplifications were undertaken: 1/ Unchanged solvent- and solution-volume throughout the process: consequently it is justified to calculate with quantities instead of concentrations. 2/ They dissolved material is immediately, uniformly dispersed in the solvent, the viscosity of the solution remains unchanged. 3/ The dissolution is taking place irreversibly through unchanged surface-areas and at constant temperatures. 4/ Velocity constant values are not changing throughout the process.

In a system like this the retarding effect of the dispersing medium may be interpreted according to the following example.

Model A in Figure I. demonstrates a set closely fitting drug particles /surface: dF; elongation: l_A/ located perpendicularly to the direction of dissolution, and model D shows a part of a continuous matrix, having an elongation of l_D. The dissolution equation according to first order kinetics may be put down without limiting conditions in the case of both models separately, both for the active agent /m_A/ and for the matrix /m_D/, resp.:

$$m_A = M_{A\infty}/1-\exp-k_A t/ \quad m_D = M_{D\infty}/1-\exp-k_D t/ \qquad 1./$$

The partial dissolution periods of the consecutive drug particles are Δt_{A1}, Δt_{A2}, etc., and those of the corresponding matrix particles Δt_{D1}, etc. The overall dissolution time of all drug particles is t_A, and that of the matrix t_D. In the case of a solid dispersion the particles A are dispersed in matrix D.

Figure 2. demonstrates a set of active agent particles incorporated in a random way into a matrix.

From the model there follows, that as if by virtue of the shrinking of the dissolution surface, the dissolution procedure of identical amounts of pharmacon particles incorporated in the matrix, takes a portionwise course in a given direction, to the contrary of the continuous process of model 1/A.

As in the process only the change in the amount of the favoured component, namely that of the active agent is of interest, the dissolution of the matrix and its retard effect derived from this, is demonstrated by the horizontal shifts

in the matrix, takes a portionwise course in a given direction, to the contrary of the continuous process of model 1/A.

As in the process only the change in the amount of the favoured component, namely that of the active agent is of interest, the dissolution of the matrix and its retard effect derived from this, is demonstrated by the horizontal shifts of the increasing Δt_{D1}, Δt_{D2}, etc. periods taken in the direction of the t axis. The quantity of the active agent in the solvent remains namely unchanged in the course of the dissolutions of the dispersing medium.

The overall dissolution time of the entire pharmacon-amount can be obtained by summarizing the dissolution time of the drug t_A, and the dissolution time of the dispersing medium t_D, The retard effect of the dispersing medium is proportional to its dissolution rate: low dissolution rates result in high retard effects.

From this curve these can further be established, that with increased dispersion degree the individual stages of the process become less and less pronounced, in extreme cases the diagram can be approached by a continuous curve.

Though most probably the sectional curve may be approached by a continuous one following first order kinetics, nevertheless the curve giving the best approach should be further analysed, also because of the high variability of the particle distribution of the active agent.

In the numerous communications analysing dissolution rates of solid principles incorporated in systems of various structures, three kinds of drug-dissolution-time functions are considered, namely zero- or first order processes or some proportional to $\sqrt{t}$. This formed the basis of our studies.

On our mathematical model it was studied, which of the above mentioned three ways of kinetic descriptions known from the literature, would give the best approach to the sectional curves corresponding to the various distributions.

As the sequence in a set, consisting of randomly mixed drug- and matrix-particles is highly variable, and any sequence is equally probable, that calculation was performed considering all possible distributions of the sets consisting of relatively few particles each.

It was assumed that the sample of surface F consists of numerous sets of identical elongations, each of a surface ΔF. It does not seem irreal to consider the distribution of the particles among the sets as uniform and calculating with an identical number of particle pro set. A further simplification, --never achived in reality,-- consists in the omission of particle interactions between those in the individual sets.

Corresponding to these simplifications it was assumed that a set consists of n_A drug-particles of an amount of m_A each, and of n_D matrix-particles of identical m_D quantities each. The maximal solubility of the components as well as their dissolution constants were choosen arbitrarily, in a way that value of k_A should be one order of magnitude larger than that of k_D.

By using the formulas 1./ the dissolution periods Δt_{A1}, Δt_{A2}, etc. and Δt_{D1}, Δt_{D2}, etc. of consecutive particles of identical quantities were determined for both the active agent and the matrix, as well as the overall dissolution times $\underline{t}_A$ and $\underline{t}_D$.

According to the possible number of the particle distribution $\underline{N}$, the Δt dissolution times of consecutive particles were arranged in $\underline{N}$ series. At all series the amount of the active agent was determined at close periods of t_1, t_2, etc. in the interval ranging from $t = 0$ to $t = /t_A+t_D/$ /possible curves/.

Thereafter by considering the overall period $/t_A+t_D/$ and overall amount of the active substance, the dissolution constants and ratio-factors for the obtained figures the drug amounts at periods of t_1, t_2, etc. in the interval ranging from $t=0$ to $t=/t_A+t_D/$ were determined /theoretical curves/.

The mean-square error between the quantitative parameters of the respective "possible" curve and the "theoretical" curves following the various orders of kinetics were calculated at periods of t_1, t_2, etc., as well as the sum of the squares of errors for the entire time interval.

It was observed that, independently from the number of particles, the sum of the squares of errors was the smallest, consequently the approach was the best, when the solution conforming to first order kinetics was applied.

The equation of the "theoretical" curve giving the best approach to the "possible" curve is the following:

$$m_A = M_{A\infty}/1-\exp -k_i/t_A+t_D// \qquad 2./$$

wherein k_i is the rate constant of the theoretical curve.

As relation 1./ is valid in the case of sample consisting solely of drug-particles and equation 2./ in that where the drug is incorporated in the matrix:

$$k_A . t_A = k_i/t_A+t_D/ \qquad 3./$$

from what

$$k_A . \alpha = k_i \qquad 4./$$

if

$$\alpha = t_A/t_A+t_D/ \qquad 5./$$

α = retard factor; it demonstrates to what extent the value of k_A dissolution constant of the active agent has to be decreased in order to achieve a k_i dissolution rate constant in the course of the process.

The value of the retard-factor may vary from $\underline{0}$ to $\underline{1}$. From equations 1./ and 5./ there follows:

$$\alpha = \frac{\frac{1}{k_A} \lg \frac{M_{A\infty}}{M_{A\infty}-m_A}}{\frac{1}{k_A} \lg \frac{M_{A\infty}}{M_{A\infty}-m_A} + \frac{1}{k_D} \lg \frac{M_{D\infty}}{M_{D\infty}-m_D}} \qquad 6./$$

In the case of a sample considered as a bunch of sets the values of dissolution constants k_A and k_D in the denominator of 6./ have to be modified as both matrix and drug occupy only a part of the dissolution surface F, and the dissolution rate constant is a function of the surface. On the basis of considerations not discussed in detail these surface modifications may be assumed to be, with a good approximation, proportional to the volume fractions of both components, i.e. to $\psi A^{1/3}$ and $/1-\psi A^{1/3}/$.

In the case of a real sample:

$$\alpha = \frac{\frac{1}{k_A} \lg \frac{M_{A\infty}}{M_{A\infty}-m_A}}{\frac{1}{k_A \psi A^{1/3}} \lg \frac{M_{A\infty}}{M_{A\infty}-m_A} + \frac{1}{k_D/1-\psi A^{1/3}/} \lg \frac{M_{D\infty}}{M_{D\infty}-m_D}} \qquad 7./$$

According to equation 7./, α is decreased by decreasing matrix dissolution rates /at increased molecular weights/ and increased dispersion-medium proportion, furthermore in a solid dispersion corresponding to this model --contrary to our initial assumption,-- a retard-effect exists also in that case, if $k_A \; k_D$.

To confirm these deductions in vitro experiments were pursued.

Similarly to several investigations recorded in the literature, polyethylenglycol with various degrees of polymerization as well as other water soluble, wax-like substances were applied as dispersion medium, and finely granulated Codein hydrochloride and No-Spa /2/ as the drug model.

The pharmacon was dispersed at various ratios in the molten dispersion medium. Approximately identical amounts of this molten preparation were placed into dissolution vessels, ensuring equal surfaces, after cooling they were smoothed over and weighed.

The dissolution of the active agent was measured at 37°C, at a stirring speed 50 ±2 r.p.m., by assaying in each case in identical volumes of distilled water, and the samples being taken at distinct periods and replaced by solvent.

The k_i constants and the measured α values were determined from experimental data, while the calculated α values from equation 7./.

Some results of our experiments are shown as examples to demonstrate, that similar results were obtained by using other systems, too.

Figure 3.A demonstrates the variations of the measured and calculated α values as a function of the composition, while Table 3.B sohws the same as a function of the degree of matrix--polymerization, with a model using No-Spa as pharmacon and polyethylenglycol as matrix.

It can be established, that the trend of the measured and calculated α values is identical and corresponds to our conclusions. Their values are in the same range of magnitude in nearly all cases.

The possible reason of the numerical deviations surpassing experimental errors may be that the prerequisites of the dispersion model, required for theoretical considerations, are not fully realistic in the case of our dispersion models.

On the basis of our experimental results there may be concluded that by using equation 7./, applying an appropriate dispersion medium of known parameters and setting ratios which can be calculated, α and the in vitro dissolution constant of the drug k_A can be regulated to attain the desired k_i values with a fairly good approximation.

Results of our experiments carried out on solid dispersions prepared by application of a matrix consisting of a mixture of soluble and insoluble materials, are going to be published later.

Figure I.

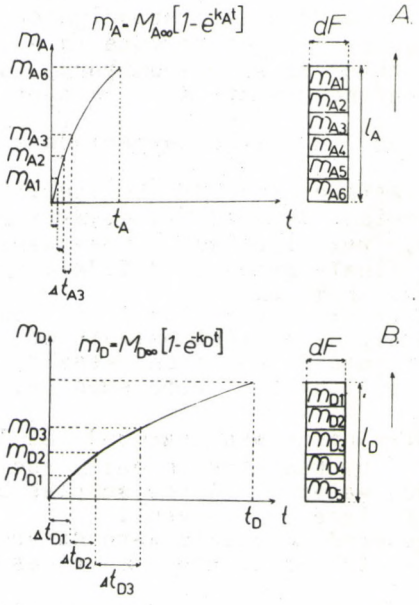

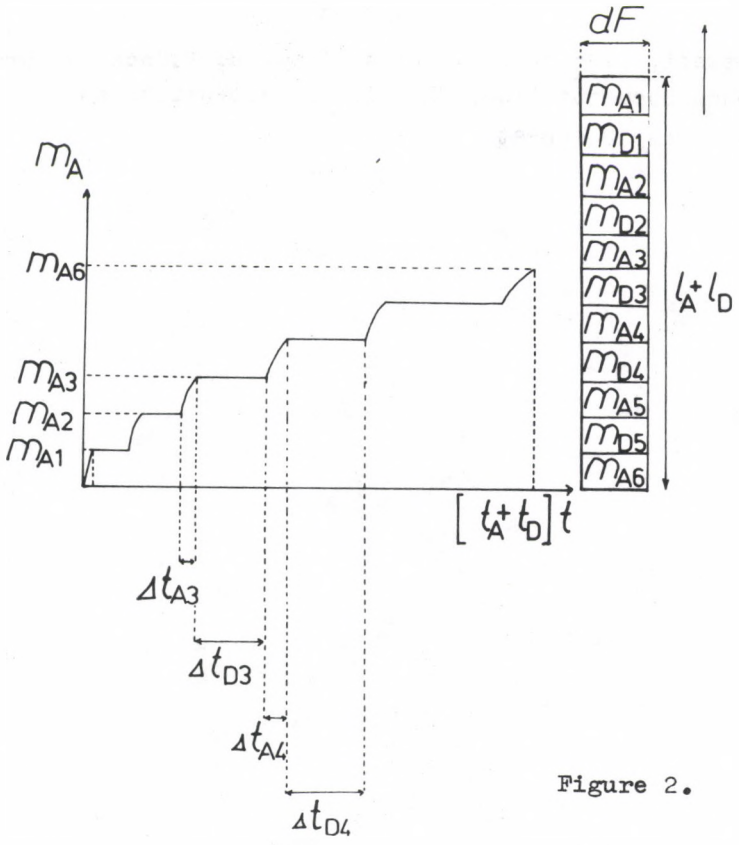

Figure 2.

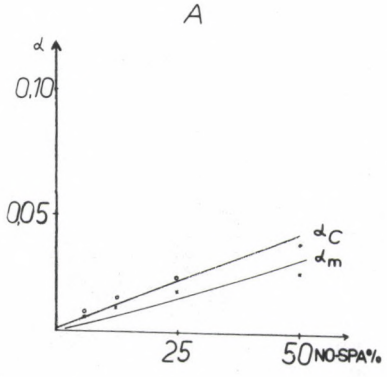

B

NO-SPA 50%

PEG	α_m	α_c
1500	0,074	0.111
4000	0,056	0.074
6000	0,025	0.038
12000	0,011	0.010

Figure 3.

REFERENCES

/1/ E.Békefi, J.Bozzay, Z.Csürös, Á.Dávid, R.Soós: in press

/2/ No-Spa Documentation, Chinoin Pharmaceutical and Chemical Works, Budapest

Group IV/2
Methods

HIGH RESOLUTION ELECTRON MICROSCOPY AND THE MOLECULAR STRUCTURE OF MONOLAYERS

W.BAUMEISTER and M.HAHN

Institute of Biophysics and Electron Microscopy, University of Düsseldorf, 4 Düsseldorf 1, Federal Republic Germany, Moorenstrasse 5

Because of its relevance to biological membranes the structure of monomolecular layer systems as formed at water-air interfaces has attracted wide attention. Irrespective of the many powerful physical techniques now available the detailed spatial organization even of relatively simple model systems is not yet really accessible. This is not so astonishing if we consider that the state of most biological membranes is more or less a fluid one (1), and that certain minimum displacements from randomness can accomplish the various membrane functions. Transient transformations of certain areas into well ordered domains could be sufficient to perform even rather complex cooperative functions. The absence of a long range order, however, excludes that methods based on an extensive use of spatial redundancy (e.g. x-ray diffraction) are capable of the structural information, which is considered to be of particular relevance in a biological context. In principle electron microscopy should provide a powerful tool for the analysis of the molecular topography of membranes and membrane model systems, as it works - at least in principle - independently on the degree of structural redundancy. Unfortunately there is still a considerable discrepancy between the instrumental resolution achievable (0,2 - 0,3 nm) and the limits to which up to now reliable spatial information can be extracted from or-

ganic materials (1,5 - 2 nm). The main reasons for this limitation are support film noise obscuring specimen details, the necessity of heavy atom labeling within the stringent requirements of isomorphism to produce suitable contrast and most fundamentally, radiation induced structural deteriorations of the specimen.

Monolayer Preparation

Monomolecular layers are spread at a water-air-interface and transferred to electron microscopic specimen supports following the well-known procedure as developed by Blodgett (2) modified such that the film pressure is maintained constant within $\pm$ .15 dyn . cm^{-1} during transfer by interconnecting the pressure sensing Langmuir- or a Wilhelmy balance with the compression mechanism by means of a feedback-loop (for review see 3). To avoid non-equilibrium structures of the layer, i.e. artificial inhomogenieties (4) careful adjustment of the compression rate (5) and integral-controller properties of the feedback are mandatory. By sequencing the deposition procedure a controlled assembly of symetric as well as asymetric bi-, oligo- or multilayers is feasible. Lipid-protein layers are formed either by adsorbing the protein onto the lipid layer following its deposition on a solid support, by injection of protein into the subphase (6) or even more elegantly by shifting the lipid layer over a protein solution in a multicompartment trough system (7).

Heavy Atom Labeling

Heavy atom labeling, which is yet scarcely explored, has to consider the effective electron scattering cross section of the heavy atom label (the higher the scattering cross section, the lower the dose L_{min} for its detection), the selectivity of the label and its influence on the supramolecular organisation of the layer. Fig. 1 shows that the electron scattering cross section and consequently also L_{min} are not simply a linear function of the atomic number Z, but depend intrinsi-

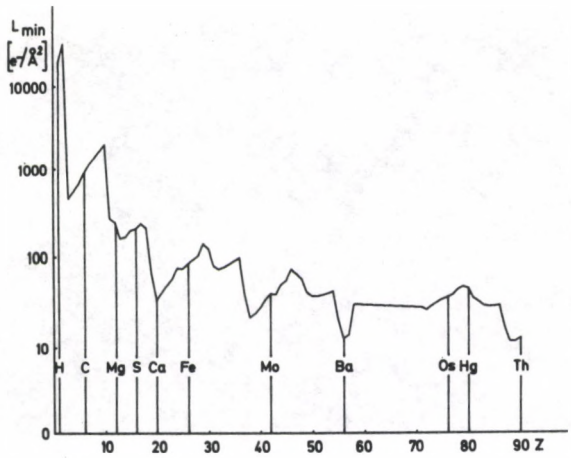

Fig.1 Minimum electron density L_{min} to image a single atom of atomic number Z with recent commercial electron microscopes at 100 keV beam energy. Processing of micrographs by a posteriori optical frequency filtering is assumed. Consideration of bonds leads to somewhat increased L_{min} values.

cally on the amount of screening by the electronic structure in the outer regions of the atoms.

Specimen Supports

While the granularity of carbon films obliterates the finest structural details, thin crystalline layers as obtained by thermic or H_2O_2 exfoliation of vermiculite (8) offer suitably smooth and "low-noise" supports for monolayer preparations. The support film problem can nearly be eliminated taking advantage of the fact that liquid-condensed and condensed monolayers span over the holes (.05 - 1 /um) of perforated support films (see Fig.2) and remain stable for sufficiently long periods of time.

Imaging Under Minimal Beam Exposure Conditions

To minimize radiation induced structural deteriorations of the specimen, focussing and correction of astigmatism must

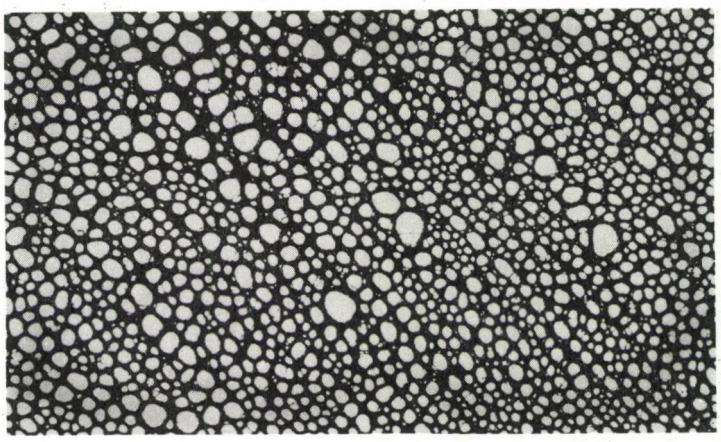

Fig. 2 Perforated gold film with "hole avenues"

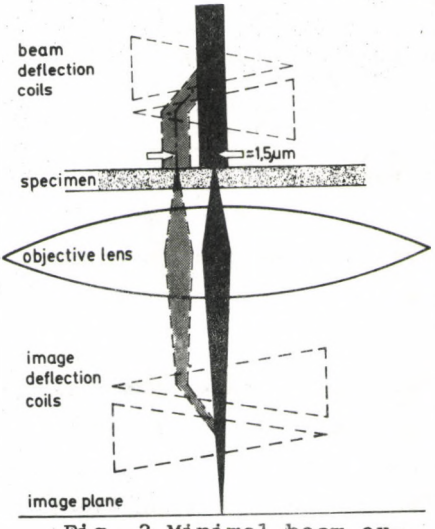

Fig. 3 Minimal beam exposure by simultaneous deflection of beam and image for all operations except the actual recording

be performed on a specimen area about 1 - 2 µm (≈ diameter of the beam) beside the area to be micrographed (9). For this purpose it is advantageous to shift beam and image by built-in magnetic deflector units (see Fig.3). For taking pictures the excitations of the deflector coils are switched to normal immediately before the shutter is opened. Perforated supports with nearly regular avenues of holes (Fig.2) offer a reasonably high probability of hitting for the actual micrograph a hole with comparable specimen areas as was viewed for focussing.

Radiation Damage And Reduction of Damage

Most of the actual damage is due to inelastic interactions between beam and specimen electrons and following secondary

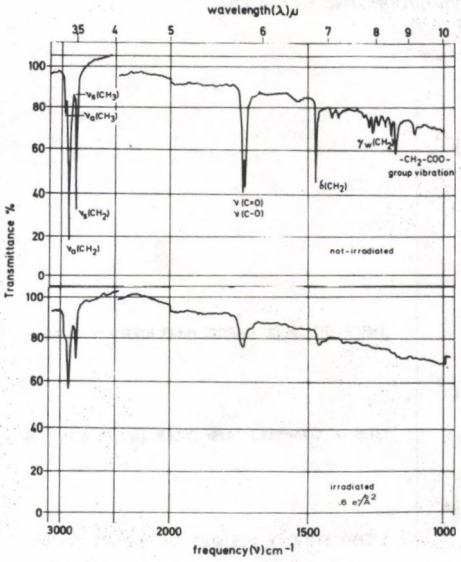

Fig.4 IR-spectra of 8 tripalmitin layers deposited on a germanium internal reflection plate: non-irradiated control plate and plate irradiated with .6 $e^-/Å^2$.

processes. Bond scissions, radical formation, migration and volatilisation of molecular fragments as well as inter-and intramolecular cross linking cause drastic changes of the layer structure which might make it impossible to relate the electron micrographs to the original structure (for reviews see 3, 10, 11). It has been shown by ATR-IR spectroscopy (see Fig.4) that the supra-molecular organisation of tripalmitin layer systems begins to degrade at doses of .3 $e^-/Å^2$. Layers irradiated with 2 $e^-/Å^2$ show almost complete destruction of pseudohexagonal order, the hydrocarbon chains are no longer in all- trans configuration and the marked decrease in the intensity of the CH_2 stretching bands indicates that chain fragmentation is followed by mass loss (12). The secondary effects of radiation damage might be reduced by low specimen temperatures (11), conductive surface coatings (13) and additional energy dissipating sandwich layers (14).

Perspectives

Tab.1 summarizes the dose requirements for various modes of structural analysis of layer systems by means of electron-diffraction and- microscopy and the corresponding damaging effects. The table can be interpreted as follows: Only the most "radiation resistant" organo-metallic monolayers can with a certain degree of reliability be investigated by

DOSE REQUIREMENTS AND DAMAGING EFFECTS

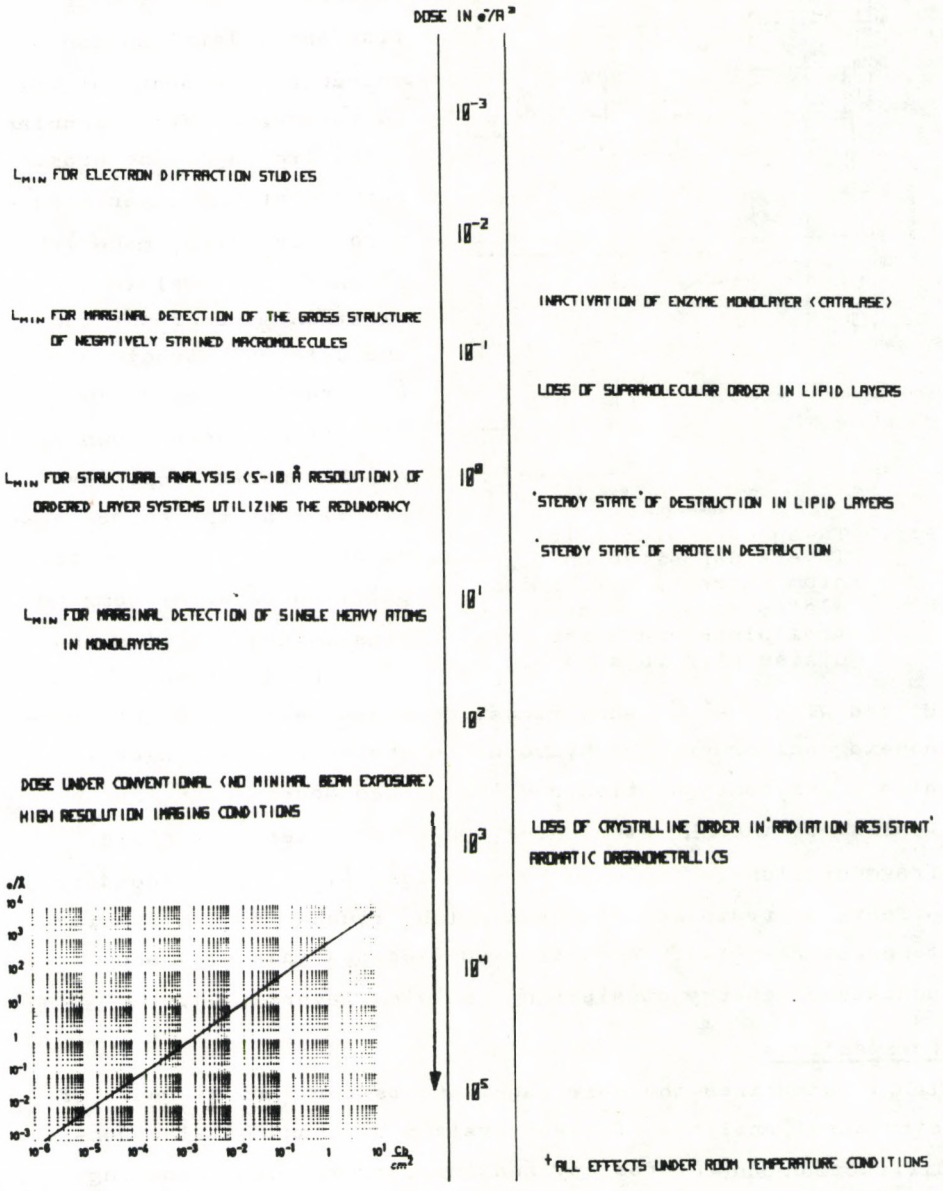

TABLE 1

direct visualisation of the heavy atom pattern (14, 15). The dose L_{min} for marginal detection of single heavy atoms in monolayers which is achievable only under optimum imaging and image processing conditions exceeds in any case the dose which is tolerated by lipid and lipid-protein layer systems without profound structural alterations. Significant progress is to be expected only, if the radiation resistance can substantially be increased or if it can be insured that, irrespective of the destruction of the light atom matrix, the labeling heavy atoms remain close to their original location. This stresses the general question whether or not the "steady state" of destruction in which further incoming radiation energy is efficiently dissipated, bears a close ressemblance to the original structure. Far better is the situation with well ordered lipid-protein layers. Here, the utilisation of structural redundancies by extracting the phase information from micrographs, exposed far below the margin of specular readibility and the amplitudes from the electron diffraction pattern offers the chance to synthesize density maps by digital reconstruction techniques with minimum destruction of the specimen as recently has been demonstrated (16). Relatively simple layer systems can be investigated by electron diffraction which is nearly uncritical with respect to radiation damage. Aging effects, i.e. the transformation of Langmuir-Blodgett layers into microcrystals as already observed by Stenhagen (17) and recently investigated by ATR-IR spectroscopy and replicatechniques (18) can also be detected on electron diffractograms. Moreover, electron diffraction offers the chance of studying the molecular structure of hydrated lipid layers by means of hydration chambers (19) and to monitor phase-transformations under controlled environmental conditions (20, 21).

1) S.J.Singer a. G.L.Nicolson, Science 175, 720 (1972)

2) K.B.Blodgett, J.Amer.Chem.Soc. 57, 1007 (1035)

3) W.Baumeister a.M.Hahn, in "Progress in Surface and Membrane Science" (J.F.Danielli and D.Cadenhead, Eds.), Acad.Press New York), in press

4) H.Zocher a.F.Siebel, Z.Phys.Chem. (Leipzig) 146, 401 (1930)

5) W.Baumeister, Fette-Seifen-Anstrichmittel 77, 109 (1975)

6) G.Colacicco, Lipids 5, 636 (1970)

7) P.Fromherz, Biochim.Biophys.Acta 225, 382 (1971)

8) W.Baumeister a. M.Hahn, J.Microsc. (London) 101, 111 (1974)

9) R.C.Williams a.H.W.Fisher, J.Mol.Biol.52, 121 (1970)

10) R.M.Glaeser, in "Electron Microscopy" (B.Siegel, Ed.), John Wiley and Sons, Inc. New York, in press

11) M.Isaacson, in "Principles and Techniques of Electron Microscopy" (M.A.Hyat, Ed.) Van Nostrand and Reinhold Co. New York, in press

12) M.Hahn, U.P.Fringeli a. W.Baumeister, 8th Inter.Congr. Electron Microscopy Canberra 1974, Vol.II, 672

13) S.M.Salih a.V.E.Cosslett, Phil.Mag.30, 225 (1974)

14) W.Baumeister a. M.Hahn, Cytobiol. 7, 244 (1973)

15) W.Baumeister a. M.Hahn, Nature (London) 241, 445 (1973)

16) P.N.T.Unwin a.R.Henderson, J.Mol.Biol. in press

17) E.Stenhagen, Trans. Faraday Soc. 34, 1328 (1938)

18) F.Kopp et al., Biophys.Struct.Mechanism 1, 75 (1975)

19) D.F.Parsons et al., Adv.Biol.Med.Phys.15, 161 (1974)

20) S.W.Hui, D.F.Parsons a. M.Cowden, Proc.Nat.Acad.Sci. USA 71, 5068 (1974)

21 S.W.Hui et al., Biochim.Biophys.Acta 382, 265 (1975)

ELECTRON MICROSCOPIC INVESTIGATIONS OF COLLOID AND POLYMER SYSTEMS

H.J. Purz

Academy of Science of the GDR, Institute of Polymer Chemistry, 153 Teltow-Seehof, German Democratic Republic

The investigation of the micromorphology of colloid and polymer systems has gained great importance. However, particular interest has been taken in the formation, change and destruction caused by various factors, as sol-gel transformation, agglomeration, ageing, film formation, etc. Observations of the formation processes of the morphology in statu nascendi depend on the preparation techniques. Generally, the electron microscopy provides no possibilities of investigating substances in dissolved or liquid state. Therefore, adequate fixation and removal of liquids is required for structural investigations. In freeze etching techniques the freeze fixation and partial removal of water by vacuum sublimation, preferentially after freeze breaking, became an appropriate means in investigating biological ([1]) and technical ([2,3]) objects. Here, the selection of a suitable cryogenic medium is of decisive importance for the quality of preparation.

The freezing rate depends on the size (surface area) and thermal conductivity of the object. Higher freezing rate was achieved by imparting high static pressure during freezing ([4]) or by injection of macroscopic droplets into the cryogenic medium ([5]) and by freezing a paraffine oil droplet with an aqueous solution finely divided in it ([6]).

In various applications the freeze etching method proved suitable for electron microscopic investigations of objects containing water and other liquids, particularly if chemical preparation would cause structural changes. However the limitations of these techniques should be considered. Artefacts result particularly from freezing and etching with systems containing high amounts of liquids, as solutions and dispersions.

This paper describes the results obtained by applying the freeze etching technique to various colloid and polymer systems to which other electron microscopic preparation techniques are less advantageously applied. The advantages of this techniques as well as possible artefacts are considered by examples, e.g. colloid and polymer sols, gels, dispersion and polymer mixtures.

By using the standard method of freeze etching (dipping the sample of about 1 mm^3 in liquid freon 22, Fp - 160 °C, propane, Fp - 189.9 °C or isopentane, Fp - 159.9 °C; breaking and etching at -100 °C) the freezing process causes segregation, that is, colloidal and dissolved substances are dislocated and concentrated between the monocrystals to form eutectic structures. The segregation can particularly be vizualised with polymer solutions and sols (Fig. 1a,3a). The solute forms a more or less regular network, which shows in some regions preferred network orientation (Fig. 3a). The size of segregation regions varies from some 100 Å to some µm in diameter, depending on concentration and properties of the polymer as well as on the freezing conditions. Segregations of this kind was found with various polymer solutions of different concentration, as polyvinylalcohol, carboxymethylcellulose, Na-cellulose xanthate, Na-polyacrylate, gelatine, non-aqueous polymer and water glass solutions. With decreasing concentration the coherent network structures are decomposed or their formation becomes impossible. On applying the emulsion droplet, spray, high static pressure method in order to increase the freezing rate the segregation can be suppressed and only partial structure formation is observed.

Quite another freezing mechanism is observed if the sol has already been fixed by coagulation, although after immobilisation the gel contains the same amount of water than the sol. Fig. 1c shows the network structure of an isotrope capillar gel (Tl-cellulose xanthate) and an optically isotrope NH_4-cx gel (Fig. 1b) as compared with the artefacts of segregation in the corresponding polyelectrolyte sols. The gel structure, which can be controlled by electrolyte coagulation and other

parameters, differs essentially from the artefacts in the sol. This gel structure was also obtained by other preparation methods, e.g. exchange of water for a series of solvents having decreasing dissolving power, freeze drying and freezing substitution as well as subsequent ultramicrotomy ([7]). Therefore, the network is suggested to be the real structure of the gel. In order to verify this difference a technique was developed, which reveals the process of electrocoagulation in statu nascendi and vizualises the sol-gel interface in one picture. The sol droplet is slightly coagulated by electrolyte solution and subsequently treated by the standard freeze etching method, as shown schematically in Fig. 2. Fig. 3 shows the "frozen kinetics" of gel formation, sol-gel interface and structure or artefacts in PVA and CMC sol systems. There is a striking difference between the sol and gel phase. The formation of primary and secondary valency bonds in the gel causes variations of the interface tension. In the interface region the gel exhibits a fine granular structure which then changes to a network structure having large mesh diameter. This is obviously caused by gradual dehydratation during gel formation. The fine granular structure in the "pre-zone gel" is probably associated with water droplets formed by segregation during gel formation (e.g. PVA 220 Å, CMC 300-500 Å). This simple experimental set-up allows to demonstrate the differences between network structures in sol and gel as well as the "frozen kinetics" of gel formation occuring on using the standard method. Using this procedure various gel structures of high liquid content, which were formed e.g. by electrolytic and thermal coagulation of immediately in polymerization (soluble polyglycolmethacrylate gel), were investigated and the results were compared with those obtained by other fixation methods and ultramicrotomy.

As another example of application of the freeze etching method the investigation of crosslinking reactions in gels should be mentioned, that is PVA crosslinked by formaldehyde. Other crosslinking processes, e.g. crosslinking by irradiation ([8]), and various states of swelling can likewise be demonstrated by this method.

Further interesting objects of investigation are dispersions, particularly latices. Here, the freeze etching technique proved suitable to provide information on the size and, including the possibilities of artefact formation, on the distribution and arrangement of latex particles and additives. Fig. 4a shows the freeze etching replica of a polyvinylacetate dispersion. A small section has just been split off from a latex particle, thus enabling differentiation of the swollen porous internal structure from the granular surface of that particle. Fig. 4b presents the same latex dispersion containing a protective colloid in the form of network-like links. Even at temperatures of -100 °C and lower plastic deformation (elevations, radial fibrillation) of the latex spheres may occur on freeze fracturing (Fig. 4c). Fig. 4d,e,f and g illustrate segregation phenomena with a dilution series of polymethacrylic acid methyl ester at -150 °C (particle diameter =600 to 900 Å). At dilution ratio 1:5 (4e) there are aggregated regions besides individual latex particles which either may be left from the concentrated dispersion /Fig. 4d/ (residual associates) or formed by segregation. At dilution ratio 1:10 (4f) the periodic chains of latex particles are caused by segregation, that is, by substance dislocation within fractions of seconds during freeze shocking of the sample in freon. At higher dilution ration (1:50) (4g) the latex particles are randomly distributed. Under consideration of these phenomena this technique allows to investigate the agglomeration of dispersions, film formation from dispersion, swelling of polymer structures etc. Further, the effect of surfactants and additives on the arrangement of particles can be studied. The "morphological kinetics" of film formation from latices by drying is shown in Fig. 5.

Fig. 6a shows the microstructure of an aqueous PVAc dispersion pigmented with TiO_2 and Fig. 6b vizualises ferric oxide pigment particles in a resin solution. These pictures demonstrate particularly the shape and distribution of pigment particles. Fig. 7 presents a clay (montmorillonite) 7a and a stearate dispersion 7b . An organic dispersion having anisometric particles (microcrystalline cellulose) is shown in Fig. 7c. This freeze

etching replica reveals a fibrillar structure of the particles in the longitudinal axis.

Fig. 8a shows dye coupling agent particles (particle diameter 500 to 2000 Å) randomly distributed in a gelatine network. On ultrasonic spraying the dispersion on a film associates are formed during drying (8b) thus disturbing the result.

These micrographs provide information on the size, shape and distribution or arrangement of particles in dispersions and allow to draw conclusions to the preparation processes and performance of dispersions.

The freeze etching method allows also to investigate the compatibility of polymer mixtures. Here no homogeneous distribution occurs, e.g. in a cellulose-polyacrylonitrile system. In compatible mixtures, e.g. cellulose and P V A, no structural differences would occur.

The importance of this technique of water removal was stressed in investigations of bacteria cellulose. Fig. 9 compares the fibrillar structure of bacteria cellulose obtained by freeze etching and other techniques. After freeze etching the fribrilar strands are embedded in an ice matrix. Here, the real state in the original sample is approximated (solid-water ratio 1:100).

The differences in state of fixation as expressed by the size of voids and specific surface area of air-dry samples and samples obtained by solvent exchange and freeze drying were determined by porosity and BET measurements. The results are shown in Fig. 10. By freeze drying and solvent exchange a more enlarged fibrillar structure is obtained than with air-dry samples. Further, the fibril diameter of air-dry samples is lower. This result explaines the importance of fixation and kind of water removal for a water containing object.

References

(1) H. Moor, Z. Zellforsch., 62, 546 (1964)

(2) H.J. Purz and A. Gröbe, Faserforsch. Textiltech., 22, 235 (1971)
H.J. Purz, J. Polym. Sci., C 38, 405 (1972)

(3) R. Menold et al., Chem.-Ing.-Techn., 44, 1226 (1972)

(4) U. Riehle, Chem.-Ing.-Techn., 40, 213 (1968)
H. Moor and U. Riehle, 4th Europ.Conf. Electron Microscopy, Rome 1968, II, 33 (1968)

(5) L. Bachmann and W.W. Schmitt, Naturwiss., 58, 217 (1971)
(6) W. Buchheim, Naturwiss. 59, 121 (1972)
(7) H.-G. Hicke et al., Faserforsch.Textiltech., 25, 425 (1974)
(8) L.D. Johnson and G.G. Cooks, 7th Intern.Conf. Electron Microscopy, Grenoble 1970, I, 381 (1970)

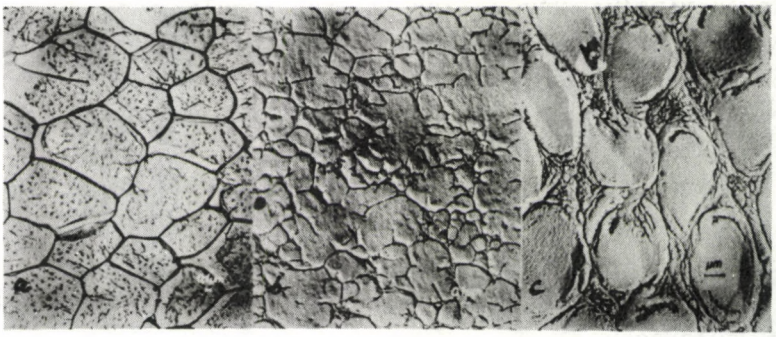

Fig. 1
1a = so
1b,1c =
ge

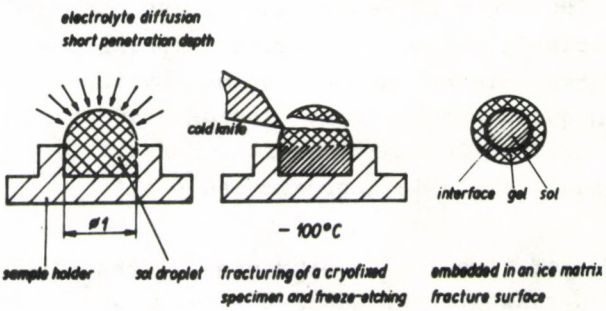

Fig. 2
preparation techniq
for investigating
the sol-gel
interface



Fig. 3
Sol-gel transformation
in a PVA and a CMC system

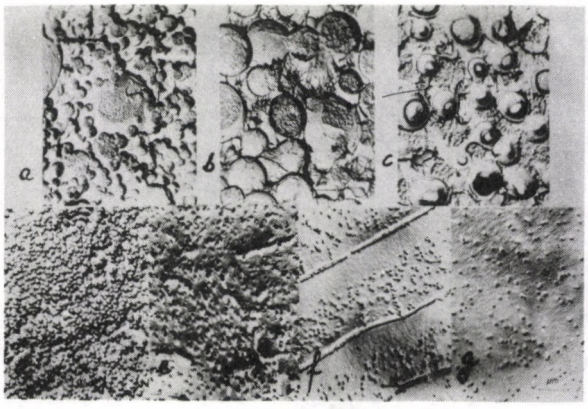

Fig. 4

Micromorphology of PVAc and polyacrylo-acidmethylether-latex and artefact structures

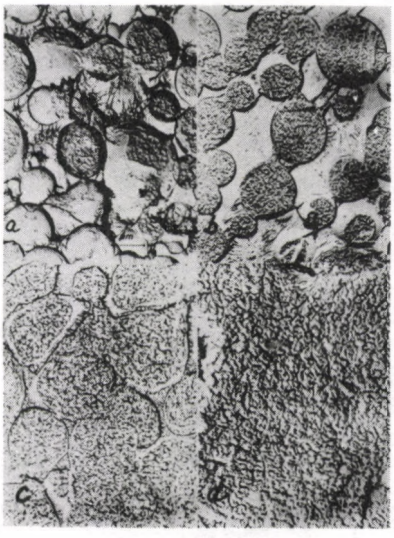

Fig. 5

"Morphological kinetics" of film formation from latices by drying



Fig. 6

Microstructure of pigmented PVAc-dispersion and resin solution

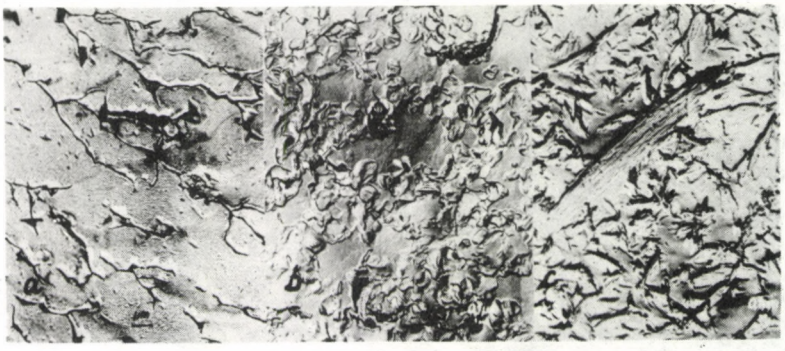

Fig. 7
Clay, stearate, MK-cellulose

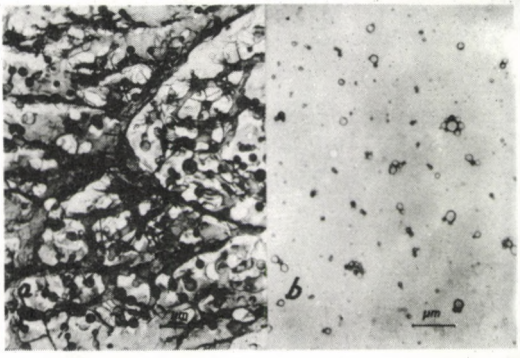

Fig. 8
Dye-coupling particles in a gelatine-gel network by freeze etching and by ultrasonic spraying

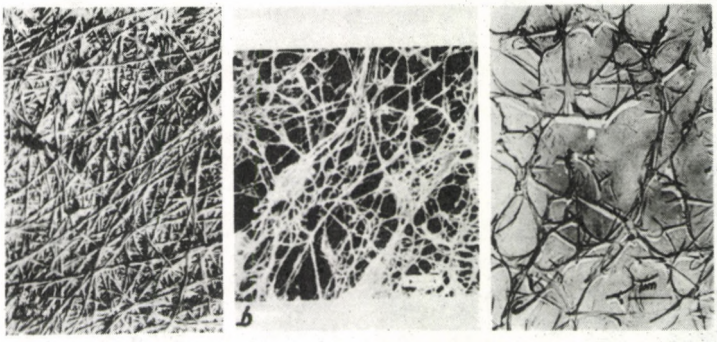

Fig. 9
Bacteria cellulose by air drying, freeze drying, and freeze etching

Bacterium cellulose sample (BC)	Adsorbent	Spec. surface area m^2/g weight	Void volume cm^3/g 0.76–0.0152 µm ø
Air – dry	Krypton	7,6	0,097
			0,101
EMB – exchange	Krypton	89	1,24
	Krypton	97	
	Nitrogen	93	
Lyophilization	Krypton	98	1,929
			1,891

Fig. 10
Void volume and specific surface area of BC depending on the conditions of water removal

DEVELOPMENT OF NEW METHODS IN ELECTROANALYTICAL AND SURFACE CHEMISTRY ON THE BASIS OF THE SUSPENSION EFFECT

Yu.M.Chernoberezhskii, K.I.Omarova, M.Sh.Shukroev

Leningrad State University, Leningrad 199004,Sredny pr.41/43
Soviet Union

There are various methods of investigation of electrical properties of the dispersed systems. Among them the method of the suspension effect (S.E.M.) begins to be used. However, in spite of the great potentialities of S.E.M. and its simplicity it has not yet attracted the due attention of scientists.

The main point of the suspension effect (S.E.) is as follows. The magnitudes of pH, pNa, pCl and pX in the general case electrometrically measured in sol, suspension, sediment or in the solution of high molecular substance of ionic type and in the solution equilibrated with them are unequal. As a rule, S.E. is characterized by the magnitude of ΔpH (or ΔpX): ΔpH= pH susp. - pH equil.liq., or by the corresponding magnitude expressed in mV (ΔE), which is the difference between e.m.f. of two circuits designed for pH determination in suspension and equilibrium liquid.

There are basically two approaches to the explanation of the nature of S.E. and to the interpretation of potentiometric data in dispersed systems. The advocates of the first approach (Marshall et al.) hold to the simplest ideas of Donnan and believe that potentiometric determinations in dispersed systems can be interpreted in a simple way in terms of the activity values of individual ions /1/. The advocates of the second viewpoint (Jenny, Overbeek, Honig et al.) believe that the cause of S.E. is a difference between junction potentials of salt bridges submerged into an equilibrium solution and into a dispersed system /2-4/. According to the latter conception, the potentiometric determinations in dispersed systems

do not give any information about the activity of individual ions in a colloidal solution. We, too, hold the second viewpoint.

If we adopt the second viewpoint we come to a sad conclusion that these determinations are quite useless. One is under the impression that S.E. should be got rid of whenever possible. And researchers often do like that nowadays, using a salt bridge filled with equilibrium liquid. Sometimes S.E. is merely neglected, and the potentiometric determinations in dispersed systems are interpreted in the same way as in true solutions.

In this paper we shall try to show potentialities that emerge if S.E. is made use of, to show what it can offer to a researcher who deals with dispersed systems. In this case S.E. becomes a new instrument of an investigator, but not an accompanying and hampering phenomenon.

1. S.E. may be used /5/ to determine the position of the isoelectric point. It follows, in particular, from the relationships between ζ, pH and ΔpH, pH determined by us for amphoteric oxides (Al_2O_3, Cr_2O_3, BeO). Fig.1a shows these relationships for Al_2O_3. At pH < 8.2, where the particles are positively charged, ΔpH is also positive; at pH > 8.2, where the particles are negatively charged, ΔpH is negative. At the isoelectric point (pH=8.2) S.E. is equal to zero.

Fig.1b shows the dependence of ΔpH and exchange capacity-g on pH for the Soviet amphoteric ion-exchanger БАК (functional groups - COOH, $-\overset{+}{N}(R)_3$). The curves for g and ΔpH are identical. At pH = 5.4 - 5.5 the magnitudes of ΔpH and g are equal to zero, and ion-exchanger is in isoelectric state.

Fig.1c shows the dependences of ΔpH, adsorption of H^+-OH^- ions, extinction coefficient -τ and viscosity -η of gelatine sols on pH of equilibrium liquid. As it follows from fig.1c, all methods show the same magnitude of pH = 4.95 for the isoelectric point of gelatine. This magnitude is in good agreement with the data obtained by other investigators.

These data prove that alongside with other methods S.E.M. may be used to locate the isoelectric point.

2. On the basis of S.E. a new method of estimation of spe-

cific surface of fine powders with surface charge carrying particles may be developed. It follows from the relationship between the magnitudes of ΔpH and particle size of quartz. (Fig.2a).

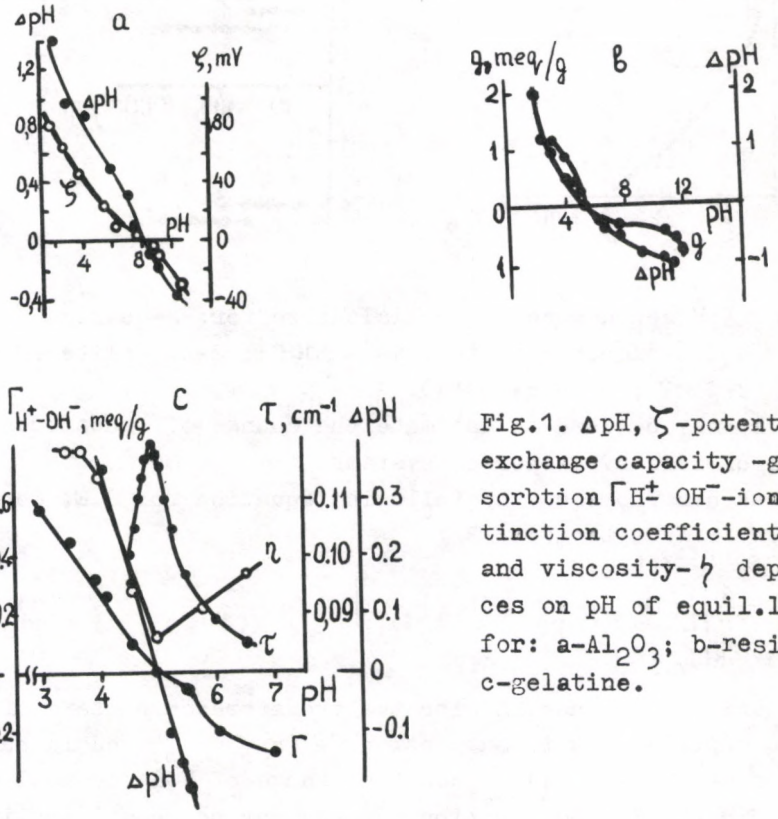

Fig.1. ΔpH, ζ-potential, exchange capacity -g, adsorbtion $\Gamma H^{\pm}$ OH^{-}-ions, extinction coefficient- τ and viscosity- η dependences on pH of equil.liq. for: a-Al_2O_3; b-resin БАК; c-gelatine.

While there is an evident dependence of ΔpH magnitude on particle size in the case of particles carrying charges only on their surface, the dependence in question is absent in the case of resins, where the charge is distributed through the whole volume. This is illustrated by Fig.2b, where data on S.E. of two Soviet resins КУ -2 (cation-exchanger) and ЭДЭ10П (anion-exchanger) and two American resins Dowex 50W10 and Amberlite IR-45 are given. The data prove that there is no ΔpH dependence upon the size (1-1000 μm) of resin particles. Thus we may also judge about the manner of charge distribu-

tion (surface or bulk) by the kind of S.E. dependence on particle size.

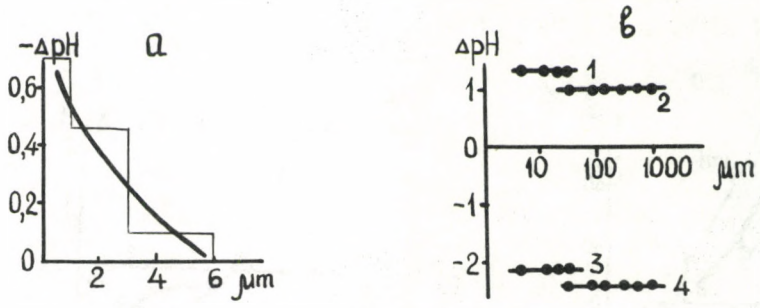

Fig.2. ΔpH dependence on particle size for: a-quartz; b-ion-exchange resins: 1-ЭДЭ10П ; 2-Amberlite IR-45; 3-КУ-2 ; 4-Dowex 50W10.

3. S.E. may be used to estimate the change of transference numbers of ions by dispersed systems.

Overbeek has proposed the following equation for S.E. (or capillary effect Loosjes)/3/:

$$\Delta E = \frac{1}{F}\int_{KCl_{dil.}}^{KCl_{sat.}} \left[(n_{Cl})_{cap.} - (n_{Cl})_{sol.}\right] d\mu_{KCl} \qquad (1)$$

Eq.(1) brings together ΔE with the transference numbers of ions in capillar (or in suspension) - $(n_{Cl})_{cap.}$ and in bulk solution of KCl - $(n_{Cl})_{sol.}$ and the change of KCl chemical potential in the liquid junction. Eq.(1) may be re-written in such a way

$$\Delta E = \frac{RT}{F}\int_{(a_{\pm})_o}^{(a_{\pm})_{s.b.}} 2\,\Delta n\, d\ln a_{\pm} \qquad (2)$$

where $(a_+)_{s.b.}$ and $(a_+)_o$ are mean activities of KCl in salt bridge and equilibrium liquid, resp., and Δn-the change of transference number of Cl^-. From eq.(2) follows that finding relationships $\Delta E, (a_+)_o$ at $(a_+)_{s.b.}$=const. or $\Delta E, (a_+)_{s.b.}$ at $(a_+)_o$=const. makes it possible to find the relation between $\Delta\bar{n}$ and $a_{\pm}$.

Experimental relations $\Delta E, (a_{\pm})_o$ and $\Delta E, (a_{\pm})_{s.b.}$ for Dowex 50W10 are shown in Fig.3.

The table 1 shows magnitudes of Δn at different KCl concentrations estimated by both S.E.M. (in two variants) and usual Hittorf method. There is a good correspondence of Δn magnitudes estimated in three ways.

The proposed method of Δn estimation by S.E.M. is quite simple and the experiment takes but a few minutes whereas the Hittorf method about an hour.

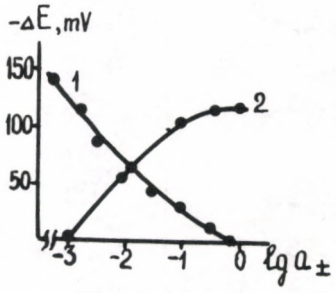

Fig.3. $\Delta E, (a_{\pm})_o^{-1}$ and $\Delta E, (a_{\pm})_{s.b.}^{-2}$ dependences for Dowex 50W10.

4. S.E. may be used to estimate the activation energy of electrical conductivity of ion-exchange resins.

Using Overbeek's general approach to a description of S.E. and Wyllie's model conception for conductivity of ion-exchanger sediment /6/ equilibrated with KCl solution we deduced the following equation

$$\Delta E = \pm \frac{RT}{F} \ln \frac{1 + \frac{\bar{\varkappa}(a+b)}{\varkappa_o}}{1 + \frac{\bar{\varkappa}(a+b)}{\varkappa_{s.b.}}} \qquad (3)$$

Eq.(3) connects ΔE with specific conductivities of resin particles $\bar{\varkappa}$ (or gel parts, if particles are heterogeneous), equilibrium liquid $\varkappa_o$, salt bridge $\varkappa_{s.b.}$ and with dispersed phase concentration which is expressed by a sum of two geometrical parameters (a + b) of Wyllie's model.

If cation-exchanger is in equilibrium with diluted solution of KCl, and saturated KCl salt bridge is used, that is, if $\varkappa_{s.b.} \gg \bar{\varkappa}(a+b) \gg \varkappa_o$, eq.(3) may be considerably simplified:

$$\Delta E = -\frac{RT}{F} \ln \frac{\bar{\varkappa}(a+b)}{\varkappa_o} \qquad (4)$$

Table 1. The change of transference number of Cl-ions estimated by S.E.M. (in two variants) and by Hittorf method

C equil.liq. N. KCl	Δn by S.E.M.: $\Delta E, \lg(a_+)_o$ salt bridge 3.5 N KCl	Δn by S.E.M.: $\Delta E, \lg(a_+)_{s.b.}$ equil.liq. 1.10^{-3} N KCl	Δn by Hittorf method
	Dowex 50W 2		
1.10^{-3}	0.51	0.50	0.50
1.10^{-2}	0.51	0.50	0.48
2.10^{-2}	0.41	0.42	0.45
4.10^{-2}	0.36	0.36	0.39
1.10^{-1}	0.34	0.33	0.30
	Dowex 50W 10		
1.10^{-3}	0.52	o.52	0.50
1.10^{-2}	0.40	0.41	0.35
2.10^{-2}	0.37	0.38	0.28
4.10^{-2}	0.28	0.34	0.25
1.10^{-1}	0.28	0.32	0.24

Table 2. Comparison of activation energy of electrical conductivity of ion-exchange resins determined by S.E.M. and by $\varkappa$,T dependence.

C equil.liq. N. KCl	$-\frac{d(\Delta E)}{dT}$, mV grad	ΔQ by S.E.M. kcal/mole	$\bar{Q}$ by S.E.M. kcal/mole	$\bar{Q}$ by $\varkappa$,T kcal/mole
		Dowex 50W 2		
1.10^{-3}	0.8	2.6	6.2	6.4
1.10^{-2}	0.4	0.5	4.1	3.6
1.10^{-1}	0.1	0	3.6	3.6
		Dowex 50W 10		
1.10^{-3}	0.9	3.8	7.4	6.8
1.10^{-2}	o.5	1,5	5.1	4.1
1.10^{-1}	0.1	0.	3.6	3.6

Using Arrhenius equations for specific conductivities of resin particles and equilibrium solution it is easy to show

$$\Delta E = -\frac{RT}{F}\ln\left[(a+b)\cdot K\right] - \frac{Q_o - \bar{Q}}{F} \qquad (5)$$

where $\bar{Q}$ and Q_o are activation energy of specific conductivities of resin and equilibrium solution, resp., and K-constant. Assuming (a + b) is independent of T we come to the conclusion that ΔE must be a linear function of T. It was proved by the experimental data obtained for Dowex 50W2 and Dowex 50W10. From eq.(5) it also follows that obtaining of temperature dependence of S.E. makes it possible to estimate $\bar{Q}$.

Table 2 contains values of $\bar{Q}$ estimated from ΔE,T dependence and $\bar{Q}$ estimated by the method of temperature dependence of electrical conductivity usually used for such purposes. Somewhat larger magnitudes of $\bar{Q}$ found by S.E.M. may be acounted for by the fact that S.E.M. enables us to determine the activation energy of resin particles (or even gel parts of the particles), whereas $\varkappa$,T dependence - the magnitude corresponding to the total sediment (particles plus the solution between them). As Q_o is less than that of resin particles the magnitude of $\bar{Q}$ estimated by S.E.M. must be somewhat greater.

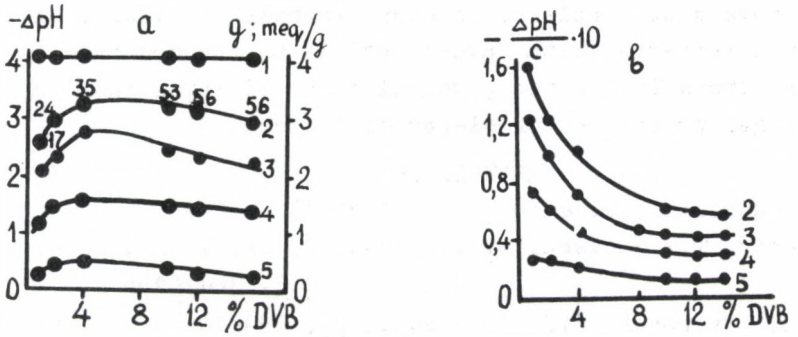

Fig.4. ΔpH and exchange capacity (g) - a and ΔpH/C - b dependences on DVB content for Dowex 50W, equilibrated with 2 -10^{-4}; 3 -10^{-3}; 4 -10^{-2}; 5 -10^{-1}.

The data obtained prove that investigation of ΔE,T dependence makes it possible to evaluate the activation energy of electrical conductivity of ion-exchange resins. The method

of $\varkappa$,T dependence is complicated by polarization of electrodes and dispersed system, which is a function of frequency. The proposed method based on S.E. has no such drawbacks.

5. S.E. may be used to estimate the properties of ion-exchange resins. Thus, Fig.4a shows the dependence of ΔE and g of a number of Dowex 50W sediments on divinilbenzene (DVB)content of resins. The different curves refer to different KCl concentrations of equilibrium liquid. The figures at particular points on the curve correspond to %-content of dry resin in sediment.The extreme dependences obtained reflect a conflict of two factors, namely, an increase in the concentration of fixed charges, hence, in that of counter-ions and at the same time, an increase of the bond-energy of counter-ions. These factors affect reversely the magnitude of ΔpH.

Of still greater interest is the relationship $\Delta pH/C$, %DVB (C is the solid content in sediment), which is shown in Fig.4b The decrease of $\Delta pH/C$ with an increase in DVB content reflects an increase of the bond-energy of counter-ions. As the concentration of KCl increases the slope of the curves decreases, which testifies to the fact that the difference in the bond-energy at different DVB contents decreases with an increase in electrolyte concentration.

All above data enable us to stop regarding S.E. as a side effect interfering with investigation. On the contrary, S.E. may be turned into a new powerful means of investigation of electrical properties of dispersed systems.

REFERENCES

1.C.E. Marshall, Science 113, 43 (1951)
2.H.Jenny, T.R.Nielsen, N.T.Coleman, D.S.Williams, Science 112, 164 (1950)
3.J.Th.G.Overbeek, J.Colloid Sci., 8, 593(1953)
4.E.P.Honig, J.Electroanal. Chem., 37, 249 (1972)
5.H.R.Kruyt, Colloid Science, vol.1, Elsevier, Amsterdam 1952
6.K.S.Spiegler, R.L.Yoest, M.R.J.Wyllie, Disc.Farad. Soc., 21, 174 (1956)

MÖSSBAUER STUDY OF THE CORROSION PRODUCTS OF IRON AND IRON ALLOYS

A. Vértes*, E.Kuzmann**, S. Nagy*, F.Nagy*, L. Domonkos**, and Z. Hegedüs**

*Department of Physical Chemistry and Radiology, L. Eötvös University of Sciences, Budapest

**Department of Physical Metallurgy and Technology, Csepel Iron and Metal Works, Budapest

Scaling is one of the surface phenomena which take place when hot steel comes into contact with air /1,2/. The scales are known to be made up mainly of wüstite ($Fe_{1-x}O$), magnetite (Fe_3O_4) and haematite. Scaling under various experimental /1/ and industrial conditions /2/ has been studied by several authors, using a variety of methods. Mössbauer spectroscopy - which we used for the qualitative and quantitative analysis of scales formed on steel bands treated in alcalic bath and on untreated steel, respectively - has so far been applied mainly to the investigation of the various types of oxides.

The Mössbauer spectrum of wüstite measured at room temperature consists of a slightly asymmetric pair of lines. This spectrum has been interpreted in different ways by the various authors: according to WERTHEIM /3/ one line corresponds to Fe^{2+}, and the other to Fe^{3+}, while SHIRANE /4/ claims that the asymmetric pair of lines is the resultant of the Fe^{2+} quadrupole doublet and Fe^{3+} single line and JOHNSON /5/ is of the opinion that there are two Fe^{2+} quadrupole pair of lines in different positions on which the singlet of Fe^{3+} is superimposed. ELLIAS /6/ interpreted the spectrum as a resultant of quadrupole pairs of lines and GREENWOOD et al. /7/ using computer fitting found that the Mössbauer spectrum of $Fe_{0.941}O$ taken at room temperature might correspond to a Fe^{3+} quadrupole doublet and two Fe^{2+} quadrupole doublets. The

transformation of wüstite into other oxide phases can be followed quickly and sensitively with the help of Mössbauer spectroscopy /8,9/.

The samples of scale were prepared in the Csepel Works and the Mössbauer spectra recorded with the spectrometer of the Department of Physical Chemistry and Radiology of the L. Eötvös University. This spectrometer uses a constant acceleration vibrator and recording by a multi-channel analyzer. The samples were steel bands of the following composition: 0.06 % of C, 0.24 % of Si, 0.41 of Mn, and were heat treated at 900° C for 30 min in air, after which the scale was removed from the surface and crushed to powder. This powder was the "untreated" sample. A similar sample of steel was immersed in alcalic bath prior to heat treatment, heat treated and the scale removed from its surface served as the sample of "treated" scale.

The Mössbauer spectra of both the treated and untreated scale samples were recorded at room temperature and at the temperature of liquid nitrogen. The parameters of the spectra recorded at room temperature are given in Table 1. Figure 1 is the Mössbauer spectrum of the untreated scale sample, recorded at room temperature. The spectrum shows a conspicuously complex, multi-line pattern, however this curve is only an envelope curve in which the majority of the 13 peaks of higher intensities can be resolved into several lines. The asymmetric pair of lines at the bottom, in the middle of the spectrum, which because of its relatively high intensity is shown discontinuously and in a smaller scale, indicates the wüstite phase in the untreated sample. On the spectrum appear the lines both of magnetite and haematite and the latter has lines of lower intensity. The small quantity of metalic iron in the sample is suggested by the slight distortion of these lines in the positions where the lines of metalic iron should be.

Figure 2 shows the Mössbauer spectrum of the sample of scale obtained from steel pretreated with alcalic bath This resembles the spectrum of the untreated sample in its

complexity, 15 main lines making up the envelope curve. Lines characteristic of wüstite, magnetite, haematite and metallic iron can be found in the spectrum. Comparison of the Mössbauer spectrum of the treated and untreated scale samples shows immediately a difference in the intensity of the same lines in the two spectra, due primarily to the difference in the quantity of the oxide phases in the treated and untreated sample. Modifications in the structures of the lines mean partly that the change in the quantities of the various oxides was not the same for all oxides in the treated sample and partly that within certain oxide phases the ion composition and structure have also changed. It appears that in the treated sample the overall quantitiy of magnetite and haematite have decreased considerably (the quantity of magnetite more than that of haematite) compared to the untreated sample.

In order to be able to observe more closely the changes in the most important scale component (wüstite), for the sake of a higher resolution the Mössbauer spectra were recorded at such a low velocity range at which the multichannel analyzer recorded only intensities corresponding to that of wüstite. These spectra recorded in greater detail in the range of low velocities are shown in Fig.3. (illustrating the middle of the Mössbauer spectrum of untreated scale recorded at room temperature) and in Fig.4. (which is the middle of the Mössbauer spectrum of treated scale recorded at room temperature) The main difference between the two spectra appears at the first glance: the spectrum of the untreated scale consists of asymmetric lines showing less splitting, while the intensities of the lines in the spectrum of the treated scale are almost the same and are situated more widely apart. The difference in the intensities of two spectra indicates that there is somewhat more wüstite in the treated sample than in the untreated one. The greater quadrupole splitting of treated sample can be attributed to a reduced symmetry round the iron atoms. The results of the resolution of these spectra by means of the computer are illustrated in Table 2,

showing that in the case of untreated scale the most favourable resolution is into four lines, and in the case of treated scale the optimum resolution is into two lines.

These results can be interpreted by assuming that the reason for the lower quantity of magnetite and haematite in the treated scale is due to the inhibitory effect of treatment on the formation of the higher iron oxides, in agreement with the data of Table 3 which also shows the ratio of Fe^{3+} in the various iron oxides.

From these measurements further conclusions can be drawn regarding the changes in the defect structure of wüstite as a result of treatment in alcalic bath. The defect structure can be brought into correlation with the quadrupole splitting observed in the Mössbauer spectra recorded at room temperature. Extensive quadrupole splitting has its origin in the neighbouring cation vacancy which influences the electric field gradient at the Fe^{2+} nucleus.

X-ray and neutron diffraction studies revealed on the one hand four cation vacancies round one tetrahedral Fe^{3+} (symbol: $\left\{{}^{t}Fe^{3+}\ (\square_{+})_4\right\}^{5-}$) and 13 cation vacancies round four tetrahedral Fe^{3+}-s (symbol: $\left\{{}^{t}Fe^{3+}_{4}(\square_{+})_{13}\right\}^{14-}$) in the defect structure of wüstite. /7/

Analysing our experimental results (Tables 2-3) in the case of the untreated sample the defect structure $\left\{{}^{t}Fe^{3+}\ (\square_{+})_4\right\}^{5-}$ seems to be more probable and in the case of the treated sample the defect structure $\left\{{}^{t}Fe^{3+}_{4}(\square_{+})_{13}\right\}^{14-}$.

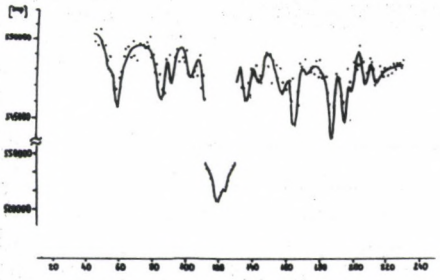

Fig. 1. channel

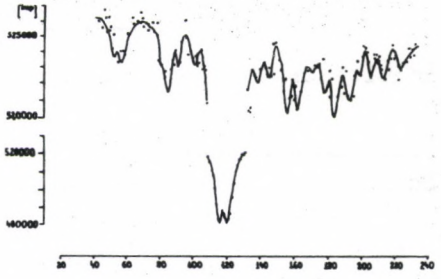

Fig. 2. channel

Table 1

Parameters of the unresolved Mössbauer spectra of untreated and treated scale samples measured at room temperature. (Position of lines in mm/s related to iron)

Number of line	Untreated sample high velocity	Treated sample range	Untreated sample low velocity	Treated sample range
1	8.71	8.82		
2	8.00	8.09		
3		5.51		
4	5.16	5.16		
5	2.90	2.90		
6	0.90	1.24	1.15	1.18
7	0.41	0.77	0.78	0.50
8	-1.08	-1.30		
9	-2.09	-2.18		
10	-3.62	-3.49		
11	-4.44	-4.21		
12	-5.39	-5.39		
13		-5.83		
14	-7.14	-6.81		
15	-8.12	-7.88		

Table 2

Results of the computer resolution of the scale spectra

Scale	χ^2	Degree of freedom	Resolved lines	
			position channel (or velocity)	intensity %
untreated	177	138	97,6; 112.4; 144.9	60.8;30;0;9
untreated	207	136	95.7;98,8; 112.8; 145.3	29.4;29;0 ; 31.2;10.4
treated	131	180	(1.23 mm/s) 96.6 (0.517 mm/s) 114.2	46.2;55.8;
treated	166	177	96.9;110.4; 115.6	50;8;42
treated	241	174	(1.22;1.21; 0.67;0.46 mm/s) 96.9; 97.0; 110.4;115.6	42;8;8;42

Table 3

Ratio of Fe/O and Fe^{3+}/Fe in the various iron oxides

	FeO	$Fe_{1-x}O$			Fe_3O_4	Fe_2O_3
Fe/O ratio	1.00	0.95	0.90	0.85	0.75	0.67
Fe^{3+}/Fe_{total}, %	0.0	10.5	22.2	35.3	66.7	100.0

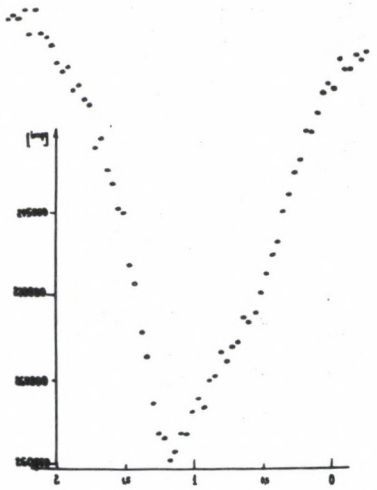

Fig. 3. mm/s

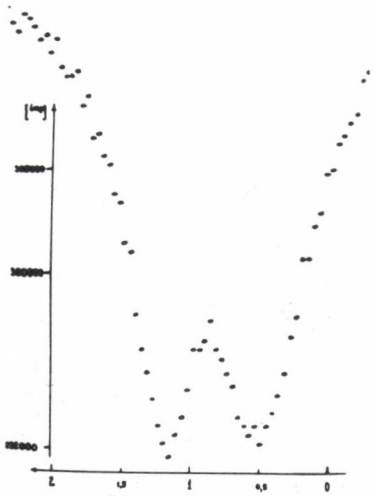

Fig. 4. mm/s

Literature

1. M.J. ENGELL, A. RAHMEL: Korrosion 23. Verlag Chemie GmbH, Weintheim, 1971.
2. A. RAHMEL: Korrosion 24. Verlag Chemie GmbH, Weinheim, 1972.
   B.E.F. FENDER, F.D. RILEY: H. Phys. Chem. Solids 30, 793 /1969/.
3. G.K. WERTHEIM: J. Appl. Phys. 32, 1105 /1961/
4. G. SHIRANE, D.E. COX, S.L. RUBY: Phys. Rev. 125, 1158 /1962/.
5. D.P. JOHNSON: Solid State Conim. 7, 1785 /1969/
6. D.J. ELIAS, J.W. Linnett: Trans.Farady Soc. 65, 2673 /1969/.
7. N.N. GREENWOOD, A.T. HAWE: J.Chem. Soc. Dalton Transl. 1, 110 /1972/.
8. N.N. GREENWOOD, A.T. HOWE: J.Chem. Soc. Dalton Transl. 1, 116 /1972/ and 1, 122 /1972/
9. D.A. CHANNING, S.M. DICKERSON, M.J. GRAHAM: Corros. Sci. 13, 933 /1973/.

THE DOUBLE LAYER INTERACTION OF TWO CHARGED COLLOIDAL SPHERES OF A CONCENTRATED DISPERSION IN A HYDROCARBON MEDIUM

S. Levine and G. R. Féat

Department of Mathematics, University of Manchester, Manchester, M13 9PL, England.

We wish to calculate the double layer interaction between two, identical, neighbouring, charged spherical particles of a concentrated dispersion in a liquid of low dielectric constant, such as a hydrocarbon[1-4]. The effect of surrounding particles is accounted for by enclosing the surfaces S_1 and S_2 of the two neighbouring particles by a symmetrical surface S_0 situated in the hydrocarbon medium, on which the normal component of the electric field is zero. Assuming the particle surfaces to carry fixed positive charge, the diffuse layer in the hydrocarbon medium contains only one ion species, the anionic (univalent) counter-ion, at such low concentrations that the mean density of anions n_- in the region enclosed by S_0 is practically uniform. Suppose that the dispersion contains N identical particles in a volume V. Then it is readily shown that the surface S_0 encloses a volume equal to $2V/N$, twice the mean volume per particle.

The potential distribution ψ in the hydrocarbon medium satisfies Poisson's equation, which is expressed in the non-dimensional form

$$a^2 \nabla^2 \phi = 1 \tag{1}$$

by introducing the dimensionless quantities

$$\bar{\kappa}^2 = \kappa^2 a^2 = \frac{4\pi n_- e_0^2}{\epsilon k T} a^2 \quad , \quad \phi = \frac{1}{\bar{\kappa}^2} \frac{e_0 \psi}{k T} \quad . \tag{2}$$

Here κ is the Debye-Huckel parameter, a the radius of a particle, ϵ the dielectric constant of the hydrocarbon medium, e_0 the proton charge, k Boltzmann's constant and T the absolute temperature.

The solution of (1) may be expressed in various co-ordinate systems. Let r_1, θ_1, λ and r_2, θ_2, λ be the spherical polar co-ordinates of a general point in the hydrocarbon medium referred respectively to the particle centres O_1 and O_2 as origin, where θ_1 and θ_2 are the angles measured from the line of centres and λ is the azimuthal angle about this line. The solution of (1) as a multipole expansion about the two particle centres, reads up to quadrupole terms,[1,2]

$$\phi = \frac{1}{12a^2}\left(r_1^2 + r_2^2\right) + B_0\left(\frac{1}{r_1} + \frac{1}{r_2}\right) + B_1\left(\frac{\cos\theta_1}{r_1^2} + \frac{\cos\theta_2}{r_2^2}\right) \qquad (3)$$

$$+\left(A_2 r_1^2 + \frac{B_2}{r_1^3}\right) P_2(\cos\theta_1) + \left(A_2 r_2^2 + \frac{B_2}{r_2^3}\right) P_2(\cos\theta_2) + \cdots$$

apart from an additive constant. The first term is a particular integral of (1) and the rest of (3) is the general solution of Laplace's equation. The terms proportional to positive powers of r_1 and r_2 are dominant at large distances from the particles since they increase indefinitely. However, the solution (3) is restricted to the volume contained by S_0 where the normal derivative of ϕ vanishes. The potential ϕ diminishes from the surface S_1 or S_2 to the outer surface S_0, reaches a 'minimum' on S_0 and then increases beyond S_0.

If the total charge on the surface S_1 equals $p e_0$, then Gauss's theorem states

$$-\epsilon \int_{S_1} \left(\frac{\partial \psi}{\partial r_1}\right)_{r_1 = a} dS = 4\pi p e_0 . \qquad (4)$$

Application of this condition to (3) yields

$$B_0 = \frac{1}{3}\left(\frac{b_0^3}{a^2}\right), \qquad (5)$$

where b_0 is the radius of the spherical volume V/N assigned per particle. The determination of the coefficients (B_1, A_2, B_2, etc.) in the higher order terms of (3) depends partly on the boundary conditions at the particle surface. In the case of dielectric particles, the potential inside a particle satisfies Laplace's equation. The conditions at the particle surface are continuity in potential and the usual relation between discontinuity in normal component of dielectric displacement and

the surface charge density. The presence of terms in the potential which are proportional to positive powers of r_1 and r_2 permit the outer surface S_0 to be varied, subject to the requirement that the volume enclosed by S_0 equals $2V/N$. With a limited number of terms retained in the multipole expansion, the boundary conditions can only be satisfied approximately. In order to isolate electrically the region contained within S_0 as much as possible from the surroundings, an additional condition on S_0 is that the potential variation on it be small.

Let S be any closed surface in the hydrocarbon medium surrounding particle O_1 only. Then if the potential ψ satisfies the Poisson-Boltzmann equation, the electric double layer force on O_1 is given by the surface integral[5]

$$\vec{X} = \int_S \left[\frac{\varepsilon}{4\pi} \left(E_n \vec{E} - \frac{1}{2} E^2 \vec{n} \right) - \Pi \vec{n} \right] dS , \tag{6}$$

where $\vec{E}$ is the electric field vector, E_n the normal component of $\vec{E}$ outwards to S, E the magnitude of $\vec{E}$, Π the ideal osmotic pressure due to the ions in the hydrocarbon medium and $\vec{n}$ the unit, outward normal vector on S. The force vector $\vec{X}$ consists of a Maxwell electrostatic stress term and of an osmotic pressure term. It is convenient to choose for S the particle surface S_1, and we need only consider the component of $\vec{X}$ in the direction O_2O_1 along the line of centres. This reads

$$X_0 = -2\pi a^2 \int_0^{\pi} \left[\frac{\varepsilon}{8\pi} \left\{ \left[\left(\frac{\partial \psi}{\partial r_1} \right)^2 - \frac{1}{a^2} \left(\frac{\partial \psi}{\partial \theta_1} \right)^2 \right] \cos\theta_1 - \frac{2}{a} \sin\theta_1 \frac{\partial \psi}{\partial r_1} \frac{\partial \psi}{\partial \theta_1} \right\} - kT\, n_a(\theta_1) \cos\theta_1 \right] \sin\theta_1 \, d\theta_1 , \tag{7}$$

where $n_a(\theta_1)$ is the volume density of counter-ions next to S_1. If only the first two terms are retained in the series (3) for ϕ (the 'monopole' approximation), then the formula (6) yields

$$X_0 = X_0^{(m)} = \frac{\gamma}{12} \frac{b_0^3}{a^4 b^2} \left(b_0^3 - 4b^3 \right) , \tag{8}$$

where γ is a unit of force defined as

$$\gamma = \frac{\varepsilon}{3} \left(\frac{kT}{e_0} \right)^2 \bar{\kappa}^4 , \tag{9}$$

and $2b = O_1O_2$, the separation between the centres of the two particles. With the convention that X_0 is the force on O_1 in the direction O_2O_1, $X_0 > 0$ represents a repulsion between O_1 and O_2 and $X_0 < 0$ an attrac-

tion. We vary the separation $2b$ from the distance of nearest approach $2a$ to a mean nearest-neighbour separation $2b_m$. For a regular close packing distribution with 12 nearest neighbours $b_m = 0.9047\, b_0$. The force X_0 in equation (8) is zero at $4b^3 = b_0^3$ or $b = 0.63\, b_0$. At particle contact the formula (8) describes a repulsive force. This repulsion diminishes with increase in separation to reach the value zero at $b = 0.63 b_0$, and then changes to an attraction at larger separations. The integral (7) for X_0 is also determined when the 'dipole' (B_1) and the 'quadrupole' (A_2, B_2) terms are retained in the potential ϕ. The corresponding successive approximations to the force, $X_0^{(m)}$, $X_0^{(d)}$, $X_0^{(q)}$ are similar, all three showing a repulsion at small b $(\lesssim 1.4a)$ but an attraction at larger b.

Table 1 illustrates this behaviour of the inter-particle force. For $\varepsilon = 2$, $T = 25°C$, $a = 0.1$ micron and 10^{-7}M counter-ion concentration in the hydrocarbon medium, $\bar{\kappa}^{-2} = 0.212$ and $\gamma = 2.2 \times 10^{-15}$ newton. The ratio $\varepsilon_p/\varepsilon = 10$, where ε_p is the dielectric constant of the particle medium. Also the volume fraction of particles equals $(a/b_0)^3$, which we choose to be 0.1. The number of (univalent) cations p on a particle surface equals the number of counter-ions per particle, so that

$$p = n_- \left[\frac{V}{N} - \frac{4\pi}{3} a^3 \right] = \frac{4\pi}{3} n_- \left(b_0^3 - a^3 \right), \qquad (10)$$

which is assumed independent of separation. This yields $p = 2.5$ for the values of n_-, b_0 and a chosen. It is readily verified that the changes in electric double layer interaction energy of the two particles in the range of separations $b = a$ to $b = b_m$ are only a fraction of thermal energy kT. This suggests that electric double layer forces play a minor role in governing stability of concentrated dispersions in hydrocarbon media.

— — — — — — — — — — — — — — —

Table

Force between two particles at different separations in various approximations

$\varepsilon = 2$, $a = 0.1\mu$, 10^{-7}M counter-ions, 10% volume fraction of particles, $\gamma = 2.2 \times 10^{-15}$ newton, T = 25°C, surface charge pe_0 independent of b, $p = 2.5$

b/a	1.0	1.2	1.4	1.6	1.8	1.95

Multipole expansion with dielectric particle; $\epsilon_p/\epsilon = 10$; (m) = monopole; (d) = dipole; (q) = quadrupole

$X_0^{(m)}/\gamma$	4.5	1.78	-0.44	-2.11	-3.44	-4.33
$X_0^{(d)}/\gamma$	3.1	1.25	-0.29	-1.70	-2.85	-3.55
$X_0^{(q)}/\gamma$	3.9	1.85	0.15	-1.20	-2.30	-3.10

Perfectly conducting particles - bispherical co-ordinates; (1) = first approximation; (2) = second approximation

$X_0^{(1)}/\gamma$	—	16.7	5.4	1.2	-1.3	-2.6
$X_0^{(2)}/\gamma$	—	3.63	0.17	-1.51	-2.80	-3.62

Perfectly conducting particles in contact ($b/a=1$) -tangent-sphere co-ordinates

— — — — — — — — — — — — — — —

In view of its apparent importance, it seems desirable to test the validity of this conclusion by seeking a different approximation to the force between the two particles. In the case where the dielectric constant of the particles is large compared with that of the hydrocarbon medium, the surfaces of the two particles may be assumed to be equipotentials, with fixed total surface charge. The solution of (1) is then conveniently expressed in terms of orthogonal bispherical co-ordinates, denoted by μ, η, λ . The spheres S_1 and S_2 are denoted by $\mu = -\mu_0$ and $\mu = \mu_0$ respectively where $\cosh \mu_0 = b/a$. The solution of (1) now reads

$$\phi = \phi(\mu,\eta) = \frac{C^2}{3}\left[\frac{\cosh\mu\cosh 2\mu_0 - \cos\eta}{(\cosh\mu - \cos\eta)(\cosh 2\mu_0 - 1)}\right] + \sqrt{\cosh\mu - \cos\eta}\sum_{n=0}^{\infty} C_n \cosh\{(n+\tfrac{1}{2})\mu\} P_n(\cos\eta) + \phi_0 \qquad (11)$$

where $C = \sinh\mu_0$ and ϕ_0 is an additive constant. The first term is the particular integral of (1) already introduced in (2) and expressed here in bispherical co-ordinates. The coefficients C_n can be determined by the condition that ϕ is constant on the surface $\mu = -\mu_0$. It is convenient to choose ϕ_0 such that $\phi = 0$ on the sphere $\mu = -\mu_0$. If $h_\mu d\mu$, $h_\eta d\eta$, $h_\lambda d\lambda$ denote elements of length along the curvilinear axes then Gauss's theorem reads

$$-2\pi \int_0^{\pi} \frac{h_\eta h_\lambda}{h_\mu} \left(\frac{\partial \psi}{\partial \mu}\right)_{\mu=-\mu_0} d\eta = \frac{4\pi p e_0}{\varepsilon} \tag{12}$$

This yields the relation

$$\sum_{n=0}^{\infty} C_n = \frac{b_0^3}{b\sqrt{2}\,\sinh\mu_0} \tag{13}$$

making use of (10). The integral (7) for the force X_0 on O_1 is readily expressed in terms in bispherical co-ordinates. This has been integrated (numerically in part), retaining the first and second terms (C_0 and C_1) in the infinite series of equation (11), which is the solution of Laplace's equation. The computed values of X_0 ($X_0^{(1)}$, $X_0^{(2)}$ denoting the first and second approximations) are shown in the Table. Calculations of the first three coefficients C_0, C_1 and C_2 in (11) that the series in (11) converges rapidly when $b/a > 1.4$, but not for smaller separations. An increasing number of terms of this series is required with decrease in particle separation, rendering calculations at very small separations ($b/a \lesssim 1.2$) impractical. Indeed, at particle contact where $\mu_0 = 0$, the sum in (13) becomes infinite so that bispherical co-ordinates cannot be used. In the Table the disparity between the first and second approximations for the force $X_0^{(1)}$ and $X_0^{(2)}$ at $b/a \lesssim 1.4$ demonstrates this poor convergence at the smaller separations.

In the particular case of conducting particles at contact it is possible to obtain an exact solution for the potential and therefore for the interparticle force with the particular model assumed here. Use is made of tangent-sphere co-ordinates,[7] which we denote by ξ, ζ, λ . The particle surfaces S_1 and S_2 are now given by $\xi = -\xi_0$ and $\xi = \xi_0$ respectively, where $\xi_0 = 1/2a$. The solution of (1) is

$$\phi = \phi(\xi, \zeta) = \frac{1}{12a^2}\left(\frac{2}{\xi^2+\zeta^2} + \frac{1}{2\xi_0^2}\right) + (\xi^2+\zeta^2)^{1/2} \int_0^{\infty} A(q)\cosh(q\xi)\, q\, J_0(q\eta)\, dq + \phi_0 \tag{14}$$

where J_0 is the Bessel function of the first kind of order zero and

$$A(q) = -\frac{e^{-q\xi_0}}{\cosh(q\xi_0)}\left\{\left(\phi_0 + \frac{1}{24a^2\xi_0^2}\right)\frac{1}{q} + \frac{1}{6\xi_0 a^2}\right\} \tag{15}$$

We choose the potential on the particle surfaces to be zero and apply Gauss's theorem, which in tangent-sphere co-ordinates reads

$$2\pi \int_0^{\infty} \left[\frac{h_\eta h_\lambda}{h_\xi} \frac{\partial \psi}{\partial \xi} \right]_{\xi=-\xi_0} d\eta = \frac{4\pi p e_0}{\varepsilon} \qquad (16)$$

Making use of (10) this yields

$$\Phi_0 = -\frac{1}{2\ln 2} \left\{ \frac{2}{3} \left(\left(\frac{b_0}{a} \right)^3 - 1 \right) + \frac{2}{3} \left(1 + \frac{\ln 2}{2} + \frac{\pi^2}{12} \right) \right\}, \qquad (17)$$

which depends only on the volume fraction of particles $(a/b_0)^3$. For a 10% fraction, $\Phi_0 = -5.371$. The force X_0 on S_1 is given by

$$X_0 = -\frac{\varepsilon}{4} \int_0^{\infty} \left[\frac{h_\eta h_\lambda}{h_\xi^3} \left(\frac{\partial \psi}{\partial \xi} \right)^2 \frac{\partial z}{\partial \xi} \right]_{\xi=-\xi_0} d\eta, \qquad (18)$$

where z is the distance along the line of centres. For the 10%, volume fraction $X_0/\gamma = 2.23$. This is smaller than the value obtained for the dielectric particles at contact, as given in the Table. Also we can expect that in bispherical co-ordinates the third approximation will reduce still further the value $X_0/\gamma = 3.63$ shown in the Table at $b/a = 1.2$.

References

1. C. S. Chen and S. Levine, J. Colloid Interface Sci., 43, 599 (1973).
2. G. R. Feat and S. Levine, Faraday Transactions II, 71, 102 (1975).
3. G. R. Feat and S. Levine, J. Colloid Interface Sci., (in press).
4. G. R. Feat and S. Levine (submitted for publication).
5. G. M. Bell and S. Levine, Trans. Faraday Soc., 54, 785 (1958).
6. P. M. Morse and H. Feshbach, Methods of Theoretical Physics, Part II, Chap. 10, 1953, McGraw-Hill.
7. P. Moon and D. E. Spencer, Field Theory Handbook, 1961, Springer-Verlag.

THEORETICAL ASPECTS OF THE RATE OF WETTING OF A POROUS MEDIUM

S. Levine* and G. Neale

Department of Chemistry, University of Victoria, Victoria, British Columbia, Canada V8W 2Y2, and Department of Chemical Engineering, University of Alberta, Edmonton, Alberta, Canada.

*Permanent address: Department of Mathematics, University of Manchester, England.

Among the different models of a porous medium, those which are most readily amenable to theoretical treatment in respect to fluid flow are assemblages of parallel plate channels or cylindrical capillaries and regular arrays of parallel identical cylindrical rods or of identical spheres. Here we shall be mainly concerned with such arrays and shall use the cell-type theories of Happel[1-3] and Kuwabara[4] to describe the hydrodynamic flow of the fluid permeating the porous medium. The model of equal spheres simulates a porous powder and that of rod-like cylinders should apply to textiles and similar materials. In representing a porous medium by these models, the following assumptions are made: (i) The advancing front of the imbibing liquid is a planar surface of a given fixed mean area. Thus we ignore the occurrence of "channelling" or "fingering" due to local inhomogeneities in the porous medium. (ii) The distribution of spheres or rod uniformly fills the whole volume of the medium and is fixed. No allowance is made for possible movement of particles constituting the porous medium (change in packing geometry) during the imbibition. (iii) The effect of entrapment of displaced vapour (e.g. air) as the penetrating liquid permeates the medium is ignored. (iv) Because of the non-uniform cross-section of the 'bore' or space between the particles with the advance of the liquid-vapour interface through the porous medium, this interface expands and contracts as the cross-section changes. The presence of hysteresis[5] between wetting and drainage indicates that energy is being dissipated irreversibly during the passage of liquid through the medium. Estimating these dissipative effects is a difficult problem which we shall only discuss briefly.

Making the approximations described above and using Darcy's law[6] a general treatment of the rate of penetration of a fluid into a porous medium can be given as follows.[7] We consider a cross-sectional area A of

the porous medium through which an incompressible fluid of density ρ and viscosity μ is advancing in a direction normal to the area A. Let z be the penetration distance of the fluid front and S the internal surface area per unit volume of porous material. In a displacement δz of the fluid front, the increase in wetted surface area is $SA\delta z$, the corresponding free energy change due to surface adhesion is $\gamma SA\,\delta z$, where γ is the adhesion tension and the equivalent suction force is γSA. If the direction of the mean flow is inclined at an angle ϕ to the vertical and ε is the void fraction (porosity) of the porous medium, then the force of gravity on the fluid when its front has advanced a distance z is $Az\varepsilon\rho g\cos\phi$. The equation of motion for the advancing front when energy dissipation is neglected is given by

$$A\varepsilon\rho\frac{d}{dt}\left(z\frac{dz}{dt}\right)=\gamma SA-Az\varepsilon\rho g\cos\phi-\frac{A\mu z}{k}\frac{dz}{dt}, \qquad (1)$$

where the left-hand side is the rate of change of linear momentum of the fluid and the last term on the right-hand side is the viscous drag according to Darcy's law, k being the permeability of the porous medium. Introducing the parameters

$$\alpha=\frac{\mu}{k\varepsilon\rho}, \quad \beta=\frac{\gamma S}{\varepsilon\rho}, \quad \lambda=\frac{kg\cos\phi}{\mu}\left(\frac{\varepsilon^3\rho^3}{\gamma S}\right)^{1/2}, \qquad (2)$$

and the variables

$$T=\alpha t, \quad Z=\frac{\alpha}{\sqrt{\beta}}z, \qquad (3)$$

equation (1) now becomes

$$\frac{d}{dT}\left(Z\frac{dZ}{dT}\right)+Z\frac{dZ}{dT}+\lambda Z=1. \qquad (4)$$

In horizontal flow $\phi=\frac{\pi}{2}$, $\lambda=0$ and the general solution of (4) is

$$Z^2=2T+Ce^{-T}+D, \qquad (5)$$

where C and D are integration constants. At large times, this simplifies to $Z^2=2T$ so that $dZ/dT=1/Z$. Reverting to the original variables z and t, this gives the velocity of penetration

$$V=\frac{dz}{dt}=\frac{k\gamma S}{\mu z}. \qquad (6)$$

For a single cylindrical capillary of radius a, the porosity $\varepsilon = 1$, $S = 2/a$ and on replacing Darcy's law by Poiseuille's law $k = a^2/8$. Hence (6) becomes

$$V = \frac{\gamma a}{4\mu Z}, \qquad (7)$$

which is Washburn's equation for a horizontal tube.[9-10] The constants C and D in the general solution (5) depend on the initial conditions but difficulties are encountered in the interpretation of (4) at entry into the porous medium $Z = 0$, if it is assumed that the fluid front has zero velocity. Thus it is seen from (4) that if $Z = 0$ and $dZ/dT = 0$ then $d^2Z/dT^2 = 1/Z = \infty$ for any λ.

Szekely, Neumann and Chuang[11] have endeavoured to overcome the difficulty of the initial conditions at the entry into the capillary. They do not start with the equation of force balance or equivalently of momentum balance, but rather with the equation of energy balance as described by Bird, Stewart and Lightfoot.[12] If we adapt their approach to the present system, then (1) is replaced by

$$A\varepsilon\rho \frac{d}{dt}\left[(Z+h)\frac{dZ}{dt}\right] = \gamma S A - AZ\varepsilon\rho g\cos\phi - \frac{A\mu Z}{k}\frac{dZ}{dt} - \frac{1}{2}A\varepsilon\rho e_v\left(\frac{dZ}{dt}\right)^2 \qquad (8)$$

By considering the flow of fluid from a reservoir into the porous medium at the entry position $Z = 0$, one is led to a pressure term which is equivalent to an additional effective length h of imbibed fluid. The last term on the right-hand side is dissipative and is based on the general expression for the rate of energy irreversibly dissipated, given by Bird, Stewart and Lightfoot,[12] namely "1/2 x mass rate of flow x mean square fluid velocity x friction loss factor e_v." No attempt is made here to estimate either h or e_v. On introducing the transformation (3), equation (8) becomes

$$(Z + C)\frac{d^2Z}{dT^2} + \left(1 + \tfrac{1}{2}e_v\right)\left(\frac{dZ}{dT}\right)^2 + Z\frac{dZ}{dT} + \lambda Z = 1, \qquad (9)$$

where $C = \alpha h/\sqrt{\beta}$

For a single vertical capillary of radius a, Szekely, Neumann and Chuang put $h = 7a/6$ and $e_v = 0.45$ and solved (9) numerically with the initial conditions $Z = dZ/dT = 0$ at $T = 0$. Their source of energy dissipation was the circulation set up near the entrance to the capillary tube because of the sharp corner, whereas hysteresis would probably be

the main dissipative effect in a porous medium. The inclusion of the additional length h removes the infinity at $T=0$. If the first and second terms are neglected (9) simplifies to

$$\frac{dZ}{dT} = \frac{1}{Z} - \lambda \quad , \tag{10}$$

which becomes Washburn's equation for a vertical capillary tube $(\phi = 0)$

$$\frac{dz}{dt} = \frac{a}{4\mu}\left(\frac{\gamma}{z} - \frac{\rho g a}{2}\right) . \tag{11}$$

From the numerical solutions of Szekely, Neumann and Chuang it would appear that in capillaries with radii of 0.01 - 0.001 cm. equation (11) is fairly good except for the initial 0.001 - 0.1 sec.

This suggests starting with the Washburn limiting form and using a series expansion. On introducing the transformation[7] $U = dT/dZ$ from which $d^2Z/dT^2 = -(dU/dZ)/U^3$, equation (9) becomes

$$-(Z+\tau)\frac{dU}{dZ} + (1+\tfrac{1}{2}e_v)U + ZU^2 = (1-\lambda Z)U^3 . \tag{12}$$

In the absence of gravity $(\lambda = 0)$, where $U = Z$ is the Washburn formula for a single capillary, a suitable expansion at large Z (large z or t) is

$$U = Z + \frac{e_v}{2Z} - \frac{\tau}{Z^2} + \frac{e_v(1-\frac{1}{4}e_v)}{Z^3} + \cdots . \tag{13}$$

Reverting to variables z and t , this becomes

$$\frac{dt}{dz} = \frac{\alpha}{\beta}z + \frac{e_v}{2\alpha z} - \frac{\sqrt{\beta}\,\tau}{(\alpha z)^2} + \frac{\beta e_v(1-\frac{1}{4}e_v)}{(\alpha z)^3} + \cdots \tag{14}$$

Integration yields t in terms of z , apart from an additive constant. The first term in (14) gives Washburn's eqn. (6), which does not depend on h or e_v . At angles $\phi < \pi/2$ when $\lambda \neq 0$, equation (12) can be solved by an iteration method which begins with the Washburn relation (10), namely

$$U = U_0 = Z/(1-\lambda Z) . \tag{15}$$

A solution of (12) which is suitable for $Z \lesssim 1/\lambda \gg 1$ is

$$U = U_0 + U_1 + U_2 + \cdots , \tag{16}$$

where

$$U_1 = \frac{(1-\lambda Z)}{Z^2}\left[(1+\tfrac{1}{2}e_v)U_0 - (Z+c)\frac{dU_0}{dZ}\right), \qquad (17)$$

$$U_2 = \frac{(1-\lambda Z)}{Z^2}\left[(1+\tfrac{1}{2}e_v)U_1 - (Z+c)\frac{dU_1}{dZ} - 2ZU_1^2\right]. \qquad (18)$$

It is readily verified that (16) reduces to the expansion (13) for $\lambda = 0$. The limiting height of rise of the fluid Z_∞ is derived from the condition $U_0 = \infty$, giving $Z_\infty = 1/\lambda$ or

$$Z_\infty = \frac{\gamma S}{\varepsilon \rho g}. \qquad (19)$$

In the unit-cell model for a porous powder of identical spherical particles, each particle of radius a is surrounded by a concentric spherical shell of fluid having an outer radius b, such that the volume fraction of particles is $(a/b)^3$. The porosity $\varepsilon = 1 - (a/b)^3$ and the specific surface area $S = 3(1-\varepsilon)/a$. Happel[1] assumed that the tangential component of the shear stress due to the fluid flow through the spherical shell is zero at the outer boundary of the shell whereas Kuwabara[4] chose zero velocity at this boundary. In the Happel theory, Darcy's permeability coefficient k in equation (1) is given by[7]

$$k = \frac{2}{9}\frac{a^2}{(1-\varepsilon)\Omega}, \qquad (20)$$

where, if $y = a/b = (1-\varepsilon)^{1/3}$,

$$\Omega = \Omega_H(y) = \frac{2(3+2y^5)}{3(2-3y+3y^5-2y^6)} \qquad (21)$$

The corresponding value of Ω in Kuwabara's theory is

$$\Omega = \Omega_K(y) = \frac{5}{(2-9y+5y^3-y^6)} \qquad (22)$$

In both cases Ω increases from the value $\Omega = 1$ at $\varepsilon = 1$ with decrease in porosity.

In the unit-cell representation of a porous medium by a swarm of identical cylindrical rods, the fluid flows through an annular space between a cylinder of radius a and an outer cylindrical envelope of radius b, where the porosity is now $\varepsilon = 1-(a/b)^2$ and the specific surface area $S = 2(1-\varepsilon)/a$. The cylinders are assumed so long that end effects are negligible and S must be evaluated over a volume of the medium $\mathcal{V}$ such that $\mathcal{V}^{1/3} \gg a$. For flow in the direction of the axes past a regular array of parallel cylinders, the Happel[2] and Kuwabara[4] models give the same prediction for the permeability of the porous medium k which may be expressed in the same form as (20), namely[2]

$$k = k_{\parallel} = \frac{a^2}{8(1-\varepsilon)\Lambda}, \tag{23}$$

where, if $y = a/b = (1-\varepsilon)^{1/2}$

$$\Lambda = \Lambda_{\parallel}(y) = -\frac{1}{3-4y^2+y^4+4\ln y}. \tag{24}$$

The reason for a common $k_{\parallel}$ is that the conditions of zero shear stress and zero vorticity at the outer envelope are equivalent. For flow perpendicular to the axes of the cylinders, the Kuwabara model gives a value for the permeability $k = k_{\perp}^{K} = \frac{1}{2}k_{\parallel}$ whereas in the Happel model $k = k_{\perp}^{H}$, which is given by (23), with

$$\Lambda = \Lambda_{\perp}^{H}(y) = -\frac{1}{(1-y^4)/(1+y^4)+2\ln y}. \tag{25}$$

These values for $k_{\perp}^{K}$ and $k_{\perp}^{H}$ will also apply to a system of cylinders oriented parallel to a single plane, to which the fluid flow is perpendicular, provided the system can be regarded as equivalent to a large number of clusters of parallel cylinders. Further, if we assume that a system of randomly arranged cylinders is equivalent to groups of cylinders parallel and perpendicular to the direction of flow, then the effective permeability k_R is given by

$$\frac{1}{k_R} = \frac{1}{3}\left(\frac{1}{k_{\parallel}} + \frac{2}{k_{\perp}}\right), \tag{26}$$

since resistance to flow is inversely proportional to permeability. For the Kuwabara model this yields $k_R = k_R^K = 0.6\,k_{\parallel}$. For the Happel

model k_R is given by (23) with

$$\Lambda = \Lambda_R^H(y) = -\frac{3}{3-4y^2+y^4+2\left(\frac{1-y^4}{1+y^4}\right)+8\ln y} \qquad (27)$$

Similarly to the $\Omega(y)$ functions in the sphere models of the porous medium, the $\Lambda(y)$ functions in the cylinder models increase with decrease in porosity. But at $\epsilon=1$, the $\Lambda(y)$ equal zero whereas the $\Omega(y)$ equal unity. Plots of these various functions are shown. We note that if the porous medium is represented by an assemblage of parallel cylindrical capillaries of radius a, then the permeability coefficient simply equals $a^2/8$.

In their theory of the rate of wetting of a cylindrical capillary, Szekely, Neumann and Chuang did not allow for the departure from Poiseuille flow of the flow pattern in the vicinity of the advancing meniscus. This was investigated by Hansen and Toong[13] who attempted to solve simultaneously Laplace's equation which governs the shape of the meniscus and the hydrodynamic equations of motion for steady state fluid flow in a cylindrical tube. However, they left unsolved the well-known apparent contradiction between the no-slip condition and the movement of the three-phase line or contact line. Similar omissions in the treatment of the advancing fluid front through a porous medium are implied in the equation (8).

References

1. J. Happel, J. Amer. Inst. Chem. Eng., 4, 197 (1958).
2. J. Happel, J. Amer. Inst. Chem. Eng., 5, 174 (1959).
3. J. Happel and H. Brenner, Low Reynolds Number Hydrodynamic (Prentice-Hall, New York, 1965).
4. S. Kuwabara, J. Phys. Soc. Japan, 14, 197 (1958).
5. T. D. Blake and J. M. Haynes, Progress in Surface and Membrane Science, Vol. 6, 125 (1973).
6. A. E. Scheidegger, The Physics of Flow Through Porous Media (Univ. of Toronto Press, 1957).
7. S. Levine and G. Neale, Faraday Transactions II, 71, 12 (1975).
8. R. E. Johnson and R. H. Dettre in Surface and Colloid Science (ed. E. Matijevic), Vol. 2, (Wiley-Interscience, New York, 1969).
9. E. W. Washburn, Phys. Rev., 17, 273 (1921).
10. E. K. Rideal, Phil. Mag., 44, 1152 (1922).
11. J. Szekely, A. W. Neumann and Y. K. Chuang, J. Coll. and Int. Sci., 35, 273 (1971).
12. R. B. Bird, W. E. Stewart and E. N. Lightfoot,"Transport Phenomena", Chap. 7 (Wiley, New York, 1960).

13. R. J. Hansen and T. Y. Toong, J. Coll. and Int. Sci., 37, 196 (1971).

Figure. Plots of Ω and Λ as functions of $1-\varepsilon$, where ε = porosity = 1 - volume fraction. Curves A, B Sphere-models of porous medium, $y = \frac{a}{b} = (1-\varepsilon)^{1/3}$ Curves C, D, E Cylinder-models, $y = \frac{a}{b} = (1-\varepsilon)^{1/2}$

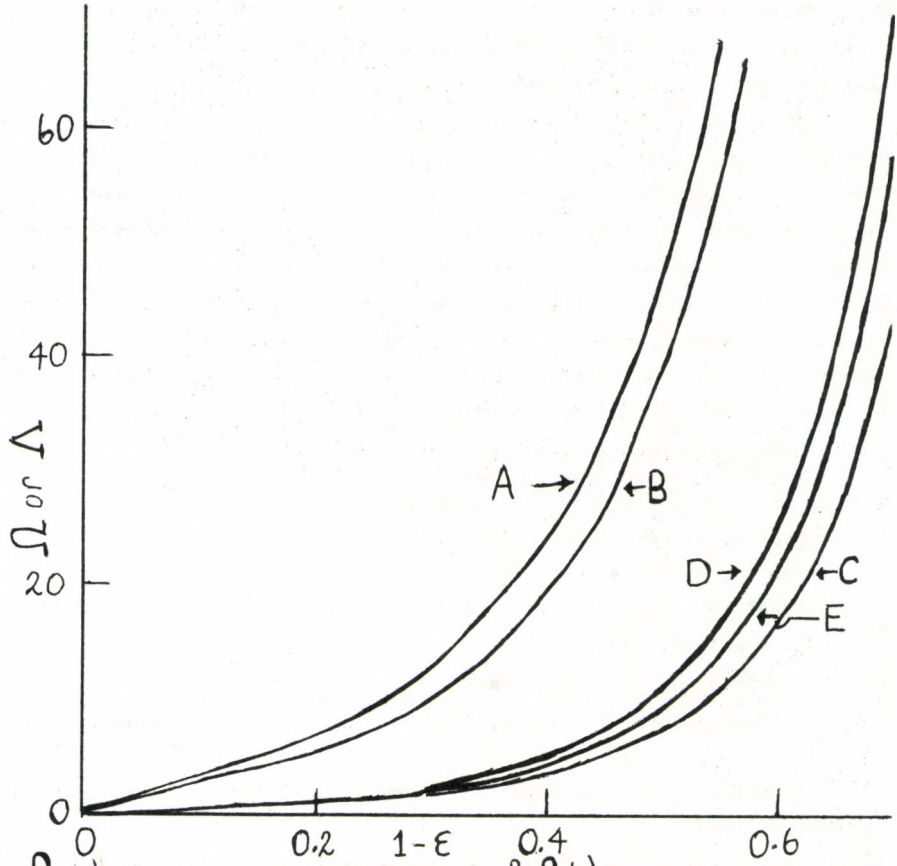

A: $\Omega_H(y)$, Happel (zero tangential stress); B: $\Omega_K(y)$ Kuwabara (zero vorticity).

C: $\Lambda_{11}(y)$ Flow parallel to cylinders (Happel and Kuwabara)

D: $\Lambda_{\perp}^{H}(y)$ Flow perpendicular to cylinders, Happel; $\Lambda_{\perp}^{K}(y) = 2\Lambda_{11}(y)$, Kuwabara

E: $\Lambda_{R}^{H}(y)$ Random orientation of cylinders, Happel; $\Lambda_{R}^{K}(y) = \frac{2}{3}\Lambda_{11}(y)$

For strict comparison at same a and ε, Λ is multiplied by factor 16/9.

BAERT, L. 75
BARAN, A. A. 283, 291
BARGEMAN, D. 439
BAUMEISTER, W. 721
BEDŐ, Zs. 517
BELOUSCHEK, P. 187
BERECZ, E. 517
BERLINER, C. 543
BIRDI, K. S. 473
BODNÁR, J. 49
BOROSS-VARGHA, É. 163
BOVKUN, O. P. 465
BOZZAY, J. 711
BRAKEL, J. van 141
BROWN, J. B. 507
CAIRNS, R. J. R. 323
CASPERS, J. 527
CHERNOBEREZHSKII, Yu. M. 737
CHIFU, E. 559
CHRISTEN, H. 481, 489
CHRISTOV, Chr. 575
CSEMPESZ, F. 299
CSÜRÖS, Z. 711
DABROWSKI, A. 83
DÁRDAI, Z. 429
DÁVID, Á. 711
DEGUCHI, K. 601
DEINEGA, U. F. 421, 655
DÉKÁNY, I. 99
DESPOTOVIC, R. 265
DIMITROV, D. S. 583
DOMONKOS, L. 745
DÖRFLER, H. D. 535, 551
DUKHIN, S. S. 349
EICKE, H. F. 481, 489
ELTEKOV, Yu. A. 213
EMMERIK, E. J. van 439
ENAULT, A. 67
EREMENKO, B. V. 363
EXEROWA, D. 575
FAZYLOVA, M. 357
FEDOROVA, E. 339
FIEBER, Ch. 157
FILIPOVIC-VINCEKOVIC, N. 265
FÓTI, G. 33, 107
FRAKNÓY-KŐRÖS, V. 695
FRIBERG, S. 507
FRIDRIKHSBERG, D. A. 357
FUJIHIRA, M. 609
FURUSAWA, K. 221
FÜREDI-MILHOFER, H. 273
GAJÁRI, J. 49, 687
GILÁNYI, T. 633
GILDE, M. 413
GRIBANOVA, E. W. 149
GRIGOROV, O. N. 149
GRIST, D. M. 331
GRÓF, P. 645
GUSTAVSSON, H. 625
HAHN, M. 721
HAYANO, S. 609
HEALY, T. W. 7
HEERTJES, P. M. 141
HEGEDÜS, Z. 745
HOLT, C. 641
HOPMANN, R. F. W. 489
HUGGINS, M. L. 3
INZELT, Gy. 645
IOANETTE, A. 559
IVANOV, I. 583
IZMAILOVA, V. N. 617
JAFFÉ, J. 527, 543
JAIN, A. K. 501
JUHÁSZ, Z. 57
KABAI-FAIX, M. 299
KARAGOUNIS, G. 671
KAZAKOVA, J. 339
KEAVEY, R. P. 307
KENDIG, M. W. 15
KERTES, A. S. 497
KLOUBEK, J. 239
KOCHERGA, I. I. 283
KONTARAKI, E. 671
KOTERA, A. 221
KOVGANICH, N. Ya. 421
KRETZSCHMAR, G. 231
KURILENKO, O. D. 283, 291
KUTY, H. 107
KUZMANN, E. 745
LANDUYT-CAUFRIEZ, M. 527
LAPCZYNSKA, I. 507
LARHER, Y. 67

LEIDHEISER, H. 15
LENGYEL, P. 687
LEVY, O. 497
LINDMAN, B. 625
LŐRINC, A. 169
LUTTER, K. 695
LYKLEMA, J. 197, 205
MÁDI, I. 315
MAGYARITS, A. 429
MALIK, W. U. 501
MANEV, E. 583
MARKINA, Z. N. 465
MARKOVITS, G. Y. 497
MAZO, U. K. 617
MÁTTYUS, H. 687
MAYER, D. 265
MEGURO, K. 133, 601
MUKHIN, L. 339
MUTO, S. 601
MÜLLER, E. 551
NAGY, F. 745
NAGY, L. G. 33, 49, 99, 107, 687
NAGY, M. 447
NAGY, S. 745
NAKANISHI, H. 221
NEUSTADTER, E. L. 323, 331
NORDE, W. 205
OGNYEVA, L. 339
OMAROVA, K. I. 737
OPOCZKY, L. 57
OVCHARENKO, F. D. 19
PANDA, A. 91
PANDI-AGATHOKLI, I. 671
PÁSZLI, I. 115
PENEV, I. 575
PESCHEL, G. 187
PLATIKANOV, D. 591
PLATONOV, B. E. 363
POPOVIC, S. 265
POSS, A. 543
PURGARIC, B. 273
PURZ, H. J. 729
RADOEV, B. P. 583
RANGELOVA, N. 591
RÉDLY, M. 703
REHAK, J. 481
RETTIG, W. 535
RICHMOND, P. 307
ROHRSETZER, S. 299
ROY, R. S. 91
RUDZINSKI, W. 83
RUSANOV, A. J. 125
RUSZNÁK, I. 687
RUYSSCHAERT, J. M. 527, 543
SACKMANN, H. 535
SCHAY, G. 107
SCHULZE, H. J. 149
SCHWUGER, M. J. 247
SHALYT, S. 339
SHILOV, V. N. 349
SHUKROEV, M. Sh. 737
SIDDIQUI, M. J. 501
SIDOROVA, M. P. 357
SMOLDERS, C. A. 439
SINYOVA, A. V. 465
SMOLKA, H. G. 247
SNUPAREK, J. 663
SOKEROV, S. 387
SOLOMENTSEVA, I. M. 283
SONNTAG, H. 157, 397
SOOS, R. 711
STERYOPOULOS, K. 169
STOYLOV, S. P. 379
STRENGE, K. 397
SUBOTIC, B. 257
SZAKSZON, M. 517
SZÁNTÓ, F. 99, 413
SZVOBODA, M. 265
TAR, I. 455
TARANENKO, V. G. 405
TARASEVICH, Yu. I. 27
TIKHOMOLOVA, K. P. 371
TOMOAIA, M. 559
TÓTH, J. 41
TÖRÖK, G. 33
TRAPEZNIKOV, A. A. 405
TRAYKOV, T. Tr. 583
TSIKURINA, N. N. 465
TSUBAKI, K. 133
UENO, M. 133, 601
ULBERG, Z. R. 655
VÁMOS, E. 679
VANDERDEELEN, J. 75
VASILJEV, N. G. 19
VASSILIEFF, Chr. St. 583
VÁRADI, T. 447
VÁRKONYI, B. 413
VASKO, J. J. 291

VÉRTES, A. 745
VLIET, T. van 197
VOLLHARDT, D. 567
VOROBEVA, T. 387
WITTINGHAM, K. P. 331
WOJCIECHOWSKI, B. W. 83
WOLFRAM, E. 163, 447, 455, 633
YAMPOLSKAYA, G. P. 617
YATES, D. 7
YEREMOVA, Yu. Ya. 349
ZASTROW, L. 567

SUBJECT INDEX

Activated carbon 49, 107

Adhesion of powders 695

Adsorption
- kinetics of 231, 239
- theory of 41, 83

Adsorption, liquid/gas
- of surfactants 231, 239

Adsorption, solid/gas
- nitric oxide on halides 67

Adsorption, solid/liquid
- of albumin 205
- of methanol-benzene mixture on silicates 100
- of organic substances on charcoal 91
- of phosphate ions on ferric oxide 75
- of polymers 197, 213, 221, 286
- of surfactants 163, 247

Aerosil 214, 405

Antimony pentoxide 33

Capillarity 371

Capillary rise 141, 149

Contact angle
- on glass 141
- on pigments 171
- on polymers 133
- theory 125

Copper phthalocyanine 169

Corrosion 745

Critical surface tension 137, 145, 170

Dipole moment of colloids 349, 379

Disjoining pressure 180, 187

Dispersions
- in non-polar media 323
- theory of concentrated 307

DLVO theory 187, 379, 443

Electrokinetics 357, 363

Electrooptical properties 379, 387

Electron microscopy 721, 729

Emulsions 331, 339

Flocculation 291
- and rheological properties 397, 413

Gelatin 455

Gels 439, 447, 455

Hamaker constant 189

Heat of immersion 115, 690

Interfacial tension
- measurement 157

Ion exchange 703

Iron oxide 7, 439

Micelles
- formation of 465, 481, 489, 497, 501
- mixed 473

Microemulsion 507, 517

Monolayers 527, 535, 543, 559, 567, 721

Montmorillonite 21, 27, 99

Mössbauer spectroscopy 36, 745

Multilayers 135

Peptization 299

Pharmaceutics 711

Polarography 551

Polymers 3, 15
- adsorption of 197, 213, 221, 367
- dispersions 655

Polymerization
- emulsion 633
- interfacial 671

Polyvinyl alcohol 448, 633, 645

Polyvinyl pyrrolidone 448

Pore structure
- of active carbon 51
- of quartz powder 150

Proteins 619, 641

Pulp 687

Quartz
- electrokinetics 357
- liquid film on 179
- powder diaphragm 150

Rheology 405, 413, 421, 429

Rutile 214

Sediment volume 99, 413

Silicates

alumo- 19

kaolinite 413

layer 27

mechanochemistry of, 57

Silver iodide 5, 7, 257. 265, 283, 291

Soils 703

Solid surfaces

energy distribution of, 41

Sols

effect of polymers on the stability of, 291, 299

formation of, 257, 265, 273

stability of, 273, 283, 299

Solubilization 466, 482, 601, 609, 619

Streaming potential , 357

Surfactants

adsorption of 163, 247
on pigments 169

interaction with polymers 633

NMR of 625

nonionics 133, 247

Suspensions 397, 413, 429

Suspension effect 737

Thin liquid films 179, 575, 583, 591

Tribology 679

Wetting

of low-energy surfaces 133, 163

theory of, 125

We recommend

ACTA CHIMICA ACADEMIAE
SCIENTIARUM HUNGARICAE

This periodical of the Hungarian Academy of Sciences publishes papers in the sphere of chemistry, including the disciplines of inorganic and analytical chemistry, physical chemistry, organic chemistry and chemical engineering.

The papers are presented in English, German, French or Russian. Published in 16 issues of some 100 to 110 pages each, making up four volumes yearly.

Size: 17×25 cm

Distributors
KULTURA
H–1389 Budapest, P.O.B. 149

Series ISBN 963 05 0877 X
Volume ISBN 963 05 0845 1